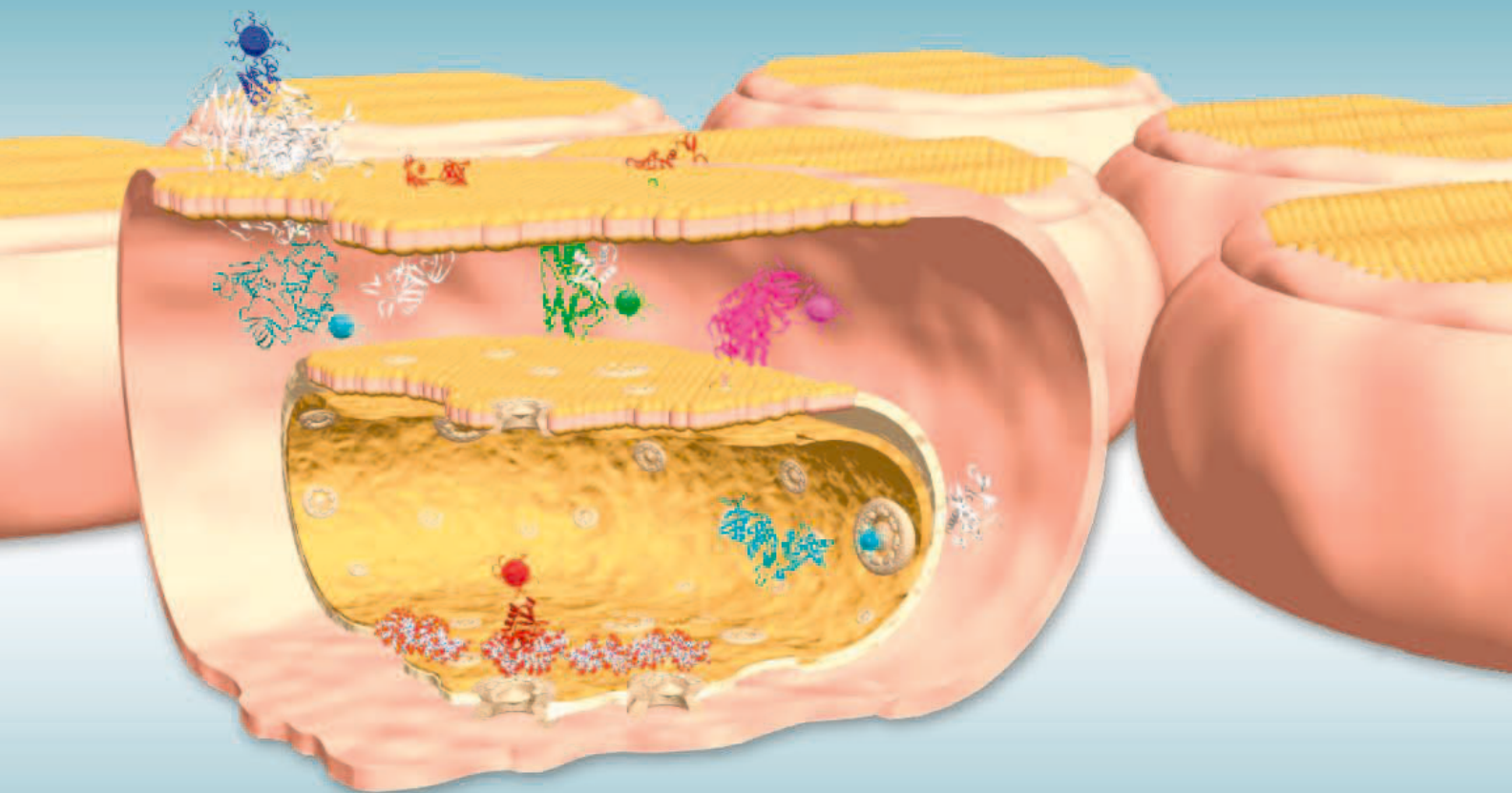


28 January 2005

Science

Vol. 307 No. 5709

Pages 465–628 \$10



125
YEARS OF GLOBAL
Science

 AAAS



Traditional Mini Preps are Over.

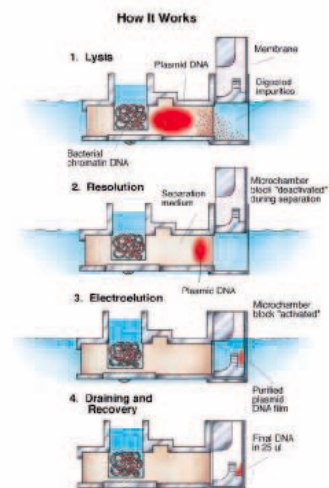


Start automating with the latest in plasmid DNA purification. The Mini Prep 96 can perform up to 96 preps in 1 hour of processing time. Up to 8 μ g of plasmid DNA per lane at less than \$1 a prep.

Start with easy operation. Disposable cassettes allow for direct loading of culture with no centrifugation.

Start the Mini Prep 96 with the push of a button. Remove high purity DNA and use in most microbiology protocols — including sequencing and cell transfection.

Start saving time and money with the Mini Prep 96.



Four Easy Steps to
Plasmid DNA Purification

Stop Manual Mini Preps



Start the Mini Prep 96™

1-800-466-7949
www.macconnell.com

Mini-Preps at the Push of a Button.
6195 Cornerstone Court, San Diego, California 92121, Fax: 858-452-6753

MACCONNELL
RESEARCH

2005 Catalog

from R&D Systems



R&D Systems 2005 catalog is now available. Our up-to-date, comprehensive product listing includes a broad selection of over 7,000 products for cancer, development, endocrinology, immunology, neuroscience, protease, and stem cell research. Please call or go online to request your copy today. Each catalog comes with our T Cell-mediated Cytotoxicity poster, featuring the new catalog art.

www.RnDSystems.com | (800) 343-7475

North America
R&D Systems, Inc.
Tel: (800) 343-7475
info@RnDSystems.com

Europe
R&D Systems Europe Ltd.
Tel: 0800 37 34 15
info@RnDSystems.co.uk

Germany
R&D Systems GmbH
Tel: 0800 909 4455
info@RnDSystems.co.uk

France
R&D Systems Europe
Tel: 0800 90 72 49
info@RnDSystems.co.uk





Amersham
Biosciences

Part of GE Healthcare



Focus on the highest level of peptide resolution.

Ettan™ MDLC is GE Healthcare's latest liquid chromatography system for proteomics applications. The system's patented nano-valve design provides ultra-low dead volumes for multidimensional and nanoscale peptide separation, resulting in unrivaled resolution and reproducibility.

This flexible and bioinert system lets you choose between dedicated high-throughput 1D-LC, online or offline 2D-LC configurations depending on your sample complexity. Its unmatched level of resolution enables you to maximize the performance of your mass spectrometer.

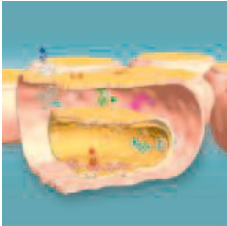
Visit www.mdlc.com



GE imagination at work

© 2004 General Electric Company - All rights reserved.
Amersham Biosciences UK Ltd, a General Electric company,
going to market as GE Healthcare.

GE02-05



COVER Artist's cutaway view through a live cell and its nucleus, showing components of a signaling pathway labeled with quantum dots of different colors (spheres). The long fluorescence lifetimes of quantum dots (semiconductor nanocrystals) will enable visualization of signal transduction pathways in real time. See page 538. [Image: Darren Keogh]

DEPARTMENTS

- 475 SCIENCE ONLINE
- 477 THIS WEEK IN SCIENCE
- 481 EDITORIAL by Rodger W. Bybee and Donald Kennedy
Math and Science Achievement
- 483 EDITORS' CHOICE
- 488 CONTACT SCIENCE
- 491 NETWATCH
- 537 AAAS NEWS AND NOTES
- 605 NEW PRODUCTS
- 610 SCIENCE CAREERS

NEWS OF THE WEEK

- 492 **DIVERSITY**
Summers's Comments Draw Attention to Gender, Racial Gaps
- 493 **VIROLOGY**
One Virus, Three Names, Three Claims
- 495 **CHEMISTRY**
Shape-Shifting Catalyst Lights Way to New Strategy for Detecting Chemicals
- 495 SCIENCE SCOPE
- 496 **CLIMATE CHANGE**
Panel Urges Unified Action, Sets 2° Target
- 496 **PLANETARY SCIENCE**
Missing Noble Gases Hint How Titan Got Its Dense Atmosphere
- 497 **GREENHOUSE WARMING**
Climate Modelers See Scorching Future as a Real Possibility
- 498 **AGRICULTURAL RESEARCH**
Centers Embrace an Alliance But Remain Wary of a Merger
- 498 **NASA BUDGET**
Hubble, Other Programs Face Cuts in 2006
- 499 **HIGHER EDUCATION**
Fundraising Begins for Network of Four African Institutes
- 499 **RESEARCH FUNDING**
Saudi Millionaire Plans an NSF for Arab Scientists
- 501 **BIODEFENSE LABS**
Boston University Under Fire for Pathogen Mishap
- 501 **CLIMATE CHANGE**
Scientist Quits IPCC Panel Over Comments



502



505



525

NEWS FOCUS

- 502 **SOUTH ASIA TSUNAMI**
A Race to Beat the Odds
Nuke Policy Leads India to Build Own Network
DNA Helps Identify Missing in the Tsunami Zone
- 505 **EVOLUTION**
Dover Teachers Want No Part of Intelligent-Design Statement
- 507 **ENVIRONMENTAL HEALTH**
Debate Continues Over Safety of Water Spiked With Rocket Fuel
- 508 **MEETING**
American Astronomical Society
Galaxy Patterns Preserve an Imprint of the Big Bang
Satellite Swiftly Catches New Bursts
An Origin for the Fiercest Cosmic Rays?
Snapshots From the Meeting
- 511 RANDOM SAMPLES

LETTERS

- 515 **Marburger Makes His Position Clear** *J. H. Marburger III. The Ethics of Deriving Gametes from ES Cells* *A. Lippman and S. A. Newman. Response* *G. Testa and J. Harris. Costs of a Rotavirus Vaccine* *J. Wecker. Preserving an Important Collection* *N. Zinder and R. J. Roberts. Science and the Bush Administration* *J. C. Gruman*
- 519 Corrections and Clarifications

BOOKS ET AL.

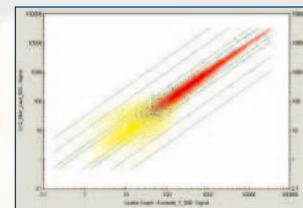
- 520 **VERTEBRATE PALEONTOLOGY**
The Dinosauria 2nd ed.
D. B. Weishampel, P. Dodson, H. Osmólska, Eds., reviewed by H. C. E. Larsson
- 521 **COMPUTING**
The SIAM 100-Digit Challenge A Study in High-Accuracy Numerical Computing
F. Bornemann, D. Laurie, S. Wagon, J. Waldvogel, reviewed by G. Strang
- 522 **HISTORY OF SCIENCE**
Pandora's Breeches Women, Science and Power in the Enlightenment
P. Fara, reviewed by A. Gopinathan

POLICY FORUM

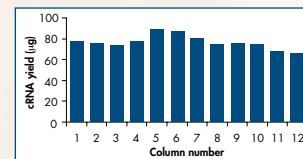
- 525 **ECOLOGY**
Do the Largest Protected Areas Conserve Whales or Whalers?
L. R. Gerber, K. D. Hyrenbach, M. A. Zacharias

Integrated Solutions — Gene Expression Analysis

Standardize your target preparation for more precise GeneChip® array results!



Good correlation with manual target preparation procedure



Average yield of cRNA from 96 RNA samples from HeLa S3 cells



Automated target preparation

The BioRobot® Gene Expression system automates the preparation of targets for Affymetrix® GeneChip arrays for more reproducible data!

Standardized target preparation is of critical importance for precise GeneChip array results. Streamline your workflow and increase reproducibility with the BioRobot Gene Expression system and Specialist Pack for GeneChip target preparation!

- **More precise array results** — through standardized target preparation, from cDNA synthesis to cRNA fragmentation
- **Reduced hands-on time** — with streamlined, automated workflow
- **Comprehensive support** — including installation, training, chemistries starter pack, and software protocols

Visit us at www.qiagen.com/automation and discover the standardized solution for precise GeneChip array results!

Trademarks: QIAGEN®, BioRobot® (QIAGEN Group); Affymetrix®, GeneChip® (Affymetrix, Inc.). QIAGEN robotic systems are not available in all countries; please inquire. IASBRTPO105S1VW 12/2004 © 2004 QIAGEN, all rights reserved.



WWW.QIAGEN.COM

PERSPECTIVES

- 527 **EVOLUTION**
An Eocene Big Bang for Bats *N. B. Simmons* *related Report page 580*
- 528 **PARASITOLOGY**
Malaria Vaccines: Back to the Future? *A. P. Waters et al.*
- 530 **PHYSIOLOGY**
A NEAT Way to Control Weight? *E. Ravussin* *related Report page 584*
- 531 **PHYSICS**
How to Create a Spin Current *P. Sharma*
- 533 **ASTRONOMY**
The Hunt for Intermediate-Mass Black Holes *G. Fabbiano*

REVIEW

- 538 **BIOCHEMISTRY**
Quantum Dots for Live Cells, in Vivo Imaging, and Diagnostics *X. Michalet et al.*

SCIENCE EXPRESS www.sciencexpress.org

PLANT SCIENCE: BZR1 Is a Transcriptional Repressor with Dual Roles in Brassinosteroid Homeostasis and Growth Responses

J.-X. He, J. M. Gendron, Y. Sun, S. S. L. Gampala, N. Gendron, C. Q. Sun, Z.-Y. Wang

A newly described transcription factor regulates both the biosynthesis of a steroid hormone in plants and how that hormone controls growth.

NEUROSCIENCE: Control of Excitatory and Inhibitory Synapse Formation by Neuroligins

B. Chih, H. Engelman, P. Scheiffele

A cell surface protein coordinates the process by which two neurons form a synapse, triggering spine formation and specifying protein accumulation.

BIOCHEMISTRY: Membrane Insertion of a Potassium-Channel Voltage Sensor

T. Hessa, S. H. White, G. von Heijne

Although it is highly charged, the voltage-sensing portion of the potassium channel can move easily through the lipid bilayer to open the channel.

PHYSICS: Heat Capacity of a Strongly Interacting Fermi Gas

J. Kinast, A. Turlapov, J. E. Thomas, Q. Chen, J. Stajic, K. Levin

A change in heat capacity of supercooled lithium atoms marks the transition between a Bose-Einstein state with strongly paired atoms and a more weakly paired superfluid state.

BREVIA

- 545 **CELL BIOLOGY:** Marine Fish Egg Hydration Is Aquaporin-Mediated

M. Fabra, D. Raldúa, D. M. Power, P. M. T. Deen, J. Cerdà

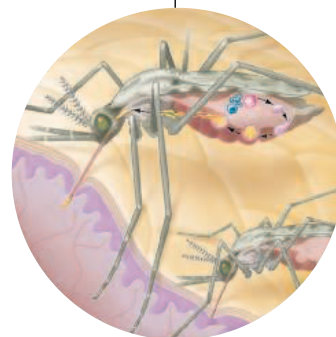
A water channel on the surface of fish eggs allows hydration that ensures proper buoyancy of the egg for dispersal in the ocean.

RESEARCH ARTICLES

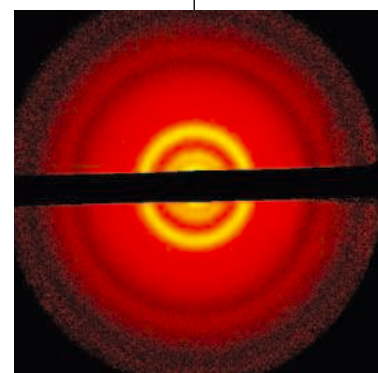
- 546 **PLANETARY SCIENCE:** A Giant Impact Origin of Pluto-Charon
R. M. Canup
Charon, Pluto's moon, may have formed when Pluto received a grazing blow from another large icy body, implying that large early collisions affected the outer solar system.
- 550 **ECOLOGY:** Farming and the Fate of Wild Nature
R. E. Green, S. J. Cornell, J. P. W. Scharlemann, A. Balmford
A model determines the consequences for wildlife of the trade-off between yield intensity of land under cultivation and amount of land under cultivation.

REPORTS

- 555 **CHEMISTRY:** Ammonia Synthesis from First-Principles Calculations
K. Honkala et al.
Calculations relating the rate of ammonia synthesis to the size distribution of ruthenium catalyst nanoparticles aid in the design of this catalyst.
- 558 **CHEMISTRY:** Dark Structures in Molecular Radiationless Transitions Determined by Ultrafast Diffraction
R. Srinivasan, J. S. Feenstra, S. T. Park, S. Xu, A. H. Zewail
Electron diffraction reveals how organic molecules excited by light release energy through a series of structural changes induced by electronic and vibrational motions.



528



558

Contents continued ►

Now! Real-time PCR results in under 40 minutes!



Real Affordable
Applied Biosystems
7300 Real-Time PCR System



Real Versatile
Applied Biosystems
7500 Real-Time PCR System



Real Fast
Applied Biosystems
7500 Fast Real-Time PCR System

Looking for faster real-time PCR results?
Our new Applied Biosystems 7500 Fast Real-Time PCR System, the choice for labs in a hurry, is

the latest addition to the innovative family of real-time PCR systems from Applied Biosystems. It enables 96-well format high-speed thermal cycling, easily integrating into your lab's workflow. Whichever system you choose, you'll get the gold standard combination of TaqMan® assays and the proven performance of the industry leader—plus unbeatable real-time chemistry choices, powerful software, and a comprehensive selection of reagents and consumables. For the real deal in real-time PCR, visit <http://info.appliedbiosystems.com/realtimepcr>



iScience. Applied Biosystems provides the innovative products, services, and knowledge resources that are enabling new, integrated approaches to scientific discovery.

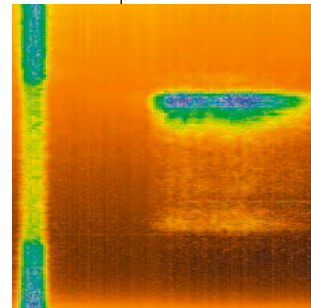


For Research Use Only. Not for use in diagnostic procedures. Practice of the patented polymerase chain reaction (PCR) process requires a license. The Applied Biosystems 7300/7500 Real-Time PCR Systems are Authorized Thermal Cyclers for PCR and may be used with PCR licenses available from Applied Biosystems. Their use with Authorized Reagents also provides a limited PCR license in accordance with the label rights accompanying such reagents. Purchase of this instrument does not convey any right to practice the 5' nuclease assay or any of the other real-time methods covered by patents owned by Roche or Applied Biosystems.

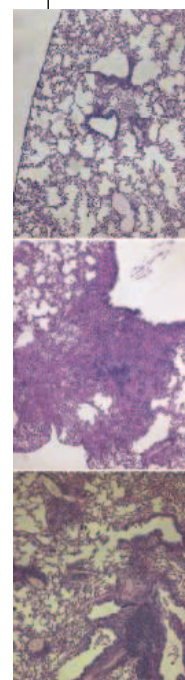
Applied Biosystems is a registered trademark and AB (Design), Applera, iScience, and iScience (Design) are trademarks of Applied Biosystems Corporation or its subsidiaries in the US and/or certain other countries. TaqMan is a registered trademark of Roche Molecular Systems, Inc. Information is subject to change without notice. © 2005 Applied Biosystems. All rights reserved.

REPORTS CONTINUED

- 563 **ATMOSPHERIC SCIENCE:** Electron Spectroscopy of Aqueous Solution Interfaces Reveals Surface Enhancement of Halides
S. Ghosal et al.
 Halides, particularly the larger ones, become concentrated at the surface of liquid salt droplets, enhancing their reactivity in Earth's atmosphere.
- 566 **PLANETARY SCIENCE:** Nightglow in the Upper Atmosphere of Mars and Implications for Atmospheric Transport
J.-L. Bertaux et al.
 Glowing, nighttime nitric oxide emissions, detected by Mars Express, track the descent of high air masses during winter above the martian south pole.
- 569 **MATERIALS SCIENCE:** Prediction of Hydrogen Flux Through Sulfur-Tolerant Binary Alloy Membranes
P. Kamakoti, B. D. Morreale, M. V. Ciocco, B. H. Howard, R. P. Killmeyer, A. V. Cugini, D. S. Sholl
 Ab initio calculations accurately predict how hydrogen diffuses through metal alloy membranes and could improve hydrogen purification.
- 573 **PLANT SCIENCE:** Micropylar Pollen Tube Guidance by Egg Apparatus 1 of Maize
M. L. Márton, S. Cordts, J. Broadhvest, T. Dresselhaus
 In flowering plants, a newly identified peptide signal guides the sperm cell-containing pollen tube to the egg for fertilization.
- 576 **EVOLUTION:** A Brief History of Seed Size
A. T. Moles, D. D. Ackerly, C. O. Webb, J. C. Tweddle, J. B. Dickie, M. Westoby
 A comprehensive seed survey shows that the evolutionarily older gymnosperms have larger seeds than flowering plants but that larger flowering plants have larger seeds.
- 580 **EVOLUTION:** A Molecular Phylogeny for Bats Illuminates Biogeography and the Fossil Record
E. C. Teeling, M. S. Springer, O. Madsen, P. Bates, S. J. O'Brien, W. J. Murphy
 New sequence data supplements an incomplete fossil record to predict a phylogeny for all living bats, identifying four groups of microbats and a likely origin in North America. *related Perspective page 527*
- 584 **PHYSIOLOGY:** Interindividual Variation in Posture Allocation: Possible Role in Human Obesity
J. A. Levine et al.
 During their daily lives, lean people spend less time sitting than do people who are overweight, even after the former have purposefully gained weight. *related Perspective page 530*
- 586 **MOLECULAR BIOLOGY:** Sequence-Directed DNA Translocation by Purified FtsK
P. J. Pease, O. Levy, G. J. Cost, J. L. Ptacin, D. Sherratt, C. Bustamante, N. R. Cozzarelli
 Individual DNA translocase molecules zip along single strands of DNA at 5 kilobases per second and reverse without dissociation upon encountering certain asymmetric sequences.
- 590 **IMMUNOLOGY:** Restoration of Tolerance in Lupus by Targeted Inhibitory Receptor Expression
T. L. McGaha, B. Sorrentino, J. V. Ravetch
 Simply increasing the number of inhibitory receptors on immune cells prevents mice from developing an apparently complicated autoimmune disorder similar to lupus.
- 593 **IMMUNOLOGY:** Endogenous MHC Class II Processing of a Viral Nuclear Antigen After Autophagy
C. Paludan, D. Schmid, M. Landthaler, M. Vockerodt, D. Kube, T. Tuschl, C. Münz
 An endogenous nuclear antigen can be presented by a pathway thought to be restricted to antigens derived from exogenous, internalized sources.
- 596 **DEVELOPMENTAL BIOLOGY:** Small CTD Phosphatases Function in Silencing Neuronal Gene Expression
M. Yeo, S.-K. Lee, B. Lee, E. C. Ruiz, S. L. Pfaff, G. N. Gill
 Cells outside the brain guard against becoming neurons by expressing an enzyme that modifies RNA polymerase in a way that prevents it from transcribing neural genes.
- 600 **NEUROSCIENCE:** Illumination of the Melanopsin Signaling Pathway
S. Panda, S. K. Nayak, B. Campo, J. R. Walker, J. B. Hogenesch, T. Jegla
 In mammals, the opsin that detects light for circadian rhythms and pupil constriction activates signaling pathways that are similar to those used in invertebrates for vision.



566



590

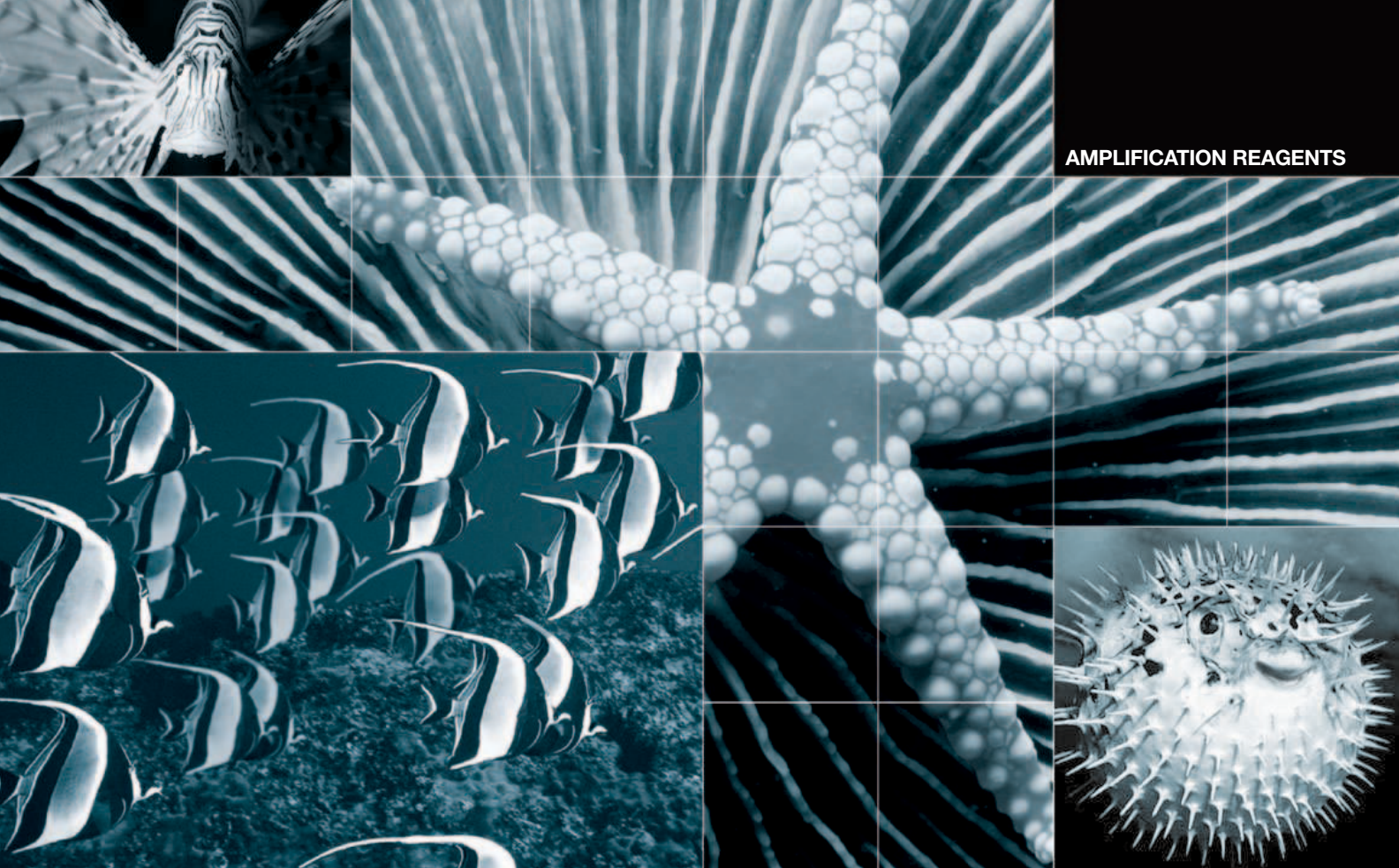


ADVANCING SCIENCE, SERVING SOCIETY

SCIENCE (ISSN 0036-8075) is published weekly on Friday, except the last week in December, by the American Association for the Advancement of Science, 1200 New York Avenue, NW, Washington, DC 20005. Periodicals Mail postage (publication No. 484460) paid at Washington, DC, and additional mailing offices. Copyright © 2005 by the American Association for the Advancement of Science. The title SCIENCE is a registered trademark of the AAAS. Domestic individual membership and subscription (51 issues): \$135 (\$74 allocated to subscription). Domestic institutional subscription (51 issues): \$550; Foreign postage extra: Mexico, Caribbean (surface mail) \$55; other countries (air assist delivery) \$85. First class, airmail, student, and emeritus rates on request. Canadian rates with GST available upon request, GST #1254 88122. Publications Mail Agreement Number 1069624. Printed in the U.S.A.

Change of address: allow 4 weeks, giving old and new addresses and 8-digit account number. Postmaster: Send change of address to Science, P.O. Box 1811, Danbury, CT 06813-1811. Single copy sales: \$10.00 per issue prepaid includes surface postage; bulk rates on request. Authorization to photocopy material for internal or personal use under circumstances not falling within the fair use provisions of the Copyright Act is granted by AAAS to libraries and other users registered with the Copyright Clearance Center (CCC) Transactional Reporting Service, provided that \$15.00 per article is paid directly to CCC, 222 Rosewood Drive, Danvers, MA 01923. The identification code for Science is 0036-8075/83 \$15.00. Science is indexed in the Reader's Guide to Periodical Literature and in several specialized indexes.

Contents continued ►



A Sea of Amplification Options

A complete selection of amplification reagents for both real-time and conventional PCR

- **Enzymes and kits for a broad array of applications** — hot-start PCR, reverse transcription, and real-time PCR using SYBR Green or probe-based detection
- **High-quality reagents designed for convenience** — easy-to-use kits and protocols simplify reaction setup to generate consistent, reproducible results
- **Products developed and supported by amplification experts** — formulated to provide sensitive detection and linear data over a wide dynamic range

To learn more about PCR and the results you can obtain, visit us on the Web at www.bio-rad.com/ad/ampreagents/



Practice of the patented polymerase chain reaction (PCR) process requires a license. SYBR is a trademark of Molecular Probes, Inc. Bio-Rad Laboratories, Inc. is licensed by Molecular Probes, Inc. to sell reagents containing SYBR Green I for use in real-time PCR for research purposes only.

Visit us on the Web at discover.bio-rad.com
 Call toll free at 1-800-4BIORAD (1-800-424-6723);
 outside the US, contact your local sales office.

BIO-RAD

Viagra for Broken Hearts?

Early experiments with mice suggest the drug has promise for treating heart failure.

Forgetting to Remember

Older people with Alzheimer-related allele may have more problems remembering future plans.

A Prolonged Demise

The mass extinction that gave rise to the dinosaurs may not have been caused by an asteroid.



Solving the tech transfer puzzle.

science's next wave www.nextwave.org CAREER RESOURCES FOR YOUNG SCIENTISTS

CANADA: Harnessing Your Discovery—Tech Transfer at Universities *A. Fazekas*

Learn how two of Canada's most successful university technology transfer offices work.

US: Educated Woman Chapter 35—Thesis Proposal Time *M.P. DeWhyse*

You must search and read the literature before you present your proposal to your thesis committee.

UK: The Fringe Benefits of Science *P. Dee*

It may not be the reason you are in the lab, but the fringe benefits of science do add up.

GRANTSNET: International Grants and Fellowships Index *Next Wave Staff*

GrantsNet updates its list of international fellowship, research funding, and prize competition opportunities.

US: Careers in Science Web Log *J. Austin*

Breaking news and observations related to science careers are updated throughout the week.

science's sage ke www.sageke.org SCIENCE OF AGING KNOWLEDGE ENVIRONMENT

PERSPECTIVE: Apoptotic Killing of Fibroblasts by Matrix-Bound Advanced Glycation Endproducts

M. E. Obrenovich and V. M. Monnier

AGE-modified extracellular matrix protein promotes programmed cell death.

NEWS FOCUS: Coming Back for Seconds *R. J. Davenport*

Extra doses of lipin protein spur obesity.

NEWS FOCUS: Led Astray *M. Leslie*

Worn-out cells prod healthy ones toward cancer.



Expanding on lipin.



School is in.

science's stke www.stke.org SIGNAL TRANSDUCTION KNOWLEDGE ENVIRONMENT

EDITORIAL GUIDE: Teaching with STKE *N. R. Gough*

STKE presents an online course supplement to a graduate course in cell signaling.

TEACHING RESOURCE: Cell Signaling Systems—A Course for Graduate Students *R. Iyengar, M. Diverse-Pierluissi, D. Weinstein, L. Devi*

Students and instructors can access information about creating and participating in an advanced course on cell signaling.

FORUM: Principles of Cell Signaling and Biological Consequences *A. Chan, R. Iyengar, S. Aaronson, A. Caplan, S. Salton, M. M. Zhou*

This online discussion supplements the first section of the Cell Signaling Systems course.

Separate individual or institutional subscriptions to these products may be required for full-text access.

GrantsNet
www.grantsnet.org
RESEARCH FUNDING DATABASE

AIDScience
www.aidscience.com
HIV PREVENTION & VACCINE RESEARCH

Members Only!
www.AAASMember.org
AAAS ONLINE COMMUNITY

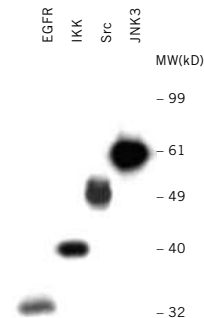
Functional Genomics
www.sciencegenomics.org
NEWS, RESEARCH, RESOURCES



Shoes are like kinases. One is never enough.

Introducing the SignalScout™ Profiling System from Stratagene for more manageable, multiplex kinase assays.

Determining the activity of protein kinases remains one of the biggest challenges in signal transduction research. Our new SignalScout™ Kinase Profiling System* allows you to screen for the activity of at least four kinases at one time, without any cross-reactivity. You can build your own multiplex kinase assays by choosing from our wide selection of kinase substrates, offered in various sizes for easy laddering. Together with our new antibodies against protein kinases, we are making your kinase research easier and faster.



DETERMINATION OF KINASE ACTIVITY USING THE SIGNALSCOUT™ KINASE SUBSTRATE LADDER KIT

GST fusion protein kinase substrates (EGFR, IKK, Src, and JNK3) were mixed to 1 µg/µl and phosphorylated by their corresponding protein kinases in the presence of ³²P ATP, separated on a 10% SDS-PAGE, and exposed for 3 hours with BioMax MR film (Kodak). Phosphorylation by each kinase on its respective substrate in the mixture is demonstrated without cross reactivity (between any kinase and the non-specific substrates in the ladder).

Need More Information? Give Us A Call:

Stratagene USA and Canada
Order: (800) 424-5444 x3
Technical Services: (800) 894-1304

Stratagene Japan K.K.
Order: 03-5159-2060
Technical Services: 03-5159-2070

Stratagene Europe
Order: 00800-7000-7000
Technical Services: 00800-7400-7400

*Patent pending

www.stratagene.com/signaling

Ask Us About These Great Products:

SignalScout™ Kinase Substrate Ladder Kit 5 assays 206330

Individual SignalScout™ kinase substrates available.
Please call for ordering information.



Images by Connecting with Dots

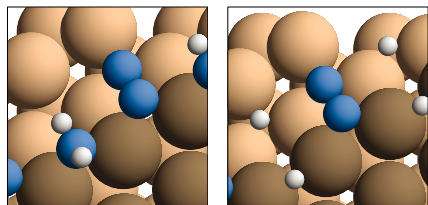
Chemical dyes have long been used to enhance contrast in biological imaging, but are limited by their rapid bleaching and a lack of tunability in their emission spectrum. Semiconductor nanoparticles, also known as quantum dots, show exceptional stability and can be easily tuned by changing the particle size and chemistry. However, to achieve widespread use, a number of techniques have been developed to synthesize, solubilize, and functionalize the particles for use in vitro and in vivo. **Michalet et al.** (p. 538; see the cover) review the state of the art in making and applying quantum dots to biological problems.

Electrons Light the Darkness

After molecules absorb light, they must somehow dissipate the excess energy. In fluorescence, much of this energy is simply re-emitted as photons. Alternatively, the molecules may undergo a range of radiationless processes, such as bond stretching and breaking, or changes in electronic structure, and the intermediates formed are termed "dark" states. **Srinivasan et al.** (p. 558) have used time-resolved electron diffraction to probe the structures of transient dark states that form after photoexcitation of benzaldehyde and several pyridine derivatives. In benzaldehyde, competing bond scission and singlet-to-triplet conversion pathways can be distinguished. The pyridine study reveals temporary C–N bond cleavage in pyridine and methylpyridine relaxation, in contrast with energy transfer to delocalized vibrations in dimethylpyridine.

Recovering Rates

One goal in catalysis is to reproduce the rate of a complex reaction from quantum chemical calculations. **Honkala et al.** (p. 555) calculated the rate of ammonia synthesis over nanosized ruthenium particles using density functional theory, with the only experimental input being the particle size distribution, from which the authors estimated the number of step sites that favor the rate-limiting N₂ dissociation step. Their rates agree with experimental data for ammonia synthesis over Ru nanoparticles supported on magnesium aluminum spinel to within factors of 3 to 20 for temperatures between 320° and 440°C. Compensation



Bumping into Your Partner-to-Be

Pluto and Charon orbit the Sun on an inclined and eccentric path that comes inside that of Neptune from time to time. Although the Pluto-Charon system is small (both objects are smaller than Earth's Moon) and has an unusual orbit, it shares some similarities with the Earth-Moon system, particularly a high angular momentum. **Canup** (p. 546) modeled the formation of Pluto-Charon with collisions between 1000-kilometer objects and found that Charon is likely to have formed as an intact satellite from a grazing collision between undifferentiated bodies. These simulations suggest that many satellites might form by collisions, and that collisions in the Kuiper Belt may have been relatively common in the early solar system.



effects between changes in activation energies and surface coverages help to make the final rates less sensitive to absolute errors in the several individual elementary reaction steps.

Martian Glow

The ultraviolet and infrared spectrometer (SPICAM) on the Mars Express spacecraft has detected a 20-kilometer-thick spherical shell of nitrous oxide (NO) at an altitude of about 70 kilometers in the martian atmosphere. **Bertaux et al.** (p. 566) found that the concentration of NO is highest (and the emission is brightest) in the south polar winter night. The emission, called night glow, occurs in a region not illuminated by the Sun, so the NO must have formed from O₂, CO₂, and N₂ that had photodissociated on the sunlit side. The N and O atoms were transported to the night side and formed NO at lower altitudes. The night glow allows scientists to track the atmospheric circulation pattern and understand climate change on Mars.

Farming-Biodiversity Face-Off

Farming is already the single greatest threat to the persistence of the other species on the planet. This threat is set to grow as human demand for food rises two- to threefold during the next 50 years. Two main solutions to the problems of coexistence of biodiversity and increased demand for agricultural products have been proposed: wildlife-friendly farming, and land-sparing permitted by high-yield farming. **Green et al.** (p. 550, published online 23 December 2004) show that the best type of farming for species persistence depends on the demand for agricultural products, and on the shapes of functions relating the population densities of different species on farmland to agricultural yield. Data for a range of taxa in developing countries suggest that high-yield farming may allow more species to persist.

Bat Origins and Diversity

Bats represent one-fifth of extant mammalian diversity, yet they are the least represented mammalian order within the fossil record. Where fossils do exist, they are often only single teeth, making it difficult to identify species and decipher the chronology of divergence events and biogeography. **Teeling et al.** (p. 580; see the Perspective by **Simmons**) have sequenced multiple genes from representatives of all bat families and have derived a phylogeny that divides the order Chiroptera into two suborders and four superfamilies, as well as resolving the phylogenetic position of *Craseonycteris thonglongai*, the smallest mammal in the world. The four microbat lineages originated 52 to 50 million years ago at the peak of Tertiary insect diversity in Laurasia. The analysis also suggests that as much as 61% of the bat fossil record may be missing.

CONTINUED ON PAGE 479



intuition. . . . scanning. . . . microarray analysis. . . . informatics. . . . discovery

**GenePix® users
get
more
published ***

GenePix and Acuity® users trust their data, trust their results and trust their conclusions. They get more done, and get more published.

Three different microarray scanners meet all your needs. GenePix Pro and Acuity microarray informatics software lead you to discovery.

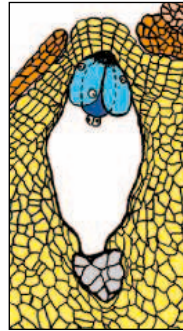
Visit our web site now and discover why we're getting so much notice.
www.moleculardevices.com/transition

 **Molecular Devices**

* *In a recent survey of PubMed entries, twice as many publications referenced GenePix than any other slide-based microarray imaging platform.*

Let ZmEA Guide You

In flowering plants, the immotile sperm cells are transported toward the egg through the pollen tube, which navigates its own path from the pollen grain to the female gametophyte. **Márton *et al.*** (p. 573) have now identified one of the signals likely to guide the pollen tube. Studying maize, a small egg apparatus-derived protein, ZmEA1, was found to light up the way for the final steps of pollen tube guidance. The *ZmEA1* gene was expressed in the egg apparatus, and the protein acted as a short-range signal required for successful fertilization. After fertilization, ZmEA1 expression was rapidly down-regulated.



Seeds Great and Small

Seed mass varies across more than ten orders of magnitude, from the dustlike seeds of orchids to the 20-kilogram double coconut. Using data from nearly 13,000 plant species, **Moles *et al.*** (p. 576) trace the history of the evolutionary radiation of seed mass, from the emergence of angiosperms to the present day. They identify the largest divergence events and those that contributed most to the spread of seed mass across present-day species. Large divergences in seed size were more consistently associated with divergences in plant-growth form than with divergences in dispersal syndrome or in latitude.

The Rewards of a Stand-Up Routine

Although purposeful exercise like jogging is well known to reduce one's risk of obesity, it is less clear whether interindividual differences in posture and body movement during the routines of daily life have an impact on body weight. Using exquisitely sensitive technology, **Levine *et al.*** (p. 584; see the Perspective by **Ravussin**) continuously measured the posture and body position of 20 volunteers during a 10-day period. All volunteers were self-proclaimed "couch potatoes," but 10 were lean and 10 were mildly obese. On average, the lean individuals stood up and moved around 2 hours longer each day than the overweight individuals, reinforcing the notion that even simple changes in behavior, such as sitting less each day, may help to prevent weight gain.

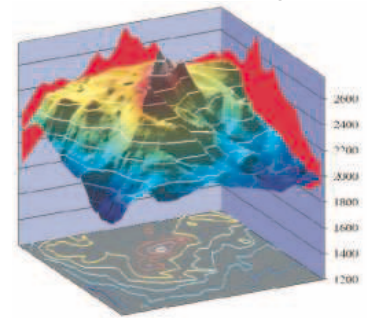
The Nuts and Bolts of an Autoimmune Disorder

Autoimmune disorders, such as systemic lupus erythematosus (SLE), arise from a breakdown of immune tolerance to the body's own constituents, and represent the culmination of multiple environmental and genetic influences. Nevertheless, it is likely that specific regulatory pathways of the immune system are perturbed. **McGaha *et al.*** (p. 590) studied genetically distinct strains of mice that share a susceptibility to developing SLE and that also express reduced levels of a particular inhibitory antibody-binding receptor. Engineering bone marrow from these animals to express the receptor gene prevented disease by partially restoring levels of the receptor on B cells. Thus, even in the context of multiple contributing factors, the modulation of a single regulatory pathway can be sufficient to dictate the course of autoimmune pathology.

Autophagy and Antigen Presentation

One-third of all eluted major histocompatibility complex (MHC) class II natural ligands are derived from endogenous cytosolic or nuclear proteins, but the underlying pathway has been difficult to pinpoint. EBNA1, the dominant CD4⁺ T cell antigen of the human oncogenic Epstein-Barr virus (EBV), is the sole viral antigen present in all EBV-associated malignancies. **Paludan *et al.*** (p. 593, published online 9 December 2004) describe how autophagy, a process by which the cell degrades defunct cytosolic components in times of stress, leads to MHC class II processing and presentation of endogenous EBNA1. The viral protein was imported into lysosomes by autophagy, where a subset of lysosomal proteases was responsible for EBNA1 degradation. Furthermore, inhibition of autophagy decreased target recognition by EBNA1-specific CD4⁺ T cell clones.

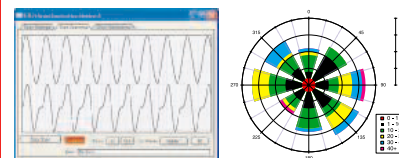
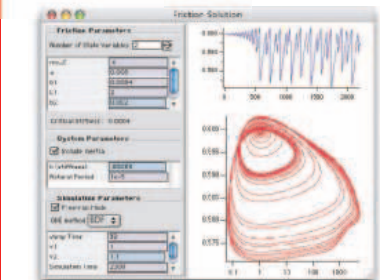
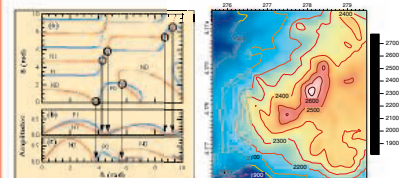
Technical Computing for Scientists and Engineers



IGOR Pro 5

for Windows and Macintosh

- Print with publication quality.
- Control every aspect of graph axes and annotations to satisfy the most demanding journals.
- Quickly graph thousands or millions of values.
- Share data and graphics cross-platform.
- Acquire data from instruments.
- Create custom graphical user interfaces.
- Analyze data using statistics, curve fitting, signal and image processing, and matrix operations.
- Automate calculations with IGOR's programming language and symbolic debugger.
- Process and display images, surfaces, and contours.
- Import Excel, binary, text, and other data.
- Export a wide variety of graphics formats.



Windows 98, Mac OS 9.1, Mac OS X 10.2 or later

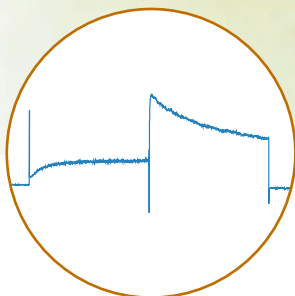
- Used by tens of thousands of scientists and engineers since IGOR debuted in 1988.
- Free highly-acclaimed technical support.
- Downloadable no-registration demo.
- 90 day money-back guarantee.

• **Science 25% off special at:**

<http://www.wavemetrics.com/sci/>
Promotion Code: SCIO5

(503) 620-3001 • (503) 620-6754 (FAX)

Ion channels need the right treatment.



We have the prescription.

Molecular Devices offers the most complete panel of products for ion channel drug discovery.

- ➔ OpusXpress® for target validation
- ➔ IonWorks HT™ for secondary screening
- ➔ PatchXpress® for safety profiling

Our revolutionary ion channel technology is only the beginning. We provide industry-leading field service and scientific support worldwide and established solutions that deliver proven results in ion channel drug discovery.

Let us help you choose the right treatment.

See us at LabAutomation 2005, Booth #1013. For a comparison of OpusXpress, IonWorks and PatchXpress, visit our web site at www.ionchanneltreatment.com.



Math and Science Achievement

The results of the Trends in International Mathematics and Science Study (TIMSS) tests for 2003 were released on 14 December 2004. They contain some important messages about what's happening globally in math and science education—messages that are taken increasingly seriously by the nearly 50 participating nations and, we hope, by the readers of *Science*. The tests, also given in 1995 and 1999, measure mathematics and science achievement at grades 4 and 8 (reflecting an average of 4 or 8 years of schooling, respectively). Because they are closely linked to school mathematics and science curricula in the participating countries, the tests yield data on student achievement that relate to the concepts learned in their own schools.

Comparative national data for mathematics and science in both grades reveal a near-monopoly by Asia in the top-scoring group, including Singapore, Korea, Hong Kong, Taiwan, and Japan. Several European nations cluster below that, and the United States and several other nations are in the next set. There is a considerable spread of scores among nations, with the average scaled scores from eighth-grade mathematics ranging from 605 (Singapore) to 264 (South Africa). Some of the “best performer” nations were those who ranked high on the United Nations Development Programme's Human Development Index (HDI), but students in Hungary, Malaysia, and South Korea, for example, did much better than their country's HDI. Between 1995 and 2003, scores for both fourth- and eighth-graders in both disciplines increased or held constant in most nations in the TIMSS samples, with improvement being especially noteworthy in fourth-grade mathematics scores. For international science, that's good news.

In the United States, mathematics and science education has been a core item in the national debate over education reform at the K–12 level, and active national and local efforts have focused on curriculum improvement. So how did U.S. students do on TIMSS? At grade 4, between 1995 and 2003, U.S. student scores held constant, although their international ranking declined slightly. But the average scores of U.S. eighth-graders made statistically significant improvements between 1995 and 2003 in both mathematics and science. In other good news, as described by the U.S. Subpopulation Performance analysis, eighth-grade African-American and Hispanic students demonstrated improvement in both mathematics and sciences over that 8-year span, and their average science scores narrowed the achievement gap that previously separated their performance from that of whites.

These gains should provide some comfort to U.S. scientists who worry about the health of elementary education. Can we find a cause? Some will surely give credit to the No Child Left Behind (NCLB) legislation, but that can be set aside as political optimism. NCLB was passed only in 2001, too late for much influence on the assessment results. On the other hand, national standards, including the National Council of Teachers of Mathematics (NCTM) Standards (1989), the American Association for the Advancement of Science (AAAS) Benchmarks for Science Literacy (1993), and the National Research Council (NRC) National Science Education Standards (1995), have been around for just about the right length of time. There has been a significant cumulative effect of these national standards on the educational system as they have influenced state standards, textbook selection, and assessments and, less directly, teacher education. So we think that a strong argument can be made for linking these standards to the improvement we see in the TIMSS results.

Education reform takes time, but the results suggest that some progress is beginning to show. TIMSS is always a sobering test for U.S. educators, because the results force a comparison of their system—which insists on the right of 50 states and 15,000 school districts to shape their own mathematics and science programs—with centrally organized systems such as that of Singapore, the world leader. The results represented by TIMSS 2003 would suggest giving accelerated emphasis to strong voluntary national standards. That is a challenging prescription for a nation devoted to local control, and one that is made more difficult by the increasing efforts in a number of school districts to mandate courses that offer religious “alternatives” to scientific theories.

Perhaps the 2003 TIMSS results will, in addition to providing a baseline for comparing international educational systems, persuade U.S. policy-makers to count the costs of leaving everything to local decision-making.

Rodger W. Bybee and Donald Kennedy

Rodger W. Bybee is executive director of the Biological Science Curriculum Study. Donald Kennedy is editor-in-chief of *Science*.





What if moving from one particular protein to the most relevant journal and patent literature were as easy as pushing a button?



It is.

Not only does SciFinder provide access to more proteins and nucleic acids than any publicly available source, but they're a single click away from their referencing patents and original research.

Coverage includes everything from the U.S. National Library of Medicine's (NLM) MEDLINE® and much more. In fact, SciFinder is the only single source of patents and journals worldwide.

Once you've found relevant literature, you can use SciFinder's powerful refinement tools to focus on a specific research area, for example: biological studies such as target organisms or diseases; expression microarrays; or analytical studies such as immunoassays, fluorescence, or PCR analysis. From each reference, you can link to the electronic full text of the original paper or patent, plus use citation tools to track how the research has evolved and been applied.

Visualization tools help you understand results at a glance. You can categorize topics and substances, identify relationships between areas of study, and see areas that haven't been explored at all.

Comprehensive, intuitive, seamless—SciFinder directs you. It's part of the process. To find out more, call us at 1-800-753-4227 (North America) or 1-614-447-3700 (worldwide) or visit www.cas.org/SCIFINDER.



SciFinder®

Part of the process.™



A division of the American Chemical Society. SciFinder is a registered trademark of the American Chemical Society. "Part of the process" is a service mark of the American Chemical Society.

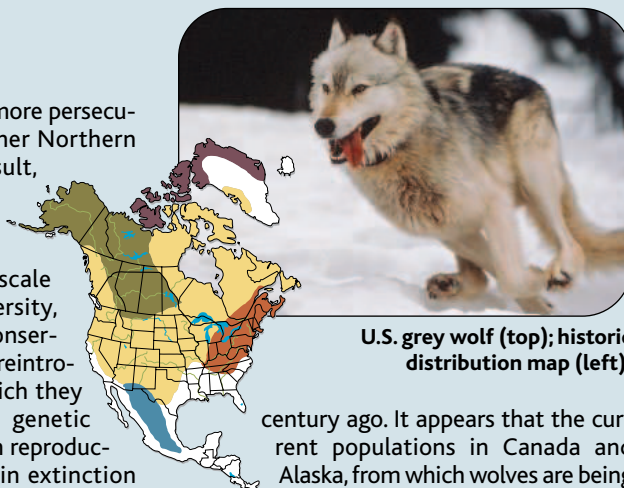
edited by Stella Hurtley

ECOLOGY/EVOLUTION

Mexicans in the Mix

Wolves have probably suffered more persecution from humans than any other Northern Hemisphere predator. As a result, wolf populations in much of Europe and North America are highly fragmented and diminished. Population loss on this scale leads to loss of genetic diversity, which can pose problems for conservation managers attempting to reintroduce animals to areas from which they have been eliminated: lower genetic diversity can mean a decrease in reproductive potential and an increase in extinction risk. It has been suggested that the high mobility of wolves might have mitigated such loss, because of the genetic mixing that would have occurred in the preextermination populations.

Leonard *et al.* quantified the loss of diversity after the 20th-century extermination programs carried out in the United States by comparing the mitochondrial DNA of present-day North American grey wolves with those from museum specimens collected a



U.S. grey wolf (top); historic distribution map (left).

century ago. It appears that the current populations in Canada and Alaska, from which wolves are being drawn for reintroduction programs in the U.S. Rocky Mountains, are missing a substantial part of the diversity of the ancestral wolves; in particular, they lack haplotypes associated with past Mexican populations. Thus, historically, the genetic diversity of grey wolves was geographically structured, and successful reintroductions to the western United States may depend on adding Mexican grey wolves to the population mix. —AMS

Mol. Ecol. 14, 9 (2005).

BIOMEDICINE

A Good Night's Sleep?

One of the distressing symptoms of progressive neurodegenerative disorders such as Alzheimer's, Parkinson's, and Huntington's diseases is the severe disruption of sleep patterns, which leads to anxiety and distress in both patients and their caregivers. Two recent papers now shed light on the cellular and molecular mechanisms of sleep disruption in Huntington's disease (HD).

Petersen *et al.* find that HD patients and R6/2 mice (which mimic many of the features of human HD) exhibit progressive loss of brain neurons in the hypothalamus—a key regulator of many different processes, including sleep. The hypothalamic neurons that die in HD patients and mice produce the neuropeptide orexin, loss of which has been implicated in narcolepsy. Decreasing amounts of orexin in the cerebrospinal fluid of HD patients could thus be used as a marker of HD progression.

Orexin neurons in the hypothalamus also innervate the suprachiasmatic nucleus, which drives circadian sleep/wake cycles by regulating the transcription of several key "clock" genes. Morton *et al.* report that progressive disruption of circadian behavior in R6/2 mice is accompanied by marked alterations in the expression of the *mPer2* and *mBmal1* clock genes. These findings help to explain why HD patients suffer from markedly increased daytime sleepiness and night wakefulness, and hopefully will contribute to better management of these distressing symptoms. —OMS

Hum. Mol. Genet. 14, 39 (2005); *J. Neurosci.* 25, 157 (2005).

CHEMISTRY

Taming SERS

The Raman effect for measuring vibrational spectra is normally quite small, but in the vicinity of rough gold or silver surfaces, localized surface plasmons can enhance signals by orders of magnitude. However, variations in surface roughness can vary the enhancement of the surface enhanced Raman effect, or SERS, which makes it difficult to use for measuring concentrations. Jackson and Halas examined the SERS effect using core-shell nanoparticles of gold or silver nanoshell coatings over silica cores. Unlike colloidal metal particles, the core-shell particles exhibit SERS enhancements caused almost entirely by the plasmon resonances set up by their geometry, not from surface roughness or regions of high field caused by particle

contact. The excitation frequency can be tuned to take full advantage of the plasmon response of the particles, which are simply deposited on glass slides. For a non-resonant excitation energy, the SERS enhancement for a typical organic molecule, p-mercaptoaniline, could be as high as 2.5×10^{10} . —PDS

Proc. Natl. Acad. Sci. U.S.A. 101, 17930 (2004).

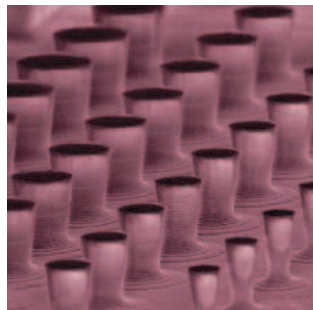
APPLIED PHYSICS

Better Single-Photon Emitters

The reliable emission of single photons in a particular direction from quantum dots and quantum well structures is an important requisite for applications in quantum information processing and quantum cryptography. However, in many implementations, the photons are emitted in bunches with poor control over

the direction in which they are emitted. Bennett *et al.* use a photolithographically defined pillar-design microcavity to restrict the optical modes into which the photons can be emitted. Using such a design for pillars 1.9 μm in diameter, they demonstrate a reproducible method providing a considerable improvement in both the single-photon emission and control over the direction of emission. —ISO

Opt. Exp. 13, 50 (2005).



Pillar design for improved single photon emission.

CONTINUED ON PAGE 485

MOVE BEYOND TRADITIONAL PCR LIMITATIONS

GENOMEPLEX™ WHOLE GENOME AMPLIFICATION

UNSURPASSED YIELD, UNLIMITED POTENTIAL

Sigma's GenomePlex Whole Genome Amplification (WGA) kit provides a rapid and straightforward method to preserve and expand very small amounts of precious DNA.

- **Robust and Accurate Amplification**
Whole genome amplification with no detectable allele or locus bias within 3 hours
- **Ultimate Flexibility**
Amplify DNA from virtually any source including blood, buccal swabs, cell culture, plants, and bacteria
- **Unlimited Genetic Analysis**
GenomePlex WGA DNA is suitable for use with common downstream applications including TaqMan® and BeadArray® or may be stored at -20°C.

Product Code	Description
WGA-1	GenomePlex WGA Kit

Call 800-325-3010 to order
or visit us on the web at
sigma-aldrich.com/wga.

sigma-aldrich.com

LEADERSHIP IN LIFE SCIENCE, HIGH TECHNOLOGY AND SERVICE
SIGMA-ALDRICH CORPORATION • BOX 14508 • ST. LOUIS • MISSOURI 63178 • USA



GenomePlex is a trademark of Rubicon Genomics, Inc.
TaqMan is a registered trademark of Roche Molecular Systems, Inc. BeadArray is a trademark of Illumina, Inc.

MICROBIOLOGY

Sleuthing *Streptococcus*

Streptococcal diseases have many disguises, ranging from minor sore throats to life-threatening toxic shock. The epidemiology of streptococcal diseases has long been problematic, manifesting as suddenly emerging and disappearing epidemics of disparate syndromes with no apparent therapeutic correlate. In a population-wide genomic study of 11 years of data from 255 isolates from Ontario, Canada, Beres *et al.* implicated the source of waves of invasive disease to the acquisition or loss of prophages, which rapidly generated unique combinations of virulence genes and their characteristic diseases: toxic shock, bacteremia, or necrotizing fasciitis. However, another 7-year Canadian study of 306 cases of invasive group A streptococcal infections revealed a population-based shift from soft tissue infections to pneumonia, especially in women. Hollm-Delgado *et al.* suggest that underlying conditions in the victims may be causing this shift. They found that the risk of soft-tissue streptococcal infections increased after varicella infections or drug injection, but ultimately could not explain the increase in pneumonia. However a statistical link could not be made between any particular serotype and specific clinical symptoms. It is possible that a prophage may be at work behind the scenes. — CA

Proc. Natl. Acad. Sci. U.S.A. 101, 11833 (2004);
Emerg. Infect. Dis. 11, 77 (2005).

MEDICINE

Mitochondria and Cancer

Human tumors often contain mutations in mitochondrial DNA (mtDNA). Whether these mutations are causally involved in tumorigenesis and the mechanisms by which they might contribute are pressing questions that remain unanswered. One hypothesis suggests that tumor-associated mtDNA mutations lead to increased production of reactive oxygen species (ROS), a by-product of mitochondrial oxidative phosphorylation, which can stimulate cell proliferation. Data from a new study of mtDNA in human prostate tumors are consistent with this hypothesis. Petros *et al.* identified mutations in two mitochondrial genes encoding

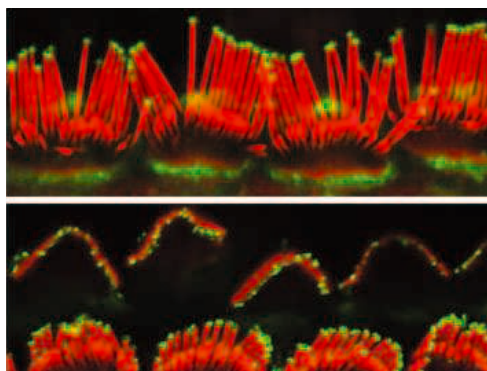
proteins involved in oxidative phosphorylation: cytochrome oxidase subunit I and ATP6. Notably, when mtDNA containing an ATP6 mutation close to the site of the tumor-associated mutation was introduced into prostate cancer cells, the cells generated significantly more ROS in comparison with wild-type controls and grew at a much faster rate in mice, supporting the notion that such mutations play a causal role in tumorigenesis. — PAK

Proc. Natl. Acad. Sci. U.S.A. 102, 719 (2005).

CELL BIOLOGY

Whirlin to the Tip

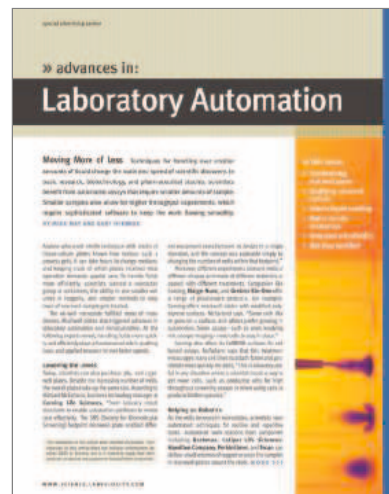
Hearing depends on the neat arrangement of stereocilia in graduated rows on the apical surface of hair cells in the inner ear. Disruption of this architecture interferes with the ability to detect both sounds and head movement. The architecture is established by the presence of actin cores within each stereocilium



Differential elongation of stereocilia (red) is initiated when myosin XVa delivers whirlin (green) to the tips.

of a defined length. Two mutant mice strains possess abbreviated stereocilia—the shaker 2 and whirler mice. Shaker 2 mice are deficient in the production of a motor protein, myosin XVa, and whirler mice are deficient in a protein termed whirlin. Belyantseva *et al.* now show that the myosin XVa protein interacts with whirlin and promotes its delivery to the tips of stereocilia. When this interaction is disrupted, stereocilia are abnormal and deafness will ensue. The whirlin transport defect, and the aberrant hair bundle pattern, in hair cells taken from shaker 2 mice could be “cured” by transfection with a fluorescently tagged version of myosin XVa. — SMH

Nature Cell Biol. 10.1038/ncb1219 (2005).



The following organization has placed an ad in the Special Advertising Section

Advances in:

Laboratory Automation
Moving More of Less

ADVERTISER	Page
Leica	606

Turn to page 607



Q

Who's helping scientists keep their heads above water?

“

Science keeps me in touch with what's happening on our planet and beyond. Reading the latest about Mars makes me appreciate the water we have here on Earth all the more.

”

AAAS Fellow Richard Cohen, consultant in lightning and electrical surge protection

AAAS



Photo: Molly E. Cohen

Richard Cohen

AAAS is committed to advancing science and giving a voice to scientists around the world. We work to improve science education, promote a sound science policy, and support human rights.

Helping our members stay abreast of their field is a key priority for AAAS. One way we do this is through *Science*, which features all the latest breakthroughs and groundbreaking research, and keeps scientists connected wherever they happen to be. Members like Richard find it essential reading.

To join the international family of science, go to www.aaas.org/join.



ADVANCING SCIENCE, SERVING SOCIETY

www.aaas.org/join

1200 New York Avenue, NW
Washington, DC 20005
Editorial: 202-326-6550, FAX 202-289-7562
News: 202-326-6500, FAX 202-321-9727

Bateman House, 82-88 Hills Road
Cambridge, UK CB2 1LQ
+44 (0) 1223 326500, FAX +44 (0) 1223 326501

SUBSCRIPTION SERVICES For change of address, missing issues, new orders and renewals, and payment questions: 800-731-4939 or 202-326-6417; FAX 202-842-1065. Mailing addresses: AAAS, P.O. Box 1811, Danbury, CT 06813 or AAAS Member Services, 1200 New York Avenue, NW, Washington, DC 20005

INSTITUTIONAL SITE LICENCES please call 202-326-6755 for any questions or information

REPRINTS Ordering/Billing/Status 800-635-7171; Corrections 202-326-6501

PERMISSIONS 202-326-7074, FAX 202-682-0816

MEMBER BENEFITS Bookstore: AAAS/Barnes&Noble.com bookstore www.aaas.org/bn; Car purchase discount: Subaru VIP Program 202-326-6417; Credit Card: MBNA 800-847-7378; Car Rentals: Hertz 800-654-2200 CDP#343457, Dollar 800-800-4000 #AA1115; AAAS Travels: Betchart Expeditions 800-252-4910; Life Insurance: Seabury & Smith 800-424-9883; Other Benefits: AAAS Member Services 202-326-6417 or www.aaasmember.org.

science_editors@aaas.org (for general editorial queries)
science_letters@aaas.org (for queries about letters)
science_reviews@aaas.org (for returning manuscript reviews)
science_bookrevs@aaas.org (for book review queries)

Published by the American Association for the Advancement of Science (AAAS), *Science* serves its readers as a forum for the presentation and discussion of important issues related to the advancement of science, including the presentation of minority or conflicting points of view, rather than by publishing only material on which a consensus has been reached. Accordingly, all articles published in *Science*—including editorials, news and comment, and book reviews—are signed and reflect the individual views of the authors and not official points of view adopted by the AAAS or the institutions with which the authors are affiliated.

AAAS was founded in 1848 and incorporated in 1874. Its mission is to advance science and innovation throughout the world for the benefit of all people. The goals of the association are to: foster communication among scientists, engineers and the public; enhance international cooperation in science and its applications; promote the responsible conduct and use of science and technology; foster education in science and technology for everyone; enhance the science and technology workforce and infrastructure; increase public understanding and appreciation of science and technology; and strengthen support for the science and technology enterprise.

INFORMATION FOR CONTRIBUTORS

See pages 135 and 136 of the 7 January 2005 issue or access www.sciencemag.org/feature/contribinfo/home.shtml

EDITOR-IN-CHIEF **Donald Kennedy**
EXECUTIVE EDITOR **Monica M. Bradford**
DEPUTY EDITORS NEWS EDITOR

R. Brooks Hanson, Katrina L. Kelner Colin Norman

EDITORIAL SUPERVISORY SENIOR EDITORS Barbara Jasny, Phillip D. Szuromi; **SENIOR EDITOR/PERSPECTIVES** Orla Smith; **SENIOR EDITORS** Gilbert J. Chin, Pamela J. Hines, Paula A. Kiberstis (Boston), Beverly A. Purnell, L. Bryan Ray, Guy Riddiough (Manila), Linda R. Rowan, David Voss; **ASSOCIATE EDITORS** Lisa D. Chong, Marc S. Lavine, H. Jesse Smith, Valda Vinson, Jake S. Yeston; **ONLINE EDITOR** Stewart Wills; **ASSOCIATE ONLINE EDITOR** Tara S. Marathe; **BOOK REVIEW EDITOR** Sherman J. Suter; **ASSOCIATE LETTERS EDITOR** Etta Kavanagh; **INFORMATION SPECIALIST** Janet Kegg; **EDITORIAL MANAGER** Cara Tate; **SENIOR COPY EDITORS** Jeffrey E. Cook, Harry Jach, Barbara P. Ordway; **COPY EDITORS** Cynthia Howe, Sabrah M. n'haRaven, Jennifer Sills, Trista Wagoner, Alexis Wynne; **EDITORIAL COORDINATORS** Carolyn Kyle, Beverly Shields; **PUBLICATION ASSISTANTS** Chris Filiatreau, Joi S. Granger, Jeffrey Hearn, Scott Miller, Jerry Richardson, Tunisia L. Riley, Brian White, Anita Wynn; **EDITORIAL ASSISTANTS** Ramatoulaye Diop, E. Annie Hall, Lisa Johnson, Patricia M. Moore, Jamie M. Wilson; **EXECUTIVE ASSISTANT** Sylvia S. Kihara; **ADMINISTRATIVE SUPPORT** Patricia F. Fisher

NEWS SENIOR CORRESPONDENTS Jean Marx; **DEPUTY NEWS EDITORS** Robert Coontz, Jeffrey Mervis, Leslie Roberts, John Travis; **CONTRIBUTING EDITORS** Elizabeth Colloff, Polly Shulman; **NEWSWRITERS** Yudhijit Bhattacharjee, Jennifer Couzin, David Grimm, Constance Holden, Jocelyn Kaiser, Richard A. Kerr, Eli Kivitsch, Andrew Lawler (New England), Gregory Miller, Elizabeth Pennisi, Charles Seife, Robert F. Service (Pacific NW), Erik Stokstad; **AMITABH AVASTHI** (intern); **CONTRIBUTING CORRESPONDENTS** Marcia Barinaga (Berkeley, CA), Barry A. Cipra, Adrian Cho, Jon Cohen (San Diego, CA), Daniel Ferber, Ann Gibbons, Robert Irion, Mitch Leslie (NetWatch), Charles C. Mann, Evelyn Strauss, Gary Taubes, Ingrid Wickelgren; **COPY EDITORS** Linda B. Felaco, Rachel Curran, Sean Richardson; **ADMINISTRATIVE SUPPORT** Scherraine Mack, Fannie Groom BUREAU: Berkeley, CA: 510-652-0302, FAX 510-652-1867, New England: 207-549-7755, San Diego, CA: 760-942-3252, FAX 760-942-4979, Pacific Northwest: 503-963-1940

PRODUCTION DIRECTOR James Landry; **SENIOR MANAGER** Wendy K. Shank; **ASSISTANT MANAGER** Rebecca Doshi; **SENIOR SPECIALISTS** Vicki J. Jorgensen, Jessica K. Moshell, Amanda K. Skelton; **SPECIALISTS** Jay R. Covert **PREFLIGHT DIRECTOR** David M. Tompkins; **MANAGER** Marcus Spiegler **ART DIRECTOR** Joshua Moglia; **ASSOCIATE ART DIRECTOR** Kelly Buckheit; **ILLUSTRATOR** Katharine Sutliff; **SENIOR ART ASSOCIATES** Holly Bishop, Laura Creveling, Preston Huey, Julie White; **ASSOCIATE** Nayomi Kevitiyagala; **PHOTO RESEARCHER** Leslie Blizard

SCIENCE INTERNATIONAL

EUROPE (science@science-int.co.uk) **EDITORIAL** INTERNATIONAL MANAGING EDITOR Andrew M. Sugden; **SENIOR EDITOR/PERSPECTIVES** Julia Fahrenkamp-Uppenbrink; **SENIOR EDITORS** Caroline Ash, Stella M. Hurlley, Ian S. Osborne, Peter Stern; **ASSOCIATE EDITOR** Stephen J. Simpson; **EDITORIAL SUPPORT** Cheryl Sharp, Emma Westgate; **ADMINISTRATIVE SUPPORT** Janet Clements, Phil Marlow, Jill White; **NEWS** INTERNATIONAL NEWS EDITOR Eliot Marshall **DEPUTY NEWS EDITOR** Daniel Clerly; **CORRESPONDENT** Gretchen Vogel (Berlin: +49 (0) 30 2809 3902, FAX +49 (0) 30 2809 8365); **CONTRIBUTING CORRESPONDENTS** Michael Balter (Paris), Martin Eserink (Amsterdam and Paris); **INTERN** Mason Inman

ASIA Japan Office: Asca Corporation, Eiko Ishioka, Fusako Tamura, 1-8-13, Hirano-cho, Chuo-ku, Osaka-shi, Osaka, 541-0046 Japan; +81 (0) 6 6202 6272, FAX +81 (0) 6 6202 6271; asca@os.gulf.or.jp **JAPAN NEWS BUREAU:** Dennis Normile (contributing correspondent, +81 (0) 3 3391 0630, FAX 81 (0) 3 5936 3531; dnormile@gol.com); **CHINA REPRESENTATIVE** Hao Xin, +86 (0) 10 6307 4439 or 6307 3676, FAX +86 (0) 10 6307 4358; haoxin@earthlink.net; **SOUTH ASIA** Pallava Bagla (contributing correspondent +91 (0) 11 2271 2896; pbagla@vsnl.com); **CENTRAL ASIA** Richard Stone (+7 3272 6413 35, rstone@aaas.org)

EXECUTIVE PUBLISHER **Alan I. Leshner**
PUBLISHER **Beth Rosner**

FULFILLMENT & MEMBERSHIP SERVICES (membership@aaas.org) **DIRECTOR** Marlene Zendell; **FULFILLMENT SYSTEMS:** MANAGER Waylon Butler; **MEMBER SERVICES:** MANAGER Michael Lung; **SENIOR SPECIALIST** Pat Butler; **SPECIALIST** Laurie Baker, Tamara Alfson; **REPRESENTATIVE** Karina Smith; **MARKETING ASSOCIATE** Deborah Stromberg

BUSINESS OPERATIONS AND ADMINISTRATION **DIRECTOR** Deborah Rivera-Wienhold; **BUSINESS MANAGER** Randy Yi; **SENIOR FINANCIAL ANALYSTS** Lisa Donovan, Jason Hendricks; **ANALYST** Jessica Tierney, Farida Yeasmin; **RIGHTS AND PERMISSIONS:** ADMINISTRATOR Emilie David; **ASSOCIATE** Elizabeth Sandler; **MARKETING:** **DIRECTOR** John Meyers; **MEMBERSHIP MARKETING MANAGER** Darryl Walter; **MARKETING ASSOCIATES** Karen Nedbal, Julianne Wielga; **RECRUITMENT MARKETING MANAGER** Allison Pritchard; **ASSOCIATES** Mary Ellen Crowley, Amanda Donathen, Catherine Featherston; **DIRECTOR OF INTERNATIONAL MARKETING AND RECRUITMENT ADVERTISING** Deborah Harris; **INTERNATIONAL MARKETING MANAGER** Wendy Sturley; **MARKETING/MEMBER SERVICES EXECUTIVE:** Linda Rusk; **JAPAN SALES AND MARKETING MANAGER** Jason Hannaford; **SITE LICENSE SALES:** **DIRECTOR** Tom Ryan; **SALES AND CUSTOMER SERVICE** Mehan Dossani, Catherine Holland, Adam Banner, Yaniv Snir; **ELECTRONIC MEDIA:** **INTERNET PRODUCTION MANAGER** Lizbeth Harman; **ASSISTANT PRODUCTION MANAGER** Wendy Stengel; **SENIOR PRODUCTION ASSOCIATES** Carla Cathey, Sheila Mackall, Lisa Stanford; **PRODUCTION ASSOCIATE** Nichele Johnston; **LEAD APPLICATIONS DEVELOPER** Carl Saffell

PRODUCT ADVERTISING (science_advertising@aaas.org): **MIDWEST** Rick Bongiovanni: 330-405-7080, FAX 330-405-7081 • **WEST COAST/TW.CANADA** B. Neil Boylan (Associate Director): 650-964-2266, FAX 650-964-2267 • **EAST COAST/ CANADA** Christopher Breslin: 443-512-0330, FAX 443-512-0331 • **UK/SCANDINAVIA/France/ITALY/BELGIUM/NETHERLANDS** Andrew Davies (Associate Director): +44 (0)1782 750111, FAX +44 (0) 1782 751999 • **GERMANY/SWITZERLAND/AUSTRIA** Tracey Peers (Associate Director): +44 (0) 1782 752530, FAX +44 (0) 1782 752531 **JAPAN** Masuyoshi Yokawa: +81 (0) 33235 5961, FAX +81 (0) 33235 5855 **ISRAEL** Jessica Nachlas +9723 54491123 • **TRAFFIC MANAGER** Carol Maddox; **SALES COORDINATOR** Deandra Simms

CLASSIFIED ADVERTISING (advertise@sciencecareers.org): **U.S. SALES DIRECTOR** Gabrielle Boguslawski: 718-491-1607, FAX 202-289-6742; **INTERNET SALES MANAGER** Beth Dwyer: 202-326-6534; **INSIDE SALES MANAGER** Daryl Anderson: 202-326-6543; **WEST COAST/MIDWEST** Kristine von Zedlitz: 415-956-2531; **EAST COAST** Jill Downing: 631-580-2445; **LINE AD SALES** Emmet Tesfaye: 202-326-6740; **SENIOR SALES COORDINATOR** Erika Bryant; **SALES COORDINATORS** Rohan Edmonson, Caroline Gallina, Christopher Normile, Joyce Scott, Shirley Young; **INTERNATIONAL SALES MANAGER** Tracy Holmes: +44 (0) 1223 326525, FAX +44 (0) 1223 326532; **SALES** Christina Harrison; **SALES ASSISTANT** Claire Griffiths; **JAPAN:** Jason Hannaford: +81 (0) 52 777 9777, FAX +81 (0) 52 777 9781; **PRODUCTION:** MANAGER Jennifer Rankin; **ASSISTANT MANAGER** Deborah Tompkins; **ASSOCIATE** Amy Hardcastle; **SENIOR TRAFFICKING ASSOCIATE** Christine Hall; **SENIOR PUBLICATIONS ASSISTANT** Robert Buck; **PUBLICATIONS ASSISTANT** Natasha Pinol

AAAS BOARD OF DIRECTORS **RETIRED PRESIDENT**, CHAIR Mary Ellen Avery; **PRESIDENT** Shirley Ann Jackson; **PRESIDENT-ELECT** Gilbert S. Omenn; **TREASURER** David E. Shaw; **CHIEF EXECUTIVE OFFICER** Alan I. Leshner; **BOARD** Rosina M. Bierbaum; John E. Burris; John E. Dowling; Karen A. Holbrook; Richard A. Meserve; Norine E. Noonan; Peter J. Stang; Kathryn D. Sullivan; Lydia Villa-Komaroff



ADVANCING SCIENCE. SERVING SOCIETY

SENIOR EDITORIAL BOARD

John I. Brauman, Chair, Stanford Univ.
Richard Losick, Harvard Univ.
Robert May, Univ. of Oxford
Marcia McNutt, Monterey Bay Aquarium Research Inst.
Linda Partridge, Univ. College London
Vera C. Rubin, Carnegie Institution of Washington
Christopher R. Somerville, Carnegie Institution

BOARD OF REVIEWING EDITORS

R. McNeill Alexander, Leeds Univ.
Richard Amasino, Univ. of Wisconsin, Madison
Kristi S. Anseth, Univ. of Colorado
Cornelia I. Bargmann, Univ. of California, SF
Brenda Bass, Univ. of Utah
Ray H. Baughman, Univ. of Texas, Dallas
Stephen J. Benkovic, Pennsylvania St. Univ.
Michael J. Bevan, Univ. of Washington
Tom Bisseling, Wageningen Univ.
Peer Bork, EMBL
Dennis Bray, Univ. of Cambridge
Stephen Buratowski, Harvard Medical School
Jillian M. Buriak, Univ. of Alberta
Joseph A. Burns, Cornell Univ.
William P. Butz, Population Reference Bureau
Doreen Cantrell, Univ. of Dundee
Mildred Cho, Stanford Univ.
David Clapham, Children's Hospital, Boston
David Cory, Oxford University
J. M. Claverie, CNRS, Marseille
Jonathan D. Cohen, Princeton Univ.
Robert Colwell, Univ. of Connecticut
Peter Crane, Royal Botanic Gardens, Kew

F. Fleming Crim, Univ. of Wisconsin
William Cumberland, UCLA
Judy DeLoache, Univ. of Virginia
Robert Desimone, NIMH, NIH
John Diffley, Cancer Research UK
Dennis Discher, Univ. of Pennsylvania
Julian Downward, Cancer Research UK
Denis Duboule, Univ. of Geneva
Christopher Dye, WHO
Richard Ellis, Cal Tech
Gerhard Ertl, Fritz-Haber-Institut, Berlin
Douglas H. Erwin, Smithsonian Institution
Barry Everitt, Univ. of Cambridge
Paul G. Falkowski, Rutgers Univ.
Tom Fenchel, Univ. of Copenhagen
Barbara Finlayson-Pitts, Univ. of California, Irvine
Jeffrey S. Flier, Harvard Medical School
Chris D. Frith, Univ. College London
R. Gadagkar, Indian Inst. of Science
Mary E. Galvin, Univ. of Delaware
Don Ganem, Univ. of California, SF
John Gearhart, Johns Hopkins Univ.
Jennifer M. Graves, Australian National Univ.
Christian Haass, Ludwig Maximilians Univ.
Dennis L. Hartmann, Univ. of Washington
Chris Hawkesworth, Univ. of Bristol
Martin Heimann, Max Planck Inst., Jena
James A. Hendler, Univ. of Maryland
Ary A. Hoffmann, La Trobe Univ.
Evelyn L. Hu, Univ. of California, SB
Meyer B. Jackson, Univ. of Wisconsin Med. School
Stephen Jackson, Univ. of Cambridge
Bernhard Keimer, Max Planck Inst., Stuttgart
Alan B. Krueger, Princeton Univ.
Antonio Lanzavecchia, Inst. of Res. in Biomedicine

Anthony J. Leggett, Univ. of Illinois, Urbana-Champaign
Michael J. Lenardo, NIAID, NIH
Norman L. Letvin, Beth Israel Deaconess Medical Center
Richard Losick, Harvard Univ.
Andrew P. MacKenzie, Univ. of St. Andrews
Raul Madariaga, École Normale Supérieure, Paris
Rick Maizels, Univ. of Edinburgh
Eve Marder, Brandeis Univ.
George M. Martin, Univ. of Washington
Edvard Moser, Norwegian Univ. of Science and Technology
Elizabeth G. Nabel, NHLBI, NIH
Naoto Nagaosa, Univ. of Tokyo
James Nelson, Stanford Univ. School of Med.
Roeland Nolte, Univ. of Nijmegen
Eric N. Olson, Univ. of Texas, SW
Erin O'Shea, Univ. of California, SF
Malcolm Parker, Imperial College
Linda Partridge, Univ. College London
John Pendry, Imperial College
Josef Perner, Univ. of Salzburg
Philippe Poulin, CNRS
David J. Read, Univ. of Sheffield
Colin Renfrew, Univ. of Cambridge
JoAnne Richards, Baylor College of Medicine
Trevor Robbins, Univ. of Cambridge
Edward M. Rubin, Lawrence Berkeley National Labs
David G. Russell, Cornell Univ.
Philippe Sansonetti, Institut Pasteur
Dan Schrag, Harvard Univ.
Georg Schulz, Albert-Ludwigs-Universität
Paul Schulze-Lefert, Max Planck Inst., Cologne
Terrence J. Sejnowski, The Salk Institute
George Somero, Stanford Univ.
Christopher R. Somerville, Carnegie Institution
Joan Steitz, Yale Univ.

Edward I. Stiefel, Princeton Univ.
Thomas Stocker, Univ. of Bern
Jerome Strauss, Univ. of Pennsylvania Med. Center
Tomoyuki Takahashi, Univ. of Tokyo
Mary Tessier-Lavigne, Genentech
Craig B. Thompson, Univ. of Pennsylvania
Michiël van der Klis, Astronomical Inst. of Amsterdam
Derek van der Kooy, Univ. of Toronto
Bert Vogelstein, Johns Hopkins
Christopher A. Walsh, Harvard Medical School
Christopher T. Walsh, Harvard Medical School
Graham Warren, Yale Univ. School of Med.
Fiona Watt, Imperial Cancer Research Fund
Julia R. Weertman, Northwestern Univ.
Daniel M. Wegner, Harvard University
Ellen D. Williams, Univ. of Maryland
R. Sanders Williams, Duke University
Ian A. Wilson, The Scripps Res. Inst.
Jerry Workman, Stowers Inst. for Medical Research
John R. Yates III, The Scripps Res. Inst.
Martin Zatz, NIMH, NIH
Walter Ziegler-Schaefer, Max Planck Inst., Munich
Huda Zoghbi, Baylor College of Medicine
Maria Zuber, MIT

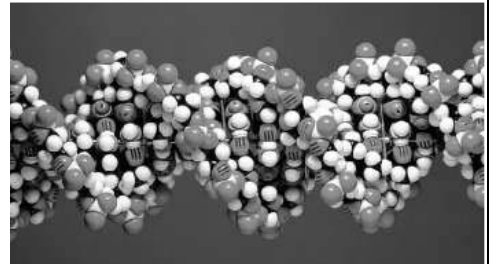
BOOK REVIEW BOARD

David Bloom, Harvard Univ.
Londa Schiebinger, Stanford Univ.
Richard Swedner, Univ. of Chicago
Robert Solow, MIT
Ed Wasserman, DuPont
Lewis Wolpert, Univ. College, London

It's Called Ground- breaking For a Reason

For more than 40 years, the leading journal in its field has driven the future of theoretical and applied biomedical engineering and biophysics. Each monthly issue of IEEE Transactions on Biomedical Engineering brings you the latest innovations in medical, molecular electronics, dentistry and aerospace applications.

**Don't miss out on the future of your world.
Subscribe today!**



**IEEE Transactions on
Biomedical Engineering**

IEEE Pub ID 018-199

ISSN: 0018-9294

Annual rate: US\$830

IEEE Member Rate: US\$60

ACCE Member Rate: US\$120

Email: subscription-service@ieee.org

Join IEEE: www.ieee.org

Submit papers: www.embs.org



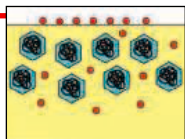
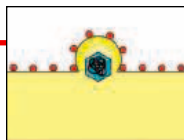
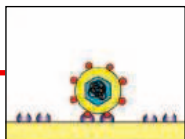
Let there
be
oligos.



Enlightenment is the reward of scientific persistence.
And in molecular biology, only the perfect oligo illuminates the secrets of nature
that you want to reveal. Our passion for your science
shines through in our custom oligos and genome oligo sets.

We cater to your visions.
www.operon.com

operon
molecules for life



IMAGES

Bringing Bugs Into Focus

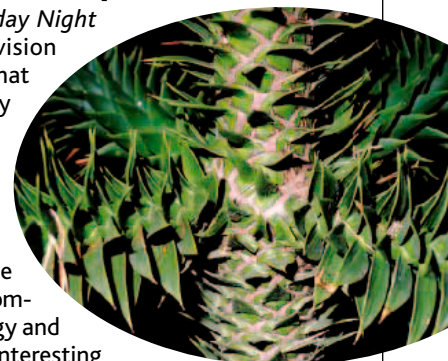
Teachers looking for just the right illustration to clarify a microbiology lab or lecture might want to visit the Microbe Library. Since last reviewed by NetWatch (9 June 2000, p. 1699), the educational site from the American Society for Microbiology has begun charging for course materials, but most of the visuals remain free. Check out more than 350 photos, diagrams, and videos from microbial mug shots to animations that explicate biological processes such as gene regulation and DNA repair. Tutorials can help students master tools and techniques such as acid-fast staining, used to identify bugs such as tuberculosis bacteria that shrug off traditional dyes. These stills (above) come from an animation that shows how a coated virus infiltrates an animal cell.

www.microbelibrary.org

WEB TEXT

A Natural History Sampler

Wayne's Word isn't a *Saturday Night Live* sketch; it's a lower-division textbook on natural history that began 10 years ago as a cheeky newsletter about topics such as avoiding mountain lion attacks. Author Wayne Armstrong, a professor at Palomar College in San Marcos, California, eventually expanded the work into an online text to accompany his courses on basic biology and botany but continued adding interesting



anecdotes about natural history subjects. For instance, Armstrong discusses speculation that Vincent Van Gogh's paintings owe something to the plant compound digoxin, which he took to treat his epilepsy. Heavy users have reported seeing rings around stars like those in Van Gogh's painting *Starry Night*. The site's roughly 2300 illustrations include many of Armstrong's photos, such as this shot of the formidable leaves of the monkey puzzle tree (above).

waynesword.palomar.edu/wayne.htm

DATABASE

Bad for the Genes

Need to know which genes the neurotoxic pesticide DDT meddles with? Wondering how the toxic metal cadmium affects erythropoietin, a hormone that spurs blood cell production? Drop by the prototype Comparative Toxicogenomics Database, sponsored by the National Institute for Environmental Health Sciences and the Mount Desert Island Biological Laboratory in Maine. The collection allows you to determine which genes respond to a particular compound, to find out which species the interaction has been studied in, and to answer other questions about hundreds of chemicals.

The information comes from papers cited in PubMed and in databases such as GenBank and SwissProt, but the site's creators hope that researchers will contribute their own findings.

RESOURCES

How to Read an Elephant

Elephants trumpet, rumble, roar, and produce a variety of other sounds, but their giant bodies are surprisingly expressive, too. Scientists and pachyderm fans can learn to interpret this sign language at ElephantVoices, hosted by two Norway-based researchers, one of whom has spent 30 years observing the beasts. The site's photo-packed Visual and Tactile Signals Database decodes more than 100 forms of African savanna elephant communication. An elephant that waggles its head usually wants to play, while the youngster below is nudging its mother to ask for a drink. The site also includes a small archive of elephant sounds and backgrounders on why and how the animals communicate.

www.elephantvoices.org



ctd.mdibl.org

BLOGS

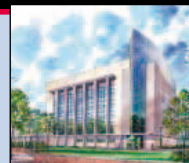
A Year in a Physicist's Life

Einstein's unkempt appearance was likely essential to his adoption as a pop icon, argues David Waller of the Sudbury Neutrino Observatory in Canada, who suggests that physicists commemorate Einstein by growing big hair. Directing a beam of protons to a detector 1000 meters away reminds Debbie Harris of Fermilab in Illinois of giving birth, because both processes have to occur in stages. These are highlights from Quantum Diaries, a new project sponsored by a coalition of particle physics labs to commemorate 2005's World Year of Physics. More than 20 physicists from around the world will chronicle their opinions, interests, successes, and failures over the next 12 months with regular dispatches, video

clips, and photos. So far, participants have weighed in on everything from how they got started in the field to the connection between physics and jazz.

interactions.org/quantumdiaries

Send site suggestions to netwatch@aaas.org. Archive: www.sciencemag.org/netwatch



DIVERSITY

Summers's Comments Draw Attention to Gender, Racial Gaps

Martin Luther King Jr. Day celebrates equality and diversity in the United States. But this year two unrelated events served to remind the scientific community how far it still has to go to reach the sort of world envisioned by the slain civil rights leader.

Just days before the 17 January national holiday, an African-American professor at the Massachusetts Institute of Technology (MIT) charged that racism was a factor in his tenure denial. And on 14 January the president of Harvard University, Lawrence Summers, triggered a national uproar when he said at an academic conference that genes and personal choices may help explain why so few women are leaders in science and engineering fields. Summers later apologized, but his contrite words aren't expected to end the controversy.

No one denies that science and engineering faculty members at major research universities remain overwhelmingly white and male, despite large numbers of women and minorities at the undergraduate and graduate levels. But why this is the case is an explosive subject. Summers lit the fuse last week at a meeting on women and minorities in science and engineering, put on by the nonprofit National Bureau of Economic Research (NBER) in Cambridge, Massachusetts, when he cited data showing that more boys than girls score at the high and low ends on standardized math and science tests. Nearly simultaneously, MIT biologist James Sherley charged publicly that colleagues undervalue his research because he is black.

According to participants at the off-the-record NBER meeting, Summers argued that women typically do not work the 80-hour weeks common to professions like law, business, or science. And while noting that socialization and bias may slow the progress of women, he cited the gender variation in test scores as a possible explanation for the larger number of men at the top of the professional ladder.

That assertion surprised and angered participants such as MIT biologist Nancy Hopkins, who led a 1999 effort to expose unconscious bias at her institution. "I thought I must not be hearing correctly," she recalls. "When I looked around, I saw other women rolling their eyes." Hopkins walked out in disgust. "He needs to listen as well as talk," says Shirley Malcom, head of education and human resources at AAAS (which publishes *Science*), who spoke after Summers. "And I got the feeling he listened but did not hear."

He did get an earful. Participants told Summers that he was misinterpreting scientific data, including their own. "High achievers are more likely to enter science, but the gender gap [in test scores] does not explain why girls—even high achievers—drop out" in significant numbers from college math and science, says Yu Xie, a sociologist at the University of Michigan, Ann Arbor. Summers cited a 2003 book by Xie and Kimberlee Shauman, *Women in Science*, that reported the performance of high-school boys varied more widely than that of girls. But Xie says this variation "is not the deciding factor" in whether women succeed in science. It's also at odds with rising numbers of women entering the scientific labor force, he notes. The decision to have a family, Xie says, seems to be the critical factor in a woman's scientific advancement. "And that," he adds, "can't be

explained by mathematical achievement."

Summers's analysis contains other flaws, Xie contended. Few researchers would argue that Asian Americans are innately more capable in math and science, he says: "The best scholarship attributes this difference mainly to culture." The phenomenon appears based in part on Asian beliefs that math is an ability that is learned, not inherited. Xie suspects that similar complex cultural differences have shaped the status of women in science.



Race and tenure. MIT's James Sherley says elite universities need to "face up to problems of racism."

Harvard's standing committee on women wrote Summers on 18 January that his comments "serve to reinforce an institutional culture at Harvard that erects numerous barriers to improving the representation of women on the faculty." Summers replied the same day, saying, "I apologize for any adverse impact on the valuable work of your committee." His NBER remarks, he added, were intended to "stimulate research on the many interrelated factors that bear on women's careers in science." Two days later Summers announced that Harvard would begin an initiative to

recruit women and back their careers.

Malcom, trained as a biologist, says that Summers's attempt to pit nature against nurture is unproductive given that the two are so clearly intertwined. Although genetic differences between men and women obviously exist, she says, they cannot explain "the systematic absence of minority males" among research professors.

That glaring absence was highlighted in an e-mail from MIT's Sherley to senior administrators after he was rejected for tenure earlier this month. The 47-year-old associate professor, the only African American in the 40-person biological engineering department, works on adult stem cell kinetics.

In a document obtained by *Science*, Sherley states that he has been denied substantial independent research space and minority career development funds, as well as being paid the least of anyone with his rank and experience. In addition, he says he waited 4 years for an invitation to give a "Meet the Lab" presentation to his colleagues. "MIT could do so much better by just facing up to the problem of racism and leading other universities in making a sincere commitment to ending it," he says. ▶



Summers's time. Harvard's Larry Summers has put the issue of women in science on the front burner with his comments at a Boston meeting.

CREDITS (TOP TO BOTTOM): MIT; LAWRENCE JACKSON/AP PHOTO

502
After the
tsunami



505
Teachers
caught in
creationist
crossfire



508
News from
the astronomy
meeting



Sherley's work, however, has been controversial. He opposes use of embryonic stem cells, and his argument that adult cells could work just as well, says one leading researcher at another university, "is a controversial hypothesis many people don't think could be true." In response, Sherley says that he considers being called controversial a badge of honor and that "findings from my laboratory have had a major impact on ideas in several related fields."

MIT officials declined to discuss the mat-

ter but called his comments "serious charges that will be handled seriously." Less than 1 year ago, MIT faculty members pledged to take "a leadership position among our peer institutions in the recruiting and success of underrepresented minority faculty and graduate students." The resolution urged MIT administrators to increase the percentage of underrepresented minorities on the faculty by "roughly a factor of two within a decade."

Meanwhile, NBER conference organizer

and economist Richard Freeman says he now regrets inviting Summers. "I didn't appreciate how Larry would take all the attention," says Freeman, who has hosted other closed-door meetings to explore other facets of the scientific workforce. But Summers's presence may have inadvertently put the issue into the national spotlight. "This provides an opportunity," says one Harvard female faculty member. "And now Larry Summers is aware he has to do something."

—ANDREW LAWLER

VIROLOGY

One Virus, Three Names, Three Claims

AMSTERDAM—Yale researchers have discovered a new cousin of the severe acute respiratory syndrome (SARS) virus that causes disease in children. Or have they?

The team has christened the agent "New Haven," and a paper published in the *Journal of Infectious Diseases (JID)* last week describes it as "a novel coronavirus." But the team admits it's the spitting image of a virus reported by Dutch researchers last year, and the paper has irked some virologists who see nothing new. Calling New Haven a new virus is "quite inappropriate," says University of Warwick virologist Craig Pringle, a former secretary of the International Committee on Taxonomy of Viruses (ICTV).

To complicate matters, the same virus was discovered and reported by not one, but two Dutch research groups last year. Each gave the virus its own name, and the two are still quibbling over who discovered it first.

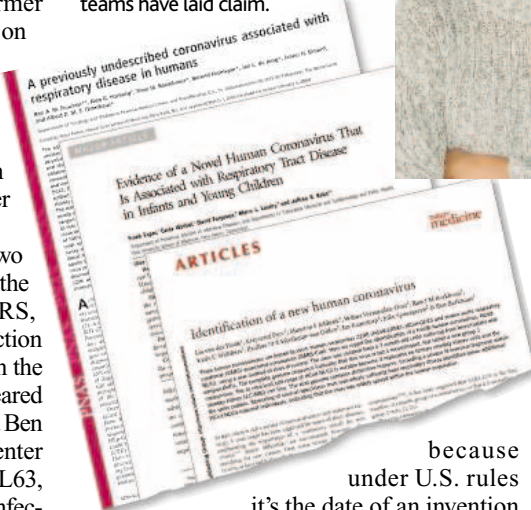
For decades, researchers knew only two human coronaviruses, which both cause the common cold. Then the third one, SARS, jolted the sleepy coronavirus field into action overnight in 2003. In a paper published in the April 2004 *Nature Medicine* (which appeared online on 21 March), Lia van der Hoek and Ben Berkhout of the Amsterdam Medical Center presented number four: a virus dubbed NL63, found in seven children with respiratory infections. The ink on that paper was barely dry when Ron Fouchier and his colleagues at nearby Erasmus Medical Center in Rotterdam reported finding the same virus, simply dubbed NL, in the 20 April *Proceedings of the National Academy Sciences*. (A note added in proof acknowledged the first paper.)

Fouchier says his team had isolated the virus more than 15 years ago but had not

gotten around to fully sequencing it and testing a series of respiratory samples for its presence. What counts is who published first, retorts Van der Hoek.

Looming behind the contest is another battle: Both groups have filed for a patent in the United States, but the Rotterdam team believes it can prevail

That's my virus. Lia van der Hoek was the first to report a new coronavirus to which the other teams have laid claim.



because under U.S. rules it's the date of an invention that matters, not when a patent was filed. A diagnostic kit could be a moneymaker, Van der Hoek says: NL63 has now been shown to cause infections, often serious, in five countries.

Now comes the "New Haven" virus, which Frank Esper, Jeffrey Kahn, and their colleagues at Yale found in children under age 5 with respiratory infections. In their paper, the team notes that New Haven, NL63, and NL are

"likely" all the same. The Yale team had named the virus before the Dutch scooped them, Kahn explains—and they stuck with the name because it's too early to tell whether the agents really are the same, he says.

That's "very unfair," says coronavirus expert Luis Enjuanes of the Universidad Autónoma in Madrid. It's up to a group claiming a new agent to show that it's really new, he notes. Even the Yale team admits that the parts of the New Haven genome sequenced so far are almost identical to that of NL63. And in a second *JID* paper linking their virus to a childhood affliction called Kawasaki disease, the group used "primers" based on NL63 to hunt for the virus in patient samples. "Apparently they're not so different at all," says Van der Hoek, who has sent a protest letter to *JID*.

Kahn declined to say whether he has filed for patents on the New Haven virus but denied that the name had anything to do with defending intellectual property rights.

ICTV will eventually decide the name of the new virus. The chair of its Coronaviridae Study Group, Willy Spaan of Leiden University Medical Center, also in the Netherlands, says a final name based on NL63 is most likely, because the Amsterdam group published first.

Meanwhile, the search for other coronaviruses goes on. In the January *Journal of Virology*, a University of Hong Kong team reports finding a fifth one, HKU1, in two pneumonia patients. It's clearly a completely new virus, Enjuanes says—and so far, it has been discovered only once.

—MARTIN ENSERINK

CREDIT: M. ENSERINK



catch the wave

2005/06

NEB catalog & technical reference is now available.

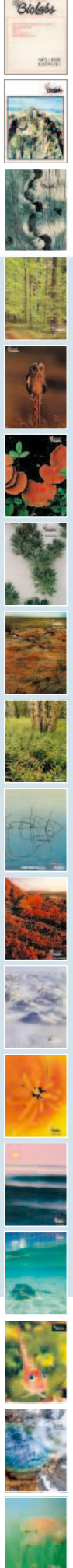
catalog highlights:

- 15 new Restriction Enzymes (not to mention 225 old favorites)
- Antarctic Phosphatase – the only commercially available phosphatase that is 100% heat inactivated in 5 minutes at 65°C; it's a better enzyme than SAP
- ShortCut siRNA Mixes – highly potent siRNA mixes that can be used at low (1-20 nM) concentration
- TransPass Transfection Reagents for siRNA and DNA
- Peptide-Carrier Kit – ligate your peptide of interest to a carrier protein for detection on Western blots or peptide arrays
- Updated Reference Appendix
- Environmental Theme – the impact of non-governmental organizations (NGOs) on the well-being of our planet

www.neb.com



The new NEB website complements our catalog and features access to an extensive library of product technical literature as well as computer tools such as Enzyme Finder and NEBcutter. The improved interface provides greater functionality when ordering products online, including customer-specific pricing, order history and shipment tracking.



1975/76

1978

1979

1980/81

1981/82

1982/83

1983/84

1985/86

1986/87

1988/89

1990/91

1992

1993/94

1995

1996/97

1998/99

2000/01

2002/03

www.neb.com



the leader in enzyme technology

New England Biolabs Inc.

32 Tozer Road • Beverly • MA 01915 USA • 1-800-NEB-LABS • Tel. (978) 927-5054 • Fax (978) 921-1350 • info@neb.com
 Canada: Tel. (800) 387-1095 • info@ca.neb.com Germany: Tel. 0800/246 5227 • info@de.neb.com
 UK: Tel. (0800) 318486 • info@uk.neb.com China: Tel. 010-82378266 • beijing@neb-china.com

For a complete list of international offices, please visit www.neb.com.

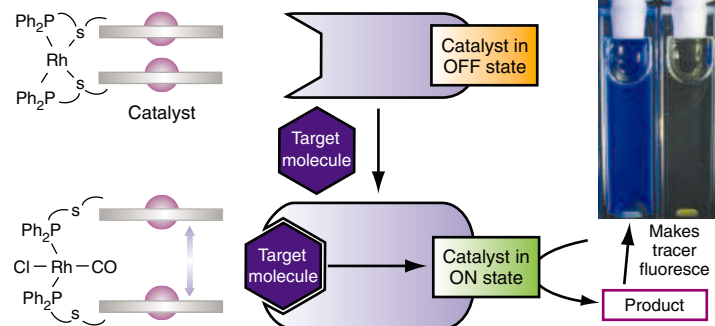
Shape-Shifting Catalyst Lights Way to New Strategy for Detecting Chemicals

Protein catalysts—or enzymes—are master shape changers. Take hemoglobin in red blood cells. When one oxygen molecule binds to the protein, the hemoglobin constricts, making it easier for the enzyme to bind additional oxygens. Chemists have rarely used shape shifting to control the activity of synthetic catalysts. But that may be set to change.

In an advanced online publication of the *Journal of the American Chemical Society*, researchers at Northwestern University in Evanston, Illinois, report that they have created a catalyst that turns on once it binds to a particular target, triggering a reaction that ultimately generates a fluorescent signal. The system is capable of revealing even minute quantities of the target molecule, they say.

“This is very novel and interesting work,” says Wenbin Lin, a chemist at the University

of North Carolina, Chapel Hill. Other groups, he says, should now be able to design novel catalysts that can lead to the detection of trace amounts of a wide variety of compounds, such as explosives and environmental pollutants. “This is a general strategy that people can use,” Lin says.



Turn on. When chloride and carbon monoxide molecules bind to catalyst’s rhodium atoms, a cavity opens between two zinc atoms (red circles). This triggers the catalyst to produce acetic acid, which in turn generates a fluorescent compound.

of North Carolina, Chapel Hill. Other groups, he says, should now be able to design novel catalysts that can lead to the detection of trace amounts of a wide variety of compounds, such as explosives and environmental pollutants. “This is a general strategy that people can use,” Lin says.

The new work is similar in spirit to the polymerase chain reaction (PCR), which amplifies snippets of DNA and attaches a fluorescent probe to the copies. This ability to detect virtually any strand of target DNA has made PCR one of the foundations of modern molecular genetics. Chemists, however, have lacked such a broadly applicable sensing technique. “One of the biggest challenges for chemistry is to do what PCR does for biology,” says Chad Mirkin, who led the Northwestern University effort. Chemists have come up with numerous schemes for detect-

ing low concentrations of different compounds, but few are generalizable for detecting a wide array of compounds. Seeking such a strategy, Mirkin and his colleagues broke the problem into two parts: detecting a target molecule and amplifying a signal so that it could be readily detected. They created an organic ring-shaped molecule with four metal atoms, two zincs and two rhodiums. The zinc atoms are the key to the molecule’s ability to act as a catalyst. These atoms work together to convert acetic anhydride into acetic acid, the same compound that gives vinegar its sour flavor. But the zincs do their job only when the two metal atoms are spaced far enough apart to let acetic anhydride molecules nuzzle in between them.

For the targeting step, Mirkin’s group designed the ring-shaped compound so that it would start off in a nonreactive, collapsed

shape. In this conformation, rhodium atoms on opposite sides of the molecule bind to two sulfur atoms and two phosphine groups (see figure, left). But when a pair of chemical targets—carbon monoxide gas and chloride ions—enter the picture, the rhodium atoms cut their ties to the sulfur atoms and latch onto the tar-

gets instead. The atomic shuffle relaxes the catalyst’s shape, thereby switching it on. The result: torrents of acetic acid.

In step two, the acetic acid donates one of its protons to another compound in the mix, known as diethylaminomethylanthracene, changing it into a highly fluorescent tracer. Mirkin and his team watched the solution light up as the catalyst detected and bound to carbon monoxide and chloride.

Mirkin notes that detecting chloride isn’t anything special. Electrochemical detectors already exist for the job. But unlike those and other detection schemes, Mirkin and others say, the new approach should make it possible to detect many different target compounds simply by altering the catalyst.

—ROBERT F. SERVICE

New Chief for Heart Institute

The new director of the National Heart, Lung, and Blood Institute (NHLBI) is a recent recruit well-versed in both clinical and basic research. Cardiologist Elizabeth Nabel, 52, now chief of clinical intramural research, will succeed Claude Lenfant, who retired in August 2003 after 21 years as head of the National Institutes of Health’s (NIH’s) third largest institute.



Nabel came to NHLBI in 1999 from the University of Michigan along with her husband, Gary Nabel, who was hired to head NIH’s new vaccine research center. Nabel, who works on vascular biology and gene therapy for damaged hearts, is a “superb scientist ... in an excellent position” to steer both basic, translational, and clinical research, says molecular cardiologist Roberto Bolli of the University of Louisville in Kentucky, a member of NHLBI’s advisory council. Nabel declined comment through a spokesperson, as her appointment had not been announced at press time.

—JOCELYN KAISER

Novel AIDS Vaccine Trial

An unusual AIDS vaccine study that began this week in seven countries aims to reduce the time needed to gauge its merit.

The 5-year study, being conducted by Merck and the HIV Vaccine Trials Network (HVTN), will recruit 1500 people at high risk of contracting the virus and will evaluate whether the vaccine can prevent sexual transmission or keep HIV levels low for those infected. Whereas clinical studies for a vaccine at this stage of development typically assess whether it triggers immune responses and is safe, this trial tries to get an early peek at whether the vaccine actually works. Researchers hope that by cutting to the chase, they can better judge whether it warrants a larger, more expensive test. The study will test the value of the body’s ability to produce “killer cells” against HIV-infected cells.

“It’s exciting,” says Susan Buchbinder, principal investigator for HVTN and an epidemiologist at the San Francisco Department of Public Health. More AIDS vaccines are in the pipeline, she notes, and “it will give us an answer about this type of approach in a more efficient way.”

—JON COHEN

CLIMATE CHANGE

Panel Urges Unified Action, Sets 2° Target

A new report from an international task force on climate change calls for the major industrial nations to join with China and India to tackle the problem together. It describes the devastating long-term impact on the environment of a 2°C rise in average global temperatures. The report is expected to help British Prime Minister Tony Blair argue his case for reductions in greenhouse gas emissions as the United Kingdom this year assumes the presidency of the G8 nations and Blair becomes president of the European Union in July.

Issued this week by a 14-member independent panel of scientists and policymakers assembled by U.S., U.K., and Australian think tanks, the report (www.americanprogress.org/climate) seeks to find common ground between nations that have ratified the 1997 Kyoto Protocol and those, including the United States and Australia, that have not. It recommends a global effort to set up a cap-and-trade system for emissions that would extend beyond the Kyoto framework that expires in 2012 and a shift in agricultural

subsidies from food crops to biofuels. It also calls on richer nations to help developing countries control their emissions as their economies grow. The panel was convened by Stephen Byers, an influential Labour member of parliament, and timed to coincide with a key speech by Blair this week at the World Economic Forum in Davos, Switzerland.

“The cost of failing to mobilize in the face of this threat is likely to be extremely high,” the report says, noting that Blair has pledged to make climate change a priority for this year.

In 2001, U.S. President George W. Bush said that “no one can say with any certainty what constitutes a dangerous level of warming and therefore what level must be avoided.” The report cites probabilistic analyses aimed at doing just that, however. Current global temperatures now hover around 0.8°C above preindustrial levels, and a 2001 report by the Intergovernmental Panel on Climate Change projects a rise of from 1.4° to 5.8° by 2100. Recent analyses conclude that even higher temperatures

can't be ruled out (p. 497).

The report makes a case that even a 2° rise could have catastrophic effects on the planet, including the decimation of coral reefs worldwide, the melting of the West Antarctic Ice Sheet, and the severe degradation and disruption of various ecosystems. The report also notes that temperatures could exceed the 2° goal before emissions controls kick in and lower the temperature by 2100.

Despite that dire scenario, policy watchers of all stripes in Washington, D.C., doubt that the report will have much impact on the Bush Administration. Patrick J. Michaels, a professor of environmental sciences at the University of Virginia, Charlottesville, and a leading climate change contrarian, called the 2° goal “arbitrary” but speculates that the White House “will be amenable to” the report's suggestions to develop clean coal technologies and push for more efficient vehicles. Administration officials declined to comment on the recommendations.

—ELI KINTISCH

PLANETARY SCIENCE

Missing Noble Gases Hint How Titan Got Its Dense Atmosphere

While the Huygens probe was discovering the weird yet familiar landscape on Titan (*Science*, 21 January, p. 330), it was failing to make some much-anticipated discoveries. The spacecraft's atmospheric analyzer never did detect the noble gases argon, krypton, or xenon, which cosmochemists expected to find lingering from the formative days of Saturn's lone big moon. “That's rather surprising,” says physicist Robert Pepin of the University of Minnesota, Twin Cities, “and a bit of a disappointment.”

Researchers had hoped to use the abundance of Titan's noble gases as a guide to how volatile elements essential to life, such as carbon and nitrogen, were divvied up among solar system bodies, including Earth, as the gases hitched a ride with water ice. The absence of detectable primordial noble gases puts a crimp in those plans.

Scientists are reasonably sure that Huygens would have detected primordial noble gases if they were there in the anticipated amounts. Huygens science team member Tobias Owen of the University of Hawaii, Manoa, noted at last week's press conference in Paris that the probe's gas chromatograph/mass spectrometer had detected argon-40, produced by radioactive decay of potassium-40 in the moon's rock. But there is as yet no sign of argon-38 or argon-36.

This means the argon-to-nitrogen ratio must be on the order of 1000 times lower on Titan than on Earth, says Owen.



No show. Huygens's failure to detect certain noble gases suggests that a moon gets an atmosphere only if it forms at a low enough temperature.

The new upper limits for titanian primordial noble gases may be frustrating, but they at least point toward an explanation for Titan's uniquely massive nitrogen atmosphere. Its surface pressure is 1.5 times that of Earth, whereas Jupiter's large moons Ganymede and Callisto have no atmospheres to speak of. This, despite their being as massive as Titan—and therefore capable of gravitationally retaining an atmosphere—and just as ice-rich, suggests that all three moons would have started with similar allotments of ice-borne gases.

Titan's dearth of noble gases suggests that the nascent Saturn system was too warm for its ices to retain the notoriously inert noble gases through adsorption or trapping within their crystalline structure, says Owen. Laboratory experiments indicate they would not be retained above 50 K, he says. But it was evidently cold enough to retain nitrogen. The Jupiter system, being little more than half Saturn's distance from the sun, was warmer still—perhaps warm enough for the ice that formed its big moons to lose not only noble gases but also the ammonia that forms a nitrogen atmosphere. So, for even a big, icy moon to have a massive atmosphere, it had best keep its distance from the sun.

—RICHARD A. KERR

CREDIT: ESA

GREENHOUSE WARMING

Climate Modelers See Scorching Future as a Real Possibility

Researchers tapping the computer power of 26,000 idling personal computers are confirming that a searing heating of the globe in the coming centuries can't be ruled out. Their new twist is twofold. It could get even hotter than the previous worst case had it. And, contrary to earlier work, no modeler can yet say that such an extreme scenario is any less likely than the moderately strong warming that most climate scientists expect. That shakes up what had seemed to be an emerging consensus, although some balk at such an extreme perspective.

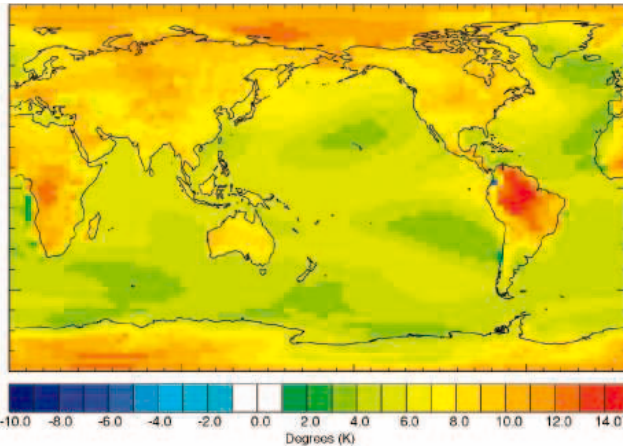
Last summer, a gathering of climate modelers, paleoclimatologists, and other climate researchers seemed to be converging on a middle ground (*Science*, 13 August 2004, p. 932). Three different kinds of studies—a collection of the latest expert-designed climate models, perturbations of a single model, and studies of past climate—addressed the question of how sensitively the climate will respond to increasing greenhouse gases. All three seemed to be pointing to a moderately strong sensitivity. When greenhouse gases are doubled, it appeared, warming would be something like 2°C to 4°C. A low, nearly harmless climate sensitivity much less than 2°C seemed quite unlikely, and an extreme one of more than 6°C or 7°C was possible but far less likely than the consensus range.

Now comes modeler David Stainforth of the University of Oxford, U.K., and 15 colleagues with their pumped-up version of the perturbed-parameter approach. In a similar study reported at last summer's workshop and in *Nature*, James Murphy of the Hadley Center for Climate Prediction and Research in Exeter, U.K., and colleagues altered 29 model variables that control physical properties such as the behavior of clouds, atmospheric convection, and winds. Given their available computing resources, they had to perturb only one parameter at a time for a total of 53 simulations. In order to extrapolate their results into the high-sensitivity range, they had to assume that changes in two parameters simply add up.

In the Stainforth study, published this week in *Nature*, the modelers varied six parameters several at a time so that they could explore

nonlinear interactions between parameters. The resulting 2578 simulations used in the study were run on personal computers whose owners—members of the general public—contributed their idle processing capacity to the *climateprediction.net* experiment.

In this distributed-computing study, perturbed parameters did in fact interact nonlinearly to heighten climate sensitivity. None of the simulations had a climate sensitivity less than 2°C, in line with expectations. And most simulations did not fall far from the model's sensitivity of 3.4°C when run with no parameters perturbed. But the inevitable long tail of results on the high-sensitivity



Ouch. If climate were as sensitive as a new study allows, greenhouse warming in coming centuries would be double-digit (oranges and reds).

side ran out to 11°C, 2°C farther than any kind of study before it.

How likely is an 11°C sensitivity? “We can’t yet give a probability for our results,” says Stainforth. “Our [high-end] results are very sensitive to our prior assumptions,” such as which parameters are perturbed and by how much. Previous studies suffer from the same limitations, he says.

Other climate researchers will take some convincing. “I just can’t believe climate sensitivity is 10°C,” says paleoclimatologist Thomas Crowley of Duke University in Durham, North Carolina. Climate’s responses to past, natural changes in greenhouse gases or equivalent climate drivers, such as volcanic eruptions, have just been too modest for that, he says. Until modelers can rein in their unruly simulations—perhaps using the tens of thousands of additional perturbed-parameter simulations now in hand at *climateprediction.net*—Crowley will stick with a moderately strong warming.

—RICHARD A. KERR

Irish Observatory to Close

Astronomers worldwide are protesting a plan to shutter Ireland’s only astronomical observatory, which has operated for 220 years.

Dunsink Observatory, in the Dublin suburb of Castleknock, houses a historic 30-centimeter telescope and conducts research on topics such as high-energy astrophysics. Last summer, however, the board of the School of Cosmic Physics of the Dublin Institute of Advanced Studies, which runs Dunsink, decided to close it by the end of the year (a date since pushed back, probably to spring 2005). Although its staff of 10 will be moved to a new building in Dublin, scientists worry that the government will reduce funding for astronomy once this national symbol is gone.

Astronomers want Ireland’s Minister for Education and Science, Mary Hanafin, to persuade the publicly funded institute to reconsider its decision and to consult with staff on the future of the observatory. “Dunsink might be used for outreach purposes, but without our involvement, it probably won’t happen in the best possible way,” says observatory director Evert J. A. Meurs. Meanwhile, 440 astronomers from around the world have signed an online petition to save the observatory (www.petitiononline.com/save_obs) and planned to present it to Hanafin this week.

—GOVERT SCHILLING

Rescue for Italian Synchrotron

ROME—The Italian government last week approved a slate of measures to support science, including a bailout of the country’s Elettra light source.

The cash-strapped synchrotron in Trieste, which produces x-rays to probe matter, had been overlooked in the government’s 2005 budget, triggering a recent strike (*Science*, 14 January, p. 192). Last week, however, the Council of Ministers approved an annual increase of \$18 million for the next few years. “The decree meets our requirements,” says *Sincrotrone* Chair Carlo Rizzuto, adding that it “acknowledges the value” of the lab.

The decree also provides for the state to act as guarantor to a high-priority \$78 million European Investment Bank loan for construction of a free-electron laser at Elettra. There is good cheer for academic researchers, too: Thanks to \$560 million added to university budgets, newly hired researchers can earn a full salary after

1 year instead of three. The change will boost their income by about 30%. Research minister Letizia Moratti calls the move “another way to keep the best youngsters in our universities.”

—SUSAN BIGGIN

CREDIT: D. A. STAINFORTH ET AL., *NATURE* 433 (27 JANUARY 2005)

Centers Embrace an Alliance But Remain Wary of a Merger

TOKYO AND NEW DELHI—The developing world's two premier agricultural research organizations have agreed to join forces on selected scientific projects. But the leaders of the International Rice Research Institute (IRRI) in Los Baños, the Philippines, and the International Maize and Wheat Improvement Center (CIMMYT), near Mexico City, rejected an outside recommendation to merge their administrative structures.

“A cynic could say that there is not much new” in this agreement, says Alex McCalla, professor emeritus of agricultural economics at the University of California, Davis, and chair of the CIMMYT board of directors. “Still, this is a set of commitments that goes way beyond anything these two centers have done before.”

The two centers are part of a global network of 16 institutions working on agricultural challenges in the developing world. The impetus for closer cooperation comes from recent research showing that the major cereals share many genes. Last year the two centers asked the Rockefeller Foundation to study various organizational options, including a full merger (*Science*, 27 February 2004, p. 1281). Meeting earlier this month in Shanghai, the centers' two boards of directors accepted the foundation's suggestion to begin

four joint research programs immediately and to pool support services related to issues such as intellectual-property rights, biosafety, and scientific publishing.

But governance issues proved more difficult. All agree that a complete merger wouldn't

the two centers under a single director-general and a single board of directors, as the foundation's working group had suggested.

McCalla says both boards felt that having a single director-general “was tantamount to a merger” and, thus, “premature.” Instead, the boards decided to set up two committees, one to oversee the joint programs and one to explore common management. They also agreed to have two members sit on both boards. “Depending on the performance of these joint programs, we may take a second step toward greater cooperation,” says Keijiro Otsuka, an agricultural economist at the Foundation for Advanced Studies on International Development in Tokyo and chair of the IRRI board.

Gurdev Khush, formerly chief breeder at IRRI and now a professor emeritus at the University of California, Davis, calls the alliance “a welcome development.” He sees the joint work on

intensive rice-wheat and rice-maize crop production systems, crop databases for breeders and farmers, and how crops can adapt to climate change as a step in the right direction. Toenniessen agrees, but adds, “We wish they would have gone further.”

—DENNIS NORMILE

With reporting by Pallava Bagla.



Multigrain? IRRI's rice researchers will soon be teaming up with CIMMYT's efforts involving wheat and maize.

work. “Dissolving two existing international institutions and replacing them with a new one raised a host of very difficult legal and procedural problems,” says Gary Toenniessen, a Rockefeller Foundation official and coordinator for the working group. The working group and the boards also agreed that the research projects should have a single leader and a unified budget. But the boards balked at putting

NASA BUDGET

Hubble, Other Programs Face Cuts in 2006

The budget ax is about to fall on several NASA science programs. Despite President George W. Bush's decision to seek a small boost in the agency's \$16.2 billion budget in 2006, sources say that the victims this year and next will include Mars data programs, aeronautics research, and the Hubble Space Telescope. The cuts, certain to be controversial, are part of the space agency's 2005 spending plan as well as the 2006 request that the president will send to Congress on 7 February.

The White House's priorities for the space agency include returning the shuttle to flight, developing new human exploration technologies, and finishing the space station. Those programs will eat up the bulk of the increases in the president's request, say sources, and starve several other activities. For example, NASA and the White House have decided to let the aging Hubble telescope fall into the

Pacific Ocean, say Administration sources, instead of mounting a servicing mission involving either robots or astronauts arriving via the shuttle. But some lawmakers have already warned the White House that they will oppose the decision not to return to Hubble to extend its life.

Although the fight over Hubble will likely produce the most fireworks on Capitol Hill, space agency managers are quietly making significant cuts this year to other science programs to cope with hundreds of millions of dollars in congressional earmarks as well as the return-to-flight costs for the shuttle. For example, NASA plans to severely curtail spending for new technologies devoted to science missions such as information systems designed to improve data return from future robotic Mars missions, Earth science probes, and the upcoming Stratospheric Observatory

for Infrared Astronomy flight, according to Administration sources. Those technologies would improve autonomy and increase the number of measurements that can be made during NASA missions. The cuts, which will be made by the exploration directorate, may surpass \$30 million.

Despite the budget squeeze, NASA managers are working hard to salvage as many science programs as possible by delaying those with later starting dates. One prime example of that strategy is the Beyond Einstein program, which was scheduled for the next decade. Sources say that the president's new budget will pledge to limit the damage to science programs inflicted by spending on human space flight. That pledge will be sorely tested, however, during the upcoming budget battles.

—ANDREW LAWLER

CREDIT: PALLAVA BAGLA

HIGHER EDUCATION

Fundraising Begins for Network Of Four African Institutes

A group of African scientists, engineers, and educators will gather this weekend in Ajuba, Nigeria, to announce plans to transform education and research in sub-Saharan Africa. Their goal is a network of four regional schools that will train 5000 scientists and engineers per year and provide world-class research facilities. And they are looking for big money to bankroll the plans—an endowment of \$500 million by 2007 for the first institute and up to \$5 billion to support all four.

“It is a big challenge,” admits Hippolyte Fofack, a World Bank senior economist involved in planning the African Institute of Science and Technology (AIST). Fofack admits there are few firm commitments yet but says that “the vibrations are very positive.”

The case for strengthening sub-Saharan Africa’s tertiary education and research efforts is easy to make. The region has only 83 scientists and engineers per million residents, one-fifth of the ratio for North Africa and one-sixth that for all developing countries. Research spending as a share of gross domestic product has actually declined since 1970, to a scant 0.47%, while spending in East Asia has quadrupled, to 1.27%, over the same period.

AIST is modeled on the Indian Institutes of Technology, a loosely affiliated group of seven institutions begun in 1963. Planners

hope for four institutes, one each in east, west, central, and south sub-Saharan Africa. The first, on land provided by the Tanzanian government in Arusha, seeks to open its doors in 2007.

The curriculum, including undergraduate and graduate programs, will emphasize “solving practical problems,” says Mohamed Hassan, executive director of the Third World Academy of Sciences and a member of the institute’s advisory committee. Degrees will be offered in science, engineering, economics, and management.

Organizers hope to build a world-class faculty by using generous salaries and first-class facilities to lure back some of the estimated 30,000 African Ph.D.s now working abroad. An even bigger challenge, says Hassan, will be finding good jobs for graduates. “Otherwise, we’ll be repeating the cycle of having talented scientists and engineers just fly away,” he says.



Setting the bar high. The World Bank’s Hippolyte Fofack agrees that financing AIST “is a big challenge.”

Teferra, director of the International Network for Higher Education in Africa at Boston College’s Center for International Higher Education.

Still, South African icon Nelson Mandela has agreed to chair the first AIST board of directors, and the Nelson Mandela Institution for Knowledge Building will manage the endowment. Fofack has amassed a long list of ministers who support the initiative in principal. “African universities aren’t really prepared to develop engineering programs with strong links to [industrial] sectors,” notes Christian

Sina Diatta, Senegal’s research minister. AIST’s planners hope that governments will back up their words with financial support during the kickoff meeting. “Politicians talk a lot about the importance of science and engineering,” says Hassan. “This will be a real test of their commitment.”

—DENNIS NORMILE

RESEARCH FUNDING

Saudi Millionaire Plans an NSF for Arab Scientists

SHARJAH, UNITED ARAB EMIRATES—Filling a void in the Persian Gulf and Middle East, a Saudi tycoon has endowed the first pan-Arab science fund.

At a technology investment forum last month in Jeddah, Saudi Arabia, Mohammed Abdul Latif Jameel announced that a holding company he heads, the Jeddah-based Abdul Latif Jameel Co., will make a \$1 million annual donation to the Arab Science and Technology Foundation (ASTF) to launch and support a new peer-reviewed research competition. The new fund, to be managed by ASTF, would select 20 proposals a year based on merit, backing each at \$50,000. Although that may seem like small potatoes, “there hasn’t been anything like this in the



Deep pockets. Mohammed Abdul Latif Jameel has pledged an annual donation of \$1 million.

Arab world,” says ASTF president Abdalla Alnajjar. “It is a wonderful beginning and an impetus to other rich Arabs and private companies to play a role in science development in the region,” adds Farouk El-Baz, director of the

Center for Remote Sensing at Boston University.

Some observers also hope the donation will spur Arab governments to strengthen their own support for science. Arab countries spend on average 7% of gross domestic product on defense but less than 0.2% on research and development. “If they don’t take drastic measures to revitalize science,” Pakistan’s science minister Atta-ur-Rahman told *Science*, then the region’s oil-fueled prosperity will seem like a mirage after the oil runs out—“from

Cadillacs back to camels,” he says.

ASTF, based in Sharjah, is hammering out guidelines for the fund and the international board that will oversee it. The foundation is best known in the West for its high-profile partnership with Sandia National Laboratories in Albuquerque, New Mexico, to support Iraqi scientists (*Science*, 14 May 2004, p. 943). ASTF intends to model the new competition, and the breadth of projects it supports, after the U.S. National Science Foundation. Only scientists from 22 Arab nations will be eligible to compete for grants, although they are allowed to have Western collaborators, Alnajjar says.

The Abdul Latif Jameel Co. started out as a Toyota dealership and has since diversified into a multinational company dealing in electronics, real estate, and other areas. Its pledge of \$1 million per year to the new fund is open-ended, says Alnajjar, who plans to woo other sponsors to follow suit. “If properly run, this could snowball into something much bigger,” he says. The fund is expected to be up and running by summer.

—RICHARD STONE



**eppendorf
& Science**
**PRIZE FOR
NEUROBIOLOGY**

You Could Be Next

Eppendorf and *Science* award an annual research prize of \$25,000 for outstanding contributions to neurobiology research based on methods of molecular and cell biology. Each year the prizewinner is selected by a committee of independent scientists, chaired by the Editor-in-Chief of *Science*, and announced at an event held during the week of the Annual Meeting of the Society for Neuroscience.

We are now accepting applications for the 2005 Prize. Young scientists who have received their PhD or MD within the past 10 years are eligible.

For more information visit:

Eppendorf at www.eppendorf.com/prize

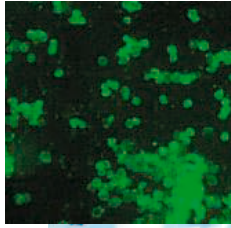
Science at www.eppendorfsienceprize.org

\$25,000 Prize
Deadline for application:
June 15, 2005

BIODEFENSE LABS

Boston University Under Fire for Pathogen Mishap

Opponents of a proposed \$128 million high-security biology lab at Boston University are crying foul following the belated revelation last week that a dangerous bacterium infected three workers at another BU lab. But the news isn't likely to derail plans for the new biodefense lab, which last week cleared its final major regulatory hurdle.



The May 2004 incident, involving a highly infectious strain of tularemia, did not become public until a week after Boston's Zoning Commission approved construction of the biosafety level 4 (BSL-4) lab. Federal, state, and city officials defend the failure to go public, insisting that the lab accident never posed a public threat. But those who argue that the BSL-4 lab should not be built in the city's crowded South End neighborhood say the incident strengthens their argument that BU is incapable of managing a laboratory that will deal with even more potent agents. Local residents have filed a suit to halt construction, and the city council may soon reconsider previously defeated legislation banning any BSL-4 lab from being built.

The trouble last year began on 22 May, when a researcher at BU's BSL-2 lab developed a fever, cough, and headache. Two days later, the same happened to a second worker; 4 months later, a third researcher was hospitalized with similar symptoms. In late October, BU scientists discovered that all three workers had handled a live strain of tularemia instead of the noninfectious variety that is typically used.

The scientists were trying to find a vaccine for what is colloquially called "rabbit fever," a sometimes-fatal illness caused by bacteria that federal officials fear could be used by bioterrorists. Paul Mead, an epidemiologist with the Centers for Disease Control and Prevention in Atlanta, Georgia, who is leading an investigation into the mix-up, says the leading suspect is a contaminated reagent. Investigators also say that workers improperly handled the bacterial sample by not placing it in a sealed chamber to filter out any infectious agents.

On 4 November, BU told lead scientist Peter Rice, chief of infectious diseases, to halt the vaccine project. But it took BU nearly a week to notify the state public health department and one more day to inform city officials. Under government guidelines, labs are

to report any such incident in an expeditious manner. "We were immediately disturbed" by the delay, says John Auerbach, chief of Boston's public health department. Anita Barry, who heads the communicable disease section of the department,



Safety first? Boston University's delayed reporting of a tularemia outbreak (inset) has stoked criticism of its plans to build a BSL-4 lab.

says BU's "lapse of 2 weeks was not that unusual, but we were unhappy."

BU eventually closed the lab space and put 11 employees on paid leave. Last week, Rice was removed from his position but

allowed to remain on the faculty. The university also failed to update a safety record report issued last summer that claimed no infections in its BSL-2 and BSL-3 labs during the past decade. That document was used in the environmental impact statement for the BSL-4 lab.

The proposed BSL-4 lab is one of six to be built around the country with National Institutes of Health funding. Although the zoning board's approval paves the way for construction to start this year, opponents say the tularemia episode gives them new ammunition. "Now BU has demonstrated they are not competent to manage even a BSL-2 [lab]," says Sujatha Byravan of the Council for Responsible Genetics in Cambridge, Massachusetts. A new lawsuit by 10 residents argues that the environmental impact statement for the proposed lab is flawed, and four city council members have pledged to push legislation banning the lab.

The city approved construction just days prior to the revelations, however, and Mayor Thomas Menino and construction unions remain staunch and powerful supporters. Their backing suggests that, for BU, the tularemia incident may turn out to be more of a temporary headache than a fatal illness.

—ANDREW LAWLER

CLIMATE CHANGE

Scientist Quits IPCC Panel Over Comments

An ugly spat has broken out among contributors to the world's leading scientific report on climate change. Chris Landsea, a hurricane expert with the National Oceanic and Atmospheric Administration in Miami, announced last week that he is resigning as a contributor to the next report of the Intergovernmental Panel on Climate Change (IPCC) because a leading co-author had "politicized" the process with pronouncements about the impact of global warming on last year's tumultuous hurricane season.

The tussle began last October when Kevin Trenberth of the National Center for Atmospheric Research in Boulder, Colorado, took part in a media phone call organized by Harvard scientists on last year's spate of hurricanes. Trenberth, who was introduced as the lead author of a chapter on climate observations for the IPCC's 2007 report, noted that warming sea temperatures and rising sea levels caused by global warming are "changing" conditions for hurricanes and warned that the 2004 hurricanes "may well be a harbinger of the future."

His widely reported comments upset Landsea, who notes that IPCC has concluded that no

such link can yet be made. Landsea threatened to resign unless IPCC leaders reprimanded or removed Trenberth. On 16 January, Landsea stepped down, saying in an e-mail to colleagues that Trenberth's actions have made it "very difficult for the IPCC process to proceed objectively" on hurricanes.

In an e-mail to *Science*, IPCC Secretary-General R. K. Pachauri repeated what he had told Landsea: "In their own individual rights, [IPCC authors] are free to express their views on any subject, including various aspects of climate change." Trenberth told *Science* that "it's ridiculous to suggest I [was] representing the IPCC"; his role as an author was mentioned during the October event merely as "part of my credentials." He also defended his view that changing sea conditions could be contributing to greater hurricane intensity.

That position is "plausible," says hurricane expert Kerry Emanuel of the Massachusetts Institute of Technology. But hurricane activity varies so much from decade to decade that "not a single person in my field thinks you can see the signal."

—JOCELYN KAISER

With reporting by Eli Kintisch and Pallava Bagla.

The tsunami ravaged settlements along the coast of Sri Lanka, but aid workers have been successful so far in preventing a mass disease outbreak

A Race to Beat the Odds

KALMUNAI, SRI LANKA—Dozens of huts, cobbled together from corrugated tin and wood scavenged from wrecked buildings, are clustered around a Hindu temple decorated with brightly painted holy figures. Inside one shelter an elderly Tamil woman squats in the sandy soil, rinsing chunks of eggplant for the evening meal. Ants crawl frenetically over a small sack of flour—her entire larder. She’s one of the lucky few survivors of the crowded beachfront neighborhoods of Kalmunai, a town in eastern Sri Lanka that was hard-hit by the tsunami.

Children are playing, barefoot, beside a pool of fetid water. “I’m really worried about this camp,” says M. A. C. Mohammed Fazal, the district’s chief medical officer. The 800 people living here, like the 437,000 other displaced survivors along Sri Lanka’s

Sri Lanka, which suffered the second highest toll after Indonesia. In the immediate aftermath, some health officials warned that disease outbreaks could double the tsunami’s toll. So far, such a crisis has been averted.

“It’s a myth that spikes in disease always follow a disaster,” says David Bradt, a WHO epidemiologist assigned to Jaffna in northern Sri Lanka. Provided people have access to chlorinated drinking water and sanitary living conditions, he says, an outbreak “is certainly not inevitable.”

But the fate of the displaced survivors hangs in the balance, and untold numbers are likely to experience serious psychological damage from this disaster. “These people are at tremendous risk,” says Denham Pole, a WHO physician in Colombo, Sri Lanka’s capital.



Survivors. Many who escaped the initial inundation, like these inhabitants of Kalmunai, are now at risk for health problems.

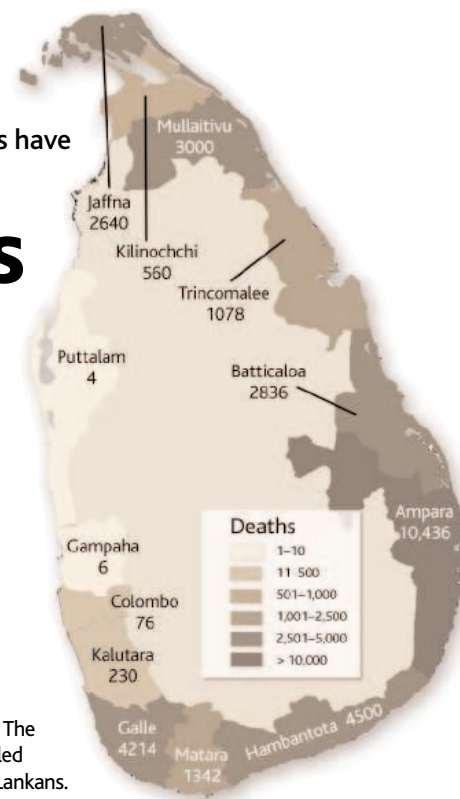
eastern and southern shores, are vulnerable to a variety of infections, including potential killers such as cholera, dysentery, and typhoid. “We’re looking for all the usual suspects,” says epidemiologist Angela Merianos, a SARS expert with the World Health Organization (WHO) temporarily assigned to Sri Lanka to help local health officials ward off diseases in the camps.

The 26 December tsunami, the third biggest natural disaster in the last 100 years, is known to have claimed more than 228,000 lives, including some 31,000 in

who had suffered a heart attack, was deteriorating. Fazal raced back, but by the time he arrived, just before 9 a.m., his father had died. “I was sobbing next to his body,” he says, “when suddenly there was panic on the streets. People were shouting, ‘The sea is coming!’” The hospital emptied.

Soon after, tsunami victims began pouring in. The first victim Fazal saw was a 5-month-old girl, cradled by her mother. “The baby was dead, but her mother didn’t believe me,” he says. Fazal, 32 and the father of an 18-month-old boy, was confronted over and over again

Death toll. The tsunami killed 31,000 Sri Lankans.



with gut-wrenching sights. “Every time I looked at a dead child, I saw my son’s face, and I cried,” he says. Later that morning Fazal found out that his wife and son and other family members had been spared.

Many victims were saved. Those whom Fazal and his staff were unable to treat were sent to the general hospital in Ampara, 25 kilometers inland. The surge of injured victims quickly abated. By early afternoon, Fazal says, only corpses were arriving at Kalmunai hospital.

On the other side of Sri Lanka, in Colombo, by late morning of 26 December “we were hearing rumors that the sea had suddenly risen to very high levels and had drowned people on the coast,” says Pole. Initial news reports said that up to 300 people had drowned, but Pole knew that Sri Lanka’s east coast was dotted with fishing villages hard up against the shore. “The death rate was incalculable at that stage,” he says.

At dawn on 27 December, WHO launched what it calls a “rapid health assessment.” Over the next few days, teams fanned out to affected areas. It wasn’t easy. For example, as one team neared the colonial-era fortress town of Galle, south of Colombo, “the roads were covered with houses,” Pole says. The assessment revealed two things: “The country as a whole was largely unaffected,” says Pole, but swaths of coastline were utterly devastated, and there were countless families whose homes were gone and children who had lost parents. “The

CREDITS (LEFT TO RIGHT): © A. WAK/PAHO-WHO; SOURCE: DISASTER OPERATION CENTRE, MINISTRY OF SOCIAL WELFARE

enormity of the disaster began to sink in.”

Foreign aid workers and Sri Lankans raced to provide basics such as clean drinking water and latrines. “The response of the government has been excellent,” Pole says. “They forgot all the usual bureaucracy and cleaned out their store.” Emergency supplies flowed to all the affected communities, including those in the northeast controlled by the Liberation Tigers of Tamil Eelam (LTTE), the rebels’ political arm.

Lack of clean water is the deficiency felt most keenly. A high water table has flooded cesspools and tainted wells, says Bipin Verma, an emergency health expert in WHO’s Colombo office. In the days after the tsunami, local health officers rode around in trucks with megaphones ordering people to boil water. “Now people understand what they have to do,” Fazal says.

Nutrition is a growing concern, says Verma. The price of vegetables has risen since the disaster, and Sri Lankans have been eating less fish out of the false fear that fish are contaminated by corpses in the water.

The risk of vector-borne diseases still looms. “To me, that’s the biggest health threat,” says Verma. Dengue and malaria, both transmitted by mosquitoes, are endemic in Sri Lanka. WHO has borrowed 50 pesticide fogging machines and distributed them throughout the country. Chlorination, sanitation, vector control: Basic measures can save lives. “We don’t have to have new science to do this,” says Bradt.

The healing process

It will be a triumph if Sri Lanka averts a major disease outbreak. Other consequences of the disaster—the psychological repercussions—cannot be avoided. “There’s an enormous amount of trauma,” says Kan Tun, WHO representative to Sri Lanka. First came shock. “People were paralyzed by despair,” says Pole.

Four weeks after the tsunami, survivors are at risk of posttraumatic stress disorder. “In my experience, adults are more vulnerable than children,” says Verma. Teams of caregivers with SHADE, a nonprofit based in Vavuniya, Sri Lanka, are working with victims in the Kalmunai region. Fear is the most prevalent emotion, says SHADE’s Jeyabalini Gopal: “Children are afraid of another wave; they even get frightened by small sounds.” Her team’s main tool is art therapy. “They draw pictures of their surroundings before and after the tsunami,” Gopal says. “That allows them to express what they can’t yet talk about.”

SHADE has worked with victims of violence in the war-torn northeast, where the government and LTTE fought a long-running civil war that was halted by a cease-fire in

Nuke Policy Leads India to Build Own Network

NEW DELHI—India’s determination to protect its seismographic secrets may result in two tsunami early-warning systems for South Asia.

Last week the government announced it would spend \$30 million on a system independent of a multinational network for the region being planned by UNESCO (*Science*, 21 January, p. 331). The decision is driven by India’s long-standing refusal to allow international parties to operate seismic monitoring stations on its territory, a policy that stems from its rejection of the global Comprehensive Test Ban Treaty (CTBT) to preserve its right to conduct underground nuclear tests.

“We are not joining a U.N.-led system,” declared Kapil Sibal, India’s minister for science, technology, and ocean development, at the end of a 2-day meeting here last week on the aftermath of the deadly South Asian earthquake and tsunami. “We will not hesitate in forging alliances with other countries, but we have to have our own tsunami warning system.”

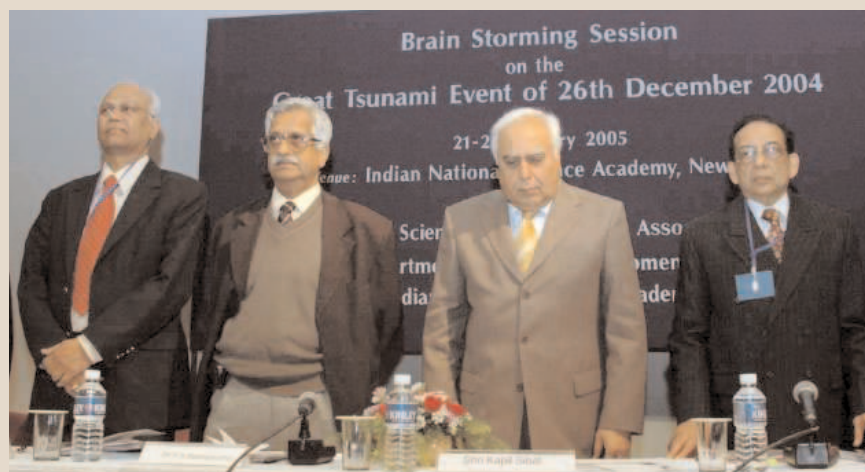
The meeting offered scientists from around the world a chance to mull over preliminary data collected since the tragedy and begin planning to mitigate the impact of future events. Indian officials said the tsunami center likely will be housed at the Indian National Centre for Ocean Information Services (INCOIS) in Hyderabad and that it will monitor other marine hazards, including cyclones. “India is the natural choice for establishing a regional early-warning center,” says Costas Synolakis, a tsunami specialist at the University of Southern California in Los Angeles and a participant at the meeting, noting that the “[scientific] backbone already exists in India.”

The Indian network would for the first time include a dozen Deep-Ocean Assessment and Reporting of Tsunamis (DART) data buoys in the Bay of Bengal, the Arabian Sea, and the southern Indian Ocean. India also plans to quadruple its current lineup of 12 online tide gauges and triple the 51 seismic stations it now operates. Officials also pledged to analyze initial earthquake reports in 10 minutes, down from 30 minutes, and improve modeling of tsunamis and their impact on land. Sibal pledged to have the key elements of the network in place in about a year.

The world’s most reliable and open seismology network is the Global Seismographic Network maintained by the Incorporated Research Institutions for Seismology (IRIS), a Washington, D.C.-based consortium. But India is not part of this network of more than 100 stations, because it never signed the CTBT. “There is a deep suspicion among the global community whether India will share online seismic data since it has never done so in the past,” says Synolakis.

Last month’s tsunami has triggered a review of that policy, however. Valangiman Subramanian Ramamurthy, secretary of the Department of Science and Technology, told *Science* that “our existing policy of not sharing online seismic data has to change” so that scientists can do a better job of understanding tsunamis. India is reassessing its relationship with IRIS, he said, hinting that one change could be a willingness to share data, in real time, on earthquakes of magnitude 5 and higher. That threshold, observers note, would be well above the level generated by any test of India’s nuclear arsenal.

—PALLAVA BAGLA



In their memory. Top Indian scientists join science minister Kapil Sibal, with head bowed, during a moment of silence for the tsunami victims.



Positive ID. Forensics experts are collaborating in Thailand.

DNA Helps Identify Missing in the Tsunami Zone

As the tsunami flood recedes, one of the recovery workers' most sensitive tasks is to put names to anonymous bodies and tell relatives when a loved one has been identified. Methods of DNA testing used in the Balkan war zone are proving their value in this work.

Before the massive effort to identify victims in the Balkans, scientists examining skeletal remains often relied on mitochondrial DNA, which degrades less rapidly than

nuclear DNA but can only identify a person's maternal lineage. Experts had assumed that nuclear DNA, which can provide a more precise match, "was not present in sufficient quantities to warrant such testing," says Ed Huffine, vice president of the Bode Technology Group Inc. in Springfield, Virginia, and a DNA program manager for the group that's helping coordinate a multinational forensics effort. But in Bosnia, "the success rate using nuclear DNA was greater than 90%," says Huffine, who helped establish the International Commission on Missing Persons identification program in the former Yugoslavia.

Many countries are taking part in the DNA studies, which help support a massive data consolidation effort in Thailand. China, for example, has offered DNA testing at no cost for all countries affected by the tsunami, according to Cai Daqing, spokesperson for the Beijing Genomics Institute. Huffine traveled to Beijing earlier this month with 100 teeth and bone samples to be tested at the institute.

Among those contributing from a distance are Sweden, which has listed about 900 people as missing, and Finland, with about 170. To help identify remains, police in Sweden are collecting DNA on mouth swabs from relatives of the missing, says Gunilla Holmlund, associate director of the department of forensic genetics at the Swedish National Board of Forensic Medicine. This is more reliable than taking DNA from toothbrushes and drinking glasses used by the missing, according to Holmlund: "There are so many errors in that."

Sweden also has temporarily suspended a ban on the use of newborn blood samples in its biobanks to identify people. Having DNA from this source "is a very great help when whole families have gone missing," Holmlund says. Finland is collecting DNA from relatives as well as from toothbrushes and other personal items of the missing.

Alec Jeffreys, a pioneer of DNA fingerprinting at the University of Leicester, U.K., says that to reduce the risk of errors, each DNA sample should be analyzed for at least 15 genetic loci. The Beijing Genomics Institute, according to Huffine, is using 16 loci, which is well within what Jeffreys calls "the safe limit." Some nations may be using fewer, which could make it harder to make a match.

In many cases, "DNA won't stand alone," Huffine says. What's required is "a composite of evidence," including medical and dental records. Every scrap of information will be put to use.

—SUSAN LADIKA

Susan Ladika is a science writer in Tampa, Florida.



Sensitive work. Without DNA testing, sorting out identities can be chancy.

2002. "In a war situation, children get angry, they can vent their feelings," says Gopal, whereas after the tsunami, "they feel powerless." Much of the northeast still bears the scars of war. For example, the countryside

around Jaffna, tightly controlled by the Sri Lankan military, is littered with bullet-scarred, burned-out shells of houses. In this region the damage from the war—to lives and property—far outstrips that of the tsunami.

In these Tamil communities, medical facilities that had deteriorated badly over the course of the civil war had been on the mend since the cease-fire. The country hadn't reported a case of cholera for 2 years running.

WHO's aim is to ensure that the aid pouring into Sri Lanka is used not only to rebuild the country's public health infrastructure but also to make it stronger. "It's a tremendous opportunity," Pole says. Kan Tun predicts it will take at least a year to restore "basic functionality" to Sri Lanka's health care system. Heightened vigilance for outbreaks can have unexpected benefits. After a cyclone devastated Orissa, India, in 1999, WHO and the local government launched a surveillance system that 3 years later gave early warning of an outbreak of leptospirosis, a rodent-borne disease new to the region.

In the meantime, Sri Lankan survivors are struggling to put their lives back together. In Kalmunai, on the morning of 22 January, a Saturday, construction crews were erecting the steel skeletons of a pair of dormitory-style buildings with concrete floors that will temporarily house 80 displaced families.

Down the road, Fazal pulls up next to a pale green mosque and points to a long mound of freshly turned earth. The bodies of several hundred victims from a largely Muslim neighborhood were washed and clothed inside the mosque before being buried in the mass grave. Fazal, a Muslim, said the burial prayer for his father here.

At Kalmunai's beach, the scale of the tragedy hits home. A new post office, freshly painted in white, is one of the few buildings with any standing walls. There's little else but flattened palm trees, scattered bricks, and twisted metal in the sand. A few women in saris and a raggedly dressed man wander through the rubble.

Less than 100 meters inland, shops are open for business. Green and yellow streamers hang from lines strung above the road to mark Id-ul-Adha, the Hajj festival day, which took place on 21 January. People were in no mood for a celebration this year. Nevertheless, says Fazal, "we're recovering a sense of normalcy." How long the recovery takes depends largely upon whether a second, preventable disaster—a major disease outbreak—visits itself upon the island.

—RICHARD STONE

With reporting by Pallava Bagla.

Dover Teachers Want No Part of Intelligent-Design Statement

A Pennsylvania school board has added “intelligent design” to its curriculum while simultaneously barring discussion of the origin of life

DOVER, PENNSYLVANIA—Jennifer Miller always wanted to be a teacher. And after “loving molecular biology” during a high school class, she decided to teach the subject at that level. For 12 years she’s shared her passion with students at Dover High School, part of the 3600-student Dover area school district here in southeastern Pennsylvania. But last week she did the unthinkable: She walked out on her three ninth-grade biology classes.

Miller wasn’t abandoning her students. Rather, she was standing up for her professional principles. The local school board had ordered her and seven colleagues to read to their biology classes a statement that attacks the theory of evolution and promotes intelligent design—the idea that the complexity of life requires action by an intelligent agent—as an alternative explanation for the origin of life. The statement also bars scientific discussion in the classroom of the origin of life, consigning that topic “to individual students and their families.”

The board’s statement (www.dover.k12.pa.us/doversd/site/default.asp) officially puts intelligent design into a U.S. public school curriculum for the first time. And that step has united the science faculty at Dover High School. “Intelligent design is not science. It is not biology. It is not an accepted scientific theory,” the teachers wrote in a 6 January letter to Dover School Superintendent Richard Nilsen, requesting that they be excused from delivering the missive. Reading the four-paragraph statement, they argued, would force them to “knowingly and intentionally misrepresent subject matter or curriculum.”

Nilsen acquiesced. So last week he and Assistant Superintendent Michael Baksa visited all nine ninth-grade biology classes to read the statement—without taking any questions afterward. Their arrival was the signal for Miller and a few of her students to leave.

Opposition to the teaching of evolution has roiled U.S. public schools for more than a century. But after the Supreme Court ruled in 1987 that teaching creationism constitutes an illegal dose of religion in the classroom, opponents began looking for a scientific anchor for their beliefs. Dover represents the latest wrinkle: The attempt to denigrate Darwin’s insight—and the overwhelming evi-

dence for it—posits it as simply one in an array of equally valid hypotheses about how life evolved on the planet. Last week a Georgia school district appealed a federal judge’s



By design. Ninth graders at Dover High School heard Superintendent Richard Nilsen (*above*) read a statement on intelligent design in their biology classes.

ruling banning textbook stickers labeling evolution as “a theory rather than a fact.” The judge said the stickers reflected the school board’s affinity for “religiously motivated individuals” (*Science*, 21 January, p. 334). And on 14 December, a group of Dover-area parents asked a U.S. District Court to declare the school board’s statement unconstitutional. A trial is scheduled for September.

In the meantime, the issue hangs over the staff at Dover High like a cloud. “It’s gotten to the point where I don’t even want to go shopping because I might be accosted,” says Bertha Spahr, a chemistry teacher who came to the school in 1965 and who chairs the science department. Miller and Robert Eshbach, a third-year environmental sciences teacher, have become media mini-

celebrities, appearing on ABC’s *World News Tonight* and the BBC as well as in the pages of *The New York Times*. “We could do three or four [interviews] a day, if we wanted,” says Miller.

The Dover controversy began more than a year ago, when the district’s current high school biology textbook came up for a routine, 7-year review by the school board. School board members quizzed the teachers and later publicly expressed their displeasure with the way the textbook handled evolution. Although the board eventually adopted the latest edition, it also accepted an anonymous donation to the school library of 50-plus copies of the 1987 book *Of Pandas and People*, which makes the case for intelligent design. On 19 November the board approved the statement that triggered the suit and led to Miller’s walkout.

Ironically, evolution occupies only a tiny part of ninth-grade biology at Dover High. Miller and the other two introductory biology teachers will spend at most three 90-minute classes on the topic—the last unit of the year before final exams—even though state curriculum guides say the unit should run for 19 days. “I’ll teach competition,” says Miller. “We’ll talk about how more things are produced than survive. I’ll teach the evidence for Darwin’s theory [on the origin of species] and talk about his trip to the Galápagos. I’ll cover natural and artificial selection. And we’ll do reproductive evolution.” But that’s it. “We don’t mention evolution anywhere else in the course.” Miller says she prefers to concentrate on the present, “and how things that are here are still evolving.”

Contrary to the claims of intelligent-design advocates, the board’s directive will narrow rather than broaden the scope of the course. “In the past, we could talk about the origins of life,” says Miller. “At least I could ask them what they might have heard [as criticism of Darwin], and we could discuss it. But now the school board has ruled that out.”

As they begin the new semester, Dover teachers are hoping for at least a respite from the hoopla. The May primary features seven (of nine) school board seats, but they won’t be filled until the general election in November. That means the controversy is likely to reignite in early June, when the next batch of students begins their brief study of evolution.

—JEFFREY MERVIS

Grasp the Proteome™

Protein:Protein Interaction

Discover

Confirm

Characterize

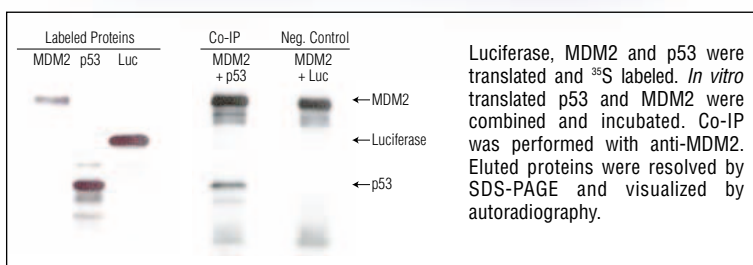
Perfect Co-IPs are within reach

Pierce Introduces ProFound™ Co-Immunoprecipitation Kits

- Couple any antibody with the universal kit or use the pre-conjugated anti-HA or c-Myc kits
- Spin columns provide higher recovery of target proteins and more consistent, reproducible results
- Kit supplied complete with resin controls



- No antibody contamination of Co-IP results because antibodies are covalently attached
- Reusable (up to 10 times) immobilized support
- Can be easily scaled up or down (10-200 µl)



Product #	Description	Product #	Description
23600	ProFound™ Co-Immunoprecipitation Kit	23615	ProFound™ Mammalian HA-Tag IP/Co-IP Kit
23605	ProFound™ Mammalian Co-Immunoprecipitation Kit	23620	ProFound™ c-Myc-Tag IP/Co-IP Kit
23610	ProFound™ HA-Tag IP/Co-IP Kit	23625	ProFound™ Mammalian c-Myc Tag IP/Co-IP Kit



FREE! Protein:Protein Interaction Guide
Request a FREE copy from Pierce, your Perbio Science branch office or distributor.

www.piercenet.com

PIERCE

Tel: 815-968-0747 or 800-874-3723 • Fax: 815-968-7316 • Customer Assistance E-mail: CS@piercenet.com

Outside the United States, visit our web site or call 815-968-0747 to locate your local Perbio Science branch office (below) or distributor

Belgium & Dist.:
Tel +32 (0)53 83 44 04
euromarketing@perbio.com

China:
Tel (8610)8048 9552
support@perbio.com.cn

France:
Tel 0800 50 82 15
euromarketing@perbio.com

Germany:
Tel 0228 9125650
de.info@perbio.com

Hong Kong:
Tel 852 2753 0686
SalesHK@perbio.com

The Netherlands:
Tel 076 50 31 880
euromarketing@perbio.com

United Kingdom:
Tel 0800 252185
uk.info@perbio.com

Switzerland:
Tel 0800 56 31 40
euromarketing@perbio.com

© Pierce Biotechnology, Inc., 2005. ProFound™ is a trademark of Pierce Biotechnology, Inc. Pierce products are supplied for laboratory or manufacturing applications only.

PERBIO



Debate Continues Over Safety of Water Spiked With Rocket Fuel

An expert panel recommends that EPA take a new approach in weighing dangers of perchlorate, but industry says precaution is trumping science

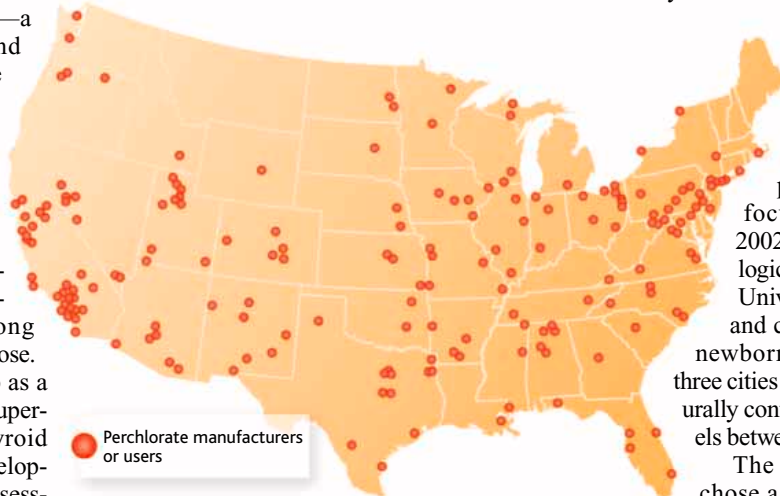
With billions of dollars in cleanup costs at stake and an intense battle being waged over the underlying science, the regulation of perchlorate is one of the hottest environmental issues around. So it is perhaps no surprise that a long-awaited report by the National Academy of Sciences (NAS) on the health risks of the chemical—a constituent of rocket fuel and explosives—hasn't calmed the debate. The report,* released 10 January, largely supports the bottom line of stringent draft regulations in progress at the Environmental Protection Agency (EPA) and state agencies. Industry scientists, however, say the report is overly conservative and takes the wrong approach in calculating a safe dose.

Perchlorate first turned up as a contaminant in 1985 at some Superfund sites. Worried about thyroid effects and damage to the developing brain, EPA drafted a risk assessment in 2002 that suggested drinking water should contain no more than 1 part per billion (ppb). But the Department of Defense and contractors argued that perchlorate is safe at concentrations up to 220 ppb. In 2003, the two sides agreed to have NAS assess the evidence and EPA's approach (*Science*, 21 March 2003, p. 1829).

Perchlorate inhibits the thyroid's uptake of iodine, which can decrease production of two thyroid hormones. These hormones help regulate metabolism and are important for healthy brain development in fetuses and infants. While EPA was working on its first risk assessment, peer reviewers pointed out that crucial data were lacking, especially about effects on the developing brain. To address this, an industry-backed consortium, called the Perchlorate Study Group, funded a range of research.

In its 2002 draft risk assessment, EPA put much weight on studies, conducted by industry-contracted scientists, of pregnant rats that had been fed doses of perchlorate. The agency took the lowest daily dose at which worrisome effects (such as changes in hormone levels and

brain shape) were noticed in the brains of the fetuses. Then they multiplied that dose by a safety factor of 300 to account for uncertainties, such as differences in metabolism between rats and humans. But industry groups and outside peer review panels that EPA consulted criticized the rat studies as unreliable.



On the map. Perchlorate is made and used all over the United States.

Enter NAS. In March 2003, it agreed to review all the published studies and evaluate EPA's approach. The committee, chaired by Richard Johnston of the University of Colorado School of Medicine in Denver, put more weight on recent human studies than the rat studies and existing epidemiological data, both of which it viewed as inconclusive. In particular, the committee relied on a 2002 study by Monte Greer of the Oregon Health and Science University in Portland and colleagues.

Greer's team fed 37 healthy adults various doses of perchlorate and monitored them for 14 days. The NAS panel took the highest daily dose at which iodide uptake by the thyroid was not inhibited and applied a 10-fold uncertainty factor to account for more sensitive individuals, particularly pregnant women with underactive thyroids or iodide deficiency.

The resulting "reference dose"—the starting point for calculating safe levels in drinking water—of 0.0007 mg/kg is broadly consistent with the dose in EPA's draft risk assessment (0.00003 mg/kg), says William

Farland, EPA's acting deputy assistant administrator for science. "It's in the ballpark." And the NAS dose is only twice that recommended by California regulators—quite a good match for the imperfect science of risk assessment, says George Alexeeff, deputy director for scientific affairs at California's Office of Environmental Health Hazard Assessment, whose group also relied on the Greer study. "As far as we're concerned, [they're] essentially identical."

Industry scientists, however, argue that EPA and the states—and now NAS—are too conservative in their calculations. "The numbers are excessively safe, unnecessarily low," says Dan Guth, a toxicologist with Boeing.

A recent study by TERA, a nonprofit risk assessment group in Cincinnati, Ohio, that consults for industry, which yielded a slightly higher reference dose of 0.002 mg/kg per day. This 2004 paper focused on two studies: Greer's 2002 research and a 2000 epidemiological study by Casey Crump of the University of Washington, Seattle, and colleagues that looked at 9784 newborn infants and 162 children in three cities in Chile, where perchlorate naturally contaminates drinking water at levels between 4 ppb and 120 ppb.

The key difference is that TERA chose a different "critical effect," or warning sign, of impending harm: the dose at which perchlorate changed levels of the thyroid hormone T4. Michael Dourson of TERA, an author, says changes in thyroid hormones are the most appropriate indicator of possible dampening of thyroid activity. The academy panel, on the other hand, picked iodide inhibition—an earlier effect—as the critical indicator, concluding that is "the most health-protective and scientifically valid approach."

EPA will now have to decide whether to follow NAS's advice on how to generate a reference dose. And that's just one step of the process; to get the concentration that's safe in drinking water, the reference dose must be adjusted for exposure. That requires regulators to decide which groups are most sensitive—fetuses or infants, for example—and make assumptions about how much perchlorate in the diet comes from water versus other sources. Given these factors, NAS's reference dose, for example, could yield a drinking water standard from 2.5 to 24.5 ppb. The low end of the range would necessitate a long and expensive cleanup: 35 states have more than 4 ppb of perchlorate in drinking water.

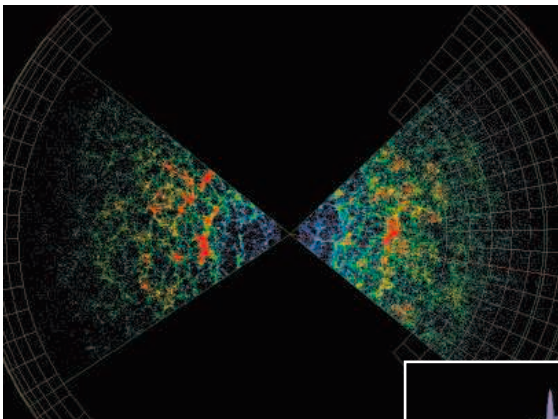
—ERIK STOKSTAD

* *Health Implications of Perchlorate Ingestion*, National Research Council of the National Academies, January 2005.

Galaxy Patterns Preserve an Imprint of the Big Bang

Graceful filigrees of galaxies stretch through today's universe like cobwebs in a long-abandoned room. Astronomers have now determined that these large-scale structures are not random. Rather, they preserve a faint echo of sound waves that reverberated through space for about 350,000 years after the big bang.

The discovery, reported jointly at the meeting by two international teams, confirmed a prediction made more than 30 years ago. However, the



Echo location. Galaxies (above) trace ripples from the big bang (inset).

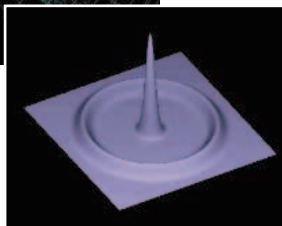
signature is so subtle that some astronomers doubted they would ever see it. Surveys of hundreds of thousands of galaxies finally revealed the imprints, in the form of enormous “ripples” where galaxies preferentially tend to congregate. “This is a very valuable confirmation of the theory of how we came to be,” says astronomer Richard Ellis of the California Institute of Technology in Pasadena.

The pattern of ripples was set in the first incandescent moments of the universe. As the baby cosmos expanded, matter and energy seethed within a dense broth. Tiny fluctuations—probably due to quantum effects—caused some regions to have more matter than others. When gravity tried to compress these denser regions, the hot particles already were so close together that they resisted being squeezed. Instead, they rebounded and then oscillated under gravity's influence. The oscillations set off sound waves, like the resonance of a ringing bell.

Today, the stretched-out remnants of these waves still pervade the universe as barely perceptible hot and cold patches in the faint glow called the cosmic microwave background (*Science*, 19 December 2003, p. 2038). In 1970, astrophysicists P. J. E. Peebles and Jer Yu of

Princeton University predicted that matter in the universe would tend to clump at the peaks of the most dominant patches, just as water tends to pile up in ripples spreading on a pond.

Unveiling the patterns required painstaking analysis of galaxies charted by two sweeping surveys: the 2-degree Field (2dF) Galaxy Redshift Survey, run by the United Kingdom and Australia, and the U.S.-led Sloan Digital Sky Survey (SDSS). Astronomers examined the spatial positions of 221,000 galaxies and 46,000 galaxies, respectively, from the two programs. Although the techniques differed, both teams found a slight excess of galaxies with separations of about 500 million light-years. That pattern—not visible to the eye—matches the expected distances from the centers to the edges of acoustic ripples that grew as space expanded, says SDSS astronomer Daniel Eisenstein of the University of Arizona, Tucson.



Astronomers now wish to use this characteristic separation between galaxies as a way to gauge accurate distances to much more remote galaxies, when the universe was younger. “It’s like a standard ruler,” says 2dF astronomer Shaun Cole of the University of Durham, U.K. “You can use it to do trigonometry and measure the geometry of the universe through time.” That’s a nifty tool, agrees astronomer Martin Rees of Cambridge University, U.K., but he’s delighted simply to confirm that galaxies behave as gravity predicts they should. “The concordant picture we have of the universe is hanging together extremely well,” he says.

Satellite Swiftly Catches New Bursts

A new satellite dedicated to spotting the most powerful cosmic explosions turned on with a bang in December. The satellite, called Swift, caught an “amazing” nine gamma ray bursts in its first 12 days of operation, reported astronomer Neil Gehrels of NASA’s Goddard Space Flight Center in Greenbelt, Maryland.

SAN DIEGO, CALIFORNIA—Nearly 2500 astronomers skirted floods and a washed-out bridge to attend the largest-ever meeting of the American Astronomical Society, 9 to 13 January.

Swift and other satellites also witnessed a whopping x-ray flare in our galaxy, an event that has scientists buzzing.

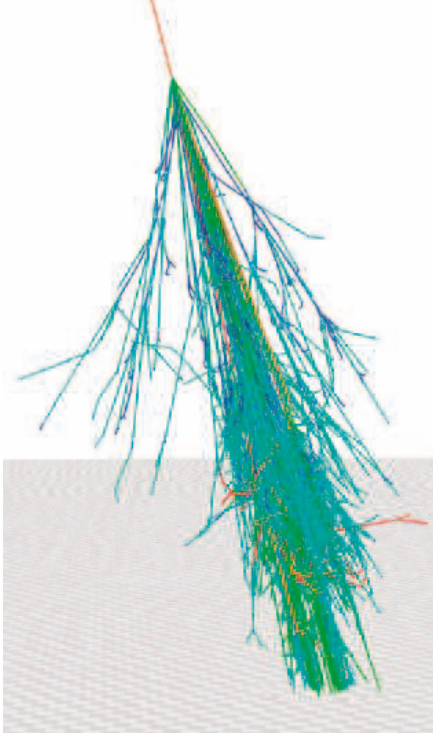
NASA launched Swift on 20 November to probe mysteries about the origins of gamma ray bursts (*Science*, 8 October 2004, p. 214). Bursts lasting longer than a few seconds probably erupt when the cores of massive stars collapse into black holes. But to confirm that scenario and find out what drives the explosions, astronomers must study bursts while their initial fires still rage. Swift swivels quickly to examine new bursts and sends the coordinates to telescopes on the ground, including fast-responding robots.

That automated sequence wasn’t yet switched on when Swift and the European Space Agency’s INTEGRAL satellite both spied a bright burst on 19 December. But even on shorter notice, two robotic telescopes on the ground had time to catch a burst in the act for just the second time: The explosion lasted 9 minutes, one of the longest ever seen. The data—in both optical and infrared light—may penetrate more deeply into a burst’s fireball than ever before. Research teams have papers in press and won’t yet discuss their findings.

As a holiday bonus 8 days later, a bizarre object about 50,000 light-years away uncorked an extraordinary blast of x-rays that pierced the sides of several satellites—including INTEGRAL and Swift—and tripped their detectors. Most telescopes could not examine the flare’s aftermath, because it was close to the sun. But astrophysicists suspect it came from a “magnetar,” a slowly spinning neutron star encased by the most intense magnetic fields known (*Science*, 23 April 2004, p. 534).

Two other magnetars have erupted with giant flares in the past 25 years, but the new flare was at least 100 times stronger. Indeed, the x-rays were so potent that a satellite called Konus-Wind saw them reflect off the moon. “This is a unique event, the mother of all giant flares,” says astrophysicist Chryssa Kouveliotou of NASA’s Marshall Space Flight Center in Huntsville, Alabama. She and other researchers are furiously completing their first analyses, which could reveal how an ultrastrong magnetic field crushes and fractures a neutron star.

Not all news from Swift is so glowing. The power supply for a cooling unit on one of the satellite’s telescopes died shortly after launch, says astronomer David Burrows of Pennsylvania State University, University Park. As a result, the electronic detectors are 25°C to 50°C



Shower of power. Highest-energy cosmic rays spark blasts of particles in the atmosphere.

warmer than anticipated. The balminess could make the x-ray telescope less sensitive to faint bursts, but Burrows and his colleagues are orienting Swift to avoid the worst heat exposure from Earth. “This makes our operations more complicated, but we think there will not be much impact on the science,” Burrows says.

An Origin for the Fiercest Cosmic Rays?

Imagine catching a golf ball driven by Vijay Singh. The most outrageous particle accelerators in space pack that much energy into single protons. These rare “ultra high-energy cosmic rays” (UHECRs) bombard Earth from all directions, so physicists can only speculate about their birthplaces. But at the meeting, theorist Glennys Farrar of New York University (NYU) made a disputed claim: identification of the first bona fide cluster of UHECRs, spat out from colliding groups of galaxies.

Farrar’s evidence comes from five UHECRs seen since 1993 within a patch of the sky several times larger than the full moon. Two networks of detectors in Japan and Utah recorded the events. Each array measures sprays of millions of particles created when UHECRs slam into the air overhead (*Science*, 21 June 2002, p. 2134).

Physicists recently recognized that four UHECRs out of a sample of about 100 formed a hot spot near the Big Dipper. In a paper accepted for publication in the *Astrophysical Journal*, 62 scientists agreed that the grouping had about a 0.5% chance of arising randomly. “That’s not significant enough to

qualify as a point source,” says physicist Pierre Sokolsky of the University of Utah in Salt Lake City, although co-author Farrar argued that the chance probability of finding such a tight cluster of four events actually is less than 0.1%.

Now, Farrar proposes two new factors. First, she found a fifth UHECR within the same hot spot by considering about 200 more cosmic rays with slightly lower energies. Second, she worked with NYU colleagues David Hogg and Andreas Berlind to examine deep-sky images of that spot from the Sloan Digital Sky Survey. They found two rich groups of about 50 galaxies crashing together, at a distance of about 600 million light-years from Earth. Virtually no other galaxies lie between the groups and us. That means the charged particles would zip to Earth along fairly straight paths instead of “smearing out,” Farrar says, because magnetic fields in the voids between galaxies are low.

It adds up to a stream of UHECRs blasting from the merging galaxies, Farrar concludes. “I’m not prepared to identify a [physical] source, but we have candidates,” she says. They include shock waves rifling through the

groups, active galactic cores powered by black holes, or even long-ago gamma ray bursts. Crucially, Farrar’s claim would rule out an entire class of models for UHECRs: the decay of exotic, ultraheavy particles left over from the big bang. Such decays, she says, would not come from a single hot spot.

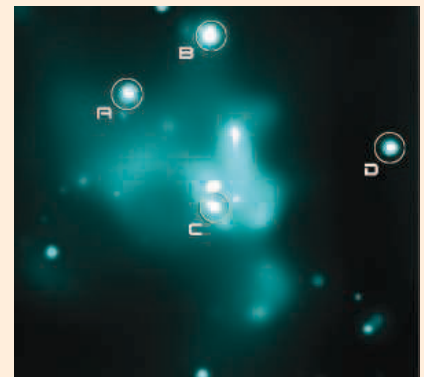
Farrar’s analysis has sparked fierce debate. “My colleagues and I simply don’t understand how she gets these small probabilities,” says Sokolsky. Adding the fifth event from a different data set introduces a risky bias, he notes. Others agree: “You can only do so much with limited data,” says Nobel laureate James Cronin of the University of Chicago.

Still, the merging galaxy groups are tantalizing, says astrophysicist Tsvi Piran of Hebrew University in Jerusalem. “This is corroborative evidence that the [UHECR] association may be real,” Piran says. All agree that a gigantic cosmic-ray observatory under construction in Argentina, called Auger, may pioneer the new science of UHECR astronomy by spotting thousands of events in the vast sky.

—ROBERT IRION

Snapshots From the Meeting

A hive of black holes. The supermassive black hole at the center of the Milky Way has attracted a throng of dark companions. NASA’s Chandra X-ray Observatory has detected flickering outbursts of x-rays from four objects (circled at right) orbiting within a few light-years of the galaxy’s core, reported Michael Muno of the University of California, Los Angeles. The likely sources are gulps of gas spiraling into small black holes, each a few times as massive as our sun, Muno and colleagues believe. Extrapolation suggests that about 10,000 black holes—most of them alone and invisible—have “migrated” toward the Milky Way’s heart by means of gravitational interactions with less-massive stars.



Dark swarm. X-ray flares (circled) point to small black holes near the Milky Way’s core.

Mega Vega disk. A famous disk of dusty debris around the bright star Vega extends much deeper into space than expected. New infrared images from NASA’s Spitzer Space Telescope reveal tiny dust particles orbiting Vega at a distance about 20 times greater than Pluto’s average distance from our sun, reported Kate Su of the University of Arizona, Tucson. Vega’s intense radiation blows away such dust grains within 1000 years, Su notes. A collision of Pluto-size objects within the past million years would have created enough fragments to grind into one another and feed the shroud, she says.

Pulsars aplenty. A knot of stars called Terzan 5 is home to our galaxy’s densest nest of pulsars, according to Scott Ransom of the National Radio Astronomy Observatory in Charlottesville, Virginia. Ransom’s team used the 100-meter Green Bank Telescope to find 21 neutron stars that spin dozens to hundreds of times each second, called “millisecond” pulsars. The startling haul of precisely calibrated radio beacons—also reported online by *Science* on 13 January (www.sciencemag.org/cgi/content/abstract/1108632)—will help astronomers create a three-dimensional map of the mass hidden deep inside the tightly packed Terzan 5 cluster, including a possible medium-size black hole.

—R.I.

Fluent in any language.

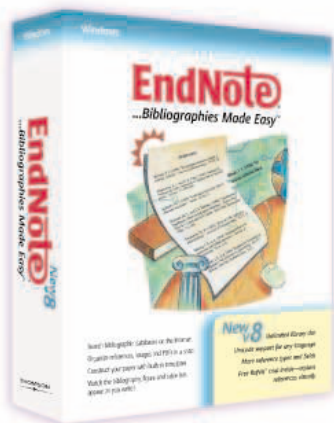
Introducing EndNote 8

EndNote is the industry standard for creating, managing, and publishing bibliographies. And with EndNote 8, your options have increased dramatically.

- *Unicode support for any language*
- *Unlimited library size*
- *New reference types and fields*
- *Enhanced support for electronic sources*
- *Perfectly formatted bibliographies for more than 1,100 publication styles*

See why millions of researchers, students, librarians, professors and writers worldwide use EndNote to search online databases, organize references, images and PDF files, and create bibliographies instantly. It's easy to use, easy to learn, saves you from retyping references, and now provides unlimited capacity. There simply is no better way to manage bibliographies.

Download your Free demo or buy online today at www.endnote.com.



"I've used EndNote since version 1, and find it to be an indispensable component of my academic toolbox. EndNote makes it easier for me to do my job well. I would not want to be without it."
—Barry J. Fishman,
School of Education,
The University of Michigan



THOMSON
TM

Sales: 800-722-1227 • 760-438-5526 • Fax: 760-438-5573
info@isiresearchsoft.com • www.endnote.com

© Copyright 2004 Thomson. EndNote is a registered trademark of Thomson.
All trademarks are the property of their respective companies.

Edited by Constance Holden

Battle of the Titans

We hate to brag OK, no, we don't. This month, the Institute for Scientific Information (ISI) in Philadelphia, Pennsylvania, reports that *Science* and *Nature* sweep the rankings of the "hottest journals of the millennium (so far)." Among "high-impact" journals, *Science* sits at the top of six categories of highly cited papers from January 1999 to August 2004, and *Nature* claimed the top spot in the other five, according to ISI's citation analysis (ScienceWatch, January/February 2005).

Several categories were almost too close to call. In molecular biology and genetics, for example, *Science* averaged 78 cites per paper from 773 published papers and *Nature* 77 for 931 papers. The two are neck and neck on cites per paper in physics, space science, neuroscience, chemistry, and immunology. Also ranking high in every field but space science is the *Proceedings of the National Academy of Sciences*.

The Mind of the Terrorist

The U.S. government has awarded \$12 million to the University of Maryland, College Park, to set up a center for behavioral and social research on terrorism—what its director Gary LaFree calls "the social science equivalent of the Manhattan Project."

The center is the fourth in a network of "centers of excellence" devoted to various aspects of terrorism funded by



Looking Into King Tut

Sounds like an episode of *CSI: Ancient Egypt*—forensic detectives want to reopen the case of King Tut's death. A 1968 x-ray of Egypt's most famous mummy, King Tutankhamen, revealed a bone chip protruding into his

skull. To some researchers, that suggested the boy-king may have been fatally struck in the head when he died in his late teens, some 3000 years ago. But the damage may have also been the result of a fall or an accident at the time of mummification.

Now 3D images from a computed tomography (CT) scan are expected to clear up the mystery. This month Egyptian archaeologists led by Zahi Hawass, secretary general of Egypt's Supreme Council of Antiquities, put a wooden box containing King Tut's remains into a portable CT scanner capable of resolving details as small as 0.5 mm. Results from the analysis of 1700 pictures are due soon.

the Department of Homeland Security. LaFree, a criminologist, says this one will study how terrorist groups form and recruit, what motivates them, and how they pick their targets. It will pull together teams from around the country to investigate areas that have received little attention in the past. "We need more than studies of the small number who become terrorists" and must explore the "pyramid" of which they are the tip, says LaFree.

Jerrold Post, head of the political psychology program at George Washington University in Washington, D.C., says the center faces a "very important challenge." He says many people fail to realize that "most terrorists are perfectly psychologically normal." Brian Jenkins, an expert on terrorists at Rand Corp. in Santa Monica, California, adds that "9/11 caused us to modify our conceptions about suicide [terrorists]."

Although lone bombers tend to be youthful non-entities who are closely managed by their handlers, he says, the September 11 killers were well-educated adults who demonstrated that they could be "left on their own for a long time isolated from a formal support structure" to carry out a multiteam mission.



Terrorists in training?

A Call to Verse

*Yet once more, O ye laurels, and once more
Ye myrtles brown, with ivy never sere,
I come to pluck your berries harsh and crude
And with forced fingers rude*
Attempt to celebrate Einstein's wonderful year.
A telescope prize and competition here†
Compels a poem—in February due.
It need not be great; it need not even rhyme.
Limerick, haiku, sestina—all that's clear
Is that if you are a poet, you
Should compose an ode about energy, space, or time
To mark the centenary of Albert's year.
Who knows? Perhaps you'll be laurel-girt,
Or perhaps you'll get a big Bronx cheer.‡*

* Educated readers will of course recognize the first four lines from Milton's *Lycidas*.

† By the British Association for the Advancement of Science, at www.the-ba.net/universe. Competitors are divided into five age groups, including adults.

‡ Poem by Charles Seife.

I have real work to do.

Getting published.

Writing my grant.

Putting together my presentation.

Discovering something meaningful.

I need time to do it.

But here I am, genotyping mice tails.

Not exactly what I had in mind when

I went into research.

With Transnetyx™, all of your genotype testing is done for you. All you have to do is clip and ship the tails, then click for your results. Testing is automated, with error-free results available in either 24 or 72 hours. It's accurate, economical, and fast. Most importantly, it frees up your time for research or anything else you'd rather be doing.

WWW.TRANSNETYX.COM

1-888-321-2113

TRANSGENIC TESTING REDEFINED

T r a n s n e t y x™

Serving Research. Saving Time.

Edited by Yudhijit Bhattacharjee

TWO CULTURES

Moving target. Can the science of visual perception help win pro basketball games? Maybe, say the Dallas Mavericks, but it's not worth the trouble.

In three of the team's games this season, employees of the NBA team attempted to coordinate crowd behavior to distract the other team's players when they shot free throws. Acting on cue, supporters in the stands waved balloons in sync rather than randomly, creating the appearance of a moving background. Contrasted with the harmless blur produced by random waving—in which the movements of individual balloons cancel one another out—this effect was expected to make the shot more difficult.

The project was a success, says Daniel Engber, a neuroscientist-turned-writer who suggested the idea to Mavericks' owner Mark Cuban (inset) and later wrote about it in the online magazine *Slate* (slate.msn.com/id/2111939). Overall, Engber claims, Mavericks' opponents were 8% less accurate at the line during the three games—all victories—than the league average.

Despite that success, Cuban decided not to stick with the strategy. "It's impossible to control 500 people sitting behind the basket," he told *Science* in an e-mail.



AWARDS

Wolf Prizes. A researcher who studies matter at its coldest has won one of the hottest prizes in physics. Daniel Kleppner, a physicist at the Massachusetts Institute of Technology in Cambridge, will receive the \$100,000 Wolf Prize for his work on the hydrogen maser,

Got any tips for this page? E-mail people@aaas.org

Rydberg atoms, and the Bose-Einstein condensate.

Gregory A. Margulis of Yale University and Sergei P. Novikov of the University of Maryland, College Park, share \$100,000 as co-winners of the Wolf mathematics prize. The selection panel cites Margulis for his "monumental contributions to algebra" and Novikov for "the introduction of algebraic-geometric methods."

DEATHS

Heart of Africa. Africa got into Bob Carsky's blood early on. Now colleagues and friends of



the agronomist, who died last fall in an air raid during the protracted civil war in Côte d'Ivoire, are trying to make sure his passion lives on. Carsky first came to Africa

with the Peace Corps, teaching science in Benin. Returning after earning a Ph.D. in agriculture from Cornell, he spent most of 15 years at the International Institute of Tropical Agriculture (IITA) in West Africa. "He was willing to tackle tough and intransigent problems such as improving the soil fertility regimes of root crops," says colleague Dyno Keatinge, now with the International Crops Research Institute for the Semi-Arid Tropics in Hyderabad, India. "This was a good man."

Last year, Carsky joined the Africa Rice Center, which was moving back to its scientific headquarters outside Bouaké, in war-torn Côte d'Ivoire. On 6 November, however, Carsky, 49, was killed while taking

shelter in a French school when rebels bombed the city.

Those who knew him are hoping to endow an African exchange program at Cornell, as well as a charitable program in Benin, where Carsky had worked with IITA. "He always gravitated toward helping people," says childhood friend Kevin Hopkins, a surgeon in Corpus Christi, Texas.

THEY SAID IT

"I had hoped that Media Lab Europe would become a virus and spread."

—Computer scientist Nicholas Negroponte, chair of MIT's Media Lab, expressing disappointment over this month's announcement that the 5-year-old Dublin center was running out of money and would be closing. The Media Lab should not have been involved in managing the center, he says. Lab officials say they will not repeat the mistake in future international ventures including an upcoming offshoot in Taiwan.



POLITICS

She's game. Former U.S. Secretary of State Madeleine Albright played the president this month in a simulated global smallpox outbreak arranged by the Center for Biosecurity at the University



of Pittsburgh Medical Center. The exercise, called Atlantic Storm, found that some European nations did not have adequate vaccine supplies to counter a terrorist attack by an Al Qaeda splinter group on Istanbul, Frankfurt, and Rotterdam. During the game, Albright warned that the U.S. public might resist attempts to share the U.S. stockpile with European countries that had opposed the war in Iraq.

CREDITS (TOP TO BOTTOM): BENJAMIN NALE; (INSET) GLEN JAMES/NBA; REBECCA KHELSEAU-CARSKY; WEBB CHAPPELL; KAVEH SARDARI/SARDARI.COM

Brilliant Signals.



New Axio Imager.
Discover New Worlds.

A new generation of microscopes is setting new standards in digital imaging. Through ultimate optimization of components, flawless integration of digital imaging and pioneering developments in optics - Axio Imager from Carl Zeiss.

Carl Zeiss
Microimaging, Inc.

Thornwood, NY
zeiss/axio-imager.com
800.233.2343



We make it visible.

UltraClone™

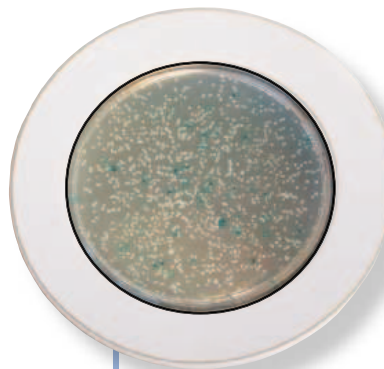
DNA Ligation & Transformation Kits

Not enough on
your plate?

Get 10X more with
UltraClone Kits.



Want a lot more recombinants from every cloning reaction? Lucigen introduces a powerful new product that dramatically increases the number of recombinants using any cloning vector. Get your genes and sequences much faster with less work.



Fill your plate with
UltraClone

UltraClone Kits:

- Incorporate Lucigen's engineered CloneSmart® DNA Ligase and unique ligation components to maximize recombinant yields.
- Just add your target DNA and vector, then transform the included *E. coli*® electrocompetent or chemically competent cells.
- No post-ligation cleanup needed.

To find out more about UltraClone call
Lucigen at 1-888-575-9695 or find us on the
web at: www.lucigen.com.

Lucigen®
The Molecular Cloning Company™

Letters to the Editor

Letters (~300 words) discuss material published in *Science* in the previous 6 months or issues of general interest. They can be submitted through the Web (www.submit2science.org) or by regular mail (1200 New York Ave., NW, Washington, DC 20005, USA). Letters are not acknowledged upon receipt, nor are authors generally consulted before publication. Whether published in full or in part, letters are subject to editing for clarity and space.

Marburger Makes His Position Clear

THE ARTICLE "BREAKDOWN OF THE YEAR: THE unwritten contract" (J. Mervis, "Breakthrough of the Year" Special Issue, 17 Dec. 2004, p. 2015) mischaracterizes my position regarding science colleagues who signed a statement accompanying a Union of Concerned Scientists report critical of the administration. The article implies that I dismissed the statement as "complaints from the Democrats." This quote and its implication directly contradicts the many statements I have made on this issue during the past year, including a previous *Science* article accurately quoting me as having "a great deal of respect" for the researchers who signed the statement but "considerably less for the report."

JOHN H. MARBURGER III

Science Advisor to the President and Director, Office of Science and Technology Policy, Executive Office of the President, Washington, DC 20502, USA.

The Ethics of Deriving Gametes from ES Cells

IN THEIR POLICY FORUM "ETHICAL ASPECTS OF ES cell-derived gametes" (17 Sept. 2004, p. 1719), G. Testa and J. Harris propose that producing gametes from embryonic stem (ES) cells derived by somatic cell nuclear transfer (SCNT) (1, 2) be considered so that same-sex couples could have offspring with genetic contributions from both partners. Their leap of faith about the technical feasibility of this proposal and their rather cavalier attitude about its health risks and social and ethical meanings demand comment.

The authors characterize risks to offspring simply in terms of whether genetic damage or misexpression (3) due to this experimental procedure is comparable to that in natural reproduction. They neglect to note that although organisms can repair DNA damage and compensate for perturbations of development, they only contain such correction mechanisms as were selected in the context of disturbances encountered in the evolutionary history of

their species. Natural selection has never acted on populations in which variants were produced by SCNT. Consequently, no specific mechanisms have evolved to deal with the associated genetic dysregulation. To learn whether general repair mechanisms can correct such damage would require experimentation on developing humans. Risks to children cannot merely be dismissed by comparisons with "other practices" as if this way of procreation was merely one more consumer choice.

Assemblages resulting from combining an ES cell-derived egg or sperm with normally produced sperm or egg via in vitro fertilization (IVF) are entities distanced not only from the physiological reproductive process but from human forebears with any socially prescribed responsibility for them. Already philosophers (4) and representatives of major research institutes (5) are claiming that human embryos produced by

“Assemblages resulting from combining an ES cell-derived egg or sperm with normally produced sperm or egg via in vitro fertilization (IVF) are entities distanced not only from the physiological reproductive process but from human forebears with any socially prescribed responsibility for them.”

—LIPPMAN AND NEWMAN

SCNT are not actually human embryos. In a culture obsessed with biological perfection, we ruefully anticipate a time when "bad" outcomes of SCNT performed with inexhaustible somatic cell nuclei and infinitely available ES cell-derived eggs and sperm are designated as not actually people.

ABBY LIPPMAN¹ AND STUART A. NEWMAN²

¹Department of Epidemiology and Biostatistics, McGill University, Montreal H3A 1A2, Canada.

²Department of Cell Biology and Anatomy, New York Medical College, Valhalla, NY 10595, USA.

References

1. K. Hubner et al., *Science* **300**, 1251 (2003).
2. Y. Toyooka, N. Tsunekawa, R. Akasu, T. Noce, *Proc. Natl. Acad. Sci. U.S.A.* **100**, 11457 (2003).
3. D. Humpherys et al., *Science* **293**, 95 (2001).
4. L. M. Guenin, *Nature Biotechnol.* **21**, 482 (2003).
5. C. Hall, *San Francisco Chronicle*, 11 December, 2002; <http://www.sfgate.com/cgi-bin/article.cgi?file=/c/a/2002/12/11/MN186283.DTL>

Response

LIPPMAN AND NEWMAN FOCUS THEIR CRITICISM on the scenario of same-sex couples parenting offspring to which both partners contribute genetically.

In the mouse, substantial progress still needs to be made to obtain bona fide gametes from ES cells and therefore much effort is required before ES-derived gametes (ESDGs) could ever be applied to human reproduction. However, we disagree that the scenario we describe constitutes a "leap of faith." Although development of science and technology has an intrinsic level of unpredictability, history of biology demonstrates that the availability of an in vitro system is a key factor to accelerate our knowledge and manipulation of biological systems. This was in fact the most salient feature of the three reports of ESDGs: not the derivation itself of so-far dysfunctional gametes, but the establishment of a system that will allow the molecular dissection of gametogenesis (1).

What other criteria should be used for evaluating risks to offspring if not the comparison with natural or currently available assisted reproduction? It is true that natural selection has never acted upon population variants generated through SCNT-derived gametes, but the same could be said for virtually every other medical or technological intervention impacting the human body. Lippman and Newman imply that SCNT would bring about a whole new sort of genetic and epigenetic damage, resistant somehow to the filter of natural repair or compensation mechanisms. The biological foundation of this prediction is unclear and should be documented. Potential defects from ESDG would be either at the genome or at the epigenome level (due to faulty reprogramming), just as for drugs, environmental factors, food, and countless other physical variables that all act, directly or indirectly, upon our genome and epigenome. Indeed, we are all new "populations variants," constantly generated by the interaction of our genomes and epigenomes with the natural and technological world. Possibly the only difference could be the scale of perturbations caused by SCNT, given our lack of understanding and control of the process of genome reprogramming. But needless to say, such issues can only be addressed through further research on scientifically and ethically appropriate models. Finally, in the case of in vitro fertilization (IVF), and especially with intracytoplasmic sperm injection, we are already curtailing natural selection to allow a "defective" genome to contribute to the offspring.

affordably
Now you can [^]monitor
Biomolecular Binding
Reactions in real time.

SR7000 New Surface Plasmon Resonance Instrument:

- High quality, kinetic data
- Affordable: a fraction of other instruments
- Flexible: you design it to do your work
- Easy to set up and use

Uses/Features:

- Response vs. time and reflectivity data
- For kinetics (on, off, equilibrium), relative affinity, sequence recognition, concentration, ligand fishing
- For epitope screening and mapping
- For method development...before running more expensive tests
- Extremely sensitive: Savitzky Golay Smoothed Data rms Noise = 0.45 μ RIU = 0.33 RU = 3.3e-05 deg. (Raw Data rms Noise = 0.97 μ RIU = 0.71 RU = 7.1e-05 deg)
- Excellent baseline stability: Maximum drift 3.1 μ RIU/hour [1 μ RIU = 0.73 RU = 7.3e-05 Deg]
- Given ready chemistry (slide with surface and analyte to test against it), the instrument can be up and producing data within an hour out of the box.
- Uses off-the-shelf HPLC fluidics

Imagine the perfect SPR instrument for you.



Reichert
Analytical Instruments

Reichert, Inc.
3374 Walden Avenue • Depew, NY 14043
Toll Free: 888-849-8955 • Tel: (716) 686-4500
Fax: (716) 686-4545 • Email: info@reichert.com
www.reichertai.com

Xenograft Studies

Immunodeficient Models

Custom
Xenograft
Studies
Nude Mice
and Rats
SCID Mice



Utilizing advanced technical practices, Charles River's Oncology Research Services Group provides customers with unsurpassed quality and timely results.

CHARLES RIVER
LABORATORIES

Accelerating the Search for Healthier Lives™

1-877-CRIVER-1 • www.criver.com/orsg



Where **Laboratory Technologies** Emerge

LabAutomation
2005

January 30 - February 3, 2005

Short Courses: January 30 - 31, 2005
Conference: January 31 - February 3, 2005
Exhibition: January 31 - February 2, 2005

San Jose McEnery Convention Center
San Jose, California

Sign up now for email updates!
Visit labautomation.org for more information, including advance registration. Or, call (866) 263-4928.



ALA is a non-profit association committed to driving progress in laboratory technologies through high-quality education that benefits the global scientific community, including its membership of scientists, academicians, and industry thought leaders.

CAA05

“It is not the enabling technology, but the choice of the word ‘assemblage,’ in its objectifying power, that distances potential humans generated through [ES-derived gametes] from the rest of society. Creatures born through ESDGs would be humans just like anybody else, whether conceived naturally or through [in vitro fertilization].”

—TESTA AND HARRIS

Lippman and Newman question the social implications of ESDGs and refer to the potential offspring of parents who have reproduced via ESDGs as “assemblages... distanced not only from the physiological reproductive process but from human forebears with any socially prescribed responsibility for them.” It is not the enabling technology, but the choice of the word “assemblage,” in its objectifying power, that distances potential humans generated through ESDGs from the rest of society. Creatures born through ESDGs would be humans just like anybody else, whether conceived naturally or through IVF.

It is also unclear why ESDGs children would be “distanced... from human forebears with any socially prescribed responsibility for them.” Isn’t it exactly the opposite, since prospective parents who take the burden and cost of medical intervention to procreate are clearly demonstrating a responsibility and commitment to their offspring that is arguably stronger, for example, than in the case of fortuitous pregnancies? Infertile heterosexual couples and homosexual couples who reproduce, now through gamete donation and surrogacy, and one day possibly through ESDGs, are asserting a responsibility toward entities that they are unlikely to view as “assemblages.” The fact that this responsibility is not “socially prescribed” for homosexual couples (short of any evidence of the inadequacy of such couples to raise children) can only be described as discriminatory.

Finally, SCNT, like any other technology, does not undermine by itself the foundations of the respect we owe to people. Robust ethical reasoning indicates that self-awareness and the capacity to value

one’s own life are the foundations of the intrinsic value of persons (2). The strength of this personhood-based framework of moral status is its independence, at least a priori, from individual or species-specific connotations. So humans conceived naturally, through IVF, or one day through ESDGs are clearly all persons.

GIUSEPPE TESTA¹ AND JOHN HARRIS²

¹Branco Weiss Fellow Society-in-Science, BioInnovationsZentrum Dresden University of Technology, Am Tatzberg 47, 01307, Dresden, Germany.

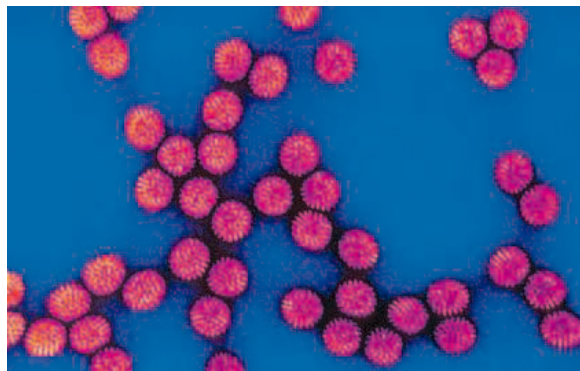
²Sir David Alliance Professor of Bioethics, Institute of Medicine, Law and Bioethics, School of Law, University of Manchester, Manchester M13 9PL, U.K.

References

1. J.A. West, G.Q. Daley, *Curr. Opin. Cell Biol.* **16**, 688 (2004).
2. John Harris, *The Value of Life* (Routledge, London, 1985).

Costs of a Rotavirus Vaccine

IN HER ARTICLE “ROTAVIRUS VACCINES’ SECOND chance” (24 Sept. 2004, p. 1890), Leslie Roberts did an excellent job of laying out the history of rotavirus vaccine development and the challenges that lie ahead in getting these vaccines to developing countries where the disease kills an estimated 440,000 children each year. Unfortunately, a quote from me may have been attributed incorrectly. In the article, she asked what would be an acceptable price for rotavirus vaccines in developing countries. She quotes me as answering, “No price is affordable for Africa.” There is a big difference between acceptable and affordable.



To arrive at an acceptable price, the value of the vaccine needs to be established. For vaccine purchasers, this requires an evidence base that includes the disease burden, the impact of the vaccine, and the cost-effectiveness relative to other interventions. Establishing the value is important to successfully engage with a manufacturer to reach agreement on a balanced price. Once an acceptable price is established, then the question of affordability can be addressed.

TRAKMATES®

If Only It Was
This Easy To
Keep Track Of
Your Car Keys.



Each tube features a permanently attached, unique 2-D Data Matrix bar code to automate sample tracking.

Ideal for tracking samples in your compound store, amongst collaborators, and from compound suppliers.

Complete line of innovative capping and racking systems offers a comprehensive storage, sampling, and shipping solution.

CONSUMABLES

www.matrixtechcorp.com



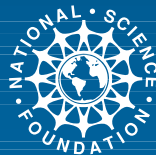
Thank you!

A very special “thank you” to all of the sponsors and supporters of the 2005 AAAS Annual Meeting.

SPONSORS



Premier Sponsor



L'ORÉAL
USA



**Pacific Northwest
National Laboratory**

Operated by Battelle for the
U.S. Department of Energy

SUPPORTERS

- ▶ Apple Computer, Inc.
- ▶ Burroughs Wellcome Fund
- ▶ CommCore Consulting Group
- ▶ European Commission
- ▶ Merck/AAAS Undergraduate Science Research Program
- ▶ Monsanto
- ▶ Sandia National Laboratories
- ▶ SEED Magazine



ADVANCING SCIENCE. SERVING SOCIETY

New vaccines, such as those against rotavirus disease, will cost more than pennies a dose. It is clear that if the poorest countries of the world are to realize the same health benefits as other countries, then the international donor community must step forward and provide financial support. The challenge to both public and private interests concerned with vaccine development and access is finding ways to meet the needs of both the consumer and the producer.

JOHN WECKER

Director, Rotavirus Vaccine Program, PATH, 1455 NW Leary Way, Seattle, WA 98107, USA. E-mail: jwecker@path.org

Preserving an Important Collection

WE, TOGETHER WITH AARON KLUG AND JIM Hudson, have been trying to save the papers of some early molecular biologists. They sit in Christie's, New York and include papers from people such as Rosalind Franklin, Aaron Klug, Max Perutz, Rollin Hotchkiss, Sven Furberg, etc. They were collected by a CalTech neuroscientist, Al Seckel, for a collector named Jeremy Norman. Norman wanted to sell them one at a time. In a lawsuit we stopped the sale so they could remain as a coherent collection. Our plan is to purchase them for 2 to 3 million dollars and donate them to Cold Spring Harbor Laboratory. Jim Watson will build an adjunct to the library to hold the history of molecular biology, including his own papers. Were this to come to pass, many of us would donate our papers. We have asked 35 people, most of whom have made a fortune in biotechnology, and have failed to obtain the funds. Time is short, so we turn to the scientific community for ideas and funds. It would be tragic if the papers from which the greatest revolution in biology came were to be dispersed.

NORTON ZINDER¹ AND RICHARD J. ROBERTS²

¹The Rockefeller University, 66th Street & York Avenue, New York, NY 10021-6399, USA. E-mail: zinder@rockvax.rockefeller.edu. ²New England Biolabs, Inc., 32 Tozer Road, Beverly, MA 01915, USA.

Science and the Bush Administration

SCIENTISTS' CURRENT OUTRAGE AT THE BUSH administration's assault on science in the U.S. is understandable but might miss the real threat—the administration's subtle yet deliberate redefinition of accepted principles of what constitutes good evidence to guide policy development. For example, the Data Quality Act, signed into law in the 2000 omnibus spending bill, gives the Office of

Management and Budget license to arbitrarily vary the quality standards for evidence for regulations. Since then, the Act has been used by industry and special interest groups to challenge health and safety warnings about smokeless tobacco, sugar, fertilizer, and asbestos; findings about climate change; and regulations about endangered species.

It is acceptable for politicians to say, "We have examined the scientific evidence on this question and have weighed it against other concerns of our constituencies and public interests in making this policy." It is not acceptable for them to arbitrarily change standards of evidence to favor their ideological or campaign contributors' interests. We must denounce such violations by political operatives lest science become a set of truths subject to change every 4 years.

It is an evidence-based truism that the best predictor of future behavior is past behavior. So there is no reason to believe that the behavior of the administration that has so perturbed the scientific community will change in the coming years. Therefore, it is critical that scientists organize, choose their battles carefully, and guard against self-serving advocacy that undermines science as an objective tool to guide decisions about medicine, public health, safety, the environment, economic development, and national security.

JESSIE C. GRUMAN

Center for the Advancement of Health, 2000 Florida Avenue, NW, Suite 210, Washington, DC 20009-1231, USA.

CORRECTIONS AND CLARIFICATIONS

News Focus: "The Indus script—write or wrong? by A. Lawler (17 Dec. 2004, p. 2026). Farmer *et al.* did not specify the number of singletons among Indus symbols. The paper can be found at <http://compling.ai.uiuc.edu/indus>. Also, the University of Pennsylvania's Greg Possehl is an archaeologist, not a linguist.

Cover Caption: (17 Dec. 2004). The image credit in the caption on p. 1989 was incorrect. The credit should be Kees Veenenbos.

News of the Week: "New TB drug promises shorter, simpler treatment" by J. Cohen (10 Dec. 2004, p. 1872). The article incorrectly stated that Johnson & Johnson was screening for a broad spectrum antibiotic. The company was screening for a TB drug from the outset. The researchers also found resistance to their new compound in vitro, not in the mouse model.

Cover Caption: (3 Dec. 2004). The image credit in the caption on p. 1637 was incorrect. The credit should be NASA/JPL/Cornell.

This Week in Science: "Staying mixed" (12 Nov. 2004, p. 1097). The half-life of C¹⁴ was incorrect in this item. It should be 5730 years, not 5370 years.

ALPHANUMERIC TUBES

One Letter.

One Number.

One Easy Way To Keep Track Of Your Samples.



Patented alphanumeric printing (A1 to H12) on the bottom of each tube allows samples to be accurately returned to a rack.

All tubes are PureFect[®] tested to ensure they are free of DNA, DNase, RNase, and other contaminants.

0.75mL and 1.4mL tubes available in Snap Racks, EcoTube Refill Packs or the innovative Latch Rack.

CONSUMABLES

www.matrixtechcorp.com

Hatching of an Accountable Science

Hans C. E. Larsson

Dinosaur research is often synonymized with science fiction or Hollywood, and it is true that most public ingestion of things dinosaur is in the form of film, adolescent stories, and children's books. Academically, dinosaur research has generally been seen as a ridiculous science—unable to stand on its own. The gap between results from this field and other sciences left many issues to fables and storytelling, but a trend during recent decades seems determined to change that.

The Dinosauria
2nd ed.
David B. Weishampel,
Peter Dodson, and
Halszka Osmólska, Eds.
University of California
Press, Berkeley, 2004.
879 pp. \$95, £62. ISBN
0-520-24209-2.

The new edition of *The Dinosauria* marks a major step in the evolution of this science (1). Advanced sciences require comparable data, methods, and languages. In dinosaur research, phylogenetic systematics (the reconstruction of genealogies) offers a foundation for progress toward meeting these requirements: Morphologies can be debated with reference to particular specimens, and accepted methodologies allow hypotheses to be refuted with some degree of confidence. To place the various dinosaurs in their phylogenetic context, all taxonomic chapters (which comprise over 70% of the text) include results from numerical cladistic analyses, with character descriptions and data matrices available online. The accountability introduced by this approach moves the discipline toward more mature sciences.

David Weishampel (Johns Hopkins), Peter Dodson (University of Pennsylvania), and Halszka Osmólska (the Institute of Paleobiology, Warsaw, Poland) recruited contributions from 41 other dinosaur workers from around the globe. Many of the authors are young, upcoming researchers, who have expanded the range of methodologies and perspectives present in the text.

The authors attempt to summarize the entire current state of dinosaur research in a single volume, and they have done so with great success. They present an astonishingly



Mark Hallett's *Yixian Faunal Scene* (detail). Some 30 species of dinosaurs have been found in the Early Cretaceous Yixian formation of China.

complete survey of the geologic age, paleogeographic distribution, and identifications of dinosaur fossils from around the globe. For every accepted group of dinosaurs, they offer particulars on included species, evolutionary relationships, morphological descriptions that diagnose the group and indicate its internal phylogenetic structure, geographic and stratigraphic distributions, and interpretations of the animals' biology.

Some chapters appear bound to traditional views of dinosaur taxonomy. For instance, single chapters are devoted to the traditional Prosauropoda and Sauropoda (dinosaurs that grace Sinclair gas stations)—two groups that together comprise half of the members of Saurischia. Other chapters are parceled out to reflect current views of dinosaur diversity, such as the nine chapters devoted to Theropoda (the carnivorous dinosaurs)—the other half of Saurischia.

Although in general each group of dinosaurs receives exceptional attention, little consideration is given to the phylogenetics of Dinosauria as a whole. The chapter on dinosaur origins devotes only two paragraphs to the monophyly (descent from a

common ancestor) of Dinosauria. The lengthy and heated history of research surrounding this topic clearly deserved inclusion in the volume.

In many of the taxonomic chapters, good, solid morphological descriptions—the bread and butter of vertebrate paleontology—are accompanied by modern illustrations. The quality of these illustrations, however, varies greatly; beautiful renditions are juxtaposed with crude line drawings. Although it may be unreasonable to expect the editors to enforce a standard graphics format in a volume of this scope, the shortcomings in some illustrations drop this work a notch below other definitive paleontological texts.

A similar variation in quality affects the volume's central unifying theme, phylogenetic systematics. Unfortunately, some authors offer only vague accounts of their data matrix and the dynamics of character evolution. Despite the editors' intentions, a number of data matrices are missing from the supporting online material (though the final revision of the text was complete by May 2003). Their absence cuts into the accountability of the work and echoes earlier days of dinosaur research. Conversely, most authors go to great lengths to discuss morphological characters, how these characters shape the phylogenetic trees, and how the character and species arrangements differ from those previously suggested. To address higher-level trends in morphological evolution, some contributors consider character changes on their phylogenetic framework. Such explorations of higher-order signals in the data introduce a new dimension to the research. Examination of the trends reinforces the phylogenetics in the way that tests of the theory of relativity lent support to fundamental aspects of Newtonian physics.

If accountability is a valid currency for the evolution of a science, the new edition of *The Dinosauria* indicates the field is moving on a progressive course. By itself, the volume stands as the current definitive summary of our knowledge of these animals. In a broader view of science, it suggests that dinosaur research may be ready to leave the nest.

Note

1. The first edition, from the same editors and publisher, was envisioned in 1984 and appeared in 1990.

10.1126/science.1107611

The reviewer is at the Redpath Museum, McGill University, 859 Sherbrooke Street West, Montreal, Quebec H3A 2K6, Canada. E-mail: hans.ce.larsson@mcgill.ca

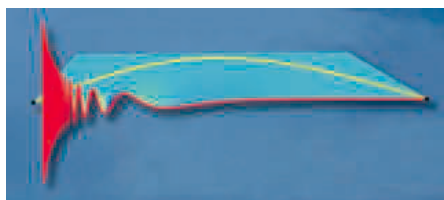
COMPUTING

Learning from 100 Numbers

Gilbert Strang

Competition and collaboration are the yang and yin that move science forward. *The SIAM 100-Digit Challenge* grew out of a contest to compute ten correct digits in the solutions to ten scientific problems, which ranged from a difficult integral to the fate of a particle diffusing in a box. The contest rules allowed entries by teams, which quickly formed. Contestants discovered new ways to achieve high accuracy, and, surprisingly, 20 entries produced what the creator of the problems never expected—100 digits, all correct.

Four of the winners—Folkmar Bornemann (Technical University of Munich, Germany), Dirk Laurie (University of Stellenbosch, South Africa), Stan Wagon (Macalester College, Minnesota), and Jörg Waldvogel (Swiss Federal Institute of Technology, Zurich)—have joined in an analysis of the ten problems for SIAM, the Society for Industrial and Applied Mathematics. A reader cannot fail



Blurry graph. The integrand in Problem 1 oscillates infinitely often inside the interval of integration.

to be struck by the unity of mathematics and the cooperation of so many mathematicians. That this teamwork happened spontaneously makes one cheerful. (The authors were completely unacquainted before the contest.) The remarkably attractive book is full of small touches, like an estimate for the totality of arithmetical operations ever carried out by man and machine: 10^{24} .

The spark for everything was Nick Trefethen. He developed the ten numerical analysis problems for his Oxford University course for entering graduate students, and in *SIAM News* for January–February 2002 (see www.siam.org/siamnews) he offered a prize for the most accurate set of solutions. The con-

The reviewer is in the Department of Mathematics, Massachusetts Institute of Technology, Cambridge, MA 02139, USA. E-mail: gs@math.mit.edu

The SIAM 100-Digit Challenge
A Study in
High-Accuracy
Numerical Computing

by Folkmar Bornemann,
Dirk Laurie, Stan Wagon,
and Jörg Waldvogel

SIAM Press, Philadelphia,
2004. 318 pp. \$57. ISBN 0-
89871-561-X.

test ran for five months, and it certainly wasn't hard to grade: each digit was right or wrong. The satisfaction of producing actual numbers (not theorems) appealed to high-school and college students and researchers from all around the world, and 94 entries were received.

The authors discuss each of the ten problems, and the techniques used to solve them, in considerable detail. An accompanying Web page (www.siam.org/books/100digitchallenge) offers further material, including source code for the methods, examples, tables, and figures. Here I will describe two of the problems. (I can't write more about the book without mathematics.)

Problem 1 requested a definite integral of the function $x^{-1}\cos(x^{-1}\log x)$. Approaching $x = 0$, the function blows up from the factor x^{-1} . Also at $x = 0$ the cosine oscillates faster and faster between 1 and -1 ; the graph of the function on the book's cover shows a blur. Most mathematicians give up quickly on such difficult integrals. (We say we have outgrown them, but the truth is more embarrassing.)

Integrals are often simplified by changing variables: Substituting t for $-\log x$ gives an integral of $\cos(te^t)$. Then integration by parts (unforgettable to all readers) eventually produces a very unpromising series that will never converge: $2^1 - 4^3 + 6^5 - 8^7 + \dots$.

On the other hand, our function is the real part of $x^{-1}x^{i/x}$. The appearance of i (the square root of -1) leads to a different and more successful idea—move into the complex plane, to escape from the oscillating blow-up around $x = 0$. When the integral is improved, it can be dealt with using Mathematica, Maple, or Matlab. I give up now. Don't send any integrals.

Problem 10 is more typical of the contest and much closer to science. A particle starts at the center of a 10 by 1 rectangle. It moves by taking infinitesimal steps in random directions (that is, it undergoes Brownian motion). What is the probability P that the particle will hit a short end of the rectangle before touching a long side?

You can discover the one significant digit in $P = 0.0000004$ by a Monte Carlo simulation. However, doing so—even when taking ten million trial walks per minute—is far too slow. After an unexpected transformation of the problem, 12 more digits can be obtained from $8e^{-5\pi/\pi}$. Ten thousand additional digits can be produced in seconds, by recognizing an elliptic function of Jacobi that is connected to Hilbert's 12th problem (proposed in the printed version of his address to the International Congress of Mathematicians in 1900).

Incredibly, an exact solution to Problem 10 can be found in a 27 February 1913 letter that Ramanujan in India sent to Hardy in

BAR CODING SERVICES

This Is Our Idea Of Designer Labels.



Available on our microplates, PCR plates, blocks or tube racks according to your exact specifications and numbering sequences.

Low minimum orders and fast turnaround times.

Reordering is simple because we keep track of all codes and specifications from previous orders.

CONSUMABLES

www.matrixtechcorp.com

Cambridge. The probability that the randomly walking particle reaches a short end of the rectangle is given by $(2/\pi) \arcsin[(3-2/2)^2 (2+\sqrt{5})^2 (\sqrt{10-3})^2 (5^{1/4}-2)^4]$. Then $P = 0.0000003837587979\dots$

This story is beautifully told by Bornemann, who was one of the solo winners (Laurie was another). His months of satisfying work earned him a grand prize of \$100—one dollar per digit. The contest was a true success and so is this book.

10.1126/science.1108288

HISTORY OF SCIENCE

Spotlight on Invisible Women

Asha Gopinathan

At a time when the issue of women in science is regularly discussed and debated, it might come as a surprise that even a few centuries ago, women played significant, visible, and valuable roles in scientific endeavors. Their participation in European science during the 17th and 18th centuries is the focus of *Pandora's Breeches: Women, Science and Power in the Enlightenment*. Patricia Fara (a historian of science at Cambridge University) provides an original and very readable account of how women have affected the development of science. Fara rejects the conventional approach

Pandora's Breeches Women, Science and Power in the Enlightenment

Patricia Fara

Pimlico (Random House), London, 2004. 288 pp. £12.50, C\$34.95. ISBN 1-8441-3082-7.

to popular writing on the history of science, which usually stresses the glorious discoveries of great men and favors heroic tales of romanticized, lone geniuses. Although Fara's stories feature relatively privileged women and mostly wealthy gentlemen,

they reflect the collaborative nature of science; the contributions of skilled artisans, practical people, and invisible assistants; and the links between scientific achievements and the rest of society.

Fara has selected eight women whose lives were entwined with those of famous male scientists of the Enlightenment. In addition, she interweaves her essays on them with stories of numerous other women who made equally significant contributions. These women played a range of roles: Some

The reviewer is at GenSci-e-Tech, E-2 Sree Vilas Lane, Laudiar, Trivandrum 695003, Kerala, India. E-mail: dend_15@yahoo.com

were devoted wives, sisters, or daughters; some were patrons to aspiring scholars; some were at the center of intellectual salons. Many ran households that enabled men to continue working in science (a circumstance seen even today). Some collected astronomical or botanical data and even published on their own, whereas others interacted with a wider audience by translating scientific works into popular languages.

For example, Elisabeth of Bohemia was celebrated as a leader of a philosophical sect, "the female Cartesians," that used Cartesian arguments against Descartes himself. One of her contemporaries, Anne Conway, was regarded by Leibniz as an important intellectual predecessor. Émilie du Châtelet, Voltaire's lover, studied, questioned, and critiqued works by Newton and Descartes. After completing a literal translation of the *Principia* into French, she prepared three further versions—a simple prose account for newcomers, a presentation in the framework of the new continental algebra, and a summary of recent mathematical research and experimental vindications of Newton's theories (which demonstrated her own deep understanding of mathematics).

During this period scientific research was regularly carried out within the domestic realm, and women such as Jane Dee, Elisabetha Hevelius, Maria Kirch, Caroline Herschel, and Marie Paulze Lavoisier conducted their work in family settings. Universities continued to be closed to all women and many men; in order to make discoveries, many of these women used such strategies as marrying established men much older than themselves. Caroline Herschel was probably the first woman to be paid a salary for scientific work, and her three letters published in the Royal Society's *Philosophical Transactions* were the first to appear under a woman's name. Paulze Lavoisier worked with her husband in his laboratory, illustrated instruments for his *Elements of Chemistry* (1789), and translated books and papers from English for him. She also ran a weekly salon in Paris where men and women met together to discuss the latest gossip, plays, and scientific experiments—and where sources of funds for research were obtained.

The Enlightenment was nevertheless a period of contradictory attitudes toward



Lithograph by unknown artist, England, c. 1830.

women in science. Whereas many men opposed exposing women to science, there were others who—as fathers, brothers, or husbands—helped women enter scientific fields. Through letters as well as meetings, Leibniz discussed science and philosophy with women throughout Europe. He relied on female patrons for financial support and praised their insights. The French and Italians were generally more tolerant of women in science than many other Europeans, although

there were differences among various fields. For example, as Fara notes, between 1650 and 1720, about 14% of German astronomers were women—probably because their participation was fostered by the strong guild tradition. Although the various scientific academies established during this period also excluded women, there were less formal networks of women engaging in similar activities and many women published under pseudonyms.

One woman who makes only a brief appearance in the book is Laura Bassi, an expert on Newton who was a university professor in Bologna during du Châtelet's time. Ambitious Italian girls followed her example by taking courses in natural philosophy, and it is unfortunate that Fara did not devote an entire essay to her.

Fara cautions against reading the lives of her subjects by light of contemporary feminist thought. They were women of their times, and their accomplishments and limitations reflect the complexities and contradictions of their circumstances. Much has changed since science became institutionalized and took its modern form during the late 18th and 19th centuries. Laboratories, museums, and hospitals have replaced the home as the locus of research. Women have finally won widespread entry to the universities and participation in research in academic and industrial settings. Nevertheless, women who wish to fully participate in contemporary science still face many barriers.

Undermining the concept of heroism in science, *Pandora's Breeches* represents subaltern history of science at its best. The stories Fara has collected should also encourage the recovery and reappraisal of the contributions of many other scientific workers who are now forgotten.

10.1126/science.1104566

SAMPLE TRACKING

Take Advantage Of The Industry's Largest Selection Of Sample Tracking Solutions.

Calendars. Date books. Electronic organizers. There are plenty of ways to keep track of things in your personal life. Fortunately, now you have access to just as many in your lab.

At Matrix, we offer the most complete selection of drug discovery solutions in the industry—from instrumentation to consumables—including the widest range of innovations for shipping, storing and tracking samples.

Whether you need the versatility to quickly trace hundreds, thousands or millions of individually marked tubes or the flexibility to add customized bar codes to your microplates, blocks or tube racks, we have the perfect solution.

For more information, visit us at www.matrixtechcorp.com or call toll-free, (866) 229-9770. Either way, you may suddenly get the feeling like today's *your* birthday.

**We'll Help You Keep Track
Of Pretty Much Everything.**

Except Your Mother's Birthday.



MATRIX
fluid thinking.

www.matrixtechcorp.com

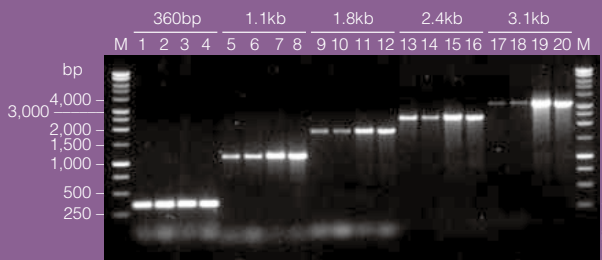
HANDHELD PIPETTING

AUTOMATED PIPETTING

CONSUMABLES



Get remarkably robust DNA amplification. Again and again and again.



Regular *Taq* vs. GoTaq DNA Polymerase over a wide range of target sizes. In each set the left two lanes are *Taq* DNA Polymerase and the right two lanes are GoTaq DNA Polymerase.

Reap the benefits of consistent, robust performance every time you amplify with GoTaq® Polymerases.

- Harvest spectacular yields with optimal enzyme and buffer
- See faster results with the all-in-one reaction buffer that doubles as a gel loading buffer
- Perform perfect gel tracking with the GoTaq Green buffer – tracks small fragments and bumper products
- Enjoy the Promega PCR Performance Guarantee

Prove it to yourself...again and again and again.

To learn more, visit www.promega.com/gotaq

ECOLOGY

Do the Largest Protected Areas Conserve Whales or Whalers?

Leah R. Gerber,¹ K. David Hyrenbach,² Mark A. Zacharias³

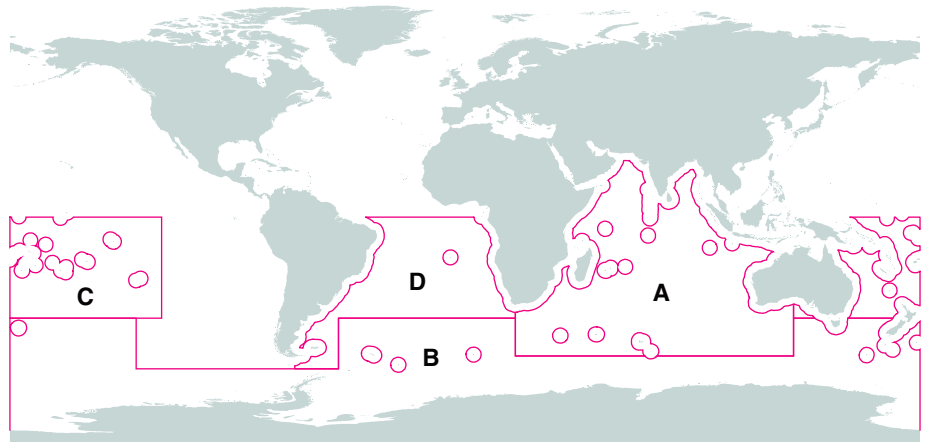
In 1946, the International Convention on the Regulation of Whaling authorized the International Whaling Commission (IWC) to designate sanctuaries that prohibit commercial or aboriginal subsistence whaling (1, 2). A sanctuary operated in the South Pacific sector of the Southern Ocean between 1938 and 1955. Since then, the Indian Ocean Sanctuary was adopted in 1979 and the Southern Ocean Sanctuary (SOS) in 1994 (1). These sanctuaries constitute the world's largest marine protected areas (see the figure, this page). Early IWC sanctuaries were emergency measures enacted to protect overexploited stocks while other measures were implemented. More recently, the establishment of IWC sanctuaries has been criticized as a political, rather than scientific, means to exclude commercial whaling from large areas of the ocean. Critics view the sanctuaries as a way to preempt the potential adoption of the Revised Management Procedure (RMP), a science-based harvest framework within the broader Revised Management Scheme (RMS) that is intended to replace the current global moratorium on commercial whaling (3).

In response to these criticisms, the IWC adopted three scientific objectives in 1998 (4). Sanctuaries were charged with promoting the recovery of whale stocks, including the establishment of appropriate monitoring of depleted populations. The effects of zero catch limits on whale stocks were to be assessed. Research was mandated on the effects of environmental change on whale populations. In 2003, the IWC directed the Scientific Committee to undertake a decadal (1994–2004) review of the SOS.

We were appointed by the IWC Scientific Committee to review the SOS and to evaluate how approaches in marine protected areas might be integrated into the IWC sanctuary program. On the basis of existing liter-

ature related to marine protected areas and cetacean biology (5–8), we have concluded (9) that the SOS in particular, and the IWC sanctuary program in general, are currently not scientifically justified. In particular, the IWC faces four main limitations:

Arbitrary boundaries. All whale species with commercial harvest potential migrate outside of the sanctuary boundaries at some point in their lives and therefore are vulnerable to commercial harvest if the global whaling moratorium is lifted (10).



Map of IWC sanctuaries in the Indian (A) and Southern (B) Oceans. Establishment of the South Pacific (C) and South Atlantic (D) Ocean sanctuaries has been proposed.

Narrow focus. Sanctuaries do not protect or mitigate other threats to Southern Ocean whale stocks and the marine ecosystems upon which these populations depend, including pollution, habitat degradation and loss, introduced species, and global climate change.

Lack of an adaptive population design. Comparative studies of the population structure and trends of harvested and unharvested whale stocks are unfeasible. An objective of the IWC Sanctuary Program is to facilitate comparisons of whale populations within and outside of the boundaries of protected areas (4). However, the size of IWC sanctuaries means that protected whales inhabiting the Indian and Southern Oceans will have to be compared with those inhabiting the Atlantic and Pacific Oceans. Because threats to whales may be different or of unequal

magnitude in different ocean basins, comparisons may not be scientifically valid.

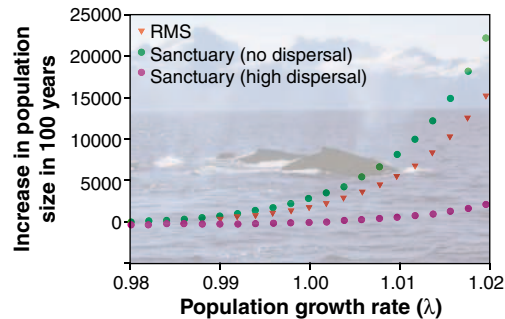
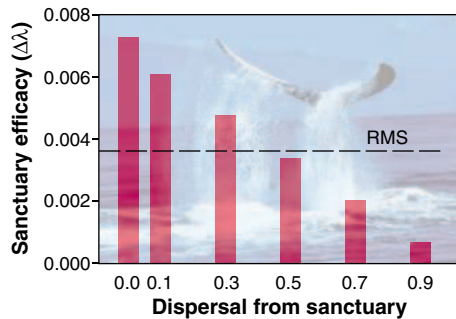
Need for baselines. Comparisons of harvested and unharvested stocks are further confounded by unregulated takes for research (i.e., scientific permit whaling), which are not limited to specific areas or time periods, and do not require adherence to catch quotas. Thus, even those populations restricted to existing IWC sanctuaries do not provide an ecological baseline for the study of the effects of climatic variability on whale populations and Southern Ocean ecosystems (11–12).

Current debate has polarized IWC members into those who advocate widespread sanctuary use and those who believe that they are redundant under the RMP/RMS. To determine whether the application of the RMP/RMS, in conjunction with a more ecologically oriented sanc-

tuary program, would represent a measurable improvement for whale management and conservation, we developed a population model to assess relative efficacy. We calculated the change in population growth rate (λ) due to sanctuary establishment for different rates of dispersal across a sanctuary boundary. We assumed typical life history parameters for baleen whales, and used demographic parameters for the gray whale *Eschrichtius robustus* (13–14). To consider the applicability of our results to other whale species, we explored the sensitivity of our results to small changes in these parameter values (15). We examined the degree to which changes in population growth resulting from alternative management schemes determine population size 100 years into the future.

The increase in λ as a result of decreas-

¹The Faculty of Ecology, Evolution and Environmental Sciences, School of Life Sciences, Arizona State University, Tempe, AZ 85287–4501, USA. E-mail: Leah.Gerber@asu.edu; ²Duke University Marine Laboratory, Beaufort, NC 28516, USA. E-mail: khyrenba@duke.edu; ³Department of Geography, University of Victoria, Victoria, BC, Canada V8W 3P5. E-mail: Mark.Zacharias@uvic.ca



Change in whale population growth rate and projected abundance. (Left) Absolute change in population growth rate (λ) resulting from a 20% reduction in adult mortality in sanctuaries with different rates of dispersal compared to the population growth rate under the RMS scenario. Take is reduced by 10% for both patches in the RMS scenario (no reserve). (Right) Projected abundance in 100 years for a range of underlying rates of population growth under alternative management schemes reflecting the small changes in λ portrayed in graph at left. "High dispersal" corresponds to a 0.9 movement rate from sanctuary to unprotected areas.

ing adult mortality (16) depended strongly on the underlying rate of dispersal (see the figure above, left). The RMP/RMS management approach was more effective than sanctuary scenarios, in cases where at least 50% of the population dispersed from the sanctuary. Furthermore, very small fluctuations in λ translated into substantial long-term changes in whale numbers (see the figure above, right). Although little is known about migratory pathways and destinations for most Southern Ocean whale populations (10, 17), it is reasonable to assume that at least 50% of whales inhabiting IWC sanctuaries move out of these areas during annual migrations (10, 18). Thus, our model suggests that a quota-based management regime (RMP/RMS) will be more effective than IWC sanctuaries as currently configured.

Although this result was robust to small (± 0.02) changes in parameter values, our model includes dispersal as diffusion, rather than as explicit migration, and does not include density dependence, demographic stochasticity, or environmental noise. However, given uncertainties concerning demographic and life-history information for whales (19) and the large number of potential sanctuary configurations, our model provides general insights into the long-term implications of different management approaches. Our results are consistent with previous work on demersal and benthic species of low motility in marine protected areas, where reserves maintain unharvested populations while supporting enhanced fishery yields outside the reserve (20, 21). Similar benefits could materialize for highly migratory species like cetaceans (8); however, this depends on how much of the species' range is encompassed by the reserve (14). Because most whale stocks that inhabit IWC sanctuaries are highly migratory (10, 17), the current sanctuaries do little for whale conservation without additional protective

measures beyond their boundaries.

IWC sanctuaries could become an important part of the IWC management approach and the broader conservation of Southern Ocean marine ecosystems. This requires better integration with other activities under the IWC mandate (e.g., RMP/RMS and scientific permit whaling) as well as with other management programs (e.g., the Convention on the Conservation of Antarctic Marine Living Resources). If IWC sanctuaries are to become a cornerstone in ecosystem management for the Southern Ocean, the IWC must work with other regional institutions and global initiatives to ensure that threats to whales, other than commercial harvest and climatic variability, are considered. However, this necessitates returning to a scientific (rather than political) approach to sanctuary designation and management. A starting point would be the establishment of IWC sanctuaries conforming to more ecologically based designation and operation criteria. Specifically, IWC sanctuaries must embrace the following principles of reserve design and management: (i) adoption of formally stated goals (e.g., biodiversity protection and fisheries enhancement) articulated in a management plan; (ii) development of measurable objectives with which to assess progress toward attaining these goals; (iii) establishment of ecologically based sanctuary boundaries; (iv) creation of a formal management plan, including the establishment of a monitoring framework; and (v) design of more appropriate review criteria reflecting the ecological objectives described in the management plan (9).

We advocate the elimination of unregulated scientific permit whaling and the application of the RMP/RMS, alongside a system of IWC sanctuaries designed to protect populations of whales during certain time periods (e.g., breeding grounds and/or feeding areas) or throughout their entire

ranges (22). If whaling were to resume under the RMP/RMS, IWC sanctuaries would only fully protect whales that migrate between the Southern Ocean and the Indian Ocean, where the overlapping sanctuaries likely encompass the entire ranges of several stocks. Nevertheless, the adherence to a quota system would enhance whale conservation by restricting the times and areas of whale harvesting, and by restricting the total catch. Moreover, the cessation of scientific permit whaling would reinstate the research value of IWC sanctuaries, by facilitating the monitoring and comparative study of harvested and unharvested stocks.

References and Notes

- International Convention for the Regulation of Whaling, Washington, DC, 2 December 1946 (U.S. Government Archives, Washington, DC).
- In accordance with the IWC, the "whaling" refers to the take of cetaceans for commercial and subsistence uses and as part of scientific studies, and "whales" are species of baleen (mysticete) and toothed (odontocete) cetaceans targeted for harvest (23).
- N. M. Young, *Understanding the Revised Management Procedure* (Center for Marine Conservation, Washington, DC, 2002).
- IWC, *Annu. Rep. Int. Whaling Comm.* **1998**, 42 (1999).
- P. D. Boersma, J. K. Parrish, *Ecol. Econ.* **31**, 287 (1999).
- C. E. Mills, J. T. Carlton, *Conserv. Biol.* **12**, 244 (1998).
- K. D. Hyrenbach, K. A. Forney, P. K. Dayton, *Aquat. Conserv.* **10**, 437 (2000).
- S. K. Hooker, L. R. Gerber, *Bioscience* **54**, 27 (2004).
- M. A. Zacharias, L. R. Gerber, K. D. Hyrenbach K. D., *Int. Whaling Comm. Pap. SC/56/SOS5* (IWC, Cambridge, 2004).
- C. R. Davis, N. Gales, *Int. Whaling Comm. Pap. SC/56/SOS2* (IWC, Cambridge, 2004).
- D. G. Ainley, *Mar. Ornithol.* **30**, 55 (2002).
- P. J. Clapham *et al.*, *Bioscience* **53**, 210 (2003).
- Values include fecundity of 0.470, adult and juvenile survival of 0.944 and 0.893, respectively, and age at sexual maturity of 8.
- S. Reilly, *Rep. Int. Whal. Comm., Special Issue* **6**, 389 (1984).
- Materials and methods are available as supporting material on Science Online.
- L. R. Gerber, S. S. Heppell, *Biol. Conserv.* **120**, 121 (2004).
- K. M. Stafford *et al.*, *Deep-Sea Res. Part 1*, **51**, 1337 (2004).
- J. L. Bannister, in *Encyclopedia of Marine Mammals*, W. F. Perrin, B. Würsig, J. G. M. Thewissen, Eds. (Academic Press, San Diego, CA, 2002), pp. 62–72.
- C. S. Baker, P. J. Clapham, *Trends Ecol. Evol.* **19**, 365 (2004).
- S. N. Murray *et al.*, *Fisheries* **24**, 11 (1999).
- G. R. Russ *et al.*, *Ecol. Appl.* **14**, 597 (2004).
- See supplemental online material.
- P. J. Clapham, C. A. Baker, in *Encyclopedia of Marine Mammals*, W. F. Perrin, B. Würsig, J. G. M. Thewissen, Eds. (Academic Press, San Diego, CA, 2002), pp. 1328–1332.
- We thank D. DeMaster and two anonymous reviewers for helpful comments, chair (A. Zerbin) and the members of the IWC SOS Review Committee for insights into the IWC Sanctuary Program; and S. Young for mapping assistance.

Supporting Online Material

www.sciencemag.org/cgi/content/full/307/5709/525/DC1
10.1126/science.1106120

EVOLUTION

An Eocene Big Bang for Bats

Nancy B. Simmons

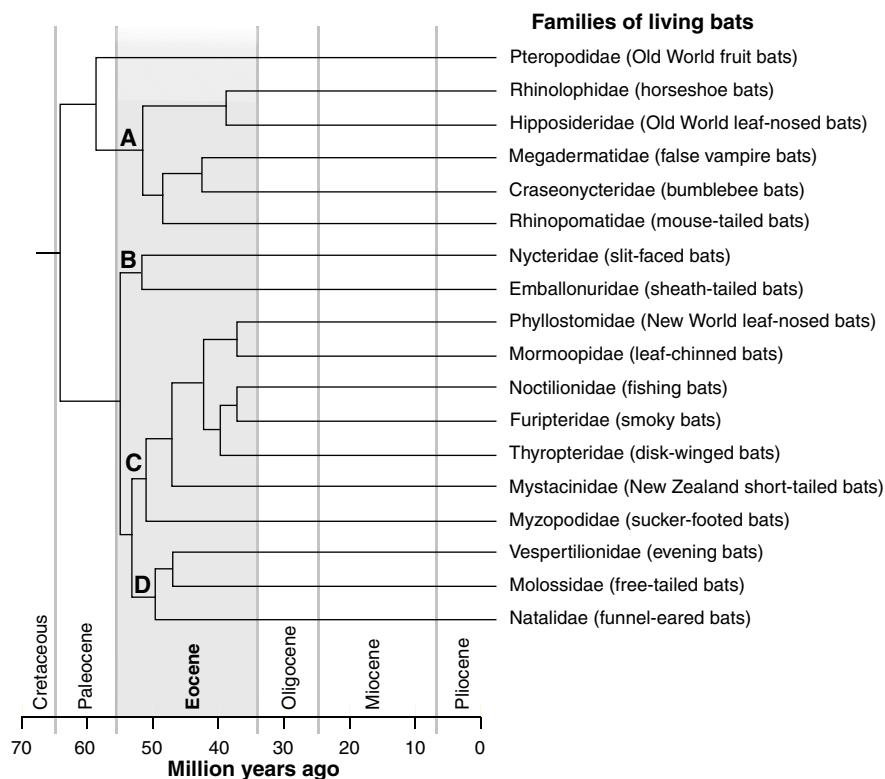
Bats, the only mammals capable of powered flight, constitute more than 20% of living mammal species (1). Unlike birds and other terrestrial vertebrates, most bats use echolocation—a biological form of sonar—to locate and track their prey (2). Bats are found on every continent except Antarctica, and they exploit a wide variety of food sources including insects, small vertebrates, fruit, nectar, pollen, and even blood (1–3). More than 110 bat species may coexist in some ecological communities, a number that far exceeds that of any other mammalian group (1, 3). Despite their prominent position among mammals, the evolutionary history of bats is largely unknown because of a limited fossil record and incomplete phylogenies. On page 580 of this issue, Teeling *et al.* (4) provide a new evolutionary tree for bats that helps to explain how, when, and where this extraordinary diversity may have originated.

Living bats are classified into 18 families on the basis of shared anatomical specializations and echolocation habits (see the figure), and another six families are known from fossils (1, 5, 6). Although biologists have long agreed that these groups represent distinct evolutionary lineages, there has been no consensus concerning relationships among them. The lack of a well-resolved phylogeny (evolutionary tree) for bats has hindered attempts to understand the origins of major specializations in these mammals, and has complicated efforts to untangle the temporal and biogeographic history of the group.

One extant family (Pteropodidae, or Old World fruit bats) lacks the sophisticated echolocation abilities of other bats. Because bat echolocation is a complex system involving specialization of the respiratory system, ear, and brain (2), it has generally been assumed that echolocation evolved only once in bats. This hypothesis has been supported by phylogenetic analyses of morphological data by a number of groups [e.g., (5)]. These analyses revealed a basal split among bats between a single lineage leading to all echolocating

bats (Microchiroptera) and another lineage leading to non-echolocating pteropodids (Megachiroptera). However, recent analyses of DNA sequence data have challenged this hypothesis, instead suggesting that some echolocating bats (rhinolophoids) are more closely related to pteropodids than to other echolocating bats [e.g., (7, 8)]. These relationships imply that echolocation either evolved twice in bats or evolved once but was later lost in pteropodids. Either scenario would require a complete rethinking of our understanding of the evolutionary history of bats, including new evolutionary explanations for more than 20 different anatomical specializations shared by living echolocating bats [but not pteropodids (5)].

Weaknesses in prior molecular studies have left some doubt about their interpretation. For example, analyses of different genes yielded incompatible phylogenetic trees, and sampling of living bat families was incomplete, leaving open the possibility that sampling biases were responsible for the surprising molecular results. The new study by Teeling *et al.* (4) overcomes these difficulties by simultaneously analyzing portions of 17 nuclear genes sampled in all extant families. The resulting phylogenetic tree, which is strongly supported by the data, confirms the results of earlier molecular studies (see the figure). Non-echolocating pteropodids nest among lineages of echolocating bats, implying a dual origin for echolocation or its loss in pteropodids. The authors do not attempt to choose between these alternatives, but a second analysis including several extinct families (4) suggests that a single origin for echolocation (followed by its loss in pteropodids) is most likely.



Temporal pattern of bat diversification. Teeling *et al.* (4) used their molecular tree and a series of fossil calibration points to reconstruct the timing of bat radiation. They calculate that living bats last shared a common ancestor at or just after the Cretaceous-Tertiary boundary. The four major lineages of living echolocating bats (A to D) appear to have subsequently originated within a narrow time frame in the Early Eocene [52 to 50 million years ago (4)]. Although divergence dates estimated from models of DNA sequence evolution are notoriously subject to biases, the Eocene dates in this study are reasonably consistent with the results of morphology-based reconstructions [e.g. (3, 6)]. The results of Teeling *et al.* suggest that all 18 of the living families of bats were distinct by the end of the Eocene (about 34 million years ago). [Adapted from (4)]

The author is in the Division of Vertebrate Zoology, American Museum of Natural History, New York, NY 10024, USA. E-mail: simmons@amnh.org

Teeling *et al.* reanalyzed a previously published morphological data set that included four extinct families (5), using their DNA tree as a constraint. The resulting trees placed the Eocene fossil families as sister taxa (close relatives) to the lineage leading to all living bats. Previous analyses of fossilized stomach contents, ear anatomy, and limb structure concluded that two of the fossil families were sophisticated echolocators similar to most living bats (5). The other fossil groups are also thought to have been capable of echolocation, although they may not have been able to track flying prey (5). Taking the relationships of these fossils into account, it seems most likely that echolocation evolved only once in bats, before diversification of the group. The lineage leading to bats was thus characterized by two remarkable specializations seen in no other land mammals: powered flight and echolocation. The coincidence of these adaptations—which may have been functionally and evolutionarily linked (9)—was probably the key that started the evolutionary diversification of the group.

The scope of this “big bang” Eocene radiation is unprecedented in mammalian history. What may have caused it? Teeling *et al.* speculate that bats diversified in the Early Eocene in response to an increase in prey diversity, and that the varied echoloca-

tion and flight strategies that characterize families may have evolved as a result of differential exploitation of ecological niches available at that time. The origin of the major bat lineages in the Eocene is apparently coincident with a rise in mean annual temperature, a significant increase in plant diversity, and the peak of Tertiary insect diversity (4). The evolutionary success of bats thus may have resulted from ancestral bats being in the right place at the right time. As flying predators capable of capturing prey on the wing, they would have had few competitors for the rich resources of the Eocene night. The only other vertebrates that exploit niches for nocturnal flying predators are the owls and nightjars. Interestingly, owls may also have undergone an adaptive radiation in the Eocene (10).

The geographic origin of bats has been a source of debate because Eocene bat fossils have been found on most continents (5, 6). Teeling *et al.* (4) seemingly have solved this problem with their new phylogeny, which unambiguously indicates a Laurasian (Northern Hemisphere) origin for bats. Once the group was established, different lineages of bats probably diversified on different continents, but the scale of the Teeling *et al.* analysis does not allow them to untangle these patterns. Indeed, it is the scale of bat diversity that makes this study

so tantalizing. Their results give us a new framework for understanding bat evolution, but it is only the tip of the iceberg. Although broad in scope, their evolutionary tree includes fewer than 40 out of more than 1100 living bat species—just 3%. Understanding the patterns of evolution of different echolocation strategies, diets, body sizes, flight styles, and reproductive habits of bats will require much more fine-grained phylogenies than are now available. As always, the devil will be in the details.

References

1. N. B. Simmons, in *Mammal Species of the World: A Taxonomic and Geographic Reference*, D. E. Wilson, D. M. Reeder, Eds. (Johns Hopkins Univ. Press, Baltimore, in press).
2. H. T. Arita, M. B. Fenton, *Trends Ecol. Evol.* **12**, 53 (1997).
3. N. B. Simmons, T. M. Conway, in *Bat Ecology*, T. H. Kunz, M. B. Fenton, Eds. (Univ. of Chicago Press, Chicago, 2003), pp. 493–535.
4. E. C. Teeling *et al.*, *Science* **307**, 580 (2005).
5. N. B. Simmons, J. H. Geisler, *Bull. Am. Mus. Nat. Hist.* **235**, 1 (1998).
6. N. B. Simmons, in *Origins of the Major Clades of Placental Mammals*, K. Rose, D. Archibald, Eds. (Johns Hopkins Univ. Press, Baltimore, in press).
7. E. C. Teeling *et al.*, *Mol. Phylogenet. Evol.* **28**, 308 (2003).
8. R. A. Van Den Bussche, S. R. Hooper, *J. Mammal.* **85**, 321 (2004).
9. J. R. Speakman, *Symp. Zool. Soc. London* **65**, 39 (1993).
10. A. Feduccia, *The Origin and Evolution of Birds* (Yale Univ. Press, New Haven, CT, ed. 2, 1999).

10.1126/science.1108871

PARASITOLOGY

Malaria Vaccines: Back to the Future?

A. P. Waters, M. M. Mota, M. R. van Dijk, C. J. Janse

Malaria is the scourge of many developing countries, particularly those in sub-Saharan Africa, claiming several million lives each year. Researchers have struggled for decades to make a successful subunit or attenuated whole-organism vaccine but with limited success. Factors that have hampered the development of a subunit vaccine include the complexity of the malaria life cycle, the wide variety of immune response induced by the malaria parasite, and an incomplete knowledge of protective immunity. In contrast, attenuated whole-organism vaccines are better understood and in principle should provide full protective immunity. Encour-

aging news in this regard comes from Mueller *et al.* reporting in a recent issue of *Nature* (1). They show that mice immunized with genetically attenuated sporozoites of the rodent malaria parasite *Plasmodium berghei* are completely protected against challenge with wild-type sporozoites.

A malaria infection is initiated by injection of sporozoites into the host blood by a female anopheline mosquito as she takes a blood meal (see the figure). The sporozoite must migrate to the liver and colonize a hepatocyte (liver cell) in order for the infection to progress. This journey is hazardous, requiring traversal of resident macrophages (Kupffer cells) lining the liver's blood vessels and passage through a number of hepatocytes before the sporozoite finds a liver cell to invade (see the figure). Here, the sporozoite differentiates, grows, and multiplies within the hepatocyte, producing

thousands of merozoites that are released into the bloodstream where they invade red blood cells, initiating the erythrocytic stage of the disease.

Of the various antimalaria vaccination strategies proposed, preventing the sporozoite from infecting a hepatocyte or blocking its subsequent intracellular development has the advantage of acting before the onset of pathology that is exclusively associated with the erythrocytic stage of infection. However, “pre-erythrocytic” vaccines must be 100% effective because a single surviving sporozoite can still cause a lethal blood-stage infection. In 1967, Nussen-zweig and colleagues (2) generated sterile protective immunity in a mouse model by administering whole *P. berghei* sporozoites that had been attenuated by gamma irradiation. These radiation-attenuated sporozoites (RAS) were incapable of infecting mice, yet when given to mice as a vaccine in a prime-boost combination, they generated long-lasting immunity to subsequent challenge with normal nonirradiated parasites. Immunity results from multifactorial responses that are thought to include sporozoite-specific antibodies, effector CD8⁺ and CD4⁺ T cells, and memory CD8⁺ T cells that recognize the infected hepatocyte (3, 4).

A. P. Waters, M. R. van Dijk, and C. J. Janse are in the Department of Parasitology, Leiden University Medical Centre, Leiden 2300 RC, Netherlands. M. M. Mota is at the Instituto Gulbenkian de Ciência, 2780-156 Oeiras, Portugal. E-mail: a.p.waters@lumc.nl

Subsequent work with the human *Plasmodium* species elicited long-lasting protection (>10 months) in human volunteers in a species-specific (although strain-independent) fashion. However, volunteers had to be immunized with sufficient sporozoites (>1000) of *P. falciparum* (the most lethal species of human malaria parasite), which had to be delivered through the bite of an irradiated infected mosquito. Numerous logistical problems surround human vaccination with RAS. These difficulties encouraged an intensive, but so far disappointing, 25-year search for sporozoite and blood-stage antigens that could be used in a subunit vaccine (5). Now, the tide has turned once more, and there is renewed and vigorous interest in a malaria vaccine comprising an attenuated whole parasite (6).

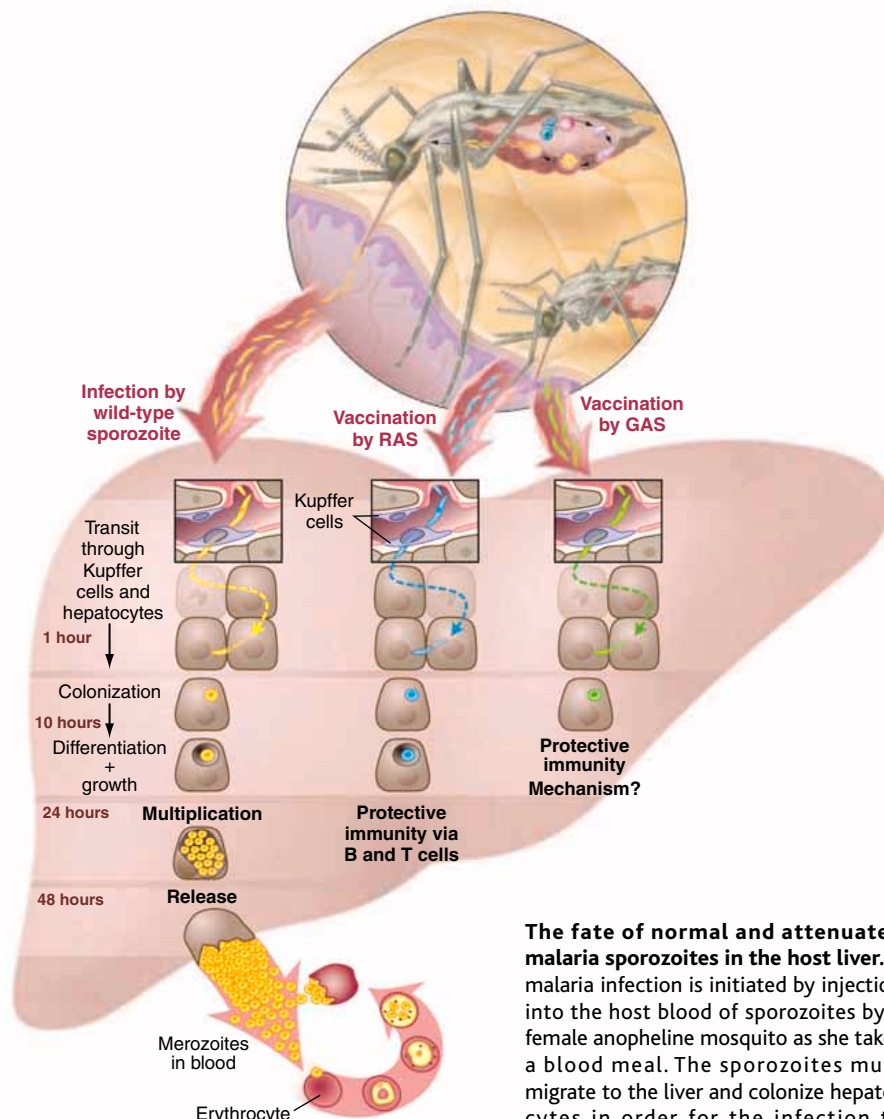
The Mueller *et al.* vaccine study resurrects the principle of RAS immunization but tosses in a twist. These investigators used genetically attenuated sporozoites (GAS) of *P. berghei* (7–9), exploiting the recent availability of complete *Plasmodium* genome sequences. In previous work (10), Mueller *et al.* had used suppression subtractive cDNA hybridization to identify 29 genes whose steady-state mRNA levels were specifically elevated in infectious *P. berghei* sporozoites in the mosquito salivary glands. This set of genes included *uis3* (up-regulated in infectious sporozoites), a small conserved transmembrane protein unique to *Plasmodium*. The UIS3 protein is thought to be located in micronemes, specialized apical secretory organelles that are essential for sporozoite motility and invasion of target cells. Using gene disruption (11), Mueller and colleagues generated a *uis3*-deficient (*uis3*⁻) strain of *P. berghei* sporozoite. The *uis3*⁻ sporozoites were motile and could invade cultured hepatocytes at wild-type efficiencies. In contrast to wild-type sporozoites that invade hepatocytes, grow, and generate merozoites within 48 hours, the mutant sporozoites started to develop and then stopped.

There are differences in growth and development between *uis3*⁻ GAS and their RAS predecessors: RAS are thought to persist within hepatocytes developing very slowly (12, 13), whereas GAS-infected hepatocytes disappear within 24 hours after infection (14). An extensive immunization/challenge study in mice demonstrated that 100% sterile protective immunity effective for at least 1 month could be generated in mice injected with *uis3*⁻ GAS sporozoites using various prime-boost protocols (the second boost was essential for full protection). Because there is an ortholog of *uis3* in *P. falciparum* (PF13_0012), it may be possible to genetically engineer a *P. falciparum* GAS that could be used in a human vaccine.

So why is the demonstration of GAS-induced protective immunity in rodents such a noteworthy advance? The first point is reproducibility. The RAS vaccine relies on irradiation of isolated sporozoites or whole infected mosquitoes with precisely the right dose of radiation—too little and the sporozoites remain fully competent to produce a complete infection; too much, and the sporozoites die and are unable to invade a liver cell and induce a protective immune response. In principle, GAS-based vaccination removes this uncertainty, offering a

standardized, reproducibly attenuated parasite. But having cleared this hurdle, there are still subsequent problems with the preparation and delivery of a GAS-based vaccine.

Currently, the only way to generate GAS (or RAS) is by using infected mosquitoes. Although the parasites can be isolated from the insect for intravenous administration, there are questions about purity. In addition, even if GAS vaccination provoked long-term immunity in humans, it is inconceivable that sufficient numbers of GAS could be produced by insectaries to immunize the



The fate of normal and attenuated malaria sporozoites in the host liver. A malaria infection is initiated by injection into the host blood of sporozoites by a female anopheline mosquito as she takes a blood meal. The sporozoites must migrate to the liver and colonize hepatocytes in order for the infection to progress. This involves traversal of resi-

dent macrophages (Kupffer cells) lining the liver's blood vessels and passage through a number of hepatocytes before invading a hepatocyte and beginning to develop. The sporozoite differentiates, grows, and multiplies within a vacuole in the host hepatocyte, giving rise to thousands of merozoites. These are released into the bloodstream where they invade red blood cells, initiating the erythrocytic stage of the disease. Sporozoites attenuated by irradiation (RAS) or by genetic manipulation (GAS) also transit through Kupffer cells and hepatocytes before invading liver cells. RAS undergo growth arrest but the infected hepatocytes remain intact, leading to the generation of a protective immune response involving B cells that attack free sporozoites and T cells that recognize infected hepatocytes. The intracellular development of GAS is different from that of RAS, as GAS-infected hepatocytes in culture disappear 24 hours after infection; the GAS-induced immune response may also be different.

rural populations of sub-Saharan Africa.

Moreover, we do not yet understand the mechanism of the protective immune response, the nature of the defect in *uis3⁻* GAS, and the role of UIS3 in the intact parasite. Clearly, *uis3⁻* GAS appear to behave differently in cultured hepatocytes than do their RAS counterparts. The possibility that the immune responses provoked by GAS and RAS are distinct is exciting and requires further investigation. The wild-type sporozoite prevents apoptosis of host liver cells that would otherwise result in destruction of the parasite (13). The behavior of *uis3⁻* GAS suggests that some colonized host cells do undergo apoptosis, and indeed evidence from our laboratories with a different gene-deficient GAS indicates that this is the case (15). The possible deleterious consequences to the host of localized hepatocyte apoptosis awaits evaluation. It should also be remembered that many individuals receiving a GAS vaccine are likely to be immunocompromised—thus, the potential for breakthrough infec-

tion with a GAS vaccine must be thoroughly assessed.

Despite this daunting list, the Mueller *et al.* work is the first concrete demonstration, since the introduction of RAS, that full sterilizing immunity against malaria infection can be achieved. *P. falciparum* is amenable to genetic engineering and it should not be too difficult to produce a nonreverting *uis3⁻* *P. falciparum* strain, which would enable a phase I efficacy trial in humans to begin soon. Vaccinating with attenuated infectious agents is as old as vaccination itself, and GAS is merely a new take on the old RAS concept. There is at least one other gene that generates a GAS phenotype when deleted from the wild-type parasite (15), and surely others will be found. GAS vaccine efficacy and safety could be improved by developing more complex GAS strains that lack multiple genes in a single parasite or that have a “GAS mix” containing sporozoites each with a different single-gene deletion. Each form of GAS must be evaluated for its immunization potential and the

best one, or combination, taken forward to human trials. Finally, the availability of attenuated blood-stage *Plasmodium* parasites indicates that an attenuated whole organism approach to malaria vaccination may be applicable to other stages of the life cycle of this vicious parasite.

References

1. A. K. Mueller *et al.*, *Nature* **433**, 164 (2005).
2. R. S. Nussenzweig *et al.*, *Nature* **216**, 160 (1967).
3. P. L. Alonso *et al.*, *Lancet* **364**, 1411 (2004).
4. A. Morrot, F. Zavala, *Immunol. Rev.* **201**, 291 (2004).
5. F. Zavala, *Res. Immunol.* **142**, 654 (1991).
6. T. C. Luke, S. L. Hoffman, *J. Exp. Biol.* **206**, 3803 (2003).
7. M. J. Gardner *et al.*, *Nature* **419**, 498 (2002).
8. J. M. Carlton, *Nature* **419**, 512 (2002).
9. N. Hall, *Science*, **307**, 82 (2005).
10. K. Matuschewski *et al.*, *J. Biol. Chem.* **277**, 41948 (2002).
11. T. F. de Koning-Ward *et al.*, *Annu. Rev. Microbiol.* **54**, 157 (2000).
12. L. F. Scheller, A. F. Azad, *Proc. Natl. Acad. Sci. U.S.A.* **92**, 4066 (1995).
13. P. Leirião *et al.*, *Cell. Microbiol.*, in press
14. A. K. Mueller *et al.*, Molecular Parasitology Meeting, Woods Hole, MA, 19 to 23 September 2004, abstract 5H.
15. M. R. van Dijk *et al.*, unpublished results.

10.1126/science.1108598

PHYSIOLOGY

A NEAT Way to Control Weight?

Eric Ravussin

In a tradition that originated in Babylon 4000 years ago, millions of us make New Year's resolutions. Such resolutions are often to lose weight by exercising more and eating less. No doubt, before January is out, most of us who swore to take a daily walk and pass up that extra snack have slunk back to our old habits. On page 584 of this issue, Levine *et al.* (1) suggest an alternative strategy for weight control. They offer evidence that differences in postural habits account for variations in body weight between the lean and the mildly obese. They propose that fidgeting, may be an unusual method of weight control.

Six years ago, Levine and co-workers introduced to *Science* readers the acronym NEAT, which stands for non-exercise activity thermogenesis (2). NEAT, we were told, is the energy expended by physical activities other than planned exercise—sitting, standing, walking, talking, fidgeting, etc. In their original study, Levine's group reported that equally overfed volunteers gained different amounts of weight, a difference that they explained by an individual's propensity for NEAT (2). Now, in a sequel to this work, Levine *et al.* attempt to pin down the source

of NEAT that accounts for this difference in energy economy (1). These investigators outfitted self-proclaimed “couch potatoes,” both lean and mildly obese, with arrays of inclinometers and triaxial accelerometers that continuously measured body posture and movements for 10 days. The authors' main observation is that obese individuals remained seated for about 2.5 hours per day longer than the lean “couch potatoes,” for an average savings of about 350 kcal/day in energy expenditure (see the figure). As this energy saving was not matched by a similar decrease in energy intake, Levine *et al.* calculate that this economy in energy expenditure would be sufficient for weight gain in the mildly obese.

In an attempt to determine whether this economy of motion is the cause or the consequence of obesity, Levine *et al.* repeated the study. This time, however, obese participants were put on a diet for 2 months and the lean ones were overfed for 2 months, resulting in a loss of 8 kg and a gain of 4 kg, respectively. Although these perturbations were small in magnitude and short in duration, both the lean and obese maintained their original posture measurements. This suggests that sedentary habits are biological rather than environmentally determined.

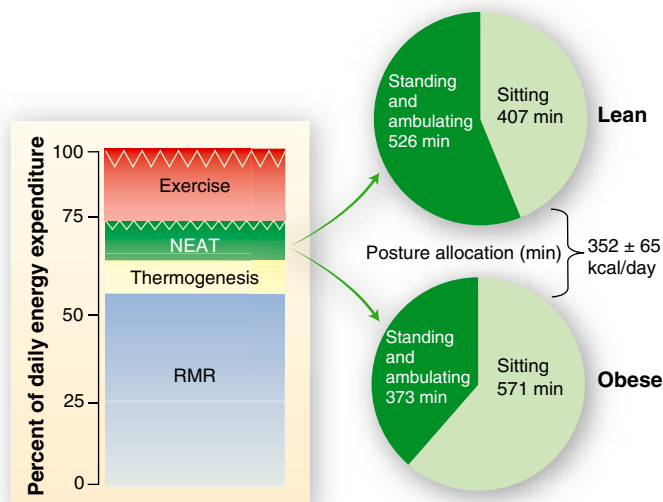
Obesity has reached epidemic proportions in developed societies, and billions of

dollars are spent on diets and health clubs in a failing effort to control weight. Weight gain is a dynamic process that results from a long-term sustained imbalance between energy intake and energy expenditure. The spectacular increase in the prevalence of obesity over the past four decades seems to indicate that environment, rather than biology, drives the epidemic (3). At present, more than two-thirds of Americans are overweight and 25% are obese, and it is expected that the prevalence of obesity in the United States will reach 40% in 2010—and the rest of the world is rapidly catching up.

Although humans have evolved thrifty mechanisms to defend energy stores during times of privation, apparently we have a much harder time preventing the storage of excess energy in times of affluence. Since the Second World War, the food industry has mass-produced increasingly palatable foods (rich in fat and refined carbohydrates) that are easily accessible and inexpensive. This has promoted excessive food intake, discouraged physical activity, and promoted obesity and its related diseases, such as diabetes, dyslipidemia, and cardiovascular disease.

The major culprit, however, is still not entirely clear: Is it increased food intake or decreased physical activity? Population data from Britain suggest that despite a doubling of the prevalence of obesity in the 1980s, the average energy intake actually declined over this period. This suggests that the adoption of a modern inactive life style is at least as important as diet in the etiology of obesity (4, 5). In this regard, it

The author is at the Pennington Biomedical Research Center, Baton Rouge, LA 70808, USA. E-mail: ravusse@pbr.edu



A moratorium on sitting. (Left) Total daily energy expenditure can be divided into three main components: resting metabolic rate (RMR), thermogenesis, and the cost of physical activity, both planned (exercise; red) and unplanned (NEAT; green). RMR represents 50 to 70% of daily energy expenditure and covers the energy necessary for body maintenance, including cellular metabolism and whole-body functions such as ventilation, circulation, and tissue oxygen uptake. RMR seems to be “fixed” for a given person, although it does decline with age. Because humans have evolved behavioral strategies (clothing) to maintain body temperature in cold environments, thermogenesis (yellow) accounts for only 10% of daily energy expenditure and encompasses the energy required to digest, absorb, transport, and store ingested food. This leaves 20 to 40% of daily energy expenditure for the most variable component, physical activity. The energy cost of physical activity can be divided into planned physical activity, such as sport and exercise, and spontaneous physical activity or NEAT, which includes all nonvolitional muscle activities such as fidgeting, muscle tone, and maintenance of posture. When people decide to increase energy expenditure for weight control purposes, usually only structured exercise is included in their calculations. Levine *et al.* propose that concentrating on modifying NEAT behaviors (standing instead of sitting, fidgeting instead of

keeping still, or simply walking) can burn the necessary extra calories to control weight (1, 2). In other words, targeting inactivity may be sufficient to fill the “energy gap” that leads to a creeping up of body weight (6). (Right) Time spent sitting versus standing and ambulating in 20 self-proclaimed “couch potatoes,” both lean (top) and mildly obese (bottom) (7). If the obese volunteers substituted a mere 164 min of sitting for standing or walking around, they would expend an extra 352 kcal/day on average. This could prevent the addition of extra pounds, assuming energy intake is unchanged.

is worth emphasizing that the “energy gap” required to explain the increased prevalence of obesity is only 100 to 200 kcal/day (6). This suggests that a sustained small change in either energy intake or energy expenditure is all that is required to prevent obesity in most of us (see the figure). Therefore, the difference in NEAT observed between obese and lean individuals is significant and implies that obesity might be prevented through simply limiting sedentary activities, or increasing behaviors such as standing, walking, and fidgeting. Indeed, a half-century ago, Widdowson (7) found that fidgeting is important for energy expenditure. In a 1986 study, spontaneous physical activity equivalent to NEAT and measured within the confines of a respiratory chamber accounted for an average energy expenditure of 348 kcal/day (8). The energy cost of

spontaneous physical activity varied among study participants from 100 to 700 kcal/day and accounted for a major portion of individual differences in 24-hour energy expenditure. Interestingly, these values are almost the same as those reported in the Levine *et al.* study in which extra “couch potato” time accounted for energy savings of 352 kcal/day on average.

The underlying mechanisms responsible for an individual’s propensity to fidget are unknown. However, studies in families (9) have shown that although the degree of spontaneous physical activity is highly variable, it is more similar among siblings than among unrelated individuals. This provides indirect evidence for the idea that NEAT is genetically determined. Furthermore, in a prospective study, weight gain was inversely related to the level of NEAT, at least in males (9). Unfortunately, if genes

do determine the true “coach potato,” then encouraging an exchange of time spent sitting for time spent standing, as suggested, is unlikely to help to control body weight. Instead, one could progressively change the environment to discourage sitting behaviors. What Levine and colleagues clearly demonstrate is that small but sustained changes in the activities of daily living can profoundly affect energy balance.

References

1. J.A. Levine *et al.*, *Science* **307**, 584 (2005).
2. J.A. Levine *et al.*, *Science* **283**, 212 (1999).
3. J. O. Hill, J. C. Peters, *Science* **280**, 1371 (1998).
4. A. M. Prentice, S.A. Jebb, *Br. Med. J.* **311**, 437 (1995).
5. M. Hayes *et al.*, *Int. J. Obes. Relat. Metab. Disord.* **29**, 151 (2005).
6. J. O. Hill *et al.*, *Science* **299**, 853 (2003).
7. E. M. Widdowson *et al.*, *Br. J. Nutr.* **8**, 147 (1954).
8. E. Ravussin *et al.*, *J. Clin. Invest.* **78**, 1568 (1986).
9. F. Zullo *et al.*, *Am. J. Physiol.* **263**, E296 (1992).

10.1126/science.1108597

PHYSICS

How to Create a Spin Current

Prashant Sharma

We usually think of a current as a flow of particles, such as the flow of electrons in a charge current generated by a battery. However, besides its charge, the electron also carries a spin, whose projection along the spin axis can point up or down. Conventional electronic devices ignore this property of the electron,

but new devices are now being built that rely on the spin (1, 2). Such devices should have faster switching times and lower power consumption than conventional devices, mainly because spins can be manipulated faster and at lower energy cost than charges can.

All currently available spin-based devices are memory devices that use the spin to store information. Spin-based electronic (spintronic) devices such as transistors (2) require spin currents, just as con-

ventional electronic devices require charge currents. Unfortunately, it is very difficult to generate and transport a spin current.

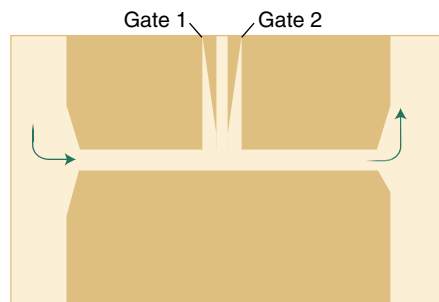
To understand what is meant by a spin current, consider an electron current that flows through a channel and contains only up-spin polarized electrons. Add to this a similar current in which all electrons are down-spin polarized and flow in the opposite direction. The result is a current of spins only; there is no net particle transfer across any cross section of the channel.

A spin current differs from a charge current in two important ways. First, it is invariant under time reversal: If the clock ran backward, spin current would flow in the same direction. Second, spin current is associated with a flow of angular momen-

The author is at Argonne National Laboratory, 9700 South Cass Avenue, Argonne, IL 60439, USA. E-mail: psharma@anl.gov

tum, which is a vector quantity. This feature allows quantum information to be sent across semiconducting structures, just as quantum optics involves distribution of information across optical networks via polarization states of the photon.

Most methods currently under investigation use ferromagnets to inject a spin current into a nonmagnetic material. However, this process is inefficient. For practical



Creating a spin current through spin pumping I. A single channel of electrons is formed in a 2D electron system through electrostatic confinement. When out-of-phase ac voltages are applied to the two gates, the channel is perturbed, resulting in a dc electron current. If one of the gates is replaced by an oscillating magnetic field, a spin current is pumped.

applications, the generation and detection of spin currents should not require strong magnetic fields and interfaces between semiconductors and ferromagnets.

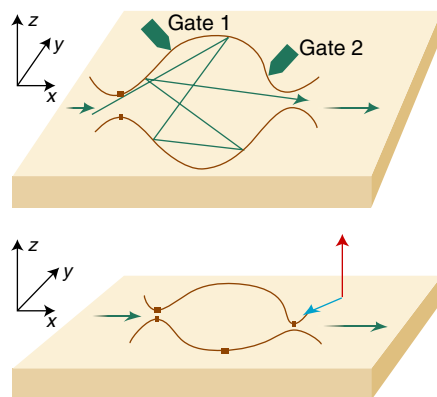
One method that meets these requirements is spin pumping, which involves the scattering of electrons off a small region (a quantum cavity). In the cavity, electrons with different spins take dissimilar paths and therefore scatter differently off the cavity walls. Through modulating the shape of the cavity periodically in time, a constant spin current can be generated.

The theory of pumping electrons without changing their spin state is based on the idea (3) that one can create a traveling wave potential for electrons to ride on. At any moment, the electrons sit in the minima of the wave and move along with it. The efficiency of this mechanism depends on the depth of the traveling wave: The deeper the potential, the greater the chance that the electrons remain trapped and are transported along with the wave.

One practical way to create such a traveling wave is to periodically modulate the transmission of the electron flow at two points in space (4). This can be done by applying two metal gates on a channel (see the first figure) or on a quantum cavity (second figure, top panel). Experimentally, these structures are created in a two-dimensional (2D) layer of electrons (an electron gas), which forms in semiconducting het-

erostructures typically made from GaAs and AlGaAs. Switkes *et al.* have shown experimentally that a quantum cavity can indeed be modulated in time (5).

These ideas have recently been generalized to create spin currents. The earliest proposal (6) was to create a traveling wave for up spin-polarized electrons that is opposite in direction to that for down spin-polarized electrons. Creation of such spin-select-



Creating a spin current through spin pumping II. (Top) A quantum cavity is perturbed through out-of-phase ac voltages applied to the two gates. Electrons entering the cavity scatter off the cavity walls several times before leaving. **(Bottom)** In a sufficiently large cavity, pumping leads to a spin current with a tunable direction of spin polarization. Both in-plane (green arrow) and out-of-plane (red arrow) polarizations are possible.

tive traveling waves requires the use of some externally controllable mechanism to break spin-rotation symmetry—that is, to define a unique spin axis in space. This can be achieved by replacing one of the metal gates in the first figure with an external, time-dependent magnetic field. To obtain efficient spin transport, one must increase the depth of the minima in the traveling waves by restricting the electrons to a long narrow channel—a quantum wire (7)—such that they repel each other.

However, the picture of a single traveling wave is inadequate for describing pumping in a finite cavity, because the electron follows a complicated path before exiting the cavity. The direction of the current is therefore determined by the details of the scattering in the cavity (8). This sensitivity to the electron's path in the cavity is an essential feature of mesoscopic semiconductor devices, which can be up to several tens of micrometers in size.

In a theoretical proposal (9) for spin pumping, this dependence of the current through the cavity on externally controllable parameters is used to generate a spin current. The proposal is to modulate the

shape of a quantum cavity through the use of two magnetic fields. A strong magnetic field applied in the plane of the cavity (see the second figure, top panel) couples only to the spin of the electrons. For such a strong in-plane magnetic field, there are more up-spin electrons (whose spins are aligned with the magnetic field) than down-spin ones inside the cavity. As a result, the pumped current is spin-polarized along the direction of the strong magnetic field and in the cavity plane; that is, it is a mixed charge and spin current.

To achieve only a spin current, a second, weak magnetic field is added. The field is weak enough not to affect the spin of an electron, but the Lorentz force exerted by this field affects the spatial motion of the charged electrons. One would therefore expect (on average) the up-spin charge current to flow in one direction while the down-spin charge current flows in the opposite direction. Spin currents have recently been produced experimentally with such a device (10).

An alternative to using magnetic fields in the cavity has also been proposed (11). It is based on the fact that the spin state of an electron moving inside a semiconductor is not independent of its momentum state. Because the quantum cavity is formed in a semiconductor—typically a GaAs/AlGaAs heterostructure—the spin of the electron is coupled to its motion inside the cavity. Because of this spin-orbit coupling, the direction of the spin of an electron follows the electron's motion. As a result, the direction of the spin polarization coming out of the cavity depends on the details of the scattering in the cavity (12). By increasing the number of times an electron scatters off the cavity walls, the in-plane spin projection of the electron can be made small, and its spin can be made to point in a direction perpendicular to the plane of the electron gas (see the second figure).

This approach should allow spin currents to be pumped through a quantum cavity without an in-plane magnetic field. Because of spin-orbit coupling, the outgoing current will be spin-polarized. By either applying a weak perpendicular magnetic field [as in the experiments in (10)] or by inducing small changes in the density of electrons in the cavity, a pure spin current can be obtained. In this method of pumping, the direction of polarization of the spin current can be changed from in-plane to out-of-plane by altering the shape and size of the quantum cavity (second figure, bottom panel). The approach has not yet been realized experimentally.

Spin pumping in mesoscopic systems allows the spin-polarization direction of currents to be manipulated without the use

of strong magnetic fields and ferromagnets. However, some experimental challenges remain before this method is ready for use in actual spintronic devices. One difficulty lies in efficiently detecting spin currents whose polarization direction is arbitrary.

Spin currents polarized in the plane of the 2D electron system have been detected electrically (10). Out-of-plane polarization in a 2D electron system may be detected (11) via the spin Hall effect. Because of this effect, an electron with its spin polarized perpendicular to its momentum is deflected in a direction orthogonal to both its momentum and its spin. Reversing the direction of either the momentum or the spin polarization reverses the direction of deflection. As a result, a spin

current with an out-of-plane polarization generates a transverse electric field in a material that shows the spin Hall effect. Recently, the spin Hall effect has been observed for the first time in a semiconducting GaAs/InGaAs heterostructure (13).

We have yet to create a spin pump that can generate spin currents with any chosen direction of spin polarization. Nonetheless, recent experimental and theoretical advances give hope that devices relying on spin currents will soon be realized.

References

1. S. A. Wolf *et al.*, *Science* **294**, 1488 (2001).
2. I. Zutic, J. Fabian, S. Das Sarma, *Rev. Mod. Phys.* **76**, 323 (2004).

3. D. J. Thouless, *Phys. Rev. B* **27**, 6083 (1983).
4. B. L. Altshuler, L. I. Glazman, *Science* **283**, 1864 (1999).
5. M. Switkes *et al.*, *Science* **283**, 1905 (1999).
6. P. Sharma, C. Chamon, *Phys. Rev. Lett.* **87**, 096401 (2001).
7. T. Giamarchi, *Quantum Physics in One Dimension* (Clarendon, Oxford, 2004).
8. P. W. Brouwer, *Phys. Rev. B* **58**, 10135 (1998).
9. E. R. Mucciolo, C. Chamon, C. Marcus, *Phys. Rev. Lett.* **89**, 146802 (2002).
10. S. K. Watson, R. M. Potok, C. M. Marcus, V. Umansky, *Phys. Rev. Lett.* **91**, 258301 (2003).
11. P. Sharma, P. W. Brouwer, *Phys. Rev. Lett.* **91**, 166801 (2003).
12. I. L. Aleiner, V. I. Fal'ko, *Phys. Rev. Lett.* **87**, 256801 (2001).
13. Y. K. Kato, R. C. Myers, A. C. Gossard, D. D. Awschalom, *Science* **306**, 1910 (2004).

10.1126/science.1099388

ASTRONOMY

The Hunt for Intermediate-Mass Black Holes

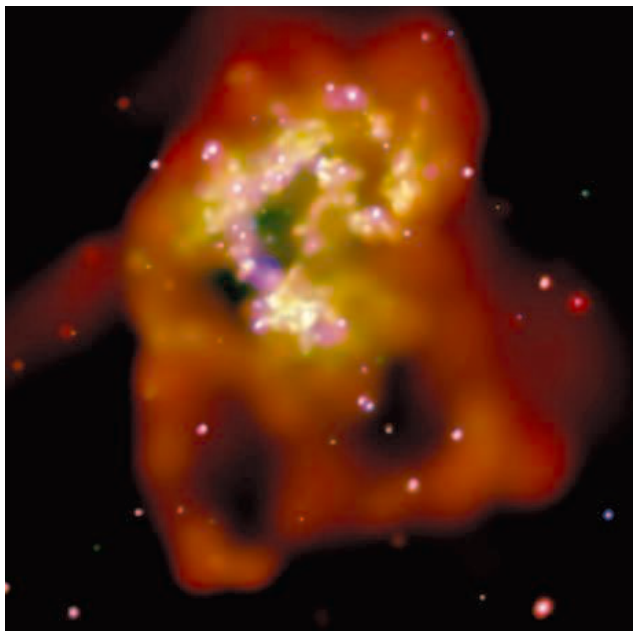
Giuseppina Fabbiano

All known black holes fall into two classes. Stellar black holes are born in the collapse of massive stars and have masses several times that of the Sun. They were discovered thanks to the x-ray emission that arises from the accretion of the outer layers of a nearby orbiting star. Supermassive black holes such as quasars have masses of millions to billions of solar masses. They are ubiquitous in elliptical galaxies and galaxy bulges. Our own Milky Way hosts both stellar black holes and a nuclear supermassive black hole.

Why have no black holes with intermediate masses of hundreds to tens of thousands of solar masses been found to date? Such black holes are thought to be produced by primordial collapse in the early universe (1) and by the gravitational collapse of the cores of dense star clusters in galaxies (2). Some astronomers have suggested that ultraluminous x-ray sources (see the figures) (3) may be the elusive intermediate-mass black holes (4, 5), but the evidence to date is inconclusive.

Ultraluminous x-ray sources are rare, pointlike x-ray sources found in galaxies farther away than our own Milky Way and its companion galaxy, Andromeda. Their x-ray luminosities are 10 to 1000 times the "Eddington luminosity" of a normal x-ray binary containing a neutron star; such binaries are the most common x-ray source in

galaxies. (The Eddington luminosity is the maximum luminosity achievable by a black hole powered by accretion from a companion star.) Ultraluminous x-ray sources are thus exceptionally bright objects, which might be powered by accretion onto black holes with masses of a few hundred solar masses or more. They could represent the missing mass range in the black hole mass distribution. But do they?



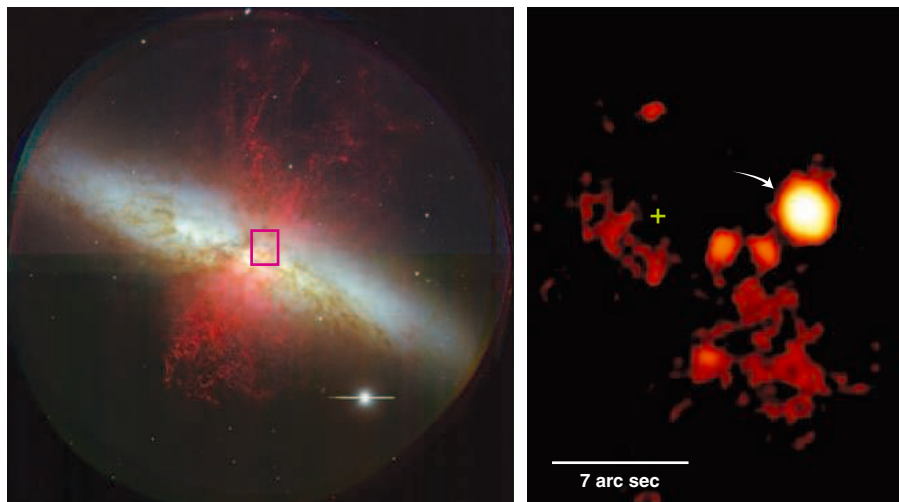
An abundance of ultraluminous x-ray sources. In this Chandra image of the "Antennae," the 14 most luminous sources are ultraluminous x-ray sources.

In the past few years, observations with NASA's Chandra x-ray observatory and the European Space Agency's XMM-Newton have greatly increased the number of known ultraluminous x-ray sources and have further elucidated their properties. The data have rekindled the debate on what these sources might be. The main alternative to intermediate-mass black holes is that they are normal black-hole x-ray binaries that only appear to exceed the Eddington luminosity because of direction-dependent (beamed) emission (6, 7). It has also been suggested that the ultraluminous x-ray emission is caused by inhomogeneities in the accretion disk, which would allow the Eddington limit to be exceeded (8).

Although the intermediate-mass black hole hypothesis has not been disproved, it is not needed to explain most of the data. Stellar-evolution calculations can account for black holes as massive as 70 solar masses, placing the fainter ultraluminous x-ray sources in the realm of stellar black holes. Evolutionary calculations of x-ray binaries can also produce luminosities in the range observed for ultraluminous x-ray sources (9). Only the brightest ultraluminous x-ray sources cannot be explained by the Eddington emission of a stellar black hole.

Variations in the intensity and color of ultraluminous x-ray sources (10) are also consistent with x-ray binaries, but this behav-

The author is at the Harvard-Smithsonian Center for Astrophysics, Cambridge, MA 02138, USA. E-mail: pepi@head.cfa.harvard.edu



The best candidate for an intermediate-mass black hole. Optical (left) and Chandra x-ray (right) images of the M82 galaxy. The arrow points to the location of the ultraluminous x-ray source that is likely to be an intermediate-mass black hole. The area covered by the right image lies within the rectangle at the center of the left image. The green cross (right image) is the galaxy nucleus.

ior does not constrain the mass of the object. In a few cases, optical and radio sources have been found in the positions of the ultraluminous x-ray sources, but they have been used to advocate both intermediate-mass black holes and beamed high-accretion binaries. However, many ultraluminous x-ray sources are found just outside star clusters, as expected for stellar black holes that were born in a supernova of a binary star; the energy of the explosion is expected to propel the black hole from its birth place (11).

Chandra observations have been crucial for explaining how ultraluminous x-ray sources relate both to the overall x-ray binary population of their parent galaxy and to the underlying stellar population. The data show that ultraluminous x-ray sources are associated with young stellar populations and are particularly numerous in galaxies with a high rate of star formation. A particularly stunning example is the galaxy pair NGC 4038/39, also known as the “Antennae.” This pair is undergoing a merger that has triggered a burst of star formation. In the Antennae, about 14 ultraluminous x-ray sources have been discovered (see the first figure) (12); normal spiral galaxies typically contain just one or two such sources.

The luminosity distribution of x-ray sources in the Antennae and other star-forming galaxies suggests a smooth transition from normal x-ray binaries to ultraluminous x-ray sources. These results are consistent with the hypothesis that ultraluminous x-ray sources are an integral part of the x-ray binary population and that the underlying objects are therefore stellar rather than intermediate-mass black holes. However, there is still some uncertainty, because the number of known sources at higher luminosities is too small to exclude the possibil-

ity that the luminosity distribution contains hidden breaks. Another argument against the intermediate-mass black hole hypothesis is given by the comparison of star-forming spiral galaxies and elliptical galaxies, which have older stellar populations. If there is a population of intermediate-mass black holes in galaxies, either from primordial collapse or from stellar cluster collapse, then one would expect all massive elliptical galaxies to have their share of ultraluminous x-ray sources, contrary to observations. However, nothing is simple in astronomy: Isolated intermediate-mass black holes may only be visible as ultraluminous x-ray sources when there is enough fuel around, and this fuel, in the form of dense clouds, is more plentiful in star-forming galaxies.

XMM-Newton is also contributing to the debate. This satellite does not have the angular resolution and sensitivity of Chandra, but it has a larger telescope area. For nearby ultraluminous x-ray sources, astronomers can thus collect spectra of very high quality and gain insights into short-term variability. The observations provide some evidence in support of intermediate-mass black holes.

XMM-Newton spectra of a few ultraluminous x-ray sources have shown evidence for low-energy (soft) spectral emissions that could be caused by accretion disks orbiting an intermediate-mass black hole (13). The more massive the black hole, the larger the inner stable orbit of the accretion disk; as a result of this geometry, the energy released by the disk per unit area is reduced, even though the total source luminosity increases. Hence, larger intermediate-mass black holes will have cooler disks than stellar black holes do, giving rise to the soft spectral components.

However, even in these cases, the debate is still open. Soft components have been reported for very few, extremely bright ultraluminous x-ray sources (other examples may still be hidden in the XMM-Newton archive). Differences in the luminosity-temperature properties of ultraluminous x-ray sources and stellar black holes have been cited in support of the intermediate-mass black holes, although the same authors note that hot-plasma emission in the vicinity of ultraluminous x-ray sources may be responsible for some of these differences (14).

By far the best candidate for an intermediate-mass black hole is an ultraluminous x-ray source in the galaxy M82 (see the second figure). The luminosity of this source exceeds by a factor of at least 1000 the Eddington luminosity of a one-solar-mass object. The surroundings of the source suggest isotropic emission, ruling out a beamed source. Its XMM-Newton spectrum and the pattern of its variability strongly support emission from an accretion disk surrounding an intermediate-mass black hole (15). This black hole could be the result of a collapsed star cluster in M82 (2) or the nucleus of a satellite galaxy captured by M82 (16).

The quest for intermediate-mass black holes is not over, in part because the nature of ultraluminous x-ray sources remains unclear. Perhaps we should not put all of them in just one category. After all, the definition of an ultraluminous x-ray source is an observational one. It could well be that this is a diverse group of sources, most of which may just be x-ray binaries in a particular state of their evolution. But some extremely bright sources may indeed be intermediate-mass black holes.

References

1. P. Madau, M. J. Rees, *Astrophys. J.* **551**, L27 (2001).
2. S. Portegies Zwart, H. Baumgardt, P. Hut, J. Makino, S. McMillan, *Nature* **428**, 724 (2004).
3. G. Fabbiano, N. E. White, in *Compact Stellar X-ray Sources*, W. H. G. Lewin, M. van der Klis, Eds. (Cambridge Univ. Press, Cambridge, in press); preprint available at <http://arxiv.org/abs/astro-ph/0307077>.
4. E. J. Colbert, R. F. Mushotzky, *Astrophys. J.* **519**, 89 (2001).
5. K. Makishima *et al.*, *Astrophys. J.* **535**, 632 (2000).
6. A. R. King *et al.*, *Astrophys. J.* **552**, L109 (2001).
7. E. Koerding, H. Falke, S. Markoff, *Astron. Astrophys.* **382**, L13 (2002).
8. M. C. Begelman, *Astrophys. J.* **568**, L97 (2002).
9. Ph. Podsiadlowski, S. Rappaport, E. Pfahl, *Rev. Mex. Astron. Astrofis. (Ser. Conf.)* **20**, 97 (2004).
10. G. Fabbiano *et al.*, *Astrophys. J.* **584**, L5 (2003).
11. P. Kaaret *et al.*, *Mon. Not. R. Astron. Soc.* **348**, L28 (2004).
12. A. Zezas *et al.*, in preparation.
13. J. M. Miller, G. Fabbiano, M. C. Miller, A. C. Fabian, *Astrophys. J.* **585**, L37 (2003).
14. J. M. Miller, A. C. Fabian, M. C. Miller, *Astrophys. J.* **614**, L117 (2004).
15. T. E. Strohmayer, R. F. Mushotzky, *Astrophys. J.* **586**, L61 (2003).
16. A. R. King, W. Dehnen, *Mon. Not. R. Astron. Soc.*, in press.

Address: <http://www.sciencemag.org/books>

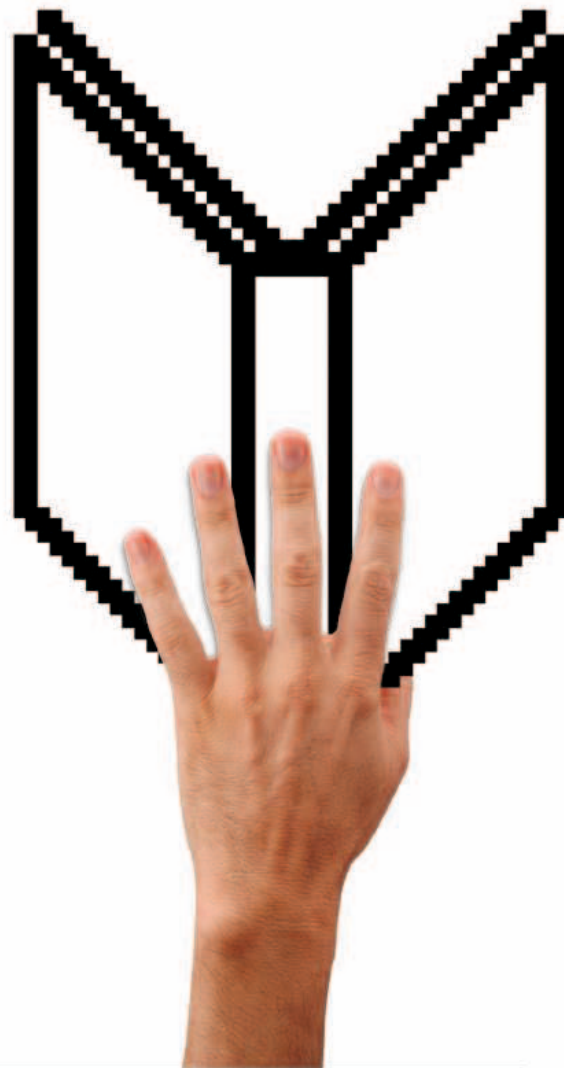
Q Where can you review new scientific books, et cetera?

A Books et al. at www.sciencemag.org/books

Read *Science's* weekly reviews of current books in all fields of science and place orders online. Peruse past reviews sorted by title, author, reviewer, and date of publication.

If you are looking for recommendations on print, audiovisual, and electronic learning tools – check out *Science Books & Films Online*.

Not a member of AAAS? Sign up today, for *Science* et cetera, books et al., and other benefits: www.aaas.org/join



Science, published by AAAS, with over 700,000 readers weekly, is the world's most widely-read general science journal. Scientists around the world submit over 12,000 papers each year for evaluation, with only one in 12 making it into final publication. This rigorous process ensures the quality of material, whether it's research on proteomics, therapeutic cloning, nanotechnology, or dark matter. To find out how to subscribe to *Science*, go to www.aaas.org/join





FOURTH ANNUAL
**PHARMACEUTICAL
 ACHIEVEMENT
 AWARDS** August 8, 2005
 State Room, Boston, MA

The Pharmaceutical Achievement Awards are comprised of eighteen high-level awards that honor industry and academic achievement in pharmaceutical science, world health and community involvement, corporate governance, and marketing. Honorees will be determined through a comprehensive international nomination process and winners selected by a cross-industry Executive Review Board. For more information about the event and the Executive Review Board, visit: www.pharmawards.com.

Nominations Are Now Being Accepted!

The nominations period for the Awards will run between now and March 30, 2005. At that time no further nominations will be accepted. The final ballot will result in the winners to be announced at the gala awards dinner. Nomination forms can be downloaded via the event website only: www.pharmawards.com

Featured Awards

WORLD HEALTH AND COMMUNITY INVOLVEMENT CATEGORY

Corporate Community Partner Award
 Award for Therapeutic Development in the Cause of World Health
 Award for Disease Prevention and Education

SCIENTIFIC ACHIEVEMENT CATEGORY

Lifetime Achievement Award
 Chief Scientific Officer of the Year
 Industry Scientist of the Year
 Academic Scientist of the Year

RESEARCH AND DEVELOPMENT CATEGORY

Outstanding Small Molecule Drug Product Award
 Outstanding Biologic Drug Product Award
 Innovative Pharmaceutical Product Award
 Rare Diseases and Conditions Award

PHARMACEUTICAL BUSINESS CATEGORY

Chief Executive Officer of the Year
 Emerging Company Executive of the Year
 Social Responsibility Award
 Business Development Deal of the Year

PHARMACEUTICAL MARKETING CATEGORY

Product Launch of the Year
 Direct to Consumer Campaign of the Year
 Marketing Campaign of the Year

Media Sponsor



part of T&F Informa plc

Cambridge Healthtech Institute Presents....



May 24-26, 2005
 Pennsylvania Convention Center
 Philadelphia, Pennsylvania



Cambridge Healthtech Institute
 1037 Chestnut Street
 Newton Upper Falls, MA 02464

The Premier Pharmaceutical R&D event of the year!

Concurrent Tracks:

Cell-Based Assays for HTS

Cheminformatics

Hit-to Lead

Driving DMPK

Drug Formulation

R&D Strategies



Register by March 1st and save \$300

**Reference Priority Code ADL35 when registering online at
www.WorldPharmaCongress.com**



INTERNATIONAL

AAAS Plays Key Role in U.S.-UNESCO Renewal

Twenty years after the United States left UNESCO, AAAS is playing a central role in building a renewed relationship and in encouraging the American science and technology (S&T) community to be more deeply involved with the international body.

In November, U.S. Secretary of State Colin Powell named AAAS to help represent S&T interests on the new United States National Commission for the United Nations Educational, Scientific and Cultural Organization, formed after President George W. Bush moved to rejoin UNESCO in 2003. That followed an international conference organized by AAAS last June, which brought officials from the United States and around the world to UNESCO headquarters in Paris for discussions on improving science education.

And at its annual meeting in Washington, D.C., next month, AAAS will host top officials for a symposium on the future of U.S.-UNESCO relations.

“Since the United States’ return to UNESCO in October 2003, interest among Americans in the work of UNESCO has been tremendous,” said Louise Oliver, the U.S. ambassador to the organization. “Although UNESCO is an inter-governmental organization, it works closely with members of the civil societies of its member states. That is why I am so pleased that we now have a national commission, and I am even more pleased that one of the key members of the commission will be the AAAS. I am confident that the AAAS will bring vast and valuable expertise to UNESCO’s crucial science and education sectors.”

Powell expressed a similar sentiment in a 15 November 2004 letter to Alan I. Leshner, CEO of AAAS and executive publisher of the journal *Science*. Leshner will represent AAAS on the commission.

Powell, who was expected to step down in late January, appointed the commission to provide the U.S. government with advice and to serve as a liaison with groups interested in UNESCO’s work. “AAAS not only has broad reach into S&T programs and communities,” Leshner said, “but it also has long experience in policy, education and media relations of concern to the commission’s work.”

UNESCO was founded in 1945, just after the end of World War II, to encourage collaboration among nations on education, science, and culture. The United States left the organization in December 1984, citing its increasingly ideological agenda and financial mismanagement.

Even then, AAAS remained engaged with the organization in areas such as science and engineering education, women in science, and sustainable development.

In announcing plans to rejoin, President Bush acknowledged UNESCO’s reforms and expressed a desire to collaborate in its efforts “to expand and improve education, promote scientific progress and press freedom, enhance understanding, and protect cultural heritage worldwide.”

The National Commission was established on 20 October 2004. The current members—nearly 90 in all—include public officials, private citizens, and nongovernmental organizations that span the spectrum of American science, culture, and education groups (see www.state.gov/p/io/unesco/).

In December, AAAS’s Consortium of Affiliates for International Programs convened a roundtable on developing the



Flags of member states of UNESCO.

commission’s agenda. “One reason we had this meeting is that many of the professional societies want to make sure that we don’t lose momentum in the activities ongoing while the commission is getting organized,” said Shere Abbott, chief international officer at AAAS.

At the AAAS Annual Meeting, the three-hour symposium “UNESCO: Opportunities Upon U.S. Reentry” is scheduled for Saturday, 19 February 2005, at 2 p.m. It will feature Ambassador Oliver as well as top officials from the State Department, the U.S. National Academy of Sciences, and AAAS, among others. For further information, see http://php.aaas.org/meetings/MPE_01.php.

AAAS

Call for Nomination of AAAS Fellows

AAAS Fellows who are current members of the Association are invited to nominate members for election as Fellows. A Fellow is defined as “a Member whose efforts on behalf of the advancement of science or its applications are scientifically or socially distinguished.” A nomination must be sponsored by three AAAS Fellows, two of whom must have no affiliation with the nominee’s institution.

Nominations undergo review by the Steering Groups of the Association’s sections (the Chair, Chair-Elect, Retiring Chair, Secretary, and four Members-at-Large of each section). Each Steering Group reviews only those nominations designated for its section. Names of Fellow nominees who are approved by the Steering Groups are presented to the AAAS Council for election.

Nominations with complete documentation must be received by 13 May 2005. Nominations received after that date will be held for the following year. The nomination form and a list of current AAAS Fellows can be found on the AAAS Web site at www.aaas.org/about/aaas_fellows. To request a hard copy of the nomination form, please contact Linda McDaniel at the AAAS Executive Office, 1200 New York Avenue, N.W., Washington, DC 20005, at 202-326-6635, or at Lmcdanie@aaas.org.

CREDIT: UNESCO/DOMINIQUE ROGER

AAAS NEWS AND NOTES

Quantum Dots for Live Cells, in Vivo Imaging, and Diagnostics

X. Michalet,^{1*} F. F. Pinaud,^{1*} L. A. Bentolila,¹ J. M. Tsay,¹ S. Doose,^{1†} J. J. Li,¹ G. Sundaresan,² A. M. Wu,² S. S. Gambhir,^{2,4} S. Weiss^{1,3*}

Research on fluorescent semiconductor nanocrystals (also known as quantum dots or qdots) has evolved over the past two decades from electronic materials science to biological applications. We review current approaches to the synthesis, solubilization, and functionalization of qdots and their applications to cell and animal biology. Recent examples of their experimental use include the observation of diffusion of individual glycine receptors in living neurons and the identification of lymph nodes in live animals by near-infrared emission during surgery. The new generations of qdots have far-reaching potential for the study of intracellular processes at the single-molecule level, high-resolution cellular imaging, long-term in vivo observation of cell trafficking, tumor targeting, and diagnostics.

The improved resolution, sensitivity, and versatility of fluorescence microscopy (1) and the development of fluorescent sensors and labeling of proteins in live cells have yielded a clearer understanding of the dynamics of intracellular networks, signal transduction, and cell-cell interaction (2). However, the monumental task of elucidating the role of all proteins and their mutual interactions in a given organism—that is, completing its proteome and its interactome—will require new approaches and tools. Single-molecule methods (3) will play a major role in this endeavor, but the complex milieu encountered inside live cells requires substantial adaptations of current in vitro techniques. Two problems associated with fluorescence microscopy—cell autofluorescence in the visible spectrum (which can mask signals from labeled molecules) and the requirement of long observation times—have created a need for new probes that emit in the near-infrared (NIR) region (wavelength >700 nm) and are more photostable than current organic fluorophores.

¹Department of Chemistry and Biochemistry, University of California, 607 Charles E. Young Drive East, Los Angeles, CA 90095, USA. ²Crump Institute for Molecular Imaging, Department of Molecular and Medical Pharmacology, ³Department of Physiology, David Geffen School of Medicine, University of California, 700 Westwood Plaza, Los Angeles, CA 90095, USA. ⁴Department of Radiology and Bio-X Program, Molecular Imaging Program at Stanford (MIPS), Stanford University School of Medicine, Stanford, CA 94305, USA.

*To whom correspondence should be addressed. E-mail: michalet@chem.ucla.edu (X.M.); fpinaud@chem.ucla.edu (F.F.P.); sweiss@chem.ucla.edu (S.W.)
†Present address: Angewandte Laserphysik & Laserspektroskopie, Universität Bielefeld, Universitätsstr. 25, 33615 Bielefeld, Germany.

Properties of Qdots

Several characteristics distinguish qdots from the commonly used fluorophores. [A more detailed description of qdot properties can be found in (4) and references listed in the online supplement.] Colloidal semiconductor quantum dots are single crystals a few nanometers in diameter whose size and shape can be precisely controlled by the duration, temperature, and ligand molecules used in the synthesis (4). This process yields qdots that have composition- and size-dependent absorption and emission (Fig. 1A). Absorption of a photon with energy above the semiconductor band gap energy results in the creation of an electron-hole pair (or exciton). The absorption has an increased probability at higher energies (i.e., shorter wavelengths) and results in a broadband absorption spectrum, in marked contrast to standard fluorophores (Fig. 1B). For nanocrystals smaller than the so-called Bohr exciton radius (a few nanometers), energy levels are quantized, with values directly related to the qdot size (an effect called quantum confinement, hence the name “quantum dots”) (4). The radiative recombination of an exciton [characterized by a long lifetime, >10 ns (5)] leads to the emission of a photon in a narrow, symmetric energy band (Fig. 1), another difference from the red-tailed emission spectra and short lifetimes of most fluorophores. The long fluorescence lifetime of qdots enables the use of time-gated detection (6) to separate their signal from that of shorter lived species (such as background autofluorescence encountered in cells).

Surface defects in the crystal structure act as temporary “traps” for the electron or hole, preventing their radiative recombination. The alternation of trapping and untrapping events

results in intermittent fluorescence (blinking) visible at the single-molecule level (7) and reduces the overall quantum yield, which is the ratio of emitted to absorbed photons. One way to overcome these problems, and to protect surface atoms from oxidation and other chemical reactions, is to grow a shell of a few atomic layers of a material with a larger band gap on top of the nanocrystal core. This shell can be designed carefully to obtain quantum yields close to 90% (8); this step also enhances qdots’ photostability by several orders of magnitude relative to conventional dyes (9).

Single qdots can be observed and tracked over an extended period of time (up to a few hours) with confocal microscopy (10), total internal reflection microscopy (11, 12), or basic wide-field epifluorescence microscopy (12–14). Single-molecule studies of qdots have revealed phenomena hidden in ensemble measurements, such as blinking (7), spectral jumps (15), or the existence of multiple long fluorescence lifetimes (16). Single-molecule microscopy is possibly one of the most exciting new capabilities offered to the biologist, as discussed below. A related technique, fluorescence correlation spectroscopy, has allowed determination of the brightness per particle and also provides a measurement of the average qdot size (17, 18) (see Fig. 1C for a comparison scale).

Qdots are also excellent probes for two-photon confocal microscopy because they are characterized by a very large absorption cross section (17). Naturally, they can be used simultaneously with standard dyes. In particular, qdots have a largely untapped potential as customizable donors of a fluorescence resonance energy transfer (FRET) pair (19).

Qdot Solubilization and Functionalization

Qdots are mostly synthesized in nonpolar organic solvents. If they are to be solubilized in aqueous buffers, their hydrophobic surface ligands must be replaced by amphiphilic ones. Different qdot solubilization strategies have been devised over the past few years (Fig. 2), including (i) ligand exchange with simple thiol-containing molecules (20, 21) or more sophisticated ones such as oligomeric

phosphines (22), dendrons (23), and peptides (24); (ii) encapsulation by a layer of amphiphilic diblock (25) or triblock copolymers (26) or in silica shells (27, 28), phospholipid micelles (29), polymer beads (30), polymer shells (31), or amphiphilic polysaccharides (32); and (iii) combinations of layers of different molecules conferring the required colloidal stability to qdots (9, 33). Recent developments include a promising water-based synthesis method (34, 35) that yields particles that emit from the visible to the NIR spectrum and are intrinsically water-soluble, but the particles have yet to be tested in biological environments.

Unless used as a nonspecific fluorescent stain, qdots require some sort of biological “interfacing.” For simple applications such as qdot tagging of a target molecule, a single recognition moiety can be grafted to the qdot (e.g., DNA oligonucleotide or aptamer, antibody, etc.) or, simpler yet, used as the qdot solubilization ligand (36). Qdot ligands containing either an amine or a carboxyl group, for instance, offer the possibility of cross-linking molecules containing a thiol group (29, 37, 38) or an *N*-hydroxysuccinimyl ester moiety (24, 27) by means of standard bioconjugation reactions. Another approach uses electrostatic interactions between qdots and charged adapter molecules, or between qdots and proteins modified to incorporate charged domains (39). These functionalization steps can be repeated to add or change functionality. For instance, streptavidin-coated qdots can be used in combination with biotinylated proteins or antibodies (13, 24, 25, 40, 41). By extension, a generic three-layer approach [using (i) an antibody against a specific target, (ii) a biotinylated secondary antibody against the first, and (iii) a streptavidin-coated qdot] allows qdot labeling of most types of target (13, 25).

The large number (10 to 100) of potential surface attachment groups can be used to “graft” different functionalities to individual qdots, resulting in multipotent probes. For instance, in addition to a recognition moiety, qdots can be equipped with a membrane-crossing or cell-internalization capability, and/or an enzymatic function. The production of biologically synthesized qdots consisting of CdS cores coated by natural peptides (42) led us to investigate the peptide-coating

approach for the surface modification of qdots (Fig. 2B). Peptides have the advantage of being easily customized, and with the correct choice of sequence, a single-step surfactant exchange can yield all necessary functions: (i) Protect the core/shell structure and maintain the original qdot photophysics, (ii) solubilize qdots, (iii) provide a biological interface, and (iv) allow the incorporation of multiple functions. The resulting particles have excellent colloidal properties, photophysics, and biocompatibility, and this “peptide toolkit” can easily be tailored to provide additional functionalities. Such functionalities can be improved by molecular evolution, a strategy that has proven extremely powerful for the recognition, synthesis, and self-assembly of nanocrystals (43).

Qdots in Cell Biology

Over the past few years, qdots have been tested in most biotechnological applications that use fluorescence, including DNA array

technology, immunofluorescence assays [reviewed in (44)], and cell and animal biology. Some of the early and most successful uses of qdots have been in immunofluorescence labeling of fixed cells and tissues; immunostaining of membrane proteins (9, 25, 37, 45, 46), microtubules (25), actin (25, 27), and nuclear antigens (25); and fluorescence in situ hybridization on chromosomes (21, 47, 48) or combed DNA (11). Qdots tend to be brighter than dyes because of the compounded effects of extinction coefficients that are an order of magnitude larger than those of most dyes (29, 49), comparable quantum yield, and similar emission saturation levels (18). But their main advantage resides in their resistance to bleaching over long periods of time (minutes to hours), allowing the acquisition of images that are crisp and well contrasted. This increased photostability is especially useful for three-dimensional (3D) optical sectioning, where a major issue is bleaching of fluorophores during acquisi-

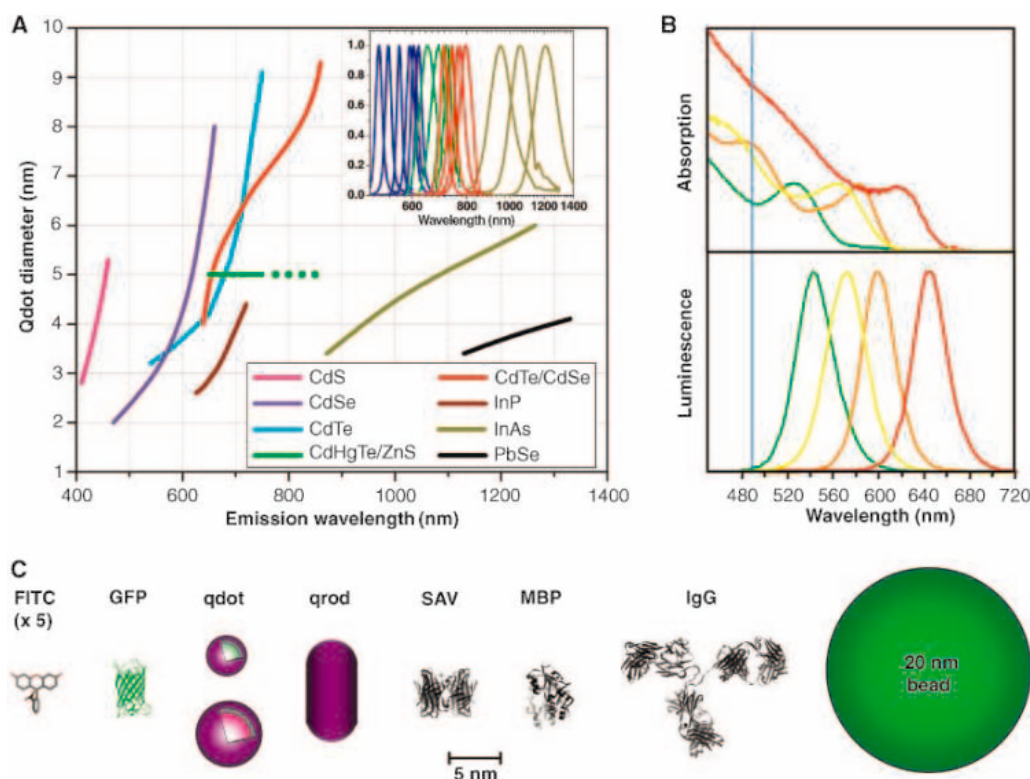


Fig. 1. (A) Emission maxima and sizes of quantum dots of different composition. Quantum dots can be synthesized from various types of semiconductor materials (II-VI: CdS, CdSe, CdTe...; III-V: InP, InAs...; IV-VI: PbSe...) characterized by different bulk band gap energies. The curves represent experimental data from the literature on the dependence of peak emission wavelength on qdot diameter. The range of emission wavelength is 400 to 1350 nm, with size varying from 2 to 9.5 nm (organic passivation/solubilization layer not included). All spectra are typically around 30 to 50 nm (full width at half maximum). Inset: Representative emission spectra for some materials. Data are from (12, 18, 27, 76–82). Data for CdHgTe/ZnS have been extrapolated to the maximum emission wavelength obtained in our group. (B) Absorption (upper curves) and emission (lower curves) spectra of four CdSe/ZnS qdot samples. The blue vertical line indicates the 488-nm line of an argon-ion laser, which can be used to efficiently excite all four types of qdots simultaneously. [Adapted from (28)] (C) Size comparison of qdots and comparable objects. FITC, fluorescein isothiocyanate; GFP, green fluorescent protein; qdot, green (4 nm, top) and red (6.5 nm, bottom) CdSe/ZnS qdot; qrod, rod-shaped qdot (size from Quantum Dot Corp.’s Web site). Three proteins—streptavidin (SAV), maltose binding protein (MBP), and immunoglobulin G (IgG)—have been used for further functionalization of qdots (see text) and add to the final size of the qdot, in conjunction with the solubilization chemistry (Fig. 2).

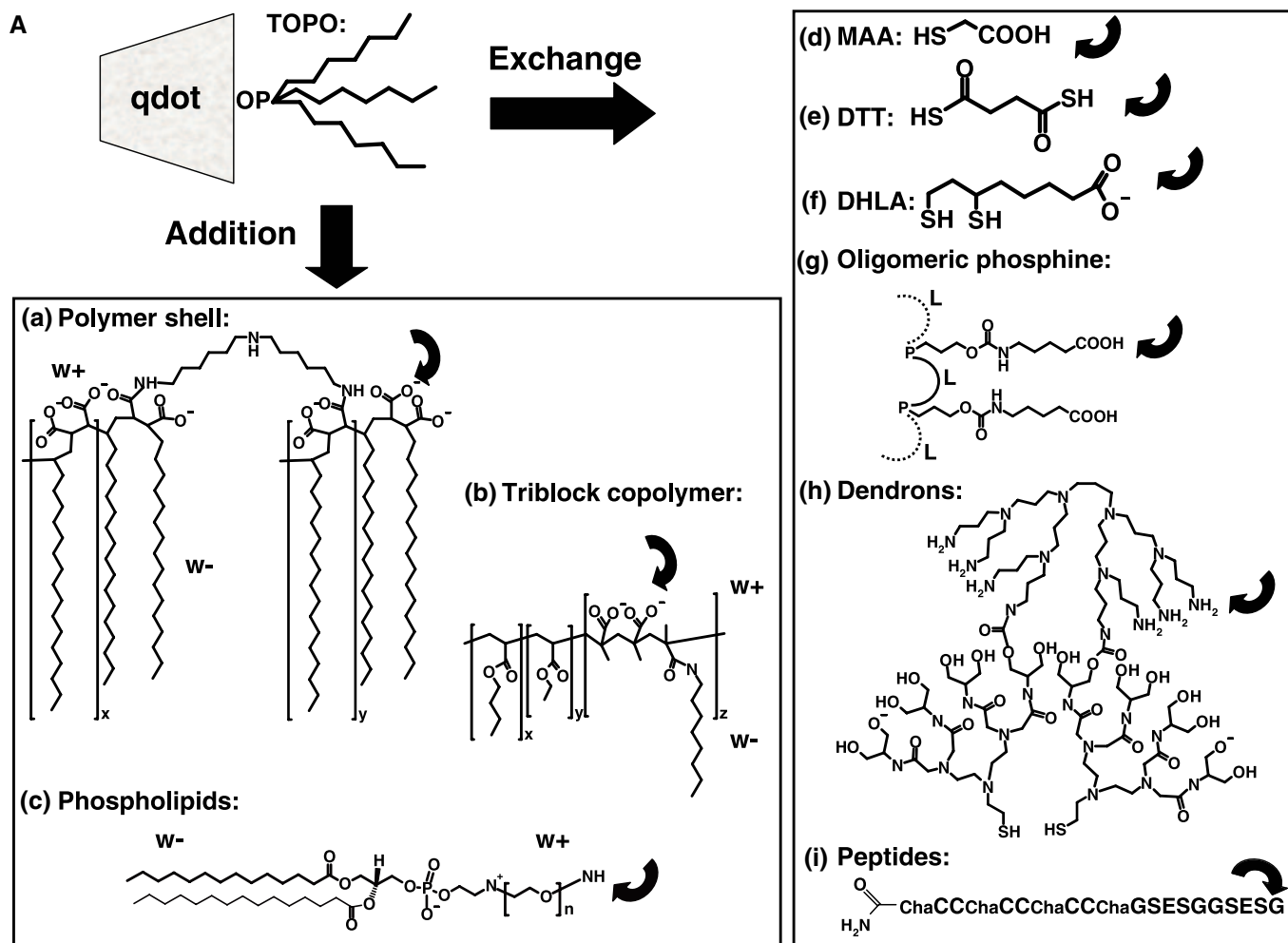
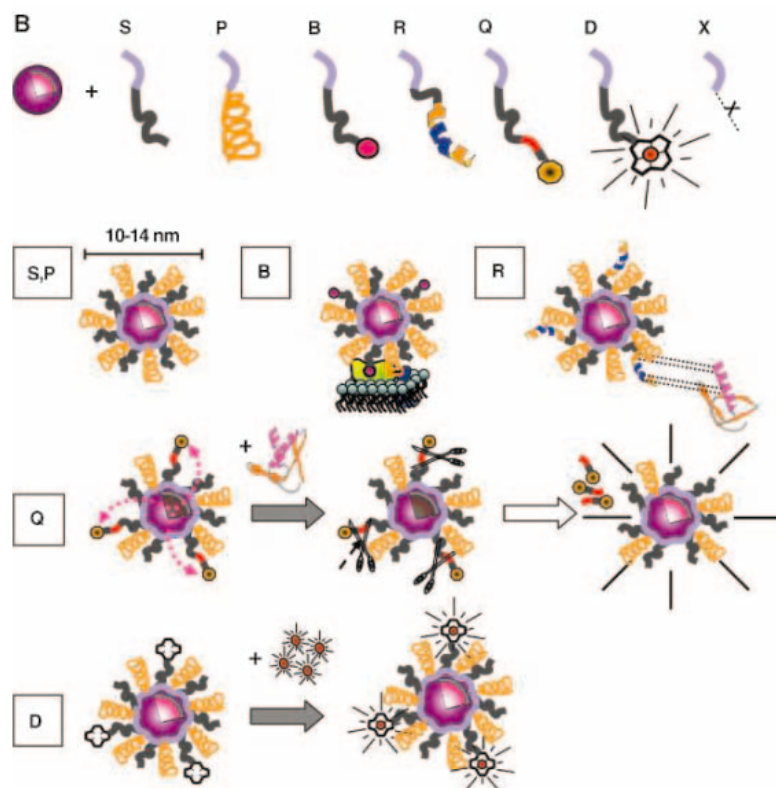


Fig. 2. Qdot solubilization and functionalization. **(A)** Surface chemistries. TOPO (trioctylphosphine oxide)-passivated qdots can be solubilized in aqueous buffer by addition of a layer of amphiphilic molecules containing hydrophilic ($w+$) and hydrophobic ($w-$) moieties, or by exchange of TOPO with molecules that have a Zn-coordinating end (usually a thiol group, SH) and a hydrophilic end. Examples of addition include (a) formation of a cross-linked polymer shell (31), (b) coating with a layer of amphiphilic triblock copolymer (26), and (c) encapsulation in phospholipid micelles (29). Examples of exchange include (d) mercaptoacetic acid (MAA) (20), (e) dithiothreitol (DTT) (21), (f) dihydrolipoic acid (DHLA) (33), (g) oligomeric phosphines (22), (h) cross-linked dendrons (23), and (i) peptides (24). The curved arrow indicates sites available for further functionalization. **(B)** Peptide toolkit. The light blue segment contains cysteines and hydrophobic amino acids ensuring binding to the qdot (24) and is common to all peptides. S, solubilization sequence; P, PEG; B, biotin; R, peptide recognition sequence; Q, quencher; D, DOTA; X, any unspecified peptide-encoded function. Qdot solubilization is obtained by a mixture of S and P. Qdots can be targeted with B, R, or other chemical moieties. Qdot fluorescence can be turned on or off by attaching a Q via a cleavable peptide link. In the presence of the appropriate enzyme, the quencher is separated from the qdot, restoring the photoluminescence and reporting on the enzyme activity. For simultaneous PET and fluorescence imaging, qdots can be rendered radioactive by D chelation of radionuclides; for simultaneous MRI and fluorescence imaging, qdots can be rendered radioactive by D chelation of nuclear spin labels.



tion of successive z-sections, which compromises the correct reconstruction of 3D structures. The gain obtained with qdots was illustrated by the high-resolution 3D confocal imaging of an unforeseen domain distribution of band3, a membrane protein involved in anion transport in erythrocytes (45) and that of clusters of overexpressed multidrug P-glycoproteins (Pgp's) in breast adenocarcinoma cell membranes (9).

The most interesting property of qdots for immunofluorescence is the very small number of qdots necessary to produce a signal. Indeed, several studies have reported flickering of some specimens, a phenomenon due to the blinking of a small number of qdots (20, 47). This demonstrates that single qdots can still be observed in immunocytological conditions, with an ultimate sensitivity limit of one qdot per target molecule. Additionally, qdots are available in a virtually unlimited number of well-separated colors, all excitable by a single wavelength (Fig. 1). Aside from simplifying image acquisition, this property could be used in confocal microscopy to perform nanometer-resolution colocalization of multiple-color individual qdots (10).

Live-cell experiments introduce a few extra levels of complexity, depending on the application: whole-cell labeling, labeling of membrane-bound proteins, and cytoplasmic or nuclear target labeling. Whole-cell labeling is of particular interest for cell or pathogen detection, cell tracking, and cell lineage studies. This can be achieved without any functionalization through microinjection (29), electroporation, or even phagocytosis of qdots (40, 50). Such internalization was observed in phagokinetic human cancer cells (51) plated on a qdot-coated coverslip. Peptide translocation domains or cationic lipids have also been shown to be efficient facilitators of endocytosis, allowing rapid labeling of whole cell populations with specific colors (50). A better specificity and efficiency can be obtained with functionalized qdots. Transferrin was used to facilitate endocytosis by mammalian cells (20), a

strategy also used successfully to label pathogenic bacteria and yeast cells (52), whereas Gram-positive bacteria were specifically detected by lectin-coated qdots (52). These and other studies have shown that qdots have a considerable advantage over standard dyes: the possibility of long-term observation with negligible photobleaching. In the experiment of Jaiswal *et al.*

however, qdots were observed to eventually end up in intracellular vesicles that could be identified in some cases as endosomes (40, 53, 54) or lysosomes (55) by organelle-specific labeling, or in a perinuclear region compatible with endosomal/lysosomal localization (29). Real-time and long-term observation of translocation of these vesicles was possible in some cases (40, 53).

Different types of functionalization have also been explored as a way to target qdots to cell surface proteins. Some examples include streptavidin (13, 25), secondary (56) or primary antibodies (40), receptor ligands such as epidermal growth factor (EGF) (46, 57) or serotonin (58), recognition peptides (56), and affinity pairs such as biotin-avidin after engineering of the target protein (24). Streptavidin-qdots were used to detect Her2 cancer markers on the surface of SK-BR-3 human breast cancer cells via a biotinylated secondary antibody to human and a humanized antibody to Her2. A similar strategy was also used in cultured spinal neurons to detect single glycine receptors, which could be successfully tracked with high resolution as they diffused in synaptic and extrasynaptic domains (13). The versatility of streptavidin-qdots makes them attractive, but the cumulative volume of qdot, streptavidin, and the two layers of antibodies may hinder their usefulness in studying the multimerization of receptors. Direct qdot functionalization with a secondary antibody reduces the number of detection layers to two; this method was used to detect the integrin α_v subunit in SK-N-SH human neuroblastoma cells (56). Partial

clustering of qdots was reported when compared to a direct integrin-recognition peptide qdot functionalization.

Another strategy consists of cross-linking primary antibodies to qdots. This was performed in two different ways in a study targeting Pgp in HeLa cells transiently transfected with a Pgp-encoding plasmid (40). The first approach involved the biotinylation of the Pgp primary antibody, which was subsequently attached to avidin-coated qdots. The

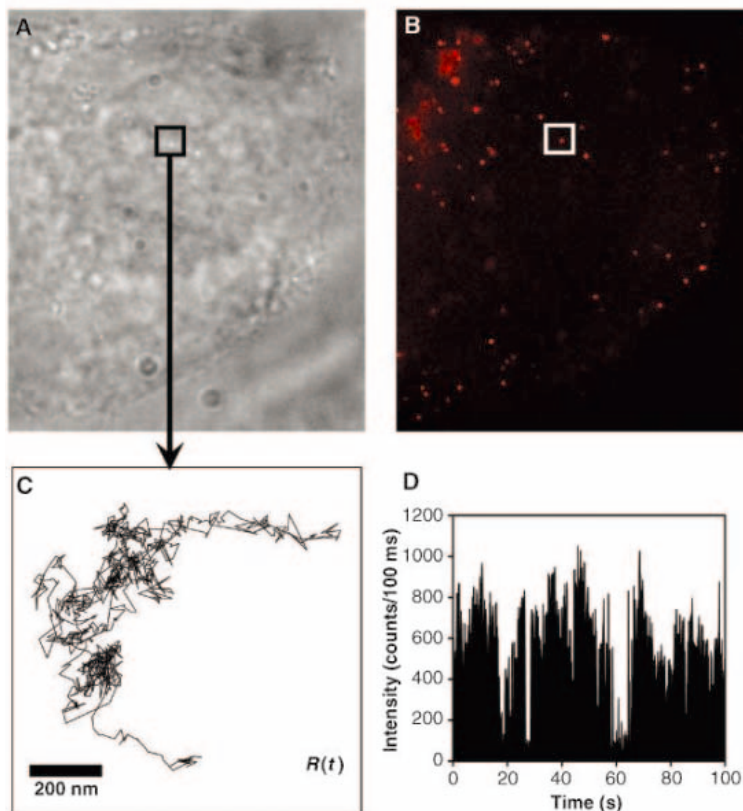


Fig. 3. Single-particle tracking in a live cell. The brightness and photostability of qdots permit single qdot observation over a long period of time. Live HeLa cells stably transfected with a plasmid expressing a chimeric avidin-CD14 receptor (24) were grown on fibronectin-coated glass coverslips, incubated with biotin-qdots (emission 630 nm), and washed with the observation medium. The cells were observed by differential interference contrast (DIC) (A) and epifluorescence (B) on an inverted microscope (Axiovert 100, Zeiss) with a simple Hg lamp and imaged with a cooled monochrome charge-coupled device camera (CoolSnap HQ, Roper Scientific). Single qdots were observed to diffuse at characteristically different rates in different regions of the membrane or inside the cytosol (data not shown). (C) The 1000-step (100 ms/step) trajectory, $R(t)$, of the qdot localized in the region marked in (A) and (B). (D) The corresponding qdot intensity, $I(t)$. The blinking pattern (succession of on and off emission) demonstrates that a single qdot was observed.

(40), *Dictyostelium discoideum* cells colored according to their starvation time could be tracked individually over several hours, allowing the determination that only starved cells contribute to the formation of aggregation centers characteristic of this species. Dubertret *et al.* (29) showed that in the *Xenopus* embryo, cells of the progeny of an injected cell still contain fluorescent qdots after several days of development. In all eukaryotic cell studies,

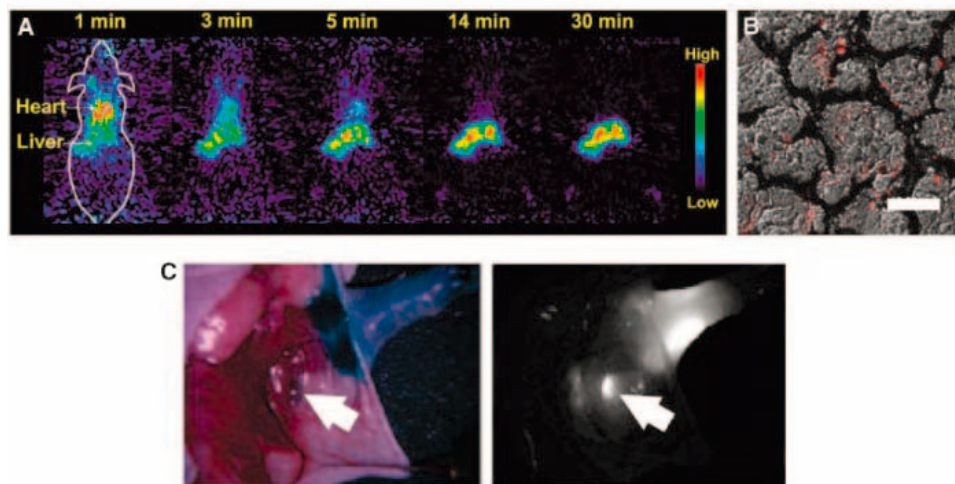


Fig. 4. Animal use of qdots. (A and B) microPET and fluorescence imaging of qdots. Qdots having DOTA (a chelator used for radiolabeling) and 600-dalton PEG on their surface were radiolabeled with ^{64}Cu (positron-emitting isotope with half-life of 12.7 hours). These qdots were then injected via the tail vein into nude mice ($\sim 80 \mu\text{Ci}$ per animal) and imaged in a small animal scanner. (A) Rapid and marked accumulation of qdots in the liver quickly follows their intravenous injection in normal adult nude mice. This could be avoided by functionalizing qdots with higher molecular weight PEG chains, as other studies have shown (49). (B) Overlay of DIC and fluorescence images of hepatocytes from a mouse shows the accumulation of qdots within liver cells. Scale bar, $20 \mu\text{m}$. A further step could involve TEM imaging of the precise localization of qdots in cells, illustrating the potential of qdots as probes at the macro-, micro-, and nanoscales. (C) Surgical use of NIR qdots. A mouse was injected intradermally with 10 pmol of NIR qdots in the left paw, 5 min after reinjection with 1% isosulfan blue and exposure of the actual sentinel lymph node. Left, color video; right, NIR fluorescence image. Isosulfan blue and NIR qdots were localized in the same lymph node (arrows). Copyright 2004 Nature Publishing Group. Reproduced with permission from (60).

second approach involved engineering an adaptor protein with both binding affinity to the Fc region of antibodies and electrostatic interactions with charged qdots (39, 40). Both experiments demonstrated specific surface labeling of the transfected cells and colocalization of the signal with that of an enhanced green fluorescent protein–fused Pgp.

In a further step to reduce the size of qdot probes, researchers have used ligands of surface receptors bound to qdots via a biotin-streptavidin link (46) or by direct cross-linking (57, 58). For instance, EGF-labeled qdots were used to study receptor-mediated signal transduction in different cancer cell lines (46). EGF-qdots bound to cell filopodia erbB1 receptors were observed to undergo a previously undetected retrograde transport (presumably along actin filaments) toward the cell body. Endocytosis of EGF-qdot–targeted erbB1 receptors in vesicles was also observed, followed by a rich dynamic pattern of diffusion, directed linear motion, and vesicular fusion.

Some proteins can be recognized by peptides, so it is attractive to use peptides for qdot functionalization. This strategy has been shown to work in human neuroblastoma with a short engineered peptide directed against integrin (56). This phenomenon was also proven to be relatively common by Akerman *et al.*, who used three different peptides to target qdots to lung endothelial cells, brain endothelial cells, and human breast carcino-

ma cells in vitro and in vivo (37). In the absence of such peptide sequences or of an identified ligand, the target molecule can be engineered to include a recognizable polypeptide. We recently illustrated this approach with the fusion of an avidin polypeptide chain to the glycosylphosphatidylinositol (GPI)–anchoring sequence of human CD14 receptors (24). Biotinylated peptide–coated qdots were used to label the avidin receptors expressed in the cytoplasmic membrane of HeLa cells. The receptors were observed with single-molecule sensitivity and were tracked for several minutes as they diffused in the membrane of live cells and trafficked in the cytosol (Fig. 3) (12). This approach allowed us to study in detail the relationship between GPI-anchored receptors and lipid rafts in the membrane (12).

In principle, the same concepts could be used to target and label cytoplasmic or nuclear targets. However, qdots need to (i) enter the cell cytoplasm and (ii) reach their target without being trapped in the endocytic pathway (40). A recent study showed that microinjection allows the delivery of qdots functionalized with the appropriate targeting peptide sequence to mitochondria or the cell nucleus (54). All other approaches seem to result in aggregation of qdots in the endosomes, but this is an area of very active research. A second level of difficulty is introduced by the impossibility of washing away probes that are in excess in the

cytoplasm, as was possible with outer-membrane labeling experiments.

Qdots in Animal Biology

The long-term stability and brightness of qdots make them ideal candidates for live animal targeting and imaging. Two-photon excitation confocal microscopy was used to image blood vessels in live mice that had received qdots by intravenous injection, showing that higher contrast and imaging depth can be obtained at a lower excitation power than with organic dyes (17). A similar study that focused on long-term imaging of live mice revealed the importance of coating qdots with high molecular weight polyethylene glycol (PEG) molecules to reduce accumulation in the liver and bone marrow (49). After several months, qdots were still visible in the bone marrow and lymph nodes of animals, illustrating the outstanding stability of these probes.

Peptide-qdots were first used to target tissue-specific vascular markers (lung blood vessels and cancer cells) by intravenous injection in live mice (37). Histological sections of different organs after 5 or 20 min of circulation showed that peptide-qdots reach their targets and are internalized by endocytosis in target cells but not in surrounding tissues, probably because of their larger size relative to dye molecules (which would stain surrounding tissues). Live animal imaging of targeted qdot delivery was recently achieved in mice by Gao *et al.*, who intravenously injected PEG-coated qdots functionalized with antibodies to prostate-specific membrane antigen (26). Because the qdots were emitting in the visible spectrum, a spectral demixing algorithm was used to separate tissue autofluorescence (59) from qdot signal in grafted tumors (26). This problem was eliminated altogether by Kim *et al.*, who injected NIR-emitting qdots (850 nm) intradermally into live mice and pigs (60). Qdots rapidly migrated to nearby lymph nodes and could be imaged virtually background-free (Fig. 4C), allowing image-guided resection of a lymph node in a pig. This latter demonstration suggests that IR imaging of qdots could possibly aid surgical procedures in humans.

Cytotoxicity

Cytotoxicity and the potential interference of qdot labeling with cellular processes are primary issues in any live-cell or animal experiment. These questions are complicated by the variety of published synthesis, solubilization, and functionalization protocols. Most of the reports discussed above did not find adverse effects on cell viability, morphology, function, or development over the

duration of the experiments (from several hours to several days) at qdot concentrations optimized for labeling efficiency. At higher concentrations, however, effects on embryo development, for instance, were noticeable (29). The less protected the core or core/shell material is, the faster the appearance of signs of interference with cell viability or function (57), with release of Cd^{2+} or Se^{2-} ion reported in both core and core-shell qdots (52, 57). Qdots are therefore not completely innocuous, but a safe range likely exists in which they can accomplish their task without major interference with the processes under study. Extensive scrutiny will naturally be needed before qdots can be used in medical procedures.

Perspectives

The current picture of qdot technology is bound to evolve rapidly on many levels. In synthesis, new compositions could entail qdots with properties such as (i) sensitivity to electric or magnetic fields (61, 62); (ii) narrower fluorescence emission and longer lifetimes (using lanthanide-doped qdots); (iii) smaller sizes and extension to the NIR spectrum, as demonstrated by ternary alloys (63); (iv) end-specific functionalizations of nanorod qdots (64); (v) suppression of blinking (14) and quantum yield enhancement (65); and (vi) built-in on-off switches or photoelectric biotransducers. An on-off switch was demonstrated for a maltose sensor (19) and can be obtained by associating the qdot to a fluorescence-quenching molecule that can be separated or cleaved upon binding to the target, or in the presence of a chemical species or enzyme. This would be of particular interest for intracellular applications, in which there is no way to get rid of unbound qdots (unlike outer cell membrane-labeling experiments). As an example of a biotransducer, light-excited qdots could transfer their charge to bound enzymes functioning as electron or hole acceptors, enabling their control by light activation. Reciprocally, qdots could be lit up by electron or hole donor enzymes through chemiluminescence (66). Peptide coating of nanomaterials is in this respect a powerful tool for imparting novel functions to the organic-inorganic interface. The simultaneous engi-

neering of the semiconductor's band gap (by rational design) with the peptide's redox potential (by molecular evolution) could be used to optimize qdot compositions and peptide sequences for binding and desired optical, electronic, magnetic, and chemical properties. In summary, different shapes, end specificities, and compositions will lead to more complex bioinorganic architectures that could be exploited as an optoelectronic interface to the cellular machinery.

Qdot functionalization is another area where new developments will be needed. Ligands of cellular proteins should be readily cross-linked to qdots by means of standard bioconjugation schemes. However, most of the potential extracellular or intracellular

one component could be easily attached or fused to the target protein, is a promising approach. Several examples of such pairs developed by molecular evolution have been reported, with fusion peptides ranging from ~200 amino acids [single chain fragment antibody targeted against fluorescein, dissociation constant $K_d \sim 50$ fM (71)] down to ~30 amino acids [peptide hairpin against Texas Red, $K_d \sim 25$ pM (72)].

Intracellular delivery remains a challenge, and strategies to escape the endocytosis pathways will be needed. Two recent publications indicate that peptide-coated qdots could have many untapped virtues: (i) 20-nm gold nanoparticles coated with protein transduction domains could enter live

cells, and further enter the nucleus with additional adenovirus nuclear localization and integrin binding domains (73); and (ii) after microinjection into the cytoplasm, PEG-coated qdots with a nuclear or mitochondrial localization sequence were successfully targeted to the nucleus or mitochondria (54). Another interesting model system, based on adenosine triphosphate-triggered release of CdS qdots encapsulated in chaperonin molecules (74), suggests using a "Trojan horse" approach to avoid the cellular defense and recycling mechanisms. Cell-permeable virus capsids, vaults, or other biocapsules could be used to translocate encapsulated qdots in cells, provided that a simple release-on-demand mechanism could be engineered in the vehicle, such

as a photolabile or pH-sensitive lock.

Qdots' photophysical properties (spectral range, brightness, long lifetimes) and their potential as single-molecule probes may justify the development of new detectors that would have the temporal resolution and sensitivity of avalanche photodiodes and the 2D spatial resolution of cameras for wide-field *in vivo* studies of protein dynamics and trafficking. Their large size and electronic density may be used for combined fluorescence and static high-resolution imaging techniques such as atomic force microscopy and electron and x-ray microscopy and tomography. Additional contrast mechanisms could be obtained by functionalization of

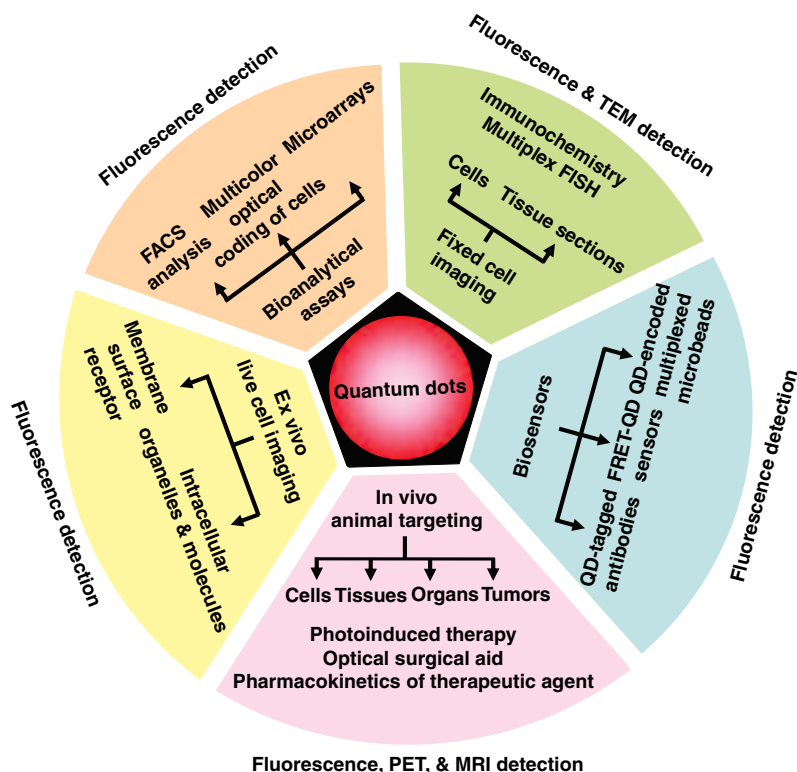


Fig. 5. Applications of quantum dots as multimodal contrast agents in bioimaging.

targets do not have any known ligands, or if they do, qdots may interfere with their interaction. The use of antibodies, which has proven successful for surface-bound proteins, may not be practical for intracellular targets because of the size of the qdot-antibody construct and delivery issues (see below). *In vivo* cross-linking strategies developed for dyes—such as the use of biarsenical ligands targeted against tetracycline motifs (67), Ni^{2+} -nitrotriacetic acid moieties targeted against hexahistidine motifs (68), and other similar approaches (69, 70)—may be adapted for qdot functionalization. The development of affinity pairs orthogonal to the biotin-avidin pair, in which

qdots. Figure 4A illustrates this idea with ^{64}Cu radioactive labeling of qdots coated with DOTA (1,4,7,10-tetraazacyclododecane-1,4,7,10 tetraacetic acid) functionalized peptides. Micro-positron emission tomography (microPET) shows that qdots injected into the tail vein in mice are rapidly accumulated in the liver. Fluorescence imaging of qdots for tracking combined with the quantitative capability of microPET should therefore permit the elucidation of targeting mechanisms, biodistribution, and dynamics in living animals with high sensitivity. Nuclear spin labels for magnetic resonance imaging (MRI) could also be incorporated into qdot coatings with the use of similar chelating groups. It should therefore be possible to image targeted qdots at all scales, from whole-body down to nanometer resolution, using a single probe.

Beyond biotechnological and cell-imaging applications (Fig. 5A), and provided that cytotoxicity issues can be resolved, one can envision the use of intravenous injection of qdots to home in on and target cellular markers of diseased tissues and organs in the human body. Qdots could then be used as contrast reagents for functional imaging with a combination of MRI, PET, computed tomography, and IR fluorescence imaging (the latter by direct imaging through the epidermis or by a catheter-based confocal fiber microscope). In vivo optical biopsy could confirm the pathology, and therapy could then be performed selectively, locally, and temporally by depositing energy (monochromatic x-rays for k-shell absorption or laser IR radiation) into the targeted qdots, in a manner similar to the recently reported photothermal tumor ablation with gold nano-shells (75). Alternatively, it might be possible to graft therapeutic enzymes to the qdot surface and activate them by light, or produce free radicals (such as singlet oxygen) by optically cycling the qdots.

Conclusion

Qdots as biological probes have lived up to the hopes of their initial promoters (20, 27). They will not replace the well-established fluorophores or fluorescent protein-fusion technologies, but will complement them for applications needing better photostability, NIR emission, or single-molecule sensitivity over long time scales. Undoubtedly, biologists will catch on to these exciting developments and will find as yet unforeseen applications for this new toolkit, thus enhancing and complementing their existing arsenal of bioimaging tools.

References and Notes

1. X. Michalet et al., *Annu. Rev. Biophys. Biomol. Struct.* **32**, 161 (2003).
2. Special issue on Biological Imaging, *Science* **300**, 75 (2003).
3. S. Weiss, *Science* **283**, 1676 (1999).
4. A. P. Alivisatos, *Science* **271**, 933 (1996).
5. A. L. Efron, S. Rosen, *Annu. Rev. Mater. Sci.* **30**, 475 (2000).
6. M. Dahan et al., *Opt. Lett.* **26**, 825 (2001).
7. M. Nirmal et al., *Nature* **383**, 802 (1996).
8. P. Reiss, J. Bleuse, A. Pron, *Nano Lett.* **2**, 781 (2002).
9. A. Sukhanova et al., *Anal. Biochem.* **324**, 60 (2004).
10. T. D. Lacoste et al., *Proc. Natl. Acad. Sci. U.S.A.* **97**, 9461 (2000).
11. X. Michalet et al., *Single Mol.* **2**, 261 (2001).
12. F. Pinaud, X. Michalet, E. Margeat, H. P. Moore, S. Weiss, unpublished data.
13. M. Dahan et al., *Science* **302**, 442 (2003).
14. S. Hohng, T. Ha, *J. Am. Chem. Soc.* **126**, 1324 (2004).
15. S. A. Empedocles, D. J. Norris, M. G. Bawendi, *Phys. Rev. Lett.* **77**, 3873 (1996).
16. A. M. Kapitonov et al., *J. Phys. Chem. B* **103**, 10109 (1999).
17. D. Larson et al., *Science* **300**, 1434 (2003).
18. S. Doose, J. M. Tsay, F. Pinaud, S. Weiss, unpublished data.
19. I. L. Medintz et al., *Nature Mater.* **2**, 630 (2003).
20. W. C. W. Chan, S. M. Nie, *Science* **281**, 2016 (1998).
21. S. Pathak, S. K. Choi, N. Arnheim, M. E. Thompson, *J. Am. Chem. Soc.* **123**, 4103 (2001).
22. S. Kim, M. G. Bawendi, *J. Am. Chem. Soc.* **125**, 14652 (2003).
23. W. Guo, J. J. Li, Y. A. Wang, X. G. Peng, *Chem. Mater.* **15**, 3125 (2003).
24. F. Pinaud, D. King, H.-P. Moore, S. Weiss, *J. Am. Chem. Soc.* **126**, 6115 (2004).
25. X. Y. Wu et al., *Nature Biotechnol.* **21**, 41 (2003).
26. X. Gao, Y. Cui, R. M. Levenson, L. W. K. Chung, S. Nie, *Nature Biotechnol.* **22**, 969 (2004).
27. M. Bruchez, M. Moronne, P. Gin, S. Weiss, A. P. Alivisatos, *Science* **281**, 2013 (1998).
28. D. Gerion et al., *J. Phys. Chem. B* **105**, 8861 (2001).
29. B. Dubertret et al., *Science* **298**, 1759 (2002).
30. X. Gao, W. C. W. Chan, S. Nie, *J. Biomed. Opt.* **7**, 532 (2002).
31. T. Pellegrino et al., *Nano Lett.* **4**, 703 (2004).
32. F. Osaki, T. Kanamori, S. Sando, T. Sera, Y. Aoyama, *J. Am. Chem. Soc.* **126**, 6520 (2004).
33. H. Mattoussi et al., *J. Am. Chem. Soc.* **122**, 12142 (2000).
34. A. L. Rogach et al., *Phys. Status Solidi B* **224**, 153 (2001).
35. N. Gaponik et al., *J. Phys. Chem. B* **106**, 7177 (2002).
36. F. Patolsky et al., *J. Am. Chem. Soc.* **125**, 13918 (2003).
37. M. E. Akerman, W. C. W. Chan, P. Laakkonen, S. N. Bhatia, E. Ruoslahti, *Proc. Natl. Acad. Sci. U.S.A.* **99**, 12617 (2002).
38. G. P. Mitchell, C. A. Mirkin, R. L. Letsinger, *J. Am. Chem. Soc.* **121**, 8122 (1999).
39. E. R. Goldman et al., *Anal. Chem.* **74**, 841 (2002).
40. J. K. Jaiswal, H. Mattoussi, J. M. Mauro, S. M. Simon, *Nature Biotechnol.* **21**, 47 (2003).
41. A. Mansson et al., *Biochem. Biophys. Res. Commun.* **314**, 529 (2004).
42. C. T. Dameron et al., *Nature* **338**, 596 (1989).
43. S. R. Whaley, D. S. English, E. L. Hu, P. F. Barbara, A. M. Belcher, *Nature* **405**, 665 (2000).
44. A. P. Alivisatos, *Nature Biotechnol.* **22**, 47 (2004).
45. F. Tokumasu, J. Dvorak, *J. Microsc.* **211**, 256 (2003).
46. D. S. Lidke et al., *Nature Biotechnol.* **22**, 198 (2004).
47. Y. Xiao, P. E. Barker, *Nucleic Acids Res.* **32**, 28E (2004).
48. L. A. Bentolila, S. Weiss, unpublished data.
49. B. Ballou, B. C. Lagerholm, L. A. Ernst, M. P. Bruchez, A. S. Waggoner, *Bioconjug. Chem.* **15**, 79 (2004).
50. L. C. Mattheakis et al., *Anal. Biochem.* **327**, 200 (2004).
51. T. Pellegrino et al., *Differentiation* **71**, 542 (2003).
52. J. A. Kloepper et al., *Appl. Environ. Microbiol.* **69**, 4205 (2003).
53. W. J. Parak et al., *Adv. Mater.* **14**, 882 (2002).
54. A. M. Derfus, W. C. W. Chan, S. N. Bhatia, *Adv. Mater.* **16**, 961 (2004).
55. K. Hanaki et al., *Biochem. Biophys. Res. Commun.* **302**, 496 (2003).
56. J. O. Winter, T. Y. Liu, B. A. Korgel, C. E. Schmidt, *Adv. Mater.* **13**, 1673 (2001).
57. A. M. Derfus, W. C. W. Chan, S. N. Bhatia, *Nano Lett.* **4**, 11 (2004).
58. S. J. Rosenthal et al., *J. Am. Chem. Soc.* **124**, 4586 (2002).
59. Y. T. Lim et al., *Mol. Imaging* **2**, 50 (2003).
60. S. Kim et al., *Nature Biotechnol.* **22**, 93 (2004).
61. M. Shim, P. Guyot-Sionnest, *Nature* **407**, 981 (2000).
62. F. V. Mikulec et al., *J. Am. Chem. Soc.* **122**, 2532 (2000).
63. R. E. Bailey, S. M. Nie, *J. Am. Chem. Soc.* **125**, 7100 (2003).
64. T. Mokari, E. Rothenberg, I. Popov, R. Costi, U. Banin, *Science* **304**, 1787 (2004).
65. J. M. Tsay, S. Doose, F. Pinaud, J. J. Li, S. Weiss, *J. Phys. Chem. B*, in press.
66. S. K. Poznyak, D. V. Talapin, E. V. Shevchenko, H. Weller, *Nano Lett.* **4**, 693 (2004).
67. S. R. Adams et al., *J. Am. Chem. Soc.* **124**, 6063 (2002).
68. A. N. Kapanidis, Y. W. Ebricht, R. H. Ebricht, *J. Am. Chem. Soc.* **123**, 12123 (2001).
69. A. Keppler, H. Pick, C. Arrivoli, H. Vogel, K. Johnsson, *Proc. Natl. Acad. Sci. U.S.A.* **101**, 9955 (2004).
70. J. Yin, F. Liu, X. Li, C. T. Walsh, *J. Am. Chem. Soc.* **126**, 7754 (2004).
71. E. T. Boder, K. S. Midelfort, K. D. Witttrup, *Proc. Natl. Acad. Sci. U.S.A.* **97**, 10701 (2000).
72. K. M. Marks, M. Rosinov, G. P. Nolan, *Chem. Biol.* **11**, 347 (2004).
73. A. G. Tkachenko et al., *Bioconjug. Chem.* **15**, 482 (2004).
74. D. Ishii et al., *Nature* **423**, 628 (2003).
75. D. P. O'Neal, L. R. Hirsch, N. J. Halas, J. D. Payne, J. L. West, *Cancer Lett.* **209**, 171 (2004).
76. W. W. Yu, J. C. Falkner, B. S. Shih, V. L. Colvin, *Chem. Mater.* **16**, 3318 (2004).
77. A. A. Guzelian, U. Banin, A. V. Kadavanich, X. Peng, A. P. Alivisatos, *Appl. Phys. Lett.* **69**, 1432 (1996).
78. A. A. Guzelian et al., *J. Phys. Chem.* **100**, 7212 (1996).
79. W. W. Yu, X. Peng, *Angew. Chem. Int. Ed.* **41**, 2368 (2002).
80. W. W. Yu, Y. A. Wang, X. Peng, *Chem. Mater.* **15**, 4300 (2003).
81. W. W. Yu, L. Qu, W. Guo, X. Peng, *Chem. Mater.* **16**, 560 (2004).
82. J. M. Tsay, M. Pflughoeft, L. A. Bentolila, S. Weiss, *J. Am. Chem. Soc.* **126**, 1926 (2004).
83. Supported by NIH grant 5-R01-EB000312, Keck Foundation grant 04074070, and Defense Advanced Research Projects Agency-Air Force Office of Scientific Research grant FA955004-10048. We are grateful for exchanges with our collaborators D. King, H.-P. Moore, A. P. Alivisatos, C. A. Larabell, D. Gerion, O. N. Witte, L. H. Rome, and G. Payne. Fluorescence microscopy images in Fig. 3 were obtained at the California NanoSystems Institute Advanced Light Microscopy/Spectroscopy Shared Facility (ALMSSF), Department of Chemistry and Biochemistry, at UCLA. We thank K. Hamadani, G. Iyer, and the referees for helpful comments on the manuscript; E. Margeat for help with the experiments described in Fig. 3; and T. Olafsen for help with the experiments described in Fig. 4, A and B. Requests for materials should be sent to qdot-info@chem.ucla.edu.

Supporting Online Material

www.sciencemag.org/cgi/content/full/307/5709/538/DC1

References

10.1126/science.1104274

Marine Fish Egg Hydration Is Aquaporin-Mediated

Mercedes Fabra,¹ Demetrio Raldúa,¹ Deborah M. Power,²
Peter M. T. Deen,³ Joan Cerdà^{1*}

The oocytes of marine pelagic teleosts swell abruptly by hydration during the reinitiation of meiosis (oocyte maturation) before ovulation. This process renders the eggs and early embryos buoyant in sea water, allowing their survival and dispersal in the ocean (1, 2). The major osmotic effectors for water uptake are free amino acids derived from the proteolysis of the oocyte major yolk proteins (3), but the membrane-associated mechanisms involved remain unknown.

The time course of oocyte hydration *in vitro* in the marine teleost gilthead sea bream (*Sparus aurata*) revealed a progressive swelling of the oocyte, which appeared to accelerate within ~2 hours after the complete proteolysis of yolk proteins (fig. S1). To investigate whether molecular water channels or aquaporins (AQPs) were involved in this process, we performed reverse transcription–polymerase chain reaction (RT-PCR) to obtain AQP cDNAs from ovarian tissue. We isolated a cDNA that had a deduced amino acid sequence with six potential transmembrane domains and two asparagine-proline-alanine motifs, the signature of the

AQP superfamily (4). Heterologous expression in *Xenopus laevis* oocytes revealed that the encoded protein, like mammalian aquaporin-1 (AQP1) (5), was selectively permeable for water, and that its permeability could be inhibited by HgCl₂ and recovered by β-mercaptoethanol (βME) (fig. S2A). However, its deduced amino acid sequence showed low identity with other vertebrate AQP1 orthologs (45 to 54%), and its mRNA was detected predominantly in the ovary (fig. S2B). On the basis of these features, we concluded that this cDNA encodes a paralog, which we named the *S. aurata* AQP1 of the ovary (SaAQP1o).

To elucidate the relationship between SaAQP1o and vertebrate AQP1-like water channels, we cloned additional sequences. In the sea bream, we identified another cDNA, the deduced protein of which was 60% identical to that of SaAQP1o, but it shared higher identity to mammalian AQP1 (57 to 59%) and was ubiquitously expressed (fig. S2B). Phylogenetic analysis revealed that SaAQP1o, together with other AQP1-like channels found in the ovaries of some fish, fall into a distant and separate

group, suggesting the fast evolution of a unique subfamily of SaAQP1o-related channels in teleosts (fig. S2C and supporting online text).

SaAQP1o peptides were localized in the cortical cytoplasm of early vitellogenic oocytes (Fig. 1A). As oocytes developed, SaAQP1o was translocated toward a more peripheral area (Fig. 1B), whereas in fully grown oocytes, it concentrated below the plasma membrane (Fig. 1C). During oocyte maturation, SaAQP1o was further translocated into the oocyte microvilli (Fig. 1D), where it can potentially mediate water influx into the oocyte. To assess the functional relevance of these findings, follicle-enclosed oocytes undergoing oocyte hydration *in vitro* were treated with HgCl₂, which inhibited hydration in a dose-dependent and reversible manner (Fig. 1E). These results paralleled the permeability properties of SaAQP1o expressed in *X. laevis* oocytes and thus provide strong support for a role of SaAQP1o in mediating sea bream oocyte hydration.

In conclusion, we found that SaAQP1o belongs to a subfamily of AQP1-like channels evolved in teleosts, which are likely derived from a common AQP1-like ancestral gene. Although SaAQP1o orthologs in other teleosts might have other, yet-unknown osmoregulatory functions, our results reveal that fish oocyte hydration is based on the interplay between protein hydrolysis and SaAQP1o, indicating a specialized physiological role for this AQP.

References and Notes

1. P. J. Mellinger, *Annee Biol.* **33**, 117 (1994).
2. B. Ådlandsvik, S. Coombs, S. Sundby, G. Temple, *Fish. Res.* **50**, 59 (2001).
3. K. Selman, R. A. Wallace, J. Cerdà, *J. Exp. Zool.* **290**, 265 (2001).
4. P. Agre *et al.*, *J. Physiol.* **542**, 3 (2002).
5. G. M. Preston, T. P. Carroll, W. B. Guggino, P. Agre, *Science* **256**, 385 (1992).
6. We thank E. Lubzens, W. W. de Jong, and F. Piferrer for critical reading of the manuscript. Supported by the Spanish Ministry of Science and Technology (MCYT) and European Commission grants (J.C.) and by a fellowship from the Catalan government (M.F.). This work is dedicated to Prof. R. A. Wallace, a pioneer in the investigation of oocyte hydration in fish, who inspired and encouraged this research.

Supporting Online Material

www.sciencemag.org/cgi/content/full/307/5709/545/DC1

Materials and Methods

SOM Text

Figs. S1 and S2

References and Notes

12 October 2004; accepted 5 November 2004

10.1126/science.1106305

¹Center of Aquaculture–Institut de Recerca i Tecnologia Agroalimentaries, Tarragona, Spain, and Reference Center in Aquaculture, Barcelona, Spain. ²Center of Marine Sciences, Universidade do Algarve, Faro, Portugal. ³Department of Physiology, Radboud University of Nijmegen Medical Center, Nijmegen, Netherlands.

*To whom correspondence should be addressed. E-mail: jcerda@icm.csic.es

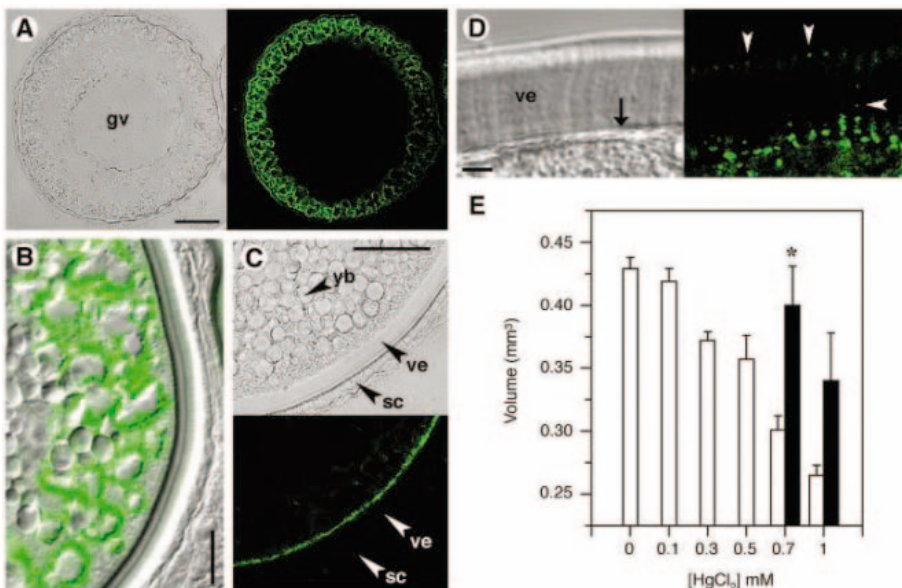


Fig. 1. (A to D) Bright-field and immunofluorescent images of SaAQP1o immunolocalization. (A) An early vitellogenic oocyte. (B) A late vitellogenic oocyte. (C) A fully grown oocyte. (D) SaAQP1o staining at the oocyte microvilli. The arrow and arrowheads indicate the plasma membrane and the microvilli, respectively. gv, germinal vesicle; yb, yolk bodies; ve, vitelline envelope; sc, somatic cells. Scale bars, (A) and (C) 50 μm; (B) 20 μm; (D) 5 μm. (E) Mercury inhibition of oocyte hydration *in vitro* (open bars) and recovery by βME (solid bars). Means ± SEM are shown; *, *P* < 0.05.

A Giant Impact Origin of Pluto-Charon

Robin M. Canup

Pluto and its moon, Charon, are the most prominent members of the Kuiper belt, and their existence holds clues to outer solar system formation processes. Here, hydrodynamic simulations are used to demonstrate that the formation of Pluto-Charon by means of a large collision is quite plausible. I show that such an impact probably produced an intact Charon, although it is possible that a disk of material orbited Pluto from which Charon later accreted. These findings suggest that collisions between 1000-kilometer-class objects occurred in the early inner Kuiper belt.

The Pluto-Charon pair shares key traits with the Earth-Moon system. Each satellite mass is substantial compared to its planet: Charon's mass is 10 to 15% of Pluto's mass, and the Moon's mass is ~1% of Earth's mass. All other satellite-to-planet mass ratios in our solar system are less than $\sim 2 \times 10^{-4}$. The orbits of Charon and the Moon are consistent with a scenario in which each satellite formed much closer to its planet, and torques due to tides raised on the planet by the satellite subsequently caused the satellite's orbit to expand to its current separation. The angular momentum of both pairs is large, within a factor of several of the critical angular momentum for rotational stability of a single object containing the total system mass.

In both cases, an origin by "giant impact," in which a large oblique collision with the growing planet produced its satellite and provided the system with its angular momentum, is favored (1–4). However, to date, the viability of this mode of origin has only been demonstrated for the Earth-Moon case. Models of lunar-forming impacts (4–7) produce disks orbiting the planet containing about 1 to 3% of the planet's mass, and as such the feasibility of forming the proportionally more massive Charon has been unknown. Although giant impacts are believed common in the final stage of terrestrial planet formation in the inner solar system (8), their role in the outer solar system and the Kuiper belt [a disk of objects orbiting exterior to Neptune between about 30 and 50 astronomical units (AU)] is more uncertain (9). The origin of Pluto-Charon provides a key constraint to this issue and to the population of objects in the primordial Kuiper belt.

Properties of the distant Pluto-Charon pair [supporting online material (SOM)

text] remain somewhat uncertain. Pluto and Charon have physical radii of $R_p \approx 1150$ to 1200 km and $R_C \approx 590$ to 620 km, and their densities are $\rho_p \approx 1.8$ to 2.1 g/cm³ and $\rho_C \approx 1.6$ to 1.8 g/cm³, indicating rock-ice compositions with about 50 to 80% rock by mass (10). Scaling the angular momentum of the Pluto-Charon binary, L_{PC} , by the quantity $L' \equiv \sqrt{GM_{PC}^2 R_{PC}}$ (where R_{PC} is the radius of an equivalent spherical object containing the total Pluto-Charon system mass, M_{PC} , and G is the gravitational constant) gives the normalized system angular momentum, $J_{PC} \equiv L_{PC}/L'$, which is in the range $0.33 < J_{PC} < 0.46$ for a Charon-to-Pluto mass ratio, q , in the range $0.1 < q < 0.15$.

Here, I present smooth particle hydrodynamic (SPH) simulations to show that giant impacts can produce Pluto-Charon-type systems with $q > 0.1$ and $J \sim 0.4$. In SPH, an object is described by a multitude of overlapping particles, each of which represent a three-dimensional (3D) distribution of matter of a specified composition, whose properties are tracked in time in a Lagrangian manner. In these simulations, particles are evolved due to gravity, compressional heating and expansion cooling, and shock dissipation (11), and the Analytic Equation of State, M-ANEOS (12, 13), is used with material constants by Pierazzo and Melosh (14). For a full description of the SPH technique, see (15), from whose work the code used here is directly descended.

The SPH simulations involved between $N = 2 \times 10^4$ and 1.2×10^5 particles and a simulated time of 1 to 4 days. Given that the appropriate differentiation state and composition of the colliding objects is uncertain, I considered three initial compositions: (i) SER: 100% undifferentiated serpentine [$Mg_3Si_2O_5(OH)_4$, a hydrated silicate containing $\approx 14\%$ H₂O by weight]; (ii) IDI: 40% water ice, 42% dunite, and 18% iron by mass and differentiated into

an ice mantle, rock core, and iron inner core; and (iii) SIM: 50% serpentine and 50% water ice in an undifferentiated mixture. These objects range from uniform to highly differentiated, with rock mass fractions between 43 and 86% and bulk densities between ~ 1.5 to 2.5 g/cm³.

I modeled a variety of impacts that were all capable of providing an angular momentum within the range for Pluto-Charon. The collision of two nonspinning equal density objects delivers a normalized angular momentum (16)

$$J_{col} \equiv \frac{L_{col}}{L'} = \sqrt{2}f(\gamma)b' \left(\frac{v_{imp}}{v_{esc}} \right) \quad (1)$$

where $b' \equiv \sin \xi$ is the scaled impact parameter, ξ is the angle between the surface normal and the impact trajectory (a grazing impact has $b' = 1$), γ is the impactor-to-total mass ratio, $f(\gamma) \equiv \gamma(1 - \gamma)\sqrt{\gamma^{1/3} + (1 - \gamma)^{1/3}}$, and (v_{imp}/v_{esc}) is the ratio of the impact velocity to the mutual escape velocity, with $v_{esc}^2 \equiv v_{esc}^2 + v_{\infty}^2$, where v_{∞} is the relative velocity at large separation. Here, $v_{esc} \equiv \sqrt{2GM_T/(R_{imp} + R_{tar})}$,

where M_T is the total colliding mass, and R_{imp} and R_{tar} are the impactor and target radii, respectively. A preimpact spin [due to earlier impacts (8, 17)] that had a component in the same rotational sense as the impact ("prograde") would increase J_{imp} . For the case of prograde spin vectors normal to the plane of the impact, the additional contribution is

$$J_{spin} = K_{imp} \frac{T_{min}}{T_{imp}} \gamma^{5/3} + K_{tar} \frac{T_{min}}{T_{tar}} (1 - \gamma)^{5/3} \quad (2)$$

where $J_{imp} = J_{col} + J_{spin}$, K_{imp} and K_{tar} are the moment of inertia constants of the colliding objects, T_{imp} and T_{tar} are the preimpact spin periods of the impactor and target, and the minimum period for rotational stability is $T_{min} \equiv \sqrt{3\pi/(G\rho)} = 2.3$ hours $(\rho/2\text{g/cm}^3)^{-1/2}$, where ρ is the density of the objects. Here, collisions with $0.5 < b' < 1$, $1 < (v_{imp}/v_{esc}) < 2.5$ (or $0 < v_{\infty} < 2.5$ km/s), $0.13 < \gamma < 0.5$, and with (18) and without preimpact spin are simulated.

Results. An impact between predifferentiated (IDI composition) identical objects, each of which contained 0.53 M_{PC} (so that $\gamma = 0.5$) and had an initial prograde 7-hour day, produces a planet-disk system (Fig. 1). This $b' = 0.83$ collision had $v_{imp} = v_{esc}$ and $J_{imp} = 0.43$, of which 14% was contained in preimpact spin. The resulting disk mass (Fig. 1) is 12% of the planet's mass, and 70% of the disk has equivalent circular orbits exterior to the

Southwest Research Institute, Boulder, CO 80302, USA, and Division of Geological and Planetary Sciences, California Institute of Technology, Pasadena, CA 91125, USA. E-mail: robin@boulder.swri.edu

Roche limit, a_R (19). Of the initial impact angular momentum, 7% escapes (contained in 1% of the mass), 44% is in orbiting material, and $\sim 50\%$ is in the final planet that forms with a spin period of 2.6 hours. The final planet-disk system has $J_f = 0.40$, where $J_f \equiv L_f / \sqrt{GM_p^3 R_f}$ is the normalized system angular momentum, with M_f the total bound mass and $R_f = (3M_f/4\pi\rho)^{1/3}$. I estimated the mass of the satellite ($M_s \equiv qM_p$) that would accumulate from the disk based on models of lunar accretion (20). Assuming that disk material with mass M_D and angular momentum L_D will either be accreted onto the planet of mass M_p or into a single satellite with semimajor axis $a_s \approx 1.2a_R$ (20, 21)

$$M_s \approx 1.9L_D / \sqrt{GM_p a_R} - 1.1M_D \quad (3)$$

For this case (Fig. 1), $q \approx 0.12$.

A collision involving undifferentiated SER objects, a smaller impactor ($\gamma = 0.3$), and no initial spin produces a planet-moon system (Fig. 2). A very grazing collision ($b' = 0.96$) is needed to supply sufficient angular momentum for this smaller γ and $v_{\text{imp}} = v_{\text{esc}}$. The result is a binary with $q = 0.125$, eccentricity $e = 0.50$, a 3500-km (or $3.25 R_p$) periapse separation, and a normalized final angular momentum $J_f = 0.36$. The planet's rotation period is 5.2 hours, with 55% of the initial angular momentum contained in the satellite.

Table 1 and table S1 detail simulations that produced a planet-moon or planet-disk system within the plausible mass-ratio range for Pluto-Charon together with $J_{\text{imp}} \geq 0.33$. Results from 120 simulations that had $0.3 < J_{\text{imp}} < 0.6$ and $M_T \sim M_{\text{PC}}$ are shown in Fig. 3 and fig. S1. Resulting planet-moon systems had satellite semimajor axes ranging from 3.7 to 21 R_p , periapses from 2.5 to 5 R_p , and $0.1 < e < 0.8$. Intermediate outcomes to those in Fig. 3 would be expected for values between those sampled here ($0.3 < \gamma < 0.5$).

The formation of intact moons is correlated with the impactor's differentiation state, with $b' > 0.8$ collisions by undifferentiated impactors typically yielding moons on stable orbits, whereas IDI impactors with $b' > 0.8$ did not. From basic thermal arguments (22), an early impactor containing ~ 30 to 50% of Pluto's mass would likely have been undifferentiated. Compared to the disk-producing impacts, the intact moon cases surround the (q, J) region of the Pluto-Charon system much more completely (Fig. 3 and fig. S1) and produce $0.1 < q < 0.15$ satellites for $b' > 0.8$, $J_{\text{imp}} > 0.3$, and $v_{\text{imp}} \leq 1.2v_{\text{esc}}$. This greater range in J_{imp} and v_{imp} than the successful disk-producing cases (SOM text and table S1) corresponds to a greater range in the other impact variables (Eqs. 1 and 2), with successful intact moon cases occurring for $0.3 \leq \gamma \leq$

0.5 and with or without initial spins. Given these data, the formation of an intact Charon appears the more probable mode of origin.

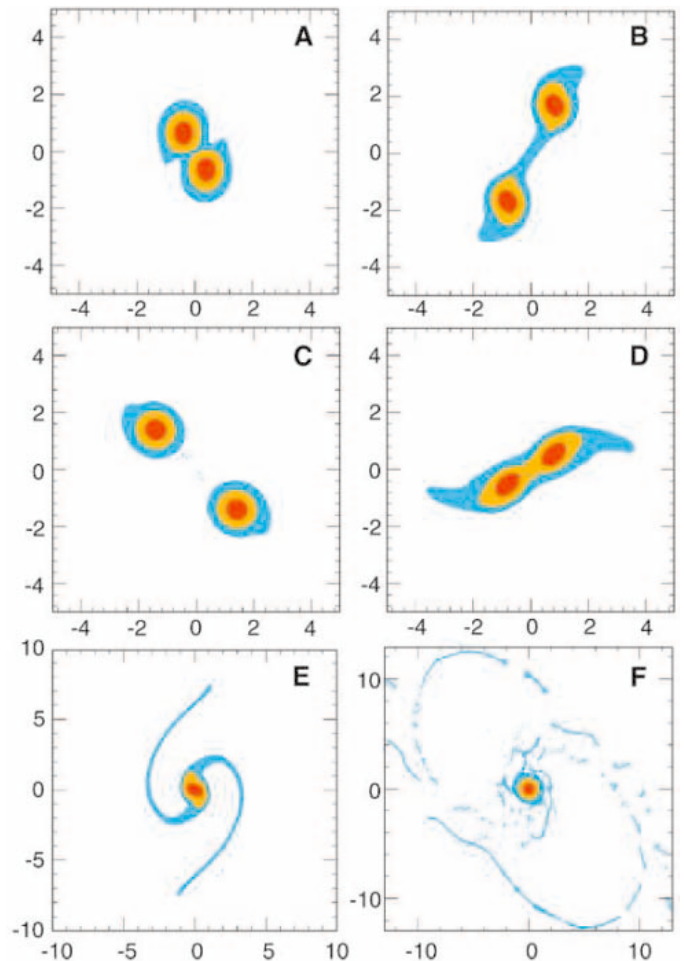
Whereas both massive disks and intact moons are produced by very oblique impacts ($b' > 0.8$), the moon cases typically involve a higher fractional partitioning of mass and angular momentum into orbiting material than the disk cases. This is primarily due to a difference in the nature of the gravitational torques that allow for orbital emplacement. For disk cases, impactor material is sheared into trailing spiral-arm structures (Fig. 1, D and E) (7), a configuration that is effective in transporting angular momentum from radially inner to outer portions. This torque causes inner arm material to accrete onto the planet, whereas the outermost material either goes into bound orbit or escapes. In the intact moon cases, the angular momentum exchange occurs primarily between the distorted figure of the target planet and a condensed region of impactor material (Fig. 2, B to E), and so in these cases the angular momentum sacrificed

to lift material into stable orbit is to a much greater degree derived from the planet, resulting in characteristically slower rotating planets and higher angular momentum and mass satellites. Intact moon formation is aided by a prograde spin of the impactor after the initial impact, which helps to counteract the shearing of impactor material due to differential Kepler motion; this can result from an initial prograde impactor or retrograde target spin, or from a highly grazing impact.

One overall implication of my simulations is that collisionally producing systems with $J \sim J_{\text{PC}}$ is correlated with the production of satellites that have $(M_s/M_p) = q \sim O(10^{-1})$. A second result is that oblique collisions with $v_{\text{imp}} \geq 1.3v_{\text{esc}}$ (or $v_{\infty} \geq 0.9$ km/s for $M_T \sim M_{\text{PC}}$) do not produce massive disks or satellites orbiting the primary, and this was true for all of the simulations.

The differentiation state and composition of Pluto and Charon could have been affected by a Charon-forming impact. For disk-producing cases, ice initially at temperatures $T \sim 150$ K

Fig. 1. Time series of a potential Pluto-Charon-forming impact yielding a planet-disk system (run 70 in table S1 with $N = 120,000$ particles). Results are shown looking down onto the plane of the impact at times $t = 1.3, 3.2, 7.5, 11.8, 14.5,$ and 24.6 hours; units shown are distance in 10^3 km. Color indicates material type (blue, water ice; orange, dunite; red, iron), with all of the particles in the 3D simulation overplotted in order of increasing density. The impacting objects are identical—both are predifferentiated into 40% ice mantles and 60% rock cores by mass with initial surface temperatures set to 150 K, increasing with depth (7) to a central temperature ≈ 800 K. After an initially oblique impact in the counter-clockwise sense (A), the two objects separate (B and C) before recolliding. After the second collision, the denser cores migrate toward the center, as a bar-type mode (36) forms in the rapidly rotating merged objects (D). From each end of the bar emanate spiral structures (D and E), whose self-gravity acts to transport angular momentum from inner to outer portions. The arms wrap up on themselves and finally disperse to yield a ring (36) of material (whose differential motion would on a longer time scale produce a disk), together with the central planet (F).



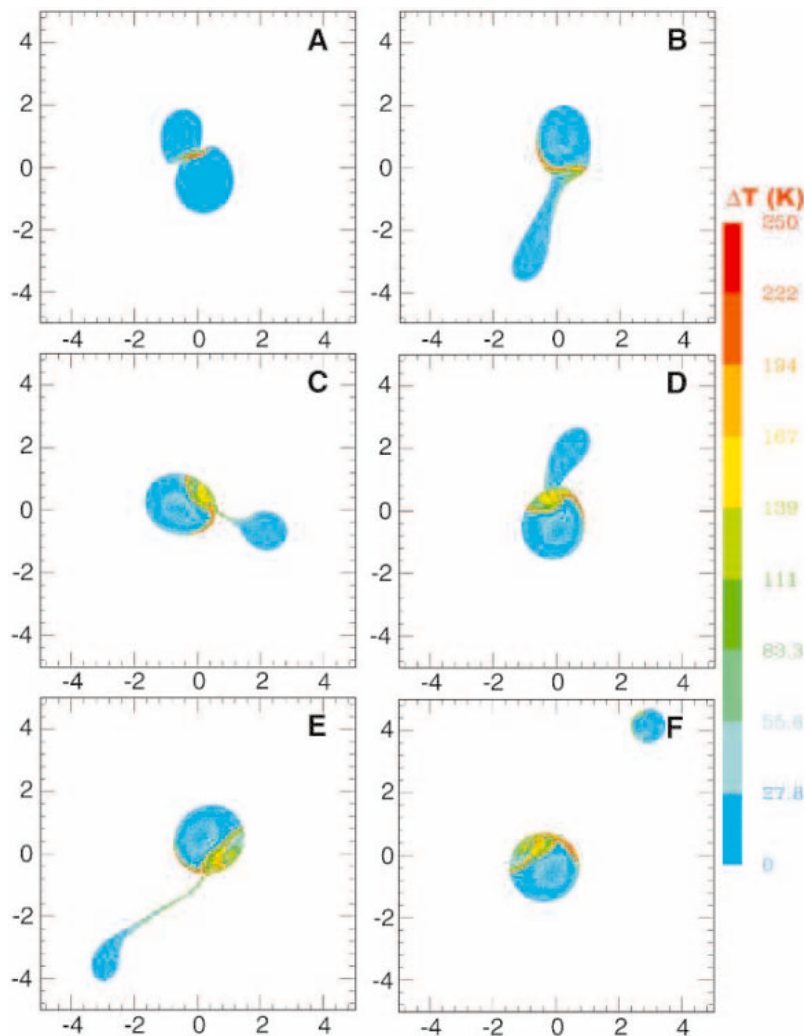


Fig. 2. Time series of a potential Pluto-Charon-forming impact yielding a planet-moon system (run 20 in Table 1 with $N = 20,000$ particles). Results are shown at times $t = 0.9, 3.2, 5.9, 7.5, 11.2,$ and 27.5 hours; distances are shown in units of 10^3 km and color scales with the change in temperature in kelvin. The impacting objects have uniform serpentine compositions. After an initially very oblique impact with a 73° impact angle (A), the two objects separate (B and C) and during this period the smaller impactor receives a net torque from the distorted figure of the target. After a second, even more grazing encounter (D), an additional portion of the impactor is accreted onto the planet, while the rest self-contracts into an intact moon containing 12% of the central planet's mass that is again torqued by the ellipsoidal figure of the target (D and E) onto a stable orbit with a semimajor axis of $6.5 R_p$ and an eccentricity of $e = 0.5$. The final moon in (F) is described by 2232 SPH particles.

Table 1. Parameters and results of impacts that yield moons with $0.1 < q < 0.15$. Simulations here involved undifferentiated objects. The preimpact spin state of the objects is shown by the fraction $(L_s/L_{\text{imp}}) = (\vec{L}_s \cdot \vec{L}_{\text{imp}})/|L_{\text{imp}}|^2$; superscripts i and it correspond, respectively, to L_s contained in the impactor or the impactor and target. L_{orb} is the angular momentum of the satellite, and J_f is the normalized final bound system angular momentum.

Run	M_T/M_{PC}	γ	b'	$v_{\text{imp}}/v_{\text{esc}}$	J_{imp}	L_s/L_{imp}	$L_{\text{esc}}/L_{\text{imp}}$	M_{esc}/M_T	$L_{\text{orb}}/L_{\text{imp}}$	J_f	q
5	1.00	0.3	0.852	1.00	0.508	0.38 ^{it}	0.06	0.010	0.378	0.486	0.102
6	1.00	0.3	0.785	1.00	0.483	0.40 ^{it}	0.01	0.002	0.365	0.480	0.108
33	1.00	0.3	0.853	1.20	0.397	0.04 ⁱ	0.00	0.000	0.514	0.397	0.115
1	1.00	0.3	0.918	1.00	0.379	0.10 ⁱ	0.00	0.000	0.584	0.379	0.120
19	1.00	0.3	0.853	1.00	0.333	0.05 ⁱ	0.00	0.000	0.529	0.333	0.125
20	1.00	0.3	0.957	1.00	0.356	0.00	0.00	0.000	0.545	0.356	0.125
7	1.00	0.3	0.958	1.00	0.379	0.06 ⁱ	0.00	0.000	0.447	0.379	0.131
16	0.95	0.5	0.899	1.00	0.452	0.12 ⁱ	0.00	0.000	0.508	0.452	0.144
21	0.95	0.5	0.862	1.05	0.454	0.11 ⁱ	0.00	0.000	0.505	0.454	0.148
22	1.00	0.3	0.924	1.05	0.372	0.03 ⁱ	0.00	0.000	0.588	0.372	0.149

in the region of the initial impact achieved a maximum $T \sim 300$ K ($\Delta T \sim 150$ K), with most of the ice heated to $T \sim 200$ K ($\Delta T \sim 50$ K), consistent with previous estimates (2). In moon-producing impacts, the satellite material experienced little heating ($\Delta T \sim 30$ K), because it had for the most part avoided direct impact with the planet, whereas the target was heated more substantially (Fig. 2).

For Pluto, the short-term heating processes associated with a large impact in combination with general accretional heating ($E_{\text{acc}}/M_p \sim 3/5[GM_p/R_p]$) could provide up to $\Delta T \sim 300$ K) and long-lived radiogenic heating ($\Delta T \leq 285$ K after 400 million years) seems most consistent with substantial melting and a differentiated state (22), although uncertainty associated with the rheology of rock-ice mixtures can affect this conclusion. The case for differentiation is much weaker for smaller Charon (22), and the results here reinforce this (23), particularly in the intact formation mode.

For $v_{\text{imp}}/v_{\text{esc}} \sim$ unity and $M_T \sim M_{PC}$, there is not appreciable vaporization of water ice, and successful impacts (Table 1 and table S1) lose only between 0 and 8% of their mass to escaping material. Thus, the increase in the overall rock-to-ice ratio of the pair as a result of a Charon-forming impact is expected to be modest to none. The intact moons contain material originating from the impactor with a similar bulk composition. In the collisions involving mixed compositions that produced disks, the denser components of the colliding objects migrated inward into the central planet (Fig. 1, D and E), leaving a disk of the preferentially lower density material (SOM text). Thus, if the impactor and proto-Pluto had similar overall ice-rock fractions, forming Charon from a disk implies $\rho_C < \rho_p$, whereas forming the satellite intact implies $\rho_C \sim \rho_p$. Both cases imply that the current total rock-ice fraction of the pair is similar to that of its progenitors.

Discussion. This work identifies a range of impacts capable of producing Pluto-Charon-type systems. The impacts are low-velocity ($v_\infty < 0.9$ km/s) oblique collisions by an impactor containing 30 to 50% of the Pluto-Charon system's mass, which often involve some preimpact spin of a magnitude similar to that estimated for other outer solar system bodies (24). The broadest range of successful impacts involves the intact formation of Charon rather than its accretion from an impact-generated disk. An intact formation implies similar planet and satellite densities, an initially eccentric satellite orbit, and characteristically larger possible satellite-to-planet mass ratios.

What is the probability of such an event? For random impact orientation (δ), $\sim 30\%$ of collisions have $b' > 0.8$. The frequency of large impacts in the early Kuiper belt is uncertain, as the current belt is believed to contain only a small portion of its original mass

(25) and to be more dynamically excited now ($\langle v_{\text{rel}}^2 \rangle^{1/2} \sim 1.5$ km/s) than when large objects formed there [$\langle v_{\text{rel}}^2 \rangle^{1/2} \ll 1$ km/s (26)]. Recent accretion simulations that produce $\sim 10^3$ -km Kuiper belt objects (KBOs) (26) predict a large-body cumulative size distribution $N_{>R} \propto R^{-q'}$ with $q' \sim 3$. This implies several tens of objects as large as those considered here ($800 < R\text{-km} < 1100$) to be consistent with the formation of $\sim 10^5$ KBOs with $R > 50$ km as estimated from current surveys (26). A “particle-in-a-box” estimate gives the characteristic time between large impacts in the Kuiper belt region

$$\begin{aligned} \tau_{\text{col}} &\approx \frac{2\pi a \Delta a H}{N_e^2 \pi (R_e + R_c)^2 v_{\text{rel}} \left[1 + \left(\frac{v_{\text{esc}}}{v_{\text{rel}}} \right)^2 \right]} \\ &\sim 10^9 \text{ years} \left(\frac{T_{\text{orb}}}{250 \text{ years}} \right) \left(\frac{50}{N_e} \right)^2 \\ &\quad \times \left(\frac{10^3 \text{ km}}{R_e} \right)^2 \left(\frac{10^2}{f} \right) \end{aligned} \quad (4)$$

where Δa and $H \approx v_{\text{rel}}/\Omega$ are the width and height of the disk annulus, respectively, $T_{\text{orb}} \equiv 2\pi/\Omega$ is the orbital period, $f \equiv [1 + (v_{\text{esc}}/v_{\text{rel}})^2]$ is the gravitational focusing factor, and v_{rel} is the relative velocity between large embryos of radius R_e and number N_e . In the current belt, $f \sim$ unity and large collisions occur too infrequently to be relevant.

If the early Kuiper belt contained a substantially greater number (27) of 10^3 -km-class KBOs than the current belt [with such objects later lost, e.g., through dynamical scattering (28)] and/or had much lower characteristic relative velocities and strong gravitational focusing, large impacts would have been more common. In the primordial accretory epoch, estimated velocities for $R \sim 10^3$ km objects are $v_{\text{rel}} \sim O(10^{-2}$ to $10^{-1})$ km/s (26) or $f > 10^2$ for $v_{\text{esc}} \sim 1$ km/s with $\tau_{\text{col}} < 10^9$ years. Large objects formed through so-called oligarchic growth with low v_{rel} could have become orbitally isolated from one another and thus have grown primarily through the accretion of small material (9, 26). However, it seems probable that such isolation would have been periodically overcome, as growing large bodies would have become increasingly dynamically crowded, leading to episodes of mutual collisions among “battling oligarchs” (9). Furthermore, the sweeping of Neptune’s mean-motion resonances through the Kuiper belt as that planet began migrating outward (29) may have itself instigated large collisions in previously dynamically stable zones and/or acted to increase the surface density of large objects captured within resonances (3).

The low-velocity impacts that produce $q > 0.1$ have $v_{\infty} < 0.9$ km/s, which is consistent with a collision in the early Kuiper belt. However, the timing of a Charon-forming impact

relative to the capture of Pluto-Charon into the 3:2 resonance with Neptune is uncertain. The binary could have formed first, at an orbital distance ~ 5 AU closer to the Sun than Pluto’s current semimajor axis, and the pair later captured as Neptune’s 3:2 migrated past them, with Pluto’s $e \approx 0.25$ orbital eccentricity obtained subsequently (29, 30). If Pluto had been captured in the 3:2 before the Charon-forming impact, an appropriate v_{∞} with a large nonresonant impactor might still have resulted (for example, in its current orbit,

Pluto’s e provides a velocity relative to circular orbits of 0.5 to 0.8 km/s at its periape and apoapse), but such an impact would have likely dislodged Pluto from resonance (31, 32). Although recapture could occur (33), the probability of this is low if the pair had a substantial orbital eccentricity (i.e., $< 10\%$ for $e > 0.15$) (34). A more promising scenario involves the collision of Pluto and an impactor both already trapped in the 3:2, as in this case, a lower relative velocity due to the difference in their forced and/or free eccentricities (32) could

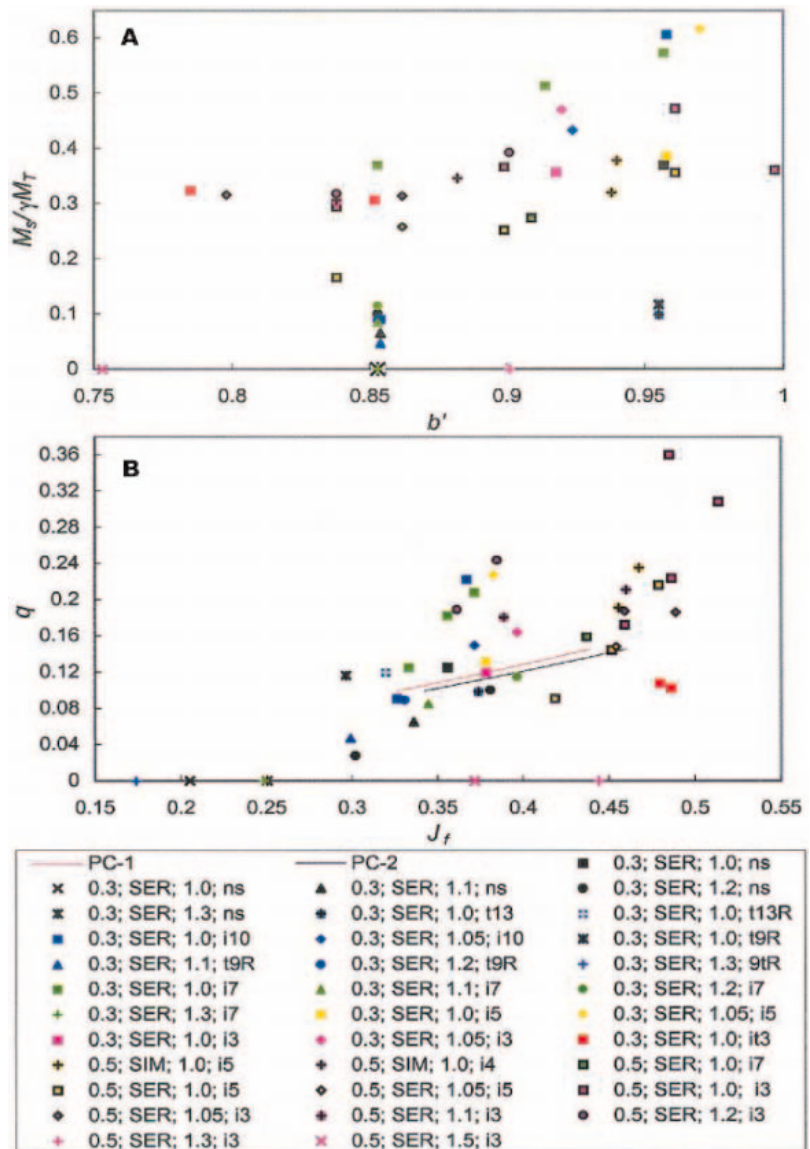


Fig. 3. Results of impact simulations that produced intact moons. Simulation parameters are shown in the legend, in which the first value is the ratio of the impactor to the total mass (γ), the second indicates the composition of the colliding objects, the third is the ratio of the impact velocity to the escape velocity, and the fourth is the preimpact prograde spin period in hours for the impactor (i) and/or target (t), with R indicating a retrograde initial spin. Cases in which an intact fragment containing 5 to 50% of the total mass escaped and little material ($< 1\%$) remained in orbit are shown as $q = 0$. (A) The mass fraction of the impactor that comprises the final moon versus the scaled impact parameter ($b' = 1$ for a grazing impact). (B) Resulting satellite-to-planet mass ratio versus the normalized angular momentum of the final bound system. In all cases, the resulting moons had periapees exterior to the co-rotation radius, $a_{\text{co}}(\sqrt{GM_T/a_{\text{co}}^3} \equiv \omega_p)$. Red and black lines bracket the parameter regime for Pluto-Charon for $0.1 < q < 0.15$ (from eq. S1).

result, and the postimpact pair might then remain in resonance.

The tendency for oblique low-velocity collisions between similarly sized objects to produce substantial amounts of material in bound orbit suggests that the impact generation of satellites is a common outcome of late-stage accretion, with the Earth-Moon ($q = 0.01$ and $J = 0.115$) and Pluto-Charon offering examples of the potential range of q and J in systems produced by such events. Requiring $(v_{\text{imp}}/v_{\text{esc}}) < 1.3$ for forming large satellites based on the simulations here implies that binary systems produced through such singular impacts would have (from Eqs. 1 and 2) $J \lesssim 0.8$.

References and Notes

- W. B. McKinnon, *Nature* **311**, 355 (1984).
- W. B. McKinnon, *Astrophys. J.* **344**, L41 (1989).
- S. A. Stern, W. B. McKinnon, J. Lunine, in *Pluto and Charon*, S. A. Stern, D. J. Tholen, Eds. (Univ. Arizona Press, Tucson, AZ, 1997), pp. 605–663.
- R. M. Canup, *Annu. Rev. Astron. Astrophys.* **42**, 441 (2004).
- A. G. W. Cameron, W. Benz, *Icarus* **92**, 204 (1991).
- R. M. Canup, E. Asphaug, *Nature* **412**, 708 (2001).
- R. M. Canup, *Icarus* **168**, 433 (2004).
- C. B. Agnor, R. M. Canup, H. F. Levison, *Icarus* **142**, 219 (1999).
- P. Goldreich, R. Sari, Y. Lithwick, *Annu. Rev. Astron. Astrophys.* **42**, 549 (2004).
- C. B. Olkin, L. H. Wasserman, O. G. Franz, *Icarus* **164**, 254 (2003).
- Our SPH simulations ignore material strength. A fluid description is valid when stresses associated with self-gravity (as well as compressional pressures associated with the impact event itself) greatly exceed the material strength, which is true for the size objects considered here (35).
- H. J. Melosh, paper presented at the 31st Lunar and

Planetary Science Conference, Houston, TX, 13 to 17 March 2000, abstract no. 1903.

- S. L. Thompson, H. S. Lauson, *Sandia Natl. Lab. Technical Report No. SC-RR-710714* (Sandia Laboratories, Albuquerque, NM, 1972).
- L. Brookshaw, Working Paper Series SC-MC-9813, Faculty of Sciences (University of Southern Queensland, Australia).
- W. Benz, in *Proceedings of the NATO Advanced Research Workshop on The Numerical Modelling of Nonlinear Stellar Pulsations*, J. R. Buchler, Ed. (Kluwer, Boston, 1990), pp. 269–288.
- R. M. Canup, W. R. Ward, A. G. W. Cameron, *Icarus* **150**, 288 (2001).
- G. Tancredi, J. A. Fernandez, *Icarus* **93**, 298 (1991).
- Rotation periods for the impactor and target between 3 and 13 hours are considered here. Estimates of rotation periods for Kuiper belt objects with $R > 10^2$ km range from about 6 (Varuna) to 14 (2001 QG298) hours (24).
- The Roche limit, $a_R \equiv 2.456R_p(\rho_p/\rho_s)^{1/3}$, is the closest distance a fluid strengthless body of density ρ_s can stably exist from a radius R_p and density ρ_p primary. At the end of each run, we classified particles as escaping (positive kinetic + potential energies), orbiting, or in the planet. A particle was considered to be orbiting if its total energy was negative, and the z component of its angular momentum exceeded that of a circular orbit at the surface of the planet. We defined an equivalent circular orbit as one having the same angular momentum as computed for a given particle but with $e = 0$. If $a_{\text{equiv}} > a_R$, the particle was considered to be on a Roche exterior orbit.
- S. Ida, R. M. Canup, G. R. Stewart, *Nature* **389**, 353 (1997).
- The resulting satellite would be smaller if substantial mass were lost from the disk subsequent to the impact or larger if angular momentum were transferred to the disk material before the satellite formed.
- W. B. McKinnon, D. P. Simonelli, G. Schubert, in *Pluto and Charon*, S. A. Stern, D. J. Tholen, Eds. (Univ. Arizona Press, Tucson, AZ, 1997), pp. 295–343.
- Tides in an initially eccentric Charon-sized satellite (Fig. 2) would circularize its orbit in $\sim 10^6$ to 10^7 years (22), yielding $\Delta T \sim 20$ K. Rapid accretion of the satellite from a disk would produce $E_{\text{acc}}/M_c \sim 3/5[GM_c/R_c]$ or up to $\Delta T \sim 80$ K for a specific heat $C \sim 1.5 \times 10^7$ erg/g K (33).
- S. S. Sheppard, D. C. Jewitt, *Astron. J.* **127**, 3023 (2004).
- M. Holman, J. Wisdom, *Astron. J.* **105**, 1987 (1993).
- S. J. Kenyon, *Publ. Astron. Soc. Pac.* **114**, 265 (2002).
- S. A. Stern, *Icarus* **90**, 271 (1991).
- J.-M. Petit, O. Mousis, *Icarus* **168**, 409 (2004).
- R. Malhotra, *Nature* **365**, 819 (1993).
- Pluto's current eccentricity suggests that it migrated outward by ~ 5 to 10 AU after its capture into Neptune's 3:2 (29).
- H. F. Levison, S. A. Stern, *Icarus* **116**, 315 (1995).
- J. Hahn, W. R. Ward, *Lunar Planet. Sci. Conf. XXVI*, 541 (1995).
- A. R. Dobrovolskis, S. J. Peale, A. W. Harris, in *Pluto and Charon*, S. A. Stern, D. J. Tholen, Eds. (Univ. Arizona Press, Tucson, 1997), pp. 159–190.
- R. Malhotra, *Astron. J.* **110**, 420 (1995).
- S. Sridhar, S. Tremaine, *Icarus* **95**, 86 (1992).
- H. A. Williams, J. E. Tohline, *Astrophys. J.* **334**, 449 (1988).
- This research was supported by the NSF under grant no. AST0307933. J. Melosh and B. Pierazzo are gratefully acknowledged for providing the M-ANEOS equation of state and related material constants. This paper has benefited from previous work and discussions with E. Asphaug, W. Ward, A. Stern, R. M. Canup, B. McKinnon, S. Kenyon, and H. Levison and from two anonymous and helpful reviews. A. Stern, L. Young, C. Olkin, and B. Bottke provided helpful comments on the manuscript, and Southwest Research Institute provided the computational resources.

Supporting Online Material

www.sciencemag.org/cgi/content/full/307/5709/546/DC1
SOM Text
Fig. S1
Table S1
References

27 October 2004; accepted 29 December 2004
10.1126/science.1106818

Farming and the Fate of Wild Nature

Rhys E. Green,^{1,2*} Stephen J. Cornell,^{1,3} Jörn P. W. Scharlemann,^{1,2} Andrew Balmford^{1,4}

World food demand is expected to more than double by 2050. Decisions about how to meet this challenge will have profound effects on wild species and habitats. We show that farming is already the greatest extinction threat to birds (the best known taxon), and its adverse impacts look set to increase, especially in developing countries. Two competing solutions have been proposed: wildlife-friendly farming (which boosts densities of wild populations on farmland but may decrease agricultural yields) and land sparing (which minimizes demand for farmland by increasing yield). We present a model that identifies how to resolve the trade-off between these approaches. This shows that the best type of farming for species persistence depends on the demand for agricultural products and on how the population densities of different species on farmland change with agricultural yield. Empirical data on such density-yield functions are sparse, but evidence from a range of taxa in developing countries suggests that high-yield farming may allow more species to persist.

Clearance for cropland or permanent pasture has already reduced the extent of natural habitats on agriculturally usable land by more than 50% (1–3), and much of the rest has been altered by temporary grazing (4).

Intensive management to increase production—through irrigation and the application of fertilizers and pesticides—can further reduce the wildlife value of farmed land. Although growth in global food production outstripped

population growth between 1961 and 1999, this was achieved through a 12% increase in the global area of cropland and a 10% rise in the area of permanent pasture (2, 3). Overall food crop yield per unit area (3) grew by 106%, but this was linked to a 97% rise in the area of land under irrigation, and 638%, 203%, and 854% increases, respectively, in the use of nitrogenous and phosphate fertilizers and the production of pesticides (2, 5, 6). These impacts look set to grow still further (5). With the human population predicted to rise to between 8 and 10 billion (7, 8) and with rapidly increasing per capita consumption (9), overall food demand is expected to increase two- to threefold by 2050 (6, 10). Here, we propose an agenda for the research needed to identify how this enormously increased demand can be met at the least cost to the other species with which we share our planet.

Agricultural change: A tale of two worlds. From the perspectives of both development and conservation, globally averaged changes in agriculture mask important spatial variation, with more pronounced recent changes in the developing world, where most species reside. For instance, since 1961 the total area of cropland in the developing world has increased by over

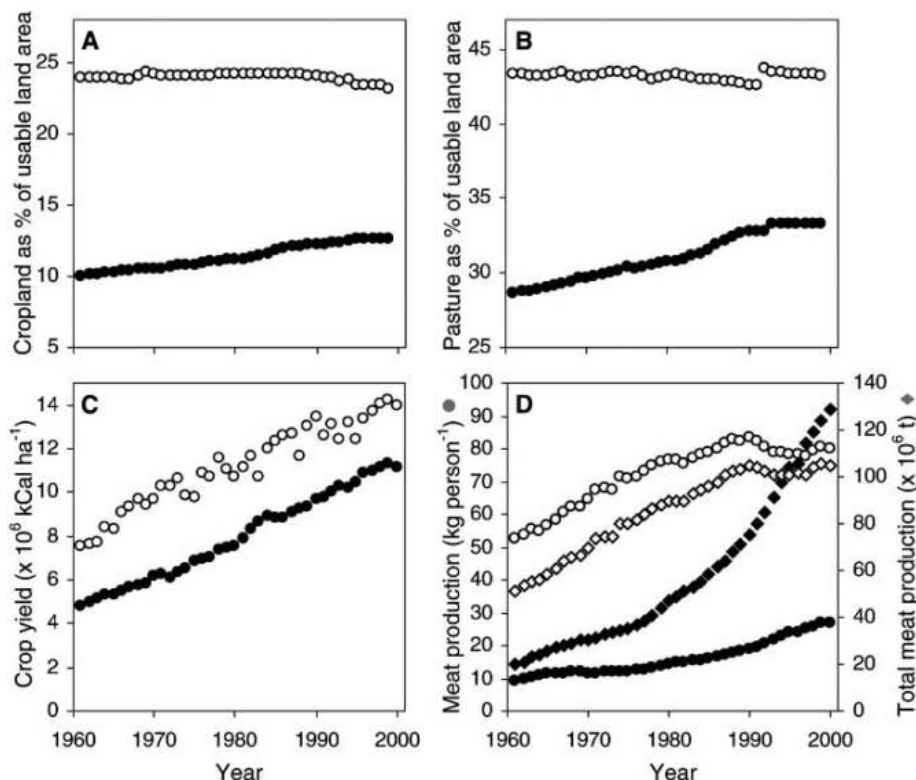


Fig. 1. Changes in agriculture in the developing and developed worlds (3), 1961 to 2000, showing annual changes in cropland (A), permanent pasture (B), mean crop yields for the 23 main food crops (3) (C), and per capita and total meat production (D). In (A) and (B), farmed areas are plotted as a percentage of usable land (3). Filled symbols are for developing world, open for developed. In (D), circles are for per capita meat production, diamonds for total meat production.

20%, whereas developed world cropland area has shrunk (Fig. 1A). A similar pattern emerges for permanent pasture (Fig. 1B). These differences in the rates of change of farmland area are not offset by lower yield growth in developing countries. Crop yields (3) have grown steadily in both the developing and developed world, with the former lagging the latter by an average of roughly 20 years (Fig. 1C). Annual growth in yield is now higher in the developing world. Further evidence that farming is changing faster in the developing world comes from trends in livestock production. Because of increasing domestic demand (9), per capita meat production is rising rapidly in the developing world, whereas elsewhere it is declining; more than half of global meat production now takes place in developing countries (Fig. 1D). How are these changes impacting wild habitats and species?

Differing impacts of farming on wild nature. Several kinds of data suggest that, although it is an important driver almost everywhere, the effect of agricultural change on wild nature is now greatest in developing countries. Coarse-scale evidence of changes in forest cover shows that recent net gains in temperate and boreal forest cover are more than offset by continued losses in tropical regions, largely by conversion to agriculture (11). Patchy data on changes in populations of temperate and tropical forest vertebrates confirm this pattern (12, 13). For a more detailed picture of the relative importance of threats to biodiversity posed by farming, we used BirdLife International's World Bird Database (3) to dissect the problems faced by all 1923 species of globally threatened and Near-Threatened birds; data for no other taxa permit such detailed and comprehensive analysis.

These data show that farming (including conversion to farmland and its intensifying use) is the single biggest source of threat to bird species listed as threatened (accounting for 37% of threats) and is already substantially more important for species in developing countries than those in developed countries (40% and 24% of threats, respectively; Fig. 2A). For developing and developed countries alike, the scale of the threat

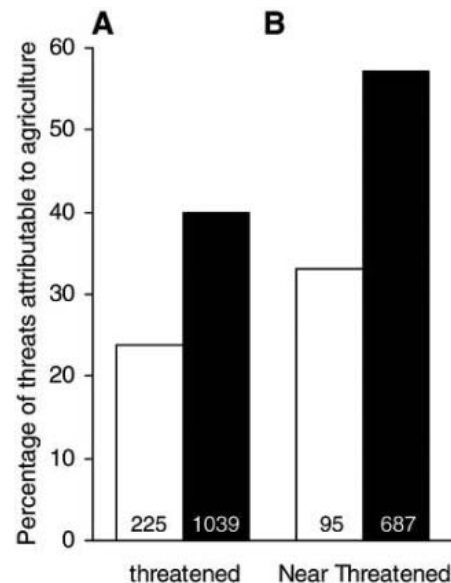


Fig. 2. The mean proportion of a species' listed threats that are attributable to agriculture plotted for threatened (A) and Near-Threatened (B) birds from the developed (white) and developing (black) world (3).

posed by agriculture is even greater for Near-Threatened species (57% and 33% of threats, respectively; Fig. 2B). Because these species are likely to become threatened in the near future (14), this implies that agriculture is a growing threat to bird species. There are also larger absolute numbers of threatened and Near-Threatened species in developing countries than in developed countries (threatened, 1039 versus 225 species; Near-Threatened, 687 versus 95). Taken together, these data indicate that agriculture is the major current and likely future threat to bird species, especially in developing countries. Given the growing scale and impacts of agriculture, how should we best resolve the need for increased food production with the desire to minimize its impact on what remains of wild nature? Two sorts of suggestions predominate.

Wildlife-friendly farming. Many conservation biologists argue that the global application of wildlife-friendly farming methods would reduce the impact of agriculture on biodiversity. Approaches include the retention of patches of natural habitat and extensively farmed seminatural habitats within the countryside and farming in ways that minimize the negative effects of fertilizers and pesticides on nontarget organisms (15–20). Such wildlife-friendly farming receives particularly strong support in Europe, where evidence of declines in the previously high biological value of long-established agroecosystems (17, 21, 22) is used to justify agri-environment payments worth over \$2.7 billion each year to European Union farmers (23). There are far fewer data on farmland biodiversity in less

¹Department of Zoology, University of Cambridge, Downing Street, Cambridge, CB2 3EJ, UK. ²Royal Society for the Protection of Birds, The Lodge, Sandy, SG19 2DL, UK. ³The Faculty of Biological Sciences, University of Leeds, Leeds, LS2 9JT, UK. ⁴Percy FitzPatrick Institute of African Ornithology, University of Cape Town, Private Bag, Rondebosch 7701, South Africa.

*To whom correspondence should be addressed. E-mail: reg29@hermes.cam.ac.uk

developed regions, but evidence that about half of Costa Rica's native forest species of birds, mammals, butterflies, and moths also occur in agricultural areas (table S1) has been used to argue that maintaining low-intensity agriculture will benefit biodiversity in developing countries as well (18–20) (table S1).

It is clear that adopting farming methods that enhance population densities of wild plant and animal species on farmland is beneficial to biodiversity, provided that the change to wildlife-friendly farming does not require a reduction in crop yield (19, 24). However, it is frequently observed that the biodiversity value of farmland declines with increasing yield (17, 21, 22), which suggests that maintaining high wild-

life interest on farmland often requires foregoing opportunities for high crop yields. Existing agri-environment schemes depend on farmers receiving large amounts of financial compensation for lost production, demonstrating that such yield penalties are perceived as real. Their existence underlies a very different school of thought on how best to simultaneously deliver food production needs and meet conservation goals.

Land sparing. This second approach hinges on moving beyond thinking solely about the farmed landscape to considering the consequences of yield penalties for the total area of farmed versus nonfarmed land. Although wildlife-friendly farming is beneficial on farmland, if it reduces yield then

a larger area must be farmed to meet any given production target. Both the Costa Rican and other results (table S1) show that even under benign agriculture, farmland usually hosts far fewer species—especially those of conservation concern—than do the relatively intact habitats from which it was derived. Hence, if yield penalties from wildlife-friendly farming are sufficiently large, the best route to meeting both food production and conservation goals may be to increase yields on already converted land, thereby reducing the need to convert remaining intact habitats, and potentially freeing up former farmland for restoration to a more natural state.

This land-sparing argument is rarely made by conservationists (25, 26), but is

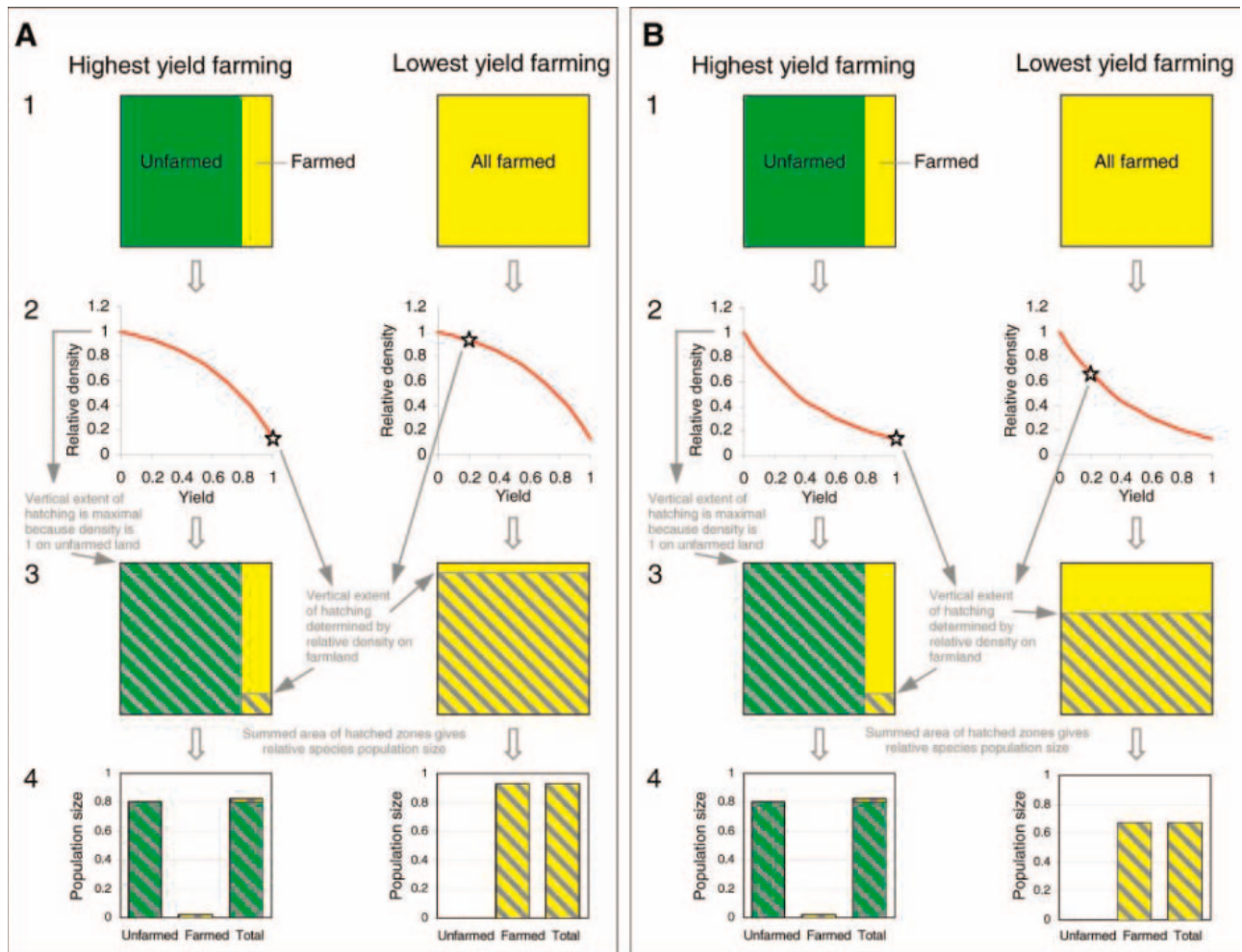


Fig. 3. Essential features of the model relating species population size to agricultural yield, shown by two examples. In the first (A), a province, shown as a map (1), is composed of farmed (yellow) and nonfarmed (green) land. The target agricultural production is $\alpha = 0.2$, which could be achieved by highest yield farming on 20% of the land area ($x = 1$, left panels) or by farming all the land at lowest possible yield ($x = 0.2$, right panels). The organism exhibits a concave density-yield function (red curve in 2), with its highest population density on nonfarmed land (where it is set to 1) and far lower density under highest yield farming than under lowest yield farming (compare stars on left and right panels in 2). The total population size of the whole province can be visualized by

shading the maps (3), so that for each habitat, the vertical extent of hatching is proportional to relative population density. The summed area of the hatched zones, relative to that of the whole province, then gives the total population size relative to the population size that would occur if the whole province were unfarmed. These relative population sizes, for nonfarmed and farmed areas and the province as a whole, are shown in the histograms (4). In this case, the total population is higher with lowest yield farming. In the second example (B), the situation is the same, except that the density-yield relationship is convex. In this example, the steep drop in density even at low yields means that land sparing is worthwhile and the total population is higher with highest yield farming.

widely advocated in the agriculture and development literature (27–33). Retrospective calculations for the United States, China, and India suggest that, without the marked increases in yields seen over recent decades, producing the amounts of food currently grown there would require 2 to 4 times more land under crops than at present (28, 33–35). Moreover, comparisons among Latin American countries provide empirical evidence that, taking other factors into account, land sparing has occurred: In the 1980s, countries with higher agricultural yield had lower deforestation rates (30), and those with higher yield increases had lower rates of increase in farmland area (27). Finally, prospective calculations show that without yield increases, even maintaining current per capita food consumption would necessitate a near doubling of the world's cropland area by 2050; by comparison, raising global average yields to those currently achieved in North America could result in very considerable land sparing (28).

Hence, although wildlife-friendly farming offers scope to increase the biodiversity value of farmed land on a per unit area basis, this may not result in a net benefit to biodiversity if it reduces crop yield. On the other hand, increasing yield could reduce the requirement for farmland and the rate of conversion of currently nonfarmed land. We may therefore face a choice between having a greater area of low-yielding wildlife-friendly farmland and less intact habitat or having a smaller area of high-yielding, less

wildlife-friendly farmland and more area available for wild nature elsewhere. Identifying the key parameters that can resolve this trade-off requires a model.

Modeling the trade-off. Our model relates the population size of individual species within a large area (“province”) to the yield per unit area of farmed land and the target agricultural production required. We focus on one species at a time to allow for evident differences between species in how they respond to changing agricultural activity. Results can later be combined across species and used to optimize province-wide metrics such as the proportion of species committed to extinction. The model province consists of a farmed part (which can include patches of natural habitat) and a nonfarmed part, and it is uniform in its potential suitability for both farming and the species of interest. We ignore any negative external effects of farming on wildlife in nonfarming areas. Crop yield x of the farmed land is scaled relative to the maximum attainable over a large area, and the target level of production of agricultural goods α is assumed to be fixed and is scaled in terms of the proportion of the province needed to grow it if yield were at the maximum (i.e., at $x = 1$). The minimum yield that can still produce the production target is $x = \alpha$ (because the whole of the province must be farmed to grow the target at this yield), and the permissible yield lies in the range $\alpha \leq x \leq 1$. For a given yield x' within this range, we assume that the production target is just

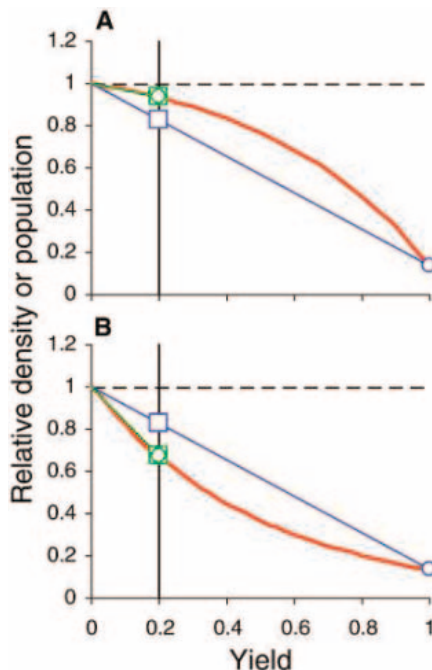
met, so that the proportion of the province that is farmed is α/x' and the proportion that is nonfarmed is $1 - (\alpha/x')$.

To see how yield then affects the population of a given species, consider a species-specific density-yield function, whereby population density is some function $f(x)$ of yield, and is scaled to 1 on nonfarmed land ($f(0) = 1$). The overall population of a species across the whole province is then the sum of its population on nonfarmed land $1 - (\alpha/x')$ and its population on farmed land $f(x') (\alpha/x')$, which is $1 + (\alpha/x') (f(x') - 1)$. Considering first a concave density-yield function (Fig. 3A, red curve), highest yield farming (at $x = 1$, summarized in the left panels) is associated with very low relative population density on farmed land (star in step 2), but with a large area of nonfarmed land with relative population density of 1 (step 3), containing most of the total population (step 4). In contrast, farming at the lowest permissible yield ($x = \alpha$, right panels) results in a far higher density on farmed land than with high-yield farming (star in step 2), which in this case more than offsets the loss of population associated with having no nonfarmed land. For this density-yield function, the total population size of this species is thus higher with lowest yield than with highest yield farming. Working through the same logic with a convex density-yield function (Fig. 3B), it can be seen that the population density on lowest yield farmed land is now considerably lower than with the concave function, and the total population is higher with highest yield farming (the sum of few individuals on farmed land plus many on the nonfarmed land spared from conversion). Comparison of these two examples therefore shows that the shape of a species' density-yield function affects which farming regime maximizes its overall population.

To explore the effects of different density-yield functions more systematically, consider a graphical version of the model (Fig. 4A). This includes both a density-yield function (red curve) and a vertical threshold line (in black) at $x = \alpha$, representing the minimum yield that can meet the production target. For any given yield x' in the permissible range ($\alpha \leq x' \leq 1$), it can be shown that the y value at which a chord drawn from $x = 0, y = 1$ to the red curve [at $x', f(x')$] intersects the vertical threshold line gives the total population size of the organism at x' , summed across the entire province and scaled relative to the population that would result if the entire province were nonfarmed [relative population size = $1 + (\alpha/x') (f(x') - 1)$]. By considering where all such permissible chords intersect the vertical threshold, one can identify the yield at which total population size is maximized.

Thus, in Fig. 4A (corresponding to Fig. 3A), the chord for lowest permissible yield

Fig. 4. A graphical version of the model. (A) A concave density-yield function $y = f(x)$ (red curve; same as 2 in Fig. 3A). The vertical threshold line (black) shows the minimum production that can meet the target agricultural production ($\alpha = 0.2$). A chord drawn from $x = 0, y = 1$ to the red curve at $x', f(x')$ at any point in the permissible range $\alpha \leq x' \leq 1$, intersects this vertical threshold at $1 + (\alpha/x') (f(x') - 1)$, which is the total population size of the organism in the entire province scaled relative to the population size that would occur if the entire province were nonfarmed. The blue line (termed the critical chord) joins the points on the red curve for $x = 0$ and $x = 1$; its intersection with the vertical threshold (blue square) gives relative population size under maximum yield farming. The green line runs from $x = 0, y = 1$ to the red curve at $0.2, f(0.2)$, and so its intersection with the vertical threshold (green square) gives the relative population size at lowest possible yield; this is greater than that under highest yield farming, and indeed that of any other chords in the permitted yield range, indicating that the total population size is maximized under lowest yield farming. These results are the same as those obtained in steps 1 to 4 of Fig. 3A. (B) Same as (A), except that the convex function from step 2 of Fig. 3B is used (with the same results as steps 1 to 4). This time the critical chord cuts the vertical threshold above the green chord and any other permissible chords, so the total population is highest when yield is highest.



(in green) intersects the vertical threshold above the line for maximum yield (in blue, termed the critical chord) and all other chords. Indeed, whenever the $f(x)$ curve is concave between $x = 0$ and $x = 1$, then the chord for lowest permissible yield always cuts the vertical threshold at the highest point of any yield in the permissible range: Thus, the total population of the species is highest at lowest possible yield. On the other hand, if as in Fig. 4B (corresponding to Fig. 3B), the $f(x)$ curve is convex between $x = 0$ and $x = 1$, the critical chord always cuts the vertical threshold above all other permissible chords, and farming at the maximum yield results in the highest population of the species. This rule also applies for species whose density increases with increasing yield (fig. S1). Results for more complex density-yield functions include dependence of the optimum on α , and an optimum at yields intermediate between the minimum and maximum [supporting online material (SOM) text].

Extension from individual species to province-wide biodiversity. Our model offers a quantitative comparison of the benefits to biodiversity of wildlife-friendly farming and land sparing, and it highlights the fundamental importance of the shape of density-yield functions. It can be extended from the single species case by considering density-yield functions for all species, or a representative sample, to estimate a province-wide metric such as the proportion of species committed to extinction under a particular farming regime. Those species with density-yield functions that exceed 1 at the selected yield value would be assumed not to be at risk of extinction, because they would have higher total populations under that regime than before agricultural modification of the landscape. For species with total populations that are lower than they would be if the whole province were nonfarmed (because their density is lower on land farmed at the chosen yield than on nonfarmed land), extinction risk might be calculated with methods derived from the species-area relationship (36). One could then calculate an optimal farming regime, which minimizes the proportion of species committed to extinction (but which would nevertheless be less favorable for some species than for others).

Limitations. Despite these potentially valuable applications, the model can be criticized for being much simpler than the real world, in various ways. First, our model assumes that farming does not affect the population density of species in nonfarmed areas. High-yield farming often leads to external effects such as pollution from pesticides and fertilizers and abstraction of water for irrigation (5, 6). However, such adverse effects can be reduced, through a combination of techni-

cal development and regulation (6, 24, 32, 37). Furthermore, low-yield farming may also affect nonfarmed habitats and, although the effect per unit of farmed area may be less severe, the total impact might be greater than for high-yield farming if larger areas of farmland are needed to meet a production target.

Second, the model supposes that agricultural production is at a fixed level for a given scenario, so that an increase in yield results in a proportionately reduced area required for farming. In practice, both empirical and theoretical evidence suggest that land sparing can sometimes be imperfect. If product demand or labor supply are elastic, or if technological changes free up rather than use up labor, increasing yields can in effect increase production targets, thereby adding to the requirement for agricultural land (24, 31, 38). The model also assumes that nonfarmed land spared from agricultural use will not be converted to some other human use unfavorable for biodiversity. Offsetting these points about likely imperfections in the operation of land sparing, it is also worth noting that there are imperfections in the real world in the delivery of biodiversity benefits by wildlife-friendly farming techniques (39).

Last, the model assumes that population size is given simply by the product of density and area. The size and distribution of patches of farmed and nonfarmed land are ignored, but fragmentation of preferred habitat would be expected to influence population density and viability. We also ignore dispersal between farmed and nonfarmed land, yet because of the effects of habitat quality on demographic rates, the population in one compartment might only persist because of net immigration from the other (40).

Although the model could be elaborated to incorporate externalities, imperfect land sparing, the spatial configuration of different land-use patches, and source-sink dynamics, we consider that our main conclusion would hold: The best way to reconcile farming and conservation depends on actual production targets and, crucially, on the relative frequency of species with different density-yield functions.

Prospects for wildlife-friendly farming versus land sparing. At present, we know little about how population densities of species on farmed land change with yield, although some forms of the density-yield function seem unlikely to be frequent (SOM text). Few studies have measured density comparably across a range of production regimes, and fewer still have simultaneously measured agricultural yields. Nevertheless, the growing number of studies indicating that half or more of all species of unmodified habitats are absent even from low-intensity farmland (table S1) suggests that many species

are likely to exhibit negative-trending convex density-yield functions (Fig. 4B). These species will fare best under maximum-yield agriculture combined with land sparing. Such beneficial land sparing is perhaps easiest to envisage in developing countries with limited histories of farming and large numbers of agriculturally naïve species, where increasing yields may reduce the pressure to clear intact habitat. However, insofar as valuable wildlife habitat can be restored or recreated on abandoned farmland, and agriculturally sensitive species still exist, land sparing through yield increases may also be important in regions with long histories of agriculture; indeed, coupling appropriately managed intensification with abandonment and restoration elsewhere may be a principal route to achieving new and ambitious programs of large-scale habitat recovery in Europe and elsewhere (41–43).

An agenda for empirical research.

What kinds of farming give the best prospect of minimizing losses of wild nature to habitat removal and change while providing food for a growing and more demanding human population? This paper does not provide an answer to that question. However, it does make explicit the nature of the quandary about whether high-yield or low-yield farming, or something in between, is best for biodiversity. Above all, our analysis highlights the need to know more about density-yield functions of real species in the real world, about how they might be modified by changes in agricultural and conservation methods, and about how far different kinds of farming influence the wildlife of nonfarmed areas. We also need to know much more about the extent and limits to which land is spared from agricultural use because of increased yields. Rapidly acquiring the data to address these issues is essential if we are to make wise and informed choices about how and where we farm. Few other decisions will have as great an influence on the fate of wild nature.

References and Notes

1. J. F. Richards, in *The Earth as Transformed by Human Action*, B. L. Turner II et al., Eds. (Cambridge Univ. Press, Cambridge, UK, 1990), pp. 163–178.
2. FAOSTAT, *FAO Statistical Databases* (Food and Agricultural Organisation of the United Nations, Rome, 2001).
3. Materials and methods are available as supporting material on Science Online.
4. B. Groombridge, M. D. Jenkins, *World Atlas of Biodiversity: Earth's Living Resources in the 21st Century* (Univ. of California Press, Berkeley, CA, 2002).
5. D. Tilman et al., *Science* **292**, 281 (2001).
6. D. Tilman, K. G. Cassman, P. A. Matson, R. Naylor, S. Polasky, *Nature* **418**, 671 (2002).
7. W. Lutz, W. Sanderson, S. Scherbov, *Nature* **412**, 543 (2001).
8. United Nations Population Division, *World Population Prospects; The 2002 Revision Highlights* (UNPD, New York, 2003), available at www.un.org/esa/population/publications/wpp2002/WPP2002-HIGHLIGHTSrev1.PDF.

9. N. Myers, J. Kent, *Proc. Natl. Acad. Sci. U.S.A.* **100**, 4963 (2003).
10. J. Bongaarts, *Popul. Dev. Rev.* **22**, 483 (1996).
11. FAO, *Global Forest Resources Assessment 2000: Main Report*, FAO Forestry Paper 140 (FAO, Rome, 2001).
12. J. Loh et al., *Living Planet Report 2002* (WWF, Gland, Switzerland, 2002), available at www.panda.org/downloads/general/LPR_2002.pdf.
13. M. Jenkins, R. E. Green, J. Madden, *Conserv. Biol.* **17**, 20 (2003).
14. IUCN Species Survival Commission, *IUCN Red List Categories and Criteria, Version 3.1* (IUCN, Gland, Switzerland, 2001).
15. A. Estrada, R. Coates-Estrada, D. A. Meritt Jr., *Biodiversity Conserv.* **6**, 19 (1997).
16. A. Estrada, R. Coates-Estrada, A. A. Dadda, P. Cammarano, *J. Trop. Ecol.* **14**, 577 (1998).
17. D. J. Pain, M. W. Pienkowski, *Farming and Birds in Europe: The Common Agricultural Policy and Its Implications for Bird Conservation* (Academic Press, London, 1997).
18. G. C. Daily, *Nature* **411**, 245 (2001).
19. M. L. Rosenzweig, *Win-Win Ecology: How the Earth's Species Can Survive in the Midst of Human Enterprise* (Oxford Univ. Press, Oxford, 2003).
20. M. L. Rosenzweig, *Oryx* **37**, 194 (2003).
21. J. R. Krebs, J. D. Wilson, R. B. Bradbury, G. M. Siriwardena, *Nature* **400**, 611 (1999).
22. P. F. Donald, R. E. Green, M. F. Heath, *Proc. R. Soc. Lond. B. Biol. Sci.* **268**, 25 (2001).
23. European Environment Agency, *Environmental Signals 2002, Benchmarking the Millennium*, Environmental Assessment Report No. 9 (Office for Official Publications of the European Communities, Copenhagen, Denmark, 2002) available at http://reports.eea.eu.int/environmental_assessment_report_2002_9/en/sig02LOW.pdf.
24. J. A. McNeely, S. J. Scherr, *Ecoagriculture: Strategies to Feed the World and Save Wild Biodiversity* (Island Press, Washington, DC, 2002).
25. J. G. Robinson, *Int. Wildl.* **24**, 30 (1994).
26. P. F. Donald, *Conserv. Biol.* **18**, 17 (2004).
27. D. Southgate, in *The Causes of Tropical Deforestation: the Economic and Statistical Analysis of Factors Giving Rise to the Loss of Tropical Forests*, K. Brown, D. W. Pearce, Eds. (UCL Press, London, 1994), pp. 134–143.
28. P. E. Waggoner, *Technol. Soc.* **17**, 17 (1995).
29. D. T. Avery, *Issues Sci. Technol.* **14**, 59 (1997).
30. E. B. Barbier, J. C. Burgess, *Land Econ.* **73**, 174 (1997).
31. A. Angelsen, D. Kaimowitz, in *Tradeoffs or Synergies? Agricultural Intensification, Economic Development and the Environment* D. R. Lee, C. B. Barrett, Eds. (CABI, Wallingford, UK, 2001), pp. 89–114.
32. D. R. Lee, C. B. Barrett, Eds., *Tradeoffs or Synergies? Agricultural Intensification, Economic Development and the Environment* (CABI, Wallingford, UK, 2001).
33. N. E. Borlaug, *In Vitro Cell. Dev. Biol.-Plant.* **38**, 221 (2002).
34. I. M. Goklany, M. W. Sprague, *Sustaining Development and Biodiversity: Productivity, Efficiency and Conservation* (Cato Institute, Washington, DC, 1992).
35. P. E. Waggoner, J. H. Ausubel, I. K. Wernick, *Popul. Dev. Rev.* **22**, 531 (1996).
36. C. D. Thomas et al., *Nature* **427**, 145 (2004).
37. J. N. Pretty, *Agri-culture: Reconnecting People, Land and Nature* (Earthscan, London, 2002).
38. M. S. Freudenberger, K. S. Freudenberger, in *Natural Resources Management in African Agriculture: Understanding and Improving Current Practices*, F. P. C. B. Barrett, A. A. Aboud, Eds. (CABI, Wallingford, UK, 2002), pp. 181–192.
39. D. Kleijn, W. J. Sutherland, *J. Appl. Ecol.* **40**, 947 (2003).
40. J. B. Hughes, G. C. Daily, P. R. Ehrlich, *Ecol. Lett.* **5**, 121 (2002).
41. RSPB, *Futurescapes: Large-Scale Habitat Restoration for Wildlife and People* (Royal Society for the Protection of Birds, Sandy, UK, 2001).
42. M. Avery, *Ecos* **22**, 3 (2001).
43. W. J. Sutherland, *Trends Ecol. Evol.* **17**, 148 (2002).
44. We thank M. Avery, J. Brashares, T. Brooks, G. Daily, D. Gibbons, and B. Grenfell for discussion and A. Stattersfield, M. Sneath, and M. Balman for access to the World Bird Database. S.J.C. acknowledges funding from the Wellcome Trust.

Supporting Online Material

www.sciencemag.org/cgi/content/full/1106049/DC1

Materials and Methods

SOM Text

Figs. S1 and S2

Table S1

References

5 October 2004; accepted 30 November 2004

Published online 23 December 2004;

10.1126/science.1106049

Include this information when citing this paper.

REPORTS

Ammonia Synthesis from First-Principles Calculations

K. Honkala,^{1,2} A. Hellman,⁴ I. N. Remediakis,^{1,2} A. Logadottir,^{1,2}
A. Carlsson,⁴ S. Dahl,⁴ C. H. Christensen,^{1,3} J. K. Nørskov^{1,2*}

The rate of ammonia synthesis over a nanoparticle ruthenium catalyst can be calculated directly on the basis of a quantum chemical treatment of the problem using density functional theory. We compared the results to measured rates over a ruthenium catalyst supported on magnesium aluminum spinel. When the size distribution of ruthenium particles measured by transmission electron microscopy was used as the link between the catalyst material and the theoretical treatment, the calculated rate was within a factor of 3 to 20 of the experimental rate. This offers hope for computer-based methods in the search for catalysts.

Detailed theoretical descriptions of the way in which solid surfaces act as catalysts for chemical reactions are now being obtained from density functional theory (DFT) calculations, which can be used to obtain the relevant activation energies. For example, Linic and Barteau have shown that a mean-field kinetic model of the selective oxidation of ethylene on an Ag catalyst, developed on the

basis of DFT calculations, can describe experimental data (1). However, the mean-field description implicitly neglects the complexity associated with interactions between adsorbed surface species and the resulting existence of many different possible reaction paths. This problem was overcome recently by Reuter et al., in a DFT-based kinetic Monte Carlo description of the oxidation of carbon monoxide over a RuO₂(110) surface (2).

Here we take the further step of developing a kinetic description that includes the full complexity of interactions and reaction paths for a complete catalytic reaction under industrial conditions over a packed bed of a high-surface-area nanoparticle catalyst. Using the

ammonia (NH₃) synthesis as the example, we show that DFT calculations can be used to directly predict a reaction rate for a supported nanoparticle Ru catalyst that is in good agreement with rate measurements performed over a wide range of industrially relevant synthesis conditions. The only experimental input included was the particle size distribution for the Ru catalyst, which was determined from transmission electron microscopy (TEM).

The synthesis of NH₃ is probably the most studied reaction in heterogeneous catalysis, and it acts as the prototype reaction that has been used to develop many key concepts in the field (3). The best elementary metal catalysts (Ru and Fe) were discovered in large-scale screening experiments almost 100 years ago (4–6), and the nature of the rate-determining step for Fe-based catalysts, N₂ dissociation, was pinpointed as early as 1934 (7, 8). About 25 years ago, surface science studies became possible and revealed a detailed picture of the N₂ dissociation process (9–13). It has been shown experimentally (14–16) and theoretically (17–19) that there is a direct link between the results of the ultra-low-pressure surface science results and NH₃ synthesis data at elevated pressure and temperature. Most recently, DFT calculations were used to quantitatively outline the complete reaction mechanism with all elementary steps on Ru (20). It has also been shown that it is possible to predict and understand the trends in reactivity when DFT calculations of

¹Center for Atomic-Scale Materials Physics, ²Department of Physics, ³Department of Chemistry, Technical University of Denmark, DK-2800 Lyngby, Denmark. ⁴Haldor Topsøe A/S, Nymøllevej 55, DK-2800 Lyngby, Denmark.

*To whom correspondence should be addressed. E-mail: norskov@fysik.dtu.dk

activation barriers and stabilities of intermediates for a series of different catalysts are combined with a simple microkinetic model (21). Our work here represents the final step in a complete first-principles description of the Ru-catalyzed NH_3 synthesis.

The starting point for our calculation is the potential energy diagram for the full reaction (20) (Fig. 1). The calculations (22) show that step sites are much more reactive for N_2 dissociation than the close-packed (001) surface, a finding that has been verified experimentally (23). By combining the results for step sites in Fig. 1 with harmonic transition state theory, we have shown that N_2 dissociation is by far the slowest step under all realistic reaction conditions (20). We will exploit these findings by treating N_2 dissociation as rate-limiting, and we only consider dissociation along step sites where the active (B_s) sites exist (23).

The results shown in Fig. 1 are for a low coverage of adsorbates. In reality, there will be other atoms and molecules adsorbed in the vicinity of the reacting molecule, and the activation energy for dissociation, $E_{a,i}$, and thus the rate constant, $k_i = \nu e^{-E_{a,i}/kT}$ where ν is the prefactor, k is the Boltzmann constant, and T is the temperature, will depend on the local environment (Fig. 2). Each local environment i will contribute to the total rate with a weight given by the probability P_i of finding this environment. The total rate r can be written as

$$r(T, p_{\text{N}_2}, p_{\text{H}_2}, p_{\text{NH}_3}) = \left(1 - \frac{p_{\text{NH}_3}^2}{p_{\text{H}_2}^3 p_{\text{N}_2} K_g}\right) \sum_i P_i k_i p_{\text{N}_2}$$

where K_g is the gas-phase equilibrium constant, and p_{N_2} , p_{H_2} , and p_{NH_3} are the pressures of N_2 , H_2 , and NH_3 , respectively.

The $\left(1 - \frac{p_{\text{NH}_3}^2}{p_{\text{H}_2}^3 p_{\text{N}_2} K_g}\right)$ term ensures that the gas phase equilibrium is established.

The probability P_i is given by the equilibrium between H_2 and NH_3 in the gas phase and adsorbed H, N, NH, NH_2 , and NH_3 ; all of the steps after the rate-limiting N_2 dissociation (Fig. 1) are in equilibrium. For this reason, we calculated the free energy of adsorption for all of the adsorbates. The entropy contributions were calculated on the basis of a complete normal mode analysis with the harmonic approximation (table S2) (22). We also calculated all possible nearest-neighbor interactions along the step (table S3). In principle, all of the interactions on the lower step should also be included. However, because we found that only H atoms appeared on the lower step, only the H-H interaction was needed. The use of grand canonical Monte Carlo simulations provides ensembles of the system in equilibrium and thus the probabilities P_i . Because N_2 dissociates with one N atom at the top of the step

and another at the bottom, an environment i is defined by having an empty site at the upper and lower step sites simultaneously and by the occupancy of the four neighboring sites.

In order to test the predictions of the rate for a real catalyst under industrially relevant conditions, we measured the activity for a Ru catalyst supported on magnesium aluminum spinel that contained 11.1 weight percent (wt %) Ru (24). The experimental results are in the form of the NH_3 productivity from a plug flow reactor loaded with a catalyst containing 0.2 g of the 11.1 wt % Ru/ MgAl_2O_4 catalyst as a function of the input partial pressures, the flow, and the temperature. We integrated the NH_3 synthesis rate down through the reactor in order to obtain the calculated NH_3 productivity.

The only information about the catalyst we needed in order to compare calculations to

experiments is the number of active sites per gram of catalyst. Thus, we characterized the activated catalyst by TEM, and we obtained the particle size distribution by analyzing $\sim 10^3$ particles. The active-site density is not directly given by the particle size distribution, because only the B_s sites are active for N_2 dissociation. Steps can be clearly observed in the TEM image of the Ru particle (Fig. 3), but it is not possible to count them. To estimate the fraction of B_s sites as a function of particle size, we calculated the surface energy of all the low-energy facets of Ru and used them in a Wulff construction to give the basic particle shape. From DFT calculations, we found that the (001)/(101) edges lower their energy by a reconstruction in which the edge row of atoms is removed. This process gives rise to the steps that contain B_s sites along the edge.

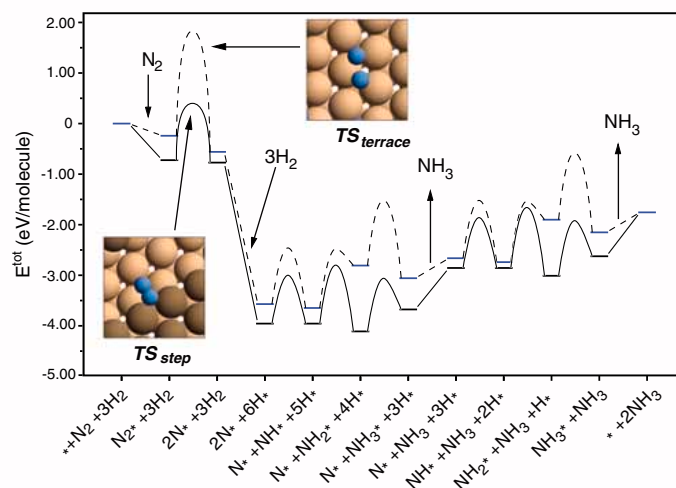


Fig. 1. The calculated potential energy (E^{tot}) diagram for NH_3 synthesis from N_2 and H_2 over close-packed (001) and stepped Ru surfaces (20). A * denotes an empty site and X^* an adsorbed species. The configuration of the transition states (TS) for N_2 dissociation over the terrace and step sites is shown in the insets.

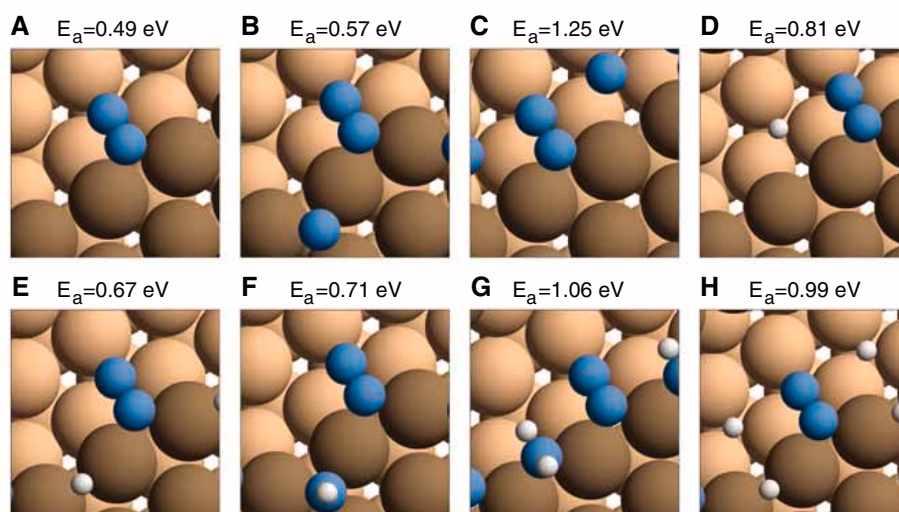


Fig. 2. Calculated activation energies (E_a) and transition state configurations for different local environments. A B_s site is shown with (A) no adsorbates in the neighboring sites, (B) adsorbed N on the upper step, (C) adsorbed N on the lower step, (D) adsorbed H on the lower step, (E) adsorbed H on the upper step, (F) adsorbed NH on the upper step, (G) adsorbed NH_2 on the upper step, and (H) adsorbed H on both the upper and lower steps. N atoms are shown in blue, H in white, and Ru in light and dark brown.

Our estimate of the particle morphology is quite crude, and it neglects the interaction with the support and changes in the surface energies caused by adsorption. However, the shape is similar to that found in the TEM image, and the fraction of B_5 (step) sites was insensitive to such details. The lack of active sites on the smallest Ru particles is in full

agreement with an experimental observation that the activity of a Ru catalyst can increase as a result of sintering the smallest Ru particles in a supported catalyst (25). The active-site density could now be calculated, and by folding it with the measured size distribution, we obtained the number of active sites per Ru mass. The largest uncertainty in

this estimate is the implicit assumption that the Wulff polyhedra are complete, i.e., that there are no partly filled layers. Our estimate is likely a lower bound to the number of active sites.

A direct comparison of the calculated and measured NH_3 productivity at a number of different conditions is shown in Fig. 4A. Given that there are no fitted parameters, the agreement is excellent. The overall rate is too small by a factor of ~ 3 to 20, and there is a tendency for the calculated inhibition by NH_3 to be slightly too weak.

The calculations provide insight into the exact nature of the active sites for the NH_3 synthesis reaction over Ru. In Fig. 4B, we give results that show the local environments contributing to the synthesis in one specific slice of the reactor. The largest contribution to the total rate does not come from the local environment with the lowest activation energy (Fig. 2). The state of the surface during synthesis conditions is such that the configuration with adsorbed H on the upper step dominates the total rate.

The agreement between theory and experiment in Fig. 4A might seem surprising, considering that the inherent accuracy of the DFT calculations is of the order 0.2 to 0.3 eV (26). An error in an activation energy of 0.25 eV, for instance, gives rise to an error in the rate of an elementary reaction of a factor of 148 at 600 K. The important point is that the total reaction rate is considerably less sensitive to the absolute error than the rate of the individual steps. We tested the sensitivity of the results to the main approximation in the DFT calculations, the exchange correlation energy functional. All of the calculations were done with the RPBE functional (26), but we also calculated all of the parameters using another functional,

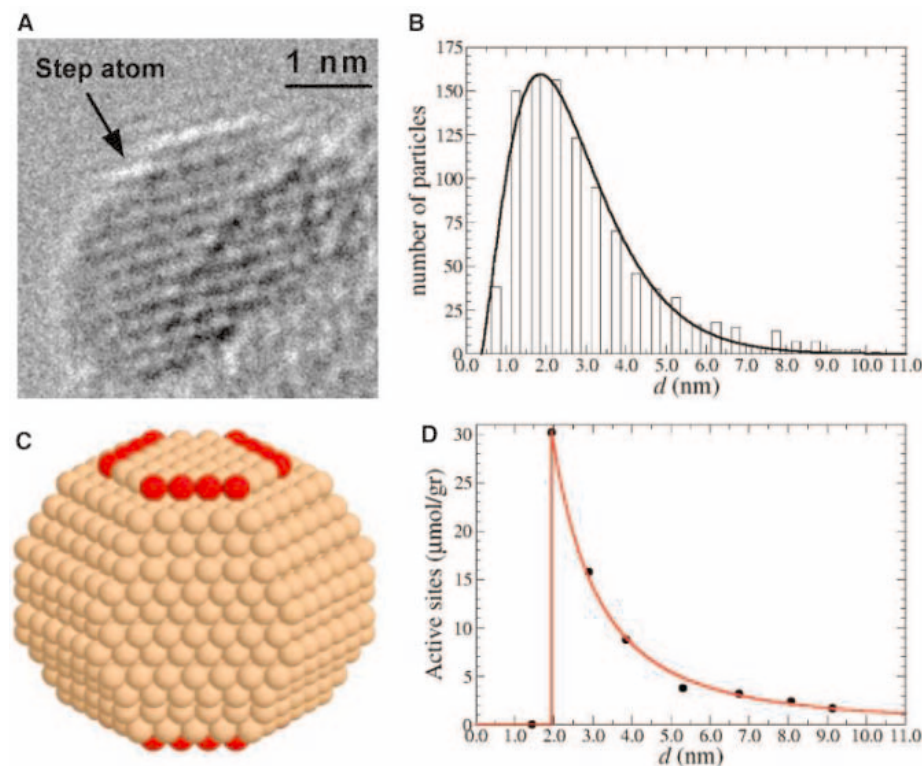


Fig. 3. (A) TEM image of a supported Ru particle with a step. (B) Particle size distribution function obtained from the TEM experiments. d , diameter. (C) A typical calculated Ru particle, with an average diameter of 2.9 nm. Atoms that belong to active B_5 sites are shown in red. (D) Density of active sites as a function of particle diameter, as calculated through analysis of the atomistic Wulff construction.

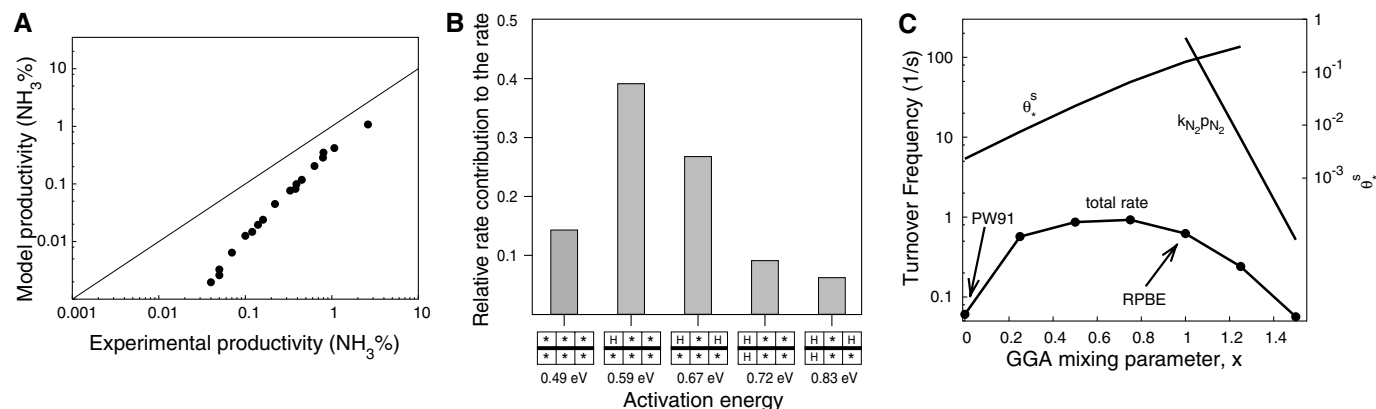


Fig. 4. (A) Comparison of the ammonia productivity from the model with experimental results. Complete agreement would mean that the results should follow the diagonal line. The total pressure was 100 bar; the ratio of N_2 to H_2 was 1:3; the total flow range over 0.2 g of catalyst was between 40 to 267 ml/min (standard temperature and pressure); the conversion range was ~ 0 to 20% of equilibrium; and the temperature range was from 320°C to 440°C. (B) The relative contributions to the rate in one slice of the reactor. On the x axis, we use a symbolic representation of the local environment,

showing the dissociation sites and four neighboring sites on the upper and lower steps. (C) Dependence of the rate on a parameter x that determines the mixing of results obtained by two different treatments of exchange-correlation effects, the generalized gradient approximation (GGA) PW91 and RPBE methods. The variation in the rate for N_2 dissociation on free sites, $p_{\text{N}_2}k_{\text{N}_2}$, and the coverage of free sites at the step, θ_s^* , are also given, showing why large variations in both compensate to give a small variation in the total rate that is proportional to both $p_{\text{N}_2}k_{\text{N}_2}$ and θ_s^* .

PW91 (27). We then interpolated all of the calculated energies between the two: $E(x) = xE_{\text{RPBE}} + (1-x)E_{\text{PW91}}$. The plot of the rate as a function of the mixing parameter x (Fig. 4C) shows a very weak dependence, because there is a compensation effect between the different steps in the total reaction (28). Changing from RPBE to PW91 decreased the barrier for N_2 dissociation substantially (by 0.6 eV) and made the dissociation of N_2 much faster. The dissociative chemisorption energy of H_2 changed simultaneously from -0.36 (RPBE) to -0.52 (PW91) eV, and the N_2 chemisorption energy changed from -0.8 (RPBE) to -1.4 (PW91) eV. These changes increased the coverage (through the equilibrium with H_2 and NH_3 in the gas phase) and decreased the number of free sites for dissociation. Because the barrier for dissociation and the stability of the intermediates on the surface vary together, a change in the overall interaction strength has only a small effect on the net rate. It is this compensation between two opposite trends that gives rise to a volcano in the catalytic activity as a function of the bond strength (28). The compensation effect is largest near to the maximum of the volcano (that is, for the best catalysts).

The insensitivity of the total catalytic rate to errors in the overall adsorption energies raises the question of the origin of the remaining discrepancy between the measured and calculated results (Fig. 4A). One possibility is that the number of active sites is underestimated. Another possible source of discrepancy could be systematic errors in the

description of the difference in bonding of different adsorbates or configurations. We tested the sensitivity of the results to such relative errors by decreasing the stability of adsorbed H relative to the NH_x species by 0.06 eV. It turns out that this is enough to make the calculated points match the measured ones completely at all temperatures and flows. Small relative errors are therefore a likely source of the underestimate of the rate in Fig. 4A. By the same token, the ability of the calculations to predict the absolute rate to within a factor of 3 to 20 suggests that the relative errors are only of the order 0.06 eV ($\sim kT$ at reaction conditions) for the exchange correlation functional used here.

Colinear variations in activation energies and bond strengths are found quite generally (21), so we would expect compensation effects to be found for other reactions. This built-in insensitivity to absolute errors, together with the higher accuracy of the DFT methods for relative energies, offers hope that DFT calculations can give a good overall description of the catalytic activity of other reactions as well.

References and Notes

- S. Linic, M. A. Barteau, *J. Am. Chem. Soc.* **125**, 4034 (2003).
- K. Reuter, D. Frenkel, M. Scheffler, *Phys. Rev. Lett.* **93**, 116105 (2004).
- M. Boudart, *Top. Catal.* **1**, 405 (1994).
- F. Haber, Nobel Prize Lecture 1918, in *Nobel Lectures, Chemistry 1901–1921* (Elsevier, Amsterdam, 1966).
- C. Bosch, Nobel Prize Lecture 1931, in *Nobel Lectures, Chemistry 1922–1941* (Elsevier, Amsterdam, 1966).
- A. Mittasch, *Adv. Catal.* **2**, 81 (1950).

- P. H. Emmett, S. Brunauer, *J. Am. Chem. Soc.* **55**, 1738 (1933).
- P. H. Emmett, S. Brunauer, *J. Am. Chem. Soc.* **56**, 35 (1934).
- F. Boszo, G. Ertl, M. Grunze, M. Weiss, *J. Catal.* **49**, 18 (1977).
- G. Ertl, M. Weiss, S. B. Lee, *Chem. Phys. Lett.* **60**, 391 (1979).
- Z. Paal, G. Ertl, S. B. Lee, *Appl. Surf. Sci.* **8**, 231 (1981).
- G. Ertl, S. B. Lee, M. Weiss, *Surf. Sci.* **114**, 527 (1982).
- G. Ertl, *J. Vac. Sci. Technol. A* **1**, 1247 (1983).
- N. D. Spencer, R. C. Schoonmaker, G. A. Somorjai, *J. Catal.* **74**, 129 (1982).
- D. R. Strongin, J. Carrazza, S. R. Bare, G. A. Somorjai, *J. Catal.* **103**, 213 (1987).
- D. R. Strongin, G. A. Somorjai, *J. Catal.* **109**, 51 (1988).
- P. Stoltze, J. K. Nørskov, *Phys. Rev. Lett.* **55**, 2502 (1985).
- J. A. Dumesic, A. A. Trivino, *J. Catal.* **116**, 119 (1989).
- M. Bunker, *Top. Catal.* **1**, 165 (1994).
- A. Logadottir, J. K. Nørskov, *J. Catal.* **220**, 273 (2003).
- A. Logadottir et al., *J. Catal.* **197**, 229 (2001).
- Materials and methods are available as supporting material on Science Online.
- S. Dahl et al., *Phys. Rev. Lett.* **83**, 1814 (1999).
- S. Dahl, J. Sehested, C. J. H. Jacobsen, E. Törnqvist, I. Chorkendorff, *J. Catal.* **192**, 391 (2000).
- C. J. H. Jacobsen et al., *J. Mol. Catal. A* **163**, 19 (2000).
- B. Hammer, L. B. Hansen, J. K. Nørskov, *Phys. Rev. B* **59**, 7413 (1999).
- J. P. Perdew et al., *Phys. Rev. B* **46**, 6671 (1992).
- T. Bligaard et al., *J. Phys. Chem. B* **107**, 9325 (2003).
- We thank the Danish Center for Scientific Computing for computer resources. Supported by EU project no. HPRN-CT-2002-00170.

Supporting Online Material

www.sciencemag.org/cgi/content/full/307/5709/555/DC1

Materials and Methods

Figs. S1 to S6

Tables S1 to S4

References and Notes

15 October 2004; accepted 17 December 2004
10.1126/science.1106435

Dark Structures in Molecular Radiationless Transitions Determined by Ultrafast Diffraction

Ramesh Srinivasan, Jonathan S. Feenstra, Sang Tae Park, Shoujun Xu,* Ahmed H. Zewail†

The intermediate structures formed through radiationless transitions are termed “dark” because their existence is inferred indirectly from radiative transitions. We used ultrafast electron diffraction to directly determine these transient structures on both ground-state and excited-state potential energy surfaces of several aromatic molecules. The resolution in space and time (0.01 angstrom and 1 picosecond) enables differentiation between competing non-radiative pathways of bond breaking, vibronic coupling, and spin transition. For the systems reported here, the results reveal unexpected dynamical behavior. The observed ring opening of the structure depends on molecular substituents. This, together with the parallel bifurcation into physical and chemical channels, redefines structural dynamics of the energy landscape in radiationless processes.

Radiationless transitions abound in chemical, physical, and biological systems, yielding such diverse phenomena as the conversion

of radiation to heat and the photodamage and photocarcinogenesis of DNA (1–5). After light absorption, a molecule can undergo ra-

diationless processes of two general types: photochemical, involving bond fragmentation or isomerization; and photophysical, involving transitions between electronic states while either conserving spin (internal conversion) or altering spin (intersystem crossing). For more than eight decades [(6) and references therein], our understanding of such radiationless processes has come from indirect evidence based on yields and decay rates of the radiative population. Theoretical studies have in turn advanced the concepts of a “heat bath” within the molecule (originally thought to violate the rules of quantum mechanics) and of conical intersections in the energy landscape (7–9).

Experimentally, the presence of nonradiative electronic relaxation processes was first deduced from the decrease in steady-state emission quantum yield of molecules at low pressures (10). With the advent of picosecond time resolution, it became possible to study the time scale of these processes [(11) and references therein]; with femtosecond time resolution, the actual nuclear motions were resolved [(12) and references

therein]. What remains unknown for these transitions are the accompanying molecular structural changes involving all nuclear motions at once. Such “dark” structures are not amenable to detection by conventional light absorption or emission. With diffraction, however, optically dark structures are as readily observed as bright ones.

Previously, we developed ultrafast electron diffraction (UED) for the study of isolated chemical reactions [(13); (14) and references therein] and for electron crystal-

lography of surfaces and surface molecular adsorbates (15–17). Here, the focus is on the nature of transient molecular structures involved in radiationless decays, believed to be nonreactively accelerated by vibrational excitation in the so-called channel-three region (18) and/or by the proximity effect (2) of electronic states. Four prototypical heteroaromatic (pyridine, 2-methylpyridine, and 2,6-dimethylpyridine) and aromatic carbonyl (benzaldehyde) organic molecules have been studied. Pyridine, which we studied before (19), is given here only as a reference. For all molecules, we determined the initial ground-state structure and followed upon excitation the changes in the diffraction pattern with time. The depletion of old bonds and emergence of new bonds elucidated the structural origin of dark transitions in the heteroaromatics and the quinoid-like excited-state

structure of triplet benzaldehyde. From these data, we gleaned the influence of parent structure on the dynamical evolution of relaxation pathways and the bifurcation into physical and chemical channels (Fig. 1) on the energy landscape.

In our laboratory, the development of the UED methodology over four generations of machines has resulted in current state-of-the-art spatial and temporal resolutions approaching 0.01 Å and 1 ps, respectively (14, 15); subpicosecond pulses have also been generated (15). The nearly million-fold increase in scattering cross section for electrons relative to x-rays, and the accompanying sensitivity to population change (~1%), make UED our technique of choice; for isolated molecules, only UED can provide such resolutions and sensitivity. Briefly, a femtosecond laser pulse initiates the change, and the ensuing structural evolution at specific time delays is probed by ultrashort bursts of electrons. Diffraction patterns are then recorded on a low-noise charge-coupled device (CCD) camera for processing and analysis. Furthermore, through the diffraction-difference method (14), careful choice of the reference image, and establishment of zero-of-time (14), it is possible to determine the particular intermediate structure of the molecular dynamics. Typically we record, at a given time delay, the scattering intensity of the molecular sample, which is converted to the molecular scattering function $sM(s)$. Fourier transform of the $sM(s)$ data generates the radial distribution curves, $f(r)$, which give the relative density of internuclear pairs.

For the studies of the pyridine series, we focused on the so-called channel-three phenomenon: At a given internal energy threshold, the nonradiative decay rate increases abruptly, with a concomitant drop in the emission quantum yield (18). In aromatics

Laboratory for Molecular Sciences, Arthur Amos Noyes Laboratory of Chemical Physics, Division of Chemistry and Chemical Engineering, California Institute of Technology, Pasadena, CA 91125, USA.

*Present address: Department of Chemistry, University of California, Berkeley, CA 94720, USA.

†To whom correspondence should be addressed. E-mail: zewail@caltech.edu

Fig. 1. Schematic of the potential energy landscape of ground and excited states in complex molecular systems. The equilibrium ground-state structure defines the initial wave packet prepared by femtosecond pulse excitation to the excited-state surface. Because of its nonequilibrium nature, the excited-state structure evolves into radiative and radiationless channels. The radiationless transitions can result from bifurcation into reactive chemical processes and nonreactive physical pathways (internal conversion/intersystem crossing).

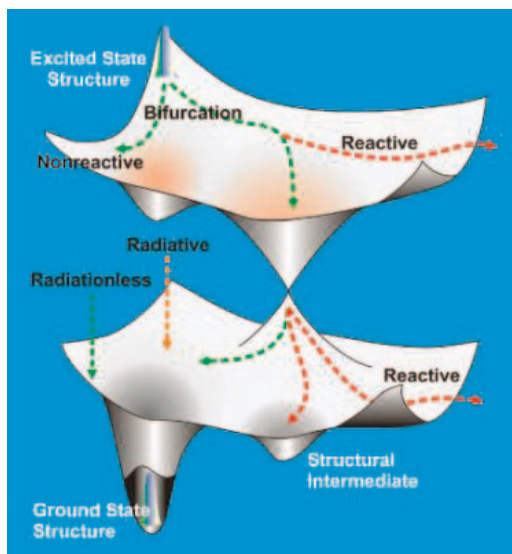
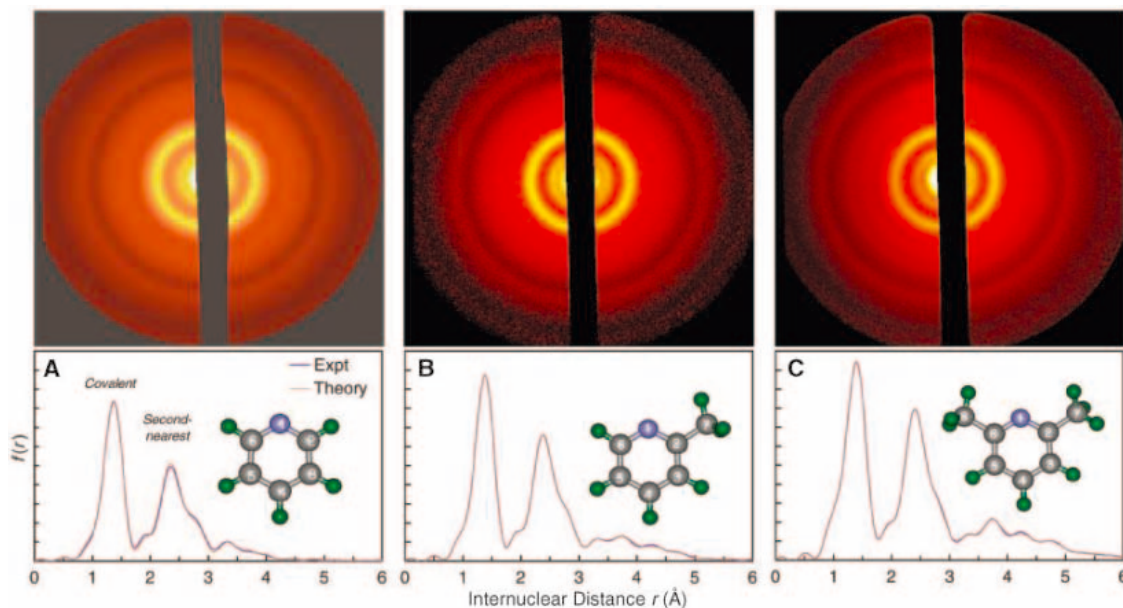


Fig. 2. Ground-state structures, as shown by 2D diffraction images and experimental radial distribution curves along with least-squares refined structural fits, for (A) pyridine, (B) picoline, and (C) lutidine. Note that the addition of methyl groups in this homologous series of molecules leaves the ring distances nearly unchanged; however, the density of longer, indirect internuclear separations increases with substitution.



such as benzenes and pyridines, upon absorption of light, a substantial portion of the energy is directed into nonradiative pathways. For pyridines, quantum yield measurements of the radiative processes (20), including picosecond studies of the total decay rates (21), have been reported. With methyl group substitution, these nonradiative yields and rates change markedly. In particular, the channel-three onset is much more pronounced for pyridine and picoline (2-methylpyridine) than for lutidine (2,6-dimethylpyridine). Such determinations of quantum yields and decay rates unfortunately contain no molecular structural information. Two fundamental questions remain as yet unanswered: What is the origin of the abrupt change in the radiationless behavior of the pyridines above a certain internal energy threshold? Further, how are such radiationless processes influenced by subtle changes in the molecular structure?

To answer these questions, we determined the transient structures involved in the radiationless transitions of the pyridine series mentioned above. First, however, we established their initial ground-state structures. Fig. 2 shows the two-dimensional (2D) diffraction images along with the experimental and refined radial distribution curves for pyridine, picoline, and lutidine. With the subsequent addition of each methyl group,

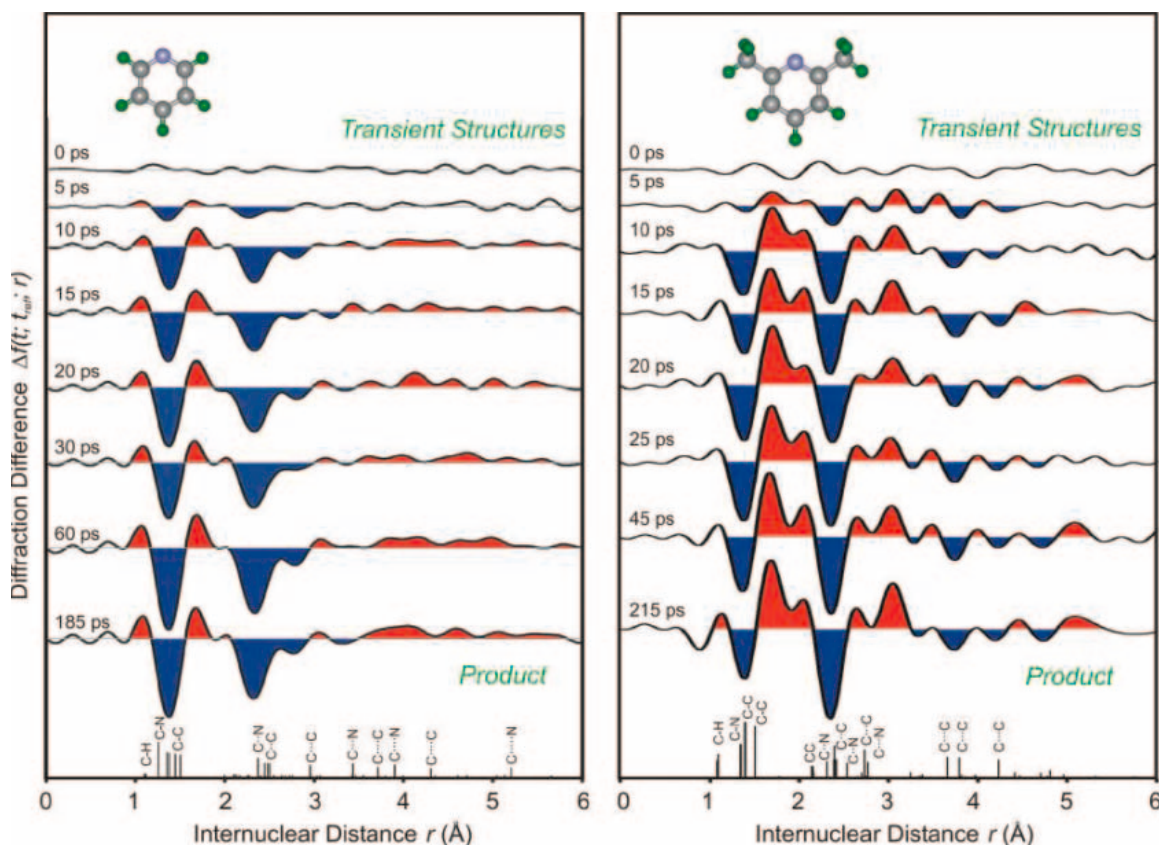
the 2D images exhibit an increasing density of rings. The starting structures for the fits were obtained from density functional theory (DFT) calculations, followed by least-squares refinement of the internuclear separations and vibrational amplitudes. The peaks in the radial distribution curves reflect the covalent C–C and C–N distances occurring near 1.3 Å, the second-nearest-neighbor C–C and C–N distances near 2.3 Å, and the third-nearest-neighbor C–C and C–N distances near 2.8 Å; all bond distances and angles were obtained for the refined structure and are summarized in figs. S1 and S2. Note that the addition of the methyl group(s) in picoline and lutidine does not affect the mean positions of the first-, second-, and third-nearest-neighbor peaks but increases their density. Simultaneously, the methylation introduces several long indirect distances with concomitant broadening of the peak at distances greater than 3.0 Å.

To resolve the structural changes during the course of the radiationless transition, we recorded diffraction patterns for a range of time delays between the exciting laser pulse (266 nm) and the probe electron pulse. The 2D diffraction-difference images show the emergence of periodic ring patterns whose intensity becomes more pronounced over time before reaching steady state. The 1D diffraction-difference curves (Fig. 3) consist

of negative peaks (blue regions), which correspond to loss of internuclear separations in the parent, and positive peaks (red regions) corresponding to gain of new interatomic distances in the transient intermediate. Note that dispersive contributions arising from vibrationally hot transient species can also lead to positive and negative contributions in the difference curves. Closer inspection of the time evolution reveals that pyridine shows greater loss of the direct covalent bond distances than the indirect ones (as is also the case for picoline). Conversely, in lutidine the noncovalent distances show much larger change.

Upon excitation, several nonradiative pathways are possible, including valence isomerization, fragmentation, and ring opening (22–29). To discriminate among the various possible reaction channels, we compared the UED data with predictions of structural models, as previously done in detail for pyridine (19). Through iterative refinement of the background and the structural parameters, we typically identify multiple best-fit structures based on χ^2 criteria. However, fitting with improper choice of the initial structure results in unphysical geometries. Fig. 4 compares experiment and theory for the refined structures, displaying both the molecular scattering and radial distribution curves for the chemical channel in pyridine

Fig. 3. One-dimensional (radial distribution) diffraction-difference curves as a function of time for pyridine (left) and lutidine (right). The negative (blue) regions reflect loss of old bonds; the positive (red) regions correspond to gain of new interatomic distances. Although pyridine shows a more pronounced depletion of the direct covalent distances, lutidine has a greater loss of indirect noncovalent distances. Also, pyridine shows emergence of positive contributions at distances greater than 3.5 Å, a feature conspicuously absent in the $f(r)$ of pyridine ground-state structure (Fig. 2A). Note that at these long distances, the baseline for pyridine at $t = 0$ only shows weak oscillatory noise; at longer times, positive contributions are present. For lutidine, the positive and negative peaks result from the dispersive contribution of the hot ground state relative to the initial cold structure (Fig. 2C).



and picoline and the physical channel in lutidine. We also considered other channels, including the formation of Dewar, Hückel, and azaprefulvene isomers, and fragmentation to HCN; however, the unsatisfactory fits for these structures exclude them from the dominant reaction channel on our time scale (Fig. 4).

On the basis of the final best-fit transient structures (Fig. 4), we conclude that upon 266-nm excitation, pyridine and picoline undergo C–N bond scission to open the aromatic ring and form a diradical structure. Lutidine does not undergo ring opening, but instead gives vibrationally hot ground-state species. The refined structures of ring-opened pyridine and picoline show alternating single (near 1.4 Å) and double-bond (near 1.3 Å) character for the skeletal distances, indicating disruption of the aromaticity of the parent ring structure. Moreover, the farthest C–N distances (reflected as positive contributions in Fig. 3A) are >4 Å, and these are absent in the $f(r)$ of the parent ground-state structure (Fig. 2A). The refined hot lutidine structure(s) are insensitive (within our resolution) to the position of the two methyl groups around the

ring; however, the distinct retention of aromatic distances in the product rules out ring opening in this molecule. A least-squares fit of the populations of these transient structures gave the temporal growth with time constants of 17 ± 1 ps, 28 ± 7 ps, and 16 ± 2 ps for pyridine, picoline, and lutidine, respectively.

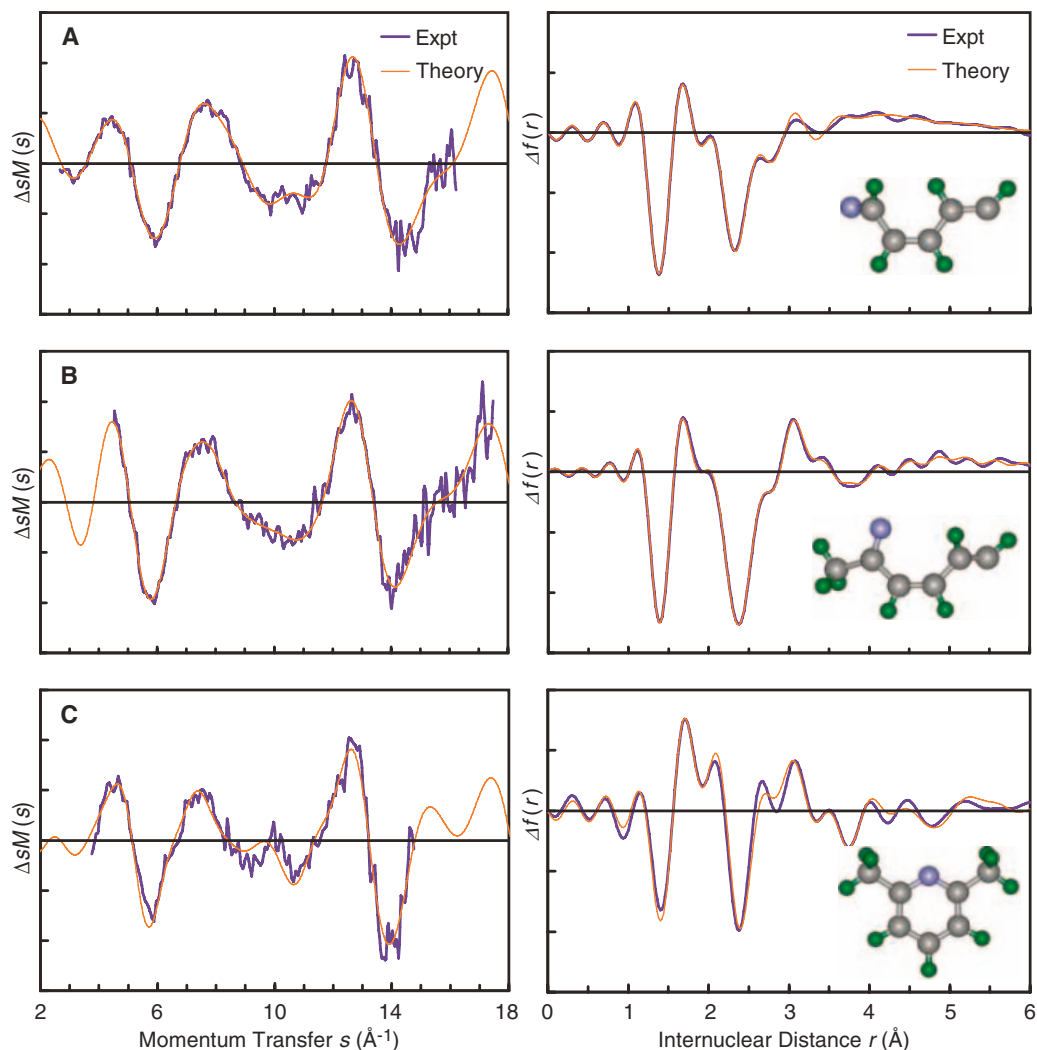
For aromatic pyridine and picoline, then, the nonradiative channel-three behavior is due to direct ring opening (30) to form the diradical structure obtained above. This observation is in stark contrast to the prevailing view that an ultrafast internal conversion pathway, mediated by the proximity of the first and second excited-state surfaces, opens up at the channel-three threshold and leads to vibrationally hot ground-state molecules. Lutidine does not undergo ring opening, consistent with its lack of channel-three behavior. The ring opening thus explains the quantum yield behavior observed in this series of molecules (31–33). In the channel-three region, pyridine and picoline show a change in quantum yield with vibronic energy (35,000 to 40,000 cm^{-1}) whereas lutidine does not, even though for all three molecules the

initial (0,0) decay is similar and the emission yield is low because of the proximity of states. The ring opening can also explain observations in gas-phase photolysis (34, 35) and in the condensed phase (27, 28).

Why are these profound differences in photophysical and photochemical behavior induced by subtle changes in the parent molecular structure? In pyridine, optical excitation at 266 nm involves transfer of a nonbonding electron on the nitrogen atom to the antibonding π^* orbital of the ring, thus lowering the strength of the C–N bond and resulting in its facile scission. If the time scale of this bond rupture is shorter than the lifetime of the state at that particular total energy, we expect this highly efficient, nonradiative photochemical process to actively deplete the radiative population, causing a decrease in emission quantum yield. The abrupt onset of the channel-three phenomenon is therefore a manifestation of the energy threshold for the ring-cleavage chemistry.

Upon methyl substitution, the electron-donating nature of these groups increases the electron density on the ring, leading to great-

Fig. 4. Transient structural determination. Experimental and theoretical difference curves are shown for (A) pyridine, (B) picoline, and (C) lutidine. Left panels: diffraction-difference molecular scattering curves; right panels: diffraction-difference radial distribution curves. The theoretical $\Delta sM(s)$ for ring-opened structures of pyridine and picoline and the hot ground-state structure of lutidine are from the least-squares refined structural fits according to χ^2 criteria (see text). Details of bond distances and angles are given in figs. S1 and S2.



er stability. Despite this increase in ring stability, structural refinement shows that 2-methylpyridine does indeed relax through ring opening, preferentially on the side opposite the methyl group. This favored scission of the bond between the nitrogen atom and the methine group can be understood in terms of its weaker character relative to other skeletal bonds in the S_1 state (36). On the other hand, the presence of two methyl groups in the 2- and 6-positions of lutidine further stabilizes the ring through increased charge density (37). Thus, it is not surprising that the lutidine nonradiative process is photophysical internal conversion rather than photochemical ring opening. Addition of electron-donating methyl substituents also tends to shrink the gap between the closely lying first ($n\pi^*$) and second ($\pi\pi^*$) excited states, which expedites the overall decay even with no excess vibrational energy.

The uniqueness of structural determination as a direct probe of molecular behavior emerges in comparison with previous spectroscopic investigations. Using femtosecond time-resolved mass spectrometry in the gas phase, our group had monitored pyridine after 277-nm excitation (22). We observed a fast decay component of 400 fs, assigned to the initial displacement of the wave packet and energy redistribution in the reactive channel. Two slower decays, with time constants of ~ 3.5 ps and ~ 15 ps, were assigned

to isomerizations to Dewar and Hückel pyridines, respectively, purely on the basis of the calculated energetics. With the direct structural information elucidated here by UED, we can reconsider these mass spectrometric results (22). The ~ 3.5 -ps time scale can still be assigned to the Dewar isomer, which is a minor channel in the time-resolved mass spectra as well as in our UED data (19). However, the time scale of the major channel (~ 15 ps) is remarkably similar to the time scale of the UED ring-opening process (17 ± 1 ps). Furthermore, the reported insensitivity of the time scales to deuteration (~ 15 ps for pyridine- h_5 versus ~ 16 ps for pyridine- d_5) would be surprising for the Hückel pathway, given that valence isomerization involves the motions of two deuterium atoms. On the basis of these considerations, therefore, we reassign the ~ 15 -ps decay rate from the mass spectrometric experiment to the ring cleavage process. This decay time is close to the reported lifetime (20 ps) of pyridine fluorescence at 1636 cm^{-1} above the S_1 origin (21).

As noted above, we have also applied UED to an aromatic carbonyl. Benzaldehyde, upon light absorption, undergoes efficient nonradiative intersystem crossing to the triplet state, as evidenced by its high phosphorescence yield (38). Previous investigations have revealed photochemical dissociation into benzene and carbon monoxide (39) above an internal energy threshold ($\sim 35,000\text{ cm}^{-1}$). We

sought to determine at 266 nm whether the photophysical and photochemical processes occur consecutively or instead proceed competitively as a result of bifurcation.

Perusal of the experimental $\Delta f(r)$ curves for excited benzaldehyde in Fig. 5B supports the rupture of covalent C–C bonds (near 1.4 Å), loss of next-nearest-neighbor distances (near 2.5 Å), and depletion of longer distances (>3.5 Å). These results suggest a fragmentation and repositioning of the atomic nuclei. As in the case of the azines, several possible candidate structures were considered, and from the molecular scattering $sM(s)$ and radial distribution $f(r)$ curves, the two best structures were found to be a quinoid-like triplet benzaldehyde and a dissociated product of benzene and carbon monoxide (Fig. 5A). The data were then fit to a sum of these two structures, with the partitioning parameter floated at each delay time. Shown in Fig. 5B is the structural fit at $t = 50$ ps, with 40% partitioned to the dissociation. In Fig. 5C, we display the temporal rise for both channels.

The quinoid structure is the optically dark, excited-state ($\pi\pi^*$) triplet benzaldehyde formed as a result of intersystem crossing (40, 41). As seen from the refined geometric parameters (Fig. 5A), this excited-state structure exhibits well-defined single and double bonds, indicating disruption of aromaticity in the ring. On the other hand, benzene formed in the dissociation pathway is in its ground electronic state, as indicated by the refined C–C bond distance in Fig. 5B. The simultaneous emergence of the photophysical and photochemical products in the diffraction data indicates a bifurcation on the excited singlet surface. The time-dependent contribution of the two pathways in the data is described by apparent rise time constants of 25 ± 4 ps and 38 ± 5 ps for excited triplet benzaldehyde and benzene, respectively (Fig. 5C). The observed difference in the rise times suggests the presence of an intermediate for the formation of benzene.

This observed bifurcation into physical and chemical pathways resolves key long-standing issues. Our quantum chemical calculations on the excited singlet surface suggest a low barrier for hydrogen shift and subsequent dissociation. Additionally, intersystem crossing from the excited singlet to the excited triplet is highly efficient. These features of the excited-state potential energy surface, combined with the similar rates of the physical and chemical channels, make these pathways competitive. When viewed in the context of previous mass spectrometry experiments, the new results account for the presence of ground-state benzene as well as triplet benzene on the nanosecond time scale, the latter produced by dissociation of excited triplet benzaldehyde (42, 43).

The UED-determined dark transient structures, including those of excited states,

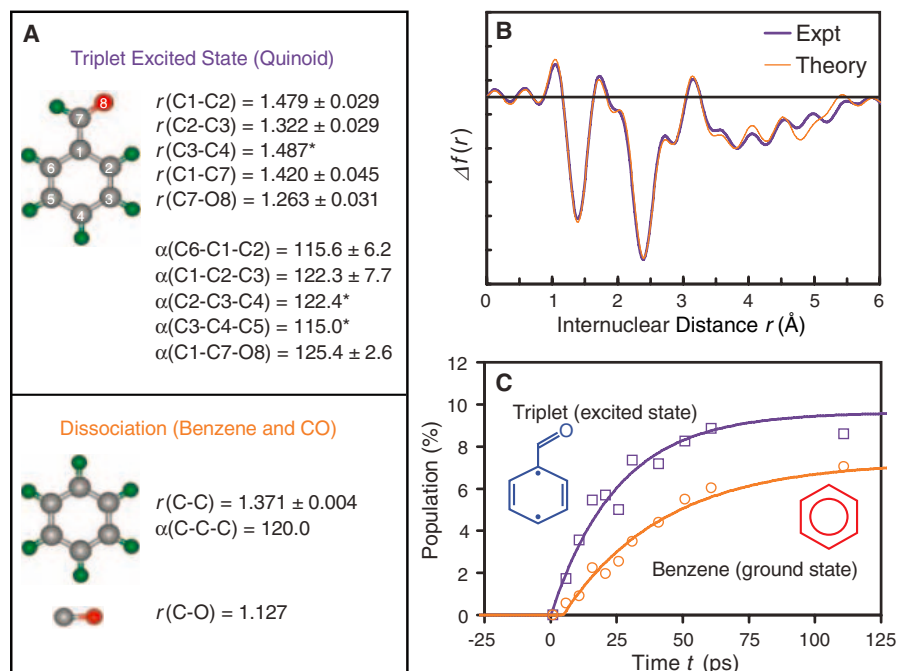


Fig. 5. Excited-state structure and bifurcation pathways in benzaldehyde. (A) Refined structural parameters for the transient species; the distances are in angstroms and the angles are in degrees. (B) Radial distribution curve of difference data and refined theoretical model for excited triplet benzaldehyde, benzene, and carbon monoxide at $t = 50$ ps. (C) Population increase and fit of a first-order exponential to the rise of excited triplet benzaldehyde and benzene with time constants of 25 ± 4 ps and 38 ± 5 ps, respectively. The parameters marked with an asterisk were not independently refined but were derived from geometric constraints.

and the time scales for bifurcation into physical and chemical channels underscore the critical importance of structural dynamics in determining the true nature of complex molecular behaviors and the energy landscapes of radiationless transitions.

References and Notes

- E. C. Lim, Ed., *Molecular Luminescence* (Benjamin, New York, 1969).
- E. C. Lim, *Adv. Photochem.* **23**, 165 (1997).
- J. D. Baldwin, in *Reactive Intermediate Chemistry*, R. A. Moss, M. S. Platz, M. Jones, Eds. (Wiley, New York, 2004), p. 899.
- E. C. Friedberg, *Nature* **421**, 436 (2003).
- C. E. Crespo-Hernandez, B. Cohen, P. M. Hare, B. Kohler, *Chem. Rev.* **104**, 1977 (2004).
- B. R. Henry, M. Kasha, *Annu. Rev. Phys. Chem.* **19**, 161 (1968).
- G. W. Robinson, R. P. Frosch, *J. Chem. Phys.* **38**, 1187 (1963).
- M. Bixon, J. Jortner, *J. Chem. Phys.* **48**, 715 (1968).
- J. Michl, in *Conical Intersections: Electronic Structure, Dynamics and Spectroscopy*, W. Domcke, D. R. Yarkony, H. Koppel, Eds. (World Scientific, Singapore, 2004), p. ix.
- G. B. Kistiakowsky, C. S. Parmenter, *J. Chem. Phys.* **42**, 2942 (1965).
- K. B. Eisenthal, Ed., *Applications of Picosecond Spectroscopy to Chemistry* (Reidel, Boston, 1984).
- A. H. Zewail, in *Les Prix Nobel: The Nobel Prizes 1999*, T. Frängsmyr, Ed. (Almqvist & Wiksell, Stockholm, 2000), pp. 103–203.
- H. Ihee *et al.*, *Science* **291**, 458 (2001).
- R. Srinivasan, V. A. Lobastov, C.-Y. Ruan, A. H. Zewail, *Helv. Chim. Acta* **86**, 1763 (2003).
- C.-Y. Ruan, F. Vigliotti, V. A. Lobastov, S. Y. Chen, A. H. Zewail, *Proc. Natl. Acad. Sci. U.S.A.* **101**, 1123 (2004).
- C.-Y. Ruan, V. A. Lobastov, F. Vigliotti, S. Y. Chen, A. H. Zewail, *Science* **304**, 80 (2004).
- J. M. Thomas, *Angew. Chem. Int. Ed. Engl.* **43**, 2606 (2004).
- J. H. Callomon, J. E. Parkin, R. Lopez-Delgado, *Chem. Phys. Lett.* **13**, 125 (1972).
- V. A. Lobastov *et al.*, *J. Phys. Chem. A* **105**, 11159 (2001).
- E. Villa, A. Amirav, E. C. Lim, *J. Phys. Chem.* **92**, 5393 (1988).
- I. Yamazaki *et al.*, *Chem. Phys. Lett.* **92**, 421 (1982).
- D. P. Zhong *et al.*, *Chem. Phys. Lett.* **298**, 129 (1998).
- K. A. Prather, Y. T. Lee, *Isr. J. Chem.* **34**, 43 (1994).
- K. E. Wilzbach, D. J. Rausch, *J. Am. Chem. Soc.* **92**, 2178 (1970).
- M. Chachivili, A. H. Zewail, *J. Phys. Chem. A* **103**, 7408 (1999).
- O. L. Chapman, C. L. McIntosh, J. Pacansky, *J. Am. Chem. Soc.* **95**, 614 (1973).
- D. E. Johnstone, J. R. Sodeau, *J. Phys. Chem.* **95**, 165 (1991).
- S. Kudoh, M. Takayanagi, M. Nakata, *J. Photochem. Photobiol. A* **123**, 25 (1999).
- A. L. Sobolewski, W. Domcke, *Chem. Phys. Lett.* **180**, 381 (1991).
- Although it is conceivable that the hot ground-state molecules could undergo further ring-opening reaction, our one-photon energy of ~ 107 kcal/mol is inadequate for complete C–N bond scission on the ground state. Furthermore, cleavage via this mechanism is known to proceed via initial loss of the α -hydrogen atom to form the pyridyl radical (44); however, there is minimal loss of hydrogen observed in pyridine upon photoexcitation (23).
- I. Yamazaki, K. Sushida, H. Baba, *J. Chem. Phys.* **71**, 381 (1979).
- I. Yamazaki, K. Sushida, H. Baba, *J. Lumin.* **18–9**, 425 (1979).
- I. Yamazaki, T. Murao, T. Yamanaka, K. Yoshihara, *Faraday Discuss.* **75**, 395 (1983).
- J. W. Pavlik, N. Kebede, M. Thompson, A. C. Day, J. A. Barltrop, *J. Am. Chem. Soc.* **121**, 5666 (1999).
- J. W. Pavlik, personal communication.
- S. Kudoh, M. Takayanagi, M. Nakata, *Chem. Phys. Lett.* **308**, 403 (1999).
- S. Porcinai, P. Foggi, *Nuovo Cimento Soc. Ital. Fis. D* **19**, 889 (1997).
- Y. Hirata, E. C. Lim, *J. Chem. Phys.* **72**, 5505 (1980).
- M. Berger, I. L. Goldblatt, C. Steel, *J. Am. Chem. Soc.* **95**, 1717 (1973).
- U. Brühlmann, M. Nonella, P. Russegger, J. R. Huber, *Chem. Phys.* **81**, 439 (1983).
- N. Ohmori, T. Suzuki, M. Ito, *J. Phys. Chem.* **92**, 1086 (1988).
- A. V. Polevoi, V. M. Matyuk, G. A. Grigor'eva, V. K. Potatov, *Khim. Vys. Energ.* **18**, 195 (1984).
- C. R. Silva, J. P. Reilly, *J. Phys. Chem. A* **101**, 7934 (1997).
- R. Liu, T. T.-S. Huang, J. Tittle, D. Xia, *J. Phys. Chem. A* **104**, 8368 (2000).
- Supported by NSF and the U.S. Air Force Office of Scientific Research.

Supporting Online Material

www.sciencemag.org/cgi/content/full/1107291/DC1
Figs. S1 and S2

9 November 2004; accepted 21 December 2004
Published online 6 January 2005;
10.1126/science.1107291
Include this information when citing this paper.

Electron Spectroscopy of Aqueous Solution Interfaces Reveals Surface Enhancement of Halides

Sutapa Ghosal,^{1,2} John C. Hemminger,^{1*} Hendrik Bluhm,³
Bongjin Simon Mun,⁴ Eleonore L. D. Hebenstreit,² Guido Ketteler,²
D. Frank Ogletree,² Felix G. Requejo,^{2,5} Miquel Salmeron²

It has been suggested that enhanced anion concentrations at the liquid/vapor interface of airborne saline droplets are important to aerosol reactions in the atmosphere. We report ionic concentrations in the surface of such solutions. Using x-ray photoelectron spectroscopy operating at near ambient pressure, we have measured the composition of the liquid/vapor interface for deliquesced samples of potassium bromide and potassium iodide. In both cases, the surface composition of the saturated solution is enhanced in the halide anion compared with the bulk of the solution. The enhancement of anion concentration is more dramatic for the larger, more polarizable iodide anion. By varying photoelectron kinetic energies, we have obtained depth profiles of the liquid/vapor interface. Our results are in good qualitative agreement with classical molecular dynamics simulations. Quantitative comparison between the experiments and the simulations indicates that the experimental results exhibit more interface enhancement than predicted theoretically.

A detailed knowledge of halide ion concentrations at solution interfaces is of great importance for understanding the chemistry of salt solutions. This is of current interest because halide ion concentrations play a key role in many atmospheric and environmental chemistry processes. For example, reactions of sea-salt aerosols with gas-phase oxidants

such as OH and ozone have been suggested as a mechanism for the introduction of substantial amounts of gas-phase chlorine and bromine compounds into the marine troposphere (1, 2). Recent field measurements have directly observed Cl₂, Br₂, and BrCl, which provides strong evidence that halogen compounds are indeed important in the

chemistry of the troposphere, both at mid-latitude and in polar regions (3–8).

Studies of the reactivity of salt solutions have suggested that there is an enhancement of the absolute anion concentrations at the interface. At first sight, such an enhancement appears contrary to thermodynamic expectations, because image-charge repulsion should move ions away from the surface and because the addition of salt to water causes an increase in surface tension. Hu *et al.* (9) suggested that Cl[−] and Br[−] ions must exist at the liquid/vapor interface of such solutions based on measurements of the uptake of Cl₂ and Br₂ gases by alkali-halide salt solutions. To explain experimental measurements of reactions of gas-phase oxidants with concentrated NaCl aerosol droplets, Knipping *et al.* (1) have also suggested that Cl[−] ion concentrations are enhanced at the liquid/vapor interface. This contention is supported by classical molecular dynamics (MD) simulations. More recently, Jungwirth and Tobias (10, 11) have elaborated on the classical MD simulations, providing additional theoretical evi-

¹Department of Chemistry, University of California, Irvine, CA 92697, USA. ²Materials Sciences Division, Lawrence Berkeley National Laboratory, Berkeley, CA 94720, USA. ³Chemical Science Division, Lawrence Berkeley National Laboratory, Berkeley, CA 94720, USA. ⁴Advanced Light Source, Lawrence Berkeley National Laboratory, Berkeley, CA 94720, USA. ⁵Departamento de Física, Facultad de Ciencias Exactas, Universidad Nacional de La Plata, 1900 La Plata, Argentina.

*To whom correspondence should be addressed. E-mail: jchemmin@uci.edu

dence for the existence of enhanced concentrations of the larger, more polarizable halogen ions at the surfaces of the corresponding aqueous solutions. Their simulations are consistent with the observed changes in surface tension with salt concentration (10).

Garrett (12) recently pointed out that “direct experimental observations of molecular structure and energetics of ions in the interfacial region are needed to corroborate the simulations.” Given both the fundamental and the atmospheric importance of the surface chemistry at the liquid/vapor interface of salt solutions, a number of laboratories have applied surface-sensitive experimental probes to shed light on the subject of surface ion concentrations in salt solutions. Nonlinear optical experiments, particularly second-harmonic generation (SHG) and vibrational sum-frequency generation (VSFG), have been shown to probe interfacial properties. Allen and co-workers (13) have used a combination of conventional Raman spectroscopy and VSFG to compare the infrared spectra from the bulk of salt solutions (Raman spectra) with spectra from the surface region (the VSFG spectra). The VSFG experiments are sensitive to the region of the sample near the surface that is noncentrosymmetric. They interpret their results to show that the noncentrosymmetric region of the solution extends farther into the bulk for the bromide and iodide salt solutions than for pure water. The enhanced disruption of the molecular symmetry when going farther into the bulk is consistent with the classical MD simulations, which show that bromide and iodide ions are enhanced near the surface, with a corresponding enhancement of the cation just below the surface (10, 13).

Raymond *et al.* (14) carried out isotopic dilution experiments in conjunction with the VSFG technique. The isotopic dilution experiments provide an elegant way to separate contributions from different species to the complex OH stretching region of the VSFG spectrum. Their results on alkali-halide solutions are consistent with the existence of anions in the near-surface region of the solution. However, they do not see any change in the hydrogen bonding of the surface water that would imply either enhanced halide ion concentrations near the surface or the separation of anions and cations in the near-surface region.

Petersen *et al.* (15) recently reported resonant SHG experiments in which they probed the surface region of NaI and KI solutions over a wide range of concentrations. Over a narrow range of low concentrations (millimolar), they showed that their results are consistent with an enhanced anion concentration in the surface region probed by the SHG experiment.

Weber *et al.* (16) reported valence-band photoemission experiments in which they were able to probe the surface region of a liquid jet of alkali-halide solution. In their

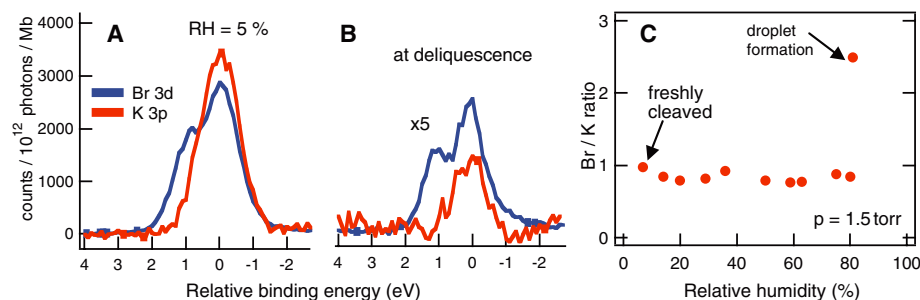


Fig. 1. Br 3d and K 3p core-level photoemission spectra acquired (A) at a relative humidity (RH) of 5% and (B) at the deliquescence point. The photon energy is adjusted so that both peaks have the same kinetic energy, 160 eV. The count rate is normalized to incident photon flux and photoemission cross section for each element. At RH = 5%, the measured ratio is Br/K = 1.1:1, close to the expected value of 1. At deliquescence there is a factor 2 enhancement of Br with respect to K (Br/K = 2.5:1). (C) The Br/K ratio as a function of water vapor relative humidity. Br/K ratio is virtually constant until deliquescence is reached.

experiments, the liquid jet is in contact with a vacuum and thus is not in equilibrium with the vapor of the solution. Although their results do not necessarily support any surface excess of anions as predicted by the classical MD simulations, they are at the same time unable to rule out the existence of such an enhancement given the particulars of their experiment. However, based on the observed change in photoemission signals as a function of the concentration of the solution used to generate the liquid jet, they suggest that there is a “negative surface excess” of ions for the case of NaI solutions—in apparent contradiction with the classical MD simulations.

We have directly measured the ion concentrations in the surface region of alkali-halide aqueous solutions by using x-ray photoelectron spectroscopy (XPS) to profile the surface composition of an alkali-halide salt in contact with water vapor. The recent development of techniques to acquire photoemission spectra in gas environments at pressures up to several torr (17) has allowed us to study an alkali-halide sample as a function of water vapor pressure, starting with the freshly cleaved, dry sample up to the deliquescence point of the salts (18). Relative humidity was varied by holding the sample at -10°C while varying the water pressure or by maintaining the pressure at ~ 2 torr while varying the sample temperature. In the experiments, the K 2p and 3p, the O 1s, and the C 1s peaks were monitored, as well as the Br 3d and I 4d peaks for KBr and KI, respectively. The C 1s peaks were monitored to quantify the small amount (submonolayer) of carbonaceous material that will always be present in such liquid/vapor interface studies. Charging of the salt surface was compensated by photoelectrons from ionized water vapor.

Quantification of the photoemission data are challenging because both gas-phase attenuation and transmission through the electron optics are energy-dependent. We overcome this problem by measuring relative anion/cation/oxygen signals for identical photo-

electron kinetic energies (KEs), obtained by choosing appropriate x-ray excitation energies and normalizing by the corresponding ionization cross sections [taken from Yeh and Lindau (19)]. The use of the same KE also ensures that the sample depth analyzed is the same for all of the elements. The energy-dependent x-ray flux was measured using a calibrated photodiode. Radiation damage from the incident x-rays was avoided by continuously displacing the sample so that the spectra are obtained in fresh spots of the sample.

The change in the surface Br/K atom ratio as a function of relative humidity is shown in Fig. 1 from an experiment in which a KBr single crystal sample was cleaved in vacuum. The XPS spectra were then obtained for different values of the water vapor relative humidity up to deliquescence of the sample, at which point a visible droplet formed at the surface. These data are typical of the results obtained in a number of experiments involving different KBr samples and in two separate analysis chambers. The spectra in Fig. 1, A and B, were obtained from a sample that was cleaved just before introduction into the vacuum system and correspond to a photoelectron KE of 160 eV. The Br/K ratio remains constant around an average value of 0.8 ± 0.1 as the water vapor pressure is increased below the deliquescence point. In the saturated solution formed at deliquescence, a significant increase of the Br/K ratio to 2.5 ± 0.2 was observed. The results were independent of the manner in which the relative humidity was varied (i.e., by varying the water vapor pressure at constant sample temperature or by varying the sample temperature at constant water pressure).

For KI, a similar abrupt change was observed from an I/K ratio of 1 below deliquescence to a value of 3.4 ± 0.2 at deliquescence. These results, along with the concentration of water, obtained using the O 1s peak, are summarized in Fig. 2. Using the O peak intensity, we obtained absolute concentration values. The values are Br/K/O(H₂O) = 15:7:78 and I/K/O(H₂O) = 25:8:67. The

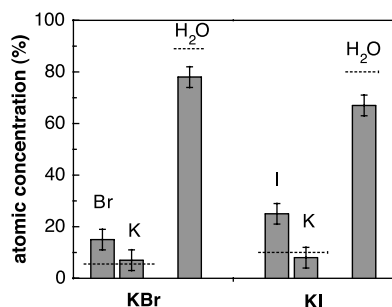


Fig. 2. Atomic concentration at the deliquescence point. The kinetic energy of the photoelectrons was 200 eV, corresponding to an escape depth of two to three atomic layers. Error bars indicating standard deviations are shown for the experimental measurements. The dashed lines indicate the expected concentrations of ions and water molecules from thermodynamic data for bulk, saturated solutions.

values expected for a saturated solution in the absence of ion segregation effects can be obtained from data on salt solubility at the appropriate temperature (20). In the absence of segregation, the ratios at -10°C are expected to be $\text{Br}/\text{K}/\text{O}(\text{H}_2\text{O}) = 5.5:5.5:84$ and $\text{I}/\text{K}/\text{O}(\text{H}_2\text{O}) = 10:10:80$. Thus, as shown in Fig. 2, there is an enhancement of the absolute anion concentrations at the interface in addition to an enhanced interfacial anion/cation ratio.

The depth into the sample probed by XPS is determined by the inelastic scattering of the electrons as they exit the sample. Electrons that undergo inelastic scattering contribute to the spectral background and are lost from the peak signal. The inelastic mean free path (IMFP) of electrons is a function of their KE, so it is possible to determine concentration depth profiles by monitoring the same elements with different photon energies (and thus different photoelectron KEs). For KEs above 100 eV, the IMFP increases with energy. Results from such experiments for deliquesced KBr and KI samples are shown in Fig. 3, in which we plot the measured anion/cation atomic ratio as a function of the photoelectron KE. Both KI and KBr show significant enhancement of the halide ion concentration in the more surface-sensitive experiments (low photoelectron KE). In both cases, a ratio of 1 (± 0.1) was obtained when the experiment was performed with photoelectrons of higher KE that probe deeper into the solution.

Our results therefore agree qualitatively with the picture derived from the MD simulations, not only in regard to the preferential enhancement of anion concentration at the surface but also in confirming the greater effect for the larger, more polarizable iodide. A more quantitative comparison between our experiments and the simulations requires a convolution of the simulation results with an exponentially decaying experimental probe

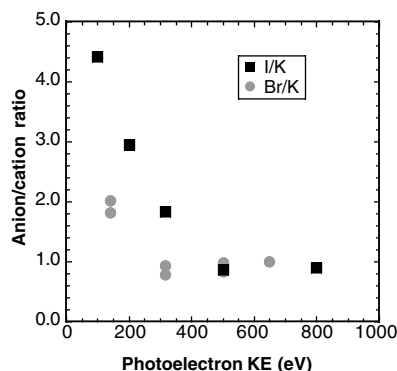


Fig. 3. Measured anion/cation atomic ratio as a function of the photoelectron kinetic energy. The circles are the measured Br/K ratios for KBr. The squares are the values of I/K for KI.

depth that would be characteristic of the XPS experiment (21). Figure 4 shows the results of the simulations for a 1.2 M NaBr solution carried out by Jungwirth and Tobias, along with an exponentially decaying experimental probe depth function for the case of an electron IMFP of 10 Å. Unfortunately, the IMFP values are not well known, particularly for liquids such as water. In the case of solid materials, reported values of IMFP vary from 5 to 10 Å at electron KEs in the range from 100 to 200 eV (22). Using these two extreme values and the density profiles of the Jungwirth and Tobias simulations (10, 11), we obtain predicted anion/cation ratios of $\text{I}^-/\text{cation} = 1.65$ (IMPF = 5.0 Å) and 1.26 (IMPF = 10 Å) and $\text{Br}^-/\text{cation} = 1.32$ (IMPF = 5.0 Å) and 1.10 (IMPF = 10 Å). It appears then that the experiments measure a larger enhancement than predicted by the classical MD simulations of Jungwirth and Tobias (10, 11).

There are several potential origins of the quantitative difference between our experiments and the simulations. For ease of handling, the experiments were carried out with KBr and KI, whereas the simulations used Na^+ as the cation. We believe that it is highly unlikely that this difference would affect the results. As mentioned previously, we have carried out the experiments at slightly reduced temperatures. In addition, because of the manner in which our experiments are done, the solutions are necessarily at saturation concentration (they are in equilibrium with both water and undissolved solid). The simulations we compare to here were carried out at a concentration of 1.2 M. The salt concentration may affect the amount of anion enhancement observed in the simulations (10, 11). Preliminary results of simulations of more concentrated KBr solutions at -10°C show results that are quite similar to the simulations at 1.2 M shown in Fig. 4 (23).

Allen and co-workers (13) carried out VSGF experiments on NaBr and NaI solutions at relatively low salt concentrations. However, the disruption of the interfacial hydrogen

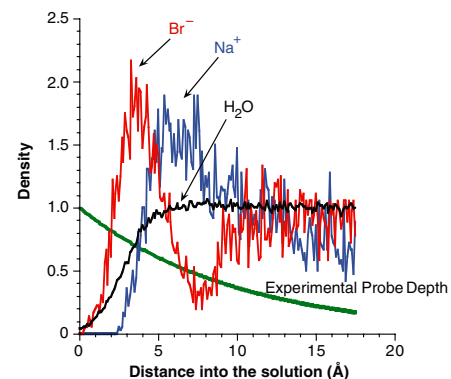


Fig. 4. Results from classical MD simulations (10, 11) of a 1.2 M NaBr solution, showing the predicted enhancement of the halide ion at the interface. An example of the experimental probe depth function for the case of an electron IMFP of 10 Å is included for comparison.

bonding of the water increased when the salt concentration was increased. Efforts are under way to provide detailed comparisons between the experiments described here and MD simulations carried out for comparable concentrations and temperatures (23). In carrying out experiments on solution interfaces, it is impossible to completely avoid contamination of the interface with impurities. As noted above, in our experiments the liquid/vapor interface contains small amounts (submonolayer) of carbonaceous material. An advantage of the XPS experiments is that we can easily quantify the amount of carbonaceous material at the interface. The anion/cation ratios that we measure are insensitive to the small amount of carbon at the interface in the submonolayer regime. Because it is likely that all liquid/vapor interface experiments have small amounts of carbonaceous material at the interface, it is important to quantify these amounts in future experiments and understand the impact on interface properties.

In making quantitative comparisons between experiments and the classical MD simulations, it should also be noted that the detailed results of such simulations are known to be particularly sensitive to the interaction potentials that are used (24). Molecular simulations have been successfully tested against and found to be consistent with bulk solution properties and even against the results of cluster studies. However, there are few quantitative results on solution interfaces to provide benchmark tests for the interaction potentials that are used for the study of liquid/vapor interfaces. As a result, it will be very important to continue close collaborative work between new experiments and simulations in this area.

References and Notes

1. E. M. Knipping *et al.*, *Science* **288**, 301 (2000).
2. S. W. Hunt *et al.*, *J. Phys. Chem. A* **108**, 11559 (2004).
3. C. W. Spicer *et al.*, *Nature* **394**, 353 (1998).
4. R. Sander *et al.*, *Atmos. Chem. Phys.* **3**, 1301 (2003).

5. C. W. Spicer *et al.*, *Atmos. Environ.* **36**, 2721 (2002).
 6. S. Ghosal, A. Shbeeb, J. C. Hemminger, *Geophys. Res. Lett.* **27**, 1879 (2000).
 7. L. A. Barrie *et al.*, *Nature* **334**, 138 (1988).
 8. L. A. Barrie, U. Platt, *Tellus* **49B**, 450 (1997).
 9. J. H. Hu *et al.*, *J. Phys. Chem.* **99**, 8768 (1995).
 10. P. Jungwirth, D. J. Tobias, *J. Phys. Chem. B* **105**, 10468 (2001).
 11. P. Jungwirth, D. J. Tobias, *J. Phys. Chem. B* **106**, 6361 (2002).
 12. B. C. Garrett, *Science* **303**, 1146 (2004).
 13. D. Liu, G. Ma, L. M. Levering, H. C. Allen, *J. Phys. Chem. B* **108**, 2252 (2004).
 14. E. A. Raymond, G. L. Richmond, *J. Phys. Chem. B* **108**, 5051 (2004).
 15. P. B. Petersen *et al.*, *Chem. Phys. Lett.* **397**, 46 (2004).
 16. R. Weber *et al.*, *J. Phys. Chem. B* **108**, 4729 (2004).
 17. D. F. Ogletree *et al.*, *Rev. Sci. Instrum.* **73**, 3872 (2002).
 18. The experiments were carried out at the Berkeley Advanced Light Source in beamlines 9.3.2 and 11.0.2. Salt crystals ~2 mm thick and ~5 mm² were mounted on a cooled copper substrate. They were cleaved in situ or just before introduction into the vacuum system. Vapor from degassed Milli-Q water (Millipore Corporation, Billerica, MA) was introduced through a leak valve and monitored with a capacitance nanometer absolute pressure gauge.

24. L. X. Dang, T. M. Chang, *J. Phys. Chem. B* **106**, 235 (2002).
 25. Supported by the Director, Office of Science, Office of Basic Energy Science, U.S. Department of Energy under contract no. DE-AC03-76SD00098 and DE-AC03-76SF00098. J.C.H. and S.G. thank the NSF for support (grants 0080806, 0209719, and 0431312). G.K. thanks the Alexander von Humboldt Foundation for support. F.G.R. thanks the Consejo Nacional de Investigaciones Científicas y Técnicas (Argentina). The authors thank D. Tobias and P. Jungwirth for providing the numerical data from their classical MD simulations of 1.2 M alkali-halide solutions, which were used for comparison with the experiments. We thank M. Roeselová for discussion of the preliminary results of classical MD simulations of higher concentration KBr solutions at -10°C. S.G. and M.S. thank M. Luna for assistance in the initial phase of this project and J. Newberg for help procuring the single-crystal samples. S.G. also thanks H. Liu for experimental help in the initial phase of these experiments. E. Wong's help and expertise with the technical aspects of the experiments are greatly appreciated.

19 October 2004; accepted 15 December 2004
 10.1126/science.1106525

Nightglow in the Upper Atmosphere of Mars and Implications for Atmospheric Transport

Jean-Loup Bertaux,^{1*} François Leblanc,¹ Séverine Perrier,¹ E. Quemerais,¹ Oleg Korabev,² E. Dimarellis,¹ A. Reberac,¹ F. Forget,³ P. C. Simon,⁴ S. A. Stern,⁵ Bill Sandel,⁶ the SPICAM team†

We detected light emissions in the nightside martian atmosphere with the SPICAM (spectroscopy for the investigation of the characteristics of the atmosphere of Mars) ultraviolet (UV) spectrometer on board the Mars Express. The UV spectrum of this nightglow is composed of hydrogen Lyman α emission (121.6 nanometers) and the γ and δ bands of nitric oxide (NO) (190 to 270 nanometers) produced when N and O atoms combine to produce the NO molecule. N and O atoms are produced by extreme UV photo-dissociation of O₂, CO₂, and N₂ in the dayside upper atmosphere and transported to the night side. The NO emission is brightest in the winter south polar night because of continuous downward transport of air in this region at night during winter and because of freezing at ground level.

of the atmosphere and ionosphere of Mars (4, 5) but also capable of providing important results on the surface albedo of Mars. A UV imaging spectrometer (118 to 320 nm, spectral resolution of 1.5 nm, intensified charge coupled device) is dedicated to nadir viewing, limb viewing, and atmospheric vertical profiling by stellar and solar occultations (6).

The UV channel of SPICAM is a full UV imaging spectrometer that spatially resolves 288 spectra along its slit, but, because of telemetry constraints, only five spectra can be transmitted for each 1-s measurement. These spectra are usually a sum of n individual spectra, with $n = 32$ in the present case, forming five band spectra (numbered from 0 to 4). The slit of the spectrometer, placed at the focus of the parabolic mirror, has two parts: a narrow part, achieving a spectral resolution of 1.5 nm, and a wide part, achieving a higher (10 times greater) photometric sensitivity for extended sources at the expense of a reduced spectral resolution (6 nm). Two band spectra were acquired with the narrow slit, and three band spectra with the wide slit, during each second in the observations reported here (7).

At the time of this observation [orbit 734, 16 August 2004, 07:00 universal time (UT)], the orbit of MEX had its pericenter on the night side, at an altitude of 266 km and a latitude of -16°. The orbit is almost polar, and MEX was descending from north to south. The attitude was fixed in an inertial system (departing from the usual nadir pointing near pericenter), so that the line of sight (LOS), which is aligned with the + Z body axis of the spacecraft, provided a grazing view of the limb while MEX was passing through its pericenter (± 10 nm). As a result, the altitude of the tangent point of the LOS [Mars nearest point (MNP)] changed from 375 km to a minimum of 15 km and back to 422 km. At the same time, the latitude changed from -11° to -70°. The whole

Airglow spectroscopy and radiometry are powerful methods for remote sensing investigations of the physics of upper atmospheres of the terrestrial planets (1). For instance, martian dayglow spectra (2, 3) reveal the effect of solar extreme ultraviolet (EUV)

radiation on upper atmosphere CO₂ as a major heating mechanism and on production of an ionosphere. On Venus, the observed UV nightglow is composed of weak O emissions, as a signature of electron precipitations capable of maintaining a nighttime ionosphere (1), and stronger spectra of O₂ and NO molecules, from radiative recombination of N and O atoms produced on the day side and transported to the night side. Thus, these NO and O₂ emissions are important tracers of atmospheric transport at high altitudes, constraining general circulation models. Up to now, however, nightglow from Mars had escaped detection.

The SPICAM (spectroscopy for the investigation of the characteristics of the atmosphere of Mars) instrument on board Mars Express (MEX) is a UV-infrared (IR) dual spectrometer dedicated primarily to the study

¹Service d'Aéronomie du CNRS/Institut Pierre-Simon Laplace (IPSL), BP.3, 91371, Verrières-le-Buisson, France. ²Space Research Institute (IKI), 84/32 Profsoyuznaya, 117810 Moscow, Russia. ³Laboratoire de Météorologie Dynamique/IPSL, University Paris 6, 75252 Paris, France. ⁴Belgian Institute for Space Aeronomy (BIRA), 3 Avenue Circulaire, B-1180 Brussels, Belgium. ⁵Southwest Research Institute, Boulder, CO 80302, USA. ⁶Lunar and Planetary Laboratory, 1541 East University Boulevard, University of Arizona, Tucson, AZ 85721, USA.

*To whom correspondence should be addressed. E-mail: bertaux@aerov.jussieu.fr

†Members of the SPICAM team and their affiliations are listed at the end of the References and Notes.

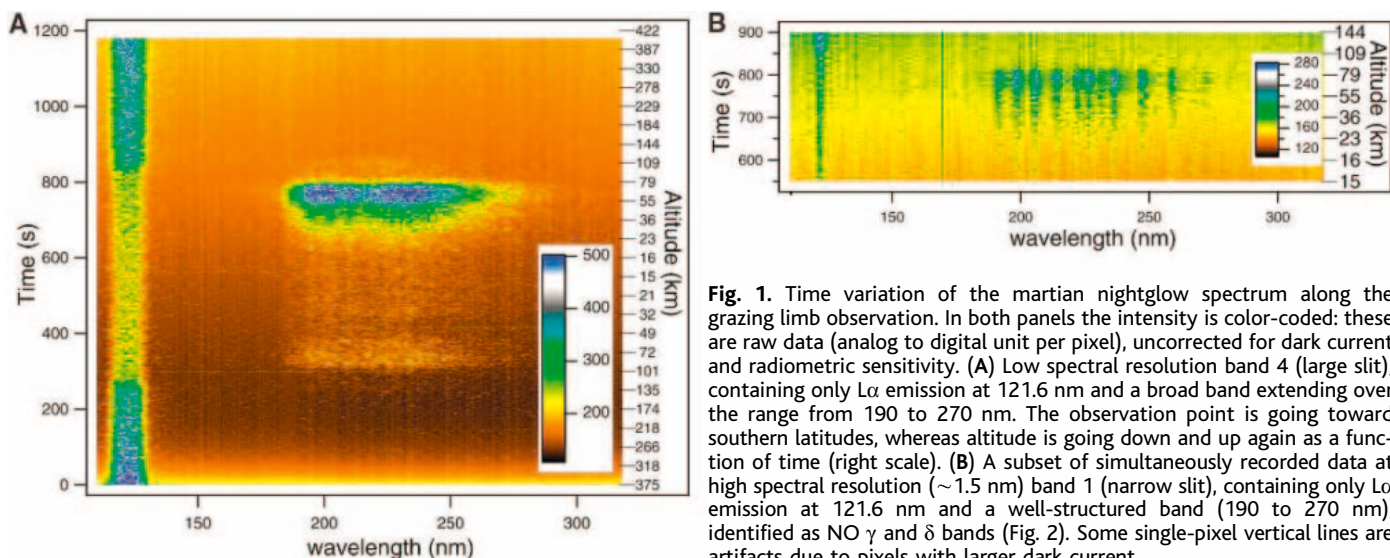


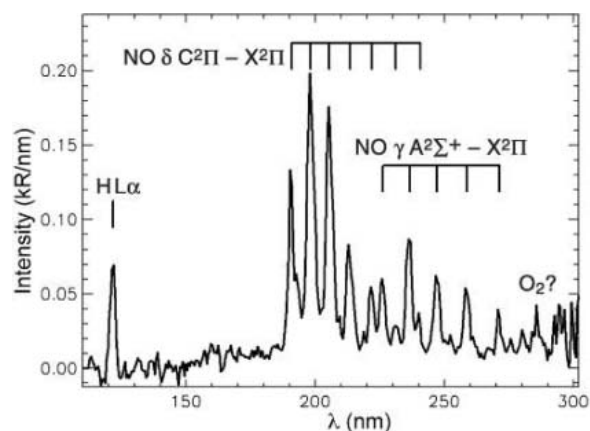
Fig. 1. Time variation of the martian nightglow spectrum along the grazing limb observation. In both panels the intensity is color-coded: these are raw data (analog to digital unit per pixel), uncorrected for dark current and radiometric sensitivity. (A) Low spectral resolution band 4 (large slit), containing only $L\alpha$ emission at 121.6 nm and a broad band extending over the range from 190 to 270 nm. The observation point is going toward southern latitudes, whereas altitude is going down and up again as a function of time (right scale). (B) A subset of simultaneously recorded data at high spectral resolution (~ 1.5 nm) band 1 (narrow slit), containing only $L\alpha$ emission at 121.6 nm and a well-structured band (190 to 270 nm), identified as NO γ and δ bands (Fig. 2). Some single-pixel vertical lines are artifacts due to pixels with larger dark current.

altitude range at the limb was therefore scanned twice but at different latitudes on the descending and ascending branches. The spectrometer slit was maintained parallel to the limb. The observations were taken around pericenter of orbit 734, Mars was at a solar distance of 1.66 AU (astronomical units), and the season was $L_s = 74^\circ$, near the northern summer (southern winter). Figure 1A is a color-coded image of the time series of spectra of band 4 (low resolution). The most obvious spectral features are the H $L\alpha$ emission, visible at all times, and a broad band emission in the region between 190 and 270 nm of variable intensity, only present when the MNP altitude is lower than ~ 80 km (Fig. 1). The higher resolution of band 0 (Fig. 1B) reveals a well-structured band, with a shape that looks constant.

By summing a number of spectra, we obtained the calibrated spectrum (Fig. 2) and identified the γ and δ bands of NO (respectively, transitions $A^2\Sigma^+ - X^2\Pi$ and $C^2\Pi - X^2\Pi$). Photons are produced when N and O atoms combine to form the NO molecule. Our identification is eased by its similarity with the case of Venus. Although some UV Venus nightglow had been detected with Mariner 5 (8) and Pioneer Venus (9), the first spectrum was acquired with International Ultraviolet Explorer (IUE) and identified as NO radiative recombination (10). It was proposed (10) that N and O atoms are produced on the Venus day side by EUV photodissociation and transported to the night side where recombination occurs, a mechanism later supported by detailed Pioneer Venus spectra (11, 12) and three-dimensional modeling of Venus atmospheric circulation (13, 14). We therefore propose that the same mechanism is responsible on Mars for our observed NO emission.

The integrated intensity of both the $L\alpha$ emission and the entire NO band region from 190 to 270 nm are plotted as a function of time (Fig. 3). The interplanetary $L\alpha$ emission and

Fig. 2. Spectrum of the martian nightglow obtained by averaging 10 consecutive individual spectra obtained in 10 s during orbit 734. Bands 0 and 1 corresponding to the narrow part of the slit (spectral resolution of 1.5 nm) have been used. Except for $L\alpha$ at 121.6 nm, all the observed lines coincide precisely with the main NO γ and δ vibrational state transitions responsible for the Venus NO nightglow. The absolute radiometric calibration comes from SPICAM observations of hot UV stars. The total NO intensity is 2.33 kR, with a 74% contribution from the δ band (and 26% from γ bands). The (0,1) line of the δ band alone is, at 475 Rayleigh, 27% of the total δ bands. Spectral features above 280 nm could be attributed to the O_2 Herzberg I system and also could be expected from the recombination of $O+O$ (as suggested by an anonymous referee).



the martian corona $L\alpha$ emission from H atoms contribute to the observed emission. The martian $L\alpha$ emission is solar radiation scattered by H atoms on the day side and transported to the night side by radiative transfer. CO_2 is a strong absorber at $L\alpha$ (15), and the atmosphere of CO_2 is opaque to $L\alpha$ below the altitude at which $\tau = 1$ (optical thickness of CO_2 along the LOS at $L\alpha$). Therefore, when the tangent point of the LOS is below this $L\alpha$ horizon, only the part of the LOS between the spacecraft and this opaque sphere will contribute to the emission. The disappearance of the interplanetary emission and possibly some contribution of the martian corona beyond the tangential point is seen at times 280 and 820 s after the start of observation, corresponding to the same altitude of 102 ± 2 km and a CO_2 slant density of $1.64 \times 10^{19} \text{ cm}^{-2}$ (15). This corresponds well to slant density estimates derived from SPICAM stellar occultations (16); around this altitude, this type of observation is a previously untested method for retrieving the CO_2 density and temperature at each limb crossing.

The light curve of the NO emission rate (Fig. 3) displays two peaks at 350 s and 770 s after the beginning of the observation (06:50:48 UT), with the second peak about 10 times brighter than the first one. Both correspond to a LOS altitude of ~ 70 km but to different latitudes, -35° and -60° , respectively. When the NO emission is displayed as a function of LOS altitude (Fig. 4), in both cases the observed emission is concentrated within the altitude range of 60 to 80 km (both γ and δ bands). This behavior can be explained by assuming a locally spherically symmetric NO-emitting layer confined to a spherical shell of thickness ~ 20 km centered at 70 km altitude, but with a much more intense emissivity rate (photons $\text{cm}^{-3} \text{ s}^{-1}$) at a latitude of -60° than at -35° . The emission seen at a tangent altitude below 60 km is essentially produced within the portion of the 60- to 80-km shell, along the LOS, before or after the MNP point (17).

The local emissivity rate of NO UV bands (in photons $\text{cm}^{-3} \text{ s}^{-1}$) is proportional to the N and O abundances, [N] and [O]. At

the altitude of their formation on the day side, [N] and [O] are too small to give rise to detectable recombination. But, when a gas parcel descends, both concentrations increase, and the emissivity rate will increase as the product [N][O] until a substantial fraction of [N] (or [O]) atoms are recombined (according to models, the abundance

of O is larger than N atoms, so [N] is the limiting factor for the NO emission). This leads to a layer of emission centered at a particular altitude. Although for Venus it was found at 115 ± 2 km (18), corresponding to a CO_2 density of $9 \times 10^{13} \text{ cm}^{-3}$ at midnight equatorial latitude (19), we find that on Mars the peak emission is at an

altitude of 70 km, corresponding to a CO_2 density of $2 \times 10^{14} \text{ cm}^{-3}$ (16). The EUV solar radiation producing O and N is ≈ 4 times larger at Venus, and the dayside mixing ratio $[\text{N}]/[\text{CO}_2]$ should be smaller on Mars than on Venus. Because the NO emission rate is related to the absolute abundance [N], it is therefore natural to have a larger CO_2 density at Mars at the level of maximum emission rate. The vertical mixing (described by an eddy diffusion coefficient) and other competing N loss reactions (without NO emission) are also playing an important role (12).

The NO band intensity may be used to estimate the downward flux of N atoms in the polar night. The peak intensity of 2.2 kilo-Rayleigh (kR) of the NO δ band measured horizontally (Fig. 4) may be converted into a vertical intensity of 85 Rayleigh, corresponding to 85×10^6 emitted photons $\text{cm}^{-2} \text{ s}^{-1}$ (20). This compares well with the prediction estimate of NO intensity at 40 to 50 Rayleigh (1). Following (21) and taking into account the fraction of photons emitted in the δ band with respect to all photons emitted, $f = 0.77$ (22), and $\epsilon = 0.45$, the efficiency (12) of the radiative N+O recombination as a loss process, we find a total of 2.5×10^8 recombinations $\text{cm}^{-2} \text{ s}^{-1}$, which must be compensated for by an equal downward flux of N atoms through the $z = 80$ km altitude level (at the place of the observation). In comparison, a much higher (17 times) average Venus nightside downward flux of 4.2×10^9 N atoms $\text{cm}^{-2} \text{ s}^{-1}$ is needed to match the average Venus NO nightglow intensity (13). Compared to the estimated production of N atoms on the Venus day side, the observed downward flux showed that about 30% of this production is transported to the night side (13).

The circulation pattern of Mars is completely different from that of Venus. The rotation is faster (1.02 days compared with 4 to 6 days), there is a strong seasonal cycle (23), and the polar night is so cold that about 30% of the whole atmosphere is actually condensing on the ground in the south polar winter. Our observations were obtained at $L_s = 74^\circ$, shortly before southern winter solstice. In this season, the part of the atmosphere where the maximum emission intensity was observed at 70°S is never illuminated by the sun. Any N and O present there must have been transported from a lower latitude where sunlight was available to photodissociate N_2 , O_2 , or CO_2 . Such an intensity can only be explained by a vertically descending flow in the upper polar atmosphere (24). This circulation pattern is consistent with prediction from a general circulation model (GCM) of the martian atmosphere (25). However, this model shows that, at this particular season, the circulation around 60 km is modulated by thermal tide

Fig. 3. (Top) Integrated intensity (wide slit band corresponding to Fig. 1A) of both the α emission (purple) and the whole NO band (black) from 190 to 270 nm, as a function of time and latitude (top scale). (Center) Altitude of the tangent point MNP. The NO emission displays two peaks, one each time the LOS crosses the 70-km altitude. The second peak is brighter by a factor of ~ 10 and is at a high southern latitude. (Bottom) sketch of the geometry of observations.

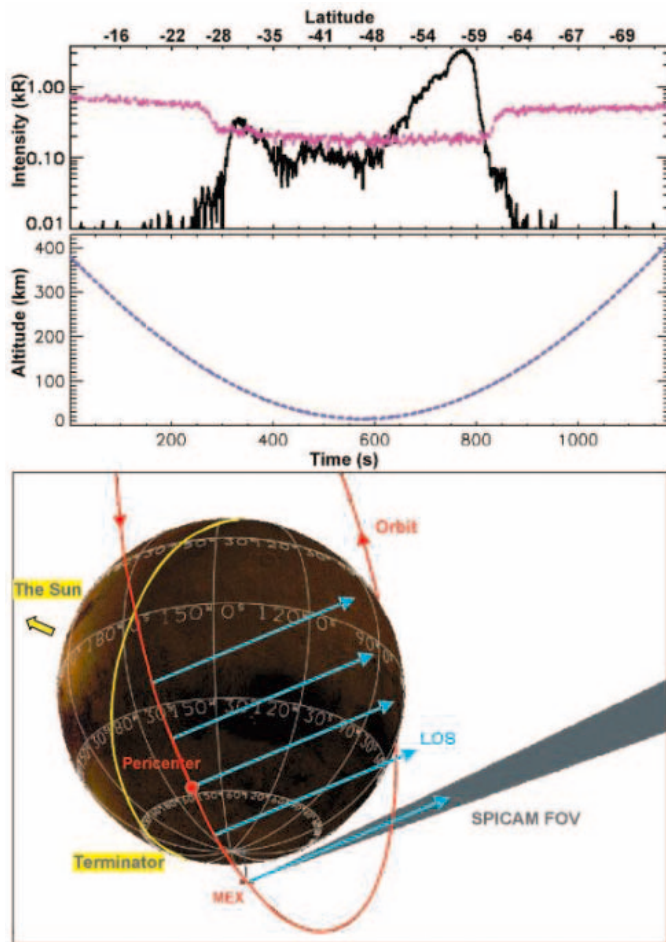
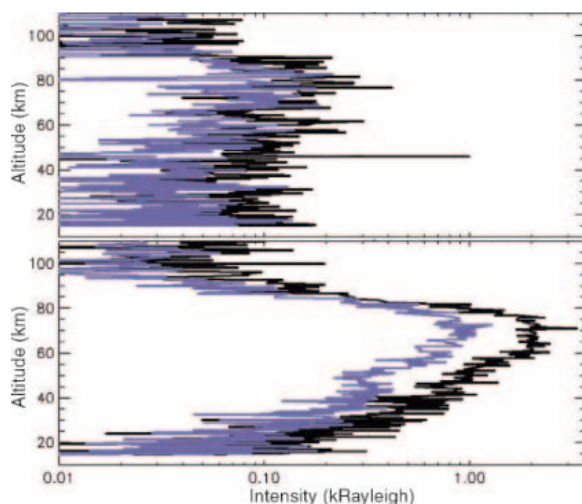


Fig. 4. Altitude profile of the limb emission of NO γ (blue) and δ (dark) system during orbit 734, around the two peaks observed on Fig. 3. (Top) First peak at time 350 s. (Bottom) Second peak at time 770 s. The blue curve is the sum of the (0,0), (0,1), (0,2), (0,3), and (0,4) bands of the γ system (at 226.2, 236.5, 247.1, 258.7, and 271.3 nm, respectively). The dark curve is the sum of the (0,0), (0,1), (0,2), (0,3), (0,4), (0,5), and (0,6) bands of the δ system (at 190.9, 198.0, 205.4, 213.4, 221.9, 231.0, and 240.6 nm, respectively). No obvious difference is seen between the two NO bands altitude behaviors. The vertical distributions of intensity peak around the 70-km altitude and are consistent with an emitting layer extending from ~ 60 to 80 km. The solar activity as seen from Mars was low, at a level $E_{10.7} = 98 \times 10^{-22} \text{ W m}^{-2} \text{ Hz}^{-1}$.



waves that propagate from the lower atmosphere and modified by the in situ heating caused by the absorption of near-IR radiation by CO₂. These processes are of key importance for our understanding of the upper atmosphere dynamics (and thus for future aeroassistance manoeuvre, for instance), but they remain poorly understood: Numerical simulations results are model-dependent (25), and few observations are available. Within this context, the NO emission process identified here provides a powerful way to constrain GCM model behavior above 60 km in conjunction with spacecraft drag measurements (26). In particular, the GCM (25) predicts that, during the opposite season, the Hadley circulation globally extends to the polar regions because of the stronger solar forcing near perihelion and a dustier atmosphere. This circulation creates a downward flow above the high northern latitudes in the polar night, which is predicted to be about several times stronger than that during the southern winter. We should expect accordingly a much more intense NO emission in July and August 2005.

References and Notes

- J. L. Fox, in *Venus and Mars: Atmospheres, Ionospheres, and Solar Wind Interactions*, J. Luhmann et al., Eds. [Geophys. Monogr. Am. Geophys. Union 66 (1992)], pp. 191–222.
- C. A. Barth et al., *J. Geophys. Res.* **76**, 2213 (1971).
- C. A. Barth et al., in *Mars*, H. Kieffer et al., Eds. (University of Arizona Press, Tucson, AZ, 1992), pp. 1054–1089, and references therein.
- J. L. Bertaux et al., *Planet. Space Sci.* **48**, 1303 (2000).
- J. L. Bertaux et al., *Adv. Space Res.*, in press.
- J. L. Bertaux et al., in *Mars Express*, A. Chicarro, Ed. (European Space Agency Special Publication SP1240, ESTEC, Netherlands, 2004), pp. 95–120.
- The instantaneous field of view for bands 0 and 1 (narrow slit) is 0.02° by 0.32° parallel to the limb and 0.2° by 0.32° for bands 2 to 4 (wide slit). Projected at the limb distance of 1200 km, it corresponds to 0.4 km by 6.7 km and 4 km by 6.7 km, respectively, for the narrow and wide slit bands.
- C. A. Barth, J. B. Pearce, K. K. Kelly, L. Wallace, W. G. Fastie, *Science* **158**, 1675 (1967).
- A. I. Stewart, D. E. Anderson Jr., L. W. Esposito, C. A. Barth, *Science* **203**, 777 (1979).
- P. D. Feldman, H. W. Moos, J. T. Clarke, A. L. Lane, *Nature* **279**, 221 (1979).
- A. I. Stewart, C. A. Barth, *Science* **205**, 59 (1979).
- A. I. Stewart, J. C. Gerard, D. W. Rusch, S. W. Bougher, *J. Geophys. Res.* **85**, 7861 (1980).
- S. W. Bougher, J. C. Gerard, A. I. F. Stewart, C. G. Fesen, *J. Geophys. Res.* **95**, 6271 (1990).
- S. W. Bougher, M. J. Alexander, H. G. Mayr, in *Venus II*, S. W. Bougher, D. M. Hunten, R. J. Phillips, Eds. (University of Arizona Press, Tucson, AZ, 1997), pp. 259–291.
- The CO₂ cross section at λ (121.5 nm) is 6.11×10^{-20} cm⁻². Optical thickness unity ($\tau = 1$, attenuation factor e) may be determined from the λ light curve occurring at an altitude of 102 ± 2 km and corresponding to 1.64×10^{19} cm⁻² CO₂ slant density (local CO₂ density integrated along a line of sight). This shows how λ emission observations on the night side can be used to determine the density profile around 100 km (and temperature from scale height).
- These results agree with our night star occultation measurements (27).
- The CO₂ cross section is 3.0×10^{-23} cm² at 190 nm, the shortest wavelength of the observed NO band, and decreases very fast with increasing wavelength, and the slant CO₂ density $1/\sigma = 3.3 \cdot 10^{22}$ cm⁻² is obtained, according to stellar occultations measurements, around 53 km. Therefore, to first order we consider that the CO₂ atmosphere is transparent to the NO emission band above 40 to 50 km. The decrease of emission with decreasing altitude is therefore more a "shell" effect than absorption or extinction by CO₂.
- J. C. Gerard, A. I. F. Stewart, S. W. Bougher, *Geophys. Res. Lett.* **8**, 633 (1981).
- A. E. Hedin, H. B. Niemann, W. T. Kasprzak, A. Seiff, *J. Geophys. Res.* **88**, 73 (1983).
- Assuming a spherical shell between 60 and 80 km with a constant NO δ band emissivity as suggested by Fig. 4, the ratio of horizontal to vertical intensity is 26.
- J. C. Gérard, E. J. Deney, H. Lehro, *Icarus* **75**, 171 (1988).
- R. P. McCoy, *J. Geophys. Res.* **88**, 3197 (1983).
- The equator of Mars is inclined by 24° to the ecliptic plane. Seasons on Mars are defined by the solar longitude L_s , with $L_s = 0^\circ$ at the northern spring equinox and $L_s = 90^\circ$ at northern summer. Seasons are asymmetric between north and south, because Mars is much nearer to the Sun during southern summer (1.38 AU) than during northern summer (1.66 AU).
- A similar diabatic subsidence of the atmosphere is also observed on Earth above the winter pole, compensated by a horizontal flow at the mesopause altitude (85 km). In view of the similarities of the atmosphere of Mars with the Earth's stratosphere, this is likely to happen also on Mars, and the CO₂ condensation process on the winter pole on Mars can only emphasize this subsidence on Mars.
- F. Forget et al., *J. Geophys. Res.* **104**, 24155 (1999).
- G. M. Keating, M. Theriot, R. Tolson, in *proceedings of Mars Atmosphere Modelling and Observations Workshop*, Grenada, Spain, CNES/ESA, 13 to 15 January 2003.
- X. Quémérais et al., in preparation.
- Mars Express is a space mission from European Space Agency (ESA). We wish to express our gratitude to all ESA members who participated in this successful mission, in particular M. Denis at European Space

Operations Center for the delicate controlling of the spacecraft and R. Pischel and T. Zeghers at ESTEC for careful planning exercises and supporting geometry graphics. We thank also Astrium for the design and construction of the spacecraft, in particular A. Clochet, responsible for the payload; our collaborators at the three institutes for the design and fabrication of the instrument (Service d'Aéronomie, France; BIRA, Belgium; and IKI, Moscow); and CNRS and CNES for financing SPICAM in France, the Belgian government, the Russian Academy of Sciences, and NASA, for support of U.S. co-investigators. The SPICAM team is composed of the following members: J.-L. Bertaux¹ (principal investigator), O. Korabev,² D. Fonteyn,³ E. Chassefière,¹ E. Dimarellis,¹ J. P. Dubois,¹ A. Hauchecorne,¹ F. Lefèvre, A. C. Lévasseur-Regourd,¹ G. Cernogora,¹ M. Cabane,¹ P. Rannou,¹ E. Quémérais,¹ C. Hermans,¹ G. Kockarts,¹ C. Lippens,¹ M. De Maziere,¹ D. Moreau,¹ C. Muller,¹ E. Neefs,¹ D. Nevejans, P. C. Simon,¹ F. Forget,⁴ F. Hourdin,⁴ O. Talagrand,⁴ V. I. Moroz,² A. Rodin,² B. Sandel,⁵ A. Stern,⁶ F. Leblanc,¹ F. Montmessin,^{1,7} O. Witasse,⁸ B. Gondet,⁹ A. Federova,² D. Fussen,³ E. Kyrölä,¹⁰ J. Tamminen,¹⁰ S. Lebonnois,⁴ S. Perrier.¹

¹Service d'Aéronomie du CNRS/IPSL, BP.3, 91371, Verrières-le-Buisson, France. ²IKI, 84/32 Profsoyuznaya, 117810 Moscow, Russia. ³BIRA, 3 Avenue Circulaire, B-1180 Brussels, Belgium. ⁴Laboratoire de Météorologie Dynamique/IPSL, Université Paris 6, 75252 Paris, France. ⁵Lunar and Planetary Laboratory, 1541 East University Boulevard, University of Arizona, Tucson, AZ 85721, USA. ⁶Southwest Research Institute, Boulder, CO 80302, USA. ⁷NASA Ames Research Center, Moffett Field, CA 94035-1000, USA. ⁸ESTEC/SCI-SR postbus 299, 2200 AG Noordwijk, Netherlands. ⁹Institut d'Astrophysique Spatiale, Orsay Campus, 91405 Orsay, France. ¹⁰Finnish Meteorological Institute, Post Office Box 503, Fin-00101 Helsinki, Finland.

1 November 2004; accepted 27 December 2004
10.1126/science.1106957

Prediction of Hydrogen Flux Through Sulfur-Tolerant Binary Alloy Membranes

Preeti Kamakoti,^{1,2} Bryan D. Morreale,¹ Michael V. Ciocco,¹ Bret H. Howard,¹ Richard P. Killmeyer,¹ Anthony V. Cugini,¹ David S. Sholl^{2*}

Metal membranes play a vital role in hydrogen purification. Defect-free membranes can exhibit effectively infinite selectivity but must also provide high fluxes, resistance to poisoning, long operational lifetimes, and low cost. Alloying offers one route to improve on membranes based on pure metals such as palladium. We show how ab initio calculations and coarse-grained modeling can accurately predict hydrogen fluxes through binary alloy membranes as functions of alloy composition, temperature, and pressure. Our approach, which requires no experimental input apart from knowledge of bulk crystal structures, is demonstrated for palladium-copper alloys, which show nontrivial behavior due to the existence of face-centered cubic and body-centered cubic crystal structures and have the potential to resist sulfur poisoning. The accuracy of our approach is examined by a comparison with extensive experiments using thick foils at elevated temperatures. Our experiments also demonstrate the ability of these membranes to resist poisoning by hydrogen sulfide.

The purification of hydrogen from gas mixtures is a crucial process in both existing and envisioned uses of hydrogen as a chemical feedstock and fuel (1, 2). Membranes made from thin films of

metal such as Pd are a well-known technology for achieving this purification. Metal membranes are also used in membrane reactors that boost reaction efficiency by selectively remov-

ing or adding hydrogen (3). Any potential metal membrane must simultaneously satisfy multiple performance objectives, such as delivering high hydrogen flux, showing long-term operability over broad ranges of temperature (T) and pressure (P), and resistance to poisoning and degradation by gas contaminants.

One route to improving on the performance of pure metal membranes is to use metal alloys as membranes (4). Binary alloys of Pd with many metals have been examined (5–13). A small number of studies have examined ternary alloys (4), but the large experimental investment required to screen even a small number of membranes poses a substantial barrier to studying such alloys in any systematic manner. This situation could be greatly aided if reliable theoretical methods were available to identify alloy compositions with promising properties or to disqualify materials from further investigation. Here we show that a combination of first-principles density functional theory (DFT) calculations and coarse-grained modeling can be used to complement experimental studies by comparing model predictions with extensive experimental measurements of hydrogen permeation through binary Pd-Cu alloys. These alloys are particularly interesting because they may resist poisoning by H_2S (8, 10, 13–15).

The permeation of hydrogen through metal

membranes is a multistep process involving dissociative chemisorption of molecular H_2 , the diffusion of atomic H into and through the bulk, and recombinative desorption of H_2 from the downstream surface (16). We modeled situations where diffusion through the bulk is the dominant resistance to mass transport; that is, where surface reactions are not rate-limiting. (Surface reactions could in principle be included within our modeling framework, but this is beyond the scope of our current work.) Under this assumption, the H concentration θ_H just inside the surface of a membrane is in equilibrium with the partial pressure of H_2 in the neighboring gas phase P_{H_2} . For dilute H concentrations, $\theta_H = K_S P_{H_2}^{1/2}$, where K_S is the Sievert's constant. The flux of H_2 through a membrane is determined by the concentration drop across the membrane and the diffusivity D of dissolved H. For dilute H concentrations, the diffusivity is well described by the self-diffusivity D_s of isolated H atoms in the metal (17). The overall throughput of a membrane is typically characterized by the permeability, which in this case is simply $k = 1/2(K_S D_s)$ (18).

The aim of our modeling approach is to characterize membrane permeability in a binary alloy membrane with composition $A_x B_{100-x}$ as a function of temperature, pressure, and alloy composition by predicting K_S and D_s . We assume that the crystal structure and the degree of local ordering within the alloy are known, but we do not use any other information that would require experimental determination. We demonstrate our method for $Pd_x Cu_{100-x}$, where x denotes atomic %. $Pd_x Cu_{100-x}$ alloys occur in multiple crystal

structures (19). A disordered face-centered cubic (fcc) phase occurs for a wide range of alloy compositions, including the region with $x > 47$. For a range of compositions centered at $x = 40$ and $T < 773$ K, an ordered body-centered cubic (bcc) phase exists.

To predict H solubility in $Pd_x Cu_{100-x}$ alloys, we consider gaseous H_2 in equilibrium with interstitial atomic H in the metal. Molecular H_2 is treated as an ideal gas, which is an accurate approach for a wide range of pressures at elevated temperatures. Interstitial sites in the alloy are treated as independent three-dimensional harmonic oscillators with classical binding energy for atomic H E_b and vibrational frequencies ν_H . The Sievert's constant is calculated by equating the chemical potentials of the interstitial and gaseous species (20, 21) giving

$$K_S = \exp\left(\beta\left[-\frac{D_E}{2} + \frac{h\nu_{H_2}}{4} - E_b - \frac{3}{2}h\nu_H\right]\right) \frac{1}{\sqrt{\alpha}} \sqrt{1 - \exp(-\beta h\nu_{H_2}/2)} \frac{1}{(1 - e^{-\beta h\nu_H})^3} \quad (1)$$

where

$$\alpha = \left(\frac{2\pi mkT}{h^2}\right)^{3/2} \frac{4\pi^2 I (kT)^2}{h^2} \quad (2)$$

Here, $D_E(\nu_{H_2})$ is the classical dissociation energy (vibrational frequency) of gaseous H_2 , I is the molecular moment of inertia, m is the mass of H_2 , h is Planck's constant, and $\beta = 1/k_B T$ (k_B is the Boltzmann constant).

We calculated E_b and ν_H for representative interstitial sites using plane wave DFT for fcc $Pd_x Cu_{100-x}$ ($x = 50, 75, \text{ and } 100$) and

¹U.S. Department of Energy National Energy Technology Laboratory, Pittsburgh, PA 15236, USA.
²Department of Chemical Engineering, Carnegie Mellon University, Pittsburgh, PA 15213, USA.

*To whom correspondence should be addressed.
E-mail: sholl@andrew.cmu.edu

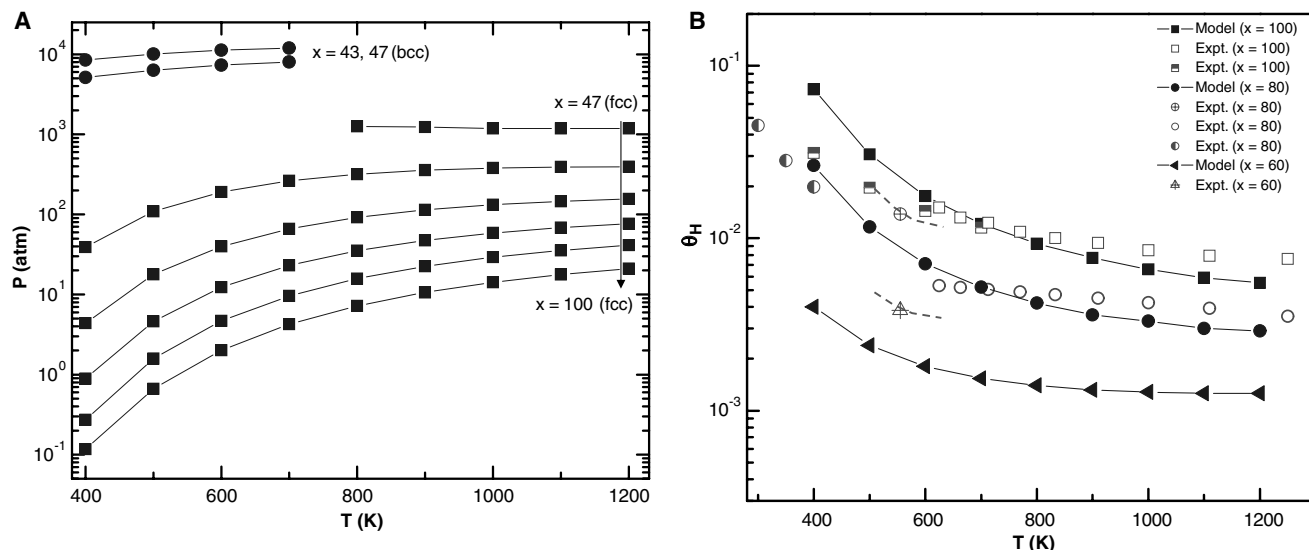


Fig. 1. (A) P - T diagram showing, for various alloys, the conditions predicted to yield $Pd_x Cu_{100-x} H_{2.5}$. Circles correspond to bcc alloys with $x = 43$ (upper curve) and 47 (lower curve). Squares show results for fcc alloys with $x = 47, 60, 70, 80, 90, \text{ and } 100$ in descending order. (B) Comparison of predicted and experimentally reported hydrogen solubilities in fcc $Pd_x Cu_{100-x}$

with $P_{H_2} = 1$ atm for $x = 100$ (squares), 80 (circles), and 60 (triangles). Predictions are indicated by solid curves and solid symbols, whereas experimental data are shown with open symbols. Dashed curves are from the partial molar enthalpy and partial molar excess entropy measured experimentally at 555 K (31). The other experimental data are from (6, 32, 33).

bcc $\text{Pd}_x\text{Cu}_{100-x}$ ($x = 35, 43, 47,$ and 50). Our DFT calculations used the PW91 GGA functional and represented interstitial H at dilute concentrations using a single H atom in computational cells containing 20 to 30 metal atoms (22, 23). Frequencies were estimated via small displacements of the H atom around local minima (or transition states), neglecting coupling of these modes with phonons in the metal (24, 25). In all, we considered 58 distinct octahedral sites and over 100 tetrahedral sites. The results for each crystal structure were used to determine simple expressions correlating the local environment of an interstitial site with the properties of H in that site. For example, for bcc $\text{Pd}_x\text{Cu}_{100-x}$ we find that tetrahedral sites with local composition $\text{Pd}_2\text{Cu}_2(\text{Pd}_2\text{Cu}_2)$, $\text{Pd}_2\text{Cu}_2(\text{PdCu}_3)$, PdCu_3 , and Cu_4 can be assigned binding energies of $E_b = 0.03, 0.07, 0.16,$ and 0.22 eV over the whole range of bcc alloy compositions. The terms in parentheses indicate the composition of the next nearest neighbor shell. We used a more complex expression involving measures of the local and overall alloy composition for the interstitial sites in the fcc alloy (23). With E_b defined in this way, the net solubility of a specified alloy is found by applying Eq. 1 to each site.

We report our solubility results by showing in Fig. 1A the P - T combinations that are predicted to have 2.5% of interstitial sites filled. The solubility drops drastically as the Pd content of the fcc alloy decreases. For bcc alloys, extremely high pressures are required to obtain even this dilute concentration. For all P - T combinations below the curve for an alloy of interest in Fig. 1A, our modeling assumption that H is dilute within a membrane is valid. Our predicted solubilities for hydrogen in fcc $\text{Pd}_x\text{Cu}_{100-x}$ ($x = 100, 80,$ and 60) are compared with experimental data in Fig. 1B. The model predictions are not perfect, but the model does accurately capture the variation in solubility with temperature and, more importantly, with alloy composition.

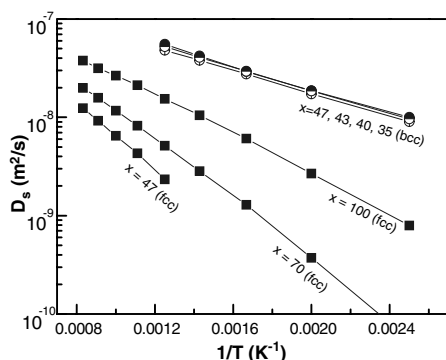


Fig. 2. Predicted diffusion coefficients for interstitial H in fcc $\text{Pd}_x\text{Cu}_{100-x}$ (squares), with $x = 100, 70,$ and 47 in descending order; and bcc $\text{Pd}_x\text{Cu}_{100-x}$ (circles), with $x = 47, 43, 40,$ and 35 in descending order.

tion. No experimental data are available for comparison for the bcc alloy.

To predict H diffusivities in $\text{Pd}_x\text{Cu}_{100-x}$ alloys, we first extended the DFT-based models described above for the binding energy of interstitial H to a similar description of the transition-state energies that define hops between adjacent sites. These energies, when used in appropriate rate expressions, predict the hopping rates between adjacent sites. We then used kinetic Monte Carlo (KMC) simulations to evaluate the diffusivities of isolated H atoms in systems with large spatial extent. For fcc alloys, quantum-corrected transition-state theory (TST) is used to predict local rates, and transition-state energies for hops between octahedral and tetrahedral sites are predicted using a DFT-based expression that accounts for both the local and overall alloy composition (23). The predicted diffusivities for several fcc alloys are shown in Fig. 2. In the range of temperatures relevant to membrane operation, the net activation energy for H diffusion increases, and the net diffusivity decreases as the Cu content of fcc $\text{Pd}_x\text{Cu}_{100-x}$ is increased.

To describe H diffusion in bcc $\text{Pd}_x\text{Cu}_{100-x}$ we used DFT calculations for materials with $x = 35, 43, 47,$ and 50 and characterized the hopping energies between examples of all possible pairs of adjacent binding sites (characterized as listed above). The classical energy barriers ranged from 0.04 to 0.13 eV and can be reasonably approximated as independent of alloy composition for each type of local

hop. Because of the large zero point energies in these materials, quantum-corrected TST for hopping rates between two tetrahedral sites, $k_{T \rightarrow T}$, at elevated temperatures can be simplified to (26) $k_{T \rightarrow T} = (k_B T/h) \exp[-\beta E^{qc}]$, where $E^{qc} = E^{\text{classical}} + (3/2)h\nu^T - h\nu^{\text{TS}}$, where $E^{\text{classical}}$ is the classical activation barrier to hopping, and $\nu^T(\nu^{\text{TS}})$ is the average vibrational frequency of H in the tetrahedral site (transition state).

Predicted H diffusion coefficients for bcc $\text{Pd}_x\text{Cu}_{100-x}$ are shown in Fig. 2. Consistent with experiments (27), the diffusivity is significantly larger than in fcc $\text{Pd}_x\text{Cu}_{100-x}$ alloys and is relatively insensitive to alloy composition. This behavior is consistent with the general observation that H diffusion is more rapid in bcc metals than in fcc metals (28). The net activation barrier for diffusion in the bcc alloys is ~ 0.12 eV. This corresponds to the energy barrier required to achieve long-range diffusion in the ordered alloy, bcc $\text{Pd}_{50}\text{Cu}_{50}$. Local hops with lower barriers also exist in this material, but these cannot lead to long-range diffusion, a point we addressed incorrectly in earlier work (22). Our prediction is in good agreement with experimental measurements in bcc $\text{Pd}_{47}\text{Cu}_{53}$ at $298 < T < 623$ K, which gave an overall activation energy of 0.11 eV (27). Our predictions do not agree with lower-temperature experiments that yielded an activation energy of 0.04 eV (26). H diffusion in bcc metals is known to yield different activation energies at low and high temperatures

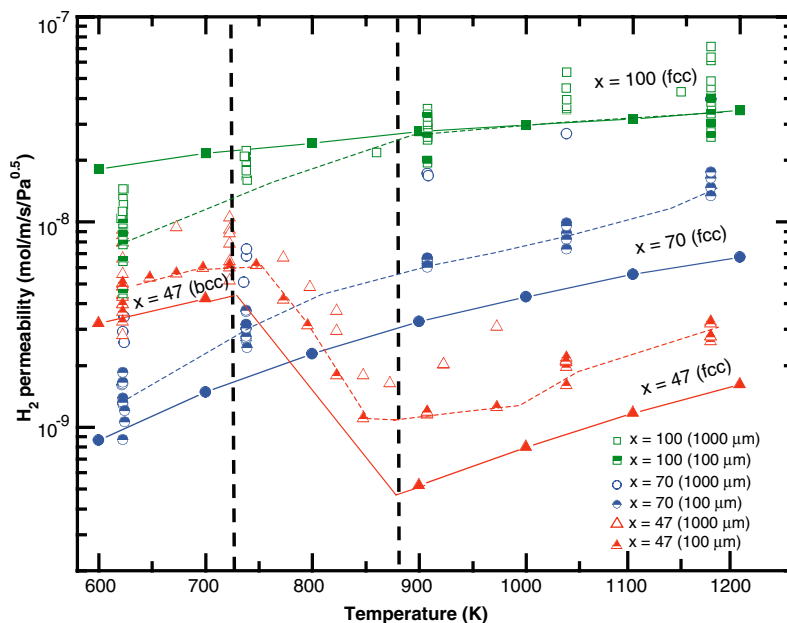


Fig. 3. Predicted and measured H_2 permeabilities through $\text{Pd}_x\text{Cu}_{100-x}$ membranes with $x = 100$ (squares), $x = 70$ (circles), and $x = 47$ (triangles), all in atomic %. The membrane thickness for each set of experiments is indicated in the legend. Theoretical predictions are shown with solid symbols and solid curves. Dashed curves indicate the experimental measurements with a 100- μm membrane (11, 18). All curves are to guide the eye only. The vertical dashed lines indicate the region where the fcc-bcc transition occurs for $\text{Pd}_{47}\text{Cu}_{53}$ (70). Theoretical predictions for this alloy are only shown in the single-phase regions. The theoretical curve indicated in the phase-transition region simply connects the theoretical predictions in the two separate phases.

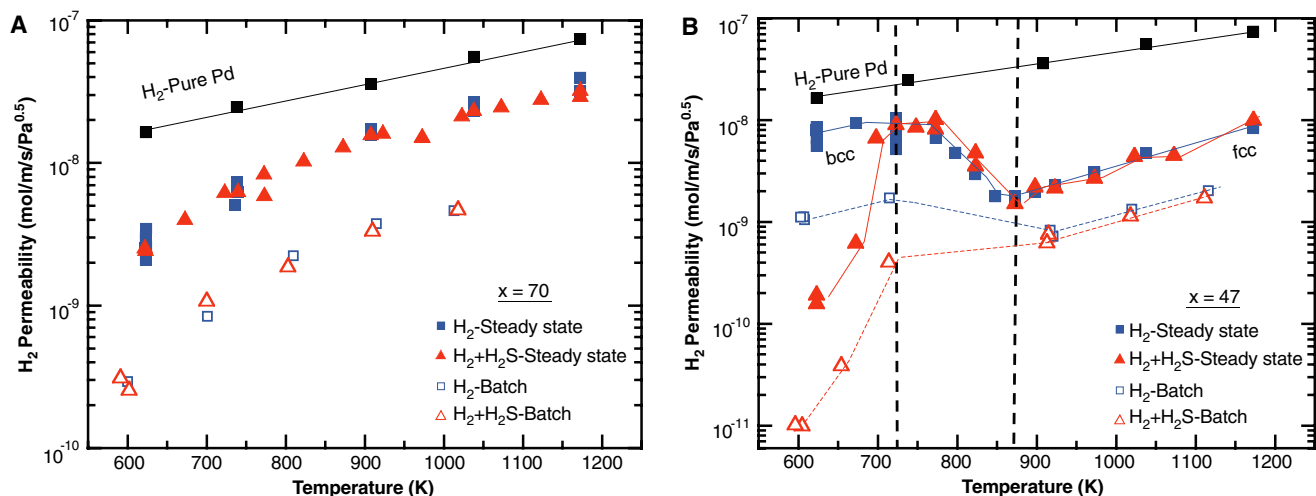


Fig. 4. Experimentally measured permeabilities of $\text{Pd}_x\text{Cu}_{100-x}$ membranes with (A) $x = 100$ and 70 and (B) $x = 100$ and 47 . Solid symbols show results from steady-state experiments with $1000\text{-}\mu\text{m}$ foils, whereas the results from transient batch experiments (10) with $100\text{-}\mu\text{m}$ foils are shown with open symbols. Experiments performed with pure H_2 and pure

Pd are shown as black squares for reference. For PdCu alloys, experiments performed with pure H_2 are shown in blue; experiments performed with H_2 containing $1000\text{ ppm H}_2\text{S}$ are shown in red. Curves are to guide the eye only. The vertical dashed lines in (B) indicate the bcc-fcc phase transition region as in Fig. 3.

because of the appearance of quantum effects at low temperatures (26). We are primarily interested in describing membranes at temperatures well above room temperature. The model described above is well suited to this regime.

Our DFT-based models of H solubility and diffusion allow us to predict the macroscopic flux of H_2 through alloy membranes. A limited knowledge of the alloy phase diagram was the only experimental information used in deriving these models. The predicted permeabilities for several representative alloys are shown in Fig. 3.

To examine the validity of our predictions, we performed extensive experiments with alloy foils of thickness 100 and $1000\text{ }\mu\text{m}$ with $623 < T < 1173\text{ K}$ and H_2 pressures ranging from 1 to 26 atm (Fig. 3). Transmembrane fluxes were measured using a steady-state flow system with a pressure drop of 1.36 atm (11, 18). The crystal structure and elemental composition of the foils were verified by x-ray diffraction and inductively coupled plasma analysis, respectively. We observed some variations in permeability as the H_2 pressure and membrane thickness were varied, which may stem from resistances to H transport other than bulk diffusion in the membrane (18, 29). The overall consistency of the data in Fig. 3, however, supports the notion that a description based only on bulk diffusion and solubility is useful for comparing relative permeabilities of different alloys.

Figure 3 compares our model predictions with our experiments for $\text{Pd}_x\text{Cu}_{100-x}$ foils. For pure Pd, the prediction lies within the scatter of the experiments, although the prediction underestimates the true increase in permeability with increasing T . For fcc $\text{Pd}_{70}\text{Cu}_{30}$, the model predicts the growth rate of permeability with T accurately, although the numeri-

cal value is underestimated at all temperatures. $\text{Pd}_{47}\text{Cu}_{53}$ provides a stringent test of our model, because we observed experimentally (19) that this material is in a bcc form for $T < 725\text{ K}$ and an fcc form for $T > 875\text{ K}$. In between these two temperature ranges, a material of mixed crystal structure exists. Our experiments and model predictions both show a dramatic decrease in membrane permeability as T is raised through this phase transition. In both phases, our model accurately predicts the temperature dependence of the permeability while underestimating the absolute values.

Achieving reasonable hydrogen flux is just one of the multiple objectives that must be satisfied by a practical metal membrane; resistance to chemical poisoning and long-term stability are also crucial. Several previous reports have hinted that PdCu alloys might have favorable behaviors in this regard (8, 10, 13–15), so we performed a series of experiments to probe the resistance of our membranes to poisoning by H_2S , a ubiquitous contaminant in many applications. Experiments were performed in a steady-state flow mode, where the feed gas contained 1000 parts per million (ppm) H_2S to complement our previous transient batch experiments (10). In the transient experiments, pure H_2 or $1000\text{ ppm H}_2\text{S}$ /balance H_2 was charged on the feed side of a membrane to pressures up to 5 atm , and the transient pressure as H_2 permeated through the membrane was monitored (10).

The key results of our H_2S tolerance experiments are summarized in Fig. 4. The batch and steady-state experiments yielded consistent results. Essentially no inhibition of H_2 flux was observed for $\text{Pd}_{70}\text{Cu}_{30}$ membranes (Fig. 4A). We exposed one $\text{Pd}_{70}\text{Cu}_{30}$ membrane to the flowing $1000\text{ ppm H}_2\text{S}$ stream

for >175 hours at temperatures ranging from 623 to 1173 K without performance degradation. For $\text{Pd}_{47}\text{Cu}_{53}$, poisoning of the membrane by H_2S was slight at temperatures where the alloy is an fcc material but stronger at temperatures where the alloy is bcc (Fig. 4B). At $T \sim 600\text{ K}$ for a H_2 feed containing $1000\text{ ppm H}_2\text{S}$, the permeability of the fcc $\text{Pd}_{70}\text{Cu}_{30}$ membrane was more than an order of magnitude larger than that of the bcc $\text{Pd}_{47}\text{Cu}_{53}$ membrane.

The picture that emerges from our modeling and experimental studies of these alloy membranes is entirely consistent. By assuming that diffusion is the rate-limiting step in permeation, our theoretical approach can predictively describe the flux of hydrogen through membranes as a function of alloy composition and temperature. Other elementary steps such as hopping from surface to subsurface sites may play a role in the performance of the ultrathin films that are desirable in practical applications (8, 29, 30). Extending our first-principles approach to examine these effects will provide useful insights into identifying physical regimes where they might become important. Similarly, identification and detailed modeling of the surface chemistry responsible for the sulfur resistance exhibited by PdCu membranes will likely open the door to the discovery of other alloys with favorable properties as H_2 membranes.

References and Notes

1. Y. S. Lin, *Separ. Purif. Technol.* **25**, 39 (2001).
2. L. Schlapbach, A. Züttel, *Nature* **414**, 353 (2001).
3. Y. She, J. Han, Y. H. Ma, *Catal. Today* **67**, 45 (2001).
4. S. N. Paglieri, J. D. Way, *Sep. Purif. Methods* **31**, 1 (2002).
5. R. B. McLellan, M. Yoshihara, *Acta Metall.* **35**, 197 (1987).
6. A. Weiss, S. Ramaprabhu, N. Rajalakshmi, *Z. Physik Chem.* **199**, 165 (1997).
7. O. M. Lovvik, R. A. Olsen, *J. Alloys Compounds* **330–332**, 332 (2002).

8. F. Roa, J. D. Way, *Ind. Eng. Chem. Res.* **42**, 5827 (2003).
 9. F. Roa, J. D. Way, R. L. McCormick, S. Paglieri, *Chem. Eng. J.* **93**, 11 (2003).
 10. B. D. Morreale et al., *J. Membr. Sci.* **241**, 219 (2004).
 11. B. H. Howard et al., *J. Membr. Sci.* **241**, 207 (2004).
 12. V. M. Gryaznov, *Z. Physik Chem.* **147**, 123 (1986).
 13. D. L. McKinley, U. S. Patent 3,350,845 (1967).
 14. A. Kulprathipanja, G. O. Alptekin, J. L. Falconer, J. D. Way, *Ind. Eng. Chem. Res.* **43**, 4188 (2004).
 15. D. Edlund, paper presented at the Advanced Coal-Fired Power Systems '96 Review Meeting, Pittsburgh, PA, 1996.
 16. T. L. Ward, T. Dao, *J. Membr. Sci.* **153**, 211 (1999).
 17. F. J. Keil, R. Krishna, M. O. Coppens, *Rev. Chem. Eng.* **16**, 71 (2000).
 18. B. D. Morreale et al., *J. Membr. Sci.* **212**, 87 (2003).
 19. M. Hansen, *Constitution of Binary Alloys* (McGraw-Hill, New York, 1958).
 20. R. H. Fowler, C. J. Smithells, *Proc. R. Soc. London Ser. A* **145**, 699 (1937).
 21. C. Wagner, *Acta Metallurgica* **21**, 1297 (1973).
 22. P. Kamakoti, D. S. Sholl, *J. Membr. Sci.* **225**, 145 (2003).
 23. P. Kamakoti, D. S. Sholl, *Phys. Rev. B* **71**, 014301 (2005).
 24. J. Greeley, W. P. Krekelberg, M. Mavrikakis, *Angew. Chem. Int. Ed. Engl.* **43**, 4296 (2004).
 25. D. E. Jiang, E. A. Carter, *Phys. Rev. B* **70**, 064102 (2004).
 26. J. Volkl, G. Alefeld, in *Hydrogen in Metals I*, G. Alefeld, J. Volkl, Eds. (Springer-Verlag, Berlin, 1978), pp. 321–348.
 27. J. Piper, *J. App. Phys.* **37**, 715 (1966).
 28. Y. Fukai, H. Sugimoto, *Adv. Phys.* **34**, 271 (1985).
 29. B. A. McCool, Y. S. Lin, *J. Mat. Sci.* **36**, 3221 (2001).
 30. Y. H. Ma et al., *Ind. Eng. Chem. Res.* **43**, 2936 (2004).
 31. O. J. Kleppa, Shamsuddin, C. Picard, *J. Chem. Phys.* **71**, 1656 (1979).
 32. E. Wicke, H. Brodowsky, in *Hydrogen in Metals 2*, G. Alefeld, J. Volkl, Eds. (Springer-Verlag, Berlin, 1978), pp. 73–151.
 33. M. Yoshihara, R. B. McLellan, *Acta Metallurgica* **31**, 66 (1983).
 34. Supported by the U.S. Department of Energy's Office of Fossil Energy. B.D.M. and M.V.C. were supported by a Parsons Inc. National Energy Technology Laboratory (NETL) Site Support contract. D.S.S. is an NETL Faculty Fellow.

2 November 2004; accepted 21 December 2004
 10.1126/science.1107041

Micropylar Pollen Tube Guidance by Egg Apparatus 1 of Maize

Mihaela L. Márton,¹ Simone Cordts,¹ Jean Broadhvest,² Thomas Dresselhaus^{1*}

Pollen tube guidance precedes the double fertilization of flowering plants. Here, we report the identification of a small maize protein of 94 amino acids involved in short-range signaling required for pollen tube attraction by the female gametophyte. *ZmEA1* is exclusively expressed in the egg apparatus, consisting of the egg cell and two synergids. Chimeric *ZmEA1* fused to green fluorescent protein (*ZmEA1:GFP*) was first visible within the filiform apparatus and later was localized to nucellar cell walls below the micropylar opening of the ovule. Transgenic down-regulation of the *ZmEA1* gene led to ovule sterility caused by loss of close-range pollen tube guidance to the micropyle.

In contrast to most animal and many lower plant species, sperm cells of flowering plants are nonmotile and are transported from the stigma to the female gametophyte (embryo sac) via pollen tube growth to allow double fertilization (1). Genetic and physiological studies have shown the involvement of both female sporophytic and gametophytic tissues in pollen tube guidance of different plant species (2). Molecules involved in sporophytic guidance have been identified as γ -aminobutyric acid (GABA), arabinogalactans, and small secreted proteins (3–6), but little is known about the molecules produced by the female gametophyte required for pollen tube guidance. The synergids have been identified as the source of producing a short-range pollen tube attractant or attractants in *Torenia fournieri*, but the molecular nature of the attractant(s) is still unknown (7).

We report the identification of *ZmEA1* (*Zea mays* *EGG APPARATUS1*) from an unfertilized maize egg cell cDNA library (8) and its role for short-range pollen tube attraction by the female gametophyte.

¹Biocenter Klein Flottbek, Developmental Biology and Biotechnology, University of Hamburg, Ohnhorststrasse 18, D-22609 Hamburg, Germany. ²Bayer BioScience N.V., Technologiepark 38, B-9052 Ghent, Belgium.

*To whom correspondence should be addressed. E-mail: dresselh@botanik.uni-hamburg.de

ZmEA1 is produced by the cells of the egg apparatus and represents a highly hydrophobic small protein of 94 amino acids with a predicted transmembrane domain (Fig. 1A). Tissue and single-cell reverse transcription polymerase chain reaction (RT-PCR) analyses showed that *ZmEA1* is exclusively expressed in the maize egg apparatus (Fig. 1, B and C) before fertilization. Lower RNA levels were detected in zygotes after in vitro fertilization and at an even lower level in two-celled proembryos. Expression of *ZmEA1* was no longer detectable at later embryo stages, which suggests a rapid down-regulation of the gene after fertilization. In situ hybridization of the maize ovary (Fig. 2B) and of female gametophyte isolated cells confirmed the restricted expression in the egg apparatus, which lacked detectable signals in the central cell, antipodals, and nucellar and integumental cells. Out of 988 ESTs generated from the originating cDNA library, 32 *ZmEA1* cDNA clones were identified, which suggests a high level of expression in mature egg cells. Further studies showed that *ZmEA1* is an intronless single gene in maize but may represent a member of a relatively heterologous gene family based on weak genomic Southern hybridization signals. Homologous sequences are also present as single genes in barley, pearl millet, and *Tripsacum dactyloides*. Interestingly, two

closely physically linked (4-kb) homologs appear to be present in rice [*Oryza sativa* *EA-like 1* (*OsEAL1*), BAC83883.1, and *OsEAL2*, BAC83885.1 (Fig. 1A)], as shown by genomic Southern and database analyses. No obvious homologs were identified in *Arabidopsis thaliana* or other dicotyledonous plant species, which suggests a possible Gramineae specific conservation of *EAL*-like genes.

The *ZmEA1* promoter (*ZmEA1p*) was isolated as 1570 base pairs of genomic sequence 5' of the AUG initiation codon and used for transgenic analyses of promoter and protein functions in the deeply embedded female gametophyte of maize (Fig. 2A). The promoter was fused to the β -glucuronidase (*Gus*) reporter gene. *GUS* activity in three of four independent functional *ZmEA1p::GUS* transgenic lines was exclusively detected in the egg apparatus of unpollinated mature ovules, confirming the egg apparatus specificity of the *ZmEA1p* transcriptional regulation (Fig. 2D). Unfertilized ovules from a transgenic maize line expressing *GUS* under control of a rice actin promoter (*OsActP::GUS*) were used to show that staining in all cells of the female gametophyte could be detected (Fig. 2E). A *ZmEA1:GFP* C-terminal fusion protein regulated by the *ZmEA1p* was secreted from the egg apparatus to the micropylar region of the nucellus of four independent transgenic lines in a manner dependent on floral developmental stage. After silk emergence, the *ZmEA1:GFP* first accumulated in the filiform apparatus (egg apparatus cell walls) (Fig. 3, A and B). After silk elongation (>10 cm), *GFP* signal was extended to a restricted area of the nucellus of unfertilized ovules (Fig. 3, C to F). The increase of *GFP* signal was well correlated with maturation of the egg apparatus during the female receptive period (9). Confocal laser scanning microscopy (CLSM) observations confirmed the presence of cell wall-localized *GFP* signals spreading from the egg apparatus toward the surface of the nucellus at the micropylar opening of the ovule (Fig. 3, E and F). This suggests possible proteolysis of the conserved C-terminal region from the predicted *ZmEA1* transmembrane domain to allow secretion and transport of

a mature protein to its target tissues. GFP fluorescence was not detectable at the surface of the inner integument (Fig. 3F) and was drastically reduced 24 hours after in vitro pollination. This rapid loss of GFP signal suggests proteolysis as a regulatory pathway to degrade ZmEA1 protein after fertilization.

We performed functional analyses of *ZmEA1* loss of activity using the highly expressing maize ubiquitin promoter via maize transgenic RNA interference (RNAi) and antisense (AS) lines A188 (R and AS lines, respectively) or hybrid A188 × H99 (Rh and AS lines, respectively). We gen-

erated 11 independent R/Rh and 5 ASH transgenic lines, and all contained multiple and complete transgene insertions (≥ 2 to >10) in multiple loci (most lines), with the exception of 4 R/Rh lines that had incomplete transgene integrations. Transgenic lines were selfed or crossed with wild-type pollen and used as pollen donor to fertilize wild-type (A188) plants (Fig. 4A). Half of the transgenic lines with complete transgene insertions (6 out of 12) showed a reduced seed set (0 to 75%) upon selfing. The four nonfunctional transgenic lines displayed a seed set comparable to wild type (95 to 100%). Clonal transgenic lines (lines with identical transgene integration pattern) displayed very similar seed set. All wild-type plants crossed with transgenic pollen displayed full seed set (Fig. 4A), which suggests that the male gametophyte was not affected by the lower *ZmEA1* activities. Although there was little variation between plants with the same integration pattern, the strong variation among independent lines is probably due to the segregation of the multiple transgenes in multiple chromosomal loci. We also assume that some integrations do not completely remove *ZmEA1* activity. Because transgenic female reproductive structures were not different from wild type, we used a transgenic pollen tube expressing GUS line (10) to visualize the fertilization process to identify the cause of transgenic female sterility. In wild-type lines, many pollen tubes reached the surface of the inner integument and continued growth toward the micropylar region (Fig. 4B), and only one pollen tube turned abruptly at the micropyle to fertilize the embryo sac (Fig. 4C). GUS staining was visible in 82% of wild-type female gametophytes 24 to 30 hours after in vitro pollination (Fig. 4F). In the two selfed transgenic lines analyzed (Rh6.1 and Rh15), pollen tubes were visible on the inner integument surface and grew close to the

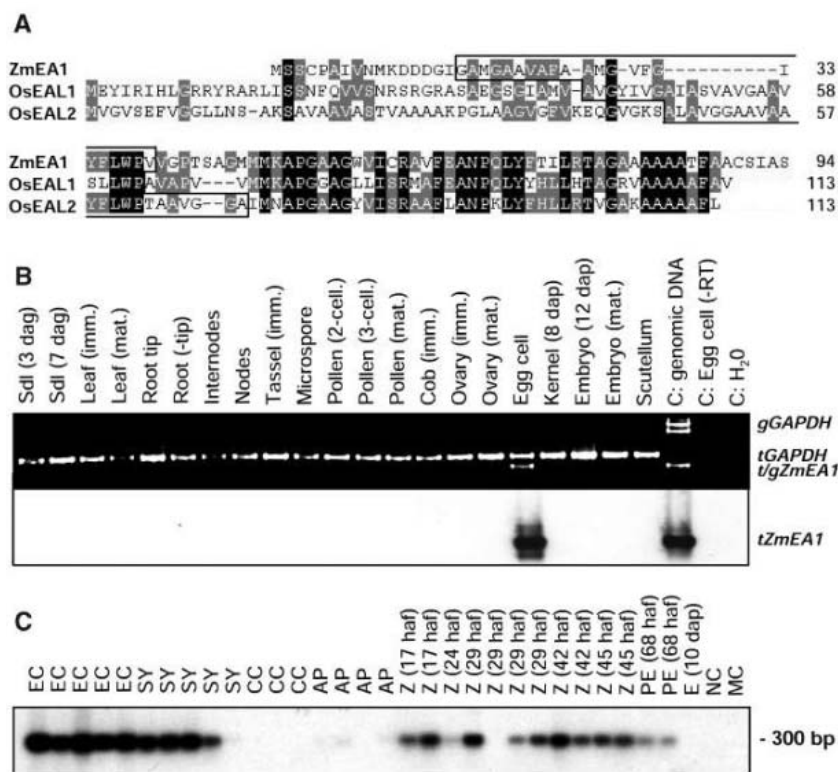
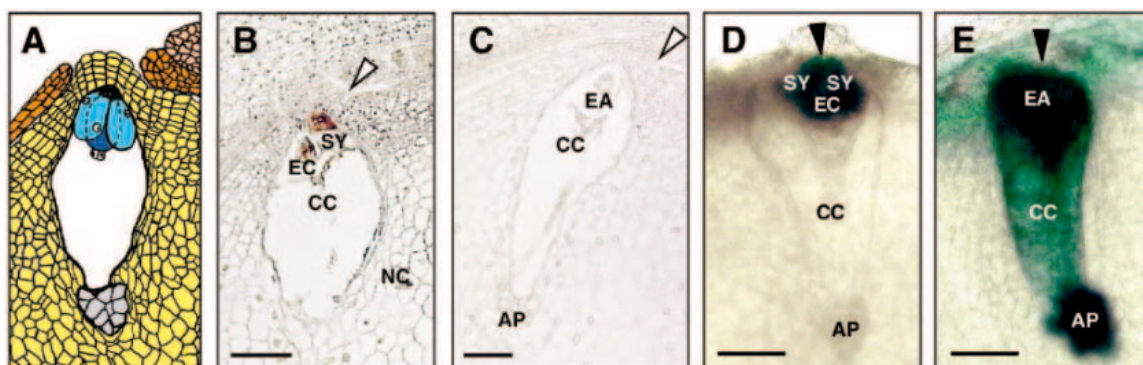


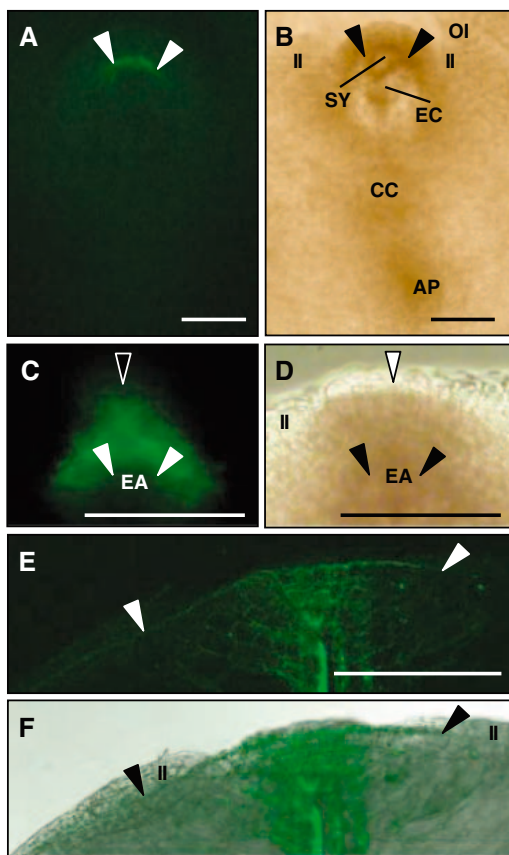
Fig. 1. *ZmEA1* gene expression and protein structure. (A) The *ZmEA1* predicted 94–amino acid protein shares C-terminal identity (shaded) and transmembrane domains (boxed) with two predicted rice proteins (*OsEAL1/2*). (B) Multiplex RT-PCR with different tissues showed *ZmEA1* expression exclusively in the egg cell. *GAPDH* mRNA is present in all tissues. (C) RT-PCR analyses of *ZmEA1* expression in maize cells and tissues. *ZmEA1* is expressed in egg cells (EC) and synergids (SY) but not in other cells of the embryo sac (CC, central cell; AP, antipodals). *ZmEA1* expression is down-regulated in in vitro zygotes (Z), and transcript amounts are even less in the two-celled proembryo (PE). *ZmEA1* mRNA was not detected in nucellus cells (NC), at later embryo stages (E), or in leaf mesophyll cells (MC). Dag, days after germination; dap, days after pollination; haf, hours after in vitro fertilization; imm., immature; mat., mature; sdl, seedling.

Fig. 2. Maize egg apparatus specificity of *ZmEA1* mRNA and promoter. (A) Schematic representation of a maize female gametophyte enclosed by the maternal tissues of the ovule. Ovary tissues are removed. Outer and inner integument are pink and orange, respectively, nucellus is yellow, and the haploid female gametophyte consists of two synergids (light blue), egg cell (blue), central cell (white), and antipodals (grey). In situ hybridization of longitudinal sections of the embryo sac were hybridized by using a *ZmEA1* antisense probe (B) and a sense probe (C), respectively. Red-purple signals show the localization of the transcript in cytoplasm of the egg cell and more profoundly in a synergid. (D) Unfertilized transgenic *ZmEA1::GUS* maize lines displayed GUS activity only in the egg apparatus.



Integuments were removed. (E) Unfertilized transgenic *OsACTp::GUS* maize line displayed GUS activity in all cells of the female gametophyte. AP, antipodals; EA, egg apparatus; EC, egg cell; CC, central cell; NC, nucellus; SY, synergids. Open arrowheads mark the surface of the micropyle, and closed arrowheads show the five to six layers of nucellar cell files of the micropyle. Scale bars, 100 μ m.

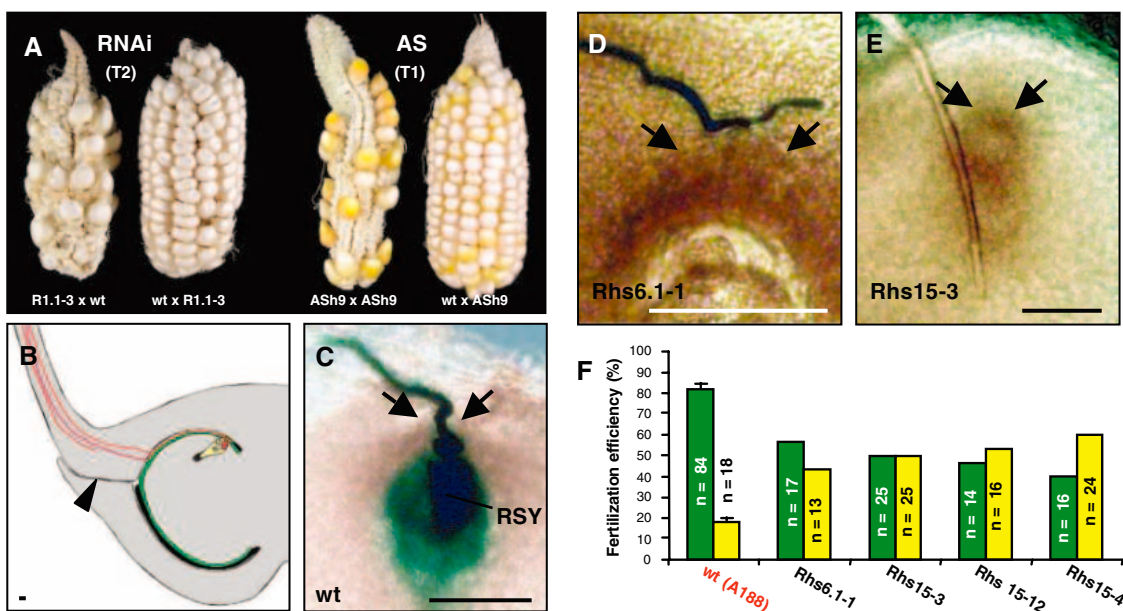
Fig. 3. Ovular localization of ZmEA1:GFP fusion protein by using epifluorescence microscopy (A and C), CLSM (E and F), and light microscopy (B and D). (A and B) GFP fluorescence is visible in the synergid cell walls (arrowheads) and filiform apparatus with faint signals within the overlying nucellus cells below the micropyle of a young ovule (silks <5 cm). (C and D). A stronger fluorescence was observed at the micropylar region of older ovules between synergid cell walls (closed arrowheads) and the surface of the nucellus cells at the micropylar opening (open arrowheads) of a mature ovule (silks >10 cm). (E and F) Fluorescence is visible within the cell walls and the surface of the six nucellus cell layers at the micropyle but not at the surface of the inner integument. Arrowheads mark the surface of the nucellus cells underlying the inner integument. AP, antipodals; EA, egg apparatus; EC, egg cell; CC, central cell; II, inner integument; OI, outer integument; SY, synergids. Scale bars, 100 μ m.



micropylar opening of the ovule (Fig. 4D), but instead of penetrating the nucellus, continued growth at random directions at the surface of the inner integument (Fig. 4E). Only 40 to 55% of the analyzed ovules of these RNAi lines showed blue staining within the female gametophyte. Such loss of pollen tube guidance was never observed in wild-type ovules and thus links transgenic expression with loss of pollen tube guidance.

All above data support a major role for ZmEA1 as a signaling molecule in maize short-range pollen tube guidance. These include transcription and protein production specific to the egg apparatus, secretion and transport to the micropylar opening of the ovule, rapid transcriptional down-regulation, and protein degradation after fertilization, as well as female sterility observed when the activity of the protein is reduced. We also found that ZmEA1:GFP was restricted only to the micropylar region, which suggests also some degradation or negative regulation of the transport in the surrounding integuments and the adjacent nucellus cells. However, even if ZmEA1 has many of the characteristics for a candidate signal, it is still unclear whether ZmEA1 represents a molecule that is directly sensed by receptors of the pollen tube tip or whether ZmEA1 stimulates secretion of pollen tube guidance signals by

Fig. 4. Loss of close-range pollen tube guidance in maize transgenic lines with reduced *ZmEA1* activity. (A) Left, seed set of the transgenic line R1.1-3 (T₂) that was propagated via pollen of the R1.1 line (T₀) to a wild-type (wt) cob is shown after self-pollination. Pollen of this line was also used as donor to fertilize the wild-type cob shown at the right. Seed set of a self-pollinated ASH9 (T₀) and out-crossed wild-type cob with pollen of this line is shown at the right. Segregation of the transgene affects female but not male fertility. (B) Schematic representation of pollen tube growth in maize. Each ovary encloses a single bitegmic ovule. In maize, the outer integument (black) is reduced compared with the inner integument (green), which itself encloses most of the nucellus except in the vicinity of the female gametophyte (yellow). This region corresponds to the micropyle. Multiple pollen tubes (red) grow through the transmitting tissues of the silk to the inner integument, but only one pollen tube penetrates the micropyle and releases sperm cells in the receptive synergid. Arrow head points toward the stylar channel. (C to E) Transgenic *OsACTp::GUS* maize pollen was used to monitor pollen tube growth and sperm discharge 24 to 30 hours after in vitro pollination in ovules of RNAi plants. (C) Direction of pollen tube growth is abruptly changed at the micropyle of a wild-type ovule where the tube penetrates the cell walls of nucellus cells and releases its contents into the receptive synergid. (D and E) Pollen tubes within



around 50% ovaries of transgenic lines (examples show lines Rhs6.1-1 and Rhs15-3) grew at the surface of the inner integument without entering the micropyle, instead continuing growth at random directions. This phenotype was never observed in wild-type ovules. (F) Summary of female gametophyte fertilization in wild-type and transgenic ovules. In wild-type, 82% of the embryo sacs were fertilized 24 to 30 hours after in vitro pollination. GUS staining and thus fertilization of embryo sacs from R lines investigated was reduced to 40 to 55%. n gives the number of excised ovules, showing the indicated phenotype; green color, fertilized female gametophyte; and yellow color, unfertilized female gametophyte. RSY, receptive synergid. Arrows mark the micropylar opening of the ovule. Scale bars, 100 μ m.

around 50% ovaries of transgenic lines (examples show lines Rhs6.1-1 and Rhs15-3) grew at the surface of the inner integument without entering the micropyle, instead continuing growth at random directions. This phenotype was never observed in wild-type ovules. (F) Summary of female gametophyte fertilization in wild-type and transgenic ovules. In wild-type, 82% of the embryo sacs were fertilized 24 to 30 hours after in vitro pollination. GUS staining and thus fertilization of embryo sacs from R lines investigated was reduced to 40 to 55%. n gives the number of excised ovules, showing the indicated phenotype; green color, fertilized female gametophyte; and yellow color, unfertilized female gametophyte. RSY, receptive synergid. Arrows mark the micropylar opening of the ovule. Scale bars, 100 μ m.

the nucellus cells. We are currently trying to identify the mature ZmEAL protein, which will then be used to study *in vitro* pollen tube guidance in maize. Nevertheless, our results bring potentially new insights into the fertilization process. It had been suggested in 1918 (11) that the filiform apparatus is required for pollen tube attraction, and in 1964, the existence of chemotropic substances, which are produced by the synergids, was postulated (12). Also, numerous secretory vesicles have been observed at the micropylar region of maize synergids but not the egg cell (13). Loss of pollen tube guidance via synergid ablation was recently substantiated in *Torenia fournieri* (7). Our data suggest that, at least in maize, not only the synergids but the whole egg apparatus could be involved in micropylar pollen tube guidance. Whether the egg cell is also involved in synthesizing a ZmEAL precursor that is transported toward the synergids via the endoplasmic reticulum or whether the egg cell is capable of ZmEAL secretion itself is a matter of further experimentation. Rapid down-regulation of the pollen tube guidance signal(s) is a major prerequisite to preventing polyspermy, and fertilization is first sensed by the synergids and egg cell, features of *ZmEAL* gene activity and protein.

The occurrence of *ZmEAL*-related genes in cereals, but not in dicotyledonous species, might be one explanation; wide crosses involving successful pollen tube guidance and fertilization are possible within genera of the Gramineae but not between species spanning wider taxonomic boundaries (14). In *Torenia fournieri*, pollen tubes of related species do not respond to the synergids attraction signal, which suggests species-specific short-range attractants (2). A similar observation was made conducting interspecific crosses using *Arabidopsis* and other Brassicaceae where pollen tubes grew normally through the transmitting tissue but rarely arrived at the funiculus and did not enter the micropyle (15). Sequence identity between ZmEAL from two maize inbred lines (A188 and H99) is 91.5% (16) and less than 45 and 43% between the maize and the two rice homologs (Fig. 1A). The low homology between EAL proteins provides further support that specific short-range guidance signals may be involved in the species-barrier concept. The identification of further molecules involved in female gametophyte pollen tube guidance in maize and other plant species should not only help understanding of many outstanding issues in plant reproductive biology but may also be used for future plant breeding to overcome some of the current crossing barriers and to allow hybridization between plant genera that cannot be crossed today.

References and Notes

1. K. Weterings, S. D. Russell, *Plant Cell* **16**, S107 (2004).
2. T. Higashiyama, H. Kuroiwa, T. Kuroiwa, *Curr. Opin. Plant Biol.* **6**, 36 (2003).
3. R. Palanivelu, L. Brass, A. F. Edlund, D. Preuss, *Cell* **114**, 47 (2003).
4. H. M. Wu, E. Wong, J. Ogdahl, A. Y. Cheung, *Plant J.* **22**, 165 (2000).
5. S. Kim *et al.*, *Proc. Natl. Acad. Sci. U.S.A.* **100**, 16125 (2003).
6. A. M. Sanchez *et al.*, *Plant Cell* **16**, S98 (2004).
7. T. Higashiyama *et al.*, *Science* **293**, 1480 (2001).
8. T. Dresselhaus, H. Lörz, E. Kranz, *Plant J.* **5**, 605 (1994).
9. R. Mól, K. Idzikowska, C. Dumas, E. Matthys-Rochon, *Planta* **210**, 749 (2000).
10. R. Brettschneider, D. Becker, H. Lörz, *Theor. Appl. Genet.* **94**, 737 (1997).
11. M. Ishikawa, *Ann. Bot. (London)* **32**, 279 (1918).
12. J. E. van der Pluijm, in *Pollen Physiology and Fertilization*, H. F. Linskens, Ed. (North Holland, Amsterdam, 1964), pp. 8–16.
13. A. G. Diboll, *Am. J. Bot.* **55**, 797 (1968).
14. H. C. Sharma, *Euphytica* **82**, 43 (1995).
15. K. K. Shimizu, K. Okada, *Development* **127**, 4511 (2000).

16. M. L. Márton, S. Cordts, J. Broadbent, T. Dresselhaus, unpublished observations.
17. We thank S. Sprunck for providing cDNA from maize zygotes and R. Brettschneider for the maize *OsACTp::GUS* line. J. Bantin, E. Kranz, S. Scholten, and P. von Wiesen are acknowledged for providing cells of the female gametophyte, *in vitro* zygotes, and proembryos for single-cell RT-PCR analyses. We are grateful to L. Viau for EST clustering and R. Reimer for support with the CLSM. The nucleotide sequence data reported is available in the European Molecular Biology Laboratory, GenBank, and DNA Databank of Japan Nucleotide Sequence Databases under the accession no. AY733074 (*ZmEAL* gene).

Supporting Online Material

www.sciencemag.org/cgi/content/full/307/5709/573/DC1
 Materials and Methods
 Figs. S1 to S5
 Table S1
 References and Notes

7 September 2004; accepted 19 November 2004
 10.1126/science.1104954

A Brief History of Seed Size

Angela T. Moles,^{1,2*} David D. Ackerly,^{3†} Campbell O. Webb,⁴
 John C. Tweddle,^{5,6} John B. Dickie,⁶ Mark Westoby²

Improved phylogenies and the accumulation of broad comparative data sets have opened the way for phylogenetic analyses to trace trait evolution in major groups of organisms. We arrayed seed mass data for 12,987 species on the seed plant phylogeny and show the history of seed size from the emergence of the angiosperms through to the present day. The largest single contributor to the present-day spread of seed mass was the divergence between angiosperms and gymnosperms, whereas the widest divergence was between Celastraceae and Parnassiaceae. Wide divergences in seed size were more often associated with divergences in growth form than with divergences in dispersal syndrome or latitude. Cross-species studies and evolutionary theory are consistent with this evidence that growth form and seed size evolve in a coordinated manner.

Seed mass affects many aspects of plant ecology. Small-seeded species are able to produce more seeds for a given amount of energy than are large-seeded species (1, 2), whereas large-seeded species have seedlings that are better able to tolerate many of the stresses encountered during seedling establishment (3). Seed mass is also correlated with the environmental conditions under which species establish (4–6) and with traits such as plant size, dispersal syndrome, plant life-span, and the ability to form a persistent

seed bank (7–13). Present-day species have seed masses ranging over 11.5 orders of magnitude, from the dust-like seeds of orchids (some of which weigh just 0.0001 mg) to the 20-kg seeds of the double coconut (Fig. 1A). Improving our knowledge of the changes in seed mass that occurred as the angiosperms radiated out of the tropics, colonized a wide range of habitats, developed a range of growth forms and dispersal strategies, and became the most abundant and diverse group of plants on earth (14–18) will greatly enhance our understanding of the ecological history of plants.

Using newly developed software (19, 20), we integrated a large seed mass data set with current best opinion for the phylogeny of seed plants. Our seed mass data set included 12,669 angiosperms and 318 gymnosperms. This is ~5% of all extant angiosperm and 38% of all extant gymnosperm species. The angiosperm species are from 3158 genera (22% of the global total) and 260 families (57%) and include representatives from all extant orders. The gymnosperm species are from 52 genera (63%) and 10 families (63%) (21).

¹National Center for Ecological Analysis and Synthesis, 735 State Street, Santa Barbara, CA 93101–5304, USA. ²Department of Biological Sciences, Macquarie University, Sydney, NSW 2109, Australia. ³Department of Biological Sciences, Stanford University, Stanford, CA 94305–5020, USA. ⁴Department of Ecology and Evolutionary Biology, Yale University, New Haven, CT 06520–8106, USA. ⁵The Natural History Museum, Cromwell Road, London, SW7 5BD, UK. ⁶Royal Botanic Gardens (RBG), Kew, Wakehurst Place, Ardingly, West Sussex, RH17 6TN, UK.

*To whom correspondence should be addressed. E-mail: amoles@bio.mq.edu.au

†Present address: Department of Integrative Biology, University of California, Berkeley, CA 94720, USA.

The resulting phylogeny has 2223 nodes (uncertain regions of the phylogeny were represented by polytomies), which we analyzed for divergences in seed size. The dense coverage of this data set allows us to locate and quantify the major divergences in seed mass.

We identified the largest divergence events and those that contributed most to the spread of seed mass across present-day species by using two indicators, width and contribution:

(1) Divergence width is a measure of the absolute size of divergences. Width was calculated as the standard deviation of \log_{10} seed mass across the clades immediately descended from the focal node. We used standard deviation instead of the absolute difference in seed mass between daughter clades (i.e., phylogenetic independent contrasts), because the former can be applied to polytomies. The 20 widest divergences are listed in Table 1 and table S1. Frequency distributions of divergence size across all divergences and across dichotomous divergences are shown in Fig. 1, B and C.

(2) Contribution is a measure of how much a divergence contributed to the variation in \log_{10} seed mass across all present-day species in the data set. Contribution takes into account the number of descendant species, the spread of seed mass among those species, and the width of the divergence in question and is analogous to a partitioning of sums of squares in an analysis of variance (22). The 20 largest contributions are listed in Table 1 and table S2.

Our analysis considers divergences rather than historical trait values of given nodes. Historical values cannot be accurately estimated from extant species, because descendant branches might have undergone parallel directional evolution and because unknown extinct branches may have had different trait values compared to surviving branches. Thus, we are highlighting major radiations in seed mass, not parts of the tree where there have been absolute changes in seed mass. Seed masses presented here are cross-species geometric means based on our sample of extant taxa in a clade. Calculations of divergence width and contribution size are based on estimated values at internal nodes using an iterative phylogenetic algorithm (22). However, we have been careful not to interpret these values as ancestral states.

Dates are presented to indicate the sequence and relative timing of major evolutionary events. Ages of major nodes were taken from the literature. These ages are derived from molecular data, calibrated on a single point in the fossil record. The ages of remaining nodes were calculated by interpolation from these “known” dates (22).

The divergence between angiosperms and gymnosperms is the most important, yet least well resolved, divergence in the tree. Molec-

ular evidence generally supports the view that the extant gymnosperms are monophyletic (23, 24), but there is still some doubt about this (25). Under the monophyletic gymnosperm hypothesis, there is a 59-fold divergence in seed mass between angiosperms (small-seeded) and gymnosperms (large-seeded), ~325 million years ago (Ma) (26) (Fig. 2, node A). This is the 54th widest divergence in the data set and contributes six times more to present-day variation in seed mass than the next highest contributing divergence (contribution = 0.43) (Fig. 1D and table S2). The alternative hypothesis, supported by morphological traits but not by molecular evidence (24, 27), is that Gnetales are the sister group of angiosperms. Under this hypothesis, the downward shift in seed mass associated with the divergence of angiosperms from Gnetales would be ~16-fold. Despite the uncer-

tainty around this node, it is clear that the evolution of the angiosperms was associated with a major reduction in seed mass. The difference in seed mass between gymnosperms and angiosperms is also apparent in the fossil record. The earliest angiosperms have much smaller seeds (averaging ~1 mm³) than coeval gymnosperms (200 mm³) (17, 28, 29).

The lower costs of pollen capture, early abortion, and reduced gametophyte size associated with the angiosperm reproductive system might have allowed angiosperms to produce smaller seeds than was economically viable for gymnosperms (30). The ability of angiosperms to produce smaller seeds than gymnosperms is demonstrated in present-day species and in the fossil record. The smallest gymnosperm seeds in our data set (*Chamaecyparis pisifera*, 0.63 mg) are almost four orders of magnitude larger than the smallest angiosperm seeds (Fig. 1A), and

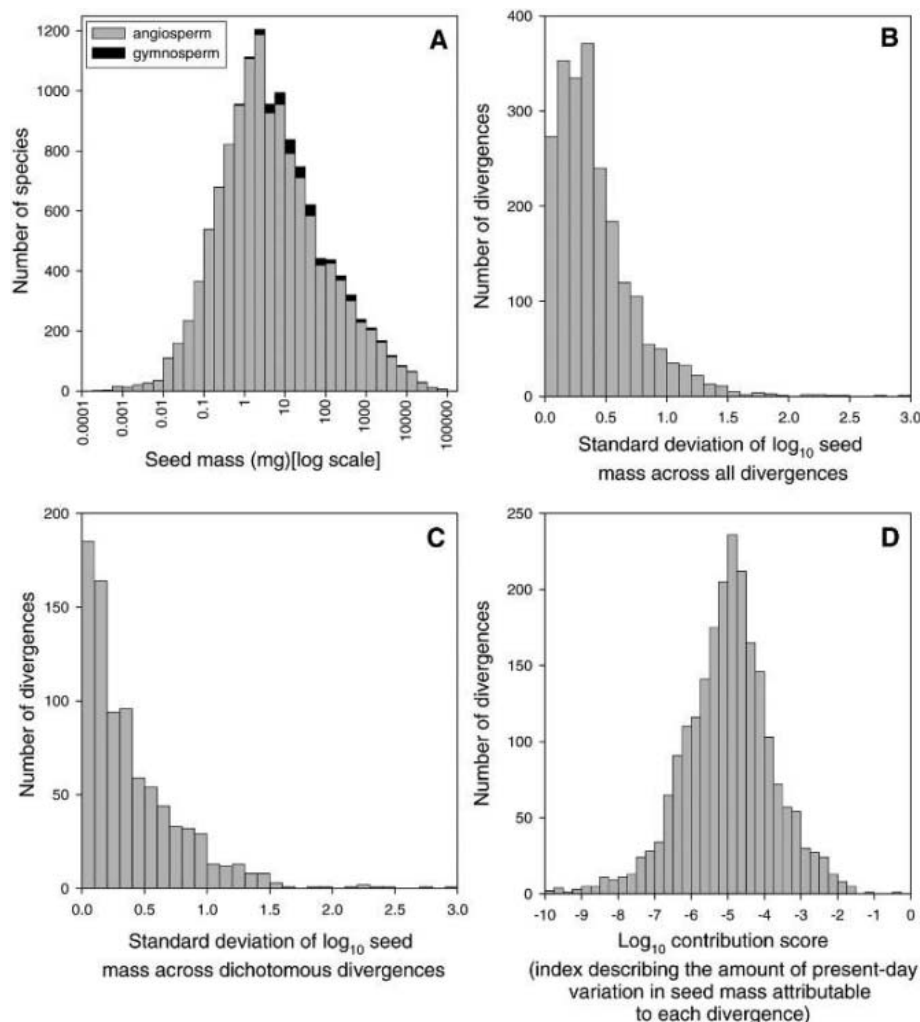


Fig. 1. Frequency distributions for seed mass, divergence size, and contribution scores. (A) Seed mass across 12,987 seed plant species. (B) Standard deviation of divergence in seed mass across all 2223 divergences. The low frequency of very small divergences results from the fact that the likelihood of all daughter nodes having the same value decreases steeply as the number of daughter nodes increases. (C) Standard deviation of divergence in seed mass across the 870 dichotomous divergences. (D) Contribution scores (22).

the smallest Cretaceous gymnosperm seeds are about two orders of magnitude larger than the smallest Cretaceous angiosperm seeds (28). The earliest divergences in the angiosperm lineage (estimated to have occurred 179 to 165 Ma) (14) were between clades with moderate-sized seeds, including *Amborella* (3.7 mg), Nymphaeaceae (water lilies, 5.9 mg), and Austrobaileyales (7.5 mg), and the remaining angiosperm clades.

Relationships among monocots, eudicots, and magnoliids are weakly resolved (31), but the sequence of these divergences does not substantially affect our results. An analysis with this node collapsed to a polytomy gave near-identical results to the analysis on the tree in Fig. 2 (nodes B and C).

Most monocots are herbaceous and have small-to-medium seeds (mean = 1.5 mg). However, the monocotyledon clade includes two notable divergences, associated with the

origin of orchids (Orchidaceae) and the origin of palms (Arecaceae) (Fig. 3A). These are the only divergences in the whole tree that rank in the top 20 both on absolute width and on their contribution to present-day variation in seed mass. The 435-fold divergence between palms and other commelinids was the second-greatest contributor to seed mass variation in the whole tree (contribution = 0.07). This divergence in seed mass was associated with a shift from herbaceous to arborescent growth forms. The massive shift in seed size associated with the divergence between “dust-seeded” orchids and the rest of the Asparagales [a clade including Iridaceae (irises), Alliaceae (onions), and Asparagaceae] was also associated with a single change in life history: the evolution of mycotrophic seedlings. Because germinating orchid seeds depend entirely on fungi for nutrition, orchids can make seeds with almost no

nutritive reserve. Seeds of most other taxa carry enough reserves to sustain a seedling until it can support itself through photosynthesis (32).

The magnoliids and Chloranthales span a wide variety of seed mass strategies (Magnoliales, 260 mg; Laurales, 470 mg; Canelales, 52 mg; Piperales, 0.64 mg; and Chloranthaceae, 1 mg), with no single divergence showing particular importance.

Most angiosperms are eudicots (Fig. 2). The earliest divergence in the eudicots separated Ranunculales (a clade including buttercups and poppies) from other eudicots. This divergence [estimated at 147 Ma (14)] was the ninth-

Table 1. The widest and most important divergences in seed mass. Clades involved in the 20 widest divergences in log₁₀ seed mass and the divergences that make the 20 largest contributions to present-day variation in seed mass. Details are given in tables S1 and S2 and in fig. S2. Semicolons separate the clades involved in the divergence of interest from their higher taxon.

Rank	Divergences
<i>Widest divergences</i>	
1	Celastraceae versus Parnassiaceae; Celastrales
2	<i>Corynocarpus</i> versus <i>Coriaria</i> ; Cucurbitales
3	Malpighiaceae versus Elatinaceae; Malpighiales
4	Rhizophoraceae mangroves versus terrestrial species
5	Connaraceae versus Oxalidaceae; Oxalidales
6	<i>Simmondsia chinensis</i> versus some other Caryophyllales
7	Dipterocarpaceae versus Cistaceae; Malvales
8	Polytomy across three <i>Bassia</i> spp.; Amaranthaceae
9	Clusiaceae versus Hypericaceae; Malpighiales
10	Arecaceae versus Poales, Commelinales, and Zingiberales
11	Orchidaceae versus other Asparagales
12	Polytomy in Proteaceae
13	Polytomy in Cornales
14	Polytomy in Clusiaceae
15	Polytomy in Calycanthaceae
16	Polytomy in Bambusoideae and Poaceae
17	Juglandaceae versus Casuarinaceae and Betulaceae
18	Polytomy in Ochnaceae
19	Combretaceae versus Lythraceae and Onagraceae; Myrtales
20	Polytomy in Lythraceae
<i>Divergences making the largest contribution</i>	
1	Angiosperms versus gymnosperms
2	Arecaceae versus Poales, Commelinales, and Zingiberales
3	Polytomy at base of Euasterid 1
4	Detarieae versus some other Fabaceae; Fabaceae
5	Polytomy in Ericales
6	Polytomy near the base of rosids
7	Saxifragales versus Vitaceae and rosids
8	Polytomy in Papilionoideae
9	Ranunculales versus other eudicots
10	Asparagales versus commelinids
11	Polytomy in Myrtaceae
12	Oleaceae versus the rest of Lamiales
13	Orchidaceae versus other Asparagales
14	Polytomy at the base of core eudicots
15	Polytomy in Lamiales
16	Polytomy in Brassicaceae
17	Euasterid 1 versus Euasterid 2
18	Polytomy in Rosaceae
19	Polytomy across Fabales, Rosales, Cucurbitales, and Fagales
20	Poales versus Commelinales and Zingiberales

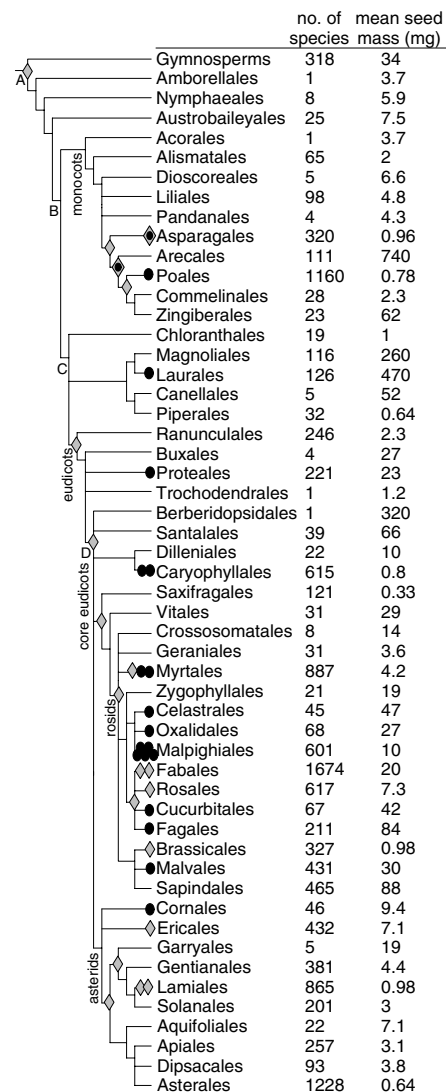


Fig. 2. Topology of the phylogenetic tree to order level, showing the location of the 20 widest divergences (black ellipses) and the 20 divergences making the largest contribution to present-day variation in seed mass (gray diamonds). Symbols at the branch tips represent changes within orders. The sample size and geometric mean seed mass presented for each order are for illustration only; all analyses were performed on species-level data. Some taxa have been omitted from this tree.

largest contributor to seed mass variation (contribution = 0.017). Ranunculales are predominantly herbaceous and have relatively small seeds (2.3 mg) compared to other eudicots.

There is uncertainty regarding the order and timing of the radiation at the base of the core eudicots, so it is represented in our tree by a five-way polytomy between Aextoxicaceae (320 mg), Dilleniaceae/Caryophyllales (0.86 mg), Saxifragales and the rosids (13 mg), Santalales (66 mg), and asterids (1.6 mg). Several of these clades became species-rich, and they range widely in seed mass, so the polytomy ranks as a high-contributing node (estimated at 129 Ma; contribution = 0.012) (Fig. 2, node D) (22). Soon after the core eudicots radiated, there was a divergence between the small-seeded, predominantly herbaceous Saxifragales (0.33 mg) and the larger-seeded rosids (14 mg) and Vitales (29 mg). This divergence was the seventh-greatest contributor to present-day variation in seed mass (contribution = 0.019).

Most present-day eudicots are rosids (represented by 5455 species in our data set) or asterids (3764 species). Wide divergences have been more frequent in the rosids (12 of the top 20) than in the asterids (one of the top 20). The greater dynamism in rosid seed-size evolution has been paralleled by their greater propensity to change growth form (33). Most of the wide divergences in the rosids were associated with a divergence

in growth form (e.g., Celastraceae versus Parnassiaceae, Connaraceae versus Oxalidaceae, Clusiaceae versus Hypericaceae, Malpighiaceae versus Elatinaceae) (Table 1 and table S1). Five of the 20 widest divergences were in Malpighiales. Seven of the 20 biggest-contributing divergences were within the rosids, including a divergence across the base of rosids; a divergence near the base of Fabaceae; a polytomy across Fabales, Rosales, Cucurbitales, and Fagales; and polytomies at the base of Papilionoideae (Fabaceae), Myrtaceae, Brassicaceae, and Rosaceae (Fig. 2 and table S2).

The asterids had 5 of the 20 biggest-contributing divergences in seed size, but only 1 of the 20 widest divergences. That is, divergences in seed mass within the asterids have given rise to a number of species-rich groups with a broad spread in seed size, though the absolute width of the divergences has not been exceptional. The widest divergence in the asterids was between Cornaceae (49 mg), Loasaceae/Hydrangeaceae (0.53 mg), and Nyssaceae (390 mg). The biggest-contributing divergences were the divergence at the base of Euasterid 1 (between Icacinaceae, Garryaceae, and the remainder of Euasterid 1; contribution = 0.026), the divergence between Oleaceae and the remainder of the Lamiales (0.014), the divergence between Euasterids 1 and 2 (0.010), a polytomy across eight families within the Lamiales (0.012),

and a polytomy near the base of the Ericales (0.020) (Fig. 2 and table S2).

Divergences in seed size appear to have been relatively consistent through time, both in terms of magnitude (fig. S1) and in the association between divergences in seed mass and divergences in explanatory variables such as growth form (table S1). That is, we have not found evidence that any particular event or period during geological history made an especially large contribution to the radiation of seed size. Our ability to ask whether radiations in traits are concentrated at particular times throughout history will increase as the precision and accuracy of divergence time estimates improves.

The widest divergence in the history of seed mass was a 13,650-fold divergence between Parnassiaceae, a small-seeded clade of temperate herbs, and Celastraceae, a large-seeded clade of tropical trees, shrubs, and lianes (Fig. 3B). The second widest divergence (6780-fold) was between *Coriaria* (Coriariaceae) and *Corynocarpus* (Corynocarpaceae) (Table 1, table S1, and fig. S2). This divergence was not associated with a divergence in dispersal syndrome (both are bird-dispersed) or with biogeographic shift (*Coriaria* has a slightly more poleward distribution than *Corynocarpus*, but their geographic ranges are mainly overlapping). However, it was associated with a shift in growth form and successional status: *Coriaria* tend to be shrubby, early successional species, whereas *Corynocarpus* tend to be later successional trees (34). The third widest divergence in seed mass (2760-fold) was between Malpighiaceae (a clade of large-seeded trees, shrubs, and lianes from tropical or warm climates) and *Elatine californica* (California waterwort, a small-seeded herb of damp habitats in California).

The three widest divergences in seed size were all associated with divergences in growth form. This was also the case for the 5th to 10th widest divergences [Connaraceae versus Oxalidaceae; Simmondsiaceae versus other Caryophyllales; Dipterocarpaceae versus Cistaceae; across *Bassia hyssopifolia*, *B. latifolia*, and *B. longifolia*; Clusiaceae versus Hypericaceae; and palms (Arecaceae) versus other commelinid monocots (Fig. 3A and table S1)]. Larger seed masses were associated with larger growth forms in 9 of the 11 dichotomous divergences in Table 1 (table S1). This association was also seen in notable changes in growth form, such as the divergence between *Pandanus* (large-seeded pachycaul trees and shrubs) and *Freycinetia* (small-seeded lianes; this was the 23rd widest divergence) and the divergence between Bambusoideae (bamboos) and the smaller Ehrhartoideae and Pooideae (grasses; this was the 122nd widest divergence). There were associations with other variables, but

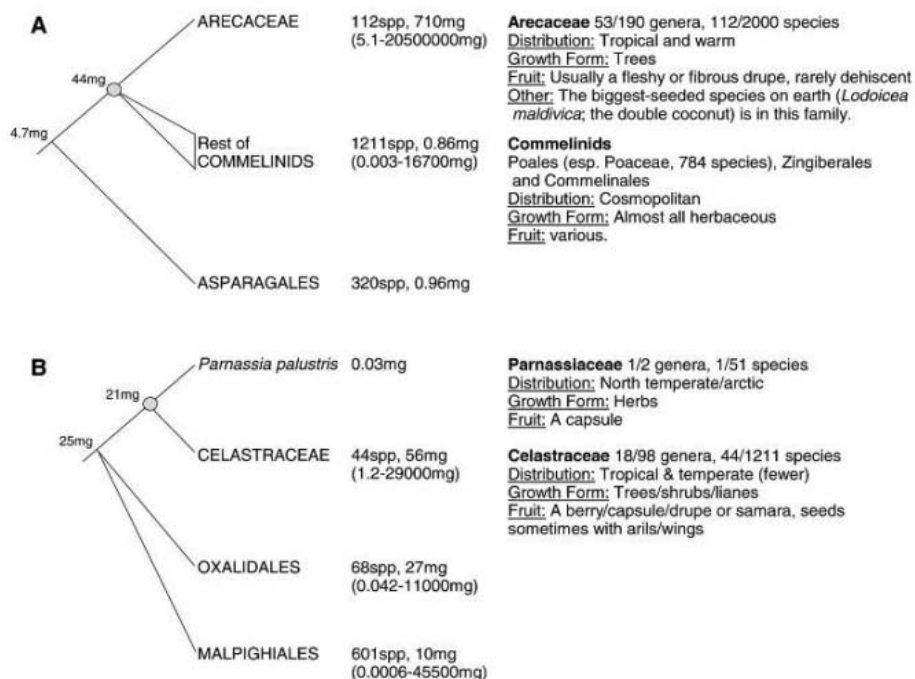


Fig. 3. Two important divergences in seed mass. (A) The divergence between palms and the remainder of the commelinid monocots. (B) The widest divergence in our tree. The text to the right shows the fraction of extant taxa in each group included in our data set and the distribution, growth form, and fruit morphology of each clade. Small numbers on interior nodes represent estimated internal means (22), and values given after clade names are geometric means taken across the tip nodes (species). Trees for the 20 widest divergences are given in fig. S2.

they were less consistent. Smaller seed mass was associated with more poleward distribution in 6 of the 11 dichotomous divergences and with a more tropical distribution in one clade. Larger seed mass was associated with biotic dispersal in 6 of the 11 dichotomous divergences and with abiotic dispersal in one divergence. An analysis across all of the divergences in the tree (based on independent contrasts) also showed that shifts in seed mass have been much more closely associated with shifts in growth form than with shifts in latitude or dispersal syndrome (35). Thus, our data are more consistent with Eriksson, Friis, and Lofgren's suggestion (29) that changes in seed mass during angiosperm evolution resulted primarily from changes in vegetation structure than with Tiffney's hypothesis (17) that changes in dispersal fauna (particularly the radiation of mammals across the Cretaceous-Tertiary boundary) allowed angiosperms to radiate into larger seed masses.

Two of the 11 top-ranking dichotomous divergences in seed mass were not associated with divergences in plant stature. One was the divergence between Juglandaceae and Casuarinaceae/Betulaceae, which was associated with a divergence between biotic and abiotic dispersal. The other was a divergence within Rhizophoraceae, between a small-seeded terrestrial habit and a large-seeded mangrove habit. A shift to a mangrove habit has generally been associated with increases in seed mass. The mangrove habit has evolved in seven families, five of them represented in our database. In four of these (Acanthaceae, Myrsinaceae, Meliaceae, and Rhizophoraceae, but not Combretaceae), mangroves have the largest seeds in the family.

The most consistent pattern we revealed was the association between changes in seed mass and changes in growth form. This result is in line with Charnov's life history theory for mammals (36). In Charnov's treatment, offspring size is coordinated with size at adulthood, because larger offspring offset the low survivorship to adulthood that would otherwise be a consequence of longer juvenile periods. This result is also consistent with cross-species studies showing that growth form is the strongest correlate of seed size (9, 10). A recent compilation of data for 2113 species from around the world (7) showed a highly significant positive relationship between seed mass and plant height ($R^2 = 0.35$). Of course, there is still great variation in seed mass for a given plant size. Some of this variation can be attributed to differences in dispersal syndrome, some to biogeography, and more variation is undoubtedly attributable to factors that we have not considered here.

The synthesis of robust phylogenies with global trait data sets holds great promise for elucidating the ecological and evolutionary

history of seed plants and of other major groups of organisms.

References and Notes

1. M. L. Henery, M. Westoby, *Oikos* **92**, 479 (2001).
2. L. W. Aarssen, C. Y. Jordan, *Ecoscience* **8**, 471 (2001).
3. M. R. Leishman, I. J. Wright, A. T. Moles, M. Westoby, in *Seeds: The Ecology of Regeneration in Plant Communities*, M. Fenner, Ed. (CAB International, Wallingford, UK, 2000), pp. 31–57.
4. E. Salisbury, *Proc. R. Soc. Lond. Ser. B* **186**, 83 (1974).
5. S. A. Foster, C. H. Janson, *Ecology* **66**, 773 (1985).
6. D. J. Metcalfe, P. J. Grubb, *Can. J. Bot.* **73**, 817 (1995).
7. A. T. Moles, D. S. Falster, M. R. Leishman, M. Westoby, *J. Ecol.* **92**, 384 (2004).
8. D. A. Levin, *Am. Nat.* **108**, 193 (1974).
9. M. R. Leishman, M. Westoby, *Am. Nat.* **143**, 890 (1994).
10. M. R. Leishman, M. Westoby, E. Jurado, *J. Ecol.* **83**, 517 (1995).
11. J. Lord *et al.*, *J. Biogeogr.* **24**, 205 (1997).
12. K. Thompson, S. R. Band, J. G. Hodgson, *Funct. Ecol.* **7**, 236 (1993).
13. D. S. Hammond, V. K. Brown, *Ecology* **76**, 2544 (1995).
14. N. Wikström, V. Savolainen, M. W. Chase, *Proc. R. Soc. Lond. Ser. B* **268**, 2211 (2001).
15. P. R. Crane, S. Lidgard, *Science* **246**, 675 (1989).
16. D. I. Axelrod, *Science* **130**, 203 (1959).
17. B. H. Tiffney, *Ann. Mo. Bot. Gard.* **71**, 551 (1984).
18. S. L. Wing, L. D. Boucher, *Annu. Rev. Earth Planet. Sci.* **26**, 379 (1998).
19. C. O. Webb, S. Kembel, D. D. Ackerly, *Phylocom*, available at www.phylodiversity.net/phylocom/ (2004).
20. C. O. Webb, M. J. Donoghue, *Mol. Ecol. Notes*, in press.
21. Percentages were calculated from the Vascular Plant Families and Genera database, available at www.rbkew.org.uk/data/vascplnt.html.
22. Materials and methods are available as supporting material on Science Online.
23. M. Schmidt, H. A. W. Schneider-Poetsch, *J. Mol. Evol.* **54**, 715 (2002).
24. J. G. Burleigh, S. Mathews, *Am. J. Bot.* **91**, 1599 (2004).

25. D. E. Soltis, P. S. Soltis, M. J. Zanis, *Am. J. Bot.* **89**, 1670 (2002).
26. W. S. Judd, C. S. Campbell, E. A. Kellogg, P. F. Stevens, M. J. Donoghue, *Plant Systematics: A Phylogenetic Approach* (Sinauer, Sunderland, MA, ed. 2, 2002).
27. M. J. Donoghue, J. A. Doyle, *Curr. Biol.* **10**, R106 (2000).
28. B. H. Tiffney, *Annu. Rev. Ecol. Syst.* **35**, 1 (2004).
29. O. Eriksson, E. M. Friis, P. Lofgren, *Am. Nat.* **156**, 47 (2000).
30. D. Haig, M. Westoby, *Evol. Ecol.* **5**, 231 (1991).
31. P. F. Stevens, Angiosperm Phylogeny Website, available at www.mobot.org/MOBOT/Research/APweb/.
32. J. A. Raven, *Funct. Ecol.* **13**, 5 (1999).
33. D. D. Ackerly, R. Nyffeler, *Evol. Ecol.* **18**, 249 (2004).
34. P. Wardle, *Vegetation of New Zealand* (Cambridge Univ. Press, Cambridge, 1991).
35. A. T. Moles *et al.*, in preparation.
36. E. L. Charnov, *Life History Invariants: Some Explorations of Symmetry in Evolutionary Ecology* (Oxford Univ. Press, Oxford, 1993).
37. We thank R. Condit, S. Diaz, P. Juniper, M. Leishman, J. Lord, M. Mayfield, B. Rice, K. Thompson, I. Wright, and S. J. Wright for access to unpublished data; R. Stevens and J. Alroy for helpful discussion; B. Tiffney and two anonymous referees for comments on the manuscript; R. Turner (RBG Kew) for checking the species list against the International Plant Names Index; and P. Stevens for APweb. Supported by the National Center for Ecological Analysis and Synthesis, the Australian Research Council (M.W.), and an NSF grant (D.D.A., C.O.W., and M. J. Donoghue). The Millennium Seed Bank Project is funded by the UK Millennium Commission, The Wellcome Trust, and Orange Plc. RBG Kew is partially funded by the UK Department of Environment, Food and Rural Affairs.

Supporting Online Material

www.sciencemag.org/cgi/content/full/307/5709/576/DC1

Materials and Methods

Figs. S1 and S2

Tables S1 to S3

References and Notes

3 September 2004; accepted 2 December 2004

10.1126/science.1104863

A Molecular Phylogeny for Bats Illuminates Biogeography and the Fossil Record

Emma C. Teeling,^{1,2*} Mark S. Springer,^{3*} Ole Madsen,⁴ Paul Bates,⁵ Stephen J. O'Brien,^{6*} William J. Murphy^{1,7}

Bats make up more than 20% of extant mammals, yet their evolutionary history is largely unknown because of a limited fossil record and conflicting or incomplete phylogenies. Here, we present a highly resolved molecular phylogeny for all extant bat families. Our results support the hypothesis that megabats are nested among four major microbat lineages, which originated in the early Eocene [52 to 50 million years ago (Mya)], coincident with a significant global rise in temperature, increase in plant diversity and abundance, and the zenith of Tertiary insect diversity. Our data suggest that bats originated in Laurasia, possibly in North America, and that three of the major microbat lineages are Laurasian in origin, whereas the fourth is Gondwanan. Combining principles of ghost lineage analysis with molecular divergence dates, we estimate that the bat fossil record underestimates (unrepresented basal branch length, UBBL) first occurrences by, on average, 73% and that the sum of missing fossil history is 61%.

Bats are a unique and enigmatic group of mammals that account for ~1,100 species (1). They are the only mammals to have achieved

true self-powered flight, are found throughout the globe, and play a major ecological role as pollinators and insect predators (2). Although

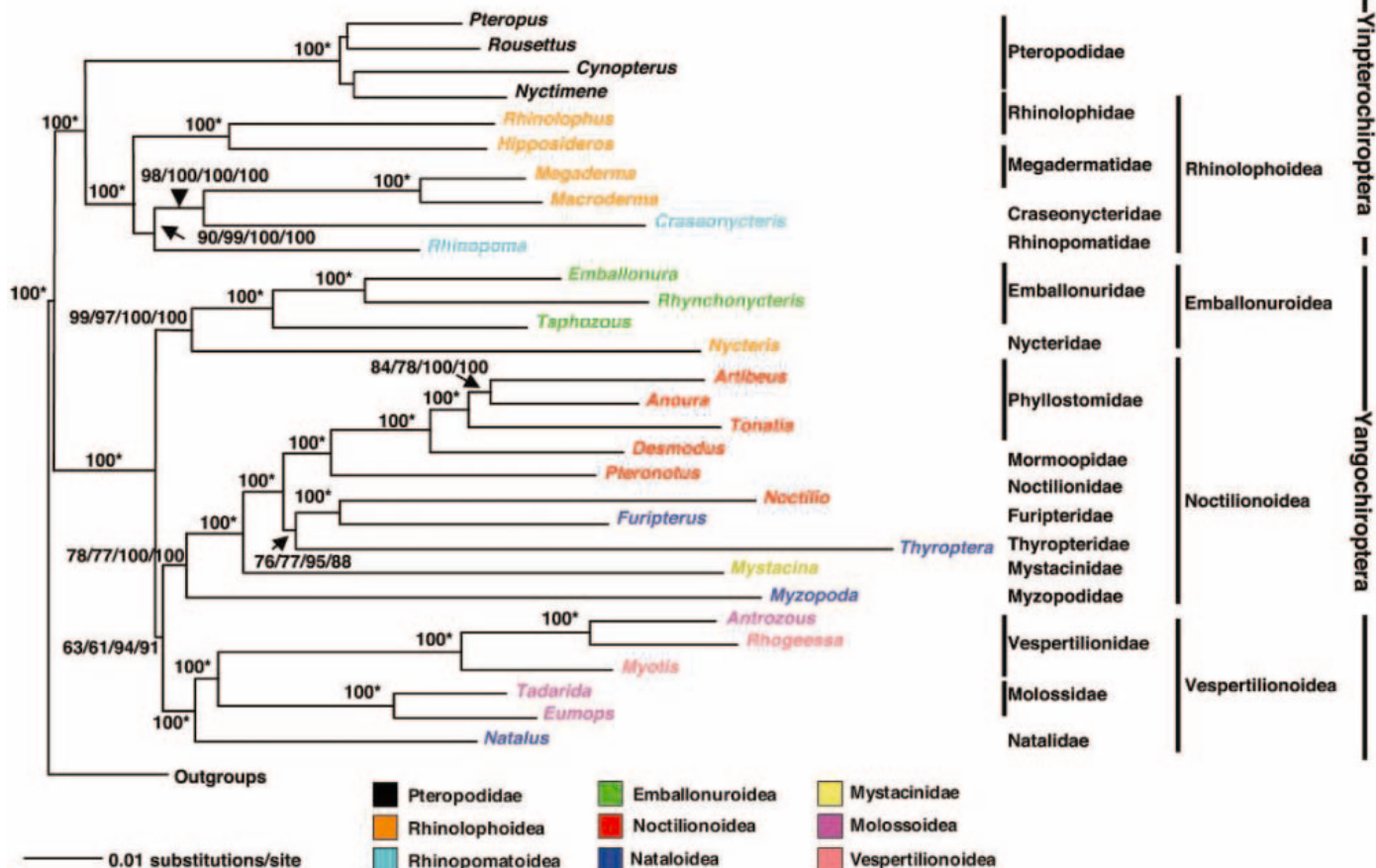


Fig. 1. The maximum likelihood tree ($-\ln$ likelihood = 92127.3772) for the concatenated data set under the GTR + Γ + I model of sequence evolution (17). Numbers at the nodes are the (ML unconstrained bootstrap values)/(ML constrained bootstrap values)/Bayesian (single-model posterior probabilities shown as percentages)/Bayesian (parti-

tioned model posterior probabilities shown as percentages). 100* signifies clades that received 100% bootstrap support in all analyses and had posterior probabilities of 1.000. The genera are color coded according to the superfamilial groups identified by the most recent morphological phylogenetic study (4).

bats originated in the early Eocene, it has been difficult to identify bat species from the fossil record, rendering the chronology of divergence events and biogeography of this order intractable from fossils alone (3). Furthermore, the evolutionary history of this order has been obscured by controversial phylogenetic hypotheses. Morphological data traditionally support the monophyly of the order and of the two suborders, Mega-

chiroptera (megabats) and Microchiroptera (microbats), implying a single origin of laryngeal echolocation and flight in bats (4). Molecular data support the monophyly of bats and thus a single origin of flight in mammals. However, molecules reveal a sister-taxon relationship between the rhinolophoid microbats and the megabats (Yinpterochiroptera), suggesting either multiple origins of laryngeal echolocation within bats or a single origin of echolocation with subsequent loss in megabats (5–10). There remains considerable uncertainty in both subordinal and superfamilial classifications within bats, where both morphological and molecular data conflict (4, 7, 10), and different molecular data sets provide varying support (8, 10).

To discriminate between the competing phylogenetic views, we analyzed 13.7 kb of nuclear sequence data from portions of 17 nuclear genes from representatives of all bat families and four laurasiatherian outgroups [30 bat genera, 4 outgroups; (11)]. Phylogenetic analyses with diverse methods resulted in a well-resolved phylogeny, dividing the order into two suborders and four super-

familial groups, rendering microbats paraphyletic (Fig. 1). Both the monophyly of the order Chiroptera and the two suborders Yinpterochiroptera (Rhinolophoidea + Pteropodidae) and Yangochiroptera received 100% bootstrap support (BSS) in all maximum likelihood (ML) analyses and had Bayesian posterior probabilities (BPP) of 1.000 (Fig. 1; table S1). Yangochiroptera is further supported by a 15-base pair (bp) deletion in *BRCA1* and a 7-bp deletion in *PLCB4*, which unites all members of Yangochiroptera, and is absent in all yinpterochiropteran and outgroup taxa (fig. S1). With the inclusion of representatives from all putative microbat families and the addition of 6.1 kb of sequence data from 13 novel nuclear genes, our results strongly support microbat paraphyly. Likewise, some of the superfamilial groupings suggested by previous molecular data are confirmed and extended by this new analysis, and many alternative hypotheses have been refuted (described in table S2).

These data provide a supported resolution for the phylogenetic placement of two enigmatic, monotypic families, Craseonycteridae and Myzopodidae (Fig. 1). *Craseonycteris*

*To whom correspondence should be addressed. E-mail: emma.teeling@ucd.ie; obrien@mail.ncicrf.gov; mark.springer@ucr.edu

thonglongai, the smallest mammal in the world, is confined to the Kanchanaburi province of western Thailand and southeast Myanmar (12, 13). Our results convincingly place Craseonycteridae within the superfamily Rhinolophoidea (100% BSS, 1.000 BPP) and provide robust support for a sister-group relationship with the megadermatids (100% ML BSS, 1.000 BPP). Further support for the inclusion of *Craseonycteris* within the Rhinolophoidea derives from the possession of pubic nipples, a unique and diagnostic rhinolophoid character (14). The phylogenetic position of the Myzopodidae (which consists of the single species *Myzopoda aurita*), endemic to Madagascar (1), is also controversial (4, 15). Our data support a basal position for the Myzopodidae within the superfamily Noctilionoidea (78% ML BBS, 1.000 BPP).

A time scale for the evolution of the order Chiroptera based on Bayesian dating analyses (11) is depicted in Fig. 2. We estimate that crown group bats last shared a common ancestor about 64 million years ago (Mya) at or following the Cretaceous-Tertiary boundary (fig. S2; table S3) (11). This date is also corroborated by a comprehensive eutherian study that primarily used non-chiropteran fossil calibration points (16). The four major microbat (echolocating)

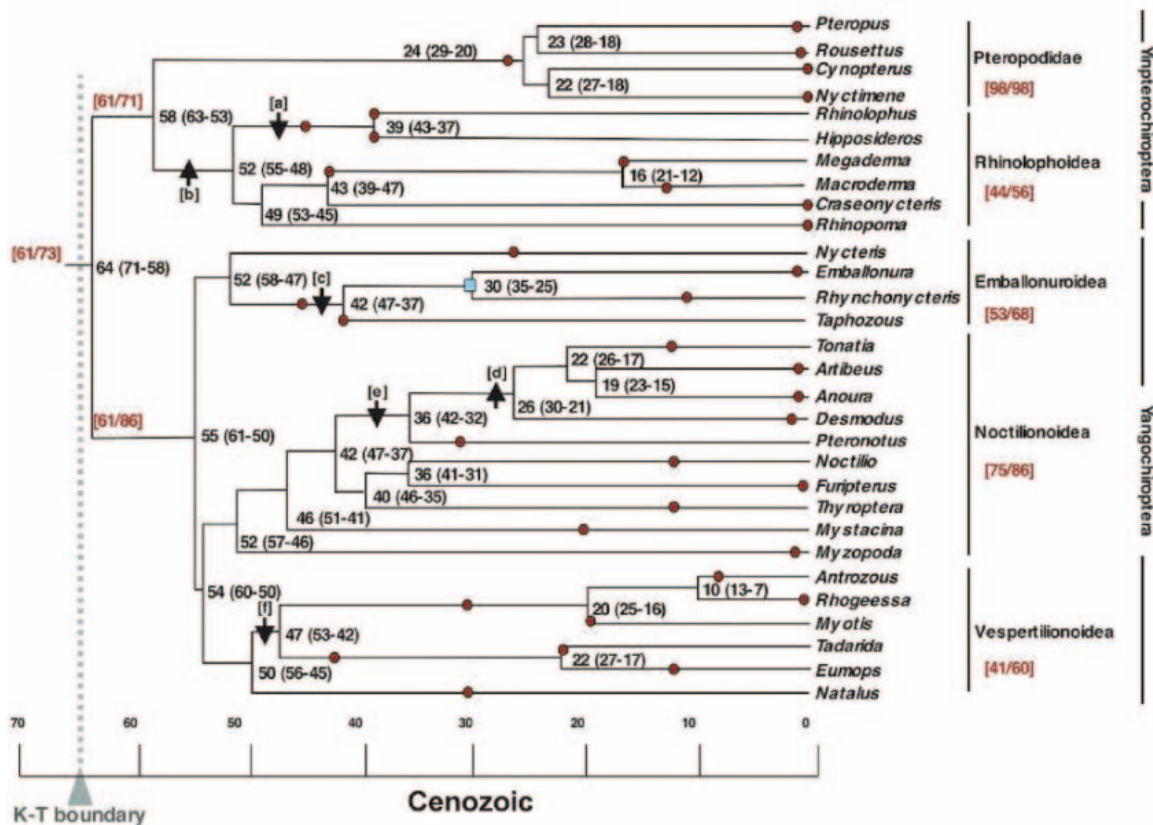
lineages [Rhinolophoidea, Emballonuroidea, Noctilionoidea, Vespertilionoidea] each originated within a narrow time frame, 52 to 50 Mya, coincident with an approximate 7° rise in mean annual temperature, a significant increase in plant diversity, and the peak of Tertiary insect diversity (17–19). We suggest that extant microbats diversified in response to an increase in prey diversity and that the varied microbat echolocation and flight strategies may have resulted from differential niche exploitation at that time.

Using this complete interfamilial phylogeny, we examined competing biogeographical hypotheses regarding the origin of bats. The oldest definitive bat fossils are early to middle Eocene, distributed in North America (*Icaronycteris*), Europe (*Hassianycteris*, *Archaeonycteris*, and *Paleochiropteryx*), and Australia (*Australonycteris*), and they were already specialized for flight and echolocation (4, 20–22). They overlapped in range with the modern extant microbat lineages, whose oldest fossil record is from the middle Eocene of Europe (4, 23, 24), and indeed appear to nest within crown group Chiroptera (25). We reanalyzed the morphological data set of Simmons and Geisler (4) for extant bat families and extinct Eocene fossils by incorporating the molecular scaffold from Fig. 1 in parsimony analyses

(Fig. 3) (11). The most parsimonious trees were used to map both current and past geographic distributions in a parsimony framework (Fig. 3) (11).

Geographic ancestral reconstructions (11) suggest that bats originated in the Laurasian land masses, possibly in North America during the early Paleocene, and fail to support a Gondwanan origin for bats, even with the inclusion of *Australonycteris* in the analyses (Fig. 3; table S4). A Southern Hemisphere origin of modern bats has been suggested [(26) and included references], but it is based mainly on current distribution of maximum bat diversity and has been confounded by unreliable phylogenies. Currently, bats are distributed throughout the globe, however, at each taxonomic level bat endemism is high (1). All ancestral reconstructions support an Asian origin for the suborder Yinpterochiroptera (Fig. 3; table S4). Since their diversification in the late Paleocene, yinpterochiropterans have had an exclusively Old World distribution (24). In contrast, the biogeographic history of Yangochiroptera is more difficult to decipher because of its panglobal distribution (1). Our results support a Laurasian, and most likely Asian/European, origin for Yangochiroptera (Fig. 3; table S4). Within this suborder, the emballonurids have an exclusively tropical

Fig. 2. Molecular time scale for the order Chiroptera based on the *divtime* analyses (11), using the ML topology depicted in Fig. 1, six fossil constraints, and a mean prior of 65 Mya for the base of the ingroup root. Numbers at the nodes are the molecular dates in millions of years; values in parentheses are the 95% credibility intervals. Letters along the branches refer to the fossil constraint age (Mya) imposed on that particular node: [a] = 37; [b] = 55; [c] = 37; [d] = 34; [e] = 30; [f] = 37. Maximum constraint is an arrow pointing up; minimum constraint is an arrow pointing down. Red circles indicate the age of the oldest fossil representing that lineage or “off-shoots” from that lineage (table S5). Red numbers in brackets to the left of the slash indicate the percentage sum missing of the fossil record for that clade, (total sum missing per lineage)/(sum age of lineage). Numbers in brackets in red to the right of the slash indicate the average percentage missing of that fossil record for



that clade or the average of the percentage missing per lineage (11) (table S5). A blue square indicates the time of separation between the New World *Rhynchonycteris* and the Old World *Emballonura*.

distribution on opposite sides of the Atlantic. The oldest fossils are middle Eocene in age from the Messel of Germany (21),

whereas the oldest New World fossils are Oligocene in age (3). Our molecular dates indicate that the split between African and

South American emballonurids (i.e., *Emballonura* versus *Rhynchonycteris*) occurred about 30 Mya (Fig. 2; fig. S2; table S3). The arrival of new world monkeys and caviomorph rodents into South America from Africa, possibly via a “vegetational raft” sailing from the Gabon to Brazil or “stepping stones” spanning the Atlantic, is also estimated to have occurred at least 31 to 25 Mya (27). We hypothesize that emballonurid bats also arrived to South America via this dispersal route and represent another mammalian lineage that made this journey.

Living noctilionoids have a disjunct distribution: phyllostomids, mormoopids, noctilionids, furpterids, and thyropterids are mainly confined to the Neotropics; mystacinids are found only in New Zealand; and myzopodids are restricted to Madagascar (1). Our ancestral reconstructions suggest that noctilionoids originated in Gondwana, perhaps in South America (Fig. 3; table S4). Their distribution and center of origin are similar to that of the flightless ratite birds (28). Molecular dating suggests that the ratites diversified as a result of vicariant speciation due to the break up of Gondwanaland (28), whereas our molecular dates estimate the origin of noctilionoids at 52 Mya (Fig. 2), too late to be explained by vicariance. At that time, dispersal was possible between the Gondwanan land masses of South America, Antarctica, and Australia. However, New Zealand, Africa, and Madagascar were already well separated (29).

Our molecular dates suggest that there are large gaps in the fossil record for most bat lineages (represented by 58 branches: 30 terminal branches, 28 internal branches; fig. S3), confirming the long held view that the bat fossil record is impoverished. By collating the oldest fossil for every branch on the tree and comparing it with the Bayesian estimated molecular divergence date for that branch, we calculated the unrepresented basal branch length (UBBL) for each lineage. Using this value, we quantified the fraction of each branch underestimated by the fossil record (11) (table S5). On average, the fossil record underestimates the origin of 58 bat lineages by 73% (Fig. 2). The four major microbat lineages are missing on average 56 to 86% of fossil history, with the Gondwanan clade (noctilionoids) missing the most (Fig. 2). Megabat lineages are missing a sum total of 98% of their fossil history (table S5). The terminal and internal branches are missing on average 58 and 88% of fossil history, respectively (table S5). With well over half of the Cenozoic history missing for microbat lineages and nearly all of the fossil history missing for megabat lineages, it is not surprising that Paleocene bat ancestors having transitional morphological adaptations for flight and echolocation have never been discovered.

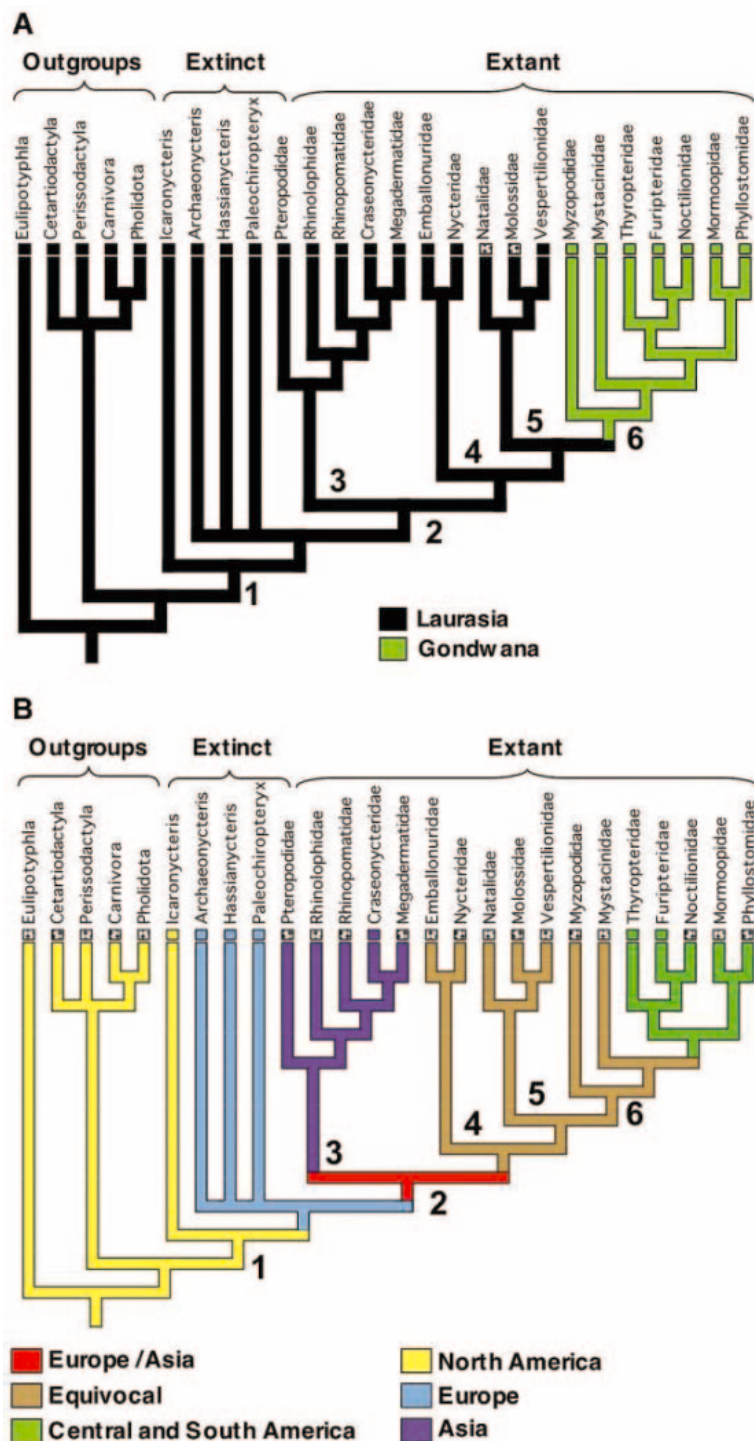


Fig. 3. Biogeographic reconstructions. The topology of the chiropteran taxa is the strict consensus topology of the six most parsimonious trees resulting from the reanalysis of the Simmons and Geisler (4) data set with the molecular constraint depicted in Fig. 1. The topology of the outgroup laurasiatherian orders is taken from Murphy *et al.* (30). All geographic characters depicted in table S7 were mapped onto each of the most parsimonious trees using accelerated and delayed transformations and the consensus results are shown as follows: (A) The earliest occurrences of each lineage in Laurasia or Gondwana, [polymorphic states indicated by a hatched box at tip of branch (11); table S4, table S7]. (B) Geographic distributions defined by nine character states (11) (table S4, table S7). Numbers at the branches identify the following clades: 1, Chiroptera; 2, Yangochiroptera; 3, Yinpterochiroptera; 4, Emballonuroidea; 5, Vespertilionoidea; and 6, Noctilionoidea. Results were considered equivocal if the delayed and accelerated transformations conflicted (table S4).

References and Notes

1. N. B. Simmons, in *Mammalian Species of the World: A Taxonomic and Geographic Reference*, D. E. Wilson, D. M. Reeder, Eds. (Johns Hopkins Univ. Press, Baltimore, in press).
2. B. D. Patterson, M. R. Willig, R. D. Stevens, in *Bat Ecology*, T. H. Kunz, M. B. Fenton, Eds. (Univ. of Chicago Press, Chicago, 2003), pp. 536–579.
3. N. J. Czaplewski, G. S. Morgan, S. A. McLeod, in *Evolution of Tertiary Mammals of North America*, vol. 2, *Marine Mammals and Smaller Terrestrial Mammals*, C. Janis, G. Gunnell, M. Uhen, Eds. (Cambridge Univ. Press, Cambridge, in press).
4. N. B. Simmons, J. H. Geisler, *Bull. Am. Mus. Nat. Hist.* **235**, 1–152 (9 March 1998).
5. J. M. Hutcheon, J. A. W. Kirsh, J. D. Pettigrew, *Philos. Trans. R. Soc. London Ser. B* **353**, 607 (1998).
6. E. C. Teeling et al., *Nature* **403**, 188 (2000).
7. E. C. Teeling et al., *Proc. Natl. Acad. Sci. U.S.A.* **99**, 1432 (2002).
8. E. C. Teeling, O. Madsen, W. J. Murphy, M. S. Springer, S. J. O'Brien, *Mol. Phylogenet. Evol.* **28**, 308 (2003).
9. R. J. Baker, J. L. Longmire, M. Maltbie, M. J. Hamilton, R. Van Den Bussche, *Syst. Biol.* **46**, 579 (1997).
10. R. A. Van Den Bussche, S. R. Hoofer, *J. Mammal.* **85**, 321 (2004).
11. Materials and methods are available as supporting material on Science Online and at the Web site of the Laboratory of Genomic Diversity, National Cancer Institute.
12. J. E. Hill, *Bull. Br. Mus. (Nat. Hist.)* **32**, 29 (1974).
13. P. J. J. Bates, T. Nwe, K. M. Swe, S. S. H. Bu, *Acta Chiropt.* **3**, 33 (2001).
14. N. B. Simmons, *Am. Mus. Novit.* **3077**, 1 (1993).
15. S. R. Hoofer, S. A. Reeder, E. W. Hansen, R. A. Van Den Bussche, *J. Mammal.* **84**, 809 (2003).
16. M. S. Springer, W. J. Murphy, E. Eizirik, S. J. O'Brien, *Proc. Natl. Acad. Sci. U.S.A.* **100**, 1056 (2003).
17. P. Wilf, C. C. Ladandera, *Science* **284**, 2153 (1999).
18. C. C. Labandera, J. Sepkoski, *Science* **261**, 310 (1993).
19. S. L. Wing, H. Sues, in *Mesozoic and Early Cenozoic Terrestrial Ecosystems in Terrestrial Ecosystems Through Time*, A. K. Behrensmeyer et al. Ed. (Univ. of Chicago Press, Chicago, 1992), pp. 327–418.
20. G. L. Jepsen, *Science* **154**, 1333 (1966).
21. J. Habersetzer, G. Storch, *Naturwissenschaften* **79**, 462 (1992).
22. S. Hand, M. Novacek, H. Godthelp, M. Archer, *J. Vertebr. Paleontol.* **14**, 375 (1994).
23. G. Storch, B. Sigé, J. Habersetzer, *Palaeontol. Z.* **76**, 189 (2002).
24. M. C. McKenna, S. K. Bell, *Classification of Mammals above the Species Level* (Columbia Univ. Press, New York, 1997).
25. M. S. Springer, E. C. Teeling, O. Madsen, M. J. Stanhope, W. W. de Jong, *Proc. Natl. Acad. Sci. U.S.A.* **98**, 6241 (2001).
26. S. J. Hand, J. A. Kirsch, in *Bat Biology and Conservation*, T. H. Kunz, P. A. Racey, Eds. (Smithsonian Institution Press, Washington, DC, 1998), pp. 72–90.
27. J. J. Flynn, A. R. Wyss, *Trends Ecol. Evol.* **13**, 449 (1998).
28. A. Cooper et al., *Nature* **409**, 704 (2001).
29. M. O. Woodburne, J. A. Case, *J. Mamm. Evol.* **3**, 121 (1996).
30. W. J. Murphy et al., *Science* **294**, 2348 (2001).
31. <http://home.ncifcrf.gov/ccr/igdl/>.
32. The research was funded and supported by federal funds from the National Cancer Institute, NIH, under contract no. N01-CO-12400, and the Darwin Initiative Grant no. 162-11-09. We would like to thank K. Jones, I. Horáček, I. Mackie, C. Mainstone, F. Catzeflis, N. Czaplewski, G. Morgan, Tin Nwe, N. Crumpler, A. Roca, and R. Stanyon for samples, technical support, and advice.

Supporting Online Material

www.sciencemag.org/cgi/content/full/307/5709/580/DC1

Materials and Methods

Figs. S1 to S3

Tables S1 to S7

References and Notes

10 September 2004; accepted 24 November 2004
10.1126/science.1105113

Interindividual Variation in Posture Allocation: Possible Role in Human Obesity

James A. Levine,* Lorraine M. Lanningham-Foster, Shelly K. McCrady, Alisa C. Krizan, Leslie R. Olson, Paul H. Kane, Michael D. Jensen, Matthew M. Clark

Obesity occurs when energy intake exceeds energy expenditure. Humans expend energy through purposeful exercise and through changes in posture and movement that are associated with the routines of daily life [called non-exercise activity thermogenesis (NEAT)]. To examine NEAT's role in obesity, we recruited 10 lean and 10 mildly obese sedentary volunteers and measured their body postures and movements every half-second for 10 days. Obese individuals were seated, on average, 2 hours longer per day than lean individuals. Posture allocation did not change when the obese individuals lost weight or when lean individuals gained weight, suggesting that it is biologically determined. If obese individuals adopted the NEAT-enhanced behaviors of their lean counterparts, they might expend an additional 350 calories (kcal) per day.

Obesity is epidemic in high-income countries. In the United States alone poor diet and physical inactivity are associated with 400,000 deaths per year (1) and obesity-related medical expenditures in 2003 approximated \$75 billion (2). Obesity is also an emerging problem in middle- and low-income countries, where the health and fiscal costs are likely to be devastating (3).

As the impact of obesity on health escalates, so too does the need to understand

its pathogenesis. Weight gain and obesity occur when energy intake exceeds energy expenditure. We are interested in a specific component of energy expenditure called NEAT and the role it might play in human obesity. NEAT is distinct from purposeful exercise and includes the energy expenditure of daily activities such as sitting, standing, walking, and talking.

We have previously shown that when humans overeat, activation of NEAT helps to prevent weight gain (4). To better understand NEAT and its role in obesity, we separated NEAT into the thermogenesis associated with posture (standing, sitting, and lying) and that associated with movement (ambulation).

To investigate whether the obese state has an effect on NEAT, we first developed and validated a sensitive and reliable technology for measuring the postural allocation of NEAT in human volunteers (5, 6). This physical activity monitoring system uses inclinometers and triaxial accelerometers to capture data on body position and motion 120 times each minute. By combining these measurements with laboratory measures of energy expenditure, we can summate NEAT and define its components (7).

To compare body posture and body motion in lean and obese people, we recruited 20 healthy volunteers who were self-proclaimed “couch potatoes.” Ten participants (five females and five males) were lean [body mass index (BMI) 23 ± 2 kg/m²] and 10 participants (five females and five males) were mildly obese (BMI 33 ± 2 kg/m²) (8) (table S1). We deliberately selected mildly obese subjects who were not incapacitated by their obesity and who had no joint problems or other medical complications of obesity. The volunteers agreed to have all of their movements measured for 10 days and to have their total NEAT measured with the use of a stable isotope technique (9). They were instructed to continue their usual daily activities and occupations and not to adopt new exercise practices. Over the 10-day period, we collected ~25 million data points on posture and movement for each volunteer.

Our analysis revealed that obese participants were seated for 164 min longer per day than were lean participants (Fig. 1A). Correspondingly, lean participants were upright for 152 min longer per day than obese participants. Sleep times (lying) were almost identical between the groups. Total

Endocrine Research Unit, Mayo Clinic, Rochester, MN 55905, USA.

*To whom correspondence should be addressed.
E-mail: jim@Mayo.edu

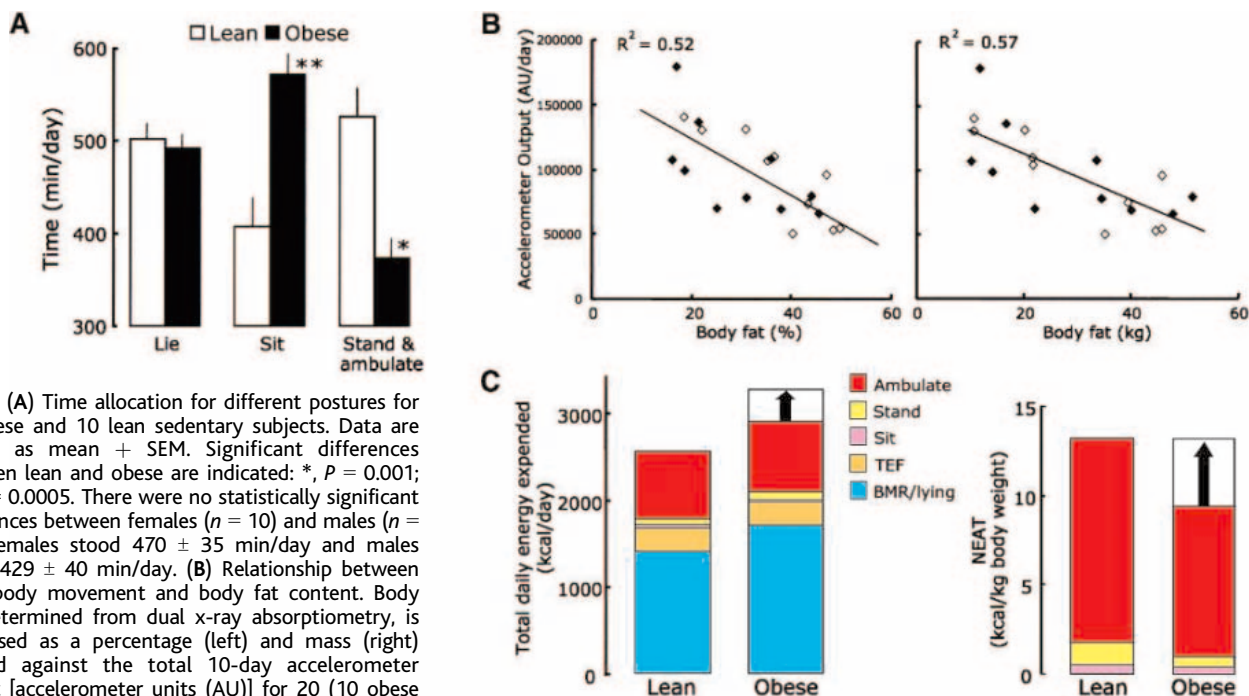


Fig. 1. (A) Time allocation for different postures for 10 obese and 10 lean sedentary subjects. Data are shown as mean + SEM. Significant differences between lean and obese are indicated: *, $P = 0.001$; **, $P = 0.0005$. There were no statistically significant differences between females ($n = 10$) and males ($n = 10$): Females stood 470 ± 35 min/day and males stood 429 ± 40 min/day. **(B)** Relationship between total body movement and body fat content. Body fat, determined from dual x-ray absorptiometry, is expressed as a percentage (left) and mass (right) plotted against the total 10-day accelerometer output [accelerometer units (AU)] for 20 (10 obese and 10 lean) sedentary subjects. The open diamonds are data for females and the filled diamonds are data for males. There was no significant relationship between fat-free mass and accelerometer output (fig. S1). The relationship between NEAT by doubly labeled water adjusted by weight versus accelerometer output is shown in fig. S2. **(C)** (Left) Total daily energy expenditure and (right) NEAT in 10 obese and 10 lean sedentary subjects. The uppermost segments of the bars for obese individuals (vertical arrows) represent the additional energy that could be

expended if these subjects were ambulatory for the same amount of time as lean subjects. BMR, basal metabolic rate; TEF, thermic effect of food. There was no significant difference in sleeping time between the lean group (423 ± 15 min) and the obese group (434 ± 17 min). The energy expenditure data and standard deviations appear in table S2. The relationship between NEAT measured with doubly labeled water and NEAT measured with the instruments is shown in fig. S3.

body movement, 89% of which was ambulation, was negatively correlated with fat mass (Fig. 1, B and C). Notably, if the obese subjects had the same posture allocation as the lean subjects, they would have expended an additional 352 ± 65 (\pm SD) (range, 269 to 477) calories (kcal) per day (Fig. 1C).

To investigate whether these differences in posture allocation are a cause or consequence of obesity, we asked seven of the original obese volunteers (four females and three males, BMI 33 ± 2 kg/m²) to undergo supervised weight loss over a period of 8 weeks. The average weight loss was 8 kg. Likewise, we recruited nine of the original lean volunteers and one additional lean volunteer (six females and four males, BMI 23 ± 2 kg/m²) to undergo supervised over-feeding over a period of 8 weeks. The average weight gain was 4 kg. After these weight perturbations, we studied posture allocation in these subjects for another 10 days. Interestingly, both the obese subjects losing weight and the lean subjects gaining weight maintained their original posture allocation (Fig. 2). Thus, it appears that interindividual differences in posture allocation are biologically determined.

It should be emphasized that this was a pilot study and that the results need to be confirmed in larger studies. Nevertheless, the current data may be important for under-

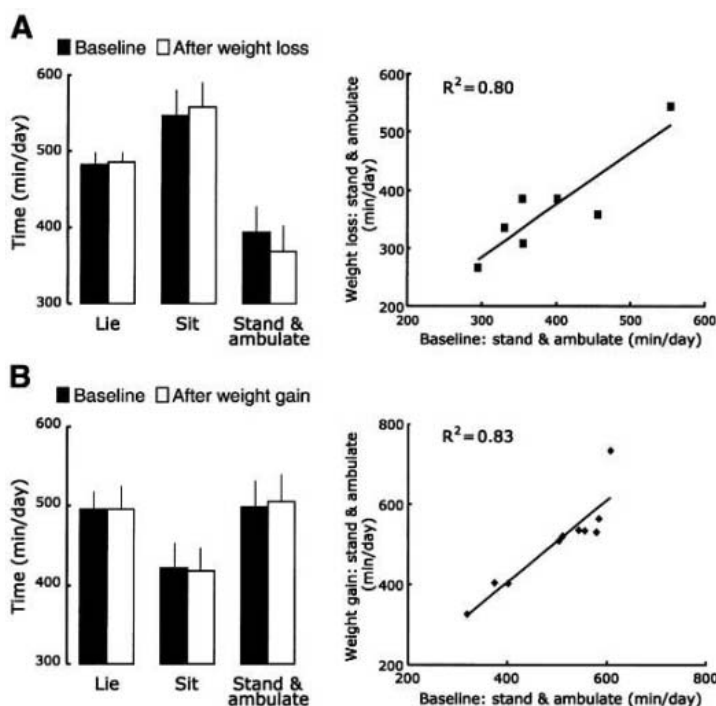


Fig. 2. (A) Posture allocation in seven obese sedentary subjects who underwent caloric restriction (8). (Left) Posture allocation data at baseline and after weight loss of 8 ± 2 kg. (Right) The time the subjects spent standing/ambulating at baseline is plotted against the time the subjects spent standing/ambulating after weight loss. **(B)** Posture allocation in 10 lean sedentary subjects who underwent experimental weight gain (8). (Left) The posture allocation data for baseline and after weight gain of 4 ± 2 kg. (Right) The time the subjects spent standing/ambulating at baseline is plotted against the time the subjects spent standing/ambulating after weight gain. Data are shown as mean + SEM.

standing the biology of obesity and how best to treat it. The propensity of obese persons to sit more than lean individuals has several potential explanations. Rodent studies support the concept that there are central and humoral mediators of NEAT (10, 11). For example, we have shown that a neuropeptide associated with arousal, orexin (12), increases NEAT in rats when injected into the paraventricular nucleus (PVN) of the hypothalamus. Preliminary data suggest that PVN injections of orexin also cause dose-dependent increases in standing posture allocation in rats (13). Thus, there may be central and humoral mediators that drive the sedentary behavior of obese individuals. The negative relationship between fat mass and movement (Fig. 1B) raises the intriguing possibility that body fat releases a factor that slows physical activity in obesity. However, these data also demonstrate that posture allocation is not the mechanism by which NEAT is modulated with short-term over-feeding. One hypothesis is that this occurs through modulation of energy efficiency; this is an area worthy of future investigation.

These data may also have implications for obesity intervention. One could argue that obese individuals have a biologically determined posture allocation and therefore are destined to become obese. If this were true, obesity would have been as common 50 years ago as it is today. However, obesity rates have increased and continue to do so

(14). We speculate that obese and lean individuals respond differently to the environmental cues that promote sedentary behavior. If the obese volunteers adopted the NEAT-enhanced behavior of their lean counterparts, they could expend an additional 350 kcal per day. Over a year, this alone could result in a weight loss of ~15 kg, if energy intake remained unchanged. Herein lies the rationale behind nationwide approaches to promote NEAT in small increments (15). For example, in Rochester, Minnesota, in 1920 before car use was commonplace the average walk to and from work was 1.6 miles (16). If walking this distance to work were reinstated by our obese subjects, all of whom currently drive to work, an extra 150 kcal per day could be expended. We will need to use similar measures to promote NEAT as an impetus to create an active and dynamic environment in which, for example, dancing supersedes television as a leisure activity. Approaches that succeed in getting people out of their chairs and moving could have substantial impact on the obesity epidemic.

References and Notes

1. A. H. Mokdad, J. S. Marks, D. F. Stroup, J. L. Gerberding, *JAMA* **291**, 1238 (2004).
2. E. A. Finkelstein, I. C. Fiebelkorn, G. Wang, *Obes. Res.* **12**, 18 (2004).
3. World Health Organization, *Obesity: Preventing and Managing the Global Epidemic* (Geneva, Switzerland, 1997).

4. J. A. Levine, N. L. Eberhardt, M. D. Jensen, *Science* **283**, 212 (1999).
5. J. A. Levine, P. A. Baulk, K. R. Westerterp, *Med. Sci. Sports Exerc.* **33**, 1593 (2001).
6. J. A. Levine, E. L. Melanson, K. R. Westerterp, J. O. Hill, *Eur. J. Clin. Nutr.* **57**, 1176 (2003).
7. J. A. Levine, E. L. Melanson, K. R. Westerterp, J. O. Hill, *Am. J. Physiol. Endocrinol. Metab.* **281**, E670 (2001).
8. Materials and methods are available as supporting material on Science Online.
9. D. A. Schoeller, C. A. Leitch, C. Brown, *Am. J. Physiol.* **251**, R1137 (1986).
10. J. A. Levine, J. Nygren, K. R. Short, K. S. Nair, *J. Appl. Physiol.* **94**, 165 (2003).
11. K. Kiwaki, C. M. Kotz, C. Wang, L. Lanningham-Foster, J. A. Levine, *Am. J. Physiol.* **286**, E551 (2004).
12. J. G. Sutcliffe, L. de Lecea, *Nature Med.* **10**, 673 (2004).
13. C. M. Kotz, personal communication.
14. J. O. Hill, H. R. Wyatt, G. W. Reed, J. C. Peters, *Science* **299**, 853 (2003).
15. More information about promoting NEAT in small increments can be found at www.smallstep.gov and www.americaonthemove.org.
16. L. Lanningham-Foster, L. J. Nysse, J. A. Levine, *Obes. Res.* **11**, 1178 (2003).
17. We thank the volunteers, dietitians, food technicians, nursing staff, and the Mass Spectrometer Core at the General Clinical Research Center, A. Oberg for assistance with statistics, and P. Baulk for technical support. Supported by NIH grants DK56650, DK63226, DK66270, and M01 RR00585, by T. S. and D. B. Ward, and by the Mayo Foundation.

Supporting Online Material

www.sciencemag.org/cgi/content/full/307/5709/584/DC1
 Materials and Methods
 Figs. S1 to S4
 Tables S1 and S2
 References

20 October 2004; accepted 7 December 2004
 10.1126/science.1106561

Sequence-Directed DNA Translocation by Purified FtsK

Paul J. Pease,^{1*} Oren Levy,^{2*} Gregory J. Cost,¹ Jeff Gore,³ Jerod L. Ptacin,¹ David Sherratt,⁵ Carlos Bustamante,^{1,3,4,†} Nicholas R. Cozzarelli^{1,2,†}

DNA translocases are molecular motors that move rapidly along DNA using adenosine triphosphate as the source of energy. We directly observed the movement of purified FtsK, an *Escherichia coli* translocase, on single DNA molecules. The protein moves at 5 kilobases per second and against forces up to 60 piconewtons, and locally reverses direction without dissociation. On three natural substrates, independent of its initial binding position, FtsK efficiently translocates over long distances to the terminal region of the *E. coli* chromosome, as it does in vivo. Our results imply that FtsK is a bidirectional motor that changes direction in response to short, asymmetric directing DNA sequences.

DNA translocases are adenosine triphosphate (ATP)-driven machines required for DNA replication, recombination, and transfer within and between cells (1–6). FtsK is a membrane-bound and septum-localized *E. coli* translocase that coordinates cell division with chromosome segregation (7). At times, the product of chromosome replication is a circular dimer rather than two monomers.

These dimers are resolved by the XerCD site-specific recombinase at a site near the terminus of replication, termed *dif* (8). Recombination between the distant *dif* sites requires FtsK. In addition, at the time of cell division some DNA may remain in the septal region, and FtsK appears to act as a pump to clear this region of DNA (9, 10). FtsK may also promote disentanglement of chromo-

some termini by means of an interaction with topoisomerase IV (11).

Translocases move along DNA or move the DNA if the translocase is anchored. In either case, translocases must be able to move in a specific direction relative to the DNA. Translocase directionality could be determined by strand polarity for single-strand tracking enzymes, nonrandom orientation of translocase binding through localized accessory factors or binding sites, or DNA sequences that affect the enzyme during translocation. In *E. coli*, provocative genetic experiments showed that lambda-phage DNA inserted near *dif* disrupted chromosome dimer resolution in a manner dependent on insertion orientation (9). Thus, DNA sequences could be directing FtsK toward *dif* so that it can activate XerCD recombination.

¹Department of Molecular and Cell Biology, ²Biophysics Graduate Group, ³Department of Physics, ⁴Howard Hughes Medical Institute, University of California, Berkeley, CA 94720–3204, USA. ⁵Division of Molecular Genetics, Department of Biochemistry, University of Oxford, OX1 3QU, UK.

*These authors contributed equally to this paper.
 †To whom correspondence should be addressed.
 E-mail: ncozzare@socrates.berkeley.edu (N.R.C.); carlos@alice.berkeley.edu (C.B.)

Here, we measured FtsK translocation on single DNA molecules and showed that FtsK moves fast (5 kb/s) and can work against a heavy load (>60 pN) in an ATP-dependent manner. We directly observed its movement along DNA and found that purified FtsK moves toward *dif*, demonstrating that DNA sequence alone is sufficient to direct FtsK toward its target. Our results are consonant with a model of FtsK in which bidirectional motors alternate activity in response to directing DNA sequences.

Our experiments used the C-terminal motor domain of FtsK (FtsK_{50C}) (12, 13). We first asked whether FtsK_{50C} is able to pull DNA against a load, as its role *in vivo* suggests. To this end, we tethered a single molecule of lambda-phage DNA between two beads, one of which was held on a micropipette (Fig. 1A). The DNA was then extended under constant tension by buffer flow. When FtsK_{50C} and ATP were introduced, the DNA tether rapidly shortened against the applied force, visualized as a decrease in the bead-to-bead distance (Fig. 1A and Movie S1). We conclude that tether shortening results from the formation of an expanding DNA loop closed off by two points of contact with FtsK_{50C}. This loop is probably topologically constrained by the translocase, because bulk assays indicate that FtsK generates twin supercoiled regions (13). Topological domain formation by translocases may be widespread, as another translocase, human Rad54, has been shown by scanning force microscopy to form supercoiled DNA loops (14).

Activity occurred in bursts that were identified by an algorithm that recognizes continuous changes in interbead distance, thus excluding periods of enzyme inactivity (12). A plot of DNA extension versus time for a typical experimental run is shown in Fig. 1B. At a constant force from 10 to 15 pN, the velocity of individual bursts from four experimental runs (totaling 108 bursts) averaged 5.0 ± 0.9 kb/s at 25°C (fig. S1), a rate comparable with those of a recent study (15). The kinetics of FtsK_{50C} are considerably faster than other DNA translocases assayed in single-molecule experiments (16–20). Not only is FtsK_{50C} exceptionally fast, it is also unusually powerful. In the same assay, against high loads of 35 to 40 pN, FtsK_{50C} velocity only drops by about half to 2.8 ± 0.5 kb/s.

Although decreasing bead-to-bead distance results from an expanding DNA loop, we also observed that the bead-to-bead distance could increase, as if the DNA loop were contracted. The rate was nearly the same during loop expansion as during loop contraction (Fig. 1B inset), which suggests that contraction too is an active process of FtsK_{50C}. This bidirectionality of FtsK_{50C} suggests that it consists of more than a single unidirectional motor (21). Occasionally, we saw an abrupt

collapse of the loop, consistent with complete release of one of the contact points between the DNA and FtsK_{50C}. Translocation and loop formation then immediately resumed, which indicates that FtsK_{50C} remained firmly bound to the DNA at at least one contact point during these events. These rapid reversals along with the small standard deviation of the observed rates make it very unlikely that there are multiple FtsK complexes acting simultaneously.

In a complementary assay for DNA translocation, a molecule of lambda DNA was tethered between two beads as in the reeling assay, but instead of being left free, the second bead was caught in an optical trap, allowing direct measurement of the force exerted on the DNA by FtsK_{50C}. As FtsK_{50C} translocated, it pulled the trapped bead toward the micropipette with a concomitant increase in force, indicative of loop formation. As the DNA loop enlarged, FtsK_{50C} experienced an increasing load that was released by reverse translocation or, less frequently, by a dissociation of the protein from one of the DNA contact points.

Visible aggregates of the enzyme, referred to here as particles, were observed at

higher protein concentrations, particularly above 100 nM. These particles bound individually to the DNA at random positions as protein was introduced to the flow cell during the optical-trap assay (Fig. 1C and Movie S2). As soon as an FtsK_{50C} particle bound to the DNA, DNA looping was initiated, as evidenced by the shortening of the tether. These particles traveled along the DNA at 4.9 ± 0.9 kb/s, the same rate measured in the reeling assay, thus making it possible to track a single active FtsK_{50C} complex.

Strikingly, the FtsK_{50C} particles consistently translocated along the lambda DNA in the same overall direction (75 out of 75 observations), even though occasionally some would temporarily reverse direction, as in the reeling assay. To be certain that unidirectionality was in fact a property of the translocase, we inverted the DNA molecule with respect to either the optical trap or the two types of beads used. The particles always moved in the same direction relative to the lambda DNA sequence. It is notable that they move in the direction predicted by genetic experiments (9). The occasional reversals show that FtsK_{50C} directionality is dynamic; it can change on

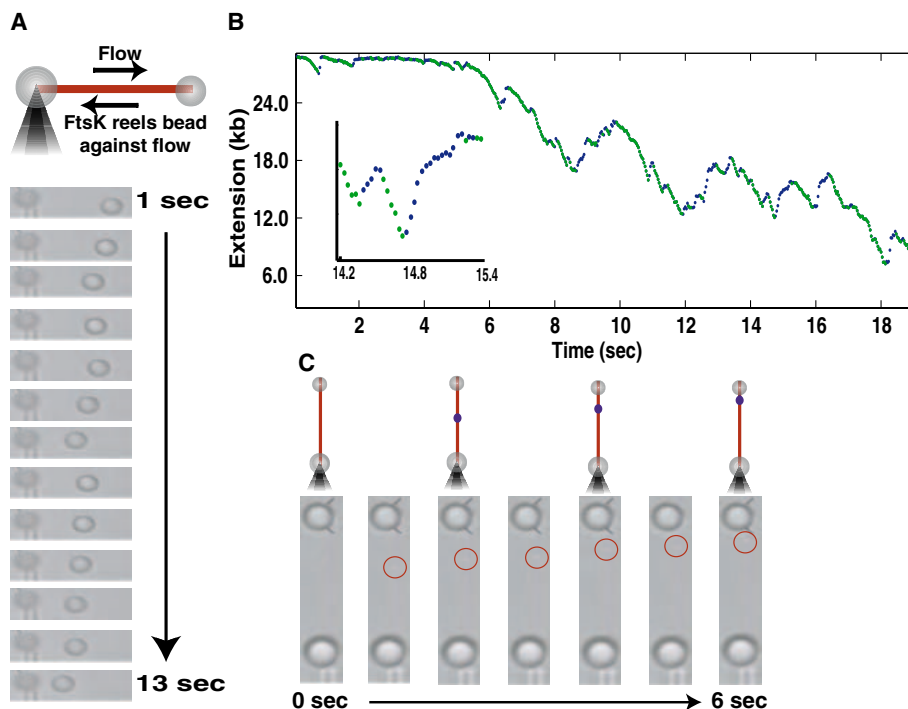


Fig. 1. Measurement of FtsK translocation with two assays. (A) In the reeling assay shown, each end of a lambda DNA molecule is attached to a bead. One bead is held by suction through a micropipette. Translocation by FtsK forms a loop in the DNA tether, which reels in the free bead against a flow force of 10 to 15 pN. The shortening of the tether with 100 nM FtsK_{50C} and 3 mM ATP is seen in the video frames spaced at 1-s intervals. (B) Tracking of free-bead position as a function of time shows bursts reeling in (green) and reeling out (blue). Reeling in and reeling out velocities are often similar (inset). (C) FtsK_{50C} translocation can be directly visualized on single lambda DNA molecules. The DNA was tethered between two beads with one held by a micropipette and the other in an optical trap. The tether was maintained at a constant tension by moving the micropipette in response to DNA looping with an automated force-feedback program. Video frames at 1-s intervals are shown with the FtsK particle surrounded by a red circle.

small scales but is ultimately unidirectional over large distances.

To test the directionality of FtsK_{50C} on its natural substrate, we constructed three DNA tethers from the *dif* region of the *E. coli* chromosome (Fig. 2A). These 27- to 30-kb substrates contain the DNA immediately to the left (L) of *dif* on the chromosome, the right (R) of *dif*, or centered (C) on *dif*. If DNA sequences neighboring *dif* are sufficient to direct FtsK, then the net movement of FtsK_{50C} particles should always be toward *dif*. The particle-tracking assay described above was used to test this hypothesis.

Every FtsK_{50C} particle observed on the L and R substrate (15 of 15) translocated to the *dif* proximal end of the DNA tether. Traces of FtsK_{50C} particles moving on L and R are shown in Fig. 2B. The rate of movement was 4.8 ± 0.9 kb/s for the bursts and 3.2 kb/s overall, the same rate as on lambda DNA. Also, as on lambda DNA, FtsK_{50C} occasionally reversed direction before turning back toward the *dif* proximal end.

In vivo, FtsK must bind to a long DNA molecule (the chromosome) and efficiently find its way to *dif*. The behavior of FtsK_{50C} on our C tether mimics the in vivo situation. Here, the FtsK_{50C} particles moved rapidly toward *dif* from either direction. Upon reaching *dif*, the particles oscillated for a number of minutes around *dif* (Fig. 2B and Movie S3), and their average position coincided with *dif*. These oscillations were only observed on the C substrate and indicate that FtsK_{50C} constantly samples DNA sequence to ensure proper directionality.

Our findings contradict the conclusion of a recent study that FtsK is a sequence-independent translocase (15). That study, however, used magnetic tweezers in which DNA is viewed down its axis. Therefore, the position or movement of FtsK could not be detected. In our assay with optical tweezers, the direction of view is perpendicular to the helix axis, and we can readily see FtsK particles. The data in the other study is readily explained by the model we present below.

We tested whether FtsK_{50C} pulls DNA into a loop from two directions at once, as does T antigen (22), by measuring simultaneously the position of the FtsK_{50C} particle and the two beads. Analysis of 25 translocation events on the C substrate showed that the DNA shortening occurred only from one direction at any given time. For example, during FtsK_{50C} translocation toward the micropipette, as diagrammed in Fig. 3A, the tether length below the particle decreased, whereas that above it increased slightly as a result of stretching caused by the high forces generated by FtsK_{50C} translocation (Fig. 3, C and D) (23, 24). We conclude that the FtsK_{50C} complex is coupled in such a way

that only one motor is active at any given time (25).

After observing that DNA enters the loop from only one side of the FtsK_{50C} complex,

we used the bead-particle correlation analysis to observe loop release. The DNA in the loop could be released from either side of the complex. However, there would only be net

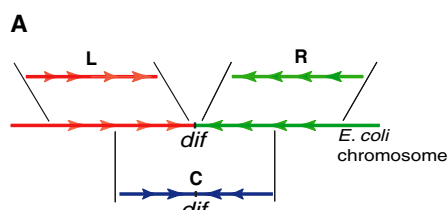


Fig. 2. FtsK translocates toward *dif* in vitro. (A) To test FtsK directionality on its natural substrate, the three DNA regions of the *E. coli* chromosome shown were amplified to give products spanning 29.5 kb to the left of *dif* (L), 28.7 kb to the right of *dif* (R), and 27.9 kb centered on *dif* (C). (B) FtsK_{50C} quickly translocated toward the *dif* proximal end with both the L (red) and R (green) substrates (15 out of 15 observations). Once the FtsK particle reached the end of the tether, it was obscured by the bead and no longer visible. The particles did not translocate back in the opposite direction even after several minutes. With the C substrate (blue), FtsK_{50C} oscillated about *dif* for 5 to 15 min. The location of *dif* is shown as a black horizontal dot-dash line.

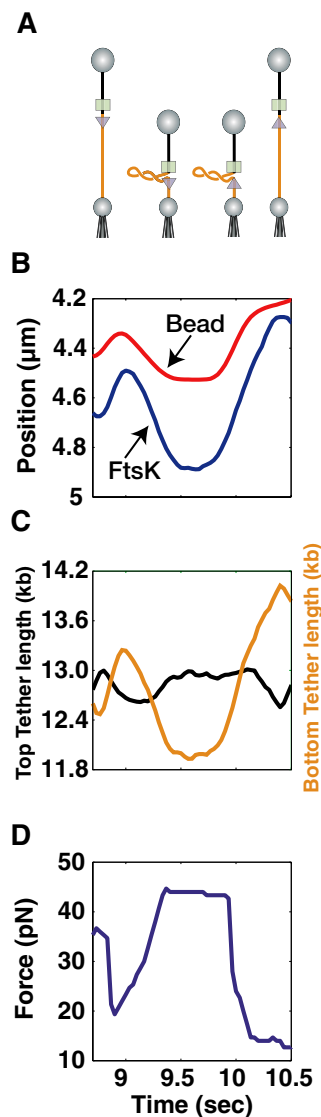
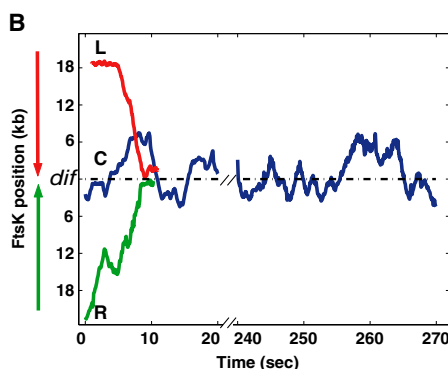


Fig. 3. Simultaneous tracking of FtsK, force on the tether, and flanking DNA lengths demonstrates that DNA is reeled from only one side at a time. (A) Diagram of the experiment showing a DNA molecule held between two beads. The portions of the tether above and below FtsK are colored black and orange, respectively, to illustrate that only the DNA below FtsK is reeled into the loop. The upper bead is in an optical trap (not shown), and the lower bead is on a micropipette. The FtsK complex is shown as two coupled bidirectional motors, with the active motor depicted as a blue triangle pointing toward the direction of movement and the inactive one as a green square. Translocation can generate a loop and displace the bead in the optical trap and also release the loop, returning the bead to the trap. (B) Correlated movement of the bead in the trap (red) and FtsK particle (blue), corresponding to the diagram in (A). The bead trace is offset to facilitate comparison. (C) As FtsK_{50C} translocates down toward the micropipette, only the tether below the FtsK_{50C} complex (orange) decreases in length (25 of 25 observations, including the opposite case in which the FtsK_{50C} complex moves up and the upper tether length decreases), which demonstrates that DNA is reeled from only one side at any one time. The tether lengths are corrected for stretching because of the high forces on the tether. (D) The force generated by FtsK_{50C} during this burst.

translocation if the loop were released from the opposite side from which it was formed. We observed all four possible movements, i.e., DNA entering the loop from either side and releasing from either side (fig. S2, A to D). The correlated movement of the bead in the optical trap and the FtsK_{50C} particle provides clear evidence that the only site of looping is at the visible FtsK_{50C} particle. The symmetry of movements seen here supports a model of two coordinated, bidirectional motors, which we propose are rectified by short, asymmetric DNA sequences.

We also observed translocation in the absence of detectable looping, especially at forces above 35 pN (fig. S2, E and F). This type of movement presumably occurs when there is no stable, static FtsK-DNA contact point. Therefore, even though translocation at low forces typically proceeds with two points of contact between the motors and DNA, only one may be needed.

We estimated the strength of the FtsK_{50C} motor using the C tether in the optical-trap assay (fig. S3). The tension in the DNA tether increases as FtsK_{50C} decreases the DNA end-to-end distance by looping and pulls the bead from the center of the trap. We measured the force at which the bead suddenly reverses direction, because the DNA loop is presumably released as a result of a slip at the contact point with the active motor. DNA loops were released at forces ranging from 15 pN to more than 60 pN, with a mean of 35 pN (fig. S3). The upper bound of this force range is close to that which causes a phase transition in DNA (26, 27).

Our working model for FtsK translocation (Fig. 4) depicts the FtsK complex as two bidirectional motors coupled in such a way that only one is active at any given time. The inactive motor remains firmly bound to the DNA, thus creating the second contact point necessary for loop formation. An expanding supercoiled domain is generated

between the two motors as one binds the DNA tightly while the other tracks the DNA helix. We propose that each motor is bidirectional to account for all of the patterns of movement we observed in our correlation analyses (fig. S2): The FtsK complex must be able to pull DNA through either motor and also release it through either motor. Net translocation of FtsK occurs, however, only when DNA is taken in through one motor and released through the opposite motor (Fig. 4). It is unclear how FtsK reverses direction, but if it tracks one strand of the DNA duplex, a switch to the complementary strand would cause translocation reversal. Although it is not shown explicitly in Fig. 4, we believe that the net directionality of FtsK is imprinted when it moves past a short, asymmetric sequence whose polarity inverts at *dif*. Directionality is then maintained over a distance long enough to give overall unidirectionality but with occasional switches.

The high speed at which FtsK translocates along DNA (5 kb/s at 25°C) is about the rate expected for this family of translocases in vivo (2, 15). Thus, the simple purified system we studied recapitulates the rate as well as the directionality of translocation in vivo. The ability of FtsK to work against a heavy load is essential for its role in vivo. FtsK is rendered stationary by its insertion into the septum and must move a considerable section of the chromosome burdened with large transcription and translation complexes. Moreover, during translocation FtsK will encounter proteins and RNA bound to the DNA, so the ability to apply force during translocation would allow FtsK to clear these potential roadblocks without slowing down appreciably. The proposed annular structure of FtsK with DNA in the lumen would make FtsK and similar translocases effective “wire-strippers,” clearing DNA (28) to reset epigenetic and cell-cycle-specific nucleo-

protein structures at the apt time of replication termination.

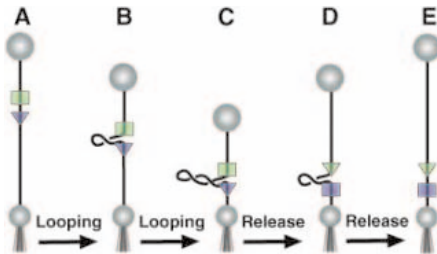
We observe that FtsK changes direction during translocation at several places on the DNA around *dif*, which suggests that the DNA sequences responsible for directionality are widespread. In fact, many short sequences with a skewed orientation flip abruptly at *dif* (29), and these have been proposed to bias the direction of FtsK translocation toward *dif* (9). The mechanism of FtsK movement could be analogous to the bipolar helicase RecBCD, which switches active motors when it encounters the skewed octamer called Chi in the correct orientation (30).

Bulk experiments with several translocases showed that these enzymes efficiently generated (+) and (–) supercoils in a circular DNA (13, 31). Our finding that FtsK forms a stable DNA loop provides a ready explanation for why these opposing supercoils did not cancel: They are segregated into separate domains delimited by the protein. FtsK and other translocases could contribute to domain formation in vivo; the mobility of the contact by FtsK is consistent with recent findings of random placement of domain boundaries in the cell (32). The rapid formation of a large loop at the terminus could concentrate catenane links, making decatenation by Topo IV more efficient (11, 33).

References and Notes

- M. R. Singleton, D. B. Wigley, *EMBO J.* **22**, 4579 (2003).
- J. Errington, J. Bath, L. J. Wu, *Nature Rev. Mol. Cell Biol.* **2**, 538 (2001).
- G. D. Recchia, M. Aroyo, D. Wolf, G. Blakely, D. J. Sherratt, *EMBO J.* **18**, 5724 (1999).
- F. X. Barre *et al.*, *Proc. Natl. Acad. Sci. U.S.A.* **98**, 8189 (2001).
- E. C. Hendricks, H. Szerlong, T. Hill, P. Kuempel, *Mol. Microbiol.* **36**, 973 (2000).
- T. L. Raoul Tan, R. Kanaar, C. Wyman, *DNA Repair (Amst.)* **2**, 787 (2003).
- G. Liu, G. C. Draper, W. D. Donachie, *Mol. Microbiol.* **29**, 893 (1998).
- G. Blakely, S. Colloms, G. May, M. Burke, D. J. Sherratt, *New Biol.* **3**, 789 (1991).
- J. Corre, J. M. Louarn, *J. Bacteriol.* **184**, 3801 (2002).
- I. F. Lau *et al.*, *Mol. Microbiol.* **49**, 731 (2003).
- O. Espeli, C. Lee, K. J. Marians, *J. Biol. Chem.* **278**, 44639 (2003).
- Materials and methods are available as supporting material on Science Online.
- L. Aussel *et al.*, *Cell* **108**, 195 (2002).
- D. Ristic, C. Wyman, C. Paulusma, R. Kanaar, *Proc. Natl. Acad. Sci. U.S.A.* **98**, 8454 (2001).
- O. A. Saleh, C. Perals, F. X. Barre, J. F. Allemand, *EMBO J.* **23**, 2430 (2004).
- M. D. Wang *et al.*, *Science* **282**, 902 (1998).
- N. R. Forde, D. Izahy, G. R. Woodcock, G. J. Wuite, C. Bustamante, *Proc. Natl. Acad. Sci. U.S.A.* **99**, 11682 (2002).
- D. E. Smith *et al.*, *Nature* **413**, 748 (2001).
- P. R. Bianco *et al.*, *Nature* **409**, 374 (2001).
- G. J. Wuite, S. B. Smith, M. Young, D. Keller, C. Bustamante, *Nature* **404**, 103 (2000).
- We use the term “motor” to mean an enzyme that translocates or binds DNA at one point, with a molecular structure yet to be established.
- R. Wessel, J. Schweizer, H. Stahl, *J. Virol.* **66**, 804 (1992).
- FtsK stopped translocating above ~63 pN, presumably because of DNA distortion, but remained bound and continued translocating if the force was lowered below the over-stretch transition.

Fig. 4. Model for FtsK translocation along a single molecule of DNA. A nicked DNA molecule is held between two beads. One bead is held with a micropipette, and the other is held in an optical trap (not shown). The two coupled motors in an FtsK complex (green and blue) are shown as a triangle when active and as a rectangle when providing a static contact point. (A) The complex binds to the DNA, and the lower motor begins moving downward. (B) The DNA is bound statically to the upper motor so that translocation by the lower motor creates a supercoiled DNA loop between the two motors, decreasing the end-to-end distance of the DNA, thus displacing the bead in the optical trap. (C) The lower motor continues enlarging the loop, further displacing the optically trapped bead. (D) The motors switch activity so that the lower motor becomes static while the upper motor begins pulling out the DNA loop, relaxing the force on the trapped bead. (E) The upper motor finishes pulling out the loop, returning the DNA tether to its full extension. The net transfer of DNA from one side of the FtsK complex to the other results in FtsK complex translocation. No net translocation is seen when the bottom motor reverses direction. This and other alternatives are illustrated in fig. S2. The reversibility of the two motors makes it possible for asymmetric DNA sequences (not shown) to dictate the overall direction of FtsK translocation by switching bidirectional motor activity.



24. S. B. Smith, Y. Cui, C. Bustamante, *Science* **271**, 795 (1996).
25. This experiment also supports our conclusion that we are observing the activity of a single FtsK complex. If multiple complexes were bound to the DNA, we would expect to see by chance occasional reeling in from above and below the observed particle.
26. It is difficult to measure a conventional stall force, because in almost all cases, the DNA loop releases before the motor velocity falls to zero.
27. Because processive motion is observed against a force of ~63 pN, we can place an upper limit of 1.6 nm (100 pN nm/63 pN) on the step size of the motor. This upper bound was calculated by assuming that a single ATP molecule is hydrolyzed per step and by recognizing that the efficiency must be less than 100%.
28. D. L. Kaplan, M. O'Donnell, *Mol. Cell* **15**, 453 (2004).
29. S. L. Salzberg, A. J. Salzberg, A. R. Kerlavage, J. F. Tomb, *Gene* **217**, 57 (1998).
30. M. Spies *et al.*, *Cell* **114**, 647 (2003).
31. J. Bath, L. J. Wu, J. Errington, J. C. Wang, *Science* **290**, 995 (2000).
32. L. Postow, C. D. Hardy, J. Arsuaga, N. R. Cozzarelli, *Genes Dev.* **18**, 1766 (2004).
33. J. Louarn, F. Cornet, V. Francois, J. Patte, J. M. Louarn, *J. Bacteriol.* **176**, 7524 (1994).
34. We thank T. H. Massey for providing the FtsK_{SOC} His-tagged construct and S. B. Smith for expert assistance. This work was supported by NIH grants GM31657 (N.R.C.), GM32543 (C.B.), GM07232-27 (J.L.P.), Wellcome Trust and the Royal Society (D.S.), Ruth L. Kirschstein National Research Service Award,

grant GM08295-15 (P.J.P.), Fannie and John Hertz Foundation (J.G.), Damon Runyon Cancer Research Foundation grant 1702-02 (G.J.C.), and U.S. Department of Energy grants DE-AC03-76DF00098, GTL2BN "Microscopies of MolecularMachines," and SNAJOB "Design of Autonomous Nanobots" (C.B.).

Supporting Online Material

www.sciencemag.org/cgi/content/full/307/5709/586/DC1

Materials and Methods
Figs. S1 to S3
Movies S1 to S3

7 September 2004; accepted 1 December 2004
10.1126/science.1104885

Restoration of Tolerance in Lupus by Targeted Inhibitory Receptor Expression

Tracy L. McGaha,¹ Brian Sorrentino,² Jeffrey V. Ravetch^{1*}

Lupus, a multigenic autoimmune condition in which a breakdown of tolerance results in the development of autoantibodies, leads to a variety of pathologic outcomes. Despite the heterogeneity of factors influencing disease susceptibility, we demonstrate that the partial restoration of inhibitory Fc receptor (FcγRIIB) levels on B cells in lupus-prone mouse strains is sufficient to restore tolerance and prevent autoimmunity. FcγRIIB regulates a common B cell checkpoint in genetically diverse lupus-prone mouse strains, and modest changes in its expression can result in either tolerance or autoimmunity. Therefore, increasing FcγRIIB levels on B cells may be an effective way to treat autoimmune diseases.

The ability of the immune system to distinguish self from nonself is central to its ability to protect against pathogens and, at the same time, maintain nonresponsiveness to self. This property is established at discrete checkpoints both during development and in the adult. To date, several early developmental checkpoint mechanisms have been identified. These include the deletion of autoreactive lymphocytes during early development of the immune system (1–3); anergy, which converts autoreactive cells to a state that precludes them from becoming activated (4, 5); and editing, a mechanism for modifying autoantibodies that renders them nonautoreactive (6, 7). Although these developmental checkpoints purge the immune repertoire of autoreactive cells, the processes of central tolerance remain incomplete, allowing self-reactive cells that express antigen receptors to escape into the periphery (8, 9). In addition, mechanisms that enhance antibody diversity, such as somatic mutation, can generate potentially autoreactive antigen

receptors in the adult (10). Thus, checkpoints that operate in the periphery of mature individuals are critical for maintaining tolerance and for establishing tolerance to self-antigens that only appear after maturity. Less is known about these peripheral checkpoints, although a principal element has emerged whereby the balance between stimulatory and inhibitory signals regulates the activation and expansion of lymphoid cells. Inhibitory signaling, in particular, is a critical feature of peripheral tolerance, providing a means for establishing thresholds for stimulation and for active deletion of autoreactive cells from the peripheral repertoire. Perturbations in inhibitory signaling pathways have been shown to be genetically associated with autoimmunity (11, 12).

Genetic studies have associated a large number of loci and candidate genes, in addition to inhibitory signaling pathways, with susceptibility to the development of autoimmune diseases (11, 13). In the context of multifactorial and multigenic diseases such as lupus, it is possible that single overriding factors may ultimately dictate whether the disease progresses or not. The selection and proliferation of immunoglobulin G (IgG)-producing B cells represents one such overriding peripheral checkpoint that is under the potential control of inhibitory signaling pathways.

Our previous work demonstrated that the expression of the inhibitory Fc receptor FcγRIIB was required for the maintenance of tolerance (14). C57BL/6 mice that are deficient in this receptor develop spontaneous lupus-like autoimmunity and progress to fulminate glomerulonephritis and premature mortality (14). Studies of bone marrow transfer into recombina-activating gene (RAG)-deficient mice suggested that FcγRIIB deficiency in the B cell compartment is most likely responsible for the loss of tolerance seen in these mice. In support of this idea, several strains of mice that develop spontaneous autoimmune disease, such as NZB, NOD, BXSB, and MRL/lpr, have also been shown to express reduced levels of FcγRIIB on activated or germinal-center B cells. This reduced expression results from a polymorphism in the promoter of this gene (15–18). These results suggest that the absolute level of FcγRIIB expressed on some B cells may regulate the ability of these cells to maintain tolerance and that relatively small changes in the expression of this inhibitory receptor may permit the survival and expansion of autoreactive cells. To test this hypothesis, we developed retroviral vectors that are capable of expressing FcγRIIB upon transduction of bone marrow cells, which can restore the wild-type level of FcγRIIB to B cells derived from autoimmune-prone strains. Bone marrow was derived from the autoimmune-susceptible strains NZM 2410, BXSB, and B6.Fcgr2b^{-/-} and transduced with either FcγRIIB-expressing retrovirus or parental (mock) virus lacking FcγRIIB. The bone marrow of irradiated recipients was reconstituted with autologous retroviral-transduced bone marrow, and the mice were followed for the development of autoimmunity and autoimmune disease. Mice that received autologous bone marrow transduced with the parent virus developed autoimmune disease and had reduced viability comparable to that of unmanipulated autoimmune-prone strains (Fig. 1A). In contrast, mice that received autologous bone marrow transduced with FcγRIIB-expressing retrovirus showed improved survival.

The basis for this protection was investigated by examination of the immune status of

¹Laboratory of Molecular Genetics and Immunology, The Rockefeller University, 1230 York Avenue, New York, NY 10021, USA. ²St. Jude Children's Research Hospital, 332 North Lauderdale, Memphis, TN 38105, USA.

*To whom correspondence should be addressed. E-mail: ravetch@rockefeller.edu

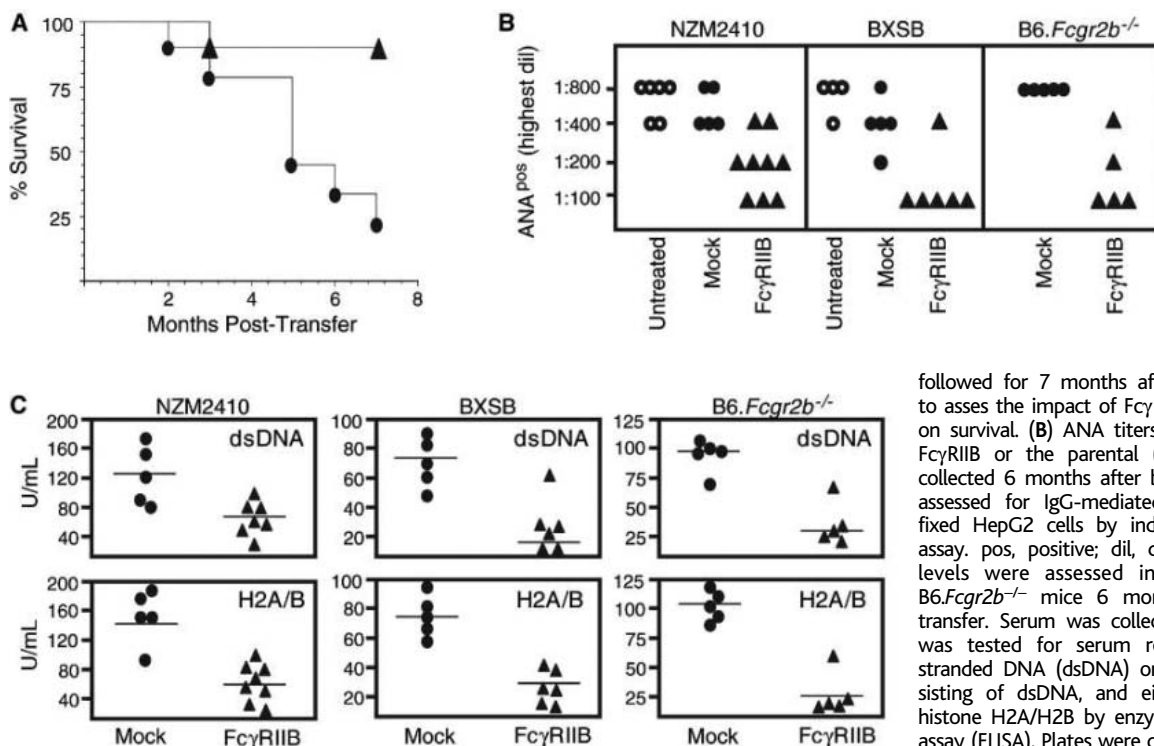


Fig. 1. Effect of FcγRIIB retroviral-mediated bone marrow transduction on spontaneous autoimmune disease in NZM2410 and BXSB mice. (A) Survival curve for NZM2410 mice transduced with the parental (mock) virus (solid circles) or the FcγRIIB-expressing retrovirus (solid diamonds). Mice were

followed for 7 months after bone marrow transfer to assess the impact of FcγRIIB retroviral transduction on survival. (B) ANA titers in mice transduced with FcγRIIB or the parental (mock) virus. Serum was collected 6 months after bone marrow transfer and assessed for IgG-mediated ANA reactivity against fixed HepG2 cells by indirect immunofluorescence assay. pos, positive; dil, dilution. (C) Autoantibody levels were assessed in NZM2410, BXSB, and B6.FcγRIIB^{-/-} mice 6 months after bone marrow transfer. Serum was collected and a 1:100 dilution was tested for serum reactivity against double-stranded DNA (dsDNA), and either histone H1 (19) or histone H2A/H2B by enzyme-linked immunosorbent assay (ELISA). Plates were coated with 100 ng of each antigen as indicated. Values represent the mean

optical density (O.D.) for duplicate wells normalized against autoimmune serum with high levels of reactivity against both dsDNA and chromatin components.

these bone marrow–recipient animals. The mice that received FcγRIIB retroviral-transduced bone marrow exhibited reduced levels of serum antinuclear antibodies (ANAs), antibodies to DNA, or antibodies to chromatin (Fig. 1, B and C), when compared with mice that received autologous bone marrow transduced with the parent retrovirus. This reduction of ANAs, antibodies to DNA, and antibodies to chromatin accounted for the lack of immune complex deposition in the kidneys of FcγRIIB retroviral-transduced NZM or BXSB recipients (Fig. 2, A and B) and thus explained the absence of renal disease in these mice (Fig. 2C). Renal function in NZM or BXSB mice whose marrow was reconstituted with marrow that was transduced with the FcγRIIB retroviral constructs was comparable to that of wild-type mice, with the majority showing little to no urine protein. In contrast, the majority of control or mock-treated mice exhibited a marked reduction in their kidney function associated with severe proteinuria (>100 mg/deciliter) (Fig. 2C). Histological examination showed that the kidneys of FcγRIIB retroviral-transduced mice resembled those of healthy mice (Fig. 3), and untreated or mock-transduced NZM2410 and BXSB mice exhibited substantial renal pathology with proliferative glomerulonephritis, tubulointerstitial inflammation, and pronounced glomerular sclerosis (Fig. 3). Similarly, FcγRIIB retroviral transduction significantly reduced vasculitis and lung inflammation in NZM

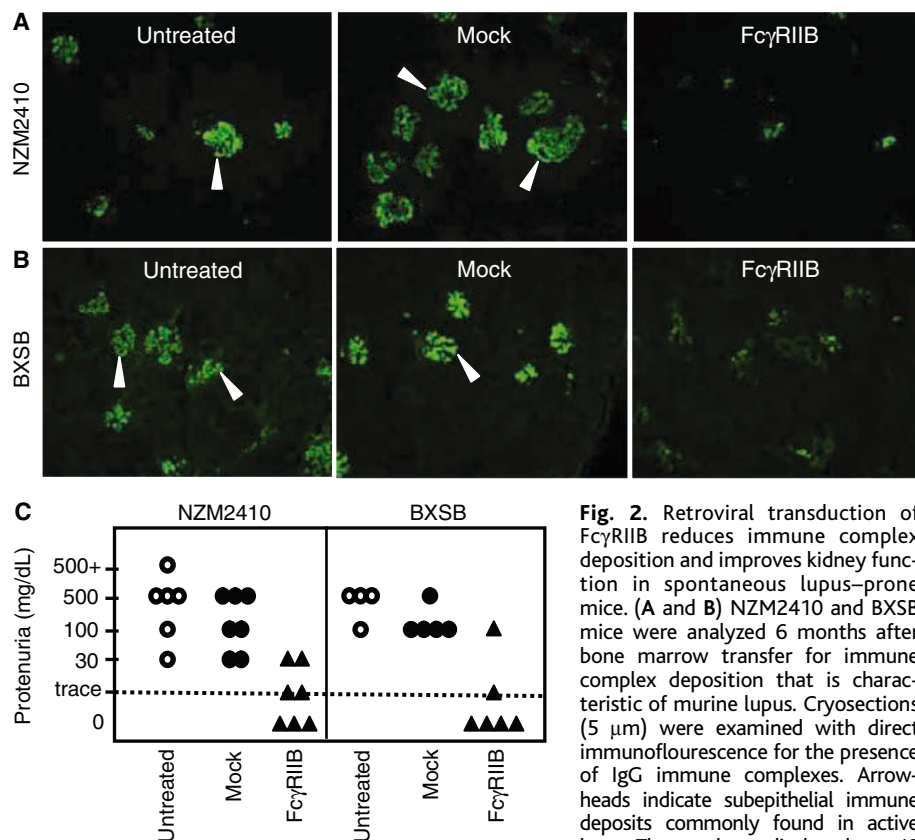


Fig. 2. Retroviral transduction of FcγRIIB reduces immune complex deposition and improves kidney function in spontaneous lupus-prone mice. (A and B) NZM2410 and BXSB mice were analyzed 6 months after bone marrow transfer for immune complex deposition that is characteristic of murine lupus. Cryosections (5 μm) were examined with direct immunofluorescence for the presence of IgG immune complexes. Arrowheads indicate subepithelial immune deposits commonly found in active lupus. The panels are displayed at ×40 magnification. (C) Kidney function was assessed 6 months after transfer by measurement of protein detectable in the urine of autoimmune-prone mice. Twenty-four-hour urine samples were collected and assayed for protein content as described elsewhere (14). The dotted horizontal line represents the normal protein levels found in mouse urine. A value of 100 mg of protein or more per deciliter is considered to be a marker of significantly altered kidney function.

2410 mice as compared with the control groups (Fig. 3).

To determine which cell populations were targeted by the retroviral transduction, we quantified levels of FcγRIIB and green fluorescent protein (GFP) by flow cytometry on lymphoid, myeloid, and dendritic cells in wild-type mice, autoimmune mice with

marrow reconstituted with FcγRIIB retrovirus, and autoimmune mice with marrow reconstituted with parental retrovirus (table S1). FcγRIIB is normally expressed on B cells, myeloid cells, and dendritic cells, and is absent from T cell populations. Reconstitution of these autoimmune strains with FcγRIIB retroviral-transduced bone

marrow resulted in a 50% increase in FcγRIIB expression on total B cells, which was contributed by the retrovirally encoded RIIB gene (Fig. 4). Because the retrovirally encoded RIIB gene was derived from a B6 donor and bears the allele recognized by the Ly17.2 antibody, it can be distinguished from the endogenous RIIB allele that is expressed by the NZM parent that is recognized by the Ly17.1 antibody. No change in Ly17.1 staining was seen on B220+ cells from untreated, mock-transduced, or RIIB-transduced animals (19). In contrast, Ly17.2 staining was noticeably enhanced in RIIB-transduced animals (Fig. 4). The efficiency of retroviral transduction in the B220+ B cell compartment for both bone marrow- and splenic-derived cells, which was determined by retroviral-encoded GFP expression, was 38% for the RIIB retrovirus and 42.5% for the parental vector alone (Fig. 4). Expression of RIIB in animals with marrow reconstituted with the RIIB-transduced bone marrow was also detected in immature T cells and a small population of myeloid cells. 20% of the immature thymocytes expressed GFP and RIIB, and 10% of the macrophages expressed these markers (figs. S1 to S3). Single positive thymocytes or single positive T cells had no detectable GFP or RIIB expression (figs. S1 and S2), and macrophages had a statistically insignificant increase in RIIB expression (fig. S3). Thus, we cannot rule out the possibility that macrophages or immature T cells play a role in the phenotype observed, although it is unlikely that they do. No overt changes in lymphoid or myeloid populations were noted in either mock- or RIIB-transduced animals (figs. S4 and S5). The basis for the apparent B cell restricted enhancement of RIIB expression may have resulted from the inactivation of the retroviral integrates in specific cellular populations (20–24).

These studies demonstrate that reestablishing tolerance in autoimmune mouse strains with diverse genetic backgrounds can be achieved by increasing the surface expression of the inhibitory FcγRIIB receptor on B cells. Although only 40% of the B cell compartment was transduced, the effect of increasing RIIB expression to wild-type levels on this percent of the population was sufficient to reestablish the peripheral checkpoint regulated by this inhibitory molecule and to prevent autoimmunity. These data are consistent with results obtained when the bone marrow of irradiated C57BL/6 recipient mice was reconstituted with mixed bone marrow derived from B6 and B6.Fcγr2b^{-/-} mice. A significant reduction in ANAs was seen when 45% of the bone marrow was of wild-type origin (fig. S6).

Although the precise mechanism by which FcγRIIB expression on B cells con-

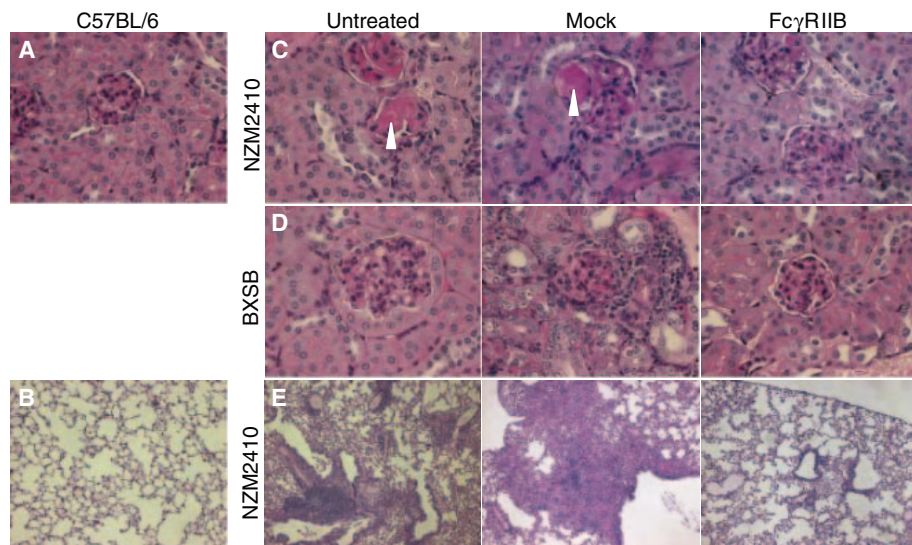


Fig. 3. Retroviral therapy with FcγRIIB reduces kidney and lung pathology in NZM2410 and BXSB mice. Periodic acid Schiff (PAS) staining of the kidney and hematoxylin and eosin (H&E) staining of the lung were done on paraformaldehyde-fixed tissue, which was then embedded in paraffin and sectioned at 5 μm thickness. Panels showing kidney sections (A, C, and D) are presented at ×63 magnification and lung sections (B and E) are presented at ×10 magnification. “Untreated” panels depict mice that received unmanipulated bone marrow, and “mock” and “FcγRIIB” panels represent mice that received cognate bone marrow transduced with the parental virus or the FcγRIIB-expressing virus, respectively. Untreated and mock-treated NZM2410 mice exhibited significant proliferative glomerulonephritis associated with obliterative sclerosis, and the presence of numerous hyaline cysts is indicated by arrowheads in (C). In contrast, BXSB mice exhibited proliferative glomerulonephritis associated with significant interstitial nephritis but little observable sclerosis as shown in (D). In all cases, the mice were assessed 6 months after bone marrow transfer. C57BL/6 panels [(A) and (B)] represent normal controls for comparison.

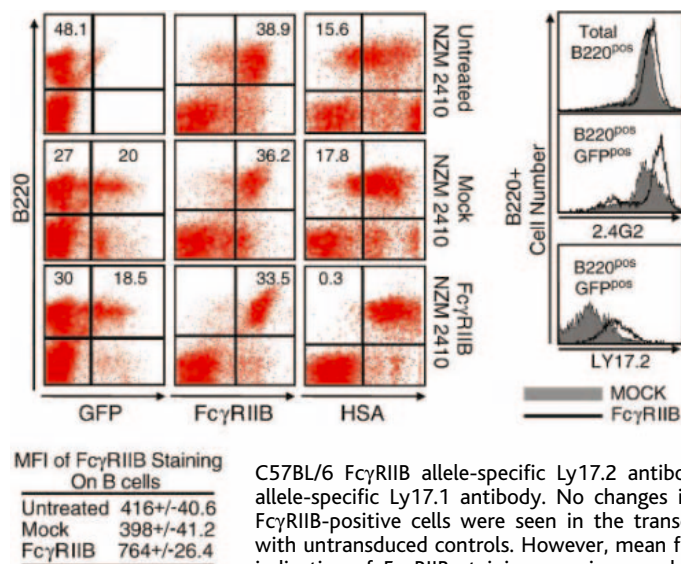


Fig. 4. FcγRIIB retroviral transduction reduces B cell activation and increases FcγRIIB expression on B cells. Five months after bone marrow transduction, B220+ splenocytes were collected and analyzed for GFP expression and FcγRIIB expression and activation. B cells were also examined for total FcγRIIB expression as assessed by staining with either the FcγRIIB/III-specific antibody 2.4G2, the C57BL/6 FcγRIIB allele-specific Ly17.2 antibody, or the NZM FcγRIIB allele-specific Ly17.1 antibody. No changes in the numbers of B220/FcγRIIB-positive cells were seen in the transduced mice as compared with untransduced controls. However, mean fluorescent intensity (MFI) indicative of FcγRIIB staining was increased by 43% on B cells. This increase in FcγRIIB expression is caused by the expression of the retroviral-encoded Ly17.2-detected FcγRIIB gene. Panels show representative samples from groups of five or six mice.

tributes to the maintenance of tolerance is still under investigation, we have recently demonstrated that RIBB expression on B cells regulates the accumulation of autoreactive plasma cells (25). Thus, relatively small changes in the surface expression of this receptor appear to be critical for determining disease progression, and these changes provide a rational basis for a therapeutic approach based on manipulating the expression of this receptor to restore tolerance in cases of autoimmune disease.

References and Notes

- J. W. Kappler, N. Roehm, P. Marrack, *Cell* **49**, 273 (1987).
- J. W. Kappler, U. Staerz, J. White, P. C. Marrack, *Nature* **332**, 35 (1988).
- D. Nemazee, K. Buerki, *Proc. Natl. Acad. Sci. U.S.A.* **86**, 8039 (1989).
- G. J. Nossal, B. L. Pike, *Proc. Natl. Acad. Sci. U.S.A.* **77**, 1602 (1980).
- R. H. Schwartz, D. L. Mueller, M. K. Jenkins, H. Quill, *Cold Spring Harbor Symp. Quant. Biol.* **54**, 605 (1989).
- S. L. Tiegs, D. M. Russell, D. Nemazee, *J. Exp. Med.* **177**, 1009 (1993).
- M. Z. Radic, J. Erikson, S. Litwin, M. Weigert, *J. Exp. Med.* **177**, 1165 (1993).
- C. Bouneaud, P. Kourilsky, P. Bousso, *Immunity* **13**, 829 (2000).
- J. Yan, M. J. Mamula, *J. Immunol.* **168**, 3188 (2002).
- T. N. Marion, M. R. Krishnan, M. A. Steeves, D. D. Desai, *Curr. Dir. Autoimmun.* **6**, 123 (2003).
- T. J. Vyse, B. L. Kotzin, *Annu. Rev. Immunol.* **16**, 261 (1998).
- N. R. Pritchard, K. G. Smith, *Immunology* **108**, 263 (2003).
- L. Morel et al., *Proc. Natl. Acad. Sci. U.S.A.* **97**, 6670 (2000).
- S. Bolland, J. V. Ravetch, *Immunity* **13**, 277 (2000).
- Y. Jiang et al., *Int. Immunol.* **11**, 1685 (1999).
- Y. Jiang et al., *Immunogenetics* **51**, 429 (2000).
- N. R. Pritchard et al., *Curr. Biol.* **10**, 227 (2000).
- Y. Xiu et al., *J. Immunol.* **169**, 4340 (2002).
- T. L. McGaha, B. Sorrentino, J. V. Ravetch, data not shown.
- P. M. Challita, D. B. Kohn, *Proc. Natl. Acad. Sci. U.S.A.* **91**, 2567 (1994).
- S. R. Cherry, D. Biniszkievicz, L. van Parijs, D. Baltimore, R. Jaenisch, *Mol. Cell. Biol.* **20**, 7419 (2000).
- C. Lange, T. Blankenstein, *Gene Ther.* **4**, 303 (1997).
- A. H. Lund, M. Duch, F. S. Pedersen, *J. Biomed. Sci.* **3**, 365 (1996).
- C. A. Klug, S. Cheshier, I. L. Weissman, *Blood* **96**, 894 (2000).
- H. Fukuyama, F. Nimmerjahn, J. V. Ravetch, *Nature Immunol.* **6**, 99 (2005).
- Supported by grants from NIH and the Alliance for Lupus Research (J.V.R.) and by a National Research Service Award (T.L.M.). We thank P. Smith and M. Patt for their technical assistance and R. Steinman, M. Nussenzweig, M. Madaio, and P. Bruhns for helpful comments.

Supporting Online Material

www.sciencemag.org/cgi/content/full/307/5709/590/DC1

Materials and Methods

Figs. S1 to S6

Table S1

References

13 September 2004; accepted 30 November 2004
10.1126/science.1105160

Endogenous MHC Class II Processing of a Viral Nuclear Antigen After Autophagy

Casper Paludan,^{1,2*} Dorothee Schmid,^{1,2*} Markus Landthaler,³ Martina Vockerodt,⁴ Dieter Kube,⁵ Thomas Tuschl,³ Christian Münz^{1,2,†}

CD4⁺ T cells classically recognize antigens that are endocytosed and processed in lysosomes for presentation on major histocompatibility complex (MHC) class II molecules. Here, endogenous Epstein-Barr virus nuclear antigen 1 (EBNA1) was found to gain access to this pathway by autophagy. On inhibition of lysosomal acidification, EBNA1, the dominant CD4⁺ T cell antigen of latent Epstein-Barr virus infection, slowly accumulated in cytosolic autophagosomes. In addition, inhibition of autophagy decreased recognition by EBNA1-specific CD4⁺ T cell clones. Thus, lysosomal processing after autophagy may contribute to MHC class II-restricted surveillance of long-lived endogenous antigens including nuclear proteins relevant to disease.

The main protein degradation machineries in eukaryotic cells are the proteasome and lysosomal proteases. The immune system monitors the products of these catabolic processes for pathogenic determinants. For this purpose, peptides generated by the proteasome are presented on MHC class I products, whereas products of lysosomal degradation are displayed on MHC class II

(1, 2). CD8⁺ and CD4⁺ T cells survey these MHC class I and II complexes, respectively. Classically, CD8⁺ T cell epitopes are of endogenous origin, synthesized in the antigen presenting cell (APC), whereas CD4⁺ T cell epitopes are of exogenous origin, endocytosed by the APC. However, analysis of natural ligands eluted from MHC class II molecules has revealed that a large proportion of MHC II-bound peptides are derived from endogenous antigens (3).

In addition, endogenous MHC class II processing has been described for self-[GAD65 (4), complement C5 (5), and immunoglobulin light chain λ 2 (6)], viral [influenza matrix protein (7), influenza nucleoprotein (8), and influenza hemagglutinin (9)], and model antigens [hen egg lysozyme (10) and neomycin phosphotransferase II (11)]. However, these studies all involved overexpression and

often ectopic expression of the antigens by transfection or infection with recombinant viral vectors. To date, the underlying endogenous MHC class II processing pathways are poorly characterized at the cell biology level.

We investigated endogenous MHC class II processing of the nuclear antigen 1 (EBNA1) of the Epstein-Barr virus (EBV). EBNA1 is the dominant EBV-latent antigen for CD4⁺ T cells and can be detected by CD4⁺ T cells after endogenous MHC class II processing in EBV-positive lymphoma cells (12). In order to address whether EBNA1 could enter MHC class II processing via lysosomal degradation, we incubated EBV-transformed lymphoblastoid cells (LCLs) with inhibitors of lysosomal acidification, ammonium chloride (Fig. 1) or chloroquine (13), for 2 days (14). On blocking of lysosomal acidification, EBNA1 accumulated in cytosolic vesicles, partially co-staining with the lysosome-resident protein LAMP1 (Fig. 1A). Subcellular fractionation confirmed that EBNA1 was enriched in microsomes on blocking of lysosomal acidification (Fig. 1B). In EBNA1 transfectants of the EBV-negative Hodgkin's lymphoma cell line L428 (L428E1PC5), EBNA1 was confined to whole-cell lysate and the nuclear fraction. After chloroquine treatment, EBNA1 could be found in the postnuclear supernatant and the high-speed pellet derived thereof. Discontinuous sucrose gradient centrifugation revealed that EBNA1 had accumulated in microsomes after chloroquine treatment. EBNA1 fractionated together with the lysosomal marker LAMP1. Accumulation of EBNA1 in microsomes after chloroquine inhibition was confirmed in the EBV-transformed B cell line LG2 (Fig. 1C). EBNA1, but not another nuclear EBV antigen and prominent CD8⁺ T cell antigen, EBNA3A, was enriched in the microsomal fraction after

¹Laboratory of Viral Immunobiology, ²Christopher H. Browne Center for Immunology and Immune Diseases, ³Laboratory of RNA Molecular Biology, Rockefeller University, New York, NY 10021, USA. ⁴Pediatrics I, ⁵Center for Internal Medicine, Hematology, and Oncology, Georg August University of Göttingen, 37099 Göttingen, Germany.

*These authors contributed equally to the presented work.

†To whom correspondence should be addressed. E-mail: munzc@mail.rockefeller.edu

chloroquine treatment. These results demonstrate that EBNA1 accumulates in cytosolic, partially lysosomal vesicles upon inhibition of acidification.

Next, we investigated whether EBNA1 follows an autophagic route to lysosomes. Autophagy is involved in the steady-state turnover of long-lived proteins and damaged organelles (15). During this process, cytoplasmic material is enveloped into double-membrane vesicles, which then fuse with lysosomes (16). This fusion can be prevented by inhibition of lysosomal acidification (17). Thus, autophagosomes accumulated in chloroquine-treated LCLs (Fig. 2A) and could be specifically visualized with the fluorescent dye monodansylcadaverine (MDC) (18). The majority of cytosolic EBNA1 was found in these large, usually less than 10 MDC⁺ vesicles (Fig. 2A), of which only a part co-stained for LAMP1 (13). To assess whether the ultrastructural features of EBNA1-containing vesicles conform to previously described autophagic vacuoles, we performed immuno-electron microscopy (IEM) on sections of EBNA1-transfected L428 Hodgkin's lymphoma cells. On inhibition of lysosomal acidification, EBNA1 could be observed in cytosolic vesicles, surrounded by double membranes (Fig. 2C, black arrows). Some of these structures had the cup-shaped appearance of forming autophagosomes (Fig. 2C, middle). An isotype control antibody produced no staining (13). Thus, autophagy participates in the delivery of EBNA1 to lysosomes.

To assess the kinetics of EBNA1 degradation via autophagosomes, we followed cytosolic EBNA1 after removal of lysosomotropic reagents. After 2 days of chloroquine or ammonium chloride treatment, a substantial amount of EBNA1 accumulated in cytosolic vesicles of LCLs (fig. S1A) (13). After removal of the lysosomotropic reagents, cytosolic EBNA1 was degraded with a half-life of around 30 min (fig. S1B). Thus, EBNA1 accumulation in autophagosomes and lysosomes represents a short-lived intermediate state of EBNA1 degradation, which can be stabilized by inhibition of lysosomal acidification.

Many long-lived proteins are substrates for autophagy (15). One well-characterized example of autophagic protein degradation is the proteasome (19–21). In chloroquine- or ammonium chloride-treated cells, the proteasome 20S core particle accumulated in cytoplasmic vesicles, most of which also co-stained for EBNA1 (fig. S2) (13). Thus, EBNA1 and a known autophagy substrate, the proteasome, accumulate in the same vesicles on inhibition of lysosomal acidification.

In order to test whether autophagy leads to endogenous MHC class II processing of EBNA1, we determined whether inhibition

of this pathway would block antigen presentation to EBNA1-specific CD4⁺ T cell clones (22, 23). Treatment with the autophagy inhibitor 3-methyladenine (24) for 2 to 4 days decreased EBNA1-specific CD4⁺ T cell recognition of EBV-transformed B cells and EBNA1-transfected Hodgkin's lymphoma cells by 30 to 70% in interferon- γ (IFN- γ) enzyme-linked immunospot (ELISPOT) assays, whereas the proteasome inhibitor lactacystin (25) had little effect (Fig. 3A). Furthermore, we used RNA interference to silence the essential autophagy gene *Atg12*. *Atg12* is a small ubiquitin-like protein, and its complex with *Atg5* is essential for autophagosome formation (26, 27). Small interfering RNAs (siRNAs) against two different regions of *Atg12* (*Atg12.1* and *Atg12.2*), but not a green fluorescent protein (GFP)-specific siRNA, down-regulated efficiently the *Atg12* mRNA level (Fig. 3B). Knockdown of *Atg12* with both siRNAs decreased the IFN- γ response of EBNA1-specific CD4⁺ T cells by 40 to 60%, whereas treatment with the GFP siRNA had no effect ($P = 0.0002$ for *Atg12.1* versus mock, $P = 0.0030$ for *Atg12.1* versus GFP, $P = 0.0004$ for *Atg12.2* versus mock, and $P = 0.0014$ for *Atg12.2* versus GFP). In contrast, EBNA3A recognition by the CD8⁺ T cell clone MS.B11 was not affected by the

Atg12 knockdown (Fig. 3C). Treatment with 3-methyladenine or *Atg12*-specific siRNAs did not affect the MHC class II levels on the B cell lines (Fig. 3D). In addition, recognition of inhibitor- or siRNA-treated target cells could be completely restored by pulsing the cells with the cognate T cell epitopes before ELISPOT or enzyme-linked immunosorbent assay (ELISA) (13). Furthermore, exogenous MHC class II processing of EBNA1 could be excluded, because LCLs were unable to sensitize bystander B cells for EBNA1-specific CD4⁺ T cell recognition (12) and EBNA1 was undetectable in the supernatants of LCL- and EBNA1-transfected L428 cells with the use of ELISAs (detection limit was 0.1 μ g/ml), whereas 1 to 10 μ g/ml were necessary to increase CD4⁺ T cell detection of EBV⁺ and EBV⁻ B cell lines (13). Thus, blocking of autophagy specifically inhibits endogenous MHC class II processing of EBNA1 but not the presentation of the MHC class I-restricted antigen EBNA3A.

Autophagy has been suggested as the main degradation pathway for long-lived proteins (15), whereas short-lived proteins are probably mainly regulated by proteasomal processing (28). A long half-life is also characteristic for EBNA1 (29) and the proteasome (20, 21). Whereas we find

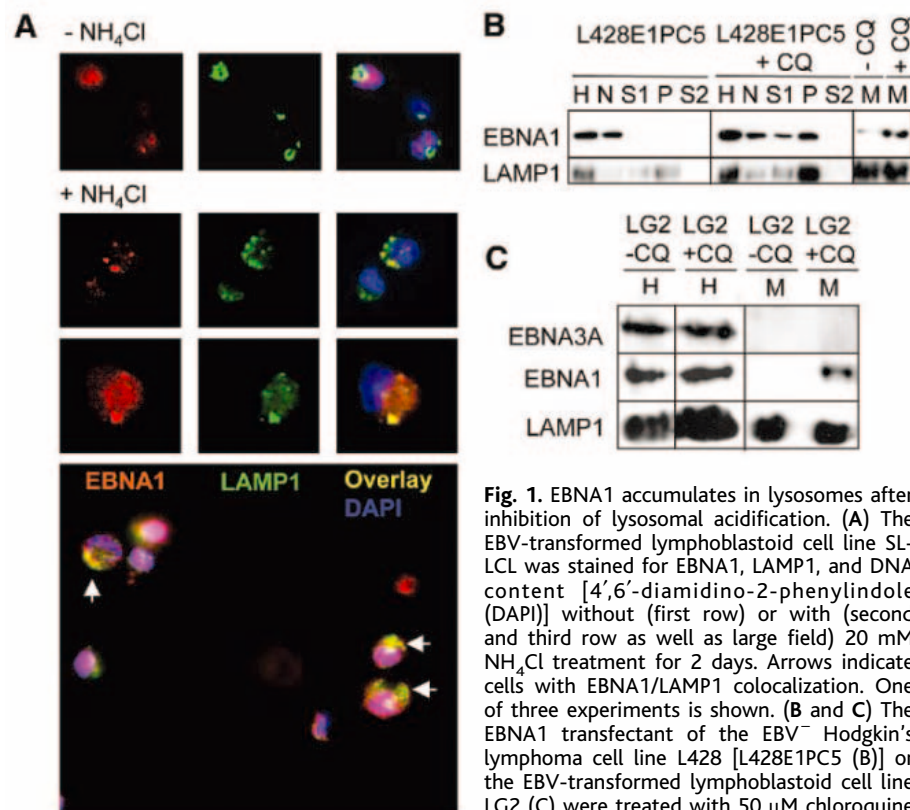


Fig. 1. EBNA1 accumulates in lysosomes after inhibition of lysosomal acidification. (A) The EBV-transformed lymphoblastoid cell line SL-LCL was stained for EBNA1, LAMP1, and DNA content [4',6'-diamidino-2-phenylindole (DAPI)] without (first row) or with (second and third row as well as large field) 20 mM NH₄Cl treatment for 2 days. Arrows indicate cells with EBNA1/LAMP1 colocalization. One of three experiments is shown. (B and C) The EBNA1 transfectant of the EBV⁻ Hodgkin's lymphoma cell line L428 [L428E1PC5 (B)] or the EBV-transformed lymphoblastoid cell line LG2 (C) were treated with 50 μ M chloroquine for 3 days (+CQ). After homogenization (H), intact cells and nuclei (N) were pelleted (twice at 3000 g for 10 min), and the postnuclear supernatant (S1) was centrifuged at 100,000 g for 1 hour to obtain a microsomal pellet (P) and a postmicrosomal supernatant (S2). Mirosomes were further purified from the interphase of a two-step sucrose gradient (2 M/0.5 M sucrose; M). EBNA1, EBNA3A, and the lysosomal marker LAMP1 were visualized by Western blot analysis (B and C). One of nine experiments is shown.

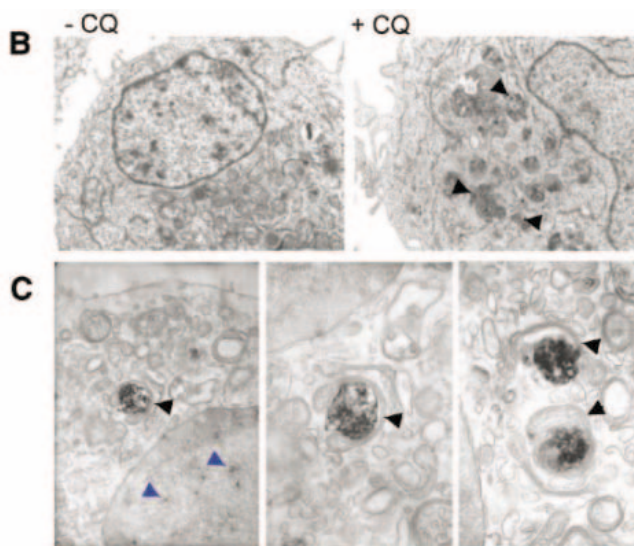
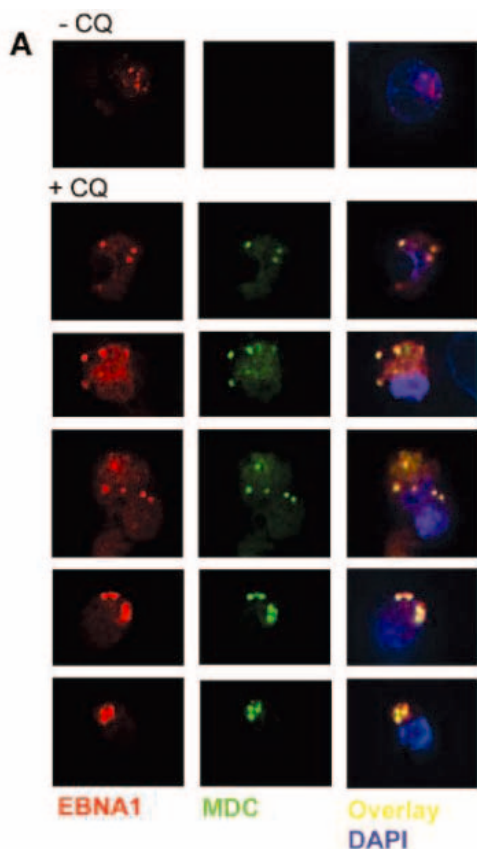


Fig. 2. EBNA1 localizes to autophagosomes upon inhibition of lysosomal acidification. (A) The lymphoblastoid cell line SL-LCL was stained for EBNA1, autophagic vesicles (MDC), and DNA content (DAPI) in the absence (-CQ) or presence (+CQ) of 50 to 100 μ M chloroquine. One of 10 experiments is shown. (B) Electron micrographs of cell organelle morphology in chloroquine-treated (+CQ) or untreated (-CQ) EBNA1-transfected L428 Hodgkin's lymphoma cells. Black arrows indicate electron-dense autophagosomes or lysosomes. (C) Electron micrographs of chloroquine-treated EBNA1-transfected L428 Hodgkin's lymphoma cells stained for EBNA1 with the monoclonal antibody 5F12. Blue arrows indicate nuclear EBNA1; black arrows, EBNA1 in forming or mature autophagosomes. One of three experiments is shown.

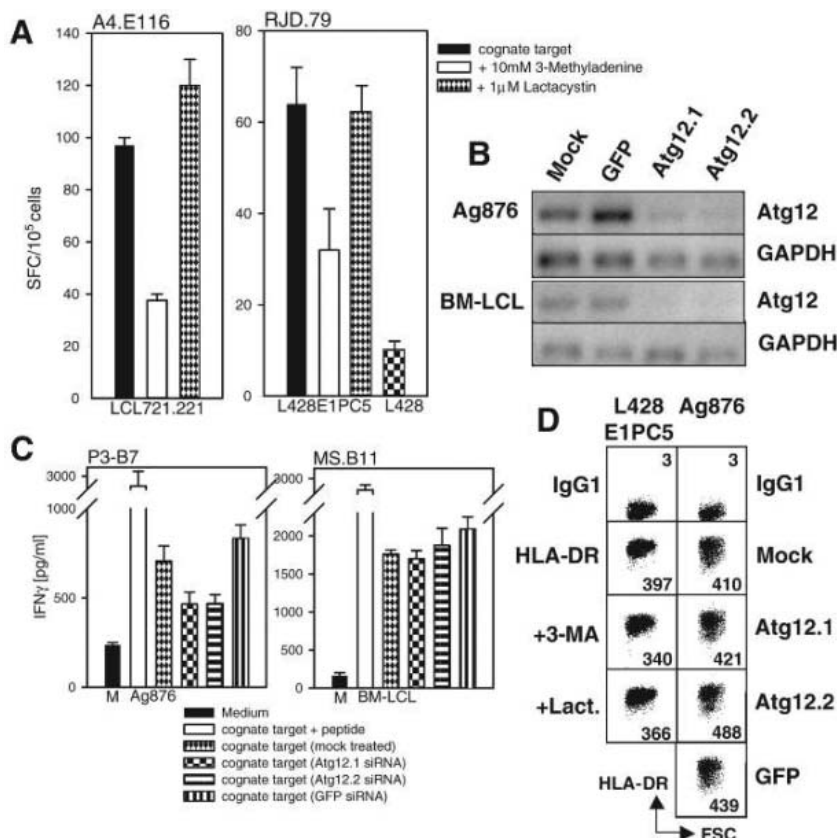


Fig. 3. Blocking of autophagy leads to down-regulation of MHC class II-restricted CD4⁺ T cell recognition of EBNA1. (A) The EBNA1-specific CD4⁺ T cell clones A4.E116 and RJD.79 were stimulated with cognate target cells [A4.E116 with human histocompatibility leukocyte antigen (HLA)-DR1+EBV+ LCL721.221, RJD.79 with HLA-DQ2/3+EBNA1+ L428E1PC5, and HLA-DQ2/3+EBNA1- L428 as a negative control] in IFN- γ ELISPOT assays. Where indicated, targets were pretreated with 10 mM 3-methyladenine or 1 μ M lactacystin for 2 to 4 days. One of four experiments is shown. Error bars indicate standard deviations. (B) mRNA levels of glyceraldehyde-3-phosphate dehydrogenase and Atg12 were analyzed on day 4 after knockdown with GFP- or Atg12-siRNAs (Atg12.1 and Atg12.2) with use of semiquantitative reverse transcription polymerase chain reaction. The results are representative of five experiments and correspond to the experiment shown in (C). (C) IFN- γ ELISAs on supernatants of the EBNA1-specific CD4⁺ T cell clone P3-B7 and the EBNA3A-specific CD8⁺ T cell clone MS.B11, co-cultured with cognate target cells (P3-B7 with HLA-DP3+ Ag876 and MS.B11 with HLA-B8+ BM-LCL). Where indicated, targets were electroporated with 10 μ M siRNA twice in 4 days before overnight culture with T cells. One of three experiments is shown. Error bars indicate standard deviations. (D) HLA-DR surface levels after treatment with 10 mM 3-methyladenine (3-MA) and 1 μ M lactacystin for EBNA1-transfected L428 Hodgkin's lymphoma cells (L428E1PC5, left) or with GFP- and Atg12-siRNAs (Atg12.1 and Atg12.2) for the EBV-transformed B cell line Ag876 (right). Mean fluorescence values are given in the flow cytometer blots. One of two experiments is shown.

autophagy and lysosomal processing of full-length EBNA1 for MHC class II presentation, glycine-alanine repeat-deleted EBNA1 and defective ribosomal products (DRiPs) of EBNA1 were described to be short-lived and processed by the proteasome for efficient presentation by MHC class I (30–33). Similarly, influenza's matrix protein follows in part a proteasome and transporter associated with antigen processing-independent, chloroquine-sensitive but brefeldin A-insensitive endogenous MHC class II processing pathway. Long-lived forms of this antigen were primarily processed onto MHC class II, but short-lived forms mainly onto MHC class I (7, 34). Lastly, the most prominent sources of natural MHC class II ligands are long-lived cytosolic or nuclear antigens, and natural MHC class I ligands primarily originate from short-lived proteins (table S1). Thus, MHC class II processing after autophagy might contribute to CD4⁺ T cell recognition of long-lived viral and tumor antigens.

Apart from APCs like EBV-transformed B cells, MHC class II presentation of endogenous antigens might be especially relevant in MHC class II-positive tissues with low phagocytic ability. At sites of inflammation, many cell types like epithelial cells up-regulated MHC class II and were found to be surrounded by cytolytic CD4⁺ T cells (35–37). Thus, CD4⁺ T cells may play a role in immune surveillance of APCs and inflamed

tissues after endogenous MHC class II processing involving autophagy, and EBNA1 is the first pathogen-derived antigen found to follow this pathway.

References and Notes

1. R. Busch, R. C. Doebele, N. S. Patil, A. Pashine, E. D. Mellins, *Curr. Opin. Immunol.* **12**, 99 (2000).
2. E. Pamer, P. Cresswell, *Annu. Rev. Immunol.* **16**, 323 (1998).
3. H. Rammensee, J. Bachmann, N. P. Emmerich, O. A. Bachor, S. Stevanovic, *Immunogenetics* **50**, 213 (1999).
4. J. D. Lich, J. F. Elliott, J. S. Blum, *J. Exp. Med.* **191**, 1513 (2000).
5. M. I. Brazil, S. Weiss, B. Stockinger, *Eur. J. Immunol.* **27**, 1506 (1997).
6. S. Weiss, B. Bogen, *Cell* **64**, 767 (1991).
7. D. Jaraquemada, M. Marti, E. O. Long, *J. Exp. Med.* **172**, 947 (1990).
8. M. S. Malnati *et al.*, *Nature* **357**, 702 (1992).
9. G. Aichinger *et al.*, *J. Biol. Chem.* **272**, 29127 (1997).
10. L. C. Bonifaz, S. Arzate, J. Moreno, *Eur. J. Immunol.* **29**, 119 (1999).
11. F. Nimmerjahn *et al.*, *Eur. J. Immunol.* **33**, 1250 (2003).
12. C. Münz *et al.*, *J. Exp. Med.* **191**, 1649 (2000).
13. C. Paludan, D. Schmid, C. Münz, unpublished data.
14. Material and methods can be found on Science Online.
15. P. E. Stromhaug, D. J. Klionsky, *Traffic* **2**, 524 (2001).
16. D. J. Klionsky, S. D. Emr, *Science* **290**, 1717 (2000).
17. A. Yamamoto *et al.*, *Cell Struct. Funct.* **23**, 33 (1998).
18. A. Biederbick, H. F. Kern, H. P. Elsasser, *Eur. J. Cell Biol.* **66**, 3 (1995).
19. A. M. Cuervo, A. Palmer, A. J. Rivett, E. Knecht, *Eur. J. Biochem.* **227**, 792 (1995).
20. K. B. Hendil, *Biochem. Int.* **17**, 471 (1988).
21. K. Tanaka, A. Ichihara, *Biochem. Biophys. Res. Commun.* **159**, 1309 (1989).
22. C. Paludan *et al.*, *J. Immunol.* **169**, 1593 (2002).
23. K. S. Voo *et al.*, *Cancer Res.* **62**, 7195 (2002).

24. P. O. Seglen, P. B. Gordon, *Proc. Natl. Acad. Sci. U.S.A.* **79**, 1889 (1982).
25. G. Fenteany *et al.*, *Science* **268**, 726 (1995).
26. N. Mizushima *et al.*, *J. Cell Biol.* **152**, 657 (2001).
27. A. Kuma, N. Mizushima, N. Ishihara, Y. Ohsumi, *J. Biol. Chem.* **277**, 18619 (2002).
28. M. F. Princiotto *et al.*, *Immunity* **18**, 343 (2003).
29. J. Levitskaya, A. Sharipo, A. Leonchiks, A. Ciechanover, M. G. Masucci, *Proc. Natl. Acad. Sci. U.S.A.* **94**, 12616 (1997).
30. S. P. Lee *et al.*, *J. Exp. Med.* **199**, 1409 (2004).
31. K. S. Voo *et al.*, *J. Exp. Med.* **190**, 459 (2004).
32. J. Tellam *et al.*, *J. Exp. Med.* **199**, 1421 (2004).
33. Y. Yim, B. Manoury, R. Fähræus, *Science* **301**, 1371 (2003).
34. M. Gueguen, E. O. Long, *Proc. Natl. Acad. Sci. U.S.A.* **93**, 14692 (1996).
35. Z. Wu, E. R. Podack, J. M. McKenzie, K. J. Olsen, M. Zakarija, *Clin. Exp. Immunol.* **98**, 470 (1994).
36. S. Muller *et al.*, *Am. J. Pathol.* **152**, 261 (1998).
37. N. Yawalkar *et al.*, *Am. J. Pathol.* **158**, 803 (2001).
38. We thank E. Sphicas of the Bio-Imaging Resource Center of Rockefeller University for expert technical assistance in electron microscopy and R. M. Steinman for critically reading the manuscript. This work was funded by the Leukemia and Lymphoma Society and by the New York Academy of Medicine (C.M.). D.S. was supported by a Deutscher Akademischer Austausch Dienst fellowship and Rockefeller University's Graduate Program.

Supporting Online Material

www.sciencemag.org/cgi/content/full/1104904/DC1
 SOM Text
 Figs S1 and S2
 Table S1
 References and Notes

7 September 2004; accepted 26 November 2004
 Published online 9 December 2004;
 10.1126/science.1104904
 Include this information when citing this paper.

Small CTD Phosphatases Function in Silencing Neuronal Gene Expression

Michele Yeo,^{1*†} Soo-Kyung Lee,^{2*‡} Bora Lee,^{2‡}
 Esmeralda C. Ruiz,² Samuel L. Pfaff,² Gordon N. Gill^{1§}

Neuronal gene transcription is repressed in non-neuronal cells by the repressor element 1 (RE-1)-silencing transcription factor/neuron-restrictive silencer factor (REST/NRSF) complex. To understand how this silencing is achieved, we examined a family of class-C RNA polymerase II (RNAPII) carboxyl-terminal domain (CTD) phosphatases [small CTD phosphatases (SCPs) 1 to 3], whose expression is restricted to non-neuronal tissues. We show that REST/NRSF recruits SCPs to neuronal genes that contain RE-1 elements, leading to neuronal gene silencing in non-neuronal cells. Phosphatase-inactive forms of SCP interfere with REST/NRSF function and promote neuronal differentiation of P19 stem cells. Likewise, small interfering RNA directed to the single *Drosophila* SCP unmasks neuronal gene expression in S2 cells. Thus, SCP activity is an evolutionarily conserved transcriptional regulator that acts globally to silence neuronal genes.

The central nervous system is derived from neuroepithelial precursor cells within the ventricular zone that are poised to produce a wide array of specialized neuronal and glial cell types upon receiving the appropriate differentiation signals. The timing and

specificity of neuronal gene expression are regulated by activator and repressor systems that gate the proper pattern of transcription. One of the best-characterized transcription factors for controlling neuronal gene expression at a global level is the repressor ele-

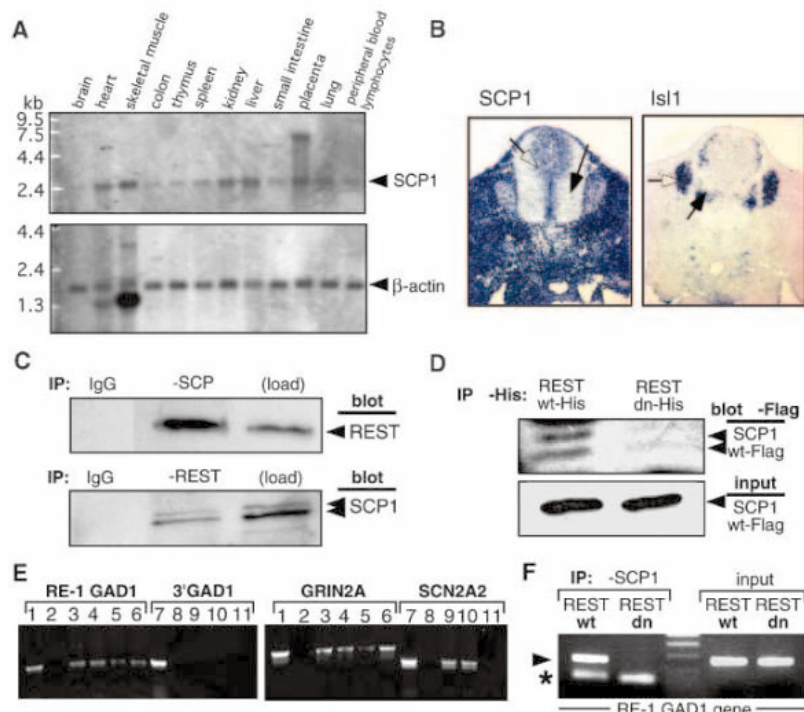
ment 1 (RE-1)-silencing transcription factor/neuron-restrictive silencer factor (REST/NRSF) repressor protein, which is involved in suppressing both premature and nonspecific neuronal gene expression (1–3). The Zn²⁺-finger-containing protein REST/NRSF binds the 23-base pair RE-1 DNA element found in many neuronal genes and then nucleates the formation of a multiprotein complex that represses gene transcription by deacetylating histones and methylating both DNA and histone H3 (4–6). These covalent modifications of chromatin reduce transcription, leading to silencing of neuronal gene expression.

We recently identified a family of three closely related human class-C phosphatases with specificity for serine 5 in the C-terminal domain (CTD) of RNA polymerase

¹Department of Medicine, University of California, San Diego, 9500 Gilman Drive, La Jolla, CA 92093, USA.
²The Gene Expression Laboratory, Salk Institute, La Jolla, CA 92037, USA.

*These two authors contributed equally to this work.
 †Present address: Neurology Division, Duke University Medical Center, Durham, NC 27710, USA.
 ‡Present address: Department of Molecular and Cellular Biology, Huffington Center on Aging, Baylor College of Medicine, One Baylor Plaza, Room 132C, Houston, TX 77030, USA.
 §To whom correspondence should be addressed.
 E-mail: ggill@ucsd.edu

Fig. 1. SCP is a component of the REST/NRSF complex (A) Northern blot analysis of the expression of SCP1 in human tissues showing lack of expression in nervous tissue. (B) In situ hybridization analysis of the expression of SCP1 and *Isl1* in E10.5 mouse cervical spinal cord. SCP1 is widely expressed in cells surrounding the developing spinal cord and in proliferating neuroepithelial cells within the ventricular zone (open arrow), but not in lateral differentiated cells (solid arrow). *Isl1* labels differentiated motor neurons (solid arrow) and dorsal root ganglion sensory neurons (open arrow), which are areas where SCP1 is not expressed. (C) Coimmunoprecipitation of SCP1 and REST/NRSF. HEK293 cell extracts were immunoprecipitated with antibodies to SCP (upper panel) or REST/NRSF (lower panel). Immunoprecipitates were resolved with SDS-polyacrylamide gel electrophoresis (SDS-PAGE), and associated proteins were identified by Western blot with antibodies to REST/NRSF and SCP1. (D) dnREST/NRSF lacks high affinity for SCP1. P19 cells were transfected with wild-type (wt) His-tagged REST (1082 amino acids) or His-tagged dnREST [DNA binding domain (DBD): 285 amino acids] together with Flag-tagged SCP1. REST-associated proteins were immunoprecipitated with antibody to His-epitope, resolved on SDS-PAGE, and probed with antibody to detect SCP1. Input controls show that Flag-SCP1 expression levels were comparable in both samples. (E) ChIP with antibody to SCP. ChIP assays of HEK293 cells with antibodies to SCP, REST/NRSF, HDAC1, HP1, or control IgG are shown. PCR primers specific for the RE-1 elements of *GAD1*, *GRIN2A*, and *SCN2A2* genes and for the 3' intron-exon region of *GAD1* were used for real time (RT)-PCR. (Left) Lanes 1 to 6 show the RE-1 element of the *GAD1* gene; lanes 7 to 11 show the 3' region of the *GAD1* gene; lanes 1 and 7 represent load controls (1%); lanes 2 and 8 are control IgG; lanes 3 and 9 used antibody to SCP; lanes 4 and 10 used antibody to REST/NRSF; lanes 5 and 11 used antibody to HDAC1; and lane 6 is antibody to HP1. (Right) Lanes 1 to 6 are the RE-1 element of the *GRIN2A* gene; lanes 7 to 11 show the RE-1 element of *SCN2A2* gene; lanes 1 and 7



are load controls (1%); lanes 2 and 8 are control IgG; lanes 3 and 9 are antibodies to SCP; lanes 4 and 10 are antibodies to REST/NRSF; lanes 5 and 11 are antibodies to HDAC1; and lane 6 is antibody to HP1. (F) ChIP demonstrates that SCP1 is recruited to the RE-1 element within the *GAD1* gene (arrowhead), whereas SCP1 is not detected at this site when the truncated dn form of REST/NRSF is present. The asterisk corresponds to a nonspecific primer band.

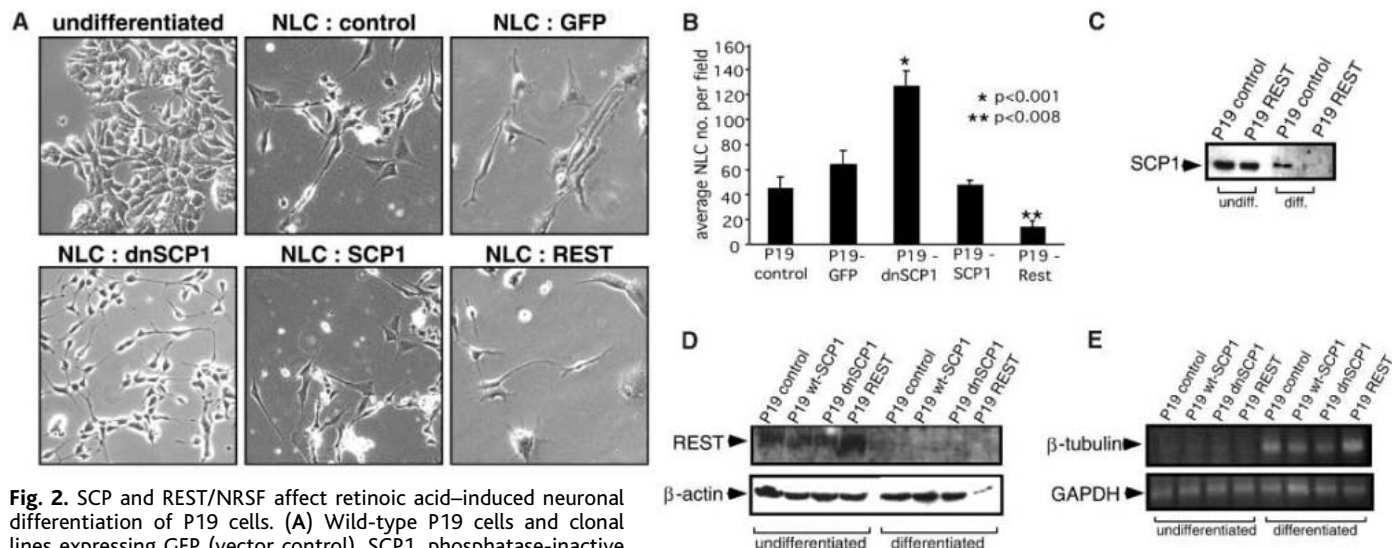


Fig. 2. SCP and REST/NRSF affect retinoic acid-induced neuronal differentiation of P19 cells. (A) Wild-type P19 cells and clonal lines expressing GFP (vector control), SCP1, phosphatase-inactive dnSCP1, or REST/NRSF were induced to differentiate into neuronlike cells (NLCs) by treatment with retinoic acid and growth in neuron-selective medium. (B) Tabulation of the number of NLCs per field. Comparisons were made to control P19 cells with Student's *t* test. (C) Western blot analysis of SCP expression in undifferentiated and retinoic acid-differentiated P19 cells. Densitometry indicates an ~85% reduction in SCP levels in differentiated P19 cells. (D) Western blot

analysis of REST/NRSF protein expression in undifferentiated and retinoic acid-induced differentiated P19 cells. The loading control, β -actin, is low in P19 cells engineered to express REST/NRSF, which reflects the very low number of differentiated cells. (E) RT-PCR quantitation of β -tubulin expression in undifferentiated and differentiated P19 cells.

II (RNAPII) (7). These small CTD phosphatases (SCPs) are localized to the nucleus in a complex with RNAPII and, like the well-characterized CTD phosphatase FCP1, they

negatively regulate RNAPII activity. The x-ray structure of SCP1 has revealed a core fold and an active center similar to those of other phosphohydrolases that share the DXDX(T/V)

amino acid signature motif with SCP1 and FCP1 (8). Although a conserved pocket in the SCPs and FCP1 adjacent to the active site is proposed to bind the CTD of RNAPII

and confer specificity (8), it remains possible that other proteins involved in gene regulation are also targeted by SCPs. The phosphatase activity of SCP1 is required for gene silencing (7). Elevated expression of SCP1 was found to repress transcription, whereas the phosphatase-inactive mutant, dominant negative SCP1 (dnSCP1), enhanced RNAPII activity (7). However, the mechanisms that recruit SCPs to promoters and the biological function of SCPs have remained unknown.

Northern blot analysis revealed that SCP1 is widely expressed in human tissues (Fig. 1A). The highest levels were observed in skeletal muscle, in contrast to the brain, which contained very low levels of SCP1 (Fig. 1A). To determine whether another SCP family member was expressed in the brain, we also probed for SCP2 and SCP3 (fig. S1). The entire SCP family is largely excluded from the adult nervous system, whereas non-neuronal tissues expressed high levels of SCP1, -2, and -3 RNA.

To define the embryonic pattern of SCP expression, *in situ* hybridization was carried out on mice at embryonic day 10.5 (E10.5). SCP1 was widely expressed in mesenchymal and ectodermal cells and in undifferentiated neuroepithelial cells (Fig. 1B). Although SCP1 was widely expressed in cervical tissues, we noted two prominent sites where it appeared to be absent: differentiating dorsal root ganglion neurons and postmitotic spinal neurons (Fig. 1B). This pattern of expression does not appear to correspond to proliferating versus nonproliferating cell populations, because SCP1 was expressed broadly in both proliferating mesenchymal and nonproliferating muscle cells. Rather, the pattern of SCP1 to -3 expression paralleled that of REST/NRSF, which is found widely in non-neuronal tissues but is excluded from neuronal cells (fig. S1) (1, 2).

The pattern of exclusion of SCPs from differentiated nervous tissue suggested that these phosphatases might function with

REST/NRSF to silence neuronal gene expression. We first examined possible interactions between SCP and REST/NRSF by using coimmunoprecipitation of the endogenous proteins in HEK293 cells. SCP immunoprecipitates were found to contain REST/NRSF, and REST/NRSF immunoprecipitates contained SCP (Fig. 1C). However, a truncated form of REST/NRSF was found to act as a dominant negative (3) and was unable to bind SCP1 (Fig. 1D). The coexpression and interaction between full-length REST/NRSF and SCP1 suggests that they form a physical complex in non-neuronal cells.

To determine whether SCP was targeted to RE-1 elements *in vivo*, we used chromatin immunoprecipitation (ChIP) with SCP antibodies and polymerase chain reaction (PCR) primers specific for the REST/NRSF binding elements of the Na⁺ channel II (*SCN2A2*), glutamate receptor (*GRIN2A*), and glutamic acid decarboxylase (*GADI*) genes (fig. S3) (9). These results were compared with ChIP by using antibody to REST/NRSF and a control immunoglobulin. As shown in Fig. 1E, both SCP and REST/NRSF are associated with RE-1 regulatory sites in the neuronal genes *GADI*, *GRIN2A*, and *SCN2A2*. As expected, this interaction was not detected with control immunoglobulin antibodies or probes for non-RE-1 sequences in the 3' end of the *GADI* gene. Likewise, neither REST/NRSF nor heterochromatin protein 1 (HP1) were detected at chromatin sites within the 3' region of *GADI*. The recruitment of SCP1 to RE-1 elements appeared to be mediated directly by REST/NRSF, because SCP1 is not detected at RE-1 elements in the presence of dnREST, which lacks the ability to recruit SCP1 (Fig. 1, D and F).

Next we examined the localization of other known components of the REST/NRSF silencing complex by using ChIP. Antibodies to histone deacetylase 1 (HDAC1), HP1, and MeCp2 detected each of these chromatin-bound proteins at RE-1 elements (Fig. 1E) (10). We did not identify HDAC1 on the *SCN2A2* promoter, which agrees with observations that this gene was not activated by the HDAC inhibitor trichostatin A (9, 11). Thus, SCP is included with other known silencer components at RE-1 REST/NRSF binding sites, although cell type and promoter differences in the exact composition of these nucleoprotein complexes probably exist.

P19 mouse embryonic stem cells can be induced to undergo neuronal differentiation by treatment with retinoic acid (12) or the basic helix-loop-helix (bHLH) transcription factor neurogenin 2 (Ngn2) (13, 14). As expected for potential negative regulators of neuronal differentiation, SCP1 and REST/NRSF are both expressed in replicating P19 stem cells but expression of both proteins is extinguished as these cells become neurons

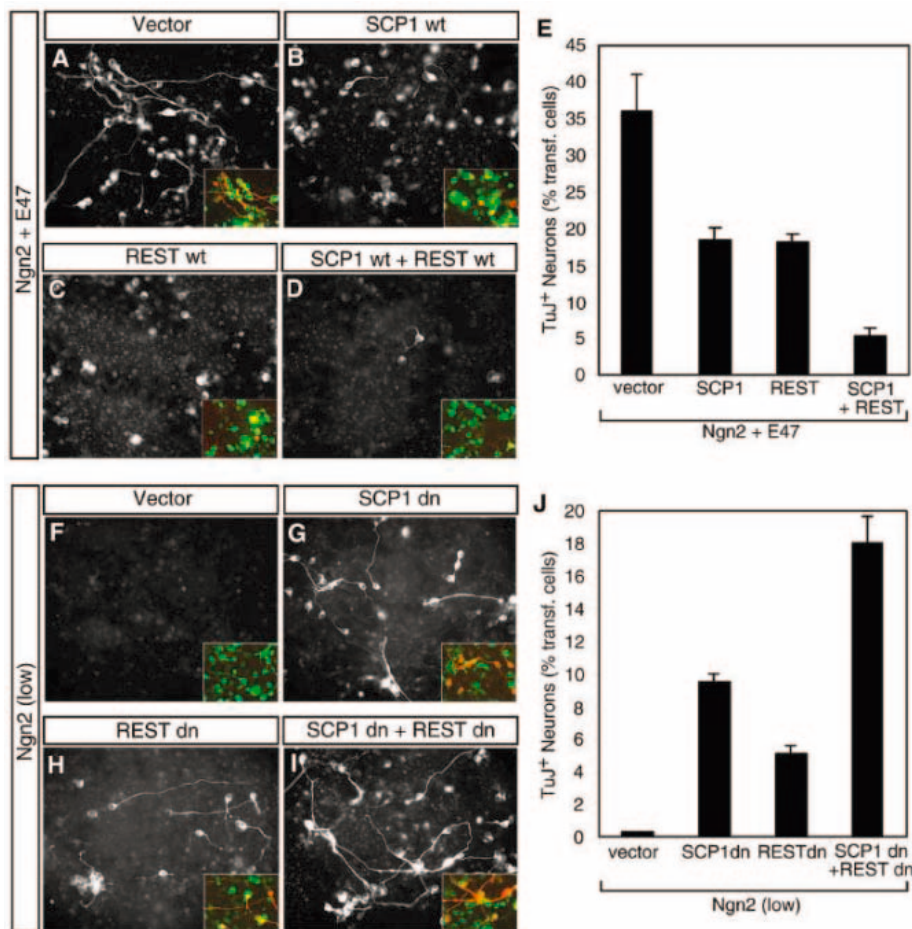


Fig. 3. SCP and REST/NRSF control Ngn2-induced neuronal differentiation (A to E) P19 stem cells were transfected with Ngn2-internal ribosome entry site (ires)-GFP plus E47 without or with SCP1 and REST/NRSF. Neurons were identified by morphology and by staining with the antibody to β III-tubulin TuJ1 (inset, red). The fraction of Ngn2-transfected cells (green) that were TuJ1-positive (red) is tabulated in (E). (F to J) P19 stem cells were transfected with Ngn2 without E47 in the absence or presence of dnSCP1 and dnREST/NRSF. The fraction of Ngn2-transfected cells (green) that were TuJ1-positive (red) is tabulated in (J).

(Fig. 2, C and D) (15). The transition point of SCP and REST/NRSF down-regulation is associated with the up-regulation of neuron-specific genes such as that which codes for β -tubulin (Fig. 2E). To examine the role of SCP1 in neuronal differentiation, we generated clonal P19 cell lines constitutively expressing the following: SCP1; a mutant phosphatase-inactive dnSCP1, where Asp⁹⁶ is replaced by Glu and Asp⁹⁸ is replaced by Asn (7); REST/NRSF; and green fluorescent protein (GFP) as a vector control. Under defined conditions with retinoic acid, >90% of viable P19 cells undergo morphological differentiation into neurons (Fig. 2, A and B). Expression of REST/NRSF did not affect the proliferation of undifferentiated P19 cells, but neuronal induction triggered the death of the transfected cells (Fig. 2, A and B). In contrast, expression of SCP1 did not block neuronal differentiation or cause cell death (Fig. 2, A and B). Blocking SCP activity with dnSCP1, however, increased neuronal differentiation ~twofold (Fig. 2, A and B). These results suggest that SCP1 function is dependent on the presence of REST/NRSF. Because REST/NRSF is down-regulated as neurons differentiate (Fig. 2D) (15), the presence of SCP1 is insufficient to disrupt neuronal differentiation. Conversely, it appears that REST/NRSF neuronal-silencing activity in undifferentiated P19 cells is antagonized by dnSCP1, leading to enhanced neuronal differentiation.

P19 cells can be driven to differentiate into postmitotic neurons in the absence of retinoic acid by the neurogenic bHLH transcription factor complex Ngn2:E47. To test whether SCP also influences this neuronal differentiation pathway, we coexpressed SCP1, Ngn2, and E47 in P19 cells and monitored their differentiation status by using cell morphology and gene expression. Neuronal differentiation driven by Ngn2:E47 was markedly attenuated in the presence of SCP1 (Fig. 3, B and E). Constitutive expression of REST/NRSF also antagonized Ngn2:E47-induced neuronal differentiation (Fig. 3, C and E); and, when coexpressed, both SCP1 and REST/NRSF were found to cooperate in blocking neuronal differentiation (Fig. 3, D and E).

Because SCP1 and REST/NRSF inhibited Ngn2-induced neuronal differentiation, we explored whether interference with SCP1 and REST/NRSF by dn forms of these proteins would conversely enhance neuronal differentiation. By lowering the concentration of Ngn2 and omitting E47, we found that neuronal differentiation was greatly reduced (Fig. 3, F and J). Under these conditions, dnSCP1 and dnREST/NRSF alone or in combination were found to strongly enhance neuronal differentiation (Fig. 3, G to J) (3). Taken together, these results indicate that

SCP1 functions in cooperation with REST/NRSF to suppress neuronal differentiation of stem cells, whether driven by retinoic acid or bHLH neurogenic transcription factors.

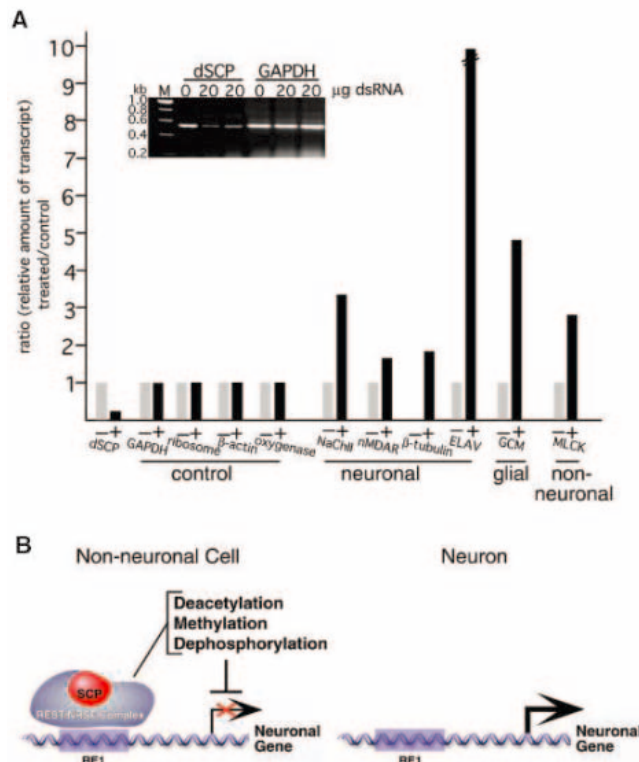
To determine whether SCP might be part of an evolutionarily conserved pathway for restricting neuronal gene expression, we next examined the role of SCP in *Drosophila*. A search of the *Drosophila* genome identified a single dSCP homolog with 75% identity to human SCP1. The dSCP protein expressed in bacteria exhibited phosphatase activity similar to that described for human SCPs (7, 10). Examination of the *Drosophila* databases revealed no P element insertions or specific deletions in the dSCP locus. Because the level of dSCP expression is relatively stable from the earliest times of analysis of *Drosophila* embryos, there is likely a strong maternal component of dSCP mRNA during early development (16).

The single SCP gene in combination with a robust RNA interference (RNAi) system in *Drosophila* prompted us to use an RNA silencing strategy [small interfering RNA (siRNA) dSCP] to knock down dSCP in S2 cells. Transfection of a 700-base pair siRNA dSCP into S2 cells reduced dSCP mRNA levels by >80% after treatment for 24 hours (Fig. 4A). After the knockdown of dSCP, glyceraldehyde phosphate dehydrogenase (GAPDH), ribosomal protein S35, non-neuronal oxygenase, and β -actin mRNA levels remained unchanged. In addition, the growth and mor-

phology of the S2 cells appeared normal after siRNA dSCP treatment. Under these conditions, however, siRNA dSCP triggered an enhancement in the expression of neuronal genes in the S2 cells. Levels of the sodium channel II protein (NaChII), the *N*-methyl-D-aspartate glutamate receptor (NMDAR), the embryonic lethal abnormal visual (ELAV), and β -tubulin all increased 2 to >10 fold (Fig. 4A and fig. S2). The mammalian orthologs of the genes encoding NaChII, NMDAR, and β -tubulin are classical neuronal genes that contain RE-1 elements (1, 2, 9). Some neuronal genes remained unchanged in response to siRNA dSCP, including those that code for synapsin, stathmin, choline acetyltransferase (ChAT), and neurofilament. Myosin light-chain kinase (MLCK), a muscle-specific protein that was highly expressed in S2 cells, was further increased by siRNA dSCP. The derepression of genes in S2 cells also extended to markers of glial cells such as glial cell missing (GCM) (17). Thus, the down-regulation of SCP and REST/NRSF in both differentiated neurons and glia correlates with their broad role in suppressing a large subset of genes normally found in mature cells of the nervous system (Fig. 1).

REST/NRSF is a DNA binding protein that assembles a repressor complex on RE-1 elements present in >1000 neuronal genes (9, 18). The proteins mSin3A/B and HDAC1/2 bind to the N terminus of REST/NRSF, and Co-REST

Fig. 4. Silencing of dSCP enhances the expression of neuronal and glial genes (A) Quantitation of transcript amounts was done with real-time quantitative (RT-qPCR). S₂ cells were either untreated (-) or treated (+) with siRNA dSCP for 24 hours. Total RNA was prepared and treated with deoxyribonuclease, and primer pairs specific for the coding sequence of each gene were used for qPCR with the dye SYBR Green. Threshold cycle (C_t) values were obtained from triplicate data points, and changes in transcript levels for treated samples were compared with untreated samples, which were assigned a value of 1. (Inset) Relative amounts of RT-PCR products for dSCP and GAPDH transcript without and with siRNA dSCP treatment. Similar results were obtained in four additional experiments. (B) Enzymatic processes involved in REST/NRSF-dependent neuronal gene silencing.



binds to the C terminus (19). In addition to these protein interactions, methylation of Lys⁹ of histone H3 creates a high-affinity binding site for HP1, providing a mechanism for localization of this protein to RE-1 elements (20, 21). Our study identifies SCPs as functional components of the REST/NRSF silencing complex (Fig. 4B). The negative influence of SCPs on the transcription of neuronal genes may be mediated by dephosphorylation of the CTD of RNAPII; it is possible, however, that other phosphatase substrates mediate these effects (22). Moreover, other related phosphatases with the DXDX(T/V) amino acid signature found in FCP1-class proteins might contribute to gene regulation by using similar mechanisms. For example, the eyes absent (Eya) transcription cofactor is a protein phosphatase belonging to this general family that serves to convert the DNA binding homeo-domain protein sine oculis from a repressor to an activator, promoting eye formation in *Drosophila* and cell proliferation required for organ formation in mice (kidney and muscle) (23, 24). In addition, SCP2 is reported to dorsalize the ventral mesoderm, indicating it might also help to negatively regulate a subset of non-neuronal genes (25).

These data provide further evidence that a variety of mechanisms are used by

REST/NRSF to suppress neuronal gene expression. Previous studies have focused on interactions with deacetylases and methylases that modify chromatin (Fig. 4B). Here we show that a mechanism involving SCPs also contributes to blocking inappropriate neuronal gene expression in developing cells. The mechanisms that inhibit the expression of any particular gene are likely to vary considerably, but our findings suggest that antagonism of the SCP pathway might help to promote neuronal differentiation from the appropriate cell types.

References and Notes

1. J. A. Chong *et al.*, *Cell* **80**, 949 (1995).
2. C. J. Schoenherr, D. J. Anderson, *Science* **267**, 1360 (1995).
3. Z. F. Chen, A. J. Paquette, D. J. Anderson, *Nature Genet.* **20**, 136 (1998).
4. M. A. Hakimi *et al.*, *Proc. Natl. Acad. Sci. U.S.A.* **99**, 7420 (2002).
5. Y. Naruse, T. Aoki, T. Kojima, N. Mori, *Proc. Natl. Acad. Sci. U.S.A.* **96**, 13691 (1999).
6. K. Kokura *et al.*, *J. Biol. Chem.* **276**, 34115 (2001).
7. M. Yeo, P. S. Lin, M. E. Dahmus, G. N. Gill, *J. Biol. Chem.* **278**, 26078 (2003).
8. T. Kamenski, S. Heilmeyer, A. Meinhart, P. Cramer, *Mol. Cell* **15**, 399 (2004).
9. V. V. Lunyak *et al.*, *Science* **298**, 1747 (2002).
10. M. Yeo *et al.*, data not shown.
11. A. Roopra *et al.*, *Mol. Cell. Biol.* **20**, 2147 (2000).
12. M. Yao, G. Bain, D. I. Gottlieb, *J. Neurosci. Res.* **41**, 792 (1995).

13. Q. Ma, C. Kintner, D. J. Anderson, *Cell* **87**, 43 (1996).
14. S. K. Lee, S. L. Pfaff, *Neuron* **38**, 731 (2003).
15. G. Bai, Z. Zhuang, A. Liu, Y. Chai, P. W. Hoffman, *J. Neurochem.* **86**, 992 (2003).
16. The gene expression database of the Berkeley *Drosophila* Genome Project is available at: www.fruitfly.org/cgi-bin/ex/bquery.pl?qttype=report&find=CG5830&searchfield=CG.
17. M. R. Freeman, J. Delrow, J. Kim, E. Johnson, C. Q. Doe, *Neuron* **38**, 567 (2003).
18. C. J. Schoenherr, A. J. Paquette, D. J. Anderson, *Proc. Natl. Acad. Sci. U.S.A.* **93**, 9881 (1996).
19. M. E. Andres *et al.*, *Proc. Natl. Acad. Sci. U.S.A.* **96**, 9873 (1999).
20. M. Lachner, D. O'Carroll, S. Rea, K. Mechtler, T. Jenuwein, *Nature* **410**, 116 (2001).
21. A. J. Bannister *et al.*, *Nature* **410**, 120 (2001).
22. T. Maile *et al.*, *Science* **304**, 1010 (2004).
23. T. L. Tootle *et al.*, *Nature* **426**, 299 (2003).
24. X. Li *et al.*, *Nature* **426**, 247 (2003).
25. I. E. Zohn, A. H. Brivanlou, *Dev. Biol.* **239**, 118 (2001).
26. The authors are grateful to V. Lunyak and I. Kalcheva for helpful advice. S.-K.L. was supported by a fellowship from the Human Frontiers Science Program, and S.L.P. was supported by the Helen McLoraine Developmental Chair in Neurobiology and the G. Harold and Leila Y. Mathers Foundation. These studies were supported by NIH grant DK13149 (G.N.G.) and NS37116 (S.L.P.).

Supporting Online Material

www.sciencemag.org/cgi/content/full/307/5709/596/DC1
Materials and Methods
Figs. S1 to S3

27 May 2004; accepted 1 December 2004
10.1126/science.1100801

Illumination of the Melanopsin Signaling Pathway

Satchidananda Panda,*†‡ Surendra K. Nayak,* Brice Campo, John R. Walker, John B. Hogenesch,§ Tim Jegla†

In mammals, a small population of intrinsically photosensitive retinal ganglion cells (ipRGCs) plays a key role in the regulation of nonvisual photic responses, such as behavioral responses to light, pineal melatonin synthesis, pupillary light reflex, and sleep latency. These ipRGCs also express melanopsin (Opn4), a putative opsin-family photopigment that has been shown to play a role in mediating these nonvisual photic responses. Melanopsin is required for the function of this inner retinal pathway, but its precise role in generating photic responses has not yet been determined. We found that expression of melanopsin in *Xenopus* oocytes results in light-dependent activation of membrane currents through the G_{αq}/G_{α11} G protein pathway, with an action spectrum closely matching that of melanopsin-expressing ipRGCs and of behavioral responses to light in mice lacking rods and cones. When coexpressed with arrestins, melanopsin could use all-*trans*-retinaldehyde as a chromophore, which suggests that it may function as a bireactive opsin. We also found that melanopsin could activate the cation channel TRPC3, a mammalian homolog of the *Drosophila* phototransduction channels TRP and TRPL. Melanopsin therefore signals more like an invertebrate opsin than like a classical vertebrate rod-and-cone opsin.

Nonvisual photoresponses in mammals, including circadian entrainment, constriction of the pupil, and regulation of sleep latency, are generated in part by a network of ipRGCs that directly innervate the brain regions that mediate these responses (1–7). The photosensitiv-

ity of these cells is dependent on melanopsin (Opn4) (2, 5, 6), an atypical vertebrate opsin first isolated from frog melanophores (8). Genetic studies have indicated that nonvisual responses to light persist in mice lacking rod and cone function but are entirely eliminated if

melanopsin is also removed (9, 10). Although these studies have established the critical role of melanopsin in photosensation within the inner retina, the underlying mechanism has remained uncharacterized.

Vertebrate and invertebrate photosensitive opsins are heterotrimeric guanine nucleotide-binding protein (G protein)-coupled receptors that use 11-*cis*-retinaldehyde (11-*cis*-retinal) or a close variant as their chromophore (11). Photoconversion of the 11-*cis*-retinal to all-*trans*-retinaldehyde (all-*trans*-retinal) creates a conformational change in these opsin proteins that triggers G protein activation and subsequent signaling. Vertebrate rod-and-cone opsins signal through photoreceptor-specific, pertussis toxin (PTX)-sensitive G proteins called transducins, whereas invertebrate opsins signal through the PTX-insensitive G_q family of G proteins (11). These responses are terminated by a combination of phosphorylation of the excited opsin and the binding of arrestin proteins (12). After signaling, re-

Genomics Institute of Novartis Research Foundation, 10675 John J. Hopkins Drive, San Diego, CA 92121, USA.

*These authors contributed equally to this work.
†To whom correspondence should be addressed.
E-mail: satchin@salk.edu, tjegla@gnf.org
‡Present address: Salk Institute for Biological Studies, La Jolla, CA 92037, USA.
§Present address: Scripps Florida, FAU-Building MC-17, 5353 Parkside Drive, Jupiter, FL 33458, USA.

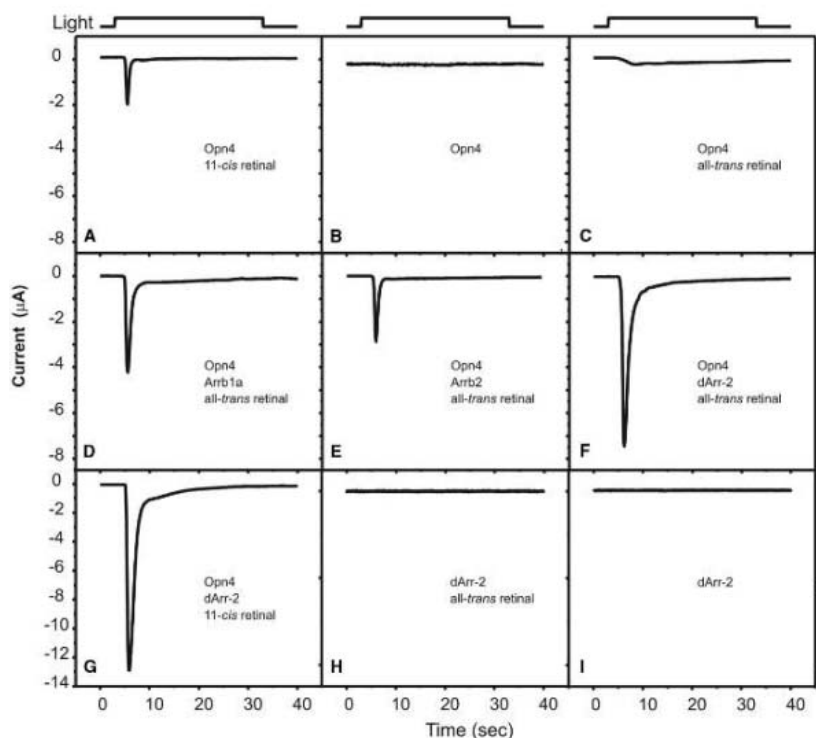
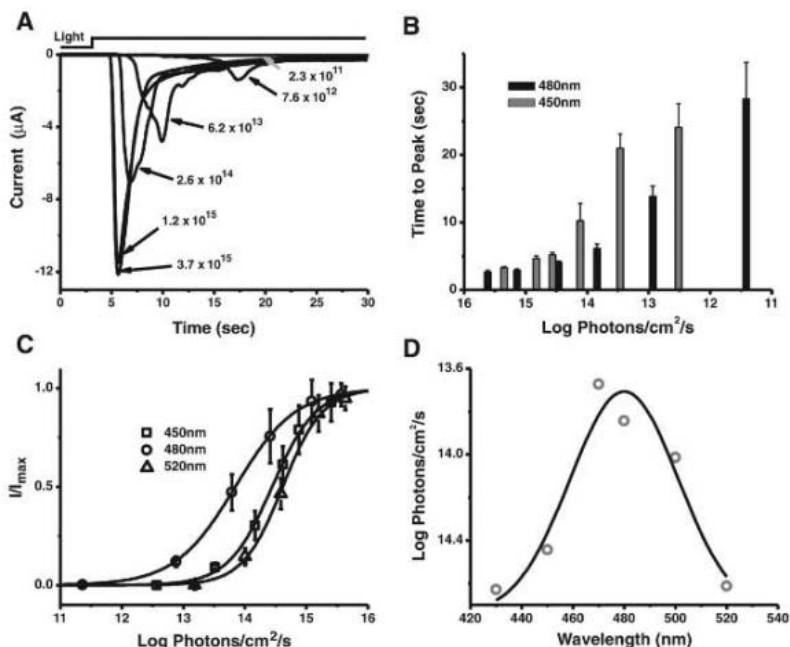


Fig. 1. Light-evoked membrane currents in *Xenopus* oocytes expressing mouse melanopsin. (A to C) *Xenopus* oocytes expressing mouse melanopsin exhibit a transient inward current at -70 mV in response to a brief saturating pulse of white light (>1000 lux) upon prior incubation with 11-*cis*-retinal (A) or all-*trans*-retinal (C), but not in the absence of exogenous retinal (B). (D to F) Coexpression of Arrb1a (D), Arrb2 (E), or dArr-2 (F) consistently produced large photocurrents in the presence of all-*trans*-retinal. (G) Enhancement of currents was also seen when 11-*cis*-retinal was used as the chromophore. (H and I) Oocytes injected with arrestin alone did not produce a photocurrent in the presence (H) or absence (I) of all-*trans*-retinal. (J) Mean peak photocurrent (\pm SEM, $n = 3$ to 9 oocytes) from oocytes under different conditions of mRNA and chromophore. All recordings were made under voltage clamp at -70 mV; see (20) for details of chromophore incubation and light application.

Fig. 2. Spectral sensitivity of melanopsin-mediated photocurrent. Photocurrents were generated from oocytes injected with mouse melanopsin and dArr-2 in response to light pulses of varying wavelength and intensity after exposure to 11-*cis*-retinal (20). (A) Representative photocurrents elicited in response to 40-s pulses of 480-nm light of varying intensity. Light pulse duration is indicated at the top with a bar; light intensity for each trace is given in photons $\text{cm}^{-2} \text{s}^{-1}$. Voltage was held at -70 mV for all recordings. The size and speed of the response correlate well with light intensity. (B) Mean time lag (\pm SEM; $n \geq 5$) from onset of the light pulse to peak of the photocurrent for pulses of 450-nm and 480-nm light of varying intensity. The time lag increases with decreasing light intensity at both wavelengths. The lag is shorter at intermediate intensities for 480-nm light, which suggests that it is more effective in eliciting the photoresponse. (C) Normalized irradiance-response curves for light wavelengths of 450, 480, and 520 nm. Bars indicate SE ($n = 4$ to 8); lines show sigmoidal fits of the data. Note the higher sensitivity of the response to 480-nm light. (D) Half-activation values, derived from sigmoidal fits of irradiance-response curves, plotted versus wavelength and fit with a Gaussian function (peak amplitude = 479.8 nm).



generation of the active chromophore is necessary to restore photosensitivity. In vertebrates, this process involves release of all-*trans*-retinal from the opsin and conversion back to 11-*cis*-retinal through an elaborate pathway resident primarily in the retinal pigment epithelium. Invertebrate opsins, such as *Drosophila* rhodopsin 1, instead photoconvert

all-*trans*-retinal back to the active form in an arrestin-dependent manner (13) and therefore also function as photoisomerases, obviating the need for an accessory pigment regeneration mechanism. Sequence comparisons have shown that melanopsin shares significant similarity to opsins from invertebrates (8), and therefore melanopsin may function more like

an invertebrate opsin than like vertebrate rod-and-cone opsins. Interestingly, both melanopsin-containing *Xenopus* melanophores (14) and ipRGCs from rodents (5) exhibit photosensitivity that persists *ex vivo* in the presence of all-*trans*-retinal, supporting this notion.

To characterize light-dependent melanopsin function, we injected mRNA encod-

ing mouse melanopsin into *Xenopus* oocytes and recorded whole-cell currents elicited in response to light pulses after exposure of the oocytes to retinaldehyde-based chromophores. *Xenopus* oocytes have been successfully used to express and functionally characterize opsins in a wide range of organisms, including bacteria and mammals (15–19). Melanopsin-expressing oocytes incubated with 11-*cis*-retinal (20) produced large, transient currents in response to illumination with saturating bright white light (>1000 lux) (Fig. 1A). Photocurrents were not observed in the absence of 11-*cis*-retinal (Fig. 1B) or in uninjected oocytes incubated with 11-*cis*-retinal (21). These results clearly indicate that melanopsin is a functional photoreceptive opsin capable of using 11-*cis*-retinal as a chromophore. Incubation of injected oocytes with all-*trans*-retinal led to small photocurrents observed in a subset of oocytes (Fig. 1C). Photoconversion of all-*trans*-retinal to the active 11-*cis* conformation is arrestin-dependent in invertebrates (13), and *Drosophila* rhodopsin 1/all-*trans*-retinal-based photocurrents in oocytes are dependent on coexpression of an arrestin (19). Thus, we reasoned that the difficulty in eliciting consistent photoresponses from oocytes incubated with all-*trans*-retinal could be corrected by coexpression of melanopsin with an arrestin. Indeed, we found that coexpression of melanopsin with mouse $\beta 1$ arrestin (Arrb1a, GenBank accession number NM_177231), mouse $\beta 2$ arrestin (Arrb2, GenBank accession number NM_145429), or fly arrestin-2 (dArr-2, GenBank accession number M32141) resulted in large, consistent photocurrents from eggs incubated with all-*trans*-retinal (Fig. 1, D, E, F, and J). The magnitude of photocurrents was also enhanced by arrestins when 11-*cis*-retinal was used as a chromophore (Fig. 1, G and J). Arrestin alone did not produce a light response (Fig. 1, H to J), thereby ruling out the possibility that the increased photosensitivity is due to coupling of arrestin to an endogenous photoreceptor. Together these observations show that melanopsin is a true photosensory opsin and that, like invertebrate opsins, it may be able to complete the retinoid cycle through intrinsic photoisomerase activity.

We next generated an action spectrum of the melanopsin-mediated photocurrent in oocytes to test whether the responses faithfully reproduced the spectral sensitivity of ipRGCs and the inner retinal nonvisual photopathway. Peak responsiveness is found at a light wavelength of about 480 nm for the excitation of ipRGCs (5) as well as for circadian entrainment (6, 22) and pupillary constriction (23) responses mediated by the inner retina pathway. We measured the irradiance-response relationship for the photocurrent at near-monochromatic light (half peak bandwidth = 10 nm) of different wavelengths from

oocytes expressing both melanopsin and arrestin (20). Reduction in light intensity led to both a reduction in the peak of the photocurrent and a delay in the onset (Fig. 2, A to C). The irradiance for half-maximal photocurrent at each wavelength was plotted to generate an action spectrum (Fig. 2D). The spectrum clearly peaks between 460 and 480 nm, and is best fitted by a Gaussian function with a peak of 480 nm ($r^2 = 0.925$). Thus, the spectral properties of melanopsin in oocytes are highly consistent with the observed function of ipRGCs. However, the absorption spectrum

of *in vitro* reconstituted melanopsin purified from cultured mammalian cells exhibits a peak absorbance in the 420- to 440-nm range (24). Cell-specific factors and/or the protein purification procedure may influence the spectral properties of the chromophore and hence may underlie this discrepancy.

We next examined the relevant G protein signaling pathway used by melanopsin to produce the observed photocurrent in oocytes. We reasoned that activation of the well-characterized native oocyte calcium-activated chloride current was largely responsible for

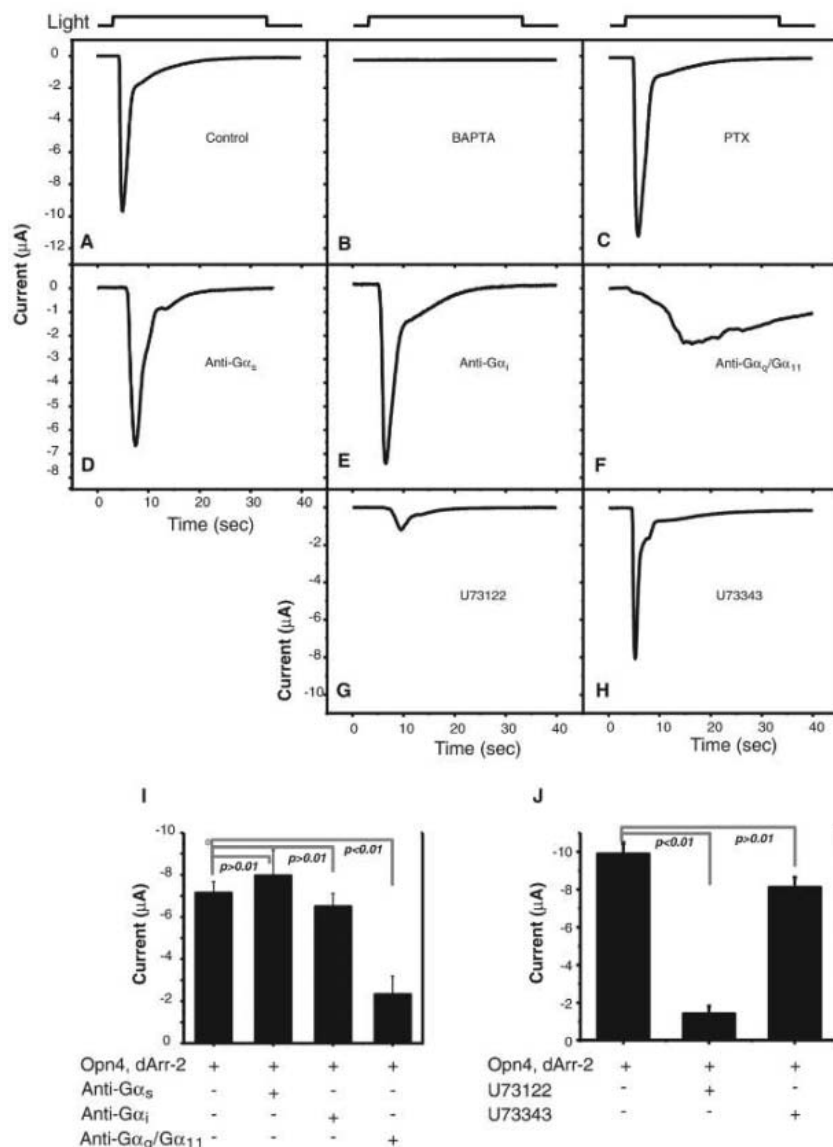


Fig. 3. Role of $G\alpha_q/G\alpha_{11}$ and PLC in generating melanopsin-dependent photocurrents. (A) A typical melanopsin-mediated photocurrent recorded in response to light (white, >1000 lux) after incubation with all-*trans*-retinal. (B and C) The photocurrent is abolished in oocytes injected with 50 nl of BAPTA (50 mM) (B) but is unaffected by injection of 50 nl of PTX (1 ng/ μ l) (C). (D and E) The photocurrent could not be blocked by injection of 50 nl of antibodies to $G\alpha_s$ (D) or $G\alpha_i$ (E) classes of G proteins. (F) Injection of antibodies recognizing a common epitope in both $G\alpha_q$ and $G\alpha_{11}$ severely attenuated the photocurrent. (G) Incubation of the oocytes with the PLC inhibitor U73122 (1 μ M) attenuated the photocurrent. (H) Incubation in solution containing an inactive analog U73343 (1 μ M) had little effect. (I) and (J) Mean values (\pm SEM, $n = 4$ to 8 oocytes) for antibody and PLC inhibitor experiments, respectively. Significance of difference was tested by Student's *t* test (equal variance); the corresponding *P* values are indicated. See (20) for details of methods.

the photocurrent, because the current reversed close to the predicted equilibrium potential for chloride and was reduced by known blockers of this channel (21). Injection of oocytes with the calcium chelator 1,2-bis(2-aminophenoxy)ethane-*N,N,N',N'*-tetraacetic acid (BAPTA) before recording eliminated the bulk of the photocurrent; this result further suggested that a rise in intracellular calcium is the trigger for the photocurrent we observed in oocytes (Fig. 3B). This response was insensitive to injection of PTX (Fig. 3C), which blocks transduction through $G_i/G_o/G_t$ class G proteins. In contrast, PTX was highly effective in blocking the potentiation of GIRK currents by the G_i -coupled M2 muscarinic receptor in the oocyte system (21). Taken together, these results imply the involvement of G_q/G_{11} class G proteins, which are the classic activators of phospholipase C- β (PLC- β). Activated PLC breaks down phosphatidylinositol 4,5-bisphosphate to inositol 1,4,5-trisphosphate and diacylglycerol (DAG), and also triggers calcium release from intracellular stores.

We found that we could block the melanopsin-induced photocurrent with injection of antibodies to $G\alpha_q/G\alpha_{11}$, but not with antibodies to $G\alpha_s$ or $G\alpha_i$ (Fig. 3, D, E, F, and I). In addition, the PLC inhibitor U73122, but

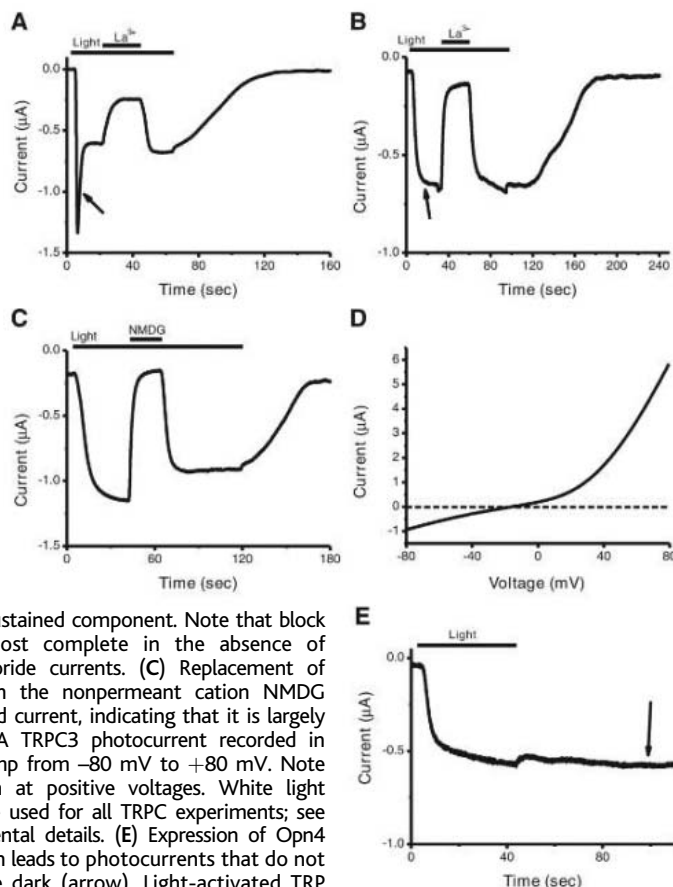
not its inactive analog U73343, was highly effective in blocking the photocurrent (Fig. 3, G, H, and J). Although we cannot rule out association of melanopsin with other G proteins under special circumstances, as has been previously shown (24), our results clearly point to a model whereby light-activated melanopsin preferentially activates the G_q/G_{11} class of G proteins, followed by activation of PLC- β .

Because this signaling mechanism is similar to that used by invertebrate opsins, we reasoned that mammalian transient receptor potential (TRP) subfamily C (TRPC) cation channels, which are paralogs of the *Drosophila* phototransduction channels Trp and Trpl (25, 26), could be involved in phototransduction in ipRGCs. Although the molecular identity of the phototransduction channel(s) in ipRGCs remains unknown, excitation of ipRGCs by light leads to both calcium influx and depolarization (5, 27, 28), as is observed in *Drosophila* photoreceptors. The current-voltage relationship of light-activated current in ipRGCs is similar to that of the TRP class of channels, in that it shows a reversal potential indicative of a nonselective cation channel and displays outward rectification at depolarized voltages (28). In addition, TRPC channels are calcium-permeable

nonselective cation channels and are activated by the G_q/G_{11} pathway (29). To test this hypothesis, we coexpressed melanopsin with mouse TRPC3 in oocytes. TRPC3 produced a novel sustained component in photocurrents that could be partially blocked with 1 mM lanthanum (La^{3+}), a known TRPC channel blocker (Fig. 4A). Injection of BAPTA before recording allowed the TRPC3 photocurrent to be observed in isolation from the transient native calcium-activated chloride currents (Fig. 4B). Insensitivity of the TRPC-based photocurrent to calcium chelation suggests activation via DAG, as has been observed for mammalian TRPC channels, including TRPC3 (29). The photocurrent was also attenuated upon prior incubation of the oocytes with U73122 (65.4% attenuation in the presence of U73122, $n = 8$). The isolated melanopsin-dependent TRPC3 photocurrents remained activated for the duration of light pulses, and they were completely blocked by La^{3+} or greatly reduced by replacement of extracellular sodium with *N*-methyl-D-glucamine (NMDG) (Fig. 4, B and C). Voltage ramps taken during light pulses show that the TRPC3 photocurrent has a profile similar to that of ipRGCs (28); it has a reversal potential typical of a nonselective cation channel and displays outward rectification at higher voltages (Fig. 4D). In the absence of arrestins, the TRPC3 photocurrent did not decrease after the end of the light pulse (Fig. 4E) and persisted for minutes (21) before returning to baseline. Therefore, arrestins may play an important role in terminating light-evoked melanopsin signaling, as they do for both invertebrate opsins and vertebrate rod-and-cone opsins. Differences in the amplitudes of TRPC3-mediated photocurrents with and without arrestin were most pronounced with multiple light pulses separated by several minutes. Responses to a second identical light pulse were greatly reduced in the absence of arrestin ($26.2 \pm 9.5\%$ of initial response, $n = 5$). In contrast, second responses were potentiated in the presence of arrestin ($195 \pm 43\%$ of initial response, $n = 4$), further suggesting the arrestin dependence of photoregeneration in melanopsin signaling. Although these observations do not constitute proof that TRPC family channels are involved in ipRGC phototransduction, members of this gene family can be considered prime candidates for the phototransduction channel of the inner retinal pathway in mammals. We were not able to demonstrate photoactivation of channels from the TRPV (TRPV1), TRPM (TRPM8), and TRPA (TRPA1) families in similar experiments (21).

Our results show that melanopsin encodes a fully functional opsin through its ability to confer photosensitivity to *Xenopus* oocytes. The action spectrum of the photocurrent closely matches that of photosensitivity of ipRGCs in

Fig. 4. Melanopsin activates TRPC channels in a light-dependent manner. (A) A photocurrent for a *Xenopus* oocyte expressing Opn4, dArr-2, and mouse TRPC3 shows the typical transient calcium-activated chloride current (arrow) but also contains a novel sustained component that is partially blocked by 1 mM lanthanum (La^{3+}) (bar). The current slowly returns to baseline after light is turned off. (B) Injection of oocytes expressing Opn4, dArr-2, and TRPC3 with 50 nl of 50 mM BAPTA before recording abolishes the calcium-activated chloride current (arrow)



but does not affect the sustained component. Note that block by 1 mM La^{3+} is almost complete in the absence of contamination from chloride currents. (C) Replacement of extracellular sodium with the nonpermeant cation NMDG greatly reduces the inward current, indicating that it is largely carried by sodium. (D) A TRPC3 photocurrent recorded in response to a voltage ramp from -80 mV to $+80$ mV. Note the outward rectification at positive voltages. White light pulses of >1000 lux were used for all TRPC experiments; see (20) for further experimental details. (E) Expression of Opn4 and TRPC3 without arrestin leads to photocurrents that do not return to baseline in the dark (arrow). Light-activated TRP currents persisted as long as recordings continued (up to 10 min), which indicates that the active form of Opn4 is very stable in this expression system. Voltage was held at -70 mV in (A), (B), (C), and (E).

rodents, which implies that melanopsin alone can account for the intrinsic photosensitivity of these RGCs. Furthermore, melanopsin functionally resembles invertebrate opsins in that it can activate both G_q/G_{11} signaling pathways and TRPC channels, and it appears to have an intrinsic photoisomerase activity. The photoisomerase activity of melanopsin may be particularly important for its function in ipRGCs because they are spatially distant from the retinal pigment epithelium, which participates in chromophore regeneration for rod-and-cone opsins. The genetic manipulation of proposed components of the signaling cascade expressed in melanopsin-containing ipRGCs will ultimately determine their role in melanopsin-based photic responses.

Note added in proof: Similar findings have recently been reported (30, 31).

References and Notes

1. N. F. Ruby *et al.*, *Science* **298**, 2211 (2002).
2. S. Hattar, H. W. Liao, M. Takao, D. M. Berson, K. W. Yau, *Science* **295**, 1065 (2002).

3. J. Hannibal, P. Hindersson, S. M. Knudsen, B. Georg, J. Fahrenkrug, *J. Neurosci.* **22**, RC191 (2002).
4. J. J. Gooley, J. Lu, T. C. Chou, T. E. Scammell, C. B. Saper, *Nature Neurosci.* **4**, 1165 (2001).
5. D. M. Berson, F. A. Dunn, M. Takao, *Science* **295**, 1070 (2002).
6. R. J. Lucas *et al.*, *Science* **299**, 245 (2003).
7. S. Panda *et al.*, *Science* **298**, 2213 (2002).
8. I. Provencio, G. Jiang, W. J. De Grip, W. P. Hayes, M. D. Rollag, *Proc. Natl. Acad. Sci. U.S.A.* **95**, 340 (1998).
9. S. Panda *et al.*, *Science* **301**, 525 (2003).
10. S. Hattar *et al.*, *Nature* **424**, 76 (2003).
11. R. C. Hardie, P. Raghur, *Nature* **413**, 186 (2001).
12. M. E. Burns, D. A. Baylor, *Annu. Rev. Neurosci.* **24**, 779 (2001).
13. A. Kiselev, S. Subramaniam, *Biochemistry* **36**, 2188 (1997).
14. M. D. Rollag, I. Provencio, D. Sugden, C. B. Green, *Methods Enzymol.* **316**, 291 (2000).
15. G. Nagel *et al.*, *Proc. Natl. Acad. Sci. U.S.A.* **100**, 13940 (2003).
16. G. Nagel *et al.*, *Science* **296**, 2395 (2002).
17. H. G. Khorana, B. E. Knox, E. Nasi, R. Swanson, D. A. Thompson, *Proc. Natl. Acad. Sci. U.S.A.* **85**, 7917 (1988).
18. B. E. Knox, R. B. Barlow, D. A. Thompson, R. Swanson, E. Nasi, *Methods Enzymol.* **316**, 41 (2000).
19. B. V. Zemelman, G. A. Lee, M. Ng, G. Miesenbock, *Neuron* **33**, 15 (2002).
20. See supporting data on Science Online.
21. S. Panda *et al.*, data not shown.

22. J. S. Takahashi, P. J. DeCoursey, L. Bauman, M. Menaker, *Nature* **308**, 186 (1984).
23. R. J. Lucas, R. H. Douglas, R. G. Foster, *Nature Neurosci.* **4**, 621 (2001).
24. L. A. Newman, M. T. Walker, R. L. Brown, T. W. Cronin, P. R. Robinson, *Biochemistry* **42**, 12734 (2003).
25. C. Montell, G. M. Rubin, *Neuron* **2**, 1313 (1989).
26. A. M. Phillips, A. Bull, L. E. Kelly, *Neuron* **8**, 631 (1992).
27. S. Sekaran, R. G. Foster, R. J. Lucas, M. W. Hankins, *Curr. Biol.* **13**, 1290 (2003).
28. E. J. Warren, C. N. Allen, R. L. Brown, D. W. Robinson, *Eur. J. Neurosci.* **17**, 1727 (2003).
29. M. Trebak, G. Vazquez, G. S. Bird, J. W. Putney Jr., *Cell Calcium* **33**, 451 (2003).
30. Z. Meylan *et al.*, *Nature*, in press; published online 26 January 2005 (10.1038/nature03344).
31. X. Qiu *et al.*, *Nature*, in press; published online 26 January 2005 (10.1038/nature03345).
32. Supported by the Novartis Research Foundation. We thank A. Patapoutian for the TRPC3 clone, R. Crouch for 11-*cis*-retinal, and K. Naik, V. Lee, and V. Piamonte for expert technical assistance.

Supporting Online Material

www.sciencemag.org/cgi/content/full/307/5709/600/DC1
 Materials and Methods
 References

10 September 2004; accepted 23 November 2004
 10.1126/science.1105121

Science sets the pace

online manuscript submission

MANUSCRIPTS

www.submit2science.org

Science can now receive and review all manuscripts electronically

online letter submission

LETTERS

www.letter2science.org

Have your voice be heard immediately



speed submission

NEW PRODUCTS

<http://science.labvelocity.com>

Proteomics Software

Version 3.0 of BioinformatIQ is designed to be a standalone software package suitable for all proteomics laboratories. Designed to provide the infrastructure for the research-scale or industrial-scale proteomics lab, BioinformatIQ integrates and controls instrumentation and manages workflow, turning the proteomics process into an integrated whole. It automates data analysis to save manual work. Through the use of powerful IBM databases, it can store up to terabytes of data.

Proteome Systems For information +61 2 9889 1830
www.proteomesystems.com

Drug Discovery Automation

Three new protocols to automate drug discovery applications are available using Millipore's Multiscreen assay systems and Caliper's Sciclone ALH 3000 Liquid Handling Workstation. The Caliper Sciclone ALH 3000 Liquid Handling Workstation offers leading-edge precision, adaptability, and scalability, enabling the efficient automated processing of 96-, 384-, and 1536-well microplates. The workstation can be configured to automate many applications, from nucleic acid and protein sample preparation protocols to molecular and cell-based screening assays. The three new protocols, Millipore's MultiScreen Solubility Assay System, Multiscreen Permeability filter plate, and Multiscreen filter plate for parallel artificial membrane permeation assays, are part of a family of optimized ADME (absorption, distribution, metabolism, and excretion) assays developed to screen compounds in the early stages of drug discovery to improve lead predictability and increase productivity. The company's ADME offering also includes the MultiScreen Caco-2 Assay System for cell-based absorption assays, MultiScreen Ultracel-PPB filter assembly for plasma protein binding, and the MultiScreen Solvint filter plate for total drug analysis.

Millipore For information 800-MILLIPORE www.millipore.com/adme

Delivery of mRNA and Viral RNA

The TransIt-mRNA Transfection Kit is optimized for efficient delivery of various types of RNA to mammalian cells. Both messenger RNA (mRNA) and viral RNA of various lengths can be delivered effectively to a wide range of cell types, with the transfection of mRNA leading to high-level protein expression with minimal cytotoxicity. As an added benefit, this kit has been optimized for use in the presence of serum containing media, thus eliminating the extra steps of media change or serum addition.

Mirus For information 608-441-2824 www.mirusbio.com

Live Laser Scanning Microscope

A live laser scanning microscope is a new addition to the LSM 5 family. With a new optical concept designed for studies on living specimens, it features a unique combination of scanning speed, image quality, and sensitivity. Collecting up to 120 confocal images per second at a resolution of 512 × 512 pixels, the LSM 5 Live scans about 20 times faster than any other confocal system so far, according to the manufacturer. It features precise optics, a

creatively designed beam splitter, and innovative beam shaping, with virtually 100% excitation efficiency and efficient emission yield, the new AchromGate beam splitter guarantees maximum performance even on thick or weakly fluorescent specimens, regardless of the color of the excitation light. Fast new Z-drive solutions permit three-dimensional image stacks to be acquired every second, which is especially useful for developmental biologists. Precisely tuned zoom optics and a sophisticated scanning concept permit the size and position of the scan field to be varied precisely, without simultaneously changing major optical parameters of the system.

Zeiss For information +49 (0) 3641 64-2770 www.zeiss.de/mikro

Cellmate II Serological Pipettor

The Cellmate II is a portable serological pipettor powered by a lithium ion battery with a lifetime guarantee. Available in five color options, the CellMate II includes a table stand, a wall mount, a universal power supply, and plug adapters for international use. Large aspirate and dispense triggers offer a comfortable finger platform and allow precise control of liquid manipulation. Separate speed buttons allow individual control of both functions.



Matrix Technologies For information 800-345-0206 www.matrixtechcorp.com

Mathematica Upgrade

Mathematica 5.1, the latest version of this science and technology software system, includes a host of new capabilities, especially for working with large-scale, diverse types of data. Innovative new algorithms have been introduced for all steps in the data handling

process, including importing, analyzing, manipulating, and plotting. A unique Automatic Algorithm Selection capability automatically applies the best algorithm to each task. There are more than 50 new functions, toolkits, and performance improvements. Highlights include industrial-strength string manipulation, built-in universal database connectivity, highly optimized binary data input/output, additional import and export formats, integrated web services support, two-dimensional and three-dimensional automated network visualization, high-performance array visualization, numerical

linear algebra performance enhancements, new algorithms for symbolic differential equations, and much more.

Wolfram Research For information 217-398-0700 www.wolfram.com

Newly offered instrumentation, apparatus, and laboratory materials of interest to researchers in all disciplines in academic, industrial, and government organizations are featured in this space. Emphasis is given to purpose, chief characteristics, and availability of products and materials. Endorsement by *Science* or AAAS of any products or materials mentioned is not implied. Additional information may be obtained from the manufacturer or supplier by visiting www.science.labvelocity.com on the Web, where you can request that the information be sent to you by e-mail, fax, mail, or telephone.

For more information visit **GetInfo**,
Science's new online product index at
<http://science.labvelocity.com>

From the pages of GetInfo, you can:

- Quickly find and request free information on products and services found in the pages of *Science*.
- Ask vendors to contact you with more information.
- Link directly to vendors' Web sites.




“To break a barrier It’s good to have Leica as a partner.”

In 1873, Ernst Abbe discovered that diffraction limits the resolution of a light microscope. Since then nobody thought that optical microscopes would ever image details much smaller than the wavelength of light.

Stefan Hell has changed this view.

Prof. Hell, today Director at the Max Planck Institute for Biophysical Chemistry in Göttingen, came up with the first physical concepts breaking the diffraction barrier. He and his team have verified nanoscale resolution in fluorescence microscopy using conventional lenses.

For his pioneering experiments, Stefan Hell has continuously relied on lenses from Leica.

 www.confocal-microscopy.com

Leica
MICROSYSTEMS

» advances in:

Laboratory Automation

Moving More of Less Techniques for handling ever smaller amounts of liquid change the scale and speed of scientific discovery. In basic research, biotechnology, and pharmaceutical studies, scientists benefit from automated assays that require smaller amounts of sample. Smaller samples also allow for higher throughput experiments, which require sophisticated software to keep the work flowing smoothly.

BY MIKE MAY AND GARY HEEBNER

Anyone who used sterile technique with stacks of tissue-culture plates knows how tedious such a process gets. It can take hours to change medium, and keeping track of which plates received what operation demands special care. To handle fluids more efficiently, scientists wanted a connected group of containers, the ability to use smaller volumes of reagents, and simpler methods to keep track of how each sample gets treated.

The 96-well microplate fulfilled many of those desires. Multiwell plates also triggered advances in laboratory automation and miniaturization. As the following experts reveal, handling fluids more quickly and efficiently plays a fundamental role in pushing basic and applied research to ever faster speeds.

Lowering the Levels

Today, scientists can also purchase 384- and 1,536-well plates. Despite the increasing number of wells, the overall plates take up the same size. According to Michael McFarland, business technology manager at **Corning Life Sciences**, “Every industry needs standards to enable automation platforms to evolve cost effectively. The SBS [Society for Biomolecular Screening] footprint microwell plate enabled differ-

ent equipment manufacturers to design to a single standard, and the concept was scaleable simply by changing the number of wells within that footprint.”

Moreover, different experiments demand wells of different shapes and made of different materials or coated with different treatments. Companies like Corning, **Nalge Nunc**, and **Greiner Bio-One** offer a range of plasticware products. For example, Corning offers microwell plates with modified polystyrene surfaces. McFarland says, “Some cells like to grow on a surface, and others prefer growing in suspension. Some assays—such as ones involving microscope imaging—need cells to stay in place.”

Corning also offers its CellBIND surfaces for cell based assays. McFarland says that this treatment encourages many cell lines to attach faster and proliferate more quickly. He adds, “This is also very useful in any situation where a scientist needs a way to get more cells, such as producing cells for high throughput screening assays or when using cells to produce biotherapeutics.”

Relying on Robotics

As the wells increase in microplates, scientists need automated techniques for routine and repetitive tasks. Automated work stations from companies including **Beckman**, **Caliper Life Sciences**, **Hamilton Company**, **PerkinElmer**, and **Tecan** can deliver small volumes of reagent or wash the samples in microwell plates around the clock. **MORE >>>**

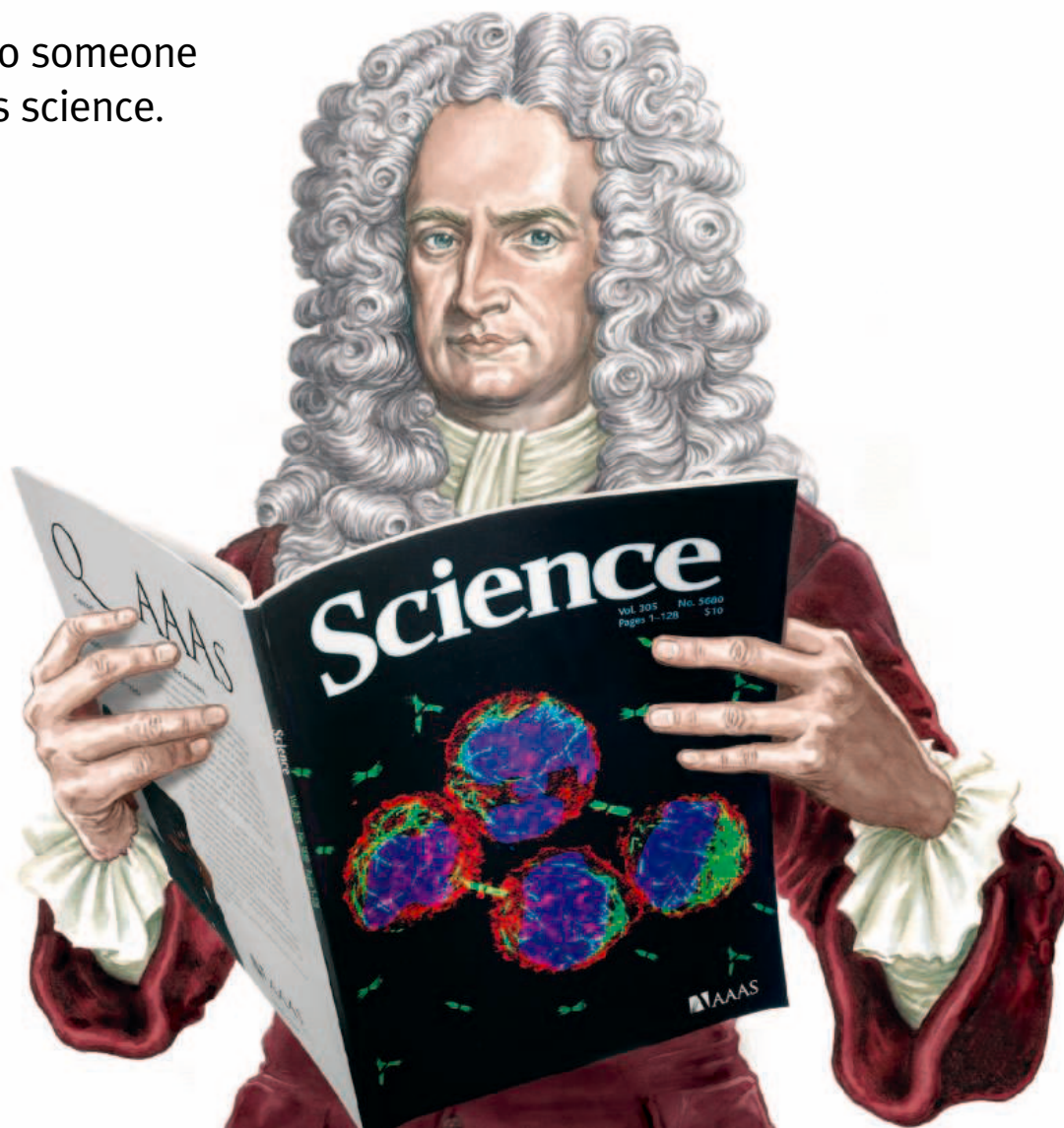
In this issue:

- > Standardizing multiwell plates
- > Modifying microwell surfaces
- > Robotic liquid handling
- > Higher density microarrays
- > Integrated microfluidics
- > Watching workflow

The companies in this article were selected at random. Their inclusion in this article does not indicate endorsement by either AAAS or Science, nor is it meant to imply that their products or services are superior to those of other companies.

Looking for a career that defies the law of gravity?

Then talk to someone who knows science.



Isaac Newton
1642–1727

If you want to head upward in the world of science, it's essential you don't leave your career to chance. At ScienceCareers.org we know science. We are committed to helping you find the right job, and to delivering the advice you need. Our knowledge is



firmly founded on the expertise of *Science*, the premier scientific journal, and the long experience of AAAS in advancing science around the world. So if you want your career to bear fruit, trust the specialist in science. Go to ScienceCareers.org

ScienceCareers.org

We know science



» advances in: Laboratory Automation

According to Joerg Pochert, director of the pharma and biotech group at Hamilton, scientists seek increasing reproducibility and process stability. This is why Pochert's company developed the Microlab STAR liquid-handling work station. Pochert says, "The STAR is something that has not been available so far. There are no syringes, no pumps, and no tubing." Instead, this system works like automated, hand-held pipettes. Pochert adds, "This technology also allows us to monitor each pipetting step, therefore achieving previously unknown process stability."

Micro Spots and Micro Flows

Although multiwell plates handle small volumes, microarrays and microfluidic devices go even smaller. Both of these technologies attract many companies, including **Affymetrix**, **Febit AG**, and **NimbleGen** for microarrays and **Agilent Technologies**, Caliper Life Sciences, and **Cepheid** for microfluidics.

In microarrays, advances often revolve around more genes on an array or processing arrays more quickly. Stephen Fodor, chairman and chief executive officer of Affymetrix, says, "The GeneChip Mapping 100K Array Set is capable of genotyping over 100,000 SNPs [single nucleotide polymorphisms]." He adds, "Jeffrey Friedman, Markus Stoffel, and Jan Breslow of the Rockefeller University are using this array technology to genotype approximately 200,000 SNPs per individual for the complete adult population of the Micronesian island of Kosrae." This population is especially interesting because it developed obesity following dietary changes—receiving Western foods—after World War II. Fodor says, "Rockefeller scientists are using genotyping microarrays to identify the exact genetic variations that might explain why only some individuals developed obesity, cardiovascular disease, and diabetes."

Scientists can combine biological assays with microscale plumbing to build what is known as a lab-on-a-chip. Kevin Hrusovsky, president and chief executive officer of Caliper Life Sciences, says, "Our LabChip technology uses miniature volumes of sample to run tests that have multiple advantages over traditional assays—accurate, information-rich data being the most important of these advantages." The microfluidic chip brings together the target and reagents, separates the analytes or cells of interest, and then the reaction can be detected directly on the chip. Hrusovsky adds, "Our LabChip 3000 Drug Discovery System, which was launched in February 2004, is gaining rapid acceptance as a very proficient way to do drug screening and drug discovery."

Tracking the Workflow

As new automation techniques allow more samples to be processed and analyzed faster, scientists need better tools to keep track of the process. A variety of companies—including **Accelrys** and **MDL Information Systems**—provide products to track data.

According to Scott Kahn, chief scientific officer at Accelrys, "The most fundamental challenge in lab automation is how to develop a workflow that doesn't just collect data but acts on it and does necessary analysis on the fly to drive the result to its ultimate destination." In other words, the analysis software helps a scientist decide how to run an experiment in real time.

Accelrys provides several new approaches to automation. Its Accord HTS manages high throughput experiments, Accord Inventory manages libraries of compounds, and Pipeline Pilot links disparate data and creates a processed result. Osman Güner, Accelrys's executive director of cheminformatics and rational drug design, says, "These tools enable a scientist to make better informed decisions, and there are lots of very expensive decisions in discovery, design, and development of a new product."

The combination of handling smaller samples in higher numbers and keeping track of the process with intelligent tools will change the experiments that scientists and clinicians can do. "To improve human health," says Fodor of Affymetrix, "we need to shift the paradigm from diagnosing and treating an existing disease, to one in which we predict disease susceptibility, determine individual response to drugs, and focus on earlier detection, more accurate diagnosis, and therapeutic management." Making more automated laboratories will help scientists push toward this arena of so-called personalized medicine and other achievements in basic research and biotechnology.

Mike May (mikemay@mindspring.com) is a freelance writer and editor based in Madison, Indiana, U.S.A. Gary Heebner (gheebner@cell-associates.com) is a marketing consultant with Cell Associates in St. Louis, Missouri, U.S.A.

ADVERTISERS

Leica [Germany]

instruments and systems for imaging analysis, including microscopes and digital cameras
+49 6441 29-0, <http://www.confocal-microscopy.com>

Leica [USA], 847-405-0123

FEATURED COMPANIES

Accelrys – a subsidiary of Pharmacoepia, bioinformatics software, <http://www.accelrys.com>

Affymetrix, DNA microarrays, <http://www.affymetrix.com>

Agilent Technologies, Inc., microfluidic devices, <http://www.agilent.com>

Beckman Coulter, Inc., automated work stations, <http://www.beckmancoulter.com>

Caliper Life Sciences, automated work stations, <http://www.calipertech.com>

Cepheid, microfluidic devices, <http://www.cepheid.com>

Corning Inc. – Life Sciences Division, plasticware for lab automation, <http://www.corning.com>

Febit AG, DNA microarrays, <http://www.febit.com>

Greiner Bio-One International, plasticware for lab automation, <http://www.gbo.com/bioscience>

Hamilton Company, automated work stations, <http://www.hamiltoncomp.com>

MDL Information Systems, Inc., bioinformatics software, <http://www.mdl.com>

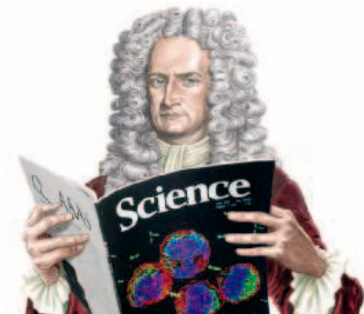
Nalge Nunc International, plasticware for lab automation, <http://www.nalgenunc.com>

NimbleGen Systems, Inc., DNA microarrays, <http://www.nimblegen.com>

PerkinElmer Life and Analytical Sciences, automated work stations, <http://las.perkinelmer.com>

Tecan, automated work stations, <http://www.tecan.com>

Classified Advertising



For full details on advertising rates, deadlines, mechanical requirements, and editorial calendar go to www.sciencecareers.org and click on **How to Advertise** or call one of our representatives.

United States & Canada

E-mail: advertise@sciencecareers.org
Fax: 202-289-6742

JILL DOWNING

(CT, DE, DC, FL, GA, MD, ME, MA, NH, NJ, NY, NC, PA, RI, SC, VT, VA)

Phone: 631-580-2445

KRISTINE VON ZEDLITZ

(AK, AR, CA, CO, HI, ID, IL, IA, KS, LA, MN, MO, MT, NE, NV, NM, ND, OK, OR, SD, TX, UT, WA, WI, WY)

Phone: 415-956-2531

BETH DWYER

(AL, IN, KY, MI, MS, OH, TN, WV and Internet Sales)

Phone: 202-326-6534

EMNET TESFAYE

(Line Advertising)

Phone: 202-326-6740

DARYL ANDERSON

(Canada and Meetings and Announcements)

Phone: 202-326-6543

Europe & International

E-mail: ads@science-int.co.uk

Fax: +44 (0) 1223-326-532

TRACY HOLMES

Phone: +44 (0) 1223-326-525

EMILIE STOTT

Phone: +44 (0) 1223-326-527

CLAIRE GRIFFITHS

Phone: +44 (0) 1223-326-528

CHRISTINA HARRISON

Phone: +44 (0) 1223-326-510

JASON HANNAFORD

Phone: +81 (0) 52-777-9777

To subscribe to *Science*:

In U.S./Canada call 202-326-6417 or 1-800-731-4939
In the rest of the world call +44 (0) 1223-326-515

Science makes every effort to screen its ads for offensive and/or discriminatory language in accordance with U.S. and non-U.S. law. Since we are an international journal, you may see ads from non-U.S. countries that request applications from specific demographic groups. Since U.S. law does not apply to other countries we try to accommodate recruiting practices of other countries. However, we encourage our readers to alert us to any ads that they feel are discriminatory or offensive.

ScienceCareers.org

We know science



POSITION OPENS

**R. JAMES COOK ENDOWED CHAIR
CROPPING SYSTEMS PATHOLOGY**
Position # 82257/82258—Search # 3917
Departments of Plant Pathology and
Crop and Soil Sciences, Pullman Campus

ASSOCIATE or FULL PROFESSOR/ASSOCIATE or FULL SCIENTIST, R. James Cook Endowed Chair in Cropping Systems Pathology: Washington State University, Pullman, Washington. The Departments of Plant Pathology and Crop and Soil Sciences, College of Agricultural, Human, and Natural Resource Sciences, invite applications for a permanent, full-time (nine to 12 months) tenure-track or tenured appointment (70 percent research, 30 percent teaching). Required: an earned Doctorate in plant pathology, crop science, soil science, or related field and experience and scholarly activity consistent with tenured faculty. For a complete notice of vacancy listing qualification for this position, visit [website: http://www.hrs.wsu.edu/employment/FAPvacancies.asp](http://www.hrs.wsu.edu/employment/FAPvacancies.asp) (Search # 3917). Submit letter of application specifically addressing each required and desired qualification, curriculum vitae, copies of college/university transcripts, and three letters of recommendation (letters should address qualifications for tenure and be sent directly from referees) to: **Dr. Dennis Johnson, Search Committee Chair, Washington State University, Department of Plant Pathology, P.O. Box 646430, Pullman, WA 99164-6430. Telephone: 509-335-3753; fax: 509-335-9581; e-mail: djohn@wsu.edu.** Screening: April 20, 2005. *Equal Employment Opportunity/Affirmative Action/ADA.*

The Department of Physiology, Louisiana State University Health Sciences Center (LSUHSC), New Orleans seeks outstanding candidates for up to four tenure-track faculty positions at the **ASSISTANT to FULL PROFESSOR** level. The successful candidate must have a Ph.D. and/or M.D. degree with a strong record of research accomplishments in one or more of the following research areas: pathophysiology of the host defense response to oral, lung, or systemic inflammation and infection; renal physiology; obesity and diabetes; angiogenesis.

There are excellent opportunities for collaboration at molecular, cellular, or systems levels of integration. Successful candidates will be expected to complement the existing research strengths of the Department, rapidly develop an extramurally funded research program, and participate in the Department's graduate and undergraduate teaching programs. An excellent startup package, competitive salary, and state-of-the-art instrumentation are available for each position. Applicants should send curriculum vitae that includes previous and current research funding, a statement of research plans, and the names of at least three references to: **Dr. Gregory Bagby (e-mail: gbagby@lsuhsc.edu), Department of Physiology, Louisiana State University Health Sciences Center, 1901 Perdido Street, New Orleans, LA 70112-1393.** *LSUHSC is an Affirmative Action/Equal Opportunity Employer.*

BIOLOGIST
ASSISTANT PROFESSOR

Tenure track, Ph.D. required. The University of South Carolina Aiken (USCA) is a predominantly undergraduate institution with a strong emphasis on teaching and research. The Department of Biology and Geology has a history of independent, funded research programs often involving undergraduates. We seek a biologist with expertise in anatomy or developmental biology to complement existing departmental strengths. Teaching duties include human anatomy and specialty area. Apply online at [website: http://uscjobs.sc.edu](http://uscjobs.sc.edu) and submit three current letters of reference to: **Dr. Hugh G. Hanlin, Chair, Search Committee, Department of Biology and Geology, University of South Carolina Aiken, Aiken, SC 29801-6309.** Complete applications received by 1 March 2005 will receive full consideration. *Women and minorities are encouraged to apply. USCA is an Affirmative Action/Equal Opportunity Employer.*

POSITION OPENS

**FACULTY POSITIONS
EXPERIMENTAL PATHOLOGY**
University of Oklahoma Health
Sciences Center

The Department of Pathology invites applications for two tenure-track positions: one at the **ASSISTANT or ASSOCIATE PROFESSOR** level, one at the **ASSOCIATE to PROFESSOR** level. Both positions will be awarded to individuals with active translational or basic molecular programs in cancer research and current ROI funding or the equivalent. Endowed positions from the Oklahoma University (OU) Cancer Center or the Department of Pathology are available for the right candidate. Individuals will be expected to participate in the departmental and interdisciplinary graduate programs, collaborate with other cancer center investigators, maintain a vigorous and funded research program, and participate in graduate and medical student education. Experimental pathologists (M.D.) or experimentalists (Ph.D. or equivalent) are encouraged to apply.

The University of Oklahoma Health Sciences Center (OUHSC) is located on a 250-acre health science campus in Oklahoma City, Oklahoma. It includes the OU Medical Center, the College of Medicine and six other graduate colleges in the health sciences. The Department of Pathology and OUHSC are undergoing major expansion, with new research space, new mouse facilities, and a cancer center building under construction. Major scientific targets for expansion include molecular genetics and cancer research. For further details visit [website: http://www3ouhsc.edu/pathology](http://www3ouhsc.edu/pathology).

Applicants should submit curriculum vitae, a concise description of research interests and goals, recent and current funding, and the names, addresses, telephone numbers, and e-mail addresses of three references to: **Dr. Ann Thor, Lloyd E. Rader Professor and Chair, Department of Pathology, P.O. Box 26901, BMSB 451, Oklahoma City, OK 73190.** Applications will be accepted until the positions are filled. *The University of Oklahoma is an Affirmative Action/Equal Opportunity Employer.*

SENIOR STAFF ASSOCIATE
Columbia University Medical Center
Department of Pathology

Position available to investigate the role of lipid metabolism in organelle trafficking, cytoskeletal dynamics, and disease-related processes using a mouse genetic approach. Applicants must hold a B.A./B.S. with eight years of research experience in mouse genetics, molecular biology, and cell culture. Must be familiar with gene targeting vector design and embryonic stem cell screening. Experience in basic biochemistry, including protein and lipid biochemistry, as well as light/fluorescence microscopy is desirable. Send curriculum vitae to: **Dr. G. Di Paolo at Columbia University, Department of Pathology, College of Physicians and Surgeons, 630 West 168th Street, Room 12-403, New York, NY 10032;** or via e-mail: gd2175@columbia.edu. *Columbia University takes Affirmative Action to ensure Equal Opportunity.*

NEUROBIOLOGY RESEARCH-TRACK (FACULTY) and POSTDOCTORAL POSITIONS, available immediately to investigate neurotransmitter actions and synaptic neurophysiology in mammalian olfactory bulb and piriform cortex. Experience with in vivo/vitro electrophysiology, patch clamping, or optical imaging required. All positions include highly competitive salary/fringe benefits, grant opportunities and interaction with neuroscientists in the Department ([website: http://www.utmem.edu/anatomy-neurobiology/](http://www.utmem.edu/anatomy-neurobiology/)) and the Neuroscience Program ([website: http://cns.utmem.edu/](http://cns.utmem.edu/)). Applicants must have a Ph.D. or M.D. Send applications (curriculum vitae and names of three references) to: **Matt Ennis (e-mail: mennis@utmem.edu), Department of Anatomy and Neurobiology, University of Tennessee Health Science Center, 855 Monroe Avenue, Suite 515, Memphis, TN 38163.** *University of Tennessee is an Affirmative Action/Equal Employment Opportunity/ADA Employer.*

CHIRON



Creating products that transform human health worldwide.

At Chiron, our aim is to prevent and treat diseases, and improve people's lives. A global biopharmaceutical leader with over 5500 employees worldwide, Chiron, headquartered in Emeryville, California, in the San Francisco Bay Area, continues to grow, and we are currently seeking experienced professionals to join us. ***Come make a difference!***

ASSOCIATE DIRECTOR, RESEARCH

Currently seeking PhD medicinal chemist responsible for directing a team of PhD and BS/MS level chemists performing research and development of small molecule therapeutics in a highly collaborative multi-disciplinary team environment. Experience in the design of therapeutics for oncology indications and in structure-guided drug design a plus. Requires PhD in Organic or Medicinal Chemistry with 8+ years of small molecule medicinal chemistry drug discovery experience. **44002996-RK**

DIRECTOR, RESEARCH

Candidate will lead projects in oncology from the antibody discovery phase up to IND-enabling studies. Requirements for this position include MD/PhD in Immunology or Oncology, along with 10 years of post-graduate experience, including 5 years in biotech or pharmaceuticals. **44002909-RK**

PRINCIPAL SCIENTIST, RESEARCH

Develop projects in immunohistochemistry, and design, implement and interpret scientific research projects between Experimental Pathology and Molecular and Cell Biology. Requires PhD in a biological scientific discipline, postdoctoral work, and 5-8 years of related experience. **44003007-RK**

PRINCIPAL SCIENTIST, RESEARCH

Support oncology drug discovery and development. Successful candidate will sit on late stage research and early development project teams for small molecule oncology drugs. Design, implement, analyze and interpret toxicology studies in-house and at CROs, write and review regulatory documents, and sit on project teams. Experience with in vitro toxicity screening useful. Requires PhD in Toxicology or related field with 5-8 years pharmaceutical industry experience. American Board of Toxicology certification desirable. **44003008-RK**

PRINCIPAL SCIENTIST, RESEARCH

Play a central role in target validation and the preclinical evaluation of antibody therapeutics for cancer. Design, plan and perform experiments to validate targets for anti-cancer therapeutic antibodies. Requires PhD in Cell Biology or related field with more than 5 years of postgraduate experience in cancer cell biology and antibody therapeutics. **44003039-RK**

SCIENTIST II, RESEARCH

Participate in and perform the design, development, execution, and interpretation of scientific research projects pertaining to the bioassays department. Contribute to small molecule drug discovery in the field of Oncology. Requires PhD in Applied Cell Biology or Biochemistry, with postdoctoral work and 3-5 years of related experience. **44003011-RK**

SPECIALIST I, RESEARCH

Support research projects in therapeutic antibodies and small molecule drug discovery. Develop purification processes and produce proteins for efficacy studies, X-ray crystallography, and high-throughput screening. Requires BS/MS in Biochemistry or a related scientific discipline, with a minimum of 5 years related experience. **44003009-RK**

SENIOR SCIENTIST, RESEARCH

Provide expertise in preclinical models, PK/PD understanding, in vivo biomarker discovery and assay development in support of projects that span from research to clinical development. Broad scientific experience in cancer biology is essential. Prior research experience with pharmacodynamic investigations using in vivo tumor models required. **44002910-RK**

SPECIALIST I, RESEARCH

Develop and perform cell-based assays as part of the hit evaluation. Employ a variety of automation instruments, signal detection technologies, and analysis techniques in this process. Ideal candidate would have experience with FACS and High-Throughput Imaging Instruments and familiarity with spreadsheet/curve-fit/graphic software. Requires BS or MS in Cell Biology, Biochemistry or related field, with minimum of 5 years work experience. **44003012-RK**

SPECIALIST I, RESEARCH

Develop and utilize in vivo models and cell-based assays to assess the efficacy and mechanism of action of novel therapeutics for oncology. Also assist in the design, development and execution of studies, analyze data, and prepare summary reports. A BS with at least five years of related experience in a research setting, or an MS with three years of experience is required, along with 3 years of in vivo model experience. **4003105-RK**

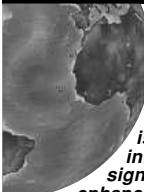
We offer an outstanding compensation/benefits package and actively promote a work-life balance.

For complete job descriptions, and to apply, please visit:

www.chiron.com

Chiron welcomes candidates from diverse backgrounds.

EXTENDING & ENHANCING HUMAN LIFE.



Bristol-Myers Squibb is a world leader in oncology, infectious diseases, diabetes, immunology, neuroscience and cardiovascular research. The Bristol-Myers Squibb Pharmaceutical Research Institute (PRI) is one of the industry's most productive and respected research organizations. It is dedicated to discovering and developing innovative, cost-effective medicines that address significant unmet medical needs that extend and enhance human life. We are currently recruiting new scientists who have the creativity and drive to discover and develop the medicines of tomorrow. You will have the support of a culture that believes in making the unattainable a reality every day. You will also have the potential for career development and mobility across our entire drug development process. We value our people and the work they do. From salary and stock options, to bonuses and medical plans, we strive to generously reward our people for their valuable efforts. Exciting Bioinformatics opportunities are available to you in our Pharmaceutical Research Institute:

SENIOR RESEARCH INVESTIGATOR II, HOPEWELL, NJ (JOB CODE 7553)

The ideal candidate will work closely with bench scientists, the Bioinformatics team, and Biostatistics team to develop tools, as well as analyze and interpret transcriptional profiling, proteomics, metabolomics, and high-content screening data in all areas of the R&D pipeline. The candidate will directly participate in experimental design and hypothesis testing in the drug discovery and development process and will contribute to both the design and delivery of data analysis to our colleagues. Open source contributions to public bioinformatics efforts such as BioPerl and BioConductor will be encouraged when aligned with BMS goals.

A Ph.D. in the Natural Sciences and a minimum of 3 years' relevant experience in the development of algorithms for analysis of profiling data are required. Statisticians with a very strong background in biological data analysis are encouraged to apply. Very strong computing skills are necessary, including but not limited to software development and programming in Perl, Web, and SQL environments. Extensive experience using sound statistical methods and programming in statistical environments such as R, SAS, and S Plus is advantageous. The successful candidate must be comfortable working in a high-performance computing Unix/Linux mainframe, cluster, and grid environment. Excellent interpersonal and oral and written communication skills are a must.

BIOINFORMATICS DEVELOPER, HOPEWELL, NJ (JOB CODE 7773)

The successful candidate will be responsible for the primary support and enhancement of BMS enterprise-wide knowledge bases for target-centric biological information and DNA sequencing informatics across all areas of R&D. The role includes support of complex Perl/Web/Oracle applications/databases and continuous enhancements to meet the evolving needs of the BMS research community. In addition, the candidate will design and develop new tools to integrate BMS genomic data with chemistry and biology experimental data in a rapid application development environment. They will work seamlessly with staff of Bioinformatics, PRI and Corporate Informatics to ensure that Genomic information is integrated into the broader BMS IT infrastructure. Open source contributions to public bioinformatics efforts such as BioPerl and BioConductor will be encouraged when aligned with BMS goals.

M.S. or equivalent in Computer Science, Bioinformatics or related discipline and 5 to 10 years' experience in Bioinformatics/Biology data management are required, preferably in an industrial research setting. Essential skills include fluency in Perl, SQL, HTML/CGI, scientific workflow analysis and scientific application design, development and support of informatics tools for managing DNA, RNA and protein sequence data; and experience in developing and supporting applications in Linux/Unix environments using RAD methodologies. Desirable skills include a working knowledge of Java, C/C++, Lisp, Oracle database design, Unix/Linux system administration and Oracle database administration, and a demonstrated ability to learn new programming environments to meet specific needs. The successful candidate will have very strong interpersonal, team working and communication skills, combined with a proven ability to work independently with senior scientists and IT professionals to develop and support integrated systems in complex multi-user environments.

Bristol-Myers Squibb offers the opportunity to work with outstanding scientists in a stimulating environment. We also offer a competitive starting salary, comprehensive benefits, and a working environment conducive to professional growth. Please paste your CV/resume text into an email and send in confidence, with Job Code ##### in subject line, to external.jobs@bms.com or visit our website at <http://www.bms.com/career/data/> for a complete listing of opportunities.

Bristol-Myers Squibb is proud to be an equal opportunity employer, M/F/D/V.



Bristol-Myers Squibb Company

www.bms.com



UNIVERSITY of VIRGINIA

PROFESSOR & CHAIR

Department of Internal Medicine

The University of Virginia School of Medicine invites applications for the position of Professor and Chair of the Department of Internal Medicine. The Department has a long tradition of excellence in basic and clinical research, education and clinical practice.

We are seeking candidates with highly developed leadership, collaborative communication and interpersonal skills. The successful candidate will be expected to have an outstanding academic record in clinical care, research and education. The candidate must be able to define and communicate a vision and strategic direction for the department, as well as provide important input into the academic direction of the School of Medicine and Medical Center. In addition, the candidate must be able to shape annual departmental objectives and plans and manage the support of these goals.

This position will have a five-year appointment. Full review commences February 1, 2005. Position is open until filled. Candidates must meet the criteria for appointment to senior faculty ranks and be Board Certified in Internal Medicine.

Please submit electronically and in hard copy a letter of interest, a curriculum vitae, and the names and addresses of three referees to:

**Search Committee for Professor and Chair of
Department of Internal Medicine
University of Virginia - School of Medicine Dean's Office
PO Box 800793, Charlottesville, VA 22908
Attention: Shirley Rothlisberger**

srr8w@virginia.edu

*The University of Virginia is an Equal
Opportunity/Affirmative Action Employer.*

ANNOUNCEMENT

The Federation of American Societies
for Experimental Biology (FASEB)

Editor-in-Chief of *The FASEB Journal*

The position of Editor-in-Chief (EIC) of *The FASEB Journal* will become available as early as July 1, 2005, but needs to be filled no later than January 1, 2006. A search committee has been appointed by the FASEB Board and the FASEB Publications Committee to initiate the search for a distinguished scientist to head this interdisciplinary journal. Candidates should have a Ph.D., M.D., or an equivalent academic degree, broad experience in experimental biological and biomedical sciences, and prior experience in editorial activities related to these scientific fields. The appointment would be for a five-year term, with potential reappointment. The EIC would report to the Board of Directors of FASEB through the FASEB Publications and Communications Committee but he or she would have extensive flexibility in selecting the Associate Editors, the Editorial Board, and future directions for the Journal. Candidates interested in the position should submit a statement of interest, along with their curriculum vitae and the names of three references to Donald A. Fischman, M.D., Chair, FASEB J. Search Committee, C/O Ms. Lynn Willis, Managing Editor, FASEB J, 9650 Rockville Pike, Bethesda, MD 20814-3998; or by email to lwillis@faseb.org. **The application deadline is May 1, 2005.**



Research Geneticist (Plants) Computational Biology/Bioinformatics

The Corn Insects and Crop Genetics Research Unit, Ames, Iowa is searching for **3 Research Geneticists** with experience in computational biology/bioinformatics who will perform research leading to success of the mission for this highly productive unit. The positions will be housed in the **Departments of Plant Pathology (ARS-X5W-0132)** and **Agronomy (ARS-X5W-0071, ARS-X5W-0137)** on the Iowa State University campus in Ames, IA. The mission of the Unit is to (1) develop strategies for genetic improvement of adapted and exotic corn germplasm under conventional and sustainable systems and improve our understanding of the relationship between these genetic improvements and genome modifications; (2) develop a basic understanding of the soybean genome by use of molecular and classical genetics and cytogenetic analysis; (3) develop a basic understanding of molecular mechanisms of interactions between cereal pathogens and their hosts; (4) develop new and improved methods and strategies for managing pest insects of corn and their biological control agents, consistent with low environmental impact; and (5) elucidate ecology, behavior, and genetics of pest insects of corn and their natural enemies.

GS-12/13 (\$60,576 - \$93,643). The successful candidate will lead a vigorous, independent research program focused on high-throughput functional genomics in plants. The candidate will interact with existing programs to integrate data from genetic and physical maps, genome and EST sequences, functional genomics, and parallel-expression profiling to investigate global gene expression in crop plants, including but not limited to effects of transgene insertion, gene duplication, and evolutionary diversity. Experience in interdisciplinary scientific computing, plant genomic and proteomic data analysis, or database development is desirable. For further information on this position contact

Dr. Roger Wise at rpwise@iastate.edu. See vacancy announcement **ARS-X5W-0132**.

GS-13/14 (\$72,035 - \$110,662). The successful candidate will conduct complex studies to develop innovative genomic and computational tools and methodology that effectively analyze DNA sequences, functional genomic data, genetic and physical maps, and genome organization of legumes. The successful candidate will be expected to interact with existing genomic programs, molecular and classical geneticists, database developers and breeders to integrate a broad range of interdisciplinary resources. Experience in computational biology, plant genomics, and database development is desirable. For further information on this position contact **Dr. Randy Shoemaker** at rcsshoe@iastate.edu. See vacancy announcement **ARS-X5W-0071**.

GS-12/13 (\$60,576 - \$93,643). The successful candidate will lead a vigorous, independent research program focused on developing genomic and biological analysis protocols and unique storage solutions for diverse data types from crop plants and will serve as the project lead for MaizeGDB, a database of genome information. The candidate will interact with existing programs to integrate genetic and physical maps, genomic and expressed sequences, assembled sequence contigs, mutant phenotype descriptions, and other related data to generate novel resources enabling plant biologists worldwide to practice a systems biology approach to understanding complex biological relationships. Experience in interdisciplinary scientific computing, biological database development, plant genomic data analysis, classical genetics, and molecular, cellular, and evolutionary biology is desirable. For further information on this position contact

Dr. M. Paul Scott at pscott@iastate.edu. See vacancy announcement **ARS-X5W-0137**.

Salary is commensurate with experience. Candidates must be U.S. citizens. A Ph.D. and postdoctoral experience preferred. Applicants must meet requirements as described in the full vacancy announcement. Incumbents will be expected to publish and present research results. A comprehensive benefits package includes paid sick and annual leave, life and health insurance, and a savings and investment plan, in addition to a federal retirement plan. The full vacancy announcement(s) and application information may be obtained by phoning 301-504-1482, via the website <http://www.afm.ars.usda.gov/divisions/hrd/>, or contacting **Janae Lentz** at **515-663-7277**. Applications in response to this ad must be postmarked by closing dates referenced in each vacancy announcement.

THE USDA/ARS IS AN EQUAL OPPORTUNITY PROVIDER AND EMPLOYER.

Director and Chief Executive

The Babraham Institute

Cambridge, UK



The Babraham Institute is an internationally renowned biomedical research institute sponsored by the Biotechnology and Biological Sciences Research Council (BBSRC). The Institute is situated on the Babraham Research Campus, a parkland site five miles south of Cambridge, which is undergoing substantial investment and development for both academic research and medical biotechnology. The Institute has about 360 staff on the campus and 60 graduate students, all of whom are registered with the University of Cambridge.

The Institute's research is focused on epigenetic, developmental and signalling events that underlie cell function, providing international leadership in key areas of post-genomic research, contributing considerably to the overall biomedical responsibility of the BBSRC. Research is exploited by Babraham Biosciences Technologies Limited (BBT), which is successfully promoting technology transfer, licensing and biocubation.

KEY ELEMENTS OF THE ROLE INCLUDE:

- Delivery of internationally competitive programmes of research.
- Development of vision for the Institute's future including its collaborations and partnerships with others nationally and internationally.
- Development of knowledge transfer and innovation activities of the Institute, including links with industry and further development of the Research Campus including executive board membership of BBT.
- Contributing both to BBSRC decisions on science priorities and strategic issues affecting institutes.
- "Head of Department" role for graduate students.

THE PERSON:

- Strong academic reputation and experience of leading internationally competitive research.
- Excellent leadership, management and communication skills.
- A track record of working effectively with senior academic scientists, government, industry and the public would be advantageous.
- Interest in the wider scientific and political environment and a desire to make a contribution to the development of science education and awareness generally in the UK.

Further information on the Institute and BBSRC can be found on www.babraham.ac.uk and www.bbsrc.ac.uk

Interested candidates should e-mail their CV to Ann Gales at search@rustonpoole.com before February 21st 2005. Alternatively, please phone +44 (0)20 7930 3001 for a confidential discussion.

Ruston Poole International plc, Cording House, 34 St. James's Street, London SW1A 1HD.



Recruiting excellence
worldwide

RUSTON POOLE
International

PRINCIPAL INVESTIGATORS

THE NATIONAL INSTITUTE OF BIOLOGICAL SCIENCES
(NIBS), BEIJING, CHINA

The National Institute of Biological Sciences (NIBS), Beijing seeks applications to fill multiple Principal Investigator (PIs) positions starting this fall. The successful candidates are expected to run their own independent research in this modern research institute studying mechanism-based aspects of biological sciences regardless of experimental systems.

The candidate should have a Ph.D. degree and several years of postdoctoral training. The initial appointment will be for 5 years, with full support by the NIBS. Renewal of appointment will be based on merit and is conditional upon passing reviews by international committees. In addition to wide open modern laboratory space, generous start-up packages, and internationally competitive salaries, NIBS aims to provide PIs with an exciting environment, collegial and interactive colleagues, efficient administrative and support mechanisms, first rate technology core facilities, outstanding graduate students, opportunities for substantial communications with the international scientific community. NIBS is particularly experienced in helping young scientists who are fresh out of their postdoctoral training to establish their laboratories quickly and efficiently so that they can start doing significant and creative research without much delay. Applicants should send in their CVs and research interests (limited to 3 pages) in English to the following email address:

wangtao@nibs.ac.cn or wangt71@yahoo.com.cn.

They should also arrange for 3 recommendation letters to be sent to the same address.



Vice President
for
Academic Programs and Dean

Applications are sought for the position of Vice President for Academic Programs and Dean at the Woods Hole Oceanographic Institution (WHOI).

The Vice President for Academic Programs and Dean is responsible for Institutional educational policy and practices, coordinates the joint graduate program with the Massachusetts Institute of Technology (MIT), oversees academic recruiting, directs the allocation of financial resources, and participates in development activities. In addition, the Vice President for Academic Programs and Dean will be expected to provide leadership in identifying new educational directions as well as interact at the national and international levels on issues of oceanographic and scientific educational policy. A strong commitment to scholarship and education is essential, demonstrated by a distinguished record in research, teaching, academic leadership, and management. A Ph.D. in a discipline related to ocean science is required, with credentials appropriate to appointment at the level of Senior Scientist (equivalent to Full Professor).

WHOI is a private research and educational institution that conducts disciplinary and interdisciplinary research in ocean-related areas of biology, chemistry, geochemistry, engineering, geology, geophysics, physical oceanography, and marine policy. The Vice President for Academic Programs and Dean is responsible for the quality and vitality of all Institution education programs, including the joint graduate program with MIT postdoctoral and undergraduate fellowships, and traineeships.

To learn more about the position, please contact the search committee chairman, **John Trowbridge**, by phone (508-289-2296) or e-mail (jtrowbridge@whoi.edu). To apply for the position, please begin the formal application process online at <http://jobs.whoi.edu>. The review of applications will begin on **March 1, 2005**. Applications will be accepted until the position is filled.

WHOI is an Affirmative Action/Equal Opportunity Employer. M/F/D/V/EOE. Women and Minorities are encouraged to apply.



**Department of Medical Oncology
Division of Hematologic Neoplasia**

The Department of Medical Oncology at the Dana-Farber Cancer Institute and the Department of Medicine, Brigham and Women's Hospital and Harvard Medical School, announce a search for two tenure-track laboratory investigators at the Assistant Professor level to join the Division of Hematologic Neoplasia. The successful applicants will develop an independent translational research program in areas relevant to hematologic malignancies. These may include hematopoietic stem cell transplantation, lymphoid malignancies, and cancer immunology. Candidates should hold an MD or MD/PhD and have training in oncology, hematology, or a related clinical field.

Applicants should submit a statement of interests, CV, and three letters of recommendation to:

Glenn Dranoff, M.D.
Chair, Search Committee
Dana-Farber Cancer Institute
Dana 510E
44 Binney Street
Boston, MA 02115

**Department of Health and Human Services
National Institutes of Health
National Institute of Mental Health
Molecular Imaging Branch
Medical Staff Physician in Positron
Emission Tomography**

The Molecular Imaging Branch at the National Institute of Mental Health, NIH has a medical staff physician position available on January 1, 2005, with a flexible start date. This Branch has embarked on major neuroimaging research to use state-of-the-art PET (positron emission tomography) techniques and newly developed neuroreceptor radioligands to study neuropsychiatric disorders. The NIH imaging facilities, radiochemistry laboratory, and multidisciplinary research team provide outstanding opportunities for productivity. Imaging is performed in animals to evaluate new radioligand and in humans to study the pathophysiology of several neuropsychiatric disorders. This senior position in the laboratory will supervise trainee(s), fellow(s), and support staff. The initial appointment is for 2 years, with option of unlimited renewals. Applicants may come from several medical specialties (e.g., Psychiatry, Neurology, or Nuclear Medicine/Radiology) but must possess a valid US medical license and have several years of experience with radiotracer imaging. Interested applicants should send CV and the names of two references to: Robert Innis, MD, PhD; Chief, Molecular Imaging Branch, NIMH, Building 1, Room B3-10, 1 Center Drive MSC-0135, Bethesda, MD 20892-0135, Email: robert.innis@nih.gov. Women and minorities are encouraged to apply.

**DHHS and NIH are Equal
Opportunity Employers**

**Department of Health and Human Services
National Institutes of Health
National Eye Institute**

Ophthalmic Genetics Branch Chief

The National Eye Institute (NEI) seeks an outstanding clinician scientist for the tenured position of Chief, Ophthalmic Genetics and Visual Function Branch (OGVFB) in the Division of Intramural Research. This recruitment is directed towards clinicians with expertise in retinal neurodegenerative disease and offers a unique opportunity for a talented individual to provide strong and stimulating leadership in an organization dedicated to uncovering new scientific knowledge, both laboratory and clinical. We welcome the full range of candidates at all levels.

The Chief, OGVFB, is expected to create a vigorous research program to elucidate mechanisms of retinal neurodegenerative disease and explore treatments. The Chief will develop broad investigational plans, independently and in collaboration with other NEI investigators and research scientists in the United States and abroad. The Chief will examine and treat patients, as well as design, implement and conduct research and clinical protocols. The OGVFB includes a molecular genetics laboratory section and provides genetic services. The Chief supervises a staff of research clinicians, basic scientists, and technicians in support of the Branch's research objectives. An opportunity exists for the Chief to recruit staff and supervise training.

The NEI provides an exceptional environment for clinical research including the infrastructure necessary for patient recruitment, a clinical protocol development group, and a Contract Research Organization that provides statistical and epidemiological expertise, data management and analysis, study monitoring, regulatory guidance, and overall operational support. The NIH Clinical Center provides additional access to exceptionally broad medical and diagnostic resources.

The position requires an ability to integrate basic, clinical and translational research, and create an intellectual synergy and an environment for state-of-the-art patient care for those suffering from eye disease. The Chief will explore translational ideas in collaboration with a newly created multidisciplinary laboratory of neurodegenerative disease. This multidisciplinary laboratory is part of a complex that houses an integrated group of investigators from a diverse set of NIH Institutes, including the National Institute of Neurological Disorders and Stroke (NINDS), the National Institute of Mental Health (NIMH), the National Human Genome Research Institute (NHGRI) and the National Institute of Allergy and Infectious Diseases (NIAID). There are unparalleled opportunities for strong interdisciplinary collaborations among these independent research groups and with other investigators throughout the NIH through several on-going Trans-Institute initiatives in neuroscience, stem cell biology, gene therapy and vascular biology and angiogenesis.

At a minimum, candidates should have a Doctor of Medicine degree from a school in the U.S. or Canada approved by a recognized accrediting body in the year of the applicant's graduation, or a Doctor of Medicine or equivalent degree from a foreign medical school which provided education and medical knowledge substantially equivalent to accredited schools in the United States. Candidates should be Board-certified and have direct clinical experience in the pathophysiology of retinal neurodegenerative disease, specifically, from the perspective of understanding biological mechanisms in any of the following areas: biochemistry, cell biology, genetics or physiology.

Applicants should submit a curriculum vitae, bibliography, copies of their five most significant publications, a summary of research accomplishments and three reference letters. Applicants should also submit a written statement with their perspective on the needs and opportunities necessary to move from the basic understanding of retinal neurodegenerative diseases to clinical therapeutic interventions and improved patient care. This statement should indicate how the applicant's particular expertise and background could contribute to this transition. Applications should be sent to: **Kimberly Ruzickova, Staff Assistant, Office of the Scientific Director, National Eye Institute, Building 31, Room 6A22, 31 Center Drive, Bethesda, MD 20892; Tel: 301-451-6763, Email: Ruzickok@nei.nih.gov**. Completed applications must be received and/or postmarked by **February 28, 2005**.



*DHHS, NIH and NEI are
Equal Opportunity Employers.*



National Oceanic and Atmospheric Administration (NOAA)

Technical Director (TD)

(A Senior Executive Service Position in the Federal Government)



Department of Commerce (DOC)
National Oceanic and Atmospheric
Administration (NOAA)
National Ocean Service (NOS)
Silver Spring, MD
\$104,927 - \$149,200 annually
Vacancy Announcement NOAA #05-03



The candidate selected for this position is responsible for providing advice to the Assistant Administrator (AA) and Deputy Assistant Administrator (DAA) and conceiving, managing, coordinating and directing the observations programs across all NOS Program Offices and must possess the following:

1. Knowledge, high level experience and recognized technical expertise in one of the principal areas of NOS: oceanography/marine, physical, chemical, biological, ecological, geodesy, cartography, and/or related environmental sciences with demonstrated experience in development of research programs/studies.
2. Broad experience in the planning, organizing, managing, coordinating and directing of multi-disciplinary programs, with particular emphasis on research to manage ocean observations, and Great Lakes, coastal and/or ocean resources. Demonstrated experience and insight to recognize opportunities for advancing the science through development of state-of-the-art, and application of innovative uses of technologies.
3. Ability to perform senior level research and/or recognized professional standing in the technical community, with particular emphasis on environmental sciences, as evidenced by publications, presentations, membership and/or offices held in professional societies.
4. Demonstrated experience in managing the transition of research into operational capabilities. Ability to translate operational requirements into research/scientific priorities.

Please contact **Dede Epstein** at 301/713-0530, x106 for an announcement package (Internet: address: dede.epstein@hrmo.noaa.gov), including mailing instructions—referring to the announcement number -OR- you may access the entire full-text vacancy from NOAA's Executive Resources Homepage (see below). Incomplete applications will be returned.
<http://www.rdc.noaa.gov/hrmo/index.htm>
This vacancy will close on February 22, 2005



"NOAA Values a Diverse Workforce and is an Equal Opportunity Employer"



Post-Doctoral Instructor in Medicine Position Harvard Medical School Massachusetts General Hospital

Innovative top laboratory (*Science* 302:1223, 2003 and *Molecular Cell Biology* 19:8646, 1999) seeks motivated candidates with interest in basic and applied immunology. Projects include: regenerative medicine NF- κ B signaling, development of highthroughput assays for clinical trials. Proficiency in cellular assays and flow cytometry are valuable tools. Preference is extended to Ph.D. candidates.

Please submit a cover letter and CV; and three contact people with phone numbers.

Send the above materials to:

Denise Faustman, MD., Ph.D.
Director, Immunobiology Laboratory
Massachusetts General Hospital
Building 149, 13th Street, Room 3601
Boston, MA 02129
LMurphy1@partners.org



Interdisciplinary Position: Research Molecular Biologist/Research Chemist (Biochemistry)/Research Molecular Geneticist; GS-401/1320/440-12/13/14

Salary Range:
\$68,530.00 - \$125,193.00 PA

The WRRC, Foodborne Contaminants Research Unit in Albany, CA is seeking a full-time research scientist. The Unit's prior research focuses on sensitive detection of infectious agents. This position allows significant latitude in methodology, but will be directed toward practical application in early detection of disease and infection (especially prior to clinical manifestations). The incumbent's research includes developing rapid, cost-effective, analytical methods for detection of prions and their components, metabolites, and/or markers in animal tissues, foods, feeds, and environmental samples.

For more details and application directions, see www.afm.ars.usda.gov/divisions/hrd/index.html Announcement number is ARS-X5W-0143. Announcement closes **March 4, 2005**. For questions you may contact **Dr. J. Mark Carter** (mcarter@pw.usda.gov) on 510-559-6053. U.S. Citizenship is required.

USDA, ARS is an Equal Opportunity Employer and Provider.

POSTDOCTORAL POSITIONS IN MAMMALIAN MOLECULAR AND DEVELOPMENTAL GENETICS

McLaughlin Research Institute is a small non-profit research organization near the east slopes of the Rocky Mountains and provides an outstanding environment to train for a career in mammalian genetics. Applicants for these positions should provide evidence, including publication in internationally recognized journals, for their potential for an independent research career. Refer to www.montana.edu/wwwmri for additional information about the following research programs.

- Genetic Regulation of Myelination (J. Bermingham)
- Genetics of Susceptibility to Neurodegenerative Disease. (G. Carlson)
- Molecular Motors & Chemical Genetics (J. Mercer)
- Development of the Auditory and Renal Systems (P. Xu)

To apply, state clearly the program to which you wish to apply, send your curriculum vitae, a statement of research interests, and the names of three individuals whom we may contact for references to:

Training Office
McLaughlin Research Institute
1520 23rd Street South
Great Falls, MT 59405
tg@po.mri.montana.edu

Associate Vice President for Research

The University of North Dakota invites applications and nominations for Associate Vice President for Research. The Associate Vice President for Research will have a primary responsibility, in coordination with the Vice President for Research, to foster and support faculty research and other creative scholarly activity across all of the academic disciplines at the University of North Dakota. Requires a Ph.D. degree or equivalent and a strong faculty scholarly record of accomplishments qualifying for tenure and appointment in an appropriate academic department. A significant record of success in securing federal grant support for the purpose of supporting scholarly research is highly desirable. Experience in the oversight of pre- and post-award administration of grants and contracts, maintaining compliance with research regulatory requirements, program development and faculty support is desired. To apply, submit a letter of application describing the applicant's experiences and characteristics in relation to satisfying the leadership needs of the position and the University. Include a current curriculum vitae, the names, addresses, e-mail addresses and telephone numbers of four references. Applications and nominations should be sent to: **James Hikins, Ph.D., Chair, Associate Vice President for Research Search Committee, University of North Dakota, Office of the Vice President for Research, Box 8367, Grand Forks, ND, 58202**. Review of applications will begin on or about **March 15, 2005** and will continue until the position is filled. Salary is commensurate with qualifications.

The University of North Dakota is an Equal Opportunity, Affirmative Action Employer, and specifically invites and encourages applications from women and minorities.

MARIE CURIE MULTI-SITE PhD FELLOWSHIPS on Tissue Engineering

Alea Jacta EST - Early Stage Training on "Shaping the Future of a New Generation of Hybrid Human Resources for the Tissue Engineering of Connective Tissues" (MEST-CT-2004-008104)

The 3B's Research Group – Biomaterials, Biodegradables and Biomimetics, U. Minho (Portugal) is seeking for top-quality highly motivated students to perform their PhD studies supported by the Marie Curie Project "Alea Jacta EST", coordinated by Rui L. Reis (U. Minho). The following vacancies are available at U. Minho:

- 4 PhD full fellowships (3 years)
- 3 short term fellowships (3 to 9 months)

The work will be carried out in a multidisciplinary field, in direct contact with researchers with engineering, materials, polymers, chemistry, biochemistry, biological and clinical backgrounds. The "Alea Jacta EST" consortium is composed of 7 European academic and industrial institutions that develop specific research expertise on different relevant complementary scientific topics. Selected candidates will have the opportunity of carrying out their PhD in direct collaboration with several of those institutions according to a well established PhD programme. They will also be connected to the Network of Excellence (NoE) EXPERTISSUES also coordinated by Rui L. Reis and the 3Bs. For further information on the entire consortium and each one of the partners, as well as further vacancies available please see: www.dep.uminho.pt/3bs (provisional site) or http://mc-opportunities.cordis.lu/show-PRJ.cfm?obj_id=7566. The typical salary will be around 2,250 Euro/ month. Grants include also allowances for travel and mobility.

Candidates should send their detailed curriculum vitae (including marks obtained in the degrees) and a motivation letter (in English) by the 11th of March 2005 to: alea.jacta.est@dep.uminho.pt. Selected candidates should start on the 1st of April. Candidates might be called for an interview, and must follow the eligibility criteria for EST Marie Curie Mobility Actions (http://europa.eu.int/comm/research/fp6/mariecurie-actions/action/eligibility_en.html). Preference will be given to candidates that obtained high marks on their first degrees and demonstrate some research experience as demonstrated by scientific publications, and knowledge of other countries and cultures. Experience in industrial driven research will also be considered.



Editor in Earth and Space Sciences

Join the editorial team at *Science*. We are seeking a new Associate Editor in the physical sciences. Applicants should have a broad range of interests and research experience in geochemistry, geophysics, planetary science, and astrophysics. Applicants should have post-doctoral experience, multiple publications, and a breadth of knowledge of cutting-edge research in these and related fields. Responsibilities include managing the review, selection, and editing of manuscripts, working with authors on revisions, solicitation of Reviews and special issues, and fostering contacts and communication with the scientific community. The position is for either our Washington, DC, or Cambridge, UK, offices. EOE. Non-smoking work environment.

For consideration, send a resume and cover letter along with salary requirements to:

AAAS
Human Resources Department, Suite #101
1200 New York Avenue
Washington, DC 20005

Applications can also be sent by e-mail to hrtemp@aaas.org or Fax to 202-682-1630. Visit us at <http://www.aaas.org>.



Think what's possible.

Are you looking to work in a global growth company where you can make a real difference? With about 81,000 associates around the globe in our affiliates in over 140 countries, we share a vision of a better today and tomorrow for patients – a vision that drives our growth and success. Our greatest job satisfaction is knowing that we improve lives, we extend lives, and we save lives – and we do it with increasing precision and efficiency through breakthrough science and innovation.

Scientific Associates – NIBR

Basel HQ, Switzerland

We are looking for highly motivated Scientific Associates to join a molecular and cellular biology research group at the Novartis Institute for Biomedical Research (NIBR) in Basel. Our focus is to understand the mechanism of action of bioactive molecules in eukaryotic cells, including model systems such as *Saccharomyces cerevisiae*. Your task will be to perform research with the state-of-the-art molecular biology and cell biology technologies and effectively contribute to drug discovery in a multidisciplinary environment.

For this challenging task we are seeking energetic candidates with the following qualifications:

- Master degree or below education level
- Proven record in the field of molecular and cell biology with knowledge in genetics
- Previous work experience with *S. cerevisiae* would be an advantage
- Keen interest to contribute to drug discovery and solve biological questions
- Highly communicative and strong team player
- Accurate and highly independent working style
- Excellent computer skills.

To find out more please visit our website www.careers.novartis.com and go to Job ID 2531BR to apply online or write to Novartis Pharma AG, Human Resources Staffing Center, WSJ-310.1.22, CH-4002 Basel, Switzerland quoting the Job ID on the envelope.



Novartis is an equal opportunity employer.

www.careers.novartis.com

POSITIONS OPEN

ASSISTANT PROFESSOR
MICROBIAL GENOMICSDepartment of Botany and Plant Pathology
Oregon State University

The Department of Botany and Plant Pathology (website: <http://www.science.oregonstate.edu/bpp/>), Oregon State University (OSU) invites applications from individuals with outstanding research accomplishments who will establish a vigorous, innovative program in genomics (functional, structural, computational, or environmental) or systems biology of prokaryotic or eukaryotic microbes. We encourage applications from candidates whose research complements existing departmental strengths, including plant biology, plant-microbe interactions, comparative biology, bacterial genomics, and fungal biology. Centralized facilities supporting genomics, proteomics, imaging, and computational research are provided by the Center for Gene Research and Biotechnology (website: <http://www.cgrb.orst.edu>). The successful candidate will contribute to the undergraduate and graduate teaching missions of the Department. Ph.D. in molecular biology or related area and relevant experience is required. Experience with or understanding techniques used by educators to ensure educational equity and excellence in a multicultural setting required. Research accomplishment in microbial genomics preferred. Position is a 12-month, 0.75 FTE tenure-track appointment. For full consideration, apply by March 1, 2005, by sending resume, a brief summary of research accomplishments and future research plans, reprints of up to five publications, and names/phone numbers of three professional references to: **Microbial Genomics Search Committee, Department of Botany and Plant Pathology, Oregon State University, 2082 Cordley Hall, Corvallis, OR 97331-2902.** Send applications by e-mail: birkye@science.oregonstate.edu or fax: 541-737-3573. Full position announcement at website: <http://oregonstate.edu/jobs>. OSU is an Affirmative Action/Equal Opportunity Employer, and has a policy of being responsive to dual-career needs.

RESEARCH FACULTY
POSITIONS

University of Missouri–Columbia

The University of Missouri School of Medicine Department of Surgery is seeking outstanding candidates for two research faculty positions. Rank and appointment status are contingent upon qualifications.

The candidate should have strong interests and experience in clinical research and demonstrate the ability to secure funding in the areas of surgical and/or clinical research. Candidate should also have interests in surgical research teaching for medical students and residents. Candidate will be expected to develop a vigorous, externally funded research program in conjunction with other Department and University research faculty members. Applicants should send curriculum vitae to: **Steve Eubanks, M.D., Chairman, Department of Surgery, University of Missouri-Columbia, Health Sciences Center, One Hospital Drive, Columbia, MO 65212.**

To request ADA accommodations, please contact ADA coordinator at telephone: 573-884-7278 (V/TTY).

Equal Opportunity/Affirmative Action/ADA Employer. Applications from minorities and women are encouraged.

(SENIOR) RESEARCH SCIENTISTS. BIATECH is a well-funded independent nonprofit biomedical research center located in Seattle area. Our mission is to discover and model the molecular mechanisms of biological processes. BIATECH invites applications from highly motivated individuals for four positions of (Senior) Scientists, responsible for research in proteomics (mass spectrometry), biochemistry/metabolomics, bioinformatics, and algorithms. These positions require relevant degree/s and documented hands-on experience. Strong publication record is a plus. For more information, visit our website: <http://www.biotech.org>. Send your curriculum vitae/resume and cover letter to e-mail: careers@biotech.org. Affirmative Action/Equal Opportunity Employer.

POSITIONS OPEN

Bacterial or Viral Systems Biology, ASSISTANT, ASSOCIATE, or FULL PROFESSOR, tenure track. The Center for Pharmaceutical Biotechnology and the Department of Microbiology and Immunology invite faculty applications in the general area of systems biology of bacterial or viral systems, including, but not limited to, such areas as microbial genomics, proteomics, or bioinformatics. Ph.D. and postdoctoral experience required. Responsibilities include developing a strong, externally funded research program, and teaching in graduate and professional programs. Candidates at the Associate or Full Professor level must have a strong record of successful extramural funding. Successful candidate will have joint appointments within the Center and the Department of Microbiology and Immunology, with extensive collaborative opportunities in a major health sciences center. Forward curriculum vitae, description of research interests, and three reference letters to: **Dr. M. Johnson, Director, Center for Pharmaceutical Biotechnology, College of Pharmacy, University of Illinois at Chicago, 900 So. Ashland - m/c 870, Chicago, IL 60607.** Review of applications will continue until position is filled. *Affirmative Action/Equal Opportunity Employer.*

Ferring Research Institute, Inc., (FRI) is the San Diego-based research division of Ferring Pharmaceuticals (website: <http://www.ferring.com>), an established company that identifies, develops, and markets innovative products in infertility, obstetrics, gastroenterology, and urology. FRI is rapidly expanding its efforts to discover new treatment approaches in these and related therapeutic areas. Currently we seek candidates for a **RESEARCH SCIENTIST II** position in the In Vitro Pharmacology Department.

Qualified candidates have a Ph.D. in biology or related discipline, postdoctoral experience, and plus four years industrial drug discovery experience in high-throughput screening, lead optimization, and molecular pharmacology. Candidates should have experience with a variety of in vitro assays related to G protein-coupled receptors, as well as workstation automation and data systems, preferably Activity-Base, for the automated analysis and storage of results. The ideal candidate will have demonstrated success working collaboratively in project teams as well as independent initiative and project leadership experience in drug discovery. In addition, the candidate must be detail-oriented, with strong communication and multitasking skills, and supervisory experience is a plus.

Ferring Research Institute, Inc., offers competitive compensation and benefits packages. Apply by sending a cover letter and resume to: **Ferring Research Institute, Inc., 3550 General Atomics Court, 2-442 (job code RS05GC-SI), San Diego, CA 92121.** Fax: 858-455-3190 or e-mail: jobs@feringr.com.

An NIH-funded **POSTDOCTORAL POSITION** is immediately available to identify genes essential for bacterial viability and inhibitors of their function. This project will exploit a novel genetic system that allows the biosynthesis of complex cyclic peptide libraries (*Chem. and Biol.* 117:1-15, 2001). Candidates must have strong background in biochemistry, microbiology, or related fields. Experience in high throughput screening, protein engineering, or enzymology is highly desirable. Publication in internationally recognized journals and strong English language skills are a must. Send detailed curriculum vitae, research summary, and contact information for three professional references to: **Dr. Ernesto Abel-Santos, Department of Biochemistry, Albert Einstein College of Medicine, Jack and Pearl Resnick Campus, 1300 Morris Park Avenue, Bronx, NY 10461.** E-mail: ecabelsan@acom.yu.edu. *Equal Opportunity Employer.*

POSITIONS OPEN

FACULTY POSITION

JUNIOR OR SENIOR LEVEL

Department of Cellular and Molecular Physiology
Yale University
School of Medicine

The Department of Cellular and Molecular Physiology seeks applicants for a Faculty Position at the junior or senior level. Candidates must hold a Ph.D., M.D., or equivalent degree. The candidate's research interest should be in the general area of cellular and molecular physiology with particular emphasis in any of the following: integrative or translational research in genetic model systems; functional genomics of ion channels, exchangers, or transporters; and/or molecular probes or computational methods. Outstanding candidates working in other areas of cellular, molecular, and systems physiology are also encouraged to apply. Excellent opportunities are available for collaborative research as well as for graduate and medical student teaching.

Applicants should include curriculum vitae, a statement of research interests and goals, and three letters of reference. Applications should be sent by e-mail: leisa.strohmaier@yale.edu in PDF format or sent to:

Dr. Steven C. Hebert, Chair
Department of Cellular and Molecular Physiology
Yale University
School of Medicine
333 Cedar Street
P.O. Box 3333
New Haven, CT 06510

Application deadline: March 31, 2005.

Yale University is an Affirmative Action/Equal Opportunity Employer.

DISTINGUISHED PROFESSOR OF
BIOLOGY

The Division of Biology of Kansas State University (KSU) invites applications for the newly established position of Alice D. Fiedler Distinguished Professor. This individual will also be affiliated with the Terry C. Johnson Center for Basic Cancer Research. We are searching for a leader in the general area of molecular, cellular, and developmental biology who is taking a model system approach relevant to some aspect of basic cancer research. A Ph.D., M.D., or equivalent is required. Applicants must have a current record of research productivity and extramural funding consistent with the very competitive salary to be provided for this tenured, endowed professorship. Generous startup funds and laboratory space (about 3,000 square feet) will be provided. This individual is expected to catalyze further excellence in an already active program in molecular, cell, and developmental biology and basic cancer research. Further information is available at website: <http://www.ksu.edu/biology/FiedlerProf>. Applicants should submit a letter of interest, curriculum vitae, and description of future research plans to: **Dr. Rob Denell, Fiedler Search Committee Chair, Division of Biology, 232 Ackert Hall, Kansas State University, Manhattan, KS 66506-4901.** Reference letters will be arranged for candidates under active consideration. Review of applications will begin January 1, 2005, and will continue until the position is filled. KSU is an Equal Employment Opportunity/Affirmative Action Employer and actively seeks diversity among its employees.

ASSISTANT PROFESSOR
FIRE SCIENCE
School of Forestry
Northern Arizona University

Nine-month, tenure-track appointment with an initial allocation of 60 percent teaching, 30 percent research, and 10 percent service responsibilities. Teaching will be at the undergraduate and graduate levels, as well as advising students. Offer specialized courses in wildland fire science and in specific areas of expertise. Anticipated start date of this position is fall of 2005 or spring 2006. More information is available at website: <http://hr.nau.edu/m/job/299/315/554776>.



**US Environmental Protection Agency
Office of Research and Development
National Health and Environmental Effects Research Laboratory
Associate Director for Ecology Research Triangle Park, NC
Announcement #EPA-05-SES-ORD-6337**

EPA is seeking a highly qualified individual for the position of Associate Director for Ecology (ADE) to provide executive leadership and management for the ecology research program within the Office of Research and Development's (ORD) National Health and Environmental Effects Research Laboratory (NHEERL). This is a Senior Executive Service (SES) position located on EPA's Research Triangle Park, NC campus. The successful candidate provides the vision and direction for the conduct of research to increase the Agency's understanding of major environmental risks of environmental stressors (natural and anthropogenic), including the development of methods to detect and track stressors and diagnostic tools to delineate and model the etiological basis for exposure-effects. Specific areas of research responsibility include programs on terrestrial and watershed ecology, ecotoxicology, multimedia ecological effects assessment and assessment and cleanup methods for contaminated aquatic and terrestrial environments. The incumbent also supervises the Directors of NHEERL's four ecology research divisions; serves as the principal ecological scientific advisor to the NHEERL Director and the ORD Assistant Administrator; and serves as the spokesperson and representative to other Federal agencies and national and international organizations with complementary research agendas to increase coordination, collaborations and communications. To learn more about NHEERL please visit our website at <http://www.epa.gov/nheerl/> or contact **Karen Dean** at (919) 541-5037.

Qualifications: A bachelors degree (or higher) is required in one of the environmental or physical sciences. Desirable applicants will have a doctoral degree (e.g., Ph.D.) in one of the biological/ecological or physical sciences and several years of experience managing a research program.

Salary Range: The salary range is \$107,550 to \$162,100, depending on qualifications.

How to Apply: The official announcement and instructions on how to apply are available at <http://www.usajobs.opm.gov/>. Click on **Search Jobs@** then type -- Associate Director for Ecology or ORD-6337. To be considered for this position, you must submit a full application in accordance with the instructions in the official announcement. Please note that all mandatory executive and technical factors must be addressed. The application must be received by **February 28, 2005**.

SES Information: Information on the SES, including good examples of how to address the five mandatory Executive Core Qualifications (ECQs), is available at <http://www.opm.gov/ses/qualify.asp#qualify>. Additional information is available by calling the **SES Vacancy Hotline** at (202) 564-0435 or writing to: **US EPA/OARM/OHROS/SES Human Resources Team, 1200 Pennsylvania Avenue, N.W. MC-3611A, Washington, DC 20460-0001, ATTN: EPA-05-SES-ORD-6337.**

US Citizenship Is Required. It is the policy of the Government of the United States to provide Equal Opportunity in Federal employment for all persons and to prohibit discrimination in employment because of race, color, religion, sex, national origin, handicap, age, or sexual orientation through a continuing affirmative program in each executive department and agency. This agency provides reasonable accommodation to applicants with disabilities. If you need a reasonable accommodation for any part of the application and hiring process, please notify the agency. The decision on granting reasonable accommodation will be on a case-by-case basis.

Keck Fellow in Cryo-EM at UCSF

Applications are being solicited for the appointment of a second Keck Imaging Fellow *specializing in single particle cryo Electron Microscopy* at the new Mission Bay campus of the University of California, San Francisco. The goal is to bring talented independent young scientists whose research is at the forefront of cryo electron microscopy and/or single particle image analysis into our diverse and interactive research community. Keck Fellows pursue their research without the obligations of faculty membership or the constraints of a conventional postdoctoral fellowship. Thus, the Fellows Program provides an alternative or a supplement to traditional postdoctoral study following the M.D. or Ph.D. degree, and an opportunity to establish a creative and successful research program prior to obtaining a faculty position.

Keck Fellows receive a salary, start-up funds and annual research funding. They may seek extramural funds to support research groups of 2-4 members. Fellowships are nonrenewable, with a maximum term of four years.

Candidates must submit a letter from a mentor or other advisor who can comment in depth on the candidate's accomplishments and potential. In addition, the application should contain the candidate's curriculum vitae, a brief research plan, 1 or 2 reprints and at least two additional reference letters. The deadline for applications is **March 1, 2005**. Applications should be sent to attention of:

Dr. David A. Agard
Chair, Keck Fellows Steering Committee
Department of Biochemistry and Biophysics
University of California, San Francisco
600 16th Street, Room S412D
San Francisco, California 94143-2240
agard@msg.ucsf.edu

The Keck Fellows Program for Imaging is sponsored by the Keck Center for Advanced Microscopy at UCSF and the W.M. Keck Foundation. The University of California is an Equal Opportunity Employer. Women and underrepresented minorities are encouraged to apply.

Department of the Interior U.S. Geological Survey Upper Midwest Environmental Sciences Center

Center Director

The United States Geological Survey (USGS), a major science Bureau of the Department of the Interior, is inviting applications for Director of its Upper Midwest Environmental Sciences Center (UMESC), La Crosse, Wisconsin. The individual selected will be expected to lead a broad and diverse ecologically and biologically based science program within the US Geological Survey. The successful candidate will interact with numerous partner and client groups, represent the Center to USGS management, to other natural resource management agencies, and to the general public. The selectee is expected to guide the research efforts of the Center, develop and maintain meaningful partnerships with other public and non-governmental natural resource agencies, possess the ability to manage budgets, experience generating revenue, and support USGS and Department of Interior missions to lend information to assist in the management of fish and wildlife trust resources.

Qualifications: The successful candidate will have a demonstrated record as a leader of diverse biological/ecological research projects in biology, ecology, or physical sciences; evidence of strong leadership and managerial skills; strong oral and written communication skills; and may possess a Ph.D or equivalent degree in a field relevant to the position. Applicants must be U.S. citizens.

Salary/Benefits: Salary range is \$96,970 – \$126,064 with possibility of recruitment bonus and relocation expenses. Generous benefit package includes health, life, and long term care insurance; retirement plan with matching contributions; pre-tax accounts for health and dependent care.

How to apply: Position requirements and detailed application procedures are provided by accessing the USGS page <http://www.usgs.gov/ohr/oars/> or the UMESC home page at <http://www.umesc.usgs.gov>.

The Federal Government is an Equal Opportunity Employer.

POSITIONS OPEN

ASSISTANT/ASSOCIATE PROFESSORS

Marine Fisheries/Marine Mammals

The Coastal Oregon Marine Experiment Station (COMES) of Oregon State University (OSU) is pleased to announce three new tenure-track research positions in fisheries ecology, cetacean biology, and pinniped ecology. These positions are part of a major strategic thrust to develop capacity for ecosystem-based science, management, and conservation of marine resources.

These positions will be based at the Hatfield Marine Science Center (HMSC) in Newport Oregon. HMSC, the largest university marine laboratory in the Pacific Northwest, is sited on Yaquina Bay and close to a wide variety of marine habitats. It also houses divisions of the Oregon Department of Fish and Wildlife, National Oceanic and Atmospheric Administration, U.S. Environmental Protection Agency, U.S. Fish and Wildlife Service, and U.S. Department of Agriculture.

The Marine Fisheries Ecologist position (001-2161) is associated with the Salmon Ecology Initiative of OSU's Agricultural Experiment Station. The Cetacean Biologist (001-2160), and Pinniped Ecologist (001-2159) positions are associated with OSU's Marine Mammal Program.

For additional information, please go to the OSU employment website: <http://oregonstate.edu/jobs>. The positions will be posted under Unclassified Vacancies - Academic Faculty and may be found by their job numbers.

Oregon State University is an Affirmative Action/Equal Opportunity Employer.

ASSISTANT/ASSOCIATE PROFESSOR
(Tenure Track/Academic Year)

Required qualifications: Ph.D. or equivalent degree in environmental sciences, biology, chemistry, physics, ecology, atmospheric science, or in a discipline related to environmental studies with an emphasis on air quality assessment; these include but are not limited to the employment of methods in environmental assessment for the study of air sheds, the study of pollutant sources, and health effects from poor air quality. Additional qualification desired: postdoctoral experience. For more information, see our website: <http://www.lsu.edu/hrm>. Deadline is February 15, 2005, or until filled. Send curriculum vitae (including e-mail address), a two-to-three page statement of research and teaching interests, names of three references, and three representative publications to: **Dr. Vincent L. Wilson, Search Committee, Department of Environmental Studies, 1285 Energy, Coast, and Environment Building, Louisiana State University, Reference: #014247, Baton Rouge, LA 70803. Telephone: 225-578-1753; fax: 225-578-4286; e-mail: vwilson@lsu.edu.** *Louisiana State University is an Equal Opportunity/Affirmative Action Employer.*

NEUROSCIENTIST
Stanford University

The Department of Neurosurgery at Stanford University invites applicants for the position of **ASSISTANT PROFESSOR (RESEARCH)**. Preference will be given to neuroscientists with expertise in molecular biology and cerebrovascular disease. Salary will be commensurate with qualifications and experience. Applicants should submit curriculum vitae, brief description of research interests, and names of three references to:

Rona Giffard, M.D., Ph.D.
Chair, Search Committee
Attention: Harriet Davis
300 Pasteur Drive R281
Stanford, CA 94305-5327
E-mail: hdavis@stanford.edu

It is expected that the candidate will develop an academic career with responsibilities including laboratory research and teaching. *Stanford University is an Equal Opportunity/Affirmative Action Employer.*

POSITIONS OPEN

SCIENTIST/SENIOR SCIENTIST POSITIONS
TRAIT DEVELOPMENT

We are seeking highly talented and creative scientists with excellent experience in plant development, physiology, and molecular biology to utilize a range of genetic, genomic, and metabolomic tools to discover and manipulate genes that will improve growth and development, nitrogen use efficiency, and stress resistance in plants. We want individuals with strong backgrounds in transgene manipulation and genetic and phenotypic analysis to focus on manipulating plant productivity. The successful applicants will lead and expand projects and collaborate with internal and external project managers in an interactive and dynamic fashion. Minimum requirements include a Ph.D. plus three to five years relevant experience. We especially encourage applications from already established scientists. Please refer to job code Sc-0105.

Ceres, Inc., is located at a new state-of-the-art research facility in the hills of Thousand Oaks, California. We offer competitive salaries and excellent benefits including equity participation and 401K. Highly motivated individuals should send applications, including current curriculum vitae, summary of research experience, and names and addresses of three references to: **Human Resources Manager, Ceres, Inc., 1535 Rancho Conejo Boulevard, Thousand Oaks, CA 91320. E-mail: ceres-hr@ceres-inc.com.** The position is available immediately.

FACULTY POSITION

Applications are invited for a tenure-track position at the **ASSISTANT or ASSOCIATE PROFESSOR** level in the Department of Physiology and Biophysics, University of Miami School of Medicine. (In exceptional cases, an appointment at tenured full professor will be considered). We seek outstanding candidates with demonstrated research interests in the neurosciences and/or biophysics. Candidates should have a Ph.D. and/or M.D. degree in a relevant field as well as postdoctoral training and publications in highly rated journals. The successful candidate will be expected to conduct an active, independent, funded research program, and to contribute teaching with excellence in medical and graduate courses in neuroscience and physiology. Send paper copies of: letter of application, curriculum vitae, statements of research and teaching interests, and copies of three publications to: **Dr. Karl Magleby, Chair, Department of Physiology and Biophysics, R-430, University of Miami School of Medicine, 1600 N.W. 10th Avenue, Miami, FL 33136.** Letters of recommendation from three references should be sent directly to the same address. Review of applications will commence when received and will continue until the position is filled. *The University of Miami is an Equal Opportunity/Affirmative Action Employer.*

Genentech is the founder of the biotechnology industry and among the world's leading biotech companies. We are instrumental in all areas of drug development from research and development to manufacturing and commercialization. We have the following opportunities available at our South San Francisco corporate headquarters:

SCIENTISTS: Must have a Ph.D. in biochemistry, immunology, medicine, or a related field, or equivalent work experience. For detailed job requirements and immediate consideration, please apply online at website: <http://www.genec.com/careers> and reference Requisition # 04-1000003647.

PHARMACEUTICAL SPECIALISTS (MICROBIOLOGY): Must have a Ph.D. in microbiology, virology, or a related field, or equivalent work experience. For detailed job requirements and immediate consideration, please apply online at website: <http://www.genec.com/careers> and reference Requisition # 88-1000005119.

Genentech offers one of the most comprehensive benefits packages in the industry. Our culture emphasizes working hard, working together, and sharing rewards. *Genentech is an Equal Opportunity Employer.*

POSITIONS OPEN

SENIOR SCIENTIST/
SIMULATIONS ANALYST

Aptima seeks candidates for open Senior Scientist/Simulations Analyst positions interested in working with a wide variety of applied projects. Responsibilities include problem formulation, solution prototyping, customer interfacing, technical writing of reports and proposals, and project management; supervising research development; design, development, testing, and evaluation of Social Networks, Quantitative Organizational Modeling, Agent-Based Simulation, and other Simulation Approaches used to capture and simulate human performance and translating human scenarios into executable modeling systems. Qualified candidates must possess a Ph.D. or M.S. degree in applied mathematics, electrical and/or systems engineering or an engineering related field, mathematics, operations research/sociology; must have experience in simulating, developing, and implementing models of complex systems in commercial modeling environments along with knowledge of the end-to-end consulting services cycle. Qualified candidates must submit a cover letter, resume, and salary requirement to: **Aptima Personnel, 12 Gill Street, Suite 1400, Woburn, MA 01801,** or by e-mail: aptima_personnel@aptima.com.

UNIVERSITY OF ARKANSAS FOR
MEDICAL SCIENCES
College of Pharmacy

The Department of Pharmaceutical Sciences invites applications for tenure-track **FACULTY POSITIONS**. Rank and salary are negotiable. Successful candidates will be expected to have a Ph.D. in pharmaceutical sciences or related field, to teach in the professional and graduate programs, and to establish an extramurally funded independent and/or collaborative research program (pharmaceutics is preferred, but other areas will be considered). Numerous opportunities exist for collaborations within the campus. Application review will begin immediately and continue until the positions are filled. Interested candidates should forward a letter of interest, curriculum vitae, and contact information for at least three references to: **Russell B. Melchert, Ph.D., University of Arkansas for Medical Sciences, College of Pharmacy, Department of Pharmaceutical Sciences, 4301 W. Markham, #522-3, Little Rock, AR 72205. Telephone: 501-686-6495; fax: 501-686-6057; e-mail: melchert@uams.edu.** *The University of Arkansas for Medical Sciences is an Equal Opportunity/Affirmative Action Employer.*

FACULTY POSITION
Anatomy Department

The Department of Anatomy at Midwestern University seeks applicants for a tenure-track position at the level of **ASSISTANT PROFESSOR**. Applicants must have a Ph.D. or equivalent, postdoctoral training is preferred, and a commitment to excellence in teaching. Applicants are expected to establish an independent research program capable of attracting extramural funding. Preference will be given to individuals broadly trained in the anatomical disciplines, with an emphasis on human gross and microscopic anatomy. Send curriculum vitae, names of references, and a statement specifying teaching interests and research plans to: **Robert R. Terreberry, Ph.D., Department of Anatomy, Midwestern University, 555 31st Street, Downers Grove, IL 60515.** Review of applications will begin on February 28, 2005. *Affirmative Action/Equal Opportunity Employer. Women/Minorities/Veterans/Persons with Disabilities are encouraged to apply.*

A **POSTDOCTORAL POSITION** is available to study the mechanism of processive DNA synthesis of vaccinia virus and to discover inhibitors by rapid screening. Experience with vaccinia virus is desirable. E-mail curriculum vitae and three reference names to: **Dr. Robert Ricciardi, University of Pennsylvania, Philadelphia, PA** at e-mail: ricciardi@biochem.dental.upenn.edu.

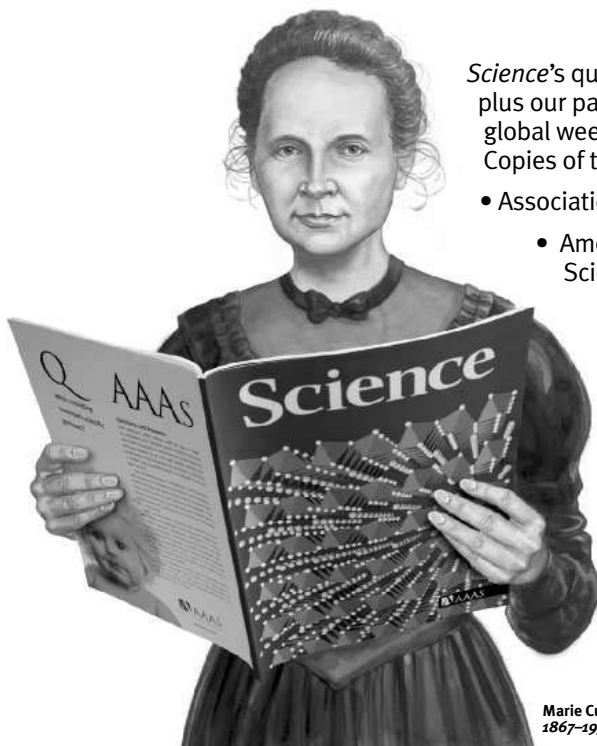
Exhibit at
the AAAS/Science
Career Fair, 21 February 2005.

Women in Science

A *Science* Advertising Supplement



To attract great scientists, talk to
someone who knows science.



Marie Curie
1867-1934

Science's qualified circulation of 129,590¹
plus our pass-along readers brings total
global weekly readership to over 710,000.²
Copies of this issue will be distributed to:

- Association for Women in Science
- American Men and Women in
Science mailing list
- University of Wisconsin Career
Fair, 2 March, Madison, WI

**ScienceCareers.org postings
available** for a nominal fee.
Post your print recruitment
ad for 8 weeks.

¹ *Science* June 2004 BPA Publisher's Statement.
² *Science* June 2004 circulation as applied to 14
January 2000 Harvey Readership Survey and
2002 Harvey Cumulative Report, publisher's
own data.

Issue date 25 February 2005

Reserve ad space by 8 February 2005

For more information, contact:
Daryl Anderson – 202-326-6543
advertise@sciencecareers.org

ScienceCareers.org

We know science



POSITION OPENS

ASSISTANT OR ASSOCIATE
PROFESSOR
Neurobiology/Neural Control of the
Circulation

The Department of Biomedical Sciences and the Dalton Cardiovascular Research Center at the University of Missouri-Columbia (MU) invite applications for a tenure-track position as Assistant or Associate Professor. This position represents a Mission Enhancement Initiative by the University of Missouri in support of the existing excellence in neurohumoral control of the circulation on campus (see **websites: <http://dalton.missouri.edu> and <http://www.cvm.missouri.edu/vbms>**). We seek applicants with demonstrated research achievements, who have, or will establish, an active nationally recognized research program that will complement ongoing work in neurohumoral control of physiological systems. Specific areas of investigation may include molecular biology, cell biology, or electrophysiology related to synaptic transmission, sensory processing, and/or receptor systems in central autonomic pathways. Outstanding candidates in related areas also are encouraged to apply. MU features a strong Interdisciplinary Neuroscience Program (**website: <http://www.neurosci.missouri.edu>**) and a major new Life Sciences initiative (**website: <http://lifesciences.missouri.edu>**). We offer competitive salaries and startup packages, modern research laboratories and support facilities, and a highly interactive faculty. Columbia, Missouri, is an attractive, progressive city with an excellent school system. Electronic submission of applications should be sent to **e-mail: neurohumoral@missouri.edu**. Attach to the e-mail a single PDF (Adobe Acrobat) or Microsoft Word document that includes your curriculum vitae, the names of three references, and a statement of research and teaching interests. Alternately, mail application materials to: **Dr. Cheryl M. Heesch, University of Missouri-Columbia, DCRC, 134 Research Park Drive, Columbia, MO 65211**. Review of applications will begin on February 15, 2005, and continue until the position is filled. To request ADA accommodations contact: **Nancy Alton at telephone: 573-882-7587**. *MU is an Equal Opportunity/Affirmative Action Employer.*

The Section of Nephrology and Functional Genomics Facility at the University of Chicago have an exciting opportunity for a junior rank **RESEARCH ASSOCIATE** to examine candidate genes relevant to kidney disease. We seek an individual who can work independently to follow-up on our microarray studies by utilizing short (or small) interfering RNA-based gene knockdown approaches in well-characterized cell culture and animal models. Applicants must have a Doctorate degree and at least two years of postdoctoral research experience. Documented expertise in cellular and molecular biology is required; experience with siRNA and animal models would be preferred. Interested applicants should send curriculum vitae, letter of interest with specific research goals, and names of three references to: **Richard Quigg, Chief, Section of Nephrology and Director, Functional Genomics Facility**. **E-mail: rquigg@uchicago.edu**. *The University of Chicago is an Affirmative Action/Equal Opportunity Employer.*

A POSTDOCTORAL POSITION is available immediately to investigate pathogenesis by the retrovirus, mouse mammary tumor virus. The project aims to identify cellular genes/factors that contribute to the development of disease using genomic and proteomic techniques. Candidates with a Ph.D. in molecular/cell biology, biochemistry, or virology and experience with tissue culture are desired. Salary competitive. Submit curriculum vitae with a description of current research and contact information for three references to: **Michael Sakalian, Ph.D., Department of Microbiology and Immunology, The University of Oklahoma Health Sciences Center, 1019 BMSB, 940 Stanton L. Young Boulevard, P.O. Box 26901, Oklahoma City, OK 73190**. **E-mail: mike-sakalian@ouhsc.edu**. Review of applications will begin immediately and continue until the position is filled.

POSITION OPENS



SCIENTIFIC CURATOR

Mount Desert Island Biological Laboratory (MDIBL) invites applications for a full-time Scientific Curator to work on the NIH-funded, publicly available Comparative Toxicogenomics Database (CTD; **website: <http://ctd.mdibl.org>**). CTD supports cross-species comparative studies of toxicologically important genes and proteins. The successful candidate will be responsible for curating gene-chemical interaction data from the biomedical literature and working with a team of biologists and software developers to develop biological ontologies, determine data curation requirements, and design user interfaces. Applicants with strong backgrounds in molecular biology and toxicology are preferred. This is not an independent research or computer science position. Candidates must have strong communication and writing skills, be highly organized and self-motivated, and work effectively in a team environment. A Ph.D. degree in Life Sciences or an M.S. with appropriate experience is required.

MDIBL, located on Mount Desert Island, Maine, home of Acadia National Park, is a 106-year-old independent research institution. The Laboratory has world class scientific and educational programs. Please send a letter describing experience, resume, and names and addresses of three references to: **Dr. Patricia Hand, Administrative Director, MDI Biological Laboratory, P.O. Box 35, Salisbury Cove, ME 04672** or **e-mail: jobs@mdibl.org**. *MDIBL is an Affirmative Action/Equal Opportunity Employer. Women and members of minority groups are encouraged to apply.*

FACULTY POSITIONS
Wright State University (WSU)
School of Medicine
in Pharmacology and Toxicology

The Department of Pharmacology and Toxicology invites applications from research scientists at the **ASSOCIATE** or **FULL PROFESSOR** level. We anticipate hiring two to three new faculty over the next few years. All applicants must have a Ph.D., D.V.M., or M.D. with an established research program supported by extramural funds. The departmental strengths are molecular endocrinology, cardiovascular sciences, cellular neuroscience, and molecular toxicology. Preference will be given to candidates whose programs complement these areas and with experience in proteomic/genomic techniques. WSU has excellent laboratory space and specialized facilities for genomics, molecular biology, neuroscience, and integrative pharmacology. Instructional responsibilities include medical and graduate teaching as well as mentoring graduate research projects. Competitive salary and startup packages are available. Review of applications will begin February 1, 2005, and continue until positions are filled. Send curriculum vitae, a description of research interests, and names of three references to: **Chair of Search Committee, Department of Pharmacology/Toxicology, Wright State University School of Medicine, 3640 Colonel Glenn Highway, Dayton, OH 45435**. **E-mail: pharmtox@wright.edu; website: <http://www.med.wright.edu/pharm/>**.

Affirmative Action/Equal Opportunity Employer.

POSTDOCTORAL OPPORTUNITY

Position available immediately for a Ph.D. or equivalent to conduct research on signaling transduction and gene regulation in vascular smooth muscle cells in the laboratory of **Drs. K. C. Kent and B. Liu**. Experience in biochemistry, cell biology, and molecular biology is required. Qualified applicants should send their curriculum vitae and names of three references to **e-mail: bol2001@med.cornell.edu** or to: **Dr. B. Liu, Department of Surgery, Weill Medical College Cornell University, P707, 1300 York Avenue, New York, NY 10021**. *Cornell University is an Equal Opportunity Employer.*

POSITION OPENS

RESEARCH ASSISTANT
PROFESSOR
Proteomics Center

Applications are currently being accepted to fill a nontenure-track Research Assistant Professor position with overall responsibility for management and day-to-day operation of the Proteomics Center within the Department of Chemistry and Biochemistry at the University of South Carolina (USC). The successful candidate will be expected to collaborate in ongoing proteomics projects with investigators at USC and also to develop an independent research program within the field of bioanalytical mass spectrometry. Duties within the Proteomics Center will include preparation and subsequent characterization and identification of proteins and peptides in user-submitted samples using matrix-assisted laser desorption/ionization-time of flight/time of flight, electrospray quadrupole time of flight, and triple-quadrupole mass spectrometers, as well as general oversight of the facility. As the Associate Director of the Proteomics Center, the candidate will consult with users on data interpretation and will assist with user training (software and hardware). Qualifications include a Ph.D. in biochemistry or bioanalytical chemistry with experience in protein microsequencing and identification using mass spectrometry. Salary is competitive and negotiable. Candidates should submit curriculum vitae, a brief description of research experience and plans, and three letters of recommendation to: **Chair, Proteomics Search Committee, Department of Chemistry and Biochemistry, 631 Sumter Street, University of South Carolina, Columbia, SC 29208** or **e-mail: vhrogers@sc.edu**. Review of applications will begin immediately and continue until the position is filled. *Affirmative Action/Equal Employment Opportunity.*

CURATOR OF MOLLUSKS
Delaware Museum of Natural History

The Delaware Museum of Natural History (DMNH) is seeking a Curator for the Mollusk collections which are among the 10 largest in the United States. Primary responsibilities include: establishing a research program centered around systematics, natural history, ecology, or behavior of mollusks, curation of the invertebrate collections, and general administration of the Mollusk department. In addition, the Curator will assist in development of exhibits and public programs.

Requirements: Ph.D. with a specialty in mollusks, one year of curatorial experience and one year of molluscan systematics experience required, demonstrated research, publication, and grant writing record. Excellent benefit package. For additional details please see the job position listed on our **website: <http://www.delmnh.org>**. Send statement of research interests, curriculum vitae, and the names and contact information for three references to: **Human Resources, Delaware Museum of Natural History, Box 3937, Wilmington, DE 19807-0937** by March 4, 2005. Please include the position title with your application. *DMNH is an Equal Opportunity Employer.*

The Heart and Vascular Research Center, MetroHealth Campus of Case Western Reserve University seeking M.D. or Ph.D. scientist for tenure-track position in cardiac electrophysiology research or related field. The candidate will have opportunity to develop an independent scientific career working with team of established basic science and clinical investigators with emphasis on integration of molecular, cell biology, biomedical engineering, and clinical approaches to cardiac electrophysiology. Candidates with background in molecular biology and interest in cell and gene therapy are of particular interest. Candidates should have qualifications for appointment at the **ASSISTANT** or **ASSOCIATE PROFESSOR** level.

Contact: **David S. Rosenbaum, M.D.** via **e-mail: drosenbaum@metrohealth.org** or **telephone: 216-778-2005**. *Case Western Reserve University and MetroHealth are Equal Opportunity/Affirmative Action Employers.*

SYMPOSIA

2nd International Immunoinformatics Symposium

Second international Congress on Immunoinformatics: Biomedicine at the Intersection of Genomics and Immunology. Jointly sponsored by the Boston University Center for Advanced Biotechnology and Brown University.

Monday, March 7, 2005 Workshop
- Immunoinformatics Tools Tutorial

Tuesday, March 8, 2005 - Wednesday, March 9, 2005 - Immunoinformatics Symposium, Boston University, Photonics Center, 8 St. Mary's Street, Boston, MA 02215

<http://www.bu.edu/bioinformatics/symposium/index.html>

For more information contact:
Caroline Lyman: clyman@bu.edu

POSITIONS OPEN

Department of Health and Human Services National Institutes of Health National Institute of Neurological Disorders and Stroke Chief, Neuroimmunology Branch Clinical Neuroscience Program Division of Intramural Research



The Neuroimmunology Branch of National Institute of Neurological Disorders and Stroke (NINDS), NIH, a component of the intramural research program within NINDS, conducts basic and clinical research into the cause and treatment of immunologically mediated diseases of the central nervous system. The major focus of the Branch is research into the cause and treatment for multiple sclerosis. The Branch is recognized both nationally and internationally as a leading research laboratory in the field of multiple sclerosis research.

The Neuroimmunology Branch is currently searching for an individual with experience in both basic immunology and clinical research to become the Chief of the Branch. The individual would be able to pursue his or her own research, focused either on basic immunological mechanisms of disease or on clinical studies of the disease process, including therapeutic trials. In addition the individual would be responsible for guiding the overall research efforts of the Branch. The Branch currently consists of four tenured individuals with interests ranging from basic molecular immunology to clinical studies of MS using MRI. Each of the tenured individuals is the chief of one of the four sections within the Branch. The successful applicant will also serve as chief of a section within the Neuroimmunology Branch. The Branch occupies approximately 4500 square feet. The Branch has access to the advanced imaging facilities at NIH as well as the Clinical Center with its world class research facilities.

Ideal candidates will have a record of outstanding research accomplishments including evidence of innovative thinking in the field of Neuroimmunology and will have demonstrated the ability to oversee a complex research organization. The position is open to individuals having either a Ph.D. or M.D. degree. Salary will be dependent on the experience of the individual. Direct questions about the position to **Dr. Story Landis, Ph.D., Director, NINDS** at landiss@ninds.nih.gov (301-496-4697). Applicants should send a cover letter, curriculum vitae and bibliography to: **Peggy Rollins, Office of the Scientific Director, 36 Convent Drive, Room 5A05, Bethesda, MD 20896** (phone 301-435-2232). Applications must be postmarked by **March 24, 2005**.



DHHS and NIH are
Equal Opportunity Employers.



GRANTS

Johnson & Johnson

CONSUMER & PERSONAL PRODUCTS WORLDWIDE
Division of Johnson & Johnson Consumer Companies, Inc.

Request for skin research proposals

The Johnson & Johnson Skin Research Training Grant Program provides funding for postdoctoral training across a broad range of skin-related biomedical research disciplines at universities and research institutions. The SRC grants are given annually to two applicants with a Ph.D. degree, from different research laboratories or teams. The SRC grants for the year 2005 will be renewable for up to three years, at \$50,000/year.

A one page preliminary proposal should be submitted by postdoctoral fellows or principal investigators as indicated below. Key points to address are the novelty of the biology or potential health or therapeutic benefits. Submission deadline is March 1st, 2005. Full proposal submission requests will be communicated on April 1st, 2005. Rejections will not be communicated. The Johnson & Johnson Skin Research Center of Johnson & Johnson Consumer & Personal Products Worldwide, Division of Johnson & Johnson Consumer Companies, Inc., does not provide individual critiques of proposals submitted. **Proposals should be mailed to:** SRC skin grant, 199 Grandview Rd, Skillman, NJ 08558, c/o RG25.

Although no proprietary claim is made on the research carried out through an SRC training grant, the relationship built between The Johnson & Johnson Skin Research Center of Johnson & Johnson Consumer & Personal Products Worldwide, Division of Johnson & Johnson Consumer Companies, Inc., and the grant recipient may lead to research agreements or business arrangements when appropriate.

ANNOUNCEMENTS

NIH-RAID (Rapid Access to Intervention Development) AN NIH ROADMAP INITIATIVE

Consultants to the Roadmap planning process advised the NIH to facilitate the development and testing of novel therapeutic interventions, particularly ones for uncommon disorders which may not attract private sector investment. Based on this advice, the NIH is establishing a new program, NIH-RAID, modeled upon the NCI's RAID program, to make available on a competitive basis, contractual resources for the preclinical development of small molecules.

NIH-RAID is not a grant program. Instead it will afford investigators access to critical resources needed for preclinical development. Services may include: creation of a product development plan, small molecule synthesis according to GMP standards, formulation, pharmacokinetic studies and animal toxicology, and help with preparation of an IND. Services actually provided will depend upon the stage of the project and the strength of the preliminary data. The final product will be returned to the applicant for further target validation and/or phase I human studies.

The deadlines for receipt of requests are **February 1, 2005** and **June 1, 2005**.

- Further information about this program and the required format for applications can be found at: <http://nihroadmap.nih.gov/raid/>.
- Inquiries can be made to the **NIH-RAID Program Coordinator** by telephone at 301-496-6325 or by e-mail to NIH-RAID@nidck.nih.gov.



NIH-RAID PILOT Program Office
NIDDK
6707 Democracy Blvd
2 Democracy Plaza, Room 634
Bethesda, MD 20892-5460



Telephone (301) 594-4660
NIH-RAID@nidck.nih.gov



POSITION OPENS

We are seeking a **POSTDOCTORAL FELLOW** to study the molecular mechanisms associated with the effects of cholesterol on the establishment and progression of serious human degenerative diseases. These diseases include cancer (primarily prostate), osteoporosis, and vascular calcification. The investigations will require the use of basic lipid/protein biochemistry techniques including membrane isolation, cholesterol measurement, and immunoblotting. Studies will also involve state-of-the-art proteomic techniques including 2-D gel/matrix-assisted laser desorption/ionization—time of flight analysis and quantitative liquid chromatography/mass spectrometry/mass spectrometry analysis. In vivo animal models will be used. Successful candidates must possess a Ph.D. or M.D. degree with relevant background in biochemistry. Experience with cholesterol and proteomics is preferred, but is not essential.

Interested candidates should send copies of their curriculum vitae including the names and addresses of three references to:

Keith R. Solomon, Ph.D.
Assistant Professor in Orthopaedic Surgery
Administrative Director, Children's
Hospital Proteomics Center
Children's Hospital
Department of Orthopaedic Surgery
Enders 1030
300 Longwood Avenue
Boston, MA 02115
Telephone: 617-919-2935
Fax: 617-730-0239
E-mail: keith.solomon@childrens.harvard.edu

CENTER DIRECTOR (HEAD), Center for Ecological Entomology (CEE), Illinois Natural History Survey (INHS), Champaign, Illinois. Successful candidate will serve as administrative head of CEE and conduct externally funded research in agricultural, medical, or environmental entomology. Requires Ph.D. in entomology or related discipline, relevant administrative experience, demonstrated leadership and team-building skills, strong record of independent research, and interest in outreach or extension education. CEE includes eight Ph.D. scientists conducting research in insect pathology, ecotoxicology, biocontrol, integrated pest management, organic production, biosystematics, insect behavior, and medical entomology, assisted by 25 research, technical, or support staff. The INHS is part of the Illinois Department of Natural Resources and an Affiliated Agency of the University of Illinois at Urbana-Champaign, IL. For more information and application requirements, see website: <http://www.inhs.uiuc.edu/opportunities/index.php>. Deadline: March 1, 2005.

BIOCHEMIST/MOLECULAR BIOLOGIST

The Division of Pharmacogenomics and Molecular Epidemiology at the National Center for Toxicological Research (NCTR) seeks an individual with biochemistry and molecular biology training to carry out both independent and collaborative studies aimed at assessment of human exposure and individual susceptibility to carcinogens, organ toxicity, and adverse drug reactions that are of regulatory or public health concern to the U.S. Food and Drug Administration. The position is at the AD-12 level (**STAFF FELLOW**; salary is \$60,718 per year). Appropriate technical support and startup funding will be provided. Interested applicants should submit curriculum vitae and the names and addresses of at least three references to: **Fred F. Kadlubar, Ph.D.** E-mail: fkadlubar@nctr.fda.gov.

NCTR is an Equal Opportunity/Affirmative Action Employer.

POSTDOCTORAL POSITIONS are available to study (1) molecular mechanism of tumorigenesis and immunoescape by adenovirus and (2) processive DNA synthesis of Kaposi's Human Herpesvirus. E-mail curriculum vitae and three reference names to: **Dr. Robert Ricciardi, University of Pennsylvania, Philadelphia, PA** at e-mail: ricciardi@biochem.dental.upenn.edu.

POSITION OPENS

POSTDOCTORAL POSITION: Department of Genetics Harvard Medical School

An exciting position to study the genetic basis of aneurysm formation. Range of projects include genotyping and identification of gene defects, the development of animal models, and molecular studies to determine the biological consequences of genetic defects. This project is a collaborative effort between **Dong H. Kim, M.D.**, and **Jonathan Seidman, Ph.D.** Work in a strong environment: terrific research community in the Department of Genetics; modern, resource-rich laboratory with more than 20 postdoctoral fellows, technicians, and students; funding for several years. We are looking for a motivated and dedicated scientist with Ph.D., M.D., or equivalent degree. Background in molecular techniques is preferable but not mandatory. Students expecting to complete their degree are encouraged to apply. Competitive salary and benefits. Interested persons should forward curriculum vitae and a list of three references to:

Dong H. Kim, M.D.
Harvard Medical School/
Brigham and Women's Hospital
75 Francis Street
Boston, MA 02115
E-mail: dkim7@partners.org

Ph.D. POSTDOCTORAL POSITION

The Gastroenterology Division of the Children's Hospital of Michigan is seeking a Ph.D. at a Post-doctoral level in the area of immunology, molecular, and cell biology with some experience in microbiology and translational research to work full time in the area of inflammatory bowel disease and gastroesophageal reflux.

Qualifications: (1) Ph.D. (molecular biology or immunology); (2) experience in cell culture, molecular biology techniques, and genomics (polymerase chain reaction, in situ hybridization, microarrays), inflammatory mediators (e.g., cytokines); (3) manuscript and grant writing skills.

Salary based on experience and qualifications. Position is available immediately.

Send curriculum vitae and names of three references to:

V. Tolia, M.D.
Director, Division of Gastroenterology
Children's Hospital of Michigan
3901 Beaubien Boulevard
Detroit, MI 48201
Telephone: 313-745-5056
Fax: 313-745-5155
E-mail: vtolia@med.wayne.edu

POSTDOCTORAL AND ASSOCIATE RESEARCH SCIENTISTS Columbia University College of Physicians and Surgeons

Positions available to perform structural and functional characterization of molecules involved in antiviral responses and RNA metabolism. Strong background in cell and molecular biology, immunology, and/or virology required. Training in biochemical analysis of RNA or RNA-binding molecules preferred. Send curriculum vitae and three references to: **Dr. P.B. Fisher, Department of Pathology, Columbia University Medical Center, 630 West 168th Street, New York, NY 10032.** Fax: 212-305-8177; e-mail: pbfl@columbia.edu. Columbia University takes Affirmative Action toward Equal Opportunity.

POSTDOCTORAL POSITION in cellular and molecular pharmacology available June 1, 2005. Applicants must have an M.D. or Ph.D. degree and less than five years of postdoctoral experience. Experience in molecular biology and animal physiology is preferred. Salary is \$35,000 per year or higher depending upon experience (NIH pay scale). For more information visit website: <http://ostrom.utm.edu>. Send curriculum vitae by e-mail: rostrom@utm.edu.

POSITION OPENS

POSTDOCTORAL POSITION is available from March 2005 in the Center for Nano Biomedicine Technology at Chung Yuan Christian University, Taiwan, Republic of China. The laboratory's research focuses on the quantum dots synthesis and its biological applications. A strong background in biochemistry as well as experience in studying nanocrystals is required. Please send curriculum vitae and the name of two references to: **Professor Dr. Walter H. Chang, Department of Biomedical Engineering.** Fax: 886-3-2654581 or e-mail: whchang@cycu.edu.tw.

ANNOUNCEMENTS

INDO-U.S. SCIENCE AND TECHNOLOGY FORUM Fulbright House, 12 Hailey Road New Delhi 110 001 CALL FOR WORKSHOP PROPOSALS

The Indo-U.S. Science and Technology Forum seeks to support collaborations between U.S. and Indian institutions in topical and frontier areas of science and technology that are of mutual interest. We aim to facilitate efforts designed to be catalytic in nature by involving best and brightest investigators in a broad distribution among all disciplines including science, engineering, biomedical research, and mathematics. The Forum would support efforts that have a strong potential for generating follow-on activities and long-term contacts that could be continued through other established bilateral funding modes. We are also interested in promoting the next generation of scientists and engineers who seek to build new and sustained relationships. The Forum solicits joint proposals by 28 February 2005 from principal investigators in academia, private research and development entities, including industry/non-governmental organizations and government institutions for holding bi-national workshop, roundtable, town hall meeting, conference, and symposia to be held either in India or the United States. The detailed proposal submission format is available on Forum website: <http://www.indoustf.org> or by e-mails: amitra@indoustf.org or mcheetham@si.edu.

COURSES AND TRAINING

2nd Annual EXPERIMENTAL NEUROGENETICS OF THE MOUSE May 15-24, 2005 University of Tennessee Health Science Center Memphis, Tennessee, U.S.A.

This lecture and hands-on workshop is to train students and researchers in the use of mice in the analysis of nervous system structure and function. Topics covered include mouse informatics, genetics of Mendelian and complex disorders of the nervous system, and various approaches to examining gene function (e.g., knockouts, N ethyl nitro sourea mutagenesis, short (or small) interfering RNA, inbred lines).

A significant part of the course will be devoted to phenotypic analysis of mice for neurological traits using behavioral, anatomical, physiological, and molecular screens. Invited speakers include: **Ellen Hess, Jacqueline Crawley, and Ilan Golani**, plus faculty affiliated with the Tennessee Mouse Genome Consortium.

Website: <http://mouseneurogenetics.utm.edu> or contact: **Pat Goss** at e-mail: pgoss@utm.edu.

Channels and Transporters: The Eric School of Biophysics will hold a European Molecular Biology Organization-sponsored lecture course on channels and transporters 30 May to 7 June 2005 in Erice, Sicily. The speakers are: **S. Amara, P. Bezannilla, R. Blakely, D. Clapham, L. DeFelice, D. Doyle, C. Fahlke, A. Gaili, R. Kaback, B. Kanner, M. Kavanaugh, C. Miller, G. Rudnick, S. Schuldiner, D. Ypey**. To learn more, and to apply online, go to website: <http://medschool.mc.vanderbilt.edu/channels.transporters2005/>.

AAAS Annual Meeting and *Science* Career Fair

The 2005 AAAS Annual Meeting is the perfect place to explore your career options and attend the *Science* Career Fair. Both the career fair and the career-related workshops are FREE to attend.

AAAS Annual Meeting

DATES: 17–21 February 2005

PLACE: Marriott Wardman
Park Hotel
Washington, DC

**CAREER WORKSHOPS (see website
for complete listing of workshops):**

- Strategic Networking
- Pathways to Multiple Career Opportunities
- AAAS Fellowship Program in Public Policy and Mass Media
- Research Training at the NIH
- How to Fire Up your Presentation

AAAS/*Science* Career Fair

DATE: 21 February 2005

PLACE: Marriott Wardman
Park Hotel
Washington, DC

TIME: 11:00 am – 4:00 pm

Science Careers offers you the chance to meet employers.

Exhibiting employers are typically from biotechnology, pharmaceutical, government, and manufacturing organizations.

For more information and updates to our exhibitor list, please visit www.sciencecareers.org and click on Career Fairs.



Registration is required to attend the career workshops. Visit www.sciencecareers.org and click on Career Fairs for instructions on how to register for free.

ScienceCareers.org

We know science



Institutional Site
License Available

Q

What can *Science* STKE give me?



A

The definitive resource on cellular regulation

STKE – Signal Transduction
Knowledge Environment offers:

- A weekly electronic journal
- Information management tools
- A lab manual to help you organize your research
- An interactive database of signaling pathways

STKE gives you essential tools to power your understanding of cell signaling. It is also a vibrant virtual community, where researchers from around the world come together to exchange information and ideas. For more information go to www.stke.org

To sign up today, visit promo.aaas.org/stkeas

Sitewide access is available for institutions. To find out more e-mail stkelicense@aaas.org



IT TAKES BOTH SIDES OF THE BRAIN.



CALL FOR ENTRIES Science & Engineering Visualization Challenge

When the left brain collaborates with the right brain, science merges with art to enhance communication and understanding of research results—illustrating concepts, depicting phenomena, drawing conclusions.

The National Science Foundation and *Science*, published by the American Association for the Advancement of Science, invite you to participate in the annual *Science and Engineering Visualization Challenge*. The competition recognizes scientists, engineers, visualization specialists, and artists for producing or commissioning innovative work in visual communications.

ENTRY DEADLINE:
May 31, 2005

AWARDS CATEGORIES:
Photos/Still Images, Illustrations, Explanatory Graphics, Interactive Media, Non-interactive media

COMPLETE INFORMATION:
www.nsf.gov/od/lpa/events/sevc

Awards in each category will be published in the September 23, 2005 issue of *Science* and *Science Online* and displayed on the NSF website.



Accept the challenge.
Show how you've mastered
the art of understanding.

MARKETPLACE

GenScript Corporation
www.genscript.com 877-436-7274

Custom Peptide
\$4.80/aa

Synthesize Any Gene
\$1.45/bp

Vector-based siRNA
CMV, U6, inducible promoters, cGFP tracking
Lentiviral, Retroviral, Adenoviral Delivery

Custom Polyclonal Antibody: \$600
Monoclonal Antibody: \$5000

**Custom Peptides
& Antibodies**

Best Service & Price! Compare and Save!
Free Sequence and Antigenicity Analyses

Alpha Diagnostic (800) 786-5777
www.4adi.com service@4adi.com

POLYCLONAL ANTIBODIES

Lets Us Design Your Antigen for FREE!

FAST DELIVERY
PEPTIDE TO ANTISERUM IN 70 DAYS
100% SATISFACTION GUARANTEED
Fax: 978-630-0021

...MADE EASY!
**NEW ENGLAND
PEPTIDE, INC.**
Tel: 888-343-5974
www.newenglandpeptide.com

POLYMORPHIC
Polymorphic DNA Technologies, Inc.™

SNP Discovery
using DNA sequencing
\$0.01 per base.

Assay design, primers, PCR, DNA sequencing and analysis included.

888.362.0888
www.polymorphicdna.com • info@polymorphicdna.com

Molecular Cloning Laboratories

High throughput DNA sequencing
Gene synthesis \$2/bp any size
Protein expression & purification
Yeast 2 hybrid/phage displaying

www.mclab.com, 888-625-2288

Pep-T-Topes

~1 mg crude (70% ave.)
1-15 mers, @ ≥ 96 peptides

\$35 / peptide

www.pepscan.com

POLYMORPHIC
Polymorphic DNA Technologies, Inc.™

Custom Gene Synthesis
\$1 per base pair

Guaranteed.
Sequence confirmation with bidirectional sequencing.

888.362.0888
www.polymorphicdna.com • info@polymorphicdna.com

DNA Sequencing Services

SNP Discovery/Resequencing/ Variant Discovery	\$0.01 per base, per direction
High throughput sequencing	\$5 per reaction
cDNA sequencing	\$5 per reaction
S.A.G.E. sequencing	\$5 per reaction



www.polymorphicdna.com
info@polymorphicdna.com

1125 Atlantic Ave., Ste. 102
Alameda, CA 94501

For research use only. © Polymorphic DNA Technologies, 2005

Custom Genomic Services

Custom Gene synthesis	\$1 per base pair
PCR	\$1 per amplicon
Real Time PCR	\$500 per assay
Whole genome scanning	\$5 per locus, per sample
Nucleic acid extraction/ purification	\$2.50 per mini-prep
Mutagenesis	\$400 any mutation within 5 bp frame
Subcloning	\$400 per clone
Library construction: Genomic, cDNA, BAC	Please inquire for pricing

888.362.0888

**For more information please visit
www.polymorphicdna.com**